VOLUME 105 PART C NUMBER 8 SEPTEMBER 1958

The Proceedings

OF

THE INSTITUTION OF ELECTRICAL ENGINEERS

FOUNDED 1871: INCORPORATED BY ROYAL CHARTER 1921

PART C

MONOGRAPHS Nos. 283–309

SAVOY PLACE . LONDON W.C.2

Price Fifteen Shillings

The Institution of Electrical Engineers

FOUNDED 1871
INCORPORATED BY ROYAL CHARTER 1921

PATRON: HER MAJESTY THE QUEEN

COUNCIL 1957–1958

President

T. E. GOLDUP, C.B.E.

Past-Presidents

W. H. ECCLES, D.Sc., F.R.S.
THE RT. HON. THE EARL OF MOUNT EDGCUMBE, T.D.
J. M. DONALDSON, M.C.
PROFESSOR E. W. MARCHANT, D.Sc.
H. T. YOUNG.
SIR GEORGE LEE, O.B.E., M.C.
SIR ARTHUR P. M. FLEMING, C.B.E., D.Eng., LL.D.
J. R. BEARD, C.B.E., M.Sc.
SIR NOEL ASHBRIDGE, B.Sc.(Eng.).
COLONEL SIR A. STANLEY ANGWIN, K.C.M.G., K.B.E., D.S.O., M.C., T.D., D.Sc.(Eng.).
SIR HARRY RAILING, D.Eng.
P. DUNSHEATH, C.B.E., M.A., D.Sc.(Eng.).
SIR VINCENT Z. DE FERRANTI, M.C.
T. G. N. HALDANE, M.A.
PROFESSOR E. B. MOULLIN, M.A., Sc.D.
SIR ARCHIBALD J. GILL, B.Sc.(Eng.).
SIR JOHN HACKING.
COLONEL B. H. LEESON, C.B.E., T.D.
SIR HAROLD BISHOP, C.B.E., B.Sc.(Eng.).
SIR JOSIAH ECCLES, C.B.E., D.Sc.
SIR GEORGE H. NELSON, BART.
SIR GORDON RADLEY, K.C.B., C.B.E., Ph.D.(Eng.).

Vice-Presidents

S. E. GOODALL, M.Sc.(Eng.).
WILLIS JACKSON, D.Sc., D.Phil., Dr.Sc.Tech., F.R.S.
G. S. C. LUCAS, O.B.E.
SIR HAMISH D. MACLAREN, K.B.E., C.B., D.F.C., LL.D., B.Sc.
C. T. MELLING, C.B.E., M.Sc.Tech.

Honorary Treasurer

THE RT. HON. THE VISCOUNT FALMOUTH.

Ordinary Members of Council

PROFESSOR H. E. M. BARLOW, Ph.D., B.Sc.(Eng.).
J. A. BROUGHALL, B.Sc.(Eng.).
C. M. COCK.
SIR JOHN DEAN, B.Sc.
B. DONKIN, B.A.
J. S. FORREST, D.Sc., M.A.
PROFESSOR J. GREIG, M.Sc., Ph.D.
E. M. HICKIN.
J. B. HIGHAM, Ph.D., B.Sc.
D. MCDONALD, B.Sc.
F. C. MCLEAN, C.B.E., M.Sc.
B. L. METCALF, B.Sc.(Eng.).
J. R. MORTLOCK, B.Sc.(Eng.).
H. H. MULLENS, B.Sc.
A. H. MUMFORD, O.B.E., B.Sc.(Eng.).
R. H. PHILLIPS, T.D.
D. P. SAYERS, B.Sc.
C. E. STRONG, O.B.E., B.A., B.A.I.
H. WATSON-JONES, M.Eng.
D. B. WELBOURN, M.A.
H. WEST, M.Sc.

Chairmen and Past-Chairmen of Sections

Measurement and Control:
H. S. PETCH, B.Sc.(Eng.).
*D. TAYLOR, M.Sc., Ph.D.

Radio and Telecommunication:
J. S. MCPETRIE, Ph.D., D.Sc.
*R. C. G. WILLIAMS, Ph.D., B.Sc.(Eng.).

Supply:
PROFESSOR M. G. SAY, Ph.D., M.Sc., F.R.S.E.
*P. J. RYLE, B.Sc.(Eng.).

Utilization:
J. VAUGHAN HARRIES.
*H. J. GIBSON, B.Sc.

Chairmen and Past-Chairmen of Local Centres

East Midland Centre:
J. D. PIERCE.
*H. L. HASLEGRAVE, M.A., Ph.D., M.Sc. (Eng.).

Mersey and North Wales Centre:
T. MAKIN.
*P. D'E. STOWELL, B.Sc.(Eng.).

North Midland Centre:
A. J. COVENEY.
*W. K. FLEMING.

North-Eastern Centre:
T. W. WILCOX.
*J. CHRISTIE.

North-Western Centre:
F. R. PERRY, M.Sc.Tech.
*T. E. DANIEL, M.Eng.

Northern Ireland Centre:
C. M. STOUPE, B.Sc.
*DOUGLAS S. PARRY.

Western Centre:
J. F. WRIGHT.
*PROFESSOR G. H. RAWCLIFFE, M.A., D.Sc.

Scottish Centre:
E. O. TAYLOR, B.Sc.
*PROFESSOR F. M. BRUCE, M.Sc., Ph.D.

South Midland Centre:
L. L. TOLLEY, B.Sc.(Eng.).
*C. J. O. GARRARD, M.Sc.

Southern Centre:
L. G. A. SIMS, D.Sc., Ph.D.
*H. ROBSON, B.Sc.

* Past Chairman.

Secretary

W. K. BRASHER, C.B.E., M.A., M.I.E.E.

Deputy Secretary

F. JERVIS SMITH, M.I.E.E.

Assistant Secretary

F. C. HARRIS.

Editor-in-Chief

G. E. WILLIAMS, B.Sc.(Eng.), M.I.E.E.

The Institution is not, as a body, responsible for the opinions expressed by individual authors or speakers.
An example of the preferred form of bibliographical references will be found beneath the list of contents.

THE PROCEEDINGS OF
THE INSTITUTION OF ELECTRICAL ENGINEERS

EDITED UNDER THE SUPERINTENDENCE OF W. K. BRASHER, C.B.E., M.A., M.I.E.E., SECRETARY

VOL. 105. PART C. NO. 8. SEPTEMBER 1958

621.313.333

The Institution of Electrical Engineers
Monograph No. 283 U
Jan. 1958
©

A SIMPLIFIED ELECTROMAGNETIC THEORY OF THE INDUCTION MOTOR, USING THE CONCEPT OF WAVE IMPEDANCE

By Professor A. L. CULLEN, Ph.D., B.Sc., and T. H. BARTON, Ph.D., B.Eng., Associate Members.

(*The paper was first received 8th July, and in revised form 30th October*, 1957. *It was published as an* INSTITUTION MONOGRAPH *in January*, 1958.)

SUMMARY

Electromagnetic field theory is applied to the analysis of performance of an induction-motor rotor when it is exposed to a rotating magnetic field of constant amplitude. An idealized model of the rotor is taken and the analysis is simplified by the application of the concept of wave impedance. The model rotor is capable of simulating the effects of tooth-top and zigzag leakage fluxes, but end effects are neglected. The equations of performance thus obtained are shown to be identical with those obtained by the conventional theory when the latter includes skin effect. The model motor used by Mishkin (*Quarterly Journal of Mechanics and Applied Mathematics*, 1954, **7**, p. 472) is shown to give results widely different from those obtained in practice, since it neglects the zigzag leakage fluxes. The analogy between the tangential force acting on the rotor and radiation pressure is indicated, and it is shown that a change of variable familiar in microwave theory leads to the theory of the variable-speed induction motor developed by Williams and Laithwaite [*Proceedings I.E.E.*, Paper No. 2097 U, June, 1956 (**104**, A, p. 102)].

LIST OF PRINCIPAL SYMBOLS

a = Depth of tooth-top region of rotor.
b = Depth of rotor bars.
b_s = Width of rotor bars.
B_m = Maximum magnetic flux density.
d = Width of opening between tops of teeth on rotor.
E_z = Electric field strength in equivalent uniform rotor.
f_x = Force per unit volume on equivalent uniform rotor.
F = Force per unit area of rotor surface.
H_x, H_y = Magnetic field components in equivalent uniform rotor.
J_z = Current density in equivalent uniform rotor.
p_s = Slot pitch.
R = Rotor-bar resistance.
s = Slip.
X_0 = Equivalent standstill rotor-bar reactance.
x, y = Rectangular co-ordinates.
Z_{01}, Z_{02} = Wave impedances in tooth-top and rotor-bar regions respectively.
α = Skin effect parameter: α^{-1} = skin depth.
β = Phase-change coefficient of flux wave.
γ_1, γ_2 = Propagation coefficients looking into rotor through tooth-top and rotor-bar regions respectively.
μ_0 = Absolute permeability of free space.
μ_r = Relative permeability.
μ_x, μ_y, μ_x', μ_y' = Absolute permeabilities of equivalent uniform anisotropic media.

(1) INTRODUCTION

The induction motor, like all other electrical devices, must obey the laws of electricity and magnetism as formulated in Maxwell's equations of the electromagnetic field. However, a practical induction motor is so complicated in its geometry that an exact solution of these equations is quite impracticable, even if the effects of non-linearity and hysteresis in the iron are ignored.

A working theory of the induction motor has, however, been developed by making use of a.c. circuit theory. The parameters introduced into this theory can be evaluated theoretically by individual field calculations, usually of an approximate character.

In a rather indirect sense, this theory can be regarded as an approximate solution of Maxwell's equations, for the a.c. circuit equations themselves follow as a consequence of Maxwell's equations, subject to certain definable limitations.

Recently, however, an approximate solution of Maxwell's equations for an idealized model of an induction motor has been obtained by Mishkin.[1] His model is linear and replaces the practical toothed structure of stator and rotor by continuous though inhomogeneous regions, having appropriately averaged resistivities, and different permeabilities in directions parallel to, and perpendicular to, the air-gap. The effect of end windings is taken into account in the theory. The analysis, though approximate, leads to results which are exceedingly complicated, so that the connection between Mishkin's equations and the usual

Correspondence on Monographs is invited for consideration with a view to publication.
Prof. Cullen is Professor of Electrical Engineering, University of Sheffield.
Dr. Barton, who was formerly in the Department of Electrical Engineering, University of Sheffield, is now in the Department of Electrical Engineering, McGill University, Montreal.

© 1958: The Institution of Electrical Engineers

performance equations of the induction motor are not readily discernible. His analysis ignores the large part played by tooth-top and zigzag leakage flux in a practical machine. This omission leads to performance equations in which a principal component of leakage reactance is that of the rotor-slot, which, as is well known, is exceedingly dependent upon the slip. As a consequence, a current locus which diverges considerably from the circle diagram is given in a particular numerical example, and Mishkin attributes the divergence to skin effect. In fact, skin effect would be negligible over a practicable speed range in the example taken. Such divergence as is observed in practice is primarily attributable to saturation of the leakage-flux paths.

The purpose of the present paper is to present a more elementary electromagnetic theory of the induction motor in which, for simplicity, end effects are neglected, but which pays due attention to the part played by tooth-top leakage fluxes. The use of a simpler model facilitates comparison with conventional theory and moreover makes possible an exact solution of the problem.

The solution of the field equations is simplified, and given a clear physical significance, by making use in the analysis of the concept of wave impedance, which has for many years been a corner-stone of microwave theory, but which, so far as the authors are aware, has not previously been invoked in the theory of electrical machinery.

A further point of interest is that a simple change of variable, familiar in microwave circuit theory, leads at once to the theory of the brushless variable-speed induction motor of Williams and Laithwaite.[3]

It is shown, furthermore, that the theory of the squirrel-cage induction motor is closely related to the theory of radiation pressure and to the theory of electromagnetic surface waves. The force acting on the rotor of such a machine can in fact be legitimately described as the radiation stress due to a surface wave incident on the rotor at a complex angle of incidence of the form $\pi/2 + j\psi$, where ψ is much greater than unity.

(2) CIRCUIT ANALYSIS

The purpose of this Section is to state briefly the results of the circuit method of analysis of the induction motor, for comparison with the field-analysis results which are obtained in the following Section.

We consider a motor in which the flux density in the air-gap is a sinusoidal travelling wave of maximum value B_m. The time-average tangential force F per unit area of rotor surface is given by

$$F = \frac{\omega_0 \tau B_m^2}{2\pi p_s} \frac{sR}{R^2 + s^2 X_0^2} \quad . \quad . \quad . \quad . \quad (1)$$

where ω_0 is the stator frequency; s, the slip; τ, the pole pitch; p_s the slot pitch; R, the resistance per unit length of the rotor bars; and X_0, the rotor-bar reactance per unit length at standstill.

If R and X_0 can be regarded as constants, eqn. (1) gives the relationship between torque and slip for an induction motor quoted in elementary textbooks. In fact, however, R and X_0 depend on the rotor frequency because of skin effect. Formulae allowing for skin effect are given by Alger.[4] For our case and our notation they can be written

$$R = \frac{\alpha}{\sigma_0 b_s} \frac{\sinh 2\alpha b + \sin 2\alpha b}{\cosh 2\alpha b - \cos 2\alpha b} \quad . \quad . \quad . \quad . \quad . \quad (2)$$

$$X_0 = \omega_0 \mu_0 \left(\frac{a}{d} + \frac{1}{s\omega_0 \mu_0} \frac{\alpha}{\sigma_0 b_s} \frac{\sinh 2\alpha b - \sin 2\alpha b}{\cosh 2\alpha b - \cos 2\alpha b} \right) \quad (3)$$

where σ_0 is the conductivity of the rotor bars and

$$\alpha = \sqrt{\frac{s\omega_0 \mu_0 \sigma_0}{2}} \quad . \quad . \quad . \quad . \quad . \quad (4)$$

The rest of the notation is given in Fig. 1.

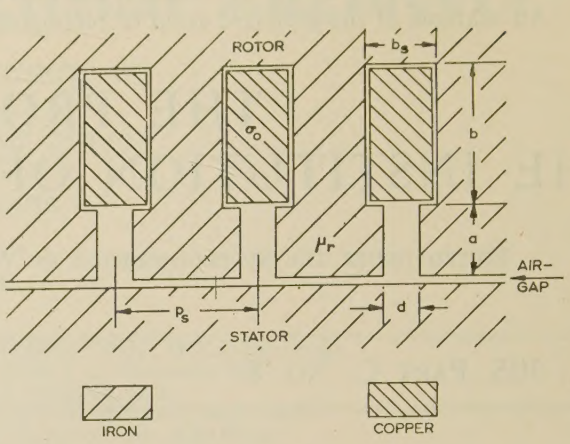

Fig. 1.—Slotted linear model motor.

The term $\omega_0 \mu_0 (a/d)$ in eqn. (3) is the reactance due to tooth-top leakage, which is dependent solely on the total conductor current and is unaffected by a non-uniform current density.

Eqns. (2) and (3) can, of course, be expanded in powers of αb, and the familiar formulae for R and X_0 neglecting skin effect can easily be derived in this way. To a first approximation, we find that

$$R \simeq \frac{1}{\sigma_0 b b_s} \quad . \quad . \quad . \quad . \quad . \quad . \quad . \quad (2a)$$

$$X_0 \simeq \omega_0 \mu_0 \left(\frac{a}{d} + \frac{b}{3b_s} \right) \quad . \quad . \quad . \quad . \quad (3a)$$

These formulae are applicable if $2\alpha b \ll 1$.

(3) FIELD ANALYSIS

The first step in applying the field method of analysis is to formulate a model of an induction motor which is simple enough to make such an analysis possible.

(3.1) Formulation of Idealized Problem

We first ignore the curvature of the air-gap and take a linearized cross-section of the actual machine as shown in Fig. 1. The effect of stator slots is also ignored. To facilitate analysis, the toothed structure of Fig. 1 is replaced by the continuous structure comprising regions 1 and 2 of Fig. 2. It is assumed that the

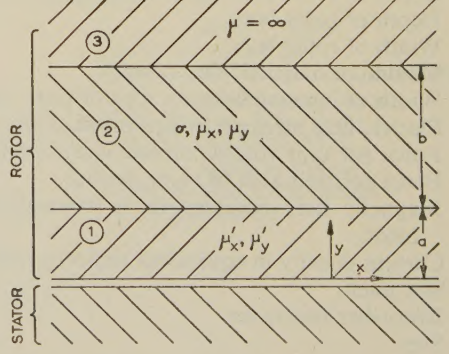

Fig. 2.—Uniform linear model motor.

rotor core, region 3, and the stator are of infinite permeability and zero conductivity. Region 1 represents the air-gap and tooth tops of Fig. 1, and therefore its conductivity is taken as

zero, whilst region 2 represents the conductor region of Fig. 1 and has a mean conductivity of

$$\sigma = \frac{b_s}{p_s}\sigma_0 \quad . \quad . \quad . \quad . \quad . \quad . \quad . \quad (5)$$

The effective permeability, on the other hand, is more difficult to evaluate. It is clear, in the first place, that the average reluctance of a path parallel to the rotor surface and passing through the slots is much greater than that in a direction perpendicular to the rotor surface. Thus the continuous region 2 in Fig. 2, which corresponds to the slotted region in Fig. 1, must be anisotropic in its magnetic properties. Similar remarks apply to region 1 in Fig. 2, which corresponds to the tooth-top region in Fig. 1.

An exact determination of the effective permeabilities is very difficult, but if fringing is neglected, simple magnetic-circuit ideas can be applied to give very crude approximations.

For region 1:

$$\left.\begin{aligned} \mu_x' &\simeq \mu_0 \frac{p_s}{d} \\ \mu_y' &\simeq \mu_r \mu_0 \frac{p_s - d}{p_s} \end{aligned}\right\} \quad . \quad . \quad . \quad . \quad (6)$$

For region 2:

$$\left.\begin{aligned} \mu_x &\simeq \mu_0 \frac{p_s}{b_s} \\ \mu_y &\simeq \mu_r \mu_0 \frac{p_s - b_s}{p_s} \end{aligned}\right\} \quad . \quad . \quad . \quad . \quad (7)$$

In these equations μ_r is the relative permeability of the iron. This will in practice be of the order of 4000, and has been taken as infinite elsewhere in formulating eqns. (6) and (7). It is also taken as infinite in region 3, which represents the unslotted rotor core.

(3.2) Field Analysis

Maxwell's equations in region 2 are:

$$-j\omega\mu_x H_x = \frac{\partial E_z}{\partial y} \quad . \quad . \quad . \quad . \quad . \quad . \quad . \quad (8)$$

$$-j\omega\mu_y H_y = -\frac{\partial E_z}{\partial x} \quad . \quad . \quad . \quad . \quad . \quad . \quad . \quad (9)$$

$$\sigma E_z = \frac{\partial H_y}{\partial x} - \frac{\partial H_x}{\partial y} \quad . \quad . \quad . \quad . \quad (10)$$

In these equations a time factor $\varepsilon^{j\omega t}$ is assumed, and $\omega = s\omega_0$ is the angular frequency of the rotor currents. The co-ordinates x and y are measured in a co-ordinate system fixed to the rotor. Derivatives with respect to z have been set equal to zero since end effects are neglected, and current flow is assumed to be wholly in the z-direction, so that H_z has been put equal to zero. Displacement currents have also been neglected.

All field quantities vary with x as $\varepsilon^{-j\beta x}$, where $\beta = 2\pi/\lambda = \pi\tau$; λ, the wavelength of the travelling wave, is equal to twice the pole pitch. Subsituting $-j\beta$ for $\partial/\partial x$ in (9) and (10) and eliminating H_y between these two equations, we get

$$\left(\sigma - j\frac{\beta^2}{\omega\mu_y}\right)E_z = -\frac{\partial H_x}{\partial y} \quad . \quad . \quad . \quad (11)$$

If a solution of eqns. (8) and (11) for E_z can be found the problem is solved, for H_y can easily be found from E_z using eqn. (9). Thus (8) and (11) are the basic equations. Their solution is easily found by making use of the wave-impedance concept and employing a transmission-line analogue. Corresponding quantities in the analogue are most easily seen by setting out the relevant equations side by side, as Booker has done in dealing with other electromagnetic problems.[2]

Induction motor	Transmission line
$-\frac{\partial E_z}{\partial y} = j\omega\mu_x H_x$	$-\frac{\partial V}{\partial y} = ZI$
$-\frac{\partial H_x}{\partial y} = \left(\sigma + \frac{\beta^2}{j\omega\mu_y}\right)E_z$	$-\frac{\partial I}{\partial y} = YV$

There is clearly a one-to-one correspondence between the following quantities

$$\left.\begin{aligned} E_z &\rightarrow V \\ H_x &\rightarrow I \\ j\omega\mu_x &\rightarrow Z \\ \sigma + \frac{\beta^2}{j\omega\mu_y} &\rightarrow Y \end{aligned}\right\} \quad . \quad . \quad . \quad . \quad . \quad (12)$$

Since Z and Y represent respectively the series impedance and shunt admittance per unit length of the transmission line, we can construct for the induction motor a transmission line equivalent which represents exactly the relationship between E_z and H_x in region 2. An elementary section of this line is shown in Fig. 3.

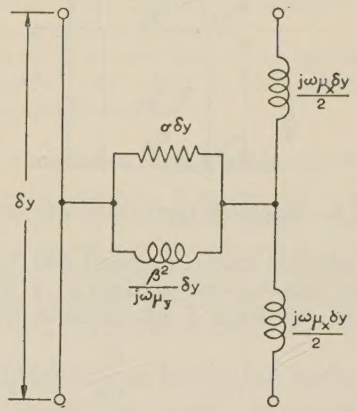

Fig. 3.—Element of equivalent transmission line.

The characteristic wave impedance and the propagation coefficient for the y-direction can be written down by inspection

$$\left.\begin{aligned} z_{02} &= \sqrt{\left(\frac{j\omega\mu_x}{\sigma + \frac{\beta^2}{j\omega\mu_y}}\right)} = \frac{j\omega\mu_x}{\gamma_2} \\ \gamma_2 &= \sqrt{\left[j\omega\mu_x\left(\sigma + \frac{\beta^2}{j\omega\mu_y}\right)\right]} \end{aligned}\right\} \quad . \quad . \quad (13)$$

The suffix '2' refers to region 2 of the induction-motor model in Fig. 2.

By exactly the same argument, we can set up a transmission-line model for region 1. The characteristic wave impedance and the propagation coefficient can be obtained from eqn. (13) by replacing μ_x by μ_x', μ_y by μ_y', and putting $\sigma = 0$. This gives

$$\left.\begin{aligned} z_{01} &= \sqrt{\frac{-\omega^2\mu_x'\mu_y'}{\beta^2}} = \frac{j\omega\mu_x'}{\gamma_1} \\ \gamma_1 &= \beta\sqrt{\frac{\mu_x'}{\mu_y'}} \end{aligned}\right\} \quad . \quad . \quad . \quad (14)$$

In order to complete the analogy, we must consider boundary conditions. At the interface between regions 1 and 2, E_z and H_x must be continuous. Thus, in the analogue, V and I must be continuous at the junction of the two dissimilar transmission lines representing regions 1 and 2. This continuity follows from Kirchhoff's laws.

In region 3, H_x must be zero everywhere since the permeability is infinite. In particular, $H_x = 0$ at the boundary between regions 3 and 2. In the analogue we must have $I = 0$ at the corresponding point. The transmission line for region 2 is therefore open-circuited at the corresponding end. The open-circuit condition can alternatively be obtained by noting that, since $\mu = \infty$ in region 3, the associated characteristic wave impedance is infinite, and this is the 'termination' of region 2.

Fig. 4 shows the transmission-line analogue of the interaction

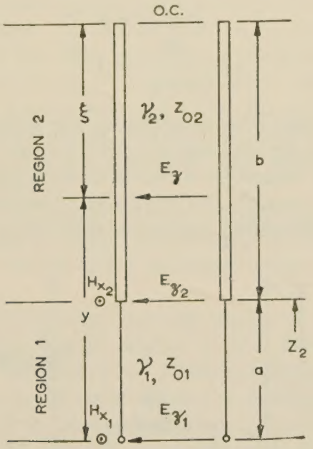

Fig. 4.—Equivalent transmission line system.

region of the induction motor, regions 1 and 2 of Fig. 2. The sending-end and receiving-end voltages of a transmission line terminated by an impedance Z_r are related as follows:

$$V_S = V_R\left(\cosh \gamma l + \frac{Z_0}{Z_R} \sinh \gamma l\right)$$

Using the equivalences set out in (12) and referring to Fig. 4, the relationship between E_{z1} and E_{z2} can be written

$$E_{z1} = E_{z2}\left(\cosh \gamma_1 a + \frac{Z_{01}}{Z_2} \sinh \gamma_1 a\right) \quad . \quad . \quad (15)$$

Here, Z_2 is the input wave impedance of region 2, which, by analogy with an open-circuited transmission line, is

$$Z_2 = Z_{02} \coth \gamma_2 b \quad . \quad . \quad . \quad . \quad . \quad (16)$$

Thus
$$E_{z1} = E_{z2}\left(\cosh \gamma_1 a + \frac{Z_{01}}{Z_{02}} \tanh \gamma_2 b \sinh \gamma_1 a\right) \quad (17)$$

Making use of the well-known formula for the voltage distribution on an open-circuited transmission line, we can express the electric field strength E_z at any distance ξ from the interface between regions 2 and 3 in terms of E_{z2} as follows:

$$E_z = E_{z2} \frac{\cosh \gamma_2 \xi}{\cosh \gamma_2 b} \quad . \quad . \quad . \quad . \quad . \quad (18)$$

Combining (17) and (18), we have

$$E_z = E_{z1} \frac{\cosh \gamma_2 \xi}{\cosh \gamma_1 a \cosh \gamma_2 b + \frac{Z_{01}}{Z_{02}} \sinh \gamma_1 a \sinh \gamma_2 b} \quad (19)$$

We have now found the form of the field distribution in region 2, but the absolute magnitude is not yet determined. We take as datum the maximum value of the magnetic flux density B_{y1} in the air-gap. Since relativistic effects can be ignored at the low velocities involved, this quantity is unaltered by transformation to co-ordinates fixed to the stator, and can be equated to B_m introduced in the circuit analysis.

The air-gap flux density can be written

$$B_{y1} = B_m e^{-j\beta x} \quad . \quad . \quad . \quad . \quad . \quad (20)$$

Since the normal component of magnetic flux density is continuous at an interface, eqn. (20) also applies just inside region 1. But in region 1 eqn. (9) applies if μ_y is replaced by μ_y'. Also $B_y = \mu_y' H_y$. Hence

$$E_{z1} = -\frac{\omega}{\beta} B_{y1} \quad . \quad . \quad . \quad . \quad . \quad (21)$$

Combining (19) and (21) we have

$$E_z = -\frac{\omega B_{y1}}{\beta} \frac{\cosh \gamma_2 \xi}{\left(\cosh \gamma_1 a \cosh \gamma_2 b + \frac{Z_{01}}{Z_{02}} \sinh \gamma_1 a \sinh \gamma_2 b\right)} \quad . \quad . \quad . \quad . \quad (22)$$

This is the exact solution for the rather highly idealized model we have chosen to consider.

To calculate the tangential force on the rotor, we start with the force per unit volume exerted in the x-direction by the magnetic field on the current. This is

$$f_x = -J_z B_y$$

If J_z and B_y are interpreted as complex amplitudes rather than instantaneous values, the time-average force density is

$$f_x = -\mathscr{R}\tfrac{1}{2} J_z B_y^* \quad . \quad . \quad . \quad . \quad . \quad (23)$$

Using eqn. (21) and remembering that $J_z = \sigma E_z$, we have

$$f_x = \frac{\sigma\beta}{2\omega} E_z E_z^* \quad . \quad . \quad . \quad . \quad . \quad (24)$$

Substituting (22) in (24) and remembering that $|B_{y1}| = B_m$, we get

$$f_x = \frac{\sigma\omega}{2\beta} B_m^2 \frac{\cosh \gamma_2 \xi \cosh \gamma_2^* \xi}{\left|\cosh \gamma_1 a \cosh \gamma_2 b + \frac{Z_{01}}{Z_{02}} \sinh \gamma_1 a \sinh \gamma_2 b\right|^2} \quad (25)$$

To find the force per unit area of rotor surface we must integrate (25) with respect to ξ between the limits 0 and b. The result is

$$F_x = \frac{\sigma\omega B_m^2}{2\beta} \frac{\gamma_2 \sinh \gamma_2 b \cosh \gamma_2^* b - \gamma_2^* \sinh \gamma_2^* b \cosh \gamma_2 b}{(\gamma_2^2 - \gamma_2^{*2}) \left|\cosh \gamma_1 a \cosh \gamma_2 b + \frac{Z_{01}}{Z_{02}} \sinh \gamma_1 a \sinh \gamma_2 b\right|} \quad . \quad . \quad . \quad . \quad (26)$$

This equation can be put into a form more convenient for practical application. In the first place, for all reasonable values of γ_1 and a, it is perfectly adequate to write

$$\left.\begin{aligned} \cosh \gamma_1 a &\simeq 1 \\ \sinh \gamma_1 a &\simeq \gamma_1 a \end{aligned}\right\} \quad . \quad . \quad . \quad . \quad . \quad (27)$$

Secondly, γ_2 can be approximated as

$$\gamma_2 \simeq \sqrt{j\omega\mu_x\sigma} = \sqrt{\left(\frac{s\omega_0\mu_x\sigma}{2}\right)}(1 + j)$$

But, from eqns. (6) and (7), we see that $\mu_x\sigma = \mu_0\sigma_0$. Thus γ_2 can be expressed in terms of the parameter α defined by eqn. (4), as follows,

$$\gamma_2 = \alpha(1 + j) \quad . \quad . \quad . \quad . \quad . \quad (28)$$

Substituting (27) and (28) in (26), putting $\beta = \pi/\tau$ and simplifying, we get

$$F_x = \frac{\omega_0 \tau B_m^2}{2\pi p_s} \frac{\sigma_0 b_s s}{2\alpha} \frac{\sinh 2\alpha b + \sin 2\alpha b}{\left[\begin{array}{l} 2\eta^2 (\cosh 2\alpha b - \cos 2\alpha b) \\ \quad + 2\eta (\sinh 2\alpha b - \sin 2\alpha b) \\ \quad\quad + (\cosh 2\alpha b + \cos 2\alpha b) \end{array}\right]} \quad (29)$$

where

$$\eta = \frac{\alpha a b_s}{d} \quad . \quad . \quad . \quad . \quad . \quad . \quad (30)$$

It is not immediately obvious from eqn. (29) that the field-theory result agrees with that obtained by circuit analysis. However, if eqns. (2) and (3) are substituted in (1), the resulting formula can be reduced exactly to eqn. (29).

It is at first sight remarkable that this exact agreement should be found between the two formulae, for approximations have been made in deriving both, and the approximations are not obviously equivalent. However, a deeper examination of the problem shows the agreement is not unreasonable. The traditional analysis is founded upon the superposition theorem, in that the fields produced by the rotor currents are considered separately from the externally applied field which produces these currents. Further there is the axiom, usually unstated, that the tangential force on the rotor due to the interaction of its currents and their own field is zero. This follows from the magnetic uniformity of the rotor and stator in the tangential direction. Hence it follows that the only relevant force is that between the radial component of the externally applied field and the conductor cross-section. Because of the high permeability of the teeth it can be assumed that the flux density is independent of depth, and hence the force per conductor per unit width is equal to the product of flux density and total conductor current, and this in fact is the manner of derivation of eqn. (1).

In applying the field theory the position is complicated since the resultant of the externally applied and the self-generated fields is considered. However, using the previous axiom it is evident that the answer must be identical with that obtained by considering only the externally applied component.

The term $\beta^2/(j\omega\mu_y)$ in eqn. (13) determines the decay of the externally applied field in the rotor slot region. This is easily seen by putting $\sigma = 0$ in that equation; there are then no rotor currents and no magnetic field other than the externally applied field. Neglecting $\beta^2/j\omega\mu_y$ in comparison with σ, as in eqn. (28), is therefore equivalent to neglecting the decay of the externally applied field in the rotor slot region. The approximation (27) is equivalent to neglecting the decay of the externally applied field in the tooth-top region. Hence the exact equivalence of the two results.

(3.3) Numerical Example

To illustrate the formulae numerically we have taken a machine with the following rotor dimensions:

Tooth top depth	$a = 1$ cm
Slot depth	$b = 2$ cm
Slot width	$b_s = 1$ cm
Slot pitch	$p_s = 2$ cm
Slot opening	$d = 0{\cdot}5$ cm

The apparently excessive tooth top depth has been chosen to make some allowance for the zigzag reactance which would occur in a normal machine. In Fig. 5, torque/slip curves at constant air-gap flux density have been plotted. Curve (*a*) is the result obtained from the field theory or from the usual eqn. (1) together with (2) and (3). Curve (*b*) is obtained from (1) using (2*a*) and (3*a*); i.e. it neglects skin effect.

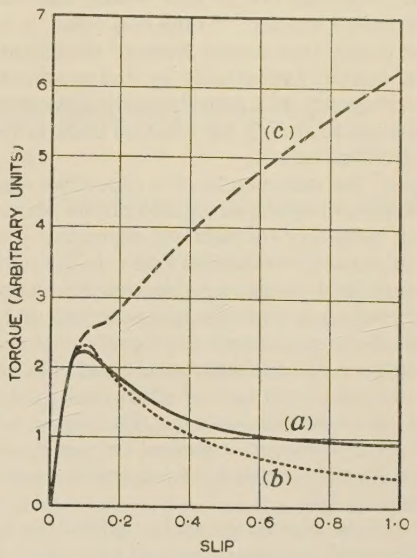

Fig. 5.—Torque/slip characteristics.

(*a*) Double-layer theory.
(*b*) Neglecting skin effect.
(*c*) Single-layer theory.

A deep-bar rotor has been selected to emphasize the well-known importance of skin effect in such cases; the standstill torque is approximately doubled.

(3.4) Comparison with Mishkin's Analysis

In Mishkin's paper[1] the rotor is represented by a much simpler model than that used in the present paper, though he has, of course, taken end effects into account and dealt with the stator as well as the rotor. Without going into so much detail, however, we shall show that his model of the rotor is too simple to represent the facts accurately, and in fact it greatly over-exaggerates skin effect.

Mishkin's analysis does not take proper account of the shape of the slot or of the fact that the rotor bars are embedded in the rotor and are separated from the rotor surface by a non-conducting (ideally) mixture of iron and air. Whilst we have taken account of this fact by using a double-region model for the electromagnetic field analysis with one region (No. 2) to represent the conductor region and a second region (No. 1) to represent the tooth-top region, Mishkin has used a single region to represent both. Our formulae can easily be applied to a single-region model by putting $a = 0$. The effective conductivity of the single layer is easily obtained, and the average values $\overline{\mu_x}$ and $\overline{\mu_y}$ can be obtained from μ_x and μ_x', and μ_y and μ_y', by combining reluctances for horizontal and vertical flux paths in parallel and in series respectively. When this is done, the single-layer theory yields the result shown as curve (*c*) in Fig. 5. It is clear that skin-effect is much exaggerated.

It should be noted that the Mishkin results can be made to fit the case of a practical machine if the permeability of the air-gap in the x-direction is increased so as to allow for the effects of tooth-top and zigzag leakage fluxes.

(4) FIELD THEORY OF THE BRUSHLESS VARIABLE-SPEED INDUCTION MOTOR

A simplified theory of the very elegant motor described by Williams and Laithwaite[4] can be derived by the methods used

in this paper. We shall not go into details, but merely indicate the main features of interest. In the first place, it is well known in microwave theory that certain types of discontinuity in waveguides can be treated theoretically by first examining the corresponding discontinuity in a parallel-plate line carrying a TEM wave, and then transforming the solution back to the waveguide case by simple substitutions.

For example,[5] the susceptance of a capacitive diaphragm in a rectangular dominant-mode waveguide can be obtained from the corresponding strip-line formula by replacing λ by λ_g. This transformation arises from the fact that a 3-dimensional problem with a harmonic field variation in say the z-direction leads to a wave equation which is formally identical with a 2-dimensional wave equation if the wavelength is properly chosen. Physically, the waveguide mode can be constructed from obliquely-travelling plane waves, the velocity of each of which measured normal to its wavefront has the constant value c. The phase velocity of the composite wave is, however, increased to $c \sec \theta$, where θ is the angle between the plane-wave direction and the axis of the waveguide, and $\sec \theta = \lambda_g/\lambda$.

Exactly the same argument can be applied to the induction motor, and the speed increase associated with obliquely travelling air-gap flux waves follows at once.

(5) CONCLUSIONS

It has been shown that the concept of wave impedance can be used in developing a simple electromagnetic field theory of the induction motor which leads to identically the same formula for the torque-slip relationship as the conventional circuit analysis with skin-effect corrections.

Thus *the same equation may be regarded either from a circuit point of view as an approximate solution of the actual problem, or from a field point of view as the exact solution of an idealized problem.*

An inadequacy in Mishkin's earlier electromagnetic theory of the induction motor has emerged, and the need for a 2-region model of the rotor has been demonstrated.

The fundamental connection between the action of an induction motor and the phenomenon of radiation pressure should be mentioned. The closest analogy is with the tangential stress due to radiation obliquely incident on an absorbing surface. This effect has been observed by Barlow and Poynting when light falls obliquely on a blackened surface.

In the induction motor, the incident wave is not a simple plane wave but a surface wave. The principle is the same, however. In both cases the incident field sets up currents which are acted upon by the magnetic field of the incident wave to produce a mechanical force. That the forces are so different in magnitude in the two cases tends to conceal the underlying unity; this is essentially due to the enormous difference in wave velocity in the two cases.

For the induction motor at standstill $F = P/v$, where P is the power delivered to the rotor and v is the velocity of the flux wave. The radiation stress due to light, on the other hand, is of the order of P/c, where c is the velocity of light. Bearing in mind that in the optical case P could hardly exceed 1 watt, the difference in the magnitudes of the forces is easily understandable.

Finally, having established a link between microwaves and induction motors, it is suggested that some of the theoretical methods developed for microwaves might usefully be examined by the machine designer. In particular, the variational methods for dealing with discontinuities, and the various techniques for handling periodic structures of various kinds, might find new application in the field of electrical machinery.

(6) REFERENCES

(1) MISHKIN, E.: 'Theory of the Squirrel-Cage Induction Motor derived directly from Maxwell's Field Equations', *Quarterly Journal of Mechanics and Applied Mathematics*, 1954, **7**, p. 472.

(2) BOOKER, H. G.: 'The Elements of Wave Propagation using the Wave-Impedance Concept', *Journal I.E.E.*, 1947, **94**, Part III, p. 171.

(3) WILLIAMS, F. C., LAITHWAITE, E. R., and PIGGOTT, L. S.: 'Brushless Variable-Speed Induction Motors', *Proceedings I.E.E.*, Paper No. 2097 U, June, 1956 (**104** A, p. 102).

(4) ALGER, P. L.: 'The Nature of Polyphase Induction Machines' (John Wiley and Sons, New York, 1952), pp. 244–245.

(5) LEWIN, L.: 'Advanced Theory of Waveguides' (Iliffe), p. 37.

621.318.13.017.31

The Institution of Electrical Engineers
Monograph No. 284 M
Feb. 1958
©

EDDY-CURRENT LOSSES IN THIN FERROMAGNETIC SHEETS

By E. W. LEE, B.Sc., Ph.D.

(*The paper was first received* 19*th August, and in revised form* 19*th October*, 1957. *It was published as an* INSTITUTION MONOGRAPH *in February*, 1958.)

SUMMARY

In very weak fields the eddy-current losses in a lamination may be calculated exactly but the observed loss is always somewhat greater. Most of this extra loss varies with frequency and field in the same way as eddy-current loss, and if a quantity η equal to the ratio of the observed to calculated loss is defined it is found that it increases rapidly with decreasing thickness of sheet. It is suggested that this effect arises from neglect of the true mechanism of magnetization, and it is shown that the classical calculation of eddy-current loss is invalid when the distance between domain walls becomes comparable with the sheet thickness. Theoretical predictions seem to be in good agreement with observations made by Richards, Walker and Lynch.

LIST OF PRINCIPAL SYMBOLS

c = Velocity of light, cm/sec.
d = Thickness of ferromagnetic sheet, cm.
e = Electronic charge.
g = Landé splitting factor.
m = Mass of electron, g.
m' = Effective oscillating mass of domain wall, g.
n = Odd integer.
p, q = Numerical constants.
t = Time, sec.
α = Restoring force on a domain wall, dynes/cm^2.
β = Domain-wall viscous damping parameter.
β_e = Domain-wall viscous damping parameter due to micro-eddy currents.
β_r = Domain-wall viscous damping parameter due to spin relaxation.
δ = Loss angle, rad.
δ_e = Loss angle due to micro-eddy currents, rad.
δ_r = Loss angle due to spin-relaxation wall damping, rad.
δ_R = Loss angle due to rotational spin relaxation, rad.
η = Ratio of measured to calculated eddy-current loss.
λ = Spin relaxation damping constant, sec^{-1}.
μ = Total magnetic permeability, gauss/oersted.
μ_W = Magnetic permeability due to wall movement, gauss/oersted.
μ_R = Magnetic permeability due to domain rotation, gauss/oersted.
ρ = Electrical resistivity, e.m.u.
χ_W = Magnetic susceptibility due to wall movement.
χ_R = Magnetic susceptibility due to domain rotation, i.e. rotational susceptibility.
$\chi_{R,\omega}$ = Rotational susceptibility at angular frequency ω.
$\chi_{R,0}$ = Rotational susceptibility at zero frequency.
ω = Angular frequency of magnetic field and magnetization, rad/sec.
A = Exchange energy per unit volume, ergs/cm^3.
H = Magnetic field, oersteds.
M_s = Saturation intensity of magnetization.
K = Magneto-crystalline anisotropy constant, ergs/cm^3.
l = Half-thickness of ferromagnetic domain, cm.

Correspondence on Monographs is invited for consideration with a view to publication.
Dr. Lee is in the Department of Physics, The University, Nottingham.

(1) INTRODUCTION

In recent years considerable progress has been made in producing magnetic alloys possessing very high initial permeability and low hysteresis loss. The most important of these are developments of binary alloys of iron and nickel containing about 78% Ni. Addition of copper and/or molybdenum enables initial permeabilities of over 100 000 to be attained.

These alloys, hereafter referred to simply as high-permeability alloys, have been developed for use as cores for small transformers where lightness and compactness are the overriding requirements. In order to design transformers which will operate satisfactorily at high frequencies the practice adopted is the usual one of making the cores with laminations sufficiently thin so that, at the operative frequency, the skin depth is greater than the thickness of the lamination. For frequencies higher than a few kilocycles per second, very thin laminations have to be used, and the production of sheets of the required thickness presents a difficult task. It is therefore all the more perturbing to find that, when the very considerable technical difficulties have been overcome and the sheet thickness has been adequately reduced (usually by cold-rolling), the properties of the material in thin sheet form are by no means as desirable as they were originally. Most important from the designer's point of view is that the eddy-current losses* in very thin sheets are always greater than those calculated from the standard classical formulae. The paper is concerned with the characteristics of this anomalous loss. A possible explanation is given which seems to be borne out by the experimental results available.

(2) CHARACTERISTICS OF THE ANOMALOUS LOSS

It has become the practice to describe the anomalous loss in terms of the ratio of the measured loss to that calculated from classical eddy-current formulae. It is unfortunate that this ratio has been given different symbols by various authors. Richards, Walker and Lynch[1] use the symbol g, but in order to avoid confusion with the Landé splitting factor, the symbol η, which is used by Feldtkeller, is used in this paper. η is a meaningful quantity only if the frequency is specified. However, it appears that it is substantially independent of frequency below about 100 kc/s. In other words, the anomalous loss behaves like an eddy-current loss as far as its frequency dependence is concerned. This rules out immediately any explanation in terms of hysteresis and losses of the Jordan type[2] since they give rise to loss angles independent of frequency, and so, if they were present, η would tend to infinity at zero frequency.

Anomalous losses of the type under consideration seem to occur in all materials, although most information exists for high-permeability alloys of the Permalloy type. This is probably solely due to the fact that these are the alloys which have been rolled thinnest. It thus appears that the anomalous eddy-current losses are not a prerogative of high-permeability materials, and there is no close correlation between η and μ.

The most striking and characteristic feature of η is its marked

* In the paper the term 'eddy-current loss' is used in a restricted sense to mean the loss measured in a sinusoidally varying field of such small amplitude that the permeability is sensibly constant and hysteresis loss negligible. Similarly, the term 'permeability' is taken to mean initial permeability throughout.

dependence on sheet thickness. It increases sharply with decreasing thickness, and for a 3-micron Permalloy strip Abgrall and Epelboin[3] found that η equals 18. Measurements by Richards, Walker and Lynch show that, for a Mo–Permalloy of composition Ni 77%, Cu 5%, Mo 4% and Fe 14%, the loss ratio can be expressed as $\eta - 1 = ka^{-3/2}$ where k is a constant and a is the strip thickness. Moreover, for values of a greater than about 200 microns, $\eta = 1{\cdot}0$ within the limits of experimental error. This is important since it indicates that there is nothing seriously wrong with the classical eddy-current calculation for sheets whose thickness is, by ordinary engineering standards, quite small.

An explanation often given for these facts is the presence of surface layers whose permeability is less than that of the bulk material. These could arise quite naturally from surface closure domains or could be due to impurities existing only on the surface. Evidence for the existence of such layers has been put forward by Peterson and Wrathall,[4] who inferred their presence from measured eddy-current losses, and more directly by Epelboin,[5] who measured the initial permeability of a Permalloy tape at each stage in the removal of successive layers from the surface by electropolishing. Feldtkeller[6] showed that low-permeability surface layers would give rise to loss ratios greater than unity, but the maximum value of η predicted by his analysis is about $1{\cdot}6$, which is much too low to account for the observed values. Furthermore Richards, Walker and Lynch consider that the low-permeability surface layers encountered by Peterson and Wrathall are definitely attributable to impurities. These layers do not exist in special high-purity alloys. The anomalous losses, however, still persist. It thus appears that Feldtkeller's mechanism, if present at all, can only account for part of the excess loss.

A more realistic approach to a somewhat similar problem is that of Aspden,[7] who calculates the power loss to be expected in a sheet containing a single-domain wall in the plane of the sheet. The results are compared with the power loss measured at times at which the induction is instantaneously zero. The good agreement obtained by Aspden is, in the author's opinion, to be expected, since this model of the domain structure is probably quite good for the conditions under which the experimental results were obtained, i.e. large peak induction, measured at a field near the coercive force where large domains of reverse magnetization are expanding rapidly. There is, however, no reason to expect Aspden's model to be appropriate to the situation in the very low fields considered here.

It seems that the only way of explaining the anomalous eddy-current loss in such a way that the loss ratio η is independent of frequency (or very nearly so) is through the agency of a relaxation mechanism. In this paper the suggestion is put forward that such a relaxation mechanism appears quite naturally if a more realistic approach is made to eddy-current losses, taking into account what is known about the domain structure existing in ferromagnetic materials.

(3) THEORY

It is generally believed that, in low fields, magnetization takes place by the reversible displacement of walls separating regions magnetized in directions determined by the crystal anisotropy of the material. Considering two such regions separated by a domain boundary, it is clear that the net change in magnetization is produced by very large changes in local magnetization in the immediate neighbourhood of the domain boundary. At points far removed from the boundary the material is unaffected by an external field (apart from any rotational permeability which is neglected for the time being). In other words, one must attribute a very large local permeability to the domain wall since the permeability at large distances from it is unity. A moving domain wall giving rise to large local changes in magnetization will set up micro-eddy currents which will act in such a way as to oppose the wall movement. This effect was considered in some detail by Williams, Shockley and Kittel,[8] who showed that micro-eddy currents thus produced act so as to introduce a damping term in the equation of motion of the wall. In addition, a damping of the wall movement will occur owing to inherent damping of the spins in the domain wall. This damping, first discussed by Landau and Lifshitz,[9] is of obscure origin. The mechanism is the same as that which gives rise to the finite width of the ferromagnetic resonance line, and for ferrites (in which eddy-current damping of all kinds is negligible) the damping parameter obtained from domain-wall experiments is in good agreement with that found from the resonance experiments.[10]

To take account of domain-wall damping, consider a model such as is depicted in Fig. 1, with a 90° wall lying in the zx-plane

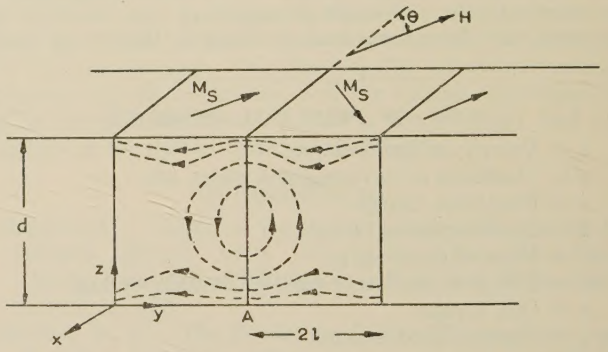

Fig. 1.—Cross-section of part of a ferromagnetic sheet.
The sheet is supposed to be of infinite extent in the x and y directions.
The domain wall at A is moving from left to right.
The dotted lines show the approximate distribution of eddy currents.

at A. Let the depth of the domains be d, which is taken parallel to the z-axis. If a field H is applied in the xy-plane into the plane of the diagram, the wall at A will tend to move to the right. In an alternating field $H_0\varepsilon^{j\omega t}$ the equation of motion of the wall will be

$$m'\ddot{y} + \beta\dot{y} + \alpha y = pHM_s \cos\theta\varepsilon^{j\omega t} \quad . \quad . \quad . \quad (1)$$

where p equals $\sqrt{2}$ for a 90° wall and 2 for a 180° wall. The effects of wall inertia do not begin to make themselves felt until frequencies of the order of some megacycles per second have been reached,[11] and hereafter the first term will be neglected. Eqn. (1) becomes

$$\beta\dot{y} + \alpha y = pHM_s \cos\theta\varepsilon^{j\omega t} \quad . \quad . \quad . \quad . \quad (2)$$

which has as its solution

$$y = \frac{pHM_s \cos\theta}{\alpha} \frac{1}{1 + j\omega\beta/\alpha}\varepsilon^{j\omega t} \quad . \quad . \quad . \quad (3)$$

If the distance between successive domain walls is $2l$ this displacement will produce a change of magnetization in the direction of the field equal to $pM_s y \cos\theta/2l$. The susceptibility is then

$$\chi = \frac{p^2M_s^2}{3\alpha 2l} \frac{1}{1 + j\omega\beta/\alpha} \quad . \quad . \quad . \quad . \quad . \quad (4)$$

in which $\cos^2\theta$ has been replaced by its average value of one-third. The frequency variation is thus of a relaxation type with a relaxation frequency equal to α/β. The loss angle for wall

movement, δ, is given by $\tan\delta = \omega\beta/\alpha$ and is thus independent of the type of wall.

As previously mentioned the damping constant, β, is in general made up of two parts, β_e caused by micro-eddy currents and β_r due to intrinsic damping of the spins. The calculation of β_e has been carried out by Williams, Shockley and Kittel[8] for a single wall and by Polivanov.[12] The latter's results are to be preferred, since he considers an array of walls transverse to the plane of the sheet. He thus obtains a result which takes into account the fact that the z-components of the currents set up by neighbouring moving walls tend to cancel out between the walls, and therefore the result converges to a limiting case as the distance between neighbouring domain walls is decreased. The current distribution is shown diagrammatically in Fig. 1. Polivanov obtains the following result for the loss tangent produced by micro-eddy currents:

$$\tan\delta_e = \frac{32\mu\omega d^2}{\pi^2\rho}\frac{l}{d}\Sigma' n^{-3}\coth\frac{n\pi l}{d} \quad . \quad . \quad . \quad (5)$$

where Σ' indicates a summation over odd values of n. This result holds for an array of domain walls which extend through the sheet perpendicular to the plane of the sheet and along the direction of the applied field. It also assumes that the domain walls remain plane, so that the following calculation is valid only for the case in which the skin depth is greater than the sheet thickness and the field penetrates the sheet without significant change of amplitude. In an actual polycrystalline sheet the domain walls will not necessarily extend through the sheet but will be bounded by the crystal grains. Each moving domain wall will set up its own system of eddy currents, and although these may cancel out in the interior of the sheet, there will be no cancellation at the surfaces. Thus the model of transverse domains extending through the sheet is likely to be a good one. It remains to show that eqn. (5) reduces to the classical value for a sheet of thickness d and uniform permeability μ when the distance between the domain walls becomes zero.

Now $$\lim_{l/d\to 0}\frac{l}{d}\Sigma' n^{-3}\coth\frac{n\pi l}{d} = \frac{1}{\pi}\Sigma' n^{-4}$$

$$= \pi^3/96$$

and so as $l/d \to 0$,

$$\tan\delta_e = \frac{\pi\omega\mu d^2}{3\rho}$$

which is just the classical value.

The damping parameter $\beta_e = \frac{\alpha}{\omega}\tan\delta_e$. From eqn. (4) $\alpha = \frac{2p^2\pi M_s^2}{3\mu l}$ if $\mu \gg 1$ and $\omega = 0$, and so

$$\beta_e = \frac{64p^2M_s^2 d\,\Sigma' n^{-3}\coth\frac{n\pi l}{d}}{3\pi\rho} \quad . \quad . \quad . \quad (6)$$

It is necessary to add that part of the damping caused by intrinsic damping of the spin system within the wall. Galt[13] calculates this spin relaxation term to be

$$\beta_r = \frac{q\lambda|K|^{1/2}}{2\gamma^2 A^{1/2}}$$

in which q is a constant approximately equal to 2 for a 180° wall and unity for a 90° wall. The total loss tangent is therefore given by

$$\tan\delta = \frac{\omega\beta}{\alpha} = \frac{\omega(\beta_e+\beta_r)}{\alpha}$$

and therefore the loss ratio η, i.e. the ratio of the actual loss to that calculated from classical eddy-current theory, is

$$\eta = \frac{9\rho l}{2p^2\pi^2 M_s^2 d^2}\left(\frac{64p^2M_s^2 d\,\Sigma' n^{-3}\coth\frac{n\pi l}{d}}{3\pi\rho} + \frac{q\lambda|K|^{1/2}}{2\gamma^2A^{1/2}}\right) \quad (7)$$

This is an exact expression for the case in which magnetization occurs solely by domain-wall displacements, i.e. for all except very-high-permeability materials in which the rotational permeability may form an appreciable factor of the whole in small fields. The necessary modification for these materials is made at the end of Section 4.

In the absence of spin relaxation effects, eqn. (7) reduces to the simple form

$$\eta = \frac{96}{\pi^3}\frac{l}{d}\Sigma' n^{-3}\coth\frac{n\pi l}{d} \quad . \quad . \quad . \quad . \quad (8)$$

This expression is plotted in Fig. 2. Empirically, by plotting $\eta - 1$ against l/d it is found that, for values of l/d less than

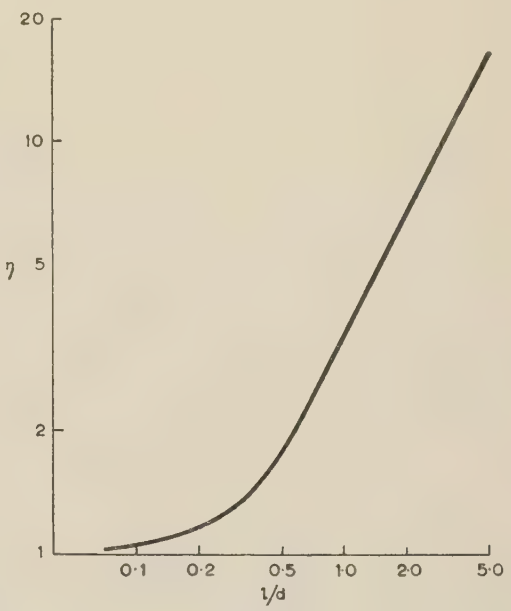

Fig. 2.—Variation of the loss ratio η as a function of ratio l/d.
This curve represents only the eddy-current losses and does not include the spin relaxation contribution.

unity, eqn. (8) can be simulated fairly accurately by an expression of the form

$$\eta = 1 + kd^{-r}$$

where k is a constant and the exponent r lies between 1·5 and 1·7. Although detailed comparison with experiment is deferred until a later Section, simple order-of-magnitude estimates of the quantities in eqn. (7) show quite generally that the spin relaxation term is not important unless d is very small—about 10 microns. The variation of η with d predicted by eqn. (7) is then approximately as d^{-r} for large values of d. As d is decreased the sum in the numerator becomes $\Sigma' n^{-3}$, independent of d, and so a d^{-1} law obtains. If d is decreased further the spin-relaxation term takes control and is manifested as a d^{-2} dependence. It is probable that this would not occur until d was reduced to a few microns. This assumes that l is constant. In fact, there will certainly be a distribution of values of l for a given (polycrystalline) specimen. Moreover it is by no means certain that l will be independent of d. Recent work by Martin[14] indicates

that the most likely relation between these two quantities is that l is proportional to $d^{1/2}$. These effects will tend to smooth out the complicated variation of η with d and will also make η decrease less rapidly with d than is predicted by eqn. (8). Eqn. (7) will then lead to an approximate law of the form

$$\eta = 1 + kd^{-r}$$

for values of d greater than a certain quantity and in which $r \simeq 1{\cdot}6$.

(4) COMPARISON WITH EXPERIMENT

The most comprehensive set of measurements with which to compare this result are those of Richards, Walker and Lynch[1] on an alloy containing 77% Ni, 14% Fe, 5% Cu and 4% Mo. This alloy has, after suitable purification, initial permeabilities ranging from 20 to 40 000 and a resistivity of $5{\cdot}7 \times 10^4$ e.m.u. Measurements made in this laboratory give $M_s = 600$ gauss. There is a considerable body of evidence to support the view that in soft magnetic materials the movement of 90° walls makes the greatest contribution to the initial permeability. The most telling evidence for this is that in these materials the highest initial permeability is developed in those alloys for which the magnetostriction constant in the direction of easy magnetization is a minimum. Since movement of a 180° wall is not accompanied by magnetostriction it is difficult to see why zero magnetostriction should be so essential to high permeability if 180° walls make an appreciable contribution. Accordingly it is assumed that $p = \sqrt{2}$. For this alloy $\lambda = 2 \times 10^8\,\mathrm{sec}^{-1}$ (see Reference 15), $\gamma = ge/2mc = 1{\cdot}76 \times 10^7$ if $g = 2$. The values of K and A are not known, but no great error will be incurred by putting $K = 500$ ergs/cm^3 and $A = 2 \times 10^{-6}$ ergs/cm^3, the latter being the value for pure iron. Substitution then gives $\beta_r \simeq 10^{-2}$. Similarly β_e becomes $40d$, taking the sum equal to unity. This implies that, for a sheet thickness of $2{\cdot}5 \times 10^{-4}$ cm, the spin relaxation and micro-eddy current terms are equal. Strips of such thickness do not appear to be available at present. For a thickness of 25 microns the spin-relaxation effects contribute only about one-tenth of the total loss, and for thicknesses of 50 microns and more they are negligible.

All the terms in eqn. (7) are now known except l. The quantity $2l$ is the distance between successive domain walls. Nothing is known about this quantity for an alloy of the composition under discussion, but one may reasonably expect that $2l$ should not be greater than the crystallite dimensions since domain walls crossing grain boundaries are not normally envisaged in unoriented material. In view of the present lack of knowledge of the factors which determine the domain sizes in polycrystalline metals it is felt to be extremely dangerous to use *a priori* values for $2l$. (For a criticism of this procedure see Reference 16.) Instead the empirical relation of Reference 1 is used, namely

$$\eta - 1 = kd^{-3/2} \quad . \quad . \quad . \quad . \quad . \quad . \quad (9)$$

where $k = 90$ if d is in microns, and eqn. (7) is 'fitted' to the value of η given by this expression for a thickness at which the spin-relaxation effects are negligible. Putting $d = 50$ microns, eqn. (9) gives $\eta = 1{\cdot}25$. This leads to a value for l of $13{\cdot}5$ microns, so that the domain width is 27 microns. For a strip of this thickness the grain size is stated[1] to be 45–50 microns so that there are then about two domain walls per crystallite. This seems to be quite a reasonable result. In the absence of any evidence to the contrary, this value of l is used for all values of d. This is probably not strictly true but it has the advantage of simplicity.

One final modification must now be made. Eqn. (7) applies only to wall movements. There will also be a contribution to the initial permeability from domain vector rotations. These give rise to a permeability

$$\mu_R = \frac{4\pi M_s^2}{3K}$$

For $K = 500$ ergs/cm^3 as used here, $\mu_R = 3\,000$. This is nearly one-tenth of the initial permeability found for these alloys. To a first approximation, relaxation losses associated with the rotational permeability may be neglected, and so μ_R will give rise to purely classical eddy-current losses for which $\eta = 1$. The expected loss ratio η' is then

$$\eta' = \frac{\mu_W}{\mu}\eta + \frac{\mu_R}{\mu} \quad . \quad . \quad . \quad . \quad . \quad (10)$$

where η is obtained from eqn. (7). Values of η' calculated from eqns. (7) and (10) are shown in Fig. 3 as a function of d. The results are in good agreement with experiment. Perhaps the most surprising result is that eqns. (7) and (10) predict a dependence of η' on thickness which is almost exactly an inverse three-halves power law. Eqn. (9) is shown in Fig. 3 for comparison.

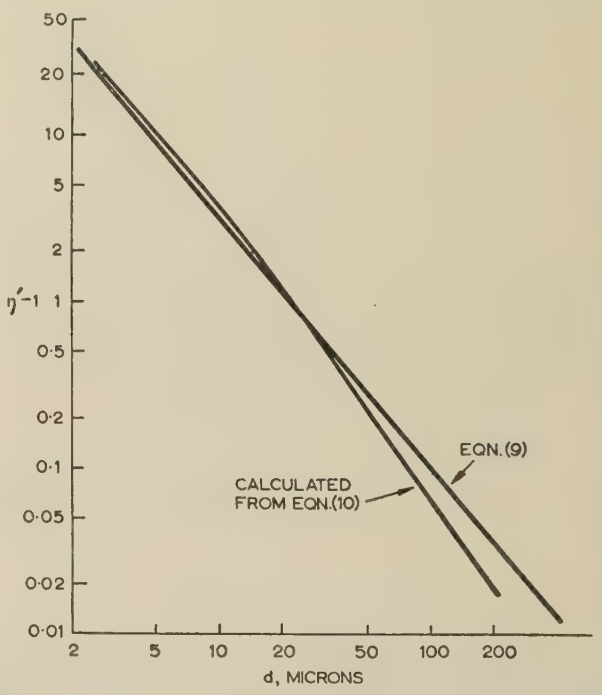

Fig. 3.—Variation of loss ratio η with sheet thickness for an alloy containing 77% Ni, 14% Fe, 5% Cu, 4% Mo.

The curve is calculated from eqn. (10).
The straight line is the empirical relation [eqn. (9)] deduced by Richards *et al.*[1] from a large number of experimental observations.

Actually there is some evidence that, in this alloy, the grain size increases with the strip thickness, and it is very possible that, provided that the crystallites are less than a certain size, the domain size is a constant fraction of the crystallite dimensions. This is in keeping with the concept of 'closed flux shell' introduced by Martius[17] and suggested by Kittel.[18] The effect would be to make η' vary less rapidly with d than is given by eqn. (7).

(5) DISCUSSION

Apart from the spin-relaxation term the factors which influence η are purely the geometrical ones of domain size and specimen thickness, so that there is no reason why large values of η should be confined to one group of magnetic materials. Broadly

speaking, eddy-current losses will be greater than those calculated on a classical basis, whenever the distance between domain walls becomes comparable with the thickness of the sheet. Very little is known about domain widths in random polycrystals, but it seems unlikely that they would be as large as the thickness of ordinary hot-rolled silicon-iron transformer sheet. Thus one would expect the eddy-current losses measured in very low fields to be equal to the values obtained from classical formulae. In fact, measurements made in this laboratory show that $\eta = 1$ within the limits of experimental error for types of 0·013 in thick commercial transformer sheet so far investigated.

The situation is somewhat different in the case of grain-oriented material. Here there is a considerable likelihood of domain walls crossing grain boundaries, and the distance between walls may be quite large. These conditions have been revealed by the powder-pattern technique. Unfortunately, the patterns become indistinct in zero applied field, which is just the region of interest. Measurements by Bates and Hart[19] on a crystallite in a disc of grain-oriented silicon iron indicate domain widths which extrapolate roughly to 250 microns in zero field. Since the thickness of this disc was 0·32 mm, $l/d \simeq 0{\cdot}4$, which, from eqn. (8), implies that $\eta \simeq 1{\cdot}6$. However, these measurements applied only to one crystallite, and the others may have contained much smaller domains. Thus, even in grain-oriented silicon iron, $\eta \simeq 1$ for the usual sheet thicknesses.

It is nevertheless to be expected that, in grain- or domain-oriented materials in which comparatively few domain walls are believed to exist, high values of η will set in at higher thicknesses than for random material, and this seems to be borne out by the measurements of Parkin[20] on a 50/50 nickel-iron alloy where grain orientation increased η by about 50%, and on a 65/36 nickel-iron in which a magnetic anneal increased η from 1·18 to 2·20. Similar results have been obtained by Buckley *et al.*[21]

In the previous Section it was suggested that, if the domain size were a constant fraction of the grain size, η would be proportional to the latter. Some measurements made by Parkin[20] on a Mumetal-type alloy seem to support this view and are shown in Fig. 4, from which it is evident that $\eta = 1$ when the

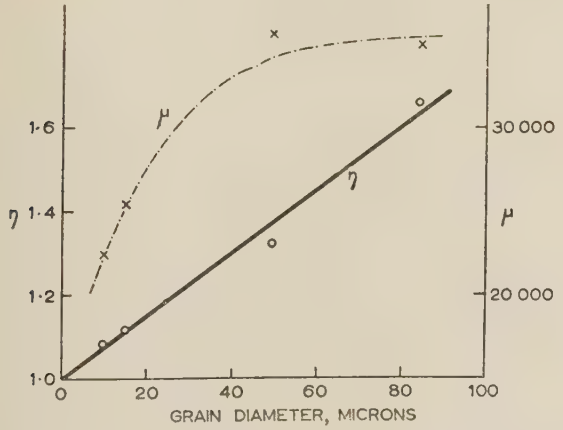

Fig. 4.—Observed variation of loss ratio η and permeability with grain diameter for a Mumetal-type alloy—Parkin.[20]

grain diameter is reduced to zero. At present, however, there is insufficient evidence to show that this is a typical result.

There next arises the possibility of a correlation between η and μ. For the spin-relaxation part, the situation is simple. On most inclusion models $|K|^{1/2} \propto \mu^{-1}$, and so η varies as μ^{-1}. It is not so easy to decide in connection with the eddy-current damping term. From eqn. (7) it would appear that, since η is proportional to l and $\mu = 2p^2\pi M_s^2/3\alpha l$, then $\eta \propto \mu^{-1}$. However, this ignores the fact that α is not independent of l. Much more likely, in the author's view, is that α increases as l decreases, and so the variation of η with μ depends on the manner in which α varies with l. Thus, although for a given set of experimental conditions, i.e. heat treatment, etc., one may observe a definite correlation between η and μ, it is not possible *a priori* to predict the form of this correlation.

These considerations also apply to the possible temperature dependence of η. Broadly speaking, one would expect η to be almost temperature independent, but if η does, in fact, vary with μ, a temperature variation in one will be reflected in the other. Genuine temperature variations in η seem to be possible only through the intervention of the spin-relaxation term. For most materials K increases rapidly at low temperatures, and, in addition, λ increases at high temperatures,[20, 23] and so the spin relaxation should become more important at both high and low temperatures.

It is perhaps pertinent to ask whether, for a given thickness of sheet, it is possible to reduce η in any way. One way might be to reduce the domain size by decreasing the grain size. The danger is that, if the reduction in grain size increases α more rapidly than it decreases the domain size, the permeability will fall. This is, in fact, the case with the measurements of Parkin shown in Fig. 4, which indicate a serious drop in permeability when the grain diameter becomes less than about 40 microns. A more hopeful way of reducing η would seem to be to reduce the anisotropy more nearly to zero. This would have the effect of increasing the domain-wall width, since this is proportional to $K^{-1/2}$, until ultimately the whole material would be composed of walls and a pure rotational permeability would result. In either case the permeability would still be subject to inherent damping of the spin in much the same way as the spin system is damped in a ferromagnetic resonance experiment. Kittel[24] obtained the following expression for the frequency dependence of the rotational susceptibility (equal to a good approximation to $\mu_R/4\pi$ for the high permeabilities considered here):

$$\frac{\chi_{R,\omega}}{\chi_{R,0}} = \frac{\omega_0^2 + \frac{\lambda}{\chi'}\left(j\omega + \frac{\lambda}{\chi'}\right)}{\omega_0^2 - \omega^2 + \left(\frac{\lambda}{\chi'}\right)^2 + 2j\omega\frac{\lambda}{\chi'}}$$

in which $\omega_0 = \gamma(2K/M_s)$ and χ' is an average rotational susceptibility approximately equal to $M_s^2/3K$. For frequencies low compared with ω_0, this gives rise to the following loss tangent:

$$\tan\delta_R = \frac{\omega\lambda}{\chi'}\frac{1}{\omega_0^2}$$

Rotational processes produce a uniform change in magnetization for which the classical eddy-current formulae should be correct and so the rotational relaxation gives

$$\eta - 1 = \frac{27\rho\lambda}{16\pi^2 M_s^2\gamma^2 d^2}$$

For the alloy considered in Section 4, $\eta - 1 = 2 \times 10^{-8} \times d^{-2}$, so that $\eta = 3$ when $d = 1$ micron. The smallness of this value, especially for large values of d, is the justification for neglecting rotational losses in eqn. (10). It also indicates that, if domain walls can be removed and a sufficiently high permeability obtained from rotations alone, η would be much reduced. However, in order that $\mu = 40\,000$, K would have to be no greater than 40 ergs/cm^3. In an alloy this would probably be difficult, since, in a typical nickel-iron alloy, it requires a precision in the nickel content of $\pm 0{\cdot}01$%. Local variations in composition might change K by this amount from one point to another through

the material unless the degree of homogeneity were unusually good.

(6) CONCLUSIONS

It is concluded that, in any ferromagnetic material subject to an alternating magnetic field of sufficiently small amplitude so that hysteresis loss is negligible, the measured losses will always be greater than those calculated on the assumption of a uniform permeability. This discrepancy should exist in all materials, not merely high-permeability alloys, and it becomes more serious as the thickness of the sheet is reduced. The ratio η may be expected to vary with d according to an approximate law of the form $\eta = 1 + kd^{-r}$, in which r may itself be a function of d but always lies between 1 and 2. The effect is caused by properties inherent in a ferromagnetic body and can never be entirely eradicated. It is possible, in principle, to reduce it by increasing the number of domain walls, i.e. by reducing the average domain size. Practically, the only way of doing this is to reduce the grain size of the material. Since such a reduction would almost inevitably be accompanied by a decrease in permeability some compromise would have to be reached in any practical arrangement.

(7) ACKNOWLEDGMENTS

The author would like to express his thanks to Professor L. F. Bates for his interest in this work. He is indebted to Mr. A. C. Lynch of the Post Office Research Station, who introduced him to the subject, for numerous helpful discussions and for many improvements made to the manuscript. He would also like to express his thanks to Mr. A. G. H. Troughton for permission to quote the result in Section 5.

(8) REFERENCES

(1) Richards, C. E., Walker, E. V., and Lynch, A. C.: 'An Experimental Study of High-Permeability Nickel-Iron Alloys', *Proceedings I.E.E.*, Paper No. 2136 M, August, 1956 (**104** B, p. 343).

(2) Jordan, H.: 'Ferromagnetische Konstanten für schwache Schwingungsfelder', *Elektrishe Nachrichtentechnik*, 1924, **1**, p. 7.

(3) Abgrall, C., and Epelboin, I.: 'Sur l'étude en fonction de la température de rubans minces en Mumetal soumis à des champs alternatifs faibles', *Comptes Rendus*, 1952, **234**, p. 1265.

(4) Peterson, E., and Wrathall, L. R.: 'Eddy Currents in Composite Laminations', *Proceedings of the Institute of Radio Engineers*, 1936, **24**, p. 275.

(5) Epelboin, I.: 'Délimitation des domains de Rayleigh dans les champs alternatifs à la lumière de récents travaux théoriques et expérimentaux', *Journale de Physique et le Radium*, 1951, **12**, p. 361.

(6) Feldtkeller, R.: 'Spulen und Überträger' (Hirzel, Stuttgart, 1949).

(7) Aspden, H.: 'The Eddy-Current Anomaly in Electrical Sheet Steel', *Proceedings I.E.E.*, Monograph No. 164 M, January, 1956 (**103** C, p. 272).

(8) Williams, H. J., Shockley, W., and Kittel, C.: 'Studies of the Propagation Velocity of a Ferromagnetic Domain Boundary', *Physical Review*, 1950, **80**, p. 1090.

(9) Landau, L., and Lifshitz, E.: 'On the Theory of the Dispersion of Magnetic Permeability in Ferromagnetic Bodies', *Physikalische Zeitschrift der Sowjetunion*, 1935, **8**, p. 153.

(10) Galt, J. K., Andrus, J., and Hopper, H. G.: 'Motion of Domain Walls in Ferrite Crystals', *Reviews of Modern Physics*, 1953, **25**, p. 93.

(11) Rado, G. T., Wright, W. R., and Emerson, W. H.: 'Ferromagnetism at Very High Frequencies. III. Two Mechanisms of Dispersion in a Ferrite', *Physical Review*, 1950, **80**, p. 273.

(12) Polivanov, K. M.: 'Dynamic Characteristics of Ferromagnetic Materials', *Izvestia Akademii Nauk S.S.S.R., Seria Fiziki*, 1952, **16**, p. 449.

(13) Galt, J. K.: 'Motion of Individual Domain Walls in a Nickel-Iron Ferrite', *Bell System Technical Journal*, 1954, **33**, p. 1023.

(14) Martin, D. H.: 'Surface Structures and Ferromagnetic Domain Sizes', *Proceedings of the Physical Society*, 1957, Section B, **70**, p. 77.

(15) Barlow, G. S.: Ph.D. Thesis, Nottingham University, 1957.

(16) Hoselitz, K.: Discussion in 'Soft Magnetic Materials for Telecommunications' (Pergamon Press, 1953), p. 8.

(17) Martius, U. M.: 'Ferromagnetism', *Progress in Metal Physics*, 1952, **3**, p. 140.

(18) Kittel, C.: 'Physical Theory of Ferromagnetic Domains', *Reviews of Modern Physics*, 1949, **21**, p. 541.

(19) Bates, L. F., and Hart, A.: 'A Comparison of the Powder Patterns on a Sample of Grain-Oriented Silicon-Iron with those obtained on a Single Crystal', *Proceedings of the Physical Society*, A, 1953, **66**, p. 813.

(20) Parkin, B. G.: Discussion in 'Soft Magnetic Materials for Telecommunications' (Pergamon Press, 1953), p. 319.

(21) Buckley, S. E., Jackson, G. A., and Thomas, A. G. F.: 'Some A.C. Measurements on a Material having a Rectangular Hysteresis Loop'. 'Soft Magnetic Materials for Telecommunications' (Pergamon Press, 1953), p. 313.

(22) Bloembergen, N.: 'On the Ferromagnetic Resonance in Nickel and Supermalloy', *Physical Review*, 1949, **76**, p. 743.

(23) Abrahams, E.: 'Relaxation Processes in Ferromagnetism', *Advances in Electronics and Electron Physics*, 1954, **6**, p. 47.

(24) Kittel, C.: 'Ferromagnetic Resonance', *Journale de Physique et le Radium*, 1951, **12**, p. 291.

621.396.67.012.12

The Institution of Electrical Engineers
Monograph No. 285 R
Feb. 1958

©

A THEORETICAL ANALYSIS OF SOME ERRORS IN AERIAL MEASUREMENTS

By J. BROWN, M.A., Ph.D., Associate Member.

(*The paper was first received 28th August, and in revised form 29th October*, 1957. *It was published as an* INSTITUTION MONOGRAPH *in February*, 1958.)

SUMMARY

A theoretical analysis of certain aerial problems is carried out with the help of the idea of a spectrum of plane waves introduced by Booker and Clemmow. The reciprocity theorem, which relates the behaviour of an aerial used for reception to the properties of the same aerial as a transmitter, is used to derive an expression for the power received by one aerial as a result of transmission from a second aerial at any distance from the first. It is shown that under the conditions used in aerial measurements the size of the receiving aerial can influence the errors in measured radiation patterns and power gains. In particular, the side-lobe levels obtained when too small a separation between the aerials is used can either be larger or smaller than the levels for the true radiation pattern. This result differs from that predicted by diffraction theory, which suggests that side-lobe levels measured at too small a distance are always worse than those in the true radiation pattern. Similarly, when the size of the receiving aerial is taken into account, errors in gain measurements are shown to be larger than those predicted by diffraction theory.

LIST OF PRINCIPAL SYMBOLS

a = Aperture length.
x, y, z = Cartesian co-ordinates.
r, θ, ϕ = Spherical polar co-ordinates.
i, j, k = Unit vectors in directions of x-, y- and z-axes.
i_r, i_θ, i_ϕ = Unit vectors in r, θ and ϕ directions.
ϵ_0, μ_0 = Absolute permittivity and permeability of free space.
Z_0, Y_0 = Wave impedance and admittance of a plane wave in free space.
k = Free-space plane-wave phase coefficient ($=2\pi/\lambda$).
$S_1 = \sin\theta\cos\phi$.
$S_2 = \sin\theta\sin\phi$.
$C = \cos\theta$.
$c_0 = \cos\theta_0$.
$s_0 = \sin\theta_0$.
$F(S_1, S_2)$ = Plane-wave spectrum radiated by an aerial.
$G(\theta, \phi)$ = Power gain of an aerial for the direction θ, ϕ.
$A_{eff}(\theta, \phi)$ = Effective receiving area of an aerial for the direction θ, ϕ.
B_R, B_T = Half-power beam widths of receiving and transmitting aerials.
D = Complex amplitude of signal in receiving-aerial feeder.
$L = \log_e 2$.
$p = 4L/B_R^2 - jkr$.
η = arc tan $(krB_R^2/4L)$.

(1) INTRODUCTION

In measurements of the radiation pattern or power gain of an aerial, errors can arise if the test site is insufficiently large. The calculation of these errors is usually based on classical diffraction theory and leads to the conclusion that the distance between the aerial being tested and the fixed aerial must exceed the Rayleigh range. In such calculations the size of the fixed aerial is neglected. The object of the paper is to examine the effect of this on the errors, and the method of calculation uses the concept of an angular spectrum of plane waves, introduced by Booker and Clemmow.[1] This not only provides a direct derivation of the results desired, but enables us to relate the problems arising in aerial-pattern measurements to those in the determination of the frequency spectrum of a time waveform.

(2) THE ANGULAR SPECTRUM OF PLANE WAVES

The basic principle in the method developed by Booker and Clemmow is that any electromagnetic field can be represented by the addition of plane waves, including the possibility that some of these waves may be inhomogeneous and of the type more commonly described as surface waves. In radiation problems, the amplitudes of these waves can be calculated if either the electric field or the magnetic field is known over a suitably chosen aperture plane; this aperture field can usually be calculated by optical methods relatively easily from the geometry of the aerial and a knowledge of the feed radiation pattern. The aperture distribution is then expressed as a Fourier integral, and the radiated field can be calculated by relating the component exponential terms in the integral to plane waves. The details of the calculation are described by Booker and Clemmow for 2-dimensional problems, and the method is readily extended to 3-dimensional problems.

Suppose, for example, that the electric field is linearly polarized

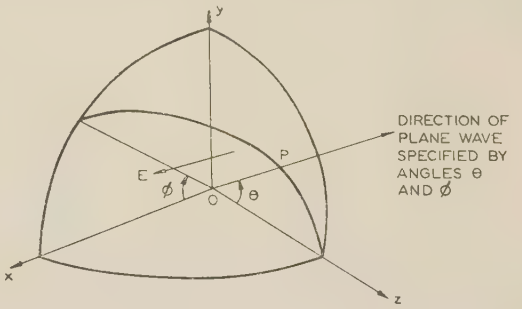

Fig. 1.—Radiating aperture, showing the co-ordinate systems used in the analysis: the aperture lies in the plane $z = 0$ and may be of infinite extent.

in the aperture plane $z = 0$ (Fig. 1), the direction of this field being parallel to the x-axis. Then

$$E_x(x, y, 0) = \frac{1}{\lambda^2}\int_{-\infty}^{\infty}\int_{-\infty}^{\infty} F(S_1,S_2)\exp(-jkS_1x - jkS_2y)dS_1dS_2 \quad \ldots (1)$$

where $F(S_1, S_2)$ is the Fourier transform of $E_x(x, y, 0)$, the aperture-plane electric field. Furthermore, the Fourier transform can be calculated from $E_x(x, y, 0)$ by the inverse relation

$$F(S_1, S_2) = \int_{-\infty}^{\infty}\int_{-\infty}^{\infty} E_x(x, y, 0)\exp(jkS_1x + jkS_2y)dxdy \quad \ldots (2)$$

Correspondence on Monographs is invited for consideration with a view to publication.

Dr. Brown is in the Department of Electrical Engineering, University College, London.

Now any plane wave travelling in a direction specified by the polar angles θ and ϕ of Fig. 1 has an x-component of electric field given by

$$E(x, y, z) = E \exp [-jk(x \sin\theta \cos\phi + y \sin\theta \sin\phi + z \cos\theta)] \quad . \quad . \quad . \quad . \quad (3)$$

E being an amplitude constant. When $z = 0$, the variation with x and y is of the same form as that in the integrand of eqn. (1), provided that

$$S_1 = \sin\theta \cos\phi \text{ and } S_2 = \sin\theta \sin\phi \quad . \quad . \quad . \quad (4)$$

We can therefore regard eqn. (1) as stating that the aperture field arises from a collection of plane waves travelling in all possible directions, the amplitude of the wave in the direction given by S_1, S_2 being $F(S_1, S_2)$. Each of these waves varies with z in the manner specified by eqn. (3), so that we find the radiated field to be

$$E_x(x, y, z) = \frac{1}{\lambda^2}\int_{-\infty}^{\infty}\int_{-\infty}^{\infty} F(S_1, S_2) \exp [-jk(S_1x + S_2y + Cz)]dS_1dS_2 \quad . \quad (5)$$

in which

$$C = (1 - S_1^2 - S_2^2)^{1/2} \quad . \quad . \quad . \quad . \quad . \quad (6)$$

When θ and ϕ are real angles, the numerical values of S_1 and S_2 are such that $(S_1^2 + S_2^2) \neq 1$, C then being real; the positive value of the square root in eqn. (6) is used. The Fourier representation, however, requires that S_1 and S_2 can assume any real values, so that C may become imaginary; if the root in eqn. (6) is now selected to make C a negative imaginary quantity, the field decays exponentially with increasing positive values of z. A wave with a progressive phase change parallel to a surface, here the plane $z = 0$, and an exponential decay perpendicular to this surface is usually called a surface wave, but can be regarded as a simple extension of the ordinary plane wave.

Expressions similar in form to eqn. (5) can be obtained for the other field components from Maxwell's equations by an equivalent generalization of the equations corresponding to (3). The component E_y is everywhere zero. Expressing the fields vectorially we find that

$$\boldsymbol{E}(x, y, z) = \frac{1}{\lambda^2}\int_{-\infty}^{\infty}\int_{-\infty}^{\infty} (C\boldsymbol{i} - S_1\boldsymbol{k})F(S_1, S_2) \exp [-jk(S_1x + S_2y + Cz)]dS_1dS_2/C \quad . \quad (7)$$

$$\boldsymbol{H}(x, y, z) = \frac{Y_0}{\lambda^2}\int_{-\infty}^{\infty}\int_{-\infty}^{\infty} [-S_1S_2\boldsymbol{i} + (1 - S_2^2)\boldsymbol{j} - CS_2\boldsymbol{k}] F(S_1, S_2) \exp [-jk(S_1x + S_2y + Cz)]dS_1dS_2/C \quad . \quad (8)$$

where $Y_0 = (\epsilon_0/\mu_0)^{1/2}$ is the free-space plane-wave admittance.

It may be noted that, when the aperture field has no y-component of electric field, this component vanishes everywhere. Corresponding results can be derived when the aperture electric field has no x-component, and the most general case can always be resolved into a sum of the two linearly polarized cases.

The field at a point sufficiently distant from the aperture plane can be calculated approximately by a double application of the stationary phase method to the integrals in eqns. (7) and (8): again this is a simple extension of the results given by Booker and Clemmow. If the distant point is specified by the spherical polar co-ordinates (r, θ, ϕ), then

$$\boldsymbol{E}(r, \theta, \phi) = \left[\frac{j \exp(-jkr)}{r\lambda}\right](\cos\phi\boldsymbol{i}_\theta - \sin\phi \cos\theta\boldsymbol{i}_\phi) F(\sin\theta \cos\phi, \sin\theta \sin\phi) \quad . \quad (9)$$

$$\boldsymbol{H}(r, \theta, \phi) = Y_0\boldsymbol{i}_r \times \boldsymbol{E}(r, \theta, \phi) \quad . \quad . \quad . \quad (10)$$

From eqn. (9) we see that the dominant contribution to the variation of the field with direction arises from the function F, which can therefore be interpreted as the amplitude radiation pattern. Restrictions on the interpretation of the plane-wave spectrum as a radiation pattern are the same as in the 2-dimensional problem, namely that the field is being considered at a distance from the aperture which is large compared with the wavelength and with the dimensions of the aperture plane over which there is appreciable illumination.

Eqn. (9) is similar to the result obtained by using the Huyghens–Kirchhoff integral method of physical optics when approximations are made appropriate to the distant point being in the Fraunhofer region. For example, when converted to the present notation, Silver's result[2] is

$$\boldsymbol{E}(r, \theta, \phi) = \left[\frac{j(1 + \cos\theta) \exp(-jkr)}{2\lambda r}\right](\cos\phi\boldsymbol{i}_\theta - \sin\phi\boldsymbol{i}_\phi) F(\sin\theta \cos\phi, \sin\theta \sin\phi) \quad . \quad (11)$$

which differs from eqn. (9) only in the angular factors multiplying the function F. For small values of θ, $\cos\theta$ can be taken as unity and then the two expressions are identical. The different angular factors, namely the extra $\frac{1}{2}(1 + \cos\theta)$ in Silver's expression and the $\cos\theta$ appearing before the vector $\boldsymbol{i}_\phi$ in eqn. (9), may be referred to as 'obliquity factors'.

The two solutions differ, although they are apparently based on identical approximations, namely the assumption that $kr \gg 1$. The most significant difference is that, whereas the Booker–Clemmow method relies only on a knowledge of the electric field in the aperture plane, the Kirchhoff method requires that both the electric and magnetic fields should be specified. These fields are not necessarily consistent, and to allow for this, additional line distributions of electric and magnetic charge are introduced along the boundary of the aperture, which is taken as finite in extent. A simple relation between the electric and magnetic fields, usually equivalent to assuming that the field in the aperture is part of a plane wave, is then postulated. It is doubtful whether this relation can ever be satisfied, so that the discrepancy between eqns. (9) and (11) probably arises from the incompatibility of the electric and magnetic aperture fields used in the derivation of eqn. (11). The difference between the two expressions is very slight, however, and in practical applications to narrow-beam aerials, θ can usually be assumed to be small enough to make $\cos\theta$ unity when, as mentioned above, the two expressions agree. In this case the magnitude of the electric field strength is directly proportional to $|F|$, which can therefore be regarded as the radiation pattern.

(3) APPLICATION OF THE ANGULAR SPECTRUM TO RECEIVING AERIALS

The idea of an angular spectrum of plane waves is of considerable help in calculating the power transferred to a receiver by an aerial when the wave incident on the aerial has a complicated form. The incident wave can be expressed as a spectrum of plane waves, the signal at the receiver being determined by summing the contributions of the individual plane waves. A knowledge of the behaviour of the aerial when illuminated by a single plane wave is required, and this can be deduced from the radiation pattern of the aerial when used as a transmitter, coupled with the reciprocity theorem.

When the reciprocity theorem of circuit theory is applied to aerials it can be shown that the radiation patterns of the aerial are identical whether it is used as a transmitter or a receiver. For the present analysis we require a slightly more general result from which the amplitude and phase in the aerial feeder can be calculated when a plane wave is incident on the aerial from any

arbitrary direction. This can be derived from the Lorentz reciprocity theorem for electromagnetic fields, and details will be given in a separate paper.

Consider the arrangement shown in Fig. 2, in which a feeder—either a waveguide or a transmission line—is connected to an

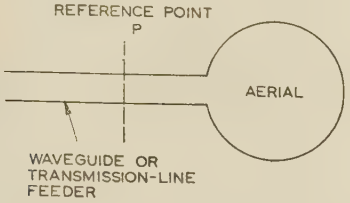

Fig. 2.—Arrangement of aerial and waveguide feed used for the derivation of the reciprocity theorem.

aerial, and select some reference point P in the feeder. Suppose that the impedance of the line is normalized, so that a wave of unit amplitude in the line carries unit power, and refer all phases to P. If a unit wave of zero phase at P travels towards the aerial, radiation will occur, and the corresponding radiation field will be of the form given by eqns. (9) and (10). To emphasize that these now correspond to a unit-amplitude wave we will attach the suffix 1 to the function F.

When the aerial is used as a receiver, a plane wave will be incident on the aerial from some arbitrary direction. We will retain our restriction that the aerial radiates waves with no y-component of electric field and choose the incident wave similarly. This will be of the form

$$E'(x, y, z) = E(C'\boldsymbol{i} + S_1'k) \exp jk(S_1'x + S_2'y + C'z) \quad . \quad (12)$$

$$\boldsymbol{H}'(x, y, z) = Y_0E\{S_1'S_2'\boldsymbol{i} - [1 - (S_2')^2]\boldsymbol{j} + C'S_2'\boldsymbol{k}\} \exp jk(S_1'x + S_2'y + C'z) \quad . \quad (13)$$

where E is a complex quantity specifying the amplitude and phase of the incoming wave, and C', S_1' and S_2' are related to θ' and ϕ' (angles defining the direction of the incoming wave) by equations similar to (4) and (6).

This incoming wave will cause a signal in the feeder travelling from the aerial towards a receiver. From the extension of the reciprocity theorem referred to above it is found that the complex quantity representing the amplitude and phase of this wave at the reference point P is given by

$$A = \tfrac{1}{2}EY_0(1 - S_2'^2)F_1(S_1', S_2') \quad . \quad . \quad . \quad . \quad . \quad (14)$$

and is therefore related to the angular spectrum F_1.

It may be noted that this equation leads to the well-known result relating power gain, $G(\theta, \phi)$, to the effective receiving area, $A(C_{eff}\theta, \phi)$, namely

$$A_{eff}(\theta, \phi) = \lambda^2G(\theta, \phi)/4\pi \quad . \quad . \quad . \quad . \quad . \quad (15)$$

Eqn. (14) also gives the phase of the wave received by the aerial.

(4) TRANSMISSION BETWEEN TWO AERIALS

(4.1) Exact Result for Received Signal

The problem of calculating the power transmitted from one aerial to a second is usually dealt with by assuming the distance between the aerials to be sufficiently great for the far-field approximation to apply. This is perfectly satisfactory when considering, for example, two stations of a relay network or the derivation of the radar equation, when the target effectively behaves both as a receiver and a transmitter. In measuring the radiation pattern and power gain of an aerial, however, the site is often so small that the far-field solution is not sufficiently accurate, and aerial designers must determine what errors can arise in the measurements and how to reduce them. Most of the calculations related to this have been based on extending the physical-optics solution to the Fresnel diffraction region, but in this method it is not easy to make appropriate allowance for the aperture sizes of both aerials. The plane-wave-spectrum approach makes it possible to derive an integral from which the power transmitted between aerials of any size can be calculated, and approximate methods of evaluating this integral can be used to estimate the effect of operating at too small a separation between the aerials. The integral will be derived for the situation of most interest, namely that of measuring the radiation pattern in one of the principal planes of the aerial.

From the reciprocity theorem it is obvious that the aerial under test can be used either as a transmitter or a receiver. In the remainder of the paper we shall assume that the test aerial is used as the transmitter and that the arrangement is as shown in Fig. 3.

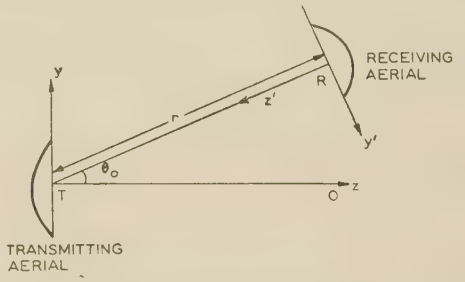

Fig. 3.—Arrangement of aerials for the measurement of the radiation pattern of aerial T, used as a transmitter.

TO is the direction of maximum radiation from T.
R is directed so that the maximum of its radiation pattern is in the direction RT.

The test aerial, T, and fixed receiving aerial, R, are arranged so that their directions of maximum radiation lie in the plane of the Figure: in addition, R is so oriented that the maximum of its radiation pattern always points towards T. The radiation pattern is then measured by rotating T about an axis perpendicular to the plane of the Figure and observing the output from a receiver connected to R as a function of the angle, θ_0, between the direction TR and the direction of maximum radiation of T. If the aerial separation, r, is sufficiently large, the observed radiation pattern will be the true far-field pattern, which is related to the plane-wave spectrum as discussed in Section 2.

The principle of the calculation is quite straightforward: the field radiated by T is expressed as an angular spectrum of plane waves. Each wave will cause a contribution to that in the waveguide connected to the aerial R, and the total received signal is obtained by adding the contributions, allowing for any phase differences, i.e. fields and not powers must be added. The generalized reciprocity theorem of Section 3.1 provides the necessary information on the phase differences between the various contributions. Suppose, for example, that the plane of Fig. 3 is taken as the plane $x = 0$ and that unit power is radiated by T. Then, the radiated field is given by eqns. (7) and (8), with F replaced by F_1^T. The component plane waves must now be referred to the co-ordinate system x, y', z', with respect to which the properties of aerial R are known. Consider one plane wave for which

$$E = E(S_1, S_2)\,(C\boldsymbol{i} - S_1k) \exp\,[-jk(S_1x + S_2y + Cz)] \quad (16)$$

The co-ordinates y and z are related to y' and z' by

$$\begin{aligned} y &= (r - z')s_0 - y'c_0 \\ z &= (r - z')c_0 + y's_0 \end{aligned} \quad . \quad . \quad . \quad . \quad (17)$$

while the unit vectors j, k can be expressed as

$$\begin{aligned} j &= -j'c_0 - k's_0 \\ k &= j's_0 - k'c_0 \end{aligned} \quad . \quad . \quad . \quad . \quad . \quad . \quad (18)$$

j', k' being unit vectors in the directions of the y'- and z'-axes respectively.

Eqn. (29) can now be written as

$$E = E(S_1, S_2)(Ci - S_1s_0j' + S_1c_0k') \exp\left[-jk(rC' - xS_1' - y'S_2' - z'C')\right] \quad . \quad (19)$$

where

$$S_1' = -S_1,\ S_2' = -Cs_0 + S_2c_0 \text{ and } C' = Cc_0 + S_2s_0 \quad (20)$$

The field is expressed in a form to which the results of Section 3.1 can be applied: it will be observed that there is a y'-component of electric field, whereas the aerial accepts only waves for which this component is zero. We can overcome this difficulty by resolving E into two perpendicularly polarized components and rejecting the one which is not accepted by the aerial. For the wave given by eqn. (19) the amplitude of the component accepted by the aerial is

$$E(S_1, S_2)(C/C') \exp(-jkrC') \quad . \quad . \quad . \quad . \quad (21)$$

so that from eqn. (23) the amplitude of the wave in the guide connected to R is

$$B = \tfrac{1}{2}Y_0(C/C')E(S_1, S_2)(1 - S_2'^2)F_1^R(S_1', S_2') \exp(-jkrC') \quad . \quad (22)$$

where $F_1^R(S_1', S_2')$ is the plane wave spectrum associated with aerial R. The total signal received by aerial R is now given by integrating with respect to S_1 and S_2. When the incident field is generated by the transmitting aerial T, inspection of eqn. (7) shows that

$$E(S_1, S_2) = F_1^T(S_1, S_2)/C\lambda^2 \quad . \quad . \quad . \quad . \quad (23)$$

Carrying out the integration over the possible range of values of S_1 and S_2, we find that the amplitude received by the waveguide connected to R when illuminated by T as in Fig. 3 is

$$D = \frac{Y_0}{2\lambda^2}\int_{-\infty}^{\infty}\int_{-\infty}^{\infty}(1 - S_2'^2)F_1^T(S_1, S_2)F_1^R(S_1', S_2')\,\epsilon^{-jkrC'}\frac{dS_1dS_2}{C} \quad . \quad . \quad . \quad (24)$$

The power received by R is given by $|D|^2$. Eqn. (24) is exact, but the evaluation of the integral in all except simple cases is extremely difficult. We will now consider certain simplifications.

(4.2) Far-Field Approximation

As already mentioned, the power received by R can be calculated fairly easily when the distance r between the aerials is sufficiently large. The integral can then be integrated by stationary phase methods, as shown in Section 7.1, the result being

$$D = \frac{jY_0c_0}{2\lambda r}\exp(-jkr)F_1^T(0, s_0)F_1^R(0, 0) \quad . \quad . \quad . \quad (25)$$

The power received by R is given by $|D|^2$, so that

$$\text{Power received} = \left(\frac{Y_0c_0}{2\lambda r}\right)^2|F_1^T(0, s_0)|^2|F_1^R(0, 0)|^2 \quad . \quad (26)$$

If the wave spectra are now replaced by the power gain for the transmitter T and the receiving area for R, eqn. (26) becomes

$$\text{Power received} = G^T\left(\theta_0, \frac{\pi}{2}\right)A^R\left(0, \frac{\pi}{2}\right)/4\pi r^2 \quad . \quad . \quad (27)$$

which is the result obtained by a simple application of the ideas of power gain and effective receiving area. Our general expression, eqn. (24), therefore reduces to the appropriate result when the distance r is sufficiently great.

(4.3) Measurement of Radiation Pattern

The radiation pattern as measured for a given distance r and known receiving aerial R is given by $|D|^2$, as calculated from eqn. (24), regarded as a function of θ_0. For sufficiently large r the measured pattern agrees with the pattern at infinite distance, $|F^T(\theta_0, \pi/2)|^2$, as shown in the last Section. To determine the errors in any particular arrangements we must evaluate $D(\theta_0)$ to a higher degree of accuracy. This will be done for one case of particular interest, namely that in which the aerial to be measured has an aperture with large horizontal and relatively small vertical dimensions. The horizontal radiation pattern then has a smaller beam-width than the vertical, and it is usually considered essential to measure the horizontal radiation pattern at a distance greater than a^2/λ, a being the horizontal aperture dimension.

Suppose that Fig. 3 represents a plan view of the arrangement used to measure the horizontal radiation pattern of T, and further assume that the fixed aerial R has a narrow horizontal radiation pattern but a relatively broad vertical pattern. The accuracy with which an integral can be evaluated by the stationary-phase method depends on the rapidity with which the integrand, excluding the exponential term, varies with the integration variable. Under the conditions postulated, the integrand, excluding the exponential term, varies relatively slowly with S_1 (corresponding to the wide vertical patterns of T and R) but rapidly with S_2. There will thus be a range of values of r, greater than some minimum value, for which the integration with respect to S_1 can be carried out exactly as in Section 7.2. If we now replace S_2 by $\sin\psi$, we have, from eqn. (49),

$$D(\theta_0) = \frac{Y_0\exp(j\pi/4)}{2(\lambda^3rc_0)^{1/2}}\int_\Gamma F_1^T(0, \sin\psi)F_1^R[0, \sin(\theta_0 - \psi)] \cos(\theta_0 - \psi)\cos^{3/2}\psi\exp\left[-jkr\cos(\theta_0 - \psi)\right]d\psi \quad . \quad (28)$$

where Γ is the integration contour of Fig. 4(a), corresponding to $\sin\psi$ ranging from $-\infty$ to ∞. Γ is selected to ensure that

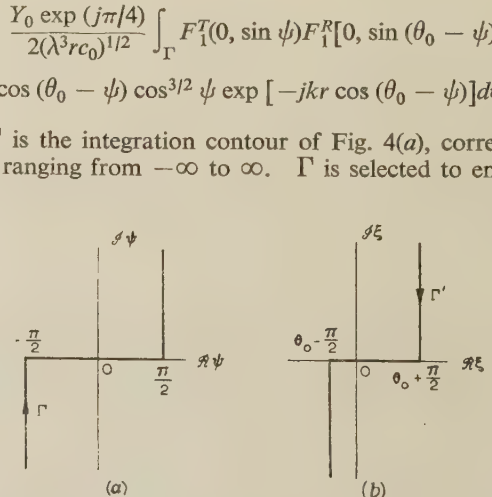

Fig. 4.—Integration contours for eqns. (41) and (43).

$\mathcal{I}\cos(\theta_0 - \psi)$ is negative to give the evanescent field decaying in the positive z-direction. This integral can be evaluated as an asymptotic series in terms of increasing powers of $(1/kr)$ by the stationary-phase method. For the present purpose it is convenient at this stage to specify the radiation pattern of the fixed aerial in more detail. The basis of our integration method is that only the plane waves travelling nearly in the direction from T to R make any significant contribution to the received signal: we therefore need consider only the form of the radiation pattern

for angles close to the normal, i.e. for values of ψ near θ_0. A good approximation to the shape of most aerial patterns in the vicinity of the direction of maximum radiation is given by a Gaussian function, so that we can use the form

$$E_1^R[0, \sin(\theta_0 - \psi)] = \lambda\left(\frac{G_R}{2\pi Y_0}\right)^{1/2} \exp\left[\frac{-2L(\theta_0 - \psi)^2}{B_R^2}\right]. \quad (29)$$

where G_R is the power gain of R in the direction of maximum radiation and B_R is the half-power beam-width of the horizontal radiation pattern of R. Substitution for F_1^R in eqn. (28) and changing the integration variable to $\xi = (\theta_0 - \psi)$ gives

$$D(\theta_0) = \left(\frac{jY_0G_R}{8\pi\lambda r c_0}\right)^{1/2} \int_{\Gamma'} F_1^T[0, \sin(\theta_0 - \xi)] \cos\xi \cos^{3/2}(\theta_0 - \xi) \exp\left(\frac{-jkr\cos\xi - 2L\xi^2}{B_R^2}\right) d\xi \quad . \quad . \quad . \quad . \quad (30)$$

Γ' being the contour in Fig. 4(*b*). The convergence of this integral on Γ' is ensured by the presence of the term $\cos\xi$ in the exponential.

Since we are considering narrow-beam aerials, $\cos\theta_0$ can be replaced by unity and corresponding approximations made in the integrand. This enables an asymptotic series to be obtained for the integral, as shown in Section 7.3, and from the results there we have

$$D(\theta_0) = \tfrac{1}{2}\exp(-jkr + \tfrac{1}{2}j\eta)\left(\frac{jY_0G_R}{\lambda r|p|}\right)^{1/2} \times \left[F_1^T(\theta_0) + \frac{\exp(j\eta)}{2|p|}F_1^{T(2)}(\theta_0) + \ldots + \frac{1\cdot 3\ldots(2n-1)}{(2n)!|p|^n}\exp(jn\eta)F_1^{T(2n)}(\theta_0) + \ldots\right] \quad . \quad (31)$$

where $$|p| = [(kr)^2 + (4L/B_R^2)^2]^{1/2} \quad . \quad . \quad . \quad (32)$$

and $$\eta = \arctan(krB_R^2/4L) \quad . \quad . \quad . \quad . \quad (33)$$

In eqn. (31), the spectrum F_1^T is shown as depending on the single angle θ_0, since we are considering only the principal plane, and $F_1^{T(n)}(\theta_0)$ is the nth derivative of the function $F_1^T(\theta)$ with respect to the angle θ, evaluated for $\theta = \theta_0$.

The expression in eqn. (31) has similarities to the corresponding result obtained by using the Kirchhoff–Huyghens method;[3] in this, no allowance is made for the beam width of the fixed aerial, and it can easily be shown that the Kirchhoff–Huyghens result is identical to that of eqn. (31) if $B_R \to \infty$, i.e. if the fixed aerial accepts incoming signals equally strongly from all directions. The more general result allows us to examine the effect of the size of the fixed aerial on the accuracy with which the radiation pattern of the transmitting aerial can be measured. At first sight it would appear that using a directive receiving aerial should cause the measured pattern $D(\theta_0)$ to approximate more closely to the desired form $F_1^T(\theta_0)$, since the magnitudes of the terms after the first on the right-hand side of eqn. (31) decrease as B_R is decreased. In the limiting case of an infinitely large receiving aerial, $B_R = 0$, $|p| \to \infty$ and $D(\theta_0) \propto F_1^T(\theta_0)$. This shows that, in principle, the pattern of T can be measured to any desired degree of accuracy at any distance, provided that a sufficiently directive receiving aerial is used. Woonton and Carruthers[4] have demonstrated this experimentally for small horns, although practical difficulties arise because of reradiation by the aerials. A problem of practical importance is how large the fixed aerial must be to give a significant degree of improvement over a non-directional aerial. The answer to this is complicated by the dependence of the phase of the various terms in eqn. (31) on B_R. We therefore resort to numerical analysis of a particular case to determine the nature of the dependence of the measured pattern on B_R.

The example which has been considered is that of a transmitting aerial which has a constant aperture distribution. Once again we restrict the analysis to large aerials, so that only small values of θ need be considered. Then, the radiation pattern of T is given sufficiently accurately by the expression

$$F_1^T(\theta) = \lambda\left(\frac{G_T}{2\pi Y_0}\right)^{1/2} \frac{\sin(\pi a\theta/\lambda)}{(\pi a\theta/\lambda)} \quad . \quad . \quad . \quad (34)$$

a being the length of the aperture of T, and the factor $\lambda(G_T/2\pi Y_0)^{1/2}$ serving to give absolute values of field strength when T radiates unit power.

When this expression for $F_1^T(\theta)$ is used, eqn. (31) can be evaluated numerically with the help of the tables prepared by Milne.[3] This has been done for a separation equal to the Rayleigh distance, a^2/λ, using several values of the parameter η corresponding to different values of B_R. The maximum number of terms used in the series of eqn. (31) in carrying out the calculations is five, i.e. derivatives up to $F_1^{T(8)}$ are included. The results are shown in Fig. 5, being normalized in each case so that the

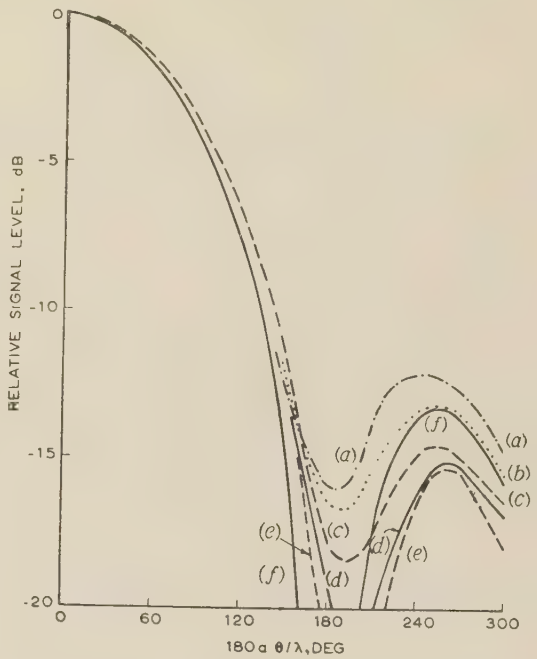

Fig. 5.—Radiation patterns for a uniformly illuminated aerial as observed at the Rayleigh distance, a^2/λ.

(*a*) $\eta = 90°$; non-directive receiver. (Pattern as calculated from the diffraction theory.)
(*b*) $\eta = 75°$; $B_R/B_T = 1{\cdot}46$.
(*c*) $\eta = 60°$; $B_R/B_T = 0{\cdot}99$.
(*d*) $\eta = 45°$; $B_R/B_T = 0{\cdot}76$.
(*e*) $\eta = 30°$; $B_R/B_T = 0{\cdot}58$.
(*f*) $\eta = 0°$; B_R/B_T (actual pattern as observed at infinite distance).

reference level corresponds to the maximum on-axis signal. The most interesting features of the set of patterns shown are:

(*a*) The measured half-power beam width is only slightly affected by the beam width of the fixed aerial.

(*b*) The first minimum becomes more marked as the fixed-aerial beam width decreases.

(*c*) The first side-lobe level at first decreases as the fixed-aerial beam width decreases, reaches a minimum and then increases to the far-field value when B_R becomes zero.

The last point is probably the most interesting from a practical point of view, and it will be noted that the side-lobe level appears too large if a small fixed aerial is used, but is too small if a very directive fixed aerial is used. The assumption frequently used in practice that side-lobe levels are apparently worse in the pattern measured at too short a range than they are in the true pattern may not therefore always be correct. The value of η for which the measured side-lobe level agrees with that in the true pattern is about 75°, corresponding to B_R/B_T 1·45 (with $B_T = 0{\cdot}88\lambda/a$ rad). For this condition the length of the fixed aerial is roughly two-thirds that of the aerial under test.

It should be stressed that the above numerical results apply only to one particular arrangement, namely the two aerials being separated by the Rayleigh range and each having a specially selected radiation pattern. It is probable that the results are not critically dependent on the shape of the fixed-aerial pattern, but on the other hand the behaviour of, for example, the measured side-lobe level may well vary with the nature of the pattern under test. One general conclusion can, however, be drawn: the problem of measuring very large aerials is not greatly eased by using a large fixed aerial. In the case being considered it is unlikely that a fixed aerial larger than the test aerial can be used, giving a minimum value for η of about 60°: while the pattern for $\eta = 60°$ in Fig. 5 approximates more closely to the actual pattern of the test aerial than does that for an omnidirectional fixed aerial, it still shows significant errors.

(4.4) Measurement of Power Gain

Most methods of power-gain measurement involve measuring the attenuation caused by transmission between two aerials and then using eqn. (27); either the gain of one aerial is known or two identical aerials are used, so that the unknown gain can be calculated. The preceding theory enables us to estimate the errors arising in any specified arrangement: one example is provided by the results in the previous Section if the received power is calculated from $|D(\theta_0)|^2$. The retention of the various constant terms in eqns. (29)–(34) permits the immediate calculation of the power received by R when unit power is transmitted from T; the 'measured gain' can then be calculated from eqn. (27). Results applicable under the conditions of the previous Section, i.e. both aerials having horizontal patterns much narrower than their vertical patterns and being separated by the Rayleigh range, are given in Fig. 6, the on-axis gain of T being plotted against η.

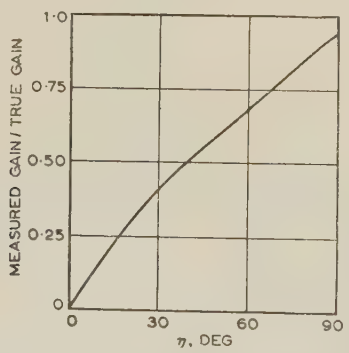

Fig. 6.—Dependence of measured gain of transmitting aerial on receiving-aerial beam width.

The ratio of the measured gain to the true gain of a transmitting aerial which has a narrow horizontal beam and a wide vertical beam is plotted against η which is expressed in terms of beam-widths in the caption to Fig. 5. The measurements are assumed to be made at distance a^2/λ.

It is immediately obvious that the measured gain depends very markedly on the size of the fixed aerial R: the least error between the measured gain and the true gain G_T occurs for an omnidirectional aerial R, the difference of 0·25 dB agreeing with calculations made by Polk[5] using Fresnel diffraction theory. The error increases very rapidly with decreasing values of B_R and becomes 1·69 dB at $\eta = 60°$, which corresponds quite closely to the situation when two identical aerials are used. For a very large receiving aerial ($\eta = 0$), the received signal tends to zero, as does the measured value of the gain of the transmitter aerial.

A more general result for two identical aerials can be obtained directly from eqn. (24); if the radiation pattern maximum is directed along the aerial axis, the gain is usually measured only for the two aerials pointing directly at each other, i.e. for $\theta_0 = 0$. Then

$$S_1' = -S_1 : S_2' = S_2 : C' = C \quad . \quad . \quad . \quad (35)$$

giving

$$D = \frac{Y_0}{2\lambda^2}\int_{-\infty}^{\infty}\int_{-\infty}^{\infty}(C^2+S_1^2)F_1(S_1, S_2)F_1(-S_1, S_2)\,\varepsilon^{-jkrC}\frac{dS_1 dS_2}{C} \quad (36)$$

where the indices T and R can now be omitted, since the two aerials are identical. We further restrict the discussion to aerials with constant phase symmetrical aperture distributions, i.e. for which

$$E_x(x, y, 0) = E_x(-x, -y, 0) = E_x^*(x, y, 0) \quad . \quad (37)$$

For such aerials $F(S_1, S_2)$ is a real symmetric function of S_1 and S_2, so that the integrand in eqn. (36) can be expressed in terms of the power gain, giving

$$D = \frac{1}{4\pi}\int_{-\infty}^{\infty}\int_{-\infty}^{\infty}G(S_1, S_2)\exp(-jkrC)dS_1 dS_2/C \quad . \quad (38)$$

The integral can again be integrated by the stationary-phase method, the dominant term corresponding to the result in eqn. (27). We shall consider in detail only the case of an aerial whose pattern is symmetrical about its axis, e.g. a paraboloid with a circularly symmetrical aperture distribution. The function G is then an even function of θ and can therefore be regarded as a function of C. The evaluation of the integral when this is so is considered in Section 7.4, and the result is applied to a uniformly illuminated circular aperture. Numerical results for the difference between the measured gain and the actual gain are shown in Fig. 7 as a function of the separation of the aerials. It will be observed that the measured gain is noticeably less than the actual gain when the separation is less than d^2/λ, d being the

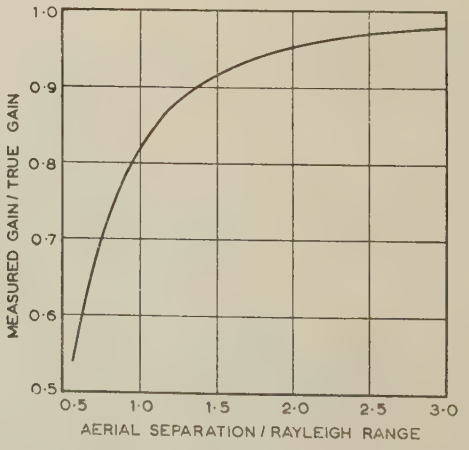

Fig. 7.—Dependence of measured gain on aerial separation.

The curve is calculated assuming that the measurement is made using two identical aerials of circular apertures, each having the diameter d: the aperture distributions are assumed constant.

aerial diameter, and that the difference is 0·86 dB at the separation d^2/λ. This figure is considerably larger than the 0·27 dB estimated by Silver* by a diffraction calculation, this corresponding to the assumption of a small receiving aerial.

(5) DISCUSSION OF RESULTS

It is apparent from the results given here that the errors in measuring aerial radiation patterns and power gains may be appreciably different from those predicted by optical diffraction theory. The reason for this difference is that diffraction theory is used to calculate the distribution of electric and magnetic field strengths and that the essential step of deriving the signal received by an aerial of finite aperture is not considered. One exception to this is Krutter's discussion† of the errors in gain measurement, where the effect of a taper in the amplitude distribution of the aperture of the receiving aerial is mentioned as a possible source of error. Krutter's suggested criterion of constancy of amplitude to within 10% is inadequate to ensure accurate gains, at least in the situation discussed in the previous Section. The errors arising from the amplitude variation can exceed those due to phase errors, and caution must therefore be used in applying correction factors of the type discussed by Polk. Similarly, examination of the radiation patterns shows that measurements on short sites can have errors of the opposite sign to those given by diffraction theory if even a moderately large receiving aerial is used. The procedure described by Bates and Elliott[6] to correct radiation-pattern measurements can be used only when small receiving aerials are used.

The plane-wave-spectrum concept introduced by Booker and Clemmow is a very powerful tool in the analysis of this type of problem. The analogy to a frequency spectrum it raises provides a convenient qualitative picture of the reasons for the influence of receiving-aerial size on the measured results. The plane-wave spectrum, which for aerials is the far-field radiation pattern, is related to the transmitter-aerial aperture distribution in the same way as is the frequency spectrum of a wave to its time variation. The measurement of radiation pattern is therefore similar to that of a frequency spectrum and is basically a filtering problem. The filtering is partly effected by the destructive interference of the waves travelling between the two aerials, which corresponds to the effect of a dispersive transmission line on a waveform. The receiving aerial, however, has also a filtering action because of its discrimination between plane waves arising from different directions. It is this additional filtering associated with the receiver which makes it essential to go a step beyond the normal diffraction treatment.

The numerical examples given in the paper have been based on the uniformly illuminated aperture to facilitate computation. For aerials with distributions of the type realized in practice, similar results will apply but may be less severe. There is a need for further numerical investigation, but to obtain a sufficiently wide range of typical results would require a considerable computation programme.

(6) REFERENCES

(1) Booker, H. G., and Clemmow, P. C.: 'The Concept of an Angular Spectrum of Plane Waves', *Proceedings I.E.E.*, Paper No. 992 R, January, 1950 (**97**, Part III, p. 11).

(2) Silver, S.: 'Microwave Antenna Theory and Design', Radiation Laboratory Series, Vol. 12 (McGraw-Hill, New York, 1949).

(3) Milne, K.: 'The Effects of Phase Errors on Simple Aperture Illuminations', Proceedings of a Conference on Centimetric Aerials for Marine Navigational Radar (H.M. Stationery Office, London, 1952), p. 86.

(4) Woonton, G. A., and Carruthers, J. A.: 'Indoor Measurements of Microwave Antenna Radiation Patterns by Means of a Metal Lens', *Journal of Applied Physics*, 1950, **21**, p. 428.

(5) Polk, C.: 'Optical Fresnel-Zone Gain of a Rectangular Aperture', *I.R.E. Transactions on Antennas and Propagation*, 1956, Vol. AP-4, p. 65.

(6) Bates, R. H. T., and Elliott, J.: 'The Determination of the True Side-Lobe Level of Long Broadside Arrays from Radiation Pattern Measurements made in the Fresnel Region', *Proceedings I.E.E.*, Monograph No. 169 R (**103**, C, p. 307).

(7) Jeffreys, H., and Jeffreys, B. S.: 'Methods of Mathematical Physics' (University Press, Cambridge), p. 501.

(8) Whittaker, E. T., and Watson, G. N.: 'Modern Analysis' (University Press, Cambridge, 1927), p. 300, ex. 9.

(7) APPENDICES

(7.1) Far-Field Approximation to Received Power

The integral to be evaluated [eqn. (24)] is

$$D = \frac{Y_0}{2\lambda^2}\int_{-\infty}^{\infty}\int_{-\infty}^{\infty}(1 - S_2'^2)F_1^T(S_1, S_2)F_1^R(S_1', S_2')\exp(-jkrC')\,dS_1dS_2/C' \quad . \quad (39)$$

When $kr \gg 1$ the exponential factor is a rapidly changing function of S_1 and S_2 and the principal contribution to D arises from the stationary-phase region. Since

$$C' = c_0(1 - S_1^2 - S_2^2)^{1/2} + s_0S_2 \quad . \quad . \quad . \quad (40)$$

the stationary point is given by

$$S_1 = 0;\ S_2 = s_0 \quad . \quad . \quad . \quad . \quad . \quad (41)$$

Near this point,

$$C' \simeq 1 - \tfrac{1}{2}S_1^2 - \tfrac{1}{2}\frac{(S_2 - s_0)^2}{c_0^2} \quad . \quad . \quad . \quad . \quad (42)$$

so that, by using a result quoted by Silver,*

$$D \simeq \frac{Y_0c_0}{2\lambda^2}F_1^T(0, s_0)F_1^R(0, 0)\exp(-jkr)\int_{-\infty}^{\infty}\int_{-\infty}^{\infty}\exp[\tfrac{1}{2}jkr(S_1^2 + U^2)]dS_1dU \quad . \quad (43)$$

where

$$U = (S_2 - s_0)/c_0 \quad . \quad . \quad . \quad . \quad . \quad (44)$$

i.e.

$$D = \frac{Y_0c_0}{2\lambda^2}F_1^T(0, s_0)F_1^R(0, 0)\exp(-jkr)\frac{2\pi\exp(j\pi/2)}{kr} \quad . \quad . \quad . \quad . \quad (45)$$

$$= \frac{jY_0c_0}{2\lambda r}F_1^T(0, s_0)F_1^R(0, 0)\exp(-jkr) \quad . \quad . \quad . \quad (46)$$

(7.2) Evaluation of Integration with Respect to S_1 by Stationary Phase

Under the conditions described in Section 4.3 the integration with respect to S_1 can be approximated by the first term of the asymptotic expansion given by the stationary-phase method. The stationary point is at $S_1 = 0$, so that from eqn. (24) we have

$$D \simeq \frac{Y_0}{2\lambda^2}\int_{-\infty}^{\infty}\int_{-\infty}^{\infty}(1 - S_2'^2)^{1/2}F_1^T(0, S_2)F_1^R(0, S_2')\exp\{-jkr[c_0(1 - S_1^2 - S_2^2)^{1/2} + s_0S_2]\}dS_1dS_2 \quad . \quad (47)$$

* Reference 2, p. 199.

† Reference 2, Section 15.14.

* Reference 2, p. 121.

in which S_1 and S_1' are made zero in all terms except the exponential.

The stationary phase method gives

$$\int_{-\infty}^{\infty} \exp\left[-jkrc_0(1 - S_1^2 - S_2)^{1/2}\right]dS_1 = \left(\frac{\lambda}{rc_0}\right)^{1/2}(1 - S_2^2)^{1/4} \exp\left[-jkrc_0\,(1 - S_2^2)^{1/2} + j\pi/4\right] \quad . \quad (48)$$

so that

$$D = \frac{Y_0 \exp(j\pi/4)}{2(\lambda^3 rc_0)^{1/2}} \int_{-\infty}^{\infty} (1 - S_2'^2)^{1/2}(1 - S_2^2)^{1/4} F_1^T(0, S_2) F_1^R(0, S_2') \exp\{-jkr[c_0(1 - S_2^2)^{1/2} + s_0 S_2]\}dS_2 \quad . \quad (49)$$

Since $S_1 = S_1' = 0$, $(1 - S_2'^2)^{1/2} = C'$, i.e. $Cc_0 + S_2 s_0$.

(7.3) Evaluation of Integral in Eqn. (30)

The integral which occurs in eqn. (30) is

$$I = \int_{\Gamma'} F_1^T[0, \sin(\theta_0 - \xi)] \cos\xi \cos^{3/2}(\theta_0 - \xi) \exp\left[-jkr\cos\xi - \frac{2L\xi^2}{B_R^2}\right]d\xi \quad . \quad (50)$$

where the integration contour Γ' is shown in Fig. 4(*b*). We are concerned with the value of I for aerials which have a narrow horizontal pattern, so that the only values of θ_0 and ξ of interest are those near to zero. The trigonometrical functions $\cos\xi$ and $\cos(\theta_0 - \xi)$ can therefore be approximated to unity, except in the exponential, where $\cos\xi$ should be replaced by $(1 - \frac{1}{2}\xi^2)$. Then

$$I = \int_{\Gamma'} F_1^T[0, \sin(\theta_0 - \xi)] \exp(-jkr - \tfrac{1}{2}p\xi^2)d\xi \quad . \quad (51)$$

where $$p = \frac{4L}{B_R^2} - jkr \quad . \quad (52)$$

We may write $$p = |p| \exp(-j\eta) \quad . \quad (53)$$

if $$\eta = \arctan(krB_R^2/4L) \quad . \quad (54)$$

Let $$\zeta = \xi \exp(-\tfrac{1}{2}j\eta) \quad . \quad (55)$$

Then, $$I = \exp(-jkr + \tfrac{1}{2}j\eta) \int F_1^T(\theta_0 - \xi) \exp(-\tfrac{1}{2}|p|\zeta^2)d\zeta \quad (56)$$

where F_1^T is now shown for convenience as a function of $(\theta_0 - \xi)$. This integration is carried out along the contour for ζ corresponding to ξ moving along Γ', but since F_1^T is a regular function, the contour can be distorted into the real axis without altering the value of the integral. The integrand vanishes as $|\xi| \to \infty$, so that no contribution results from the infinite arcs joining the ends of the original and modified contours. The integral can now be evaluated using Watson's lemma,[7] with the result

$$I = \left(\frac{2\pi}{|p|}\right)^{1/2} \exp(-jkr + \tfrac{1}{2}j\eta)\left\{[F_1^T(\theta_0 - \xi)_{\zeta=0} + \frac{1}{2|p|}\left[\frac{d^2F_1^T(\theta_0 - \xi)}{d\zeta^2}\right]_{\zeta=0} + \ldots + \frac{1\cdot 3 \ldots (2n-1)}{(2n)!\,|p|^n}\left[\frac{d^{(2n)}F_1^T(\theta_0 - \xi)}{d\zeta^{2n}}\right]_{\zeta=0} + \ldots\right\} \quad . \quad (57)$$

From eqn. (55), we see that $\xi = 0$ when $\zeta = 0$, and, furthermore,

$$\left[\frac{d^nF_1^T(\theta_0 - \xi)}{d\zeta^n}\right]_{\zeta=0} = \left[\exp(\tfrac{1}{2}jn\eta)\frac{d^nF_1^T(\theta_0 - \xi)}{d\xi^n}\right]_{\zeta=0} = \exp(\tfrac{1}{2}jn\eta)(-)^n\left[\frac{d^nF_1^T(\theta)}{d\theta^n}\right]_{\theta=\theta_0} \quad . \quad (58)$$

Let $$F_1^{T(n)}(\theta_0) = \left[\frac{d^nF_1^T(\theta)}{d\theta^n}\right]_{\theta=\theta_0} \quad . \quad (59)$$

Then

$$I = \left(\frac{2\pi}{|p|}\right)^{1/2} \exp(-jkr + \tfrac{1}{2}j\eta)\left[F_1^T(\theta_0) + \frac{\exp(j\eta)}{2|p|}F_1^{T(2)}(\theta_0) + \ldots + \frac{1\cdot 3 \ldots (2n-1)\exp(jn\eta)}{(2n)!\,|p|^n}F_1^{T(2n)}(\theta_0) + \ldots\right] \quad . \quad (60)$$

(7.4) Evaluation of Integral in Eqn. (38)

The integral to be evaluated is

$$D = \frac{1}{4\pi}\int_{-\infty}^{\infty}\int_{-\infty}^{\infty} G(S_1, S_2)\exp(-jkrC)dS_1dS_2/C = \frac{1}{\pi}\int_0^{\infty}\int_0^{\infty} G(S_1, S_2)\exp(-jkrC)dS_1dS_2/C \quad . \quad (61)$$

since $G(S_1, S_2)$ is assumed to be an even function of S_1 and S_2. Changing the integration variables to S_1 and C gives

$$D = \frac{1}{\pi}\int_0^{\infty} dS_1 \int_{\Gamma_1} dCG(C)\exp(-jkrC)/(1 - C^2 - S_1^2) \quad . \quad (62)$$

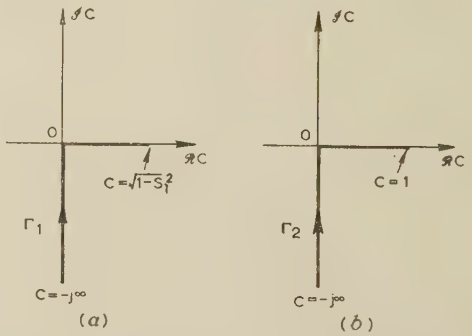

Fig. 8.—Integration contours for integrals in Section 7.4.

where Γ_1, the integration contour for C, is shown in Fig. 8(*a*), and it is assumed that G is a function of C only. Changing the order of integration in eqn. (62) gives

$$D = \frac{1}{\pi}\int_{\Gamma_2} dC \int_0^{\sqrt{(1-C^2)}} dS_1 G(C)\exp(-jkrC)/(1 - C^2 - S_1^2)^{1/2} \quad . \quad (63)$$

Γ_2 being the contour shown in Fig. 8(*b*).

In eqn. (63), the integration with respect to S_1 can be evaluated immediately, giving

$$D = \tfrac{1}{2}\int_{\Gamma_2} G(C)\exp(-jkrC)dC \quad . \quad (64)$$

Let $$C = 1 - jy \quad . \quad (65)$$

and distort the integration contour for y into the real axis: this is permissible, since the integrand is a regular function, which will vanish, as $|c| \to \infty$ for all cases of interest.

Then

$$D = \tfrac{1}{2}j\exp(-jkr)\int_0^{\infty} G(1 - jy)\exp(-kry)dy \quad . \quad (66)$$

The integral is in the standard form for integration by Watson's lemma, giving

$$D = \tfrac{1}{2}j \exp(-jkr)\left[\frac{G(1)}{kr} + \frac{1}{(kr)^2}\left(\frac{dG}{dy}\right)_{y=0} + \ldots + \frac{1}{(kr)^{n+1}}\left(\frac{d^nG}{dy^n}\right)_{y=0} + \ldots\right] \quad . \quad (67)$$

But $$\left(\frac{d^nG}{dy^n}\right)_{y=0} = (-j)^n\left(\frac{d^nG}{dC^n}\right)_{C=1} \quad . \quad . \quad . \quad (68)$$

We wish to evaluate the integral for the particular case of a uniformly illuminated circular aperture of diameter d, for which

$$G(\theta) = 4G_T J_1^2(u)/u^2 \quad . \quad . \quad . \quad . \quad . \quad (69)$$

G_T being the gain in the forward direction, $\theta = 0$, and

$$u = (\pi d/\lambda)\sin\theta \quad . \quad . \quad . \quad . \quad . \quad (70)$$

We can obtain the derivatives needed in eqn. (67) if $G(\theta)$ can be expressed as a sum of powers of $(1 - C)$.

Now,

$$\frac{J_1^2(u)}{u^2} = \frac{1}{4}\sum_{n=0}^{\infty}\frac{(-)^n(2n+2)!(u/2)^{2n}}{n!(n+2)![(n+1)!]^2} \quad . \quad . \quad (71)$$

and $$u^2 = (\pi d/\lambda)^2(1 - C^2) = (\pi d/\lambda)^2[2(1 - C) - (1 - C)^2] \quad . \quad . \quad . \quad (72)$$

Hence

$$u^{2n} = (\pi d/\lambda)^{2n}(1 - C)^n\sum_{r=0}^{n}\frac{(-)^r n!(2)^{n-r}(1 - C)^r}{r!(n - r)!} \quad . \quad (73)$$

and $$\frac{J_1^2(u)}{u^2} = \frac{1}{4}\sum_{n=0}^{\infty}\sum_{r=0}^{n}\frac{(2n+2)!(\pi d/\lambda)^{2n}[\frac{1}{2}(C-1)]^{n+r}}{r!(n-r)!(n+2)![(n+1)!]^2} \quad . \quad (74)$$

Let $$n + r = t \quad . \quad . \quad . \quad . \quad . \quad . \quad . \quad (75)$$

Then, $G(C) =$

$$G_T\sum_{t=0}^{\infty}\frac{(C-1)^t}{t!}\left\{\sum_{r=0}^{\frac{t}{2}\text{ or }\frac{t-1}{2}}\frac{(2)^{-t}t!(2t+2-2r)!(\pi d/\lambda)^{2(t-r)}}{r!(t-2r)!(t+2-r)![(t+1-r)!]^2}\right\} \quad . \quad . \quad . \quad . \quad (76)$$

from which it follows at once by inspection that

$$\left(\frac{d^tG}{dC^t}\right)_{c=1} = G_T t!\left(\frac{\pi^2d^2}{2\lambda^2}\right)^t\sum_{r=0}^{\frac{t}{2}\text{ or }\frac{t-1}{2}}\frac{(2t+2-2r)!(\pi d/\lambda)^{-2r}}{(t-2r)!(t+2-r)![(t+1-r)!]} \quad . \quad . \quad . \quad . \quad (77)$$

For large aerials, $d \gg \lambda$, so that only the first term in the series need be considered, giving

$$\left(\frac{d^tG}{dC^t}\right)_{c=1} = \frac{(2t+2)!G_T}{(t+2)![(t+1)!]^2}\left(\frac{\pi^2d^2}{2\lambda^2}\right)^t \quad . \quad . \quad (78)$$

Collecting results from eqns. (67) and (78) we have finally

$$D = \frac{jG_T\exp(-jkr)}{2kr}\sum_{t=0}^{\infty}\frac{(2t+2)!}{(t+2)![(t+1)!]^2}\left(\frac{-j\pi d^2}{4r\lambda}\right)^t \quad . \quad (79)$$

and, on using eqn. (27),

$$\left(\frac{G_m}{G_T}\right)^2 = \left|\sum_{t=0}^{\infty}\frac{(2t+2)!}{(t+2)![(t+1)!]^2}\left(\frac{-j\pi d^2}{4r\lambda}\right)^t\right|^2 \quad . \quad (80)$$

where G_m is the apparent gain if measurements are made at separation d.

621.3.013:538.3

The Institution of Electrical Engineers
Monograph No. 286
Feb. 1958
©

ELECTROMAGNETIC ENERGY TRANSFER

By P. HAMMOND, M.A., Associate Member.

(*The paper was first received 7th August, and in revised form 1st November*, 1957. *It was published as an* INSTITUTION MONOGRAPH *in February*, 1958.)

SUMMARY

Methods of calculating and measuring the flow of electromagnetic energy are compared and contrasted. The differences between the low-frequency and high-frequency approaches to energy flow problems are discussed and suggestions are made to ease the difficulties in the way of students and teachers faced with these apparently irreconcilable differences.

(1) INTRODUCTION

In teaching the principles of electromagnetism very much time is taken up with the discussion of cases of energy transfer. The aim of such discussion is to relate the primary concepts of charge and field strength to the process or mechanism of energy interchange. The term 'mechanism' is used here in accordance with Maxwell's aim of reducing electromagnetism to the study of the mechanics of electricity or of the aether.[1] This aim has by no means been completely achieved, as is borne out by two recent papers on the subject.[4,5]

In focusing attention on this mechanism we seek first for a clear and consistent mental picture or concept. Neither mathematical theory nor experimental technique is primary in this view of the matter, although the value of the mental concepts will be judged by their fruitfulness in calculation and experiment. In the words of J. J. Thomson:[6]

> Students have a great tendency to regard the whole of Maxwell's theory as a matter of the solution of certain differential equations and to dispense with any attempt to form for themselves a mental picture of the physical processes which accompany the phenomena they are investigating. I think that this state of things is to be regretted, since it retards the progress of the science of Electricity and diminishes the value of the mental training afforded by the study of that science.

The same is true, *a fortiori*, of attempts to shorten the labour of thought by conducting extensive unplanned experiments.

The process of acquiring a consistent set of concepts to deal with problems of electromagnetic energy interchange is difficult. The difficulties are increased by the accident of the historical development of the subject. Whereas some writers picture electric particles in an otherwise empty space, others see the whole of space as a seething mass of electric or magnetic whirlpools. It is no wonder that disaster sometimes overtakes the student who endeavours to reconcile these mental pictures by inserting the particles in the whirlpools. Nevertheless, the existence of such conflicting pictures, which we have inherited from the great electricians of the past, is a constant stimulus to clear thought. The paper is an attempt to clarify some of the apparent contradictions.

(2) SOME SIMPLE EXAMPLES INVOLVING ENERGY TRANSFER

In this Section examples will be discussed involving direct currents or low-frequency alternating currents in order to analyse the concepts used in what is generally called heavy-current engineering.

Correspondence on Monographs is invited for consideration with a view to publication.
Mr. Hammond is in the Department of Engineering, University of Cambridge.

(2.1) Battery Circulating Current through a Resistance Wire

Perhaps the simplest form of energy interchange is the heating effect of an electric current flowing through a wire which connects the terminals of a battery of constant voltage. If this voltage is V and the current is I, the battery supplies energy to the wire at the rate of VI per unit time. This energy is expended in overcoming the resistance of the wire. Ohm's law states that V is proportional to I, i.e. $V = RI$, where R is the resistance. This can be written as $E = \rho J$, where E is the electric force, ρ the resistivity and J the current density. In this form the law can be applied to alternating currents, whereas V loses its usefulness in the description of high-frequency effects.

Ohm's law is so simple in form that it is taken by many as almost self-evident. There is, however, a difficulty connected with it that will serve as a good introduction to the subjects discussed here. This difficulty may be expressed in the question: what is the origin of the electric force E on the current in the wire at a place considerably distant from the terminals of the battery? Clearly E can arise only from electric charges. But those at the battery terminals can act appreciably only on their immediate neighbours, since the force decreases as the square of the distance. Consider, for instance, what happens when a resistance wire is connected to the plates of a battery. Before the connection is made there is a considerable electric charge on the plates, and hence a large electric force in the vicinity of the plates. After the connection has been made and transient currents have disappeared, there is a uniform electric force $E = \rho J$ everywhere along the wire. Thus the electric force close to the plates has been reduced, while that at distant points has been increased. How has this come about? This difficulty was understood by Ohm,[8] who felt that only immediately adjacent particles of electricity could act on one another to produce the current flow. Ohm very nearly achieved a solution of this problem by his consideration of the surface charge that would also be present. He went so far as to identify the galvanic electricity of his circuit with Coulomb's static electricity. But he failed to see that this surface charge, combined perhaps with a charge distributed within the volume of the wire, provided the source of the necessary electric force. Instead, he took refuge in the analogy of the flow of heat, in which the problem does not arise.*

The analogy in general use now is that of fluid flow in a pipe. Neither of these analogies is strictly accurate, because each fails to take into account that there are in the wire positive charges as well as negative ones. Consideration shows that a current flow in a conductor implies also a surface and possibly a volume distribution of electric charge. It is this distribution which produces the uniform electric force along the wire, irrespective of the path of the wire. Far from being obvious, it is surely amazing that the current should not be altered however much the wire is twisted and contorted (we are, of course, assuming

* There is no intention here of detracting from Ohm's great achievement in clarifying a subject beset with difficulties. It must be remembered that the various quantities used at the time, such as electric strength and intensity, had not been clearly defined. There were also great experimental difficulties, owing to the absence of measuring instruments and the uncertain behaviour of batteries subject to polarization. The immense development of Ohm's thought is well seen if his paper of 1825[9] is compared with the great work of 1827.[8]

constant resistivity in this discussion). This problem is very similar to the magnetic one of providing a path for a magnetic flux by means of an iron core, where the magnetic force has to be provided by surface and volume distributions of pole strength.[10] It is well known that the leakage flux resulting from the surface distribution will depend very considerably on the configuration of the iron core. In principle, therefore, there must also be, in the electric case, some difference in the surface distribution of charge, and hence in the current flow, if the path between the battery terminals taken by the wire is altered. For magnetic forces this alteration in the flux is measurable, but in the case of current flow no such change has been observed. This is not surprising, since a coulomb of charge will give an electric force of the order of 10^{12} volts/cm at a distance of 1 cm. Thus, only a minute amount of charge is required to cause the current to flow. Nevertheless, a total absence of electric charge would also mean the cessation of current flow. The necessity for this charge distribution is hardly ever mentioned in the textbooks. In general, students have to be satisfied with references to water pipes. Pidduck,[11] however, mentions the existence of these charges. The explicit realization that they must be present will be found very helpful in understanding the subsequent discussion in the paper.

(2.2) Energy Interchange in a Simple Direct-Current Motor or Generator

Cullwick[12] has discussed in considerable detail the action of a motor or generator whose moving element is a straight conductor moving transversely to its length across a uniform magnetic field. To avoid the complication of a moving frame of reference, let us consider a simple d.c. machine in which the field poles move past stationary armature conductors. On open-circuit there is a charge separation in the armature conductors which exactly opposes the motional induced electric force Bv, where B is the magnetic flux density and v the velocity of the field system relative to the conductors; only so can the net electric force be reduced to zero. It should be noted that this charge separation will produce a distribution of charge throughout the length of the conductors and not only at the ends. The reason for this is the same as that advanced in Section 2.1. There must be zero electric force everywhere along the conductors, since no current flows on open-circuit. But charges at the ends of the conductors can act only at places close to those ends. They are not capable of producing zero electric force throughout the length of the conductors, and hence there is a need for the additional charge distribution along the conductors. It is helpful to notice explicitly that the electric force induced by the motion is equivalent to that produced by a distribution of electric charge equal and opposite to the open-circuit distribution.

Consider now the action of a motor with constant armature current. (As before we are considering the case of a stationary armature.) When the field system is at rest, a charge distribution will be required to produce everywhere an electric force ρJ. This charge distribution will correspond to a terminal potential difference $V_t = IR$. When the motor is running, this charge distribution will no longer be sufficient to cause the current to flow, because the induced electric force will be equivalent to an opposing charge distribution. In order to produce a resultant electric force ρJ, an additional charge distribution is required. This is expressed by the well-known motor equation $V_t = V_i + IR$, where V_t is the terminal voltage, V_i the induced electromotive force, and I and R are the armature current and resistance, respectively. The charge distribution has had to be increased by $(V_i + IR)/IR$.

All this is rather obvious and the terms 'potential difference' and 'induced e.m.f.' are well understood. But it is rather surprising to find that an exploring test charge would not be able to differentiate between the case when the motor is stationary and when it is running. In either event the observed electric force would be ρJ. Neither the applied p.d. nor the induced e.m.f. can be observed separately. The equation $V_t = V_i + IR$ is written in this form chiefly in order to present a clear mental picture and to separate the energy loss from the gross mechanical output. Since only the resultant force can be observed, we propose to call V_t and V_i the partial fields, whereas IR represents the total or resultant field. It may come as a shock to some engineers to realize the largely conceptual nature of such well-known quantities as V_t and V_i.

A very similar argument holds for the case of a generator, where we have the equation $V_i = V_t + IR$. In this case the induced electric force must overcome the opposing charge distribution V_t and provide a resultant electric force equivalent to IR. Once again, only the resultant force would be observed by an exploring test charge. As long as the exploration is confined to the conductor system, it is not even possible to differentiate between motor and generator action.

(2.3) Alternating-Current Circuits Involving Inductance and Capacitance as well as Resistance

In investigations into the behaviour of time-varying currents, it was early discovered that the simple Ohm's law relationship $V = RI$ was not sufficient to describe the observed results. The two new concepts of inductance and capacitance had to be introduced. The concept of inductance arose from a consideration of Faraday's laws of electromagnetic induction. It was clear that the applied voltage and the current in a circuit were, in the absence of capacitance, connected by a relationship such as $v = Ldi/dt + Ri$, where L is the inductance. In the terms of our previous discussion, it follows that with alternating currents an additional charge distribution is required to give rise to a p.d. of Ldi/dt. Once again, however, the actual electric force within the conductor is $E = \rho J$ and this is the force which would be observed by a test charge. Faraday[13] attributed the inductance effect to the action of the magnetic field surrounding the current. In other words, Ldi/dt, like the back-e.m.f., V_i, of a motor, is an effect that could be isolated only if the conductor were removed. Since the current would then cease to flow, Ldi/dt cannot be thus isolated: it can, however, be taken to represent an electric field in free space. This is very seldom stated explicitly because, as in Ohm's law, the charge distributions accompanying the effect are ignored. A similar discussion applies to the effects of capacitance, which result in an additional charge distribution, giving a p.d. of $C \int idt$. In this case the action is attributed to the electric field surrounding the conductor.

For the motor it was found convenient to distinguish between V_t and V_i, in order to divide the input power $V_t I$ into mechanical power $V_i I$ and ohmic loss $(V_t - V_i)I$. A similar useful result is achieved by separating v and Ldi/dt. vi gives the input power and $(v - Ldi/dt)i$ is the ohmic loss; hence $(Ldi/dt)i$ can be attributed to the magnetic field. Maxwell[2] showed that this term corresponded to an energy of amount given by the volume integral $\iiint \frac{1}{2}BHdv$, where the integration is to be taken throughout all space. This result, however, applied strictly only to steady magnetic fields. A similar result was obtained for the capacitance term, and the corresponding energy was found[3] to be $\iiint \frac{1}{2}DEdv$.

If an alternator is connected to a circuit, its energy output is partly dissipated in heating the conductors. The rest of the energy can be deemed to be stored in the electric and magnetic fields surrounding the circuit. It was thought that the stored energy was fully recoverable by the alternator and its associated circuit. This, however, was questioned by Fitzgerald[14] in 1882.

Fitzgerald based his reasoning on theoretical grounds and showed that, on the basis of Maxwell's hypothesis of displacement current, some energy must be lost to the alternator and must be radiated into space.

In discussing this effect it becomes essential to abandon the terms of voltage, inductance and capacitance, but the argument is not affected. Instead of the voltage equations we now have the Lorentz force equation

$$E = -\frac{\partial A}{\partial t} + v \times B \ - \text{grad}\ \phi$$

where A is the delayed vector potential, ϕ is the delayed scalar potential, and v is the velocity of the charge through the field B. This expression for E shows separately the inductance, motional and capacitance effects. Fitzgerald's hypothesis meant that neither $\partial A/\partial t$ nor grad ϕ was necessarily in time-quadrature with the current density J. We note that at a conductor $-\partial A/\partial t + u \times B - \text{grad}\ \phi = \rho J$. The effects are isolated for ease of computation and more especially to give a clear picture of the various items in an energy balance sheet.

(2.4) Action of a Transformer

Whereas the self-inductance effect at low frequencies was found to give no net energy transfer,[14] it was apparent, from Faraday's discovery of mutual induction, that energy could be transferred from one circuit to another. In addition to the various charge distributions already mentioned, there will now be another. Moreover, the instantaneous magnitude of this distribution on the primary circuit is governed by the secondary current, and hence its phase depends on the secondary current. In terms of the Lorentz force $E = -\partial A/\partial t + u \times B - \text{grad}\ \phi$, $\partial A/\partial t$ may now have an in-phase component with the current density, and this would provide a unidirectional or irreversible energy interchange. It is of interest to point out that in a.c. rotating machines the phase of the $v \times B$ term is also generally arranged to give some unidirectional flow. This is not invariably so, however, and examples to the contrary are synchronous condensers or machines like the Kapp vibrator.

(2.5) Some Conclusions

It has been shown that energy is transferred through the action of charge distributions on the conductor. The source of power experiences back-e.m.f.'s which may or may not be in phase with the voltage generated by the source. It is extremely convenient to separate the effects into magnetic and electric field effects and into mechanical and chemical energy effects. Each one of these effects may be considered to act separately in impeding or aiding the flow of electric current from the source. However, it must be kept in mind that the actual current flow is the result of all the effects acting together, and for a particular current the resultant electric field must always be governed by the resistance of the conductor. Thus it follows that an investigation into the electric field in the conductor cannot give any indication about the energy flow from the conductor, whether it be mechanical or electromagnetic energy. The concepts so far employed show why the flow into the conductor may be impeded, but once the flow has been established these concepts tell us nothing about the method of energy flow from the conductor.

(3) ENERGY TRANSFER BY ELECTROMAGNETIC RADIATION

(3.1) Maxwell's View of Electromagnetic Action

Maxwell's proposition that light is an electromagnetic disturbance suggested to his contemporaries that new concepts would have to be found and new mathematical methods developed to account for the problems associated with energy flow. Two questions presented themselves. The first concerns the transfer of energy to distant bodies, whose action on the source of the energy can reasonably be assumed negligible. In the language of power appliances, this question concerns the possibility of power flow when the device is on open-circuit. The second and related question concerns the possibility of localizing the energy flow in space and thus using the language of optics and, in particular, of Huygen's principle in electrical problems. Maxwell's preoccupation with the properties of the aether greatly reinforced the view that such localization of energy was to be expected on physical as well as mathematical principles. He failed to convince a number of electricians, such as Lord Kelvin, who had perhaps more of an engineer's turn of mind and clung to the belief that the conducting matter in the circuits was actually both the seat and the vehicle of energy interchange. However, his success was complete with those who concerned themselves with the possibility of electromagnetic radiation. It is of interest to note that this difference of approach is to a great extent responsible for the somewhat irrational distinction between heavy-current and light-current engineering.

(3.2) Poynting's Theorem of Energy Flow

A very famous attempt at a solution of the twin problems of energy flow in space was made in 1884 by J. H. Poynting, and has since become known as Poynting's theorem.[17]

Poynting considered the rate of change of energy distribution within a closed volume. Taking Maxwell's expressions,[2,3] he writes

$$\frac{d}{dt}\iiint\left(\frac{E \,.\, D}{2} + \frac{H \,.\, B}{2}\right)dv = \iiint\left(\frac{E \,.\, \partial D}{\partial t} + \frac{H \,.\, \partial B}{\partial t}\right)dv$$

But
$$\text{curl}\ H = J + \partial D/\partial t$$
$$\text{curl}\ E = -\partial B/\partial t$$

Therefore
$$E \,.\, \partial D/\partial t + H \,.\, \partial B/\partial t = E \,.\, \text{curl}\ H - E \,.\, J - H \,.\, \text{curl}\ E = -E \,.\, J - \text{div}\,(E \times H)$$

and
$$\iiint\left(\frac{E \,.\, \partial D}{\partial t} + \frac{H \,.\, \partial B}{\partial t}\right)dv + \iiint E \,.\, J dv = -\iint (E \times H) \,.\, ds$$

Thus the increase in stored energy, together with the ohmic loss, equals the in-flow of a vector $E \times H$ across the surface bounding the volume considered. (Poynting also considered terms due to the motion of the circuits. These have been omitted here for the sake of simplicity.) The Poynting vector $E \times H$ could thus be interpreted as the vector indicating the density of energy flow at any part of the surface, or indeed anywhere in space.

The possibility of energy flow on open-circuit, which would be akin to the method by which solar energy reaches the earth, was thus shown by Poynting to depend merely on the magnitude of E and H. It could readily be shown that on Maxwell's hypothesis E and H would have components varying inversely as the distance. Thus $\iint (E \times H) \,.\, ds$ would be finite at even the largest distances, and Fitzgerald's suggestion[14] could be demonstrated mathematically. Poynting himself applied his theorem to some simple cases of current flow including d.c. problems. In every case the same answer could be obtained by his method as by the older view of pushing an electric current through a wire against opposing forces. In particular, for a straight wire carrying a current, he showed that by his view the

energy would pass into the wire through its insulation at right angles to its length. In a second paper[18] he went further and discussed the actual velocities of the tubes of electric and magnetic flux.

(3.3) Criticism of Poynting's Theorem

Soon after Poynting's theorem had been published, it was shown by Sir. J. J. Thomson[7] that the expression for the power-flow vector given by the theorem was not unique. Another arbitrary vector $\boldsymbol{P} = \text{curl } \boldsymbol{Q}$ could be added, since $\int\int \text{curl } \boldsymbol{Q} \,.\, d\boldsymbol{s} = 0$. Thus the local energy density was not uniquely determined by Poynting's theorem. Various other forms of the vector have been proposed[15,19,20] which still give the same surface integral. But Poynting's vector has the great advantage of simplicity and has secured practically universal acceptance. Sumpner,[21] however, discussed the question of energy flow on the basis of Huygen's principle and reached the conclusion that the Poynting vector did not describe the actual movement of energy. Sumpner was confirmed in his view by Poynting's result in his 1885 paper[18] of a velocity for the electric flux of nearly 60 million times the velocity of light.

A more serious attack on Poynting's theorem was made as early as 1902 by Macdonald.[22] He pointed out that Poynting's expression for the magnetic field energy in a closed volume $\int\int\int \tfrac{1}{2}\boldsymbol{H} \,.\, \boldsymbol{B} dv$ had been derived by Maxwell[2] for static magnetic fields only. Moreover Maxwell's volume integration had to be carried out over all space. Macdonald proposed, as the correct power flow vector, the expression

$$\boldsymbol{E} \times \boldsymbol{H} + \tfrac{1}{2}\left(\frac{\partial \boldsymbol{A}}{\partial t} \times \boldsymbol{H} + \boldsymbol{A} \times \frac{\partial \boldsymbol{H}}{\partial t}\right)$$

where $\boldsymbol{A}$ is the vector potential or, as Macdonald terms it, the 'electrokinetic momentum'. Because Macdonald's expression for the magnetic field energy is different from that used by Poynting, the surface integral of the energy-flow vector is also different. It is surprising that Macdonald did not point out that Poynting's expression for the electric field energy was open to the same objections as that for the magnetic field energy. Once again Poynting had applied Maxwell's expression for a static unbounded field[3] to that of a time-varying and bounded one. This point also seems to have escaped the attention of later writers. Stratton[25] discusses the question in detail and justifies Poynting's treatment by postulating that Maxwell's result could be applied to a bounded space if the bounding surface had not yet been reached by the wavefront of the disturbance. This argument had, however, already been shown by Macdonald to be invalid.[23] The question naturally arises if an experiment can be devised to test the validity of Poynting's theorem. Macdonald points out that such an experiment would have to be able to deal with times shorter than the periodicity of the time-varying currents.[24] Under ordinary time-varying conditions there is no possibility of differentiating between Macdonald's and Poynting's theorems. Slepian,[19] in a very ingenious derivation of the energy-flow theorem, has given nine alternative forms for the flow vector, showing that the choice is far wider than either Poynting or Macdonald supposed.

It would appear that Poynting's theorem fails to achieve its aim. It does not give the insight, hoped for by its author, into the mechanism of energy flow in space. Nor is its mathematical basis sound. But it does provide a simple method of calculating the open-circuit energy flow. However, the mental picture of energy flow suggested by Poynting is perhaps best avoided in elementary teaching. It is possible that nature does not give an answer to Poynting's question about the localization of energy. Certainly his approach would require research into the behaviour of wavefronts, and such investigations at present lack both experimental technique and mathematical formulation.

(3.4) Application of Poynting's Theorem

The mathematical formulation of Poynting's theorem is beautifully simple. Very severe difficulties are, however, encountered in the application of the theorem to an actual example of energy flow. We state the theorem as

$$\int\int (\boldsymbol{E} \times \boldsymbol{H}) d\boldsymbol{s} = \int\int\int \left(-\boldsymbol{H} \,.\, \frac{\partial \boldsymbol{B}}{\partial t} - \boldsymbol{E} \,.\, \frac{\partial \boldsymbol{D}}{\partial t} - \boldsymbol{E} \,.\, \boldsymbol{J}\right) dv$$

i.e. outflow of energy = (decrease of stored energy) − (ohmic loss)

Consider fields that are varying harmonically; there will then be no net decrease of stored energy over a complete cycle. The statement thus becomes

inflow of energy = ohmic loss

and there is apparently no allowance for radiation of energy.

This problem is best elucidated by taking an actual case. Consider the Hertzian oscillator, which is discussed in detail in the Appendix (Section 8). The charges and current of this oscillator are postulated. The fields of these charges and this current are determined in the usual manner and the Poynting integral then gives the well-known expression for the radiated energy. But in postulating charges and current nothing has been said as to the physical possibility of causing them to be disposed in the postulated manner. We realize, following our earlier discussion, that additional charges and currents have to be present because the total current flow is governed by the ohmic relationship $E = \rho J$. The Poynting vector has, in fact, been calculated by using only the partial fields. The Poynting integral is here

$$\int\int (\boldsymbol{E}_p \times \boldsymbol{H}_p) \,.\, d\boldsymbol{s}$$

where $\boldsymbol{E}_p = \boldsymbol{E} - \boldsymbol{E}'$

and $\boldsymbol{H}_p = \boldsymbol{H} - \boldsymbol{H}'$

the suffix p denoting partial fields. $\boldsymbol{E}$ and $\boldsymbol{H}$ are the total fields and $\boldsymbol{E}'$ and $\boldsymbol{H}'$ are the additional fields to make the current flow in the oscillator physically possible. Thus Poynting's theorem applied to the partial fields becomes

$$\int\int (\boldsymbol{E}_p \times \boldsymbol{H}_p) d\boldsymbol{s} = \int\int\int \left(-\boldsymbol{H}_p \,.\, \frac{\partial \boldsymbol{B}_p}{\partial t} - \boldsymbol{E}_p \,.\, \frac{\partial \boldsymbol{D}_p}{\partial t} - \boldsymbol{E}_p \,.\, \boldsymbol{J}_p\right) dv$$

Thus, for harmonically varying quantities, the Poynting integral now gives the product of the postulated partial current and the partial electric force opposing its flow, and this is the radiated power. It will be noticed that the Poynting method is exactly analogous to the back-e.m.f. method used in power devices, because the back-e.m.f. is also essentially a partial field, which it is convenient to keep separate for the purposes of computation.

It should be noted explicitly that the partial fields are invariably used in calculations of the energy radiated from an aerial. The total fields are in general unknown and very complicated, except on the actual material of the conductors. However, if it is desired, for instance, to calculate the power input into the metal inside an induction furnace, the total fields must be used. In such a case the power input looked for is, of course, equal to the ohmic loss. It is clear that the Poynting integral using total fields must be taken around the sink and not about the source of the energy. A similar integral taken around an aerial or a transformer winding or other source of energy would, in general, give the ohmic loss in the aerial or the winding, and would supply no information about the power radiated or transferred.

If Poynting's theorem is to be used as a guide for taking measurements, it is clear that only the total fields can be observed. It is therefore desirable to investigate what information, besides that of ohmic loss, can be obtained in this manner.

It should be noted that the statement of Poynting's theorem has assumed that all energy is electromagnetic: chemical, thermal and kinetic energies have been excluded. This implies that the surface of integration is chosen so as to exclude all generators and batteries. Thus the surface must at some point intersect the supply leads (see Fig. 1). It has been shown that if we

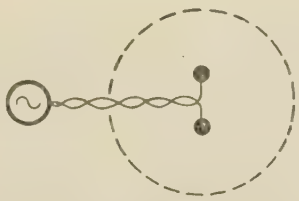

Fig. 1.—Radiation of power from a Hertzian oscillator.
The surface of integration for the Poynting flux vector intersects the supply leads.

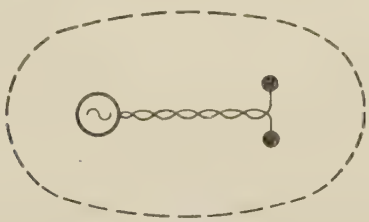

Fig. 2.—Radiation of power from a Hertzian oscillator.
The surface of integration for the Poynting flux vector encloses the alternator.

calculate $\int\int(E \times H)ds$ over such a surface we shall arrive at the ohmic loss in the conductors. Such an integral will give no information about radiated power. The integral $\int\int(E_p \times H_p)ds$ will, however, give this power. If, on the other hand, the surface of integration is chosen so as to enclose the alternator (see Fig. 2), additional electric forces due to the energy source will have to be taken into consideration. We can now write $E + E_s = \rho J$, where E_s is the additional electric force.

This additional force may arise from a wide variety of causes. Perhaps the simplest example is that of a battery, in which it is caused by chemical action. If, on the other hand, the electromagnetic energy is derived from a prime mover, such as a turbine, additional terms would have to be introduced into the energy equations to account for the shaft work done on the generator. Such further terms are not essential to the present discussion and have been omitted to simplify the treatment.

Hence

$$\int\int(E \times H) \,.\, ds = \int\int\int\left(-\frac{H \,.\, \partial B}{\partial t} - \frac{E \,.\, \partial D}{\partial t} - E \,.\, J\right)dv$$

$$= \int\int\int\left(-\frac{H \,.\, \partial B}{\partial t} - \frac{E \,.\, \partial D}{\partial t} - \rho J^2 + E_s \,.\, J\right)dv$$

Hence, for harmonic variation,

Poynting integral = (work done on the current) − (ohmic loss)

In such a case the Poynting integral gives the radiated power correctly. On the other hand, the integral using the partial fields fails. This does not matter in computation because the partial fields still give the correct answer if the term containing E_s is omitted. In other words, the supply leads have to be lengthened to exclude the generator from the volume of integration. It is clear, in any case, that the concept of back-e.m.f. would have to be abandoned if the generator were inside the volume. This consideration shows the dominance in the Poynting integral of that part of the surface which intersects the supply leads.

(3.5) Use of Alternative Forms of Poynting Vector

The simplicity of the expression $E_p \times H_p$ in calculation is such that it seems unlikely that a better form can be found. Hines,[26] however, shows that Macdonald's form gives somewhat simpler expressions in certain cases. Slepian in an early paper[27] favours Poynting's expression, but more recently[20] supports the expression $V(J + \partial D/\partial t) + H \times \partial A/\partial t$. This expression has the considerable advantage that for direct current it becomes VJ, i.e. power = voltage × current density, and thus fits into the ordinary engineering framework. Moreover, it disposes of the somewhat repugnant notion that a static condenser and a permanent magnet placed near one another engage in a process of unending and unmeasurable exchange of energy.

Attempts at building wattmeters capable of measuring the Poynting energy flow by direct measurement of the electric and magnetic fields are met by the extreme difficulty of measuring the electric force in space. At high frequencies this can be done by a monitor aerial embodying a thermocouple. For low frequencies, e.g. in eddy-current heating, a variant of the Poynting vector has been proposed to the author by Dr. R. W. Sillars, namely $\Omega\partial B/\partial t$, where Ω is the *magnetic* scalar potential. Since this form involves measurements of magnetic quantities only, it is far more convenient than the various possible alternatives. The derivation of this vector is given in the Appendix (Section 8.1).

(4) RADIATION RESISTANCE

(4.1) Induction and Radiation Effects

Poynting's work of 1884 had given a mathematical basis to the Fitzgerald suggestion of open-circuit transmission of energy. Hertz, in 1886, provided the experimental basis for the study of electromagnetic radiation. His use of high-frequency oscillations, to obtain measurable effects, gave scientists the impression that these were different in kind as well as in magnitude from the well-known effects of electromagnetic induction. Indeed, Hughes, who demonstrated Hertz's effect as early as 1879 before the President of the Royal Society,[16] was told that his effect was due to ordinary electromagnetic induction. This curious division of induction and radiation effects persists in present-day teaching, in spite of the fact that both induction and radiation effects are calculated by the identical Maxwell relationships. This is the cause of much puzzlement amongst students.

The difficulty is overcome when it is pointed out that there is no difference in kind between those alternating currents which radiate energy and those used in devices like induction motors. Once it is found that Ampère's equivalence of magnets and currents, expressed by the relationship curl $H = J$, is valid only for steady currents, it becomes apparent to the student that the magnetic field of alternating currents is not in phase with the currents. Hence the electric force always contains a component in antiphase to the current and there is a unidirectional energy flow away from the circuit. The magnitude and relative importance of this anti-phase electric force depends on the frequency and it becomes dominant at high frequencies. At low frequencies the quadrature effect is more important. This relative importance should not, however, obscure the fact that it is not possible to have pure induction fields or pure radiation fields. Conductors arranged in certain geometrical shapes may produce the superposition and cancellation of some of the field components, and this cancellation may cause the apparatus to radiate relatively

more strongly if the frequency is increased beyond a certain value. But these are special cases. The question whether a certain apparatus will radiate not infrequently betrays a lack of understanding of the fact that any alternating current cannot help but send out energy by radiation.

(4.2) Calculation of Radiation Resistance

In determining the energy transmitted by radiation it is frequently helpful to use the term 'radiation resistance'. By analogy with the ohmic resistance this is defined as the average power divided by the square of the r.m.s. current.

Most writers obtain this resistance by a method of calculation involving $\int\int(\boldsymbol{E}_p \times \boldsymbol{H}_p) \,.\, d\boldsymbol{s}$. We have shown that an alternative approach would be to use $\int\int\int(-\boldsymbol{E}_p \,.\, \boldsymbol{J}_p)dv$ and thus to apply the concept of back-e.m.f. to the problem of radio aerials. With certain exceptions, notably that of Moullin,[28] this second method is avoided and the repugnance to it is well expressed by Aharoni,[29] who states that there is no such physical quantity as radiation resistance. Many writers feel that the flux of energy described by the Poynting integral gives clear physical insight, whereas the back-e.m.f. concept does not do so. The term 'aperture' is frequently employed in this discussion and is regarded as an

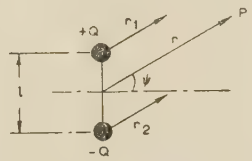

Fig. 3.—Field of a Hertzian oscillator.

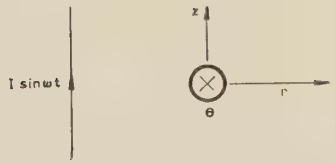

Fig. 4.—Field of a line current.

opening to allow the Poynting flux to emerge. But our discussion strongly suggests that 'physical reality' can be claimed for neither method. The Poynting integral uses partial fields, as does the back-e.m.f. method. Both methods are essentially tools for the purposes of calculation. There is, however, much to be said for the back-e.m.f. method, because frequently the volume integral is easier to determine than the surface integral, if the currents are confined to paths involving a simple geometry. A comparison of the two methods applied to a Hertzian oscillator and a line current is given in the Appendix (Section 8.2).

(5) CONCLUSION

In such a vast subject as that of electrical engineering a teacher can best serve his students by attempting to lay a sound foundation of physical concept as well as of mathematical analysis. The subject of energy transfer is taught by means of apparently irreconcilable concepts, the choice being governed by the largely irrelevant considerations of the frequency employed or the physical size of the apparatus. In power devices the concept is that of back-e.m.f. and in radio devices Poynting's theorem is used. It has been shown that the two methods are identical and related by a simple mathematical transformation. Moreover, neither method is able to give any information about localized distribution of energy in space, and both ignore the charge distributions on the conductors, which make the current flow possible. It is hoped that a knowledge of these matters will be of help to the student and will add to his enjoyment of the subject.

(6) ACKNOWLEDGMENT

The author gratefully acknowledges the unfailing encouragement extended to him by Professor E. B. Moullin.

(7) REFERENCES

(1) Maxwell, J. C.: 'Electricity and Magnetism' (Clarendon Press, 1881), Preface and throughout the treatise.
(2) *Ibid.*, Sections 634–638.
(3) *Ibid.*, Sections 630–631.
(4) Cullwick, E. G.: 'Electromagnetic Momentum and Electron Inertia in a Current Circuit', *Proceedings I.E.E.*, Monograph No. 150, September, 1955 (**103** C, p. 159).
(5) Cullwick, E. G.: 'Magnetic Energy and Electron Inertia in a Superconducting Sphere', *ibid.*, Monograph No. 184, June, 1956 (**103** C, p. 441).
(6) Thomson, Sir J. J.: 'Recent Researches in Electricity and Magnetism' (Clarendon Press, 1893), Preface.
(7) *Ibid.*, p. 280.
(8) Ohm, G. S.: 'Die galvanische Kette, mathematisch bearbeitet' (T. H. Riemann, Berlin, 1827), pp. 2–3 and 107–111.
(9) Ohm, G. S.: 'Vorlänfige Anzeige des Gesetzes, nach welchem Metalle die Contaktelektricität leiten', *Annalen der Physik und Chemie*, 1825, **4**, p. 79.
(10) Hammond, P.: 'Leakage Flux and Surface Polarity in Iron Ring Stampings', *Proceedings I.E.E.*, Monograph No. 116, January, 1955 (**102** C, p. 138).
(11) Pidduck, F. B.: 'A Treatise on Electricity' (Cambridge University Press, 1916), p. 305.
(12) Cullwick, E. G.: 'The Fundamentals of Electromagnetism' (Cambridge University Press, 1949), Chapter 2.
(13) Faraday, M.: 'Experimental Researches in Electricity, Ninth Series', *Philosophical Transactions of the Royal Society*, 1835, p. 41.
(14) Whittaker, Sir E.: 'A History of the Theories of Aether and Electricity' (Nelson, 1951), Vol. 1, pp. 311–312.
(15) *Ibid.*, p. 314.
(16) *Ibid.*, p. 323.
(17) Poynting, J. H.: 'On the Transfer of Energy in the Electromagnetic Field', *Philosophical Transactions of the Royal Society*, 1884, **175**, p. 343.
(18) Poynting, J. H.: 'On the Connection Between Electric Current and the Electric and Magnetic Inductions in the Surrounding Field', *ibid.*, 1885, **176**, p. 277.
(19) Slepian, J.: 'Energy and Energy Flow in the Electromagnetic Field', *Journal of Applied Physics*, 1942, **13**, p. 512.
(20) Slepian, J.: 'Energy Flow in Electric Systems—the VI Energy Flow Postulate', *Transactions of the American I.E.E.*, 1942, **61**, p. 835.
(21) Sumpner, W. E.: 'Radiation and Electrical Power Transmission', *Journal I.E.E.*, 1934, **75**, p. 512.
(22) Macdonald, H. M.: 'Electric Waves' (Cambridge University Press, 1902), Chapters 4 and 8.
(23) *Ibid.*, p. 33.
(24) *Ibid.*, p. 72.
(25) Stratton, J. A.: 'Electromagnetic Theory' (McGraw-Hill, 1941), Section 2.19.
(26) Hines, C. O.: 'Electromagnetic Energy Density and Flux', *Canadian Journal of Physics*, 1951, **30**, p. 123.

(27) SLEPIAN, J.: 'The Flow of Power in Electrical Machines', *Electrical Journal of Pittsburgh*, 1919, **17**, p. 303.
(28) MOULLIN, E. B.: 'Radio Aerials' (Clarendon Press, 1949).
(29) AHARONI, J.: 'Antennae' (Clarendon Press, 1946), p. 18.
(30) WATSON, G. N.: 'Theory of Bessel Functions' (Cambridge University Press, 1944), p. 76.

(8) APPENDIX

(8.1) Derivation of an Alternative Form of Poynting's Vector Suitable for Measurements at Power Frequencies

At low frequencies the magnetic field H can be approximately derived from a scalar potential function Ω. Thus $\boldsymbol{H} \simeq -\text{grad}\,\Omega$.

Therefore $$\iint(\boldsymbol{E}\times\boldsymbol{H})\,.\,d\boldsymbol{s} = \iint(-\boldsymbol{E}\times\text{grad}\,\Omega)\,.\,d\boldsymbol{s}$$
$$= \iint(\text{curl}\,\Omega\boldsymbol{E} - \Omega\,\text{curl}\,\boldsymbol{E})\,.\,d\boldsymbol{s} = \iint(-\Omega\,\text{curl}\,\boldsymbol{E})\,.\,d\boldsymbol{s}$$
$$-\iint\left(\Omega\frac{\partial B}{\partial t}\right).\,d\boldsymbol{s}$$

Hence the alternative vector is $\Omega\partial B/\partial t$. This expression is not applicable to high-frequency problems.

(8.2) Comparison of Calculation of Radiation Resistance by Poynting's Theorem and the Back-E.M.F. Method

(8.2.1) Hertzian Oscillator.

Let the charges vary as $Q\cos\omega t$. The retarded scalar potential at a distant point P is given by

$$V = \frac{Q}{4\pi\epsilon_0}\left[\frac{\cos\left(\omega t-\frac{\omega r_1}{c}\right)}{r_1} - \frac{\cos\left(\omega t-\frac{\omega r_2}{c}\right)}{r_2}\right]$$
$$= \frac{Ql\sin\psi}{4\pi\epsilon_0}\left[\frac{1}{r^2}\cos\left(\omega t-\frac{\omega r}{c}\right) - \frac{\omega}{cr}\sin\left(\omega t-\frac{\omega r}{c}\right)\right]$$

The retarded vector potential at P is parallel to the current and is given by

$$A_z = -\frac{Ql\omega\mu_0}{4\pi r}\sin\left(\omega t-\frac{\omega r}{c}\right)$$

The magnetic and electric fields are given by the following relationships:

$$\boldsymbol{H} = \frac{\text{curl}\,\boldsymbol{A}}{\mu_0},\quad E_r = -\frac{\partial V}{\partial r} - \frac{\partial A_r}{\partial t},\quad E_\psi = -\frac{1}{r}\frac{\partial V}{\partial\psi} - \frac{\partial A_\psi}{\partial t}$$

At large distances all terms decreasing more rapidly than $1/r$ can be neglected.

Hence $$H = -\frac{Ql\omega^2}{4\pi cr}\cos\psi\cos\left(\omega t-\frac{\omega r}{c}\right)$$
$$E_r = 0$$
$$E_\psi = \frac{Ql\omega^2}{4\pi r}\mu_0\cos\psi\cos\left(\omega t-\frac{\omega r}{c}\right)$$

It will be noted that these are all partial fields. The Poynting integral is given by

$$\iint(\boldsymbol{E}\times\boldsymbol{H})\,.\,d\boldsymbol{s} = \frac{Q^2l^2\omega^4}{16\pi^2c}\mu_0\cos^2\left(\omega t-\frac{\omega r}{c}\right)\int_{-\pi/2}^{+\pi/2}2\pi\cos^3\psi\,d\psi$$
$$= \frac{Q^2l^2\omega^4}{6\pi c}\mu_0\cos^2\left(\omega t-\frac{\omega r}{c}\right)$$

The radiation resistance $R = \frac{l^2\omega^2}{6\pi c}\mu_0$ ohms.

To achieve the same result by the back-e.m.f. method, we need the component of the electric force at the wire in antiphase to the current.

Close to the dipole, terms in $1/r$ can be neglected.

$$E_r = \frac{Ql\sin\psi}{4\pi\epsilon_0}\left[\frac{2}{r^3}\cos\left(\omega t-\frac{\omega r}{c}\right) - \frac{\omega}{cr^2}\sin\left(\omega t-\frac{\omega r}{c}\right)\right.$$
$$\left. - \frac{\omega}{cr^2}\sin\left(\omega t-\frac{\omega r}{c}\right)\right]$$

The component of E_r in $\sin\omega t$ is given by

$$E_r = \frac{Ql\sin\psi}{4\pi\epsilon_0}\,\frac{2}{3}\,\frac{\omega^3}{c^3} = \frac{Ql\omega^3\mu_0}{6\pi c}\sin\psi\sin\omega t$$

This is independent of r and gives the field at the dipole. We need $\psi = 90°$.

Therefore $$E_r = \frac{Ql\omega^3\mu_0}{6\pi c}\sin\omega t$$

Therefore $$E_rI = -\frac{Q^2l\omega^4}{6\pi c}\mu_0\sin^2\omega t$$

Hence radiation resistance $R = \frac{l^2\omega^2}{6\pi c}\mu_0$ ohms, as before. It will be noted that the second method avoids the integration and is slightly quicker.

(8.2.2) Long Current Filament.

$$V = 0$$
$$A_z = \frac{\mu_0 I}{4}\left[-\text{Y}_0\left(\frac{\omega r}{c}\right)\sin\omega t - \text{J}_0\left(\frac{\omega r}{c}\right)\cos\omega t\right]$$

where Y_0 and J_0 are Bessel functions of order zero.

$$E_z = -\frac{\partial A_z}{\partial t} = \frac{\mu_0\omega I}{4}\left[+\text{Y}_0\left(\frac{\omega r}{c}\right)\cos\omega t - \text{J}_0\left(\frac{\omega r}{c}\right)\sin\omega t\right]$$

$$H_\theta = -\frac{\partial A}{\partial r} = \frac{\mu_0\omega I}{4c}\left[-\text{Y}_1\left(\frac{\omega r}{c}\right)\sin\omega t - \text{J}_1\left(\frac{\omega r}{c}\right)\cos\omega t\right]$$

The Poynting integral is $\int\int(\boldsymbol{E}\times\boldsymbol{H})\,.\,d\boldsymbol{s}$, and the power component will be

$$\frac{1}{2}\,\frac{\mu_0^2\omega^2I^2}{16c}\int_0^{2\pi}\int_0^{l}\left[\text{J}_1\left(\frac{\omega r}{c}\right)\text{Y}_0\left(\frac{\omega r}{c}\right) - \text{J}_0\left(\frac{\omega r}{c}\right)\text{Y}_1\left(\frac{\omega r}{c}\right)\right]r\,d\theta\,dl$$

The expression in brackets can be simplified[30] and then

$$\iint(\boldsymbol{E}\times\boldsymbol{H})d\boldsymbol{s} = \frac{\mu_0^2\omega I^2l}{16c}$$

If $l = \frac{1}{2}\lambda$, where λ is the wavelength, this expression leads to a radiation resistance

$$R = \sqrt{\left(\frac{\mu_0}{\epsilon_0}\right)}\frac{\pi}{4}\text{ ohms}$$

By the back-e.m.f. method,

E_z in phase with I at the filament is given by

$$E_z = -\frac{\mu_0\omega I}{4}\sin\omega t$$

Hence, radiation resistance per unit length is $-\frac{E_z}{I} = \frac{\mu_0\omega}{4}$

and $R = \mu_0\frac{\pi c}{4}$ per half-wavelength $= \sqrt{\left(\frac{\mu_0}{\epsilon_0}\right)}\frac{\pi}{4}$ ohms

In this case the back-e.m.f. method is markedly quicker.

DISCUSSION ON THE ABOVE MONOGRAPH

Dr. H. Aspden (*communicated*): The point which Mr. Hammond makes concerning the manner in which existing applications of electromagnetic theory ignore the charge distributions on conductors is most important. Indeed, it raises an interesting question because it is not inconceivable that when such a charge distribution is allowed for in the calculations the result may well be that there is no true energy radiation from electrical circuits, that is, no energy lost to all the circuits in a complete system by irrecoverable radiation to outer space.

Mr. Hammond points out that it was once believed that the energy stored in the field of an alternator was fully recoverable by the alternator but that this was later questioned by Fitzgerald in 1882 on purely theoretical grounds.

It is well to bear in mind that the same electromagnetic theory as applied by Fitzgerald in his arguments leads to the prediction that there is energy radiated from an accelerated electron at a rate given by

$$\frac{\partial W}{\partial t} = \frac{2}{3}\frac{e^2 f^2}{c^3} \text{ ergs/sec} \quad . \quad . \quad . \quad . \quad . \quad . \quad (A)$$

where e is the charge of an electron, c is the velocity of light and f is the rate of acceleration of the electron, all in C.G.S. units.

Yet, it is a known fact that an accelerated electron does not radiate energy. Indeed, if it did, the electrons of all atoms would long since have dispatched their kinetic energy to outer space.

This touches on the point emphasized by Mr. Hammond because the derivation of eqn. (A) presupposes that an electron can be accelerated without specifying the means. However, when the acceleration is produced by an electric field of intensity E, eqn. (A) becomes

$$\left(\frac{\partial W}{\partial t}\right)_x = \frac{2}{3}\frac{e^2 f^2}{c^3} - \frac{4}{3}\frac{Efex}{c} \quad . \quad . \quad . \quad . \quad . \quad (B)$$

where $(\partial W/\partial t)_x$ is the rate at which energy crosses a boundary at radius x from the electron charge e. If m is the mass of the electron, this result can be written

$$\left(\frac{\partial W}{\partial t}\right)_x = \frac{4E^2e^2x}{3m^2c^3}\left(\frac{e^2}{2x} - mc^2\right) \quad . \quad . \quad . \quad . \quad (C)$$

because $mf = eE$.

Consideration shows that this equation cannot be generally valid for all values of x, because for some values of x the energy is radiated outwards and for others inwards. This indicates some fundamental inadequacy of electromagnetic theory. If the equation holds at or outside a radius x equal to $\frac{1}{2}e^2/mc^2$ there is no outward radiation of energy. This is of interest because it so happens that $\frac{1}{2}e^2/mc^2$ is the classical radius of the electron assuming that it is a hollow spherical shell of charge. The electric field energy is $\frac{1}{2}e^2/x$ and is equal to mc^2.

Mr. P. Hammond (*in reply*): Dr. Aspden seeks to apply the conclusions of my paper to radiation by individual electrons. Such extrapolation fills me with misgivings. The paper deals entirely with classical electromagnetic theory. The basic concept is that of electric charge, and I do not discuss the action of individual electrons. The difficulties in classical electron theory have been the subject of much investigation. Dr. Aspden is right in drawing attention to the necessity for including in the equations the force on the electron. In fact the classical force equations can be applied only to cases in which the external force is large compared with the 'radiation reaction' force. But I do not follow him when he says that accelerated electrons do not radiate energy. Surely this radiation has been frequently observed and is a serious problem in the action of such accelerators as the cyclotron. Reverting to my paper I should like to stress the fact that the existence of charge distributions, which I show to be necessary to current flow in conductors, does not and cannot throw doubt on the observed facts of electromagnetic radiation. It does, however, elucidate the mechanism of energy transfer and shows under what circumstances it is possible to use Poynting's vector as a tool in calculation.

621.372.8

The Institution of Electrical Engineers
Monograph No. 287 R
Feb. 1958
©

MICROWAVE ASPECTS OF WAVEGUIDES FOR LONG-DISTANCE TRANSMISSION

By A. E. KARBOWIAK, Ph.D., B.Sc.(Eng.), Associate Member.

(*The paper was first received* 15*th August, and in revised form* 7*th November*, 1957. *It was published as an* INSTITUTION MONOGRAPH *in February*, 1958.)

SUMMARY

Principal microwave problems encountered in the design of long-range communication systems using waveguides are discussed. The reasons for choosing as the medium of transmission the circular waveguide excited in the H_{01}-mode are given, and means of bridging engineering difficulties are analysed in some detail.

In particular, it is shown that plain metal waveguides are not suitable for long-range application, unless the waveguide run is substantially straight. Practical waveguides, however, must be able to follow ground contour and other unintentional bends—a condition under which the performance of conventional waveguides is considerably degraded.

The problem of unintentional bends is analysed in detail using perturbation calculus and the concept of surface impedance. The formulae obtained lead to design criteria for waveguides which are free from the above restrictions. A number of suitable waveguides are introduced and the proportions are chosen with the help of charts given in the paper. A circular metal waveguide coated with a thin skin of a dielectric is a possible solution.

Circular anisotropic waveguides are discussed at length and, among other designs, the helical waveguide of suitable proportions is shown to be another possible solution.

Numerical examples are given to illustrate the design approach and to contrast the performance of optimum designs with conventional waveguides. These examples also show that, whereas the special waveguides can be bent—for example, to follow the ground contour—to a radius as small as 100 m (or even less) without causing any appreciable deterioration in their electrical performance, the conventional waveguides under similar conditions would be considerably degraded, even to the extent of being useless for practical applications.

LIST OF PRINCIPAL SYMBOLS

$\psi_c, \psi_1, \psi_2, \ldots$ = Various wave functions.
τ = Coupling coefficient.
θ = Angle of bend.
θ_c = Critical angle of bend.
l = Arc length.
S = Span length.
R = Radius of bend.
d = Deviation at the centre of a 10 m span.
s = Waveguide radius.
μ_0, ϵ_0 = Permeability and permittivity of free space.
f = Frequency.
$\omega = 2\pi f$ = Angular frequency.
$k_0 = \omega\sqrt{(\mu_0\epsilon_0)} = \dfrac{2\pi}{\lambda_0}$ = Free-space phase-change coefficient.
λ_0 = Free-space wavelength.
$Z_0 = \sqrt{(\mu_0/\epsilon_0)}$ = Free-space impedance.
μ, ϵ, σ = Permeability, permittivity and conductivity of a medium other than free space.
ϵ_r = Relative permittivity.
$\epsilon' = \epsilon\left(1 - \dfrac{j\sigma}{\omega\epsilon}\right) = \epsilon(1 - j\tan\delta)$ = Complex permittivity.
δ = Loss angle.
$\gamma_R = \alpha_R + j\beta_R$ = Propagation coefficient along the arc of the bent guide.
$\gamma = \alpha + j\beta$ = Propagation coefficient (axial).
α = Attenuation coefficient.
$\beta = \dfrac{2\pi}{\lambda_g}$ = Phase-change coefficient.
$h_0 = \dfrac{2\pi}{\lambda_c}$ = Cut-off coefficient.
$\delta(h), \delta(\gamma)$ = Various perturbation terms.
$h = h_0 + \delta h$ = Perturbed value of h_0.
$\alpha_R, \alpha_{ZH}, \alpha_{ZE}$ = Various attenuation coefficients.
$Z_s = R_s + jX_s$ = Surface impedance (normalized with respect to Z_0).
Z_η, Z_ζ = (Anisotropic) principal components of Z_s.
Z_ϕ, Z_z = Circumferential and axial components of surface impedance, respectively.
Z_m, Z_d = Surface impedance contribution terms due to metal backing and dielectric skin, respectively.
η, ζ = Helical co-ordinates.
ψ = Lay angle of an anisotropic surface.
p = Quantity defined by eqn. (11) in the case of isotropic waveguides and by eqn. (48) for anisotropic waveguides.

Positive time factor is understood and the wave numbers are connected by

$$k_0^2 = h^2 + \beta^2 = h_0^2 - \gamma^2$$

The quantity Z_0 is absorbed in the symbol H (magnetic field vector) and consequently all impedances and coupling coefficients are normalized with respect to that quantity. As a result (although the rationalized M.K.S. system is preferred) the units do not enter in the formulae involved: the units of distance are the same as those in which the wavelength is measured.

(1) INTRODUCTION

One of the many reasons why waveguides have not as yet been used for long-range communication is that in the well-developed decimetric and centimetric regions the waveguides are too bulky, too lossy and too expensive.[1, 16] However, now that the millimetric region is being extensively explored the interest in waveguides for long-distance transmission has been revived.[2]

For a long-range application, a waveguide, to be of any extensive use, must (apart from being an economic proposition) satisfy three conditions: it must have low attenuation (say 3 dB/mile, or less); it must have adequate bandwidth-handling capacity (low dispersion); and it must be free from various multiple-echo effects associated with small discontinuities along the line.

If the waveguide is operated at a frequency much above cut-off, large bandwidth-handling capacity is ensured[3]; at the same time low attenuation figures are obtainable, particularly if suitable

Correspondence on Monographs is invited for consideration with a view to publication.
Dr. Karbowiak is with Standard Telecommunication Laboratories Ltd.

modes of propagation are chosen, e.g. the H_{01}-mode in a hollow circular metal waveguide. This transmission system has the additional advantage of being relatively immune to imperfect joints between the individual waveguide sections.

It transpires that a circular waveguide excited in the H_{01}-mode does satisfy the above enumerated conditions and is therefore suitable for the application. Any other features of this transmission system are really incidental. Thus, for example, the indefinitely falling-off frequency-attenuation curve so often stressed is not really important and is an incidental feature common to many other transmission systems.

From an engineering point of view, however, a transmission system satisfying the above-listed conditions brings with it a number of complications and difficulties.

For example, to operate the waveguide at a frequency much above cut-off it is necessary, in order to avoid impracticably large waveguides, to work the system in the millimetric region, which is just in the course of engineering exploration. Further, the waveguide is capable of supporting a large number of modes (say 200 or more), leading at times to serious mode conversion-reconversion problems (e.g. in microwave component design).

Further, the choice of the transmission mode, H_{01}, although the right one, is unfortunate in that this mode is (in a perfect waveguide) degenerate with the E_{11}-mode. The result is that the H_{01}-mode is unstable in a waveguide other than perfectly straight, leading to engineering difficulties with practical lines which, naturally, cannot be perfectly straight.

(2) PRINCIPAL PROBLEMS ASSOCIATED WITH A LONG-RANGE WAVEGUIDE COMMUNICATION SYSTEM

The problems peculiar to a long-range waveguide communication system fall into three separate sections: the pipe line itself; the components for the pipe line; and the associated equipment.

A typical long-range waveguide communication system is shown in Fig. 1. This comprises a large number of communi-

Fig. 1.—Communication system employing circular waveguide excited in the H_{01}-mode.

cation channels feeding suitable amplifiers, whose output after an appropriate coding has been performed is made to modulate a source of microwave power, M. The microwave power is fed via a suitable transducer, T, into the pipe line. At suitable intervals along the line, repeaters, R, of appropriate construction are inserted.

The line between the repeaters calls for a number of microwave components. The transducer is designed to transform the H_{01}-mode in the rectangular guide into a pure H_{01}-mode in the circular pipe with little insertion loss. Further, at many points along the line suitably designed bends and corners will be required, for example, to negotiate fixed obstacles. Needless to say, the pipe will necessitate a large number of suitably designed joints along the whole of its run. Tapers will be employed whenever a change of waveguide dimension is required, and mode filters will be inserted whenever needed to combat mode conversion-reconversion effects.

In the design of microwave components for the pipe line the difficulties are inherent to the system, arising mainly from multi-moding effects, and there is therefore only one rule to be followed: the components must be designed with a low mode-conversion figure. The attenuation of the components as far as the H_{01}-wave is concerned is of secondary importance, since the components generally occur at relatively infrequent intervals and consequently add inappreciably to the total line loss.

The design criteria for the waveguide line itself, however, cannot be summarized in a few sentences, because of the large number of factors involved. More particularly, the signal distortion in a long-range waveguide transmission system as caused by the waveguide is due to several different phenomena: the attenuation characteristic, mode conversion-reconversion effects, multiple-echo effects, and dispersion.

If the waveguide is employed for transmission of pulse-code-modulation (p.c.m.) information only, it can be shown[3] that the distortion of the intelligence (basically governed by the pulse distortion) as a result of attenuation is negligible in comparison with dispersion effects. Consequently, by using suitable coding (p.c.m.), the first phenomenon is rendered unimportant.

Mode conversion-reconversion and multiple-echo effects, i.e. wave scattering at minute irregularities along the line, have been a subject of a limited study.[4, 5] In general, the better the waveguide tolerances (other factors being equal) the less important these phenomena become.

With lines of good tolerances the only mode conversion-reconversion effects of practical significance are those between the H_{01}- and E_{11}-modes, as brought about by a bend in the waveguide.

(3) THE PROBLEM OF BENDS

(3.1) General

Communication via a waveguide excited in the H_{01}-mode (however low its theoretical attenuation may be) cannot be a practical engineering proposition unless and until a satisfactory solution to the problem of bends is produced. A waveguide used for communication between two points will necessitate two types of bends: the intentional bend and the unintentional bend. The first type arises when one wishes to make a deliberate and sharp change of direction of the propagation (e.g. to negotiate a fixed obstacle). The design of such a bend does not bring any formidable problems; even a substantial increase in attenuation in the bend is tolerable, because the overall performance of the system is little affected by it.

The unintentional bend, on the other hand, is a different proposition: it may arise anywhere along the whole of the waveguide run, and is unavoidable for practical reasons because it it is desirable for the waveguide to follow the contour of the ground (e.g. when laid in a trench), and in addition there is a limit to the precision with which a waveguide can be laid to approximate to a straight run.

The two problems are distinct, but any modification of the waveguide which removes the degeneracy between the H_{01}- and E_{11}-modes is a step in the right direction. However, whereas any such modification (which at the same time substantially increases the waveguide attenuation) may prove satisfactory for intentional bends, it is of no advantage for unintentional bends, since over a long run the waveguide would be considerably degraded in its performance. An example is a waveguide made of a poor conductor, which eases the problem of bends but degrades attenuation; elliptical waveguide is another example.

(3.2) Review of Published Theoretical Approaches

The propagation of a H_{01}-wave in a curved circular waveguide was first investigated by Jouguet.[7] He analysed the field in the curved section of a circular waveguide interposed between two semi-infinite pieces of straight pipe of the same cross-section (see Fig. 2 overleaf).

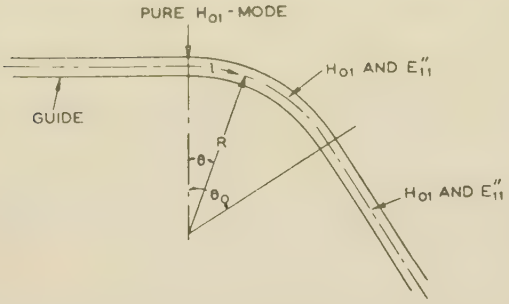

Fig. 2.—Curved circular waveguide.

If the radius of curvature is not too small in comparison with the wavelength λ and the pipe diameter $2s$, the field in the curved region is obtained (substantially) by a linear combination of H_{01}- and E_{11}-modes. The E_{11}-mode in question is polarized as shown in Fig. 3 and will be denoted by E''_{11}.

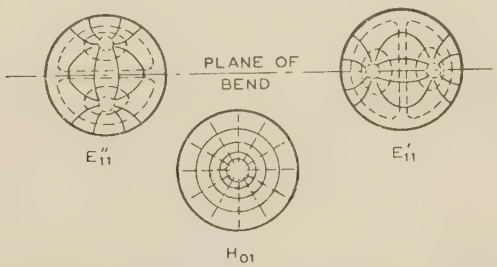

Fig. 3.—Degenerate modes of the circular waveguide.
——— Lines of electric field. – – – Lines of magnetic field.

The actual analysis of the problem, although straightforward, is rather lengthy, and only the results that have bearing on our further investigation will be discussed.

The simplest case is that of a loss-free pipe. Here the field in the curved region is given by*

$$\psi_c = A[\mathscr{H}_{01}\cos(\delta\beta_R l) + j\sqrt{(2)}\mathscr{E}''_{11}\sin(\delta\beta_R l)]\epsilon^{j\beta_0 l} \qquad (1)$$

where A is an arbitrary constant and $\delta\beta_R$ is given by

$$\delta\beta_R = \frac{k_0}{h_0 R\sqrt{2}} \quad . \quad . \quad . \quad . \quad . \quad . \quad . \quad (2)$$

Eqn. (1) has been plotted as a function of the bend angle θ in Fig. 4. It transpires that the nature of the field at a point in

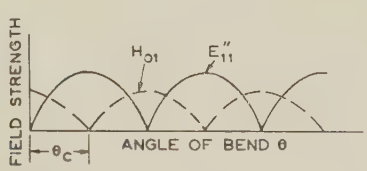

Fig. 4.—Field strength of the H_{01}- and E''_{11}-waves as a function of θ: $p \ll 1$.

the curved region is determined by θ rather than by the arc length. In particular, the field is always a mixture of the H_{01}- and E''_{11}-modes, except at the points given by

$$\theta = n\theta_c \quad (n \text{ odd}) \quad . \quad . \quad . \quad . \quad (3)$$

* $\mathscr{H}_{01}$ and $\mathscr{E}_{11}$ are algebraic symbols for the two different fields (H_{01} and E_{11}). This distinction is necessary, since the two terms in the brackets are not directly additive.

where the field is a pure E''_{11}-wave, and at the points given by

$$\theta = m\theta_c \quad (m \text{ even}) \quad . \quad . \quad . \quad . \quad (4)$$

where the field is a pure H_{01}-wave.

The angle θ_c is called the critical angle and is given by

$$\theta_c = \frac{h_0\lambda_0}{\sqrt{2}} \text{ radians} \quad . \quad . \quad . \quad . \quad . \quad (5)$$

or

$$\theta_c = 155\frac{\lambda_0}{s} \text{ degrees} \quad . \quad . \quad . \quad . \quad . \quad (6)$$

Since, after a bend angle of $2\theta_c$ has been traversed by the wave a pure H_{01}-wave is re-established, this property could be turned to advantage when designing intentional bends. However, as can be seen from eqn. (6), θ_c depends on frequency and consequently a device utilizing properties of θ_c is essentially a narrow-band device.

Jouguet applied his analysis further to the investigation of propagation in metal pipes of finite conductivity. It transpires from his results that, for a pipe of approximately 3 in diameter operated at a frequency of 35 Gc/s, bending radii of the order of several miles already add substantially to the effective waveguide attenuation.

A different analytical approach was proposed by Albersheim.[8] It is based on the theory of coupled transmission lines. The coupled transmission line equivalent of a bent circular guide is shown in Fig. 5. The lines L_0 and L_1 can carry power in H_{01}-

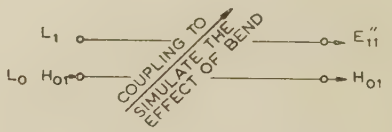

Fig. 5.—Transmission-line equivalent of a bent circular waveguide.

and E''_{11}-modes, respectively, and there is a uniform coupling between the lines to simulate the effect of the bend. The power is fed into the L_0-line and the actual proportion of power at the end of the line depends on the coupling coefficient as well as on the length of the line. Quantitative results are obtained by the application of circuit theory and can be shown to be in agreement with those obtained by Jouguet. This approach, though less rigorous, appears to be more versatile.

(3.3) A New Approach

The mathematical rigour of Jouguet's analysis and the versatility of the equivalent coupled-transmission-line approach, together with many additional advantages, are all contained in the surface-impedance approach,[9] elucidated by the author some time ago.[10]

The problem is formulated as follows. It is required to find an expression for the electromagnetic field inside a curved section of circular waveguide (Fig. 2) interposed between two semi-infinite straight pieces of waveguide of the same dimensions as the curved piece of guide, and the field at the entry to the waveguide is assumed to be a pure H_{01}-wave. The guide surface is imagined to exhibit a surface impedance of the value Z_s, and the field components are then made to assume such values at the guide surface as to satisfy that condition. It is, in fact, a problem of wave propagation inside a curved cylinder of circular cross-section whose surface impedance is Z_s. It is assumed throughout that the absolute value of the surface impedance is a small quantity.

In the solution of the problem Z_s appears as one of the parameters. If, at this stage, all conditions to be satisfied by the

waveguide (e.g. certain minimum allowable mode-conversion loss due to the bend) are inserted in the appropriate formulae, an equation determining the required value of Z_s is obtained. The second part of the problem is then of a practical nature, namely to realize physically a surface giving rise to that value of surface impedance, and this, as will be seen, can be done in a number of ways.

(4) INFLUENCE OF SURFACE IMPEDANCE ON THE PERFORMANCE OF CURVED CIRCULAR WAVEGUIDE

(4.1) Extension of Jouguet's Analysis

In the surface-impedance approach the analysis is—after an allowance has been made for minor changes in notation—the same as given in Reference 7 up to and including eqn. (51) therein. Eqn. (52) *et seq.* are, however, to be replaced by the equations given below.

In these formulae all impedances are, unless otherwise stated, normalized with respect to the free-space impedance, Z_0. Further, if we let C_0 and C_1 be the amplitude coefficients of the H_{01}- and E_{11}-waves, respectively, then the coupling coefficient τ is defined by*

$$\tau = \frac{C_1}{C_0} \quad . \quad . \quad . \quad . \quad . \quad . \quad . \quad (7)$$

(4.1.1) Propagation in Homogeneous and Isotropic Waveguides.

In homogeneous and isotropic waveguides the guide wall is characterized by a surface impedance, Z_s, such that

$$\left.\frac{E_\phi}{H_z}\right]_s = Z_s = -\left.\frac{E_z}{H_\phi}\right]_s \quad . \quad . \quad . \quad . \quad . \quad . \quad (8)$$

Using the equations appearing in Sections 3 and 4 of Reference 7 and inserting the appropriate values in the eqn. (8) above, the following will be obtained [the procedure is similar to the one used in obtaining eqn. (52) of Reference 7]:

$$j\left[\tau\frac{k_0^2\beta s}{2h^3R} - \frac{k_0}{h}\frac{J_1(hs)}{J_0(hs)}\right] = Z_s = j\left[\frac{1}{\tau}\frac{\beta s}{hR} - \frac{h_0}{k_0}\frac{J_1(hs)}{J_0(hs)}\right] \quad (9)$$

Since $h = h_0 + \delta h$ and δh is a small number, and at the same time h_0 is the first root of $J_1(hs) = 0$, consequently, on expanding the Bessel functions occurring in eqn. (9) in Taylor's series about the point $h_0 s$ and retaining the first term of each expansion only, we arrive at the following quadratic for τ:

$$\tau^2 - 2p\tau - 2 = 0 \quad . \quad . \quad . \quad . \quad . \quad (10)$$

where

$$p = \frac{h_0\beta_0}{k_0^2}\frac{R}{s}jZ_s \quad . \quad . \quad . \quad . \quad . \quad (11)$$

Eqn. (10), of course, has for its solution

$$\tau_1, \tau_2 = p \pm \sqrt{(p^2 + 2)} \quad . \quad . \quad . \quad (12)$$

There are thus two solutions for τ and correspondingly two solutions for h and γ. In other words, the H_{01}- and E_{11}-waves are unstable in the curved region, and the two independent and stable solutions are

$$\left.\begin{aligned}\psi_1 &= A_1(\mathscr{H}_{01} + \tau_1\mathscr{E}''_{11})\varepsilon^{-\gamma_1 l}\\ \psi_2 &= A_2(\mathscr{H}_{01} + \tau_2\mathscr{E}''_{11})\varepsilon^{-\gamma_2 l}\end{aligned}\right\} \quad . \quad . \quad . \quad (13)$$

Evidently the nature of the solution depends on the magnitude of p.

If p is small ($p \ll 1$)—and this occurs for sufficiently small values of surface impedance in relation to the radius of curvature —then

$$\tau_1, \tau_2 \simeq \pm\sqrt{2} + p \quad . \quad . \quad . \quad . \quad (14)$$

The corresponding value of $\delta(h)$ is obtained on substitution of expression (14) into eqn. (9). Thus, to the order indicated,

$$\delta(h)_1, \delta(h)_2 = \frac{jZ_s}{s}\frac{h^2 + k^2}{2h_0k_0} \pm \frac{k_0\beta}{h^2R\sqrt{2}} \quad . \quad (15)$$

The first term in eqn. (15) is the mean of perturbation terms (due to Z_S)[9] as would be obtained for a straight pipe when carrying the H_{01}-wave [term $\delta(h)_{ZH}$] and the E_{11}-wave [term $\delta(h)_{ZE}$]. The second term is the effect of curvature [term $\delta(h)_R$]. Thus

$$\delta(h)_1, \delta(h)_2 = \frac{\delta(h)_{ZH} + \delta(h)_{ZE}}{2} \pm \delta(h)_R \quad . \quad (16)$$

and[9]

$$\delta(\gamma)_1, \delta(\gamma)_2 = \frac{\delta(\gamma)_{ZH} + \delta(\gamma)_{ZE}}{2} \mp j\delta(\beta)_R \quad . \quad (17)$$

where

$$\delta(\beta)_R = \frac{k_0}{h_{0r}\sqrt{2}} \quad . \quad . \quad . \quad . \quad . \quad (18)$$

Here $\delta(\gamma)_{ZH}$ and $\delta(\gamma)_{ZE}$ are the perturbation terms in a straight pipe (due to Z_s) when carrying a pure H_{01}-wave and a pure E_{11}-wave, respectively.[9]

For $Z_s = 0$ these expressions reduce to the corresponding expression given in Section 3·2. As a particular application of these equations when $Z_s \neq 0$, consider the case of a metal pipe of conductivity σ. In this case the surface impedance is given by[9]

$$Z_s = (1 + j)\sqrt{\left(\frac{\pi f\mu}{\sigma}\right)}\frac{1}{Z_0} = R_s + jX_s \quad . \quad (19)$$

and for this value of surface impedance the equivalence of the above equations and those obtained by Jouguet is easy to demonstrate.

To understand the nature of the wave in a curved waveguide (Fig. 2), let us determine the coefficients A_1 and A_2 in eqn. (13). Let the wave for $\theta = 0$ be a pure H_{01}-wave, given by

$$\psi = \mathscr{H}_{01}\varepsilon^{-\gamma_0 z} \quad . \quad . \quad . \quad . \quad . \quad (20)$$

At $\theta = 0$ we equate eqns. (13) and (20), obtaining

$$\left.\begin{aligned}A_1 &= -\frac{\tau_2}{\tau_1 - \tau_2}\\ \text{and}\quad A_2 &= \frac{\tau_1}{\tau_1 - \tau_2}\end{aligned}\right\} \quad . \quad . \quad . \quad . \quad (21)$$

Consequently the field in the curved guide is given by a mixture of $H_{01}(\psi_H)$ and $E''_{11}(\psi_E)$ waves, and hence

$$\left.\begin{aligned}\psi_H &= \frac{1}{\tau_1 - \tau_2}(\tau_1\varepsilon^{-\gamma_2 l} - \tau_2\varepsilon^{-\gamma_1 l})\\ \text{and}\quad \psi_E &= \frac{\tau_1\tau_2}{\tau_1 - \tau_2}(\varepsilon^{-\gamma_2 l} - \varepsilon^{-\gamma_1 l})\end{aligned}\right\} \quad . \quad . \quad (22)$$

For small p we get for the total field

$$\psi = \psi_H + \psi_E = \left\{\mathscr{H}_{01}\cos[\delta(\beta)l] + j\sqrt{(2)}\mathscr{E}''_{11}\sin[\delta(\beta)_R l]\right\}\varepsilon^{-\gamma_0 L} \quad . \quad . \quad . \quad . \quad (23)$$

where

$$\gamma_0 = j\beta + \frac{\delta(\gamma)_{ZH} + \delta(\gamma)_{ZE}}{2} \quad . \quad . \quad (24)$$

The division of energy between the H_{01}- and E_{11}-waves is thus as shown in Fig. 4, but in addition the whole wave com-

* τ has been used instead of K, as in Jouguet's analysis.

bination suffers an attenuation which is an arithmetic average of that for H_{01}- and E_{11}-waves; similarly the phase velocity of this wave combination, ψ, is the mean of phase velocities for the H_{01}- and E_{11}-waves. We note, further, that to the first approximation (p very small) the surface impedance has no influence on the relative phase velocities of the component waves (H_{01} and E_{11}), and therefore it does not remove the degeneracy between the two waves concerned.

If p is not sufficiently small, eqn. (14) does not represent eqn. (12) adequately and consequently eqn. (23) is not applicable. Inasmuch as the case of moderate p could be dealt with exactly by using the values for τ as given by eqn. (12), the case is not of great practical interest. Accordingly, from now on we shall concern ourselves with cases for which p is a large number (say, in excess of 10), which is of great importance in that it has a direct bearing on the design of waveguides for long-distance transmission.

If p is large, then from eqn. (12) we get

$$\tau_1, \tau_2 = -\frac{1}{p}(1-\xi), 2p(1+\xi) \quad . \quad . \quad . \quad (25)$$

where ξ is the remainder of the series whose first term is

$$\xi \simeq \frac{1}{2p^2} \quad . \quad . \quad . \quad . \quad . \quad . \quad . \quad (26)$$

and this, unless otherwise stated, will be neglected.

Substitution of the coupling coefficients as given by eqn. (25) into eqn. (12) gives

$$\begin{bmatrix}\delta(h)_1\\ \delta(h)_2\end{bmatrix} = \begin{bmatrix}\delta(h)_{ZH} + \delta(h)_R\\ \delta(h)_{ZE}\end{bmatrix} \quad . \quad . \quad . \quad (27)$$

where

$$\delta(h)_R = j\frac{1}{Z_s}\frac{1}{2R}\frac{k_0}{h_0}\frac{s}{R}\left(\frac{k_0}{h_0}\right)^2 \quad . \quad . \quad . \quad (28)$$

and

$$\left.\begin{aligned}\delta(h)_{ZH} &= \frac{1}{s}\frac{h_0}{k_0}(jZ_s)\\ \delta(h)_{ZE} &= \frac{1}{s}\frac{k_0}{h_0}(jZ_s)\end{aligned}\right\} \quad . \quad . \quad . \quad . \quad (29)$$

In these expressions the various perturbation terms will be recognized as: $\delta(h)_{ZH}$, the perturbation term of a straight pipe due to Z_s, when carrying a pure H_{01}-wave; $\delta(h)_{ZE}$, the perturbation term of a straight pipe due to Z_s, when carrying a pure E_{11}-wave; and $\delta(h)_R$, the perturbation term which is a combined effect due to Z_s and guide curvature and has meaning for $R \to \infty$. (In virtue of the approximations previously made $\delta(h)_R$ has no significance for either $Z_s \to 0$ or $R \to 0$.)

The perturbation terms of the axial propagation coefficient corresponding to eqn. (27) are)

$$\begin{bmatrix}\delta(\gamma)_1\\ \delta(\gamma)_2\end{bmatrix} = \begin{bmatrix}\delta(\gamma)_{ZH} + \delta(\gamma)_R\\ \delta(\gamma)_{ZE}\end{bmatrix} \quad . \quad . \quad . \quad (30)$$

where $\delta(\gamma)_{ZH}$ and $\delta(\gamma)_{ZE}$ have meaning as explained previously, and are given by

$$\left.\begin{aligned}\delta(\gamma)_{ZH} &= \frac{1}{s}\frac{h_0^2}{k_0\beta_0}Z_s\\ \delta(\gamma)_{ZE} &= \frac{1}{s}\frac{h_0}{\beta_0}Z_s\end{aligned}\right\} \quad . \quad . \quad . \quad . \quad (31)$$

while the perturbation term due to curvature is given by

$$\delta(\gamma)_R = \frac{1}{2R}\frac{s}{R}\frac{k\beta}{h^2}\left(\frac{k_0}{\beta_0}\right)^2\frac{R_s - jX_s}{|Z_s|^2} \quad . \quad . \quad . \quad (32)$$

(4.1.2) **Nature of the Wave in a Bent Circular Waveguide.**

To examine the characteristics of the field inside a curved circular guide we use eqns. (25) and (30) in eqns. (22), obtaining

$$\psi_H = \left\{(1-\xi) + \xi\exp\left[\delta(\gamma)_2 - \delta(\gamma)_1\right]l\right\}\exp(-\gamma_1 l) \quad (33)$$

and

$$\psi_E = \frac{1}{p}\left\{\exp\left[-\delta(\gamma)_2 l\right] - \exp\left[-\delta(\gamma)_1 l\right]\right\}\exp(-j\beta l) \quad (34)$$

It will be recognized that eqn. (33) represents a 'pure' H_{01}-wave whose amplitude, apart from suffering an attenuation, varies in an oscillatory manner about the mean value $(1-\xi)$. But, since p was assumed to be large (say, over 10), $\xi\,[=1/(2p^2)]$ is a very small quantity, and consequently these variations in amplitude are negligibly small. Eqn. (34) represents an E_{11}-wave whose amplitude (of the order of $1/p$) varies in a periodic manner, apart from suffering the usual axial attenuation. For $R \to \infty$ the quantity $1/p \to 0$ and $\xi \to 0$ and consequently $\psi_E \to 0$, while the amplitude of the H_{01}-wave becomes unity, thus giving the solution for a straight pipe. The amplitude of the H_{01}-wave as a function of arc length is shown plotted in Fig. 6. The distinct nature of the field in a curved guide for the two extreme cases [of p large (Fig. 6) and p small (Fig. 4)] cannot be over-emphasized, and it is the case of large p that will occupy our attention from now on.

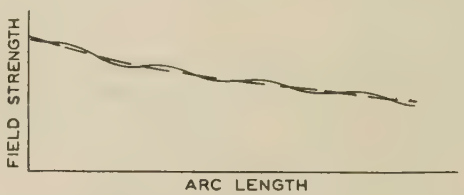

Fig. 6.—The amplitude of the H_{01}-wave in a circular waveguide: $p \gg 1$.

We have shown above that, provided that p is a large number, the wave in a curved guide will be a substantially pure H_{01}-wave. This, however, will have a propagation coefficient, γ_1, given by

$$\gamma_1 = j\beta + \delta(\gamma_1) \quad . \quad . \quad . \quad . \quad . \quad (35)$$

Thus, the attention of the H_{01}-wave in the curved guide, under these conditions, is increased by the amount

$$\left.\begin{aligned}\alpha_R &= \mathscr{R}[\delta(\gamma)_R]\\ \text{i.e.}\quad \alpha_R &= \frac{1}{2R}\frac{s}{R}\left(\frac{k_0}{\beta_0}\right)^2\frac{k\beta}{h^2}\frac{R_s}{|Z_s|^2}\end{aligned}\right\} \quad . \quad . \quad . \quad (36)$$

The attenuation of a straight guide when supporting the H_{01}-mode is given by[9] [cf. eqn. (31)]

$$\alpha_{ZH} = \frac{1}{s}\frac{h_0^2}{k_0\beta_0}R_s \quad . \quad . \quad . \quad . \quad . \quad (37)$$

Let us introduce a 'quality factor' of a bent guide defined by

$$\nu = \frac{\alpha_R}{\alpha_{ZH}} \quad . \quad . \quad . \quad . \quad . \quad . \quad (38)$$

We then find that

$$\nu = \frac{1}{2}\left[\frac{s}{R}\left(\frac{k_0}{h_0}\right)^2\frac{1}{|Z_s|}\right]^2 \quad . \quad . \quad . \quad . \quad (39)$$

This quantity, expressed as a percentage of α_{ZH}, is shown plotted in Fig. 7 as a function of λ_0 with $|Z_s|R$ as a parameter,

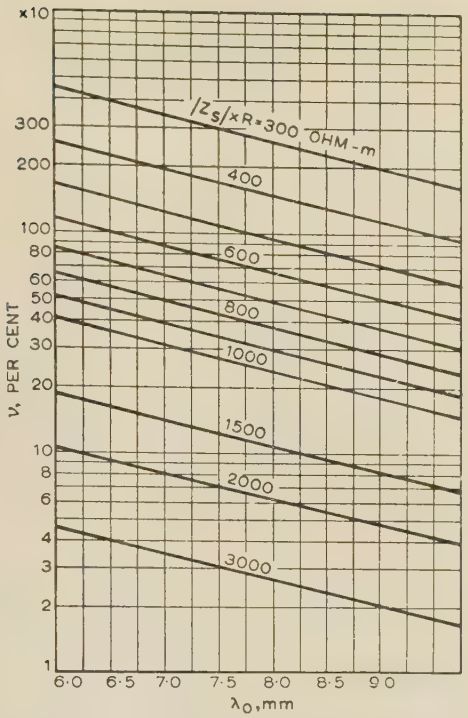

Fig. 7.—Chart for the computation of the quality factor, ν, of a curved circular waveguide of 7 cm diameter.

the curves referring to a guide whose diameter is 7 cm. Thus, using this chart we find that to negotiate a bend at $\lambda_0 = 8{\cdot}0$ mm and $\nu = 10\%$ we must have the product $|Z_s|R = 1\,600$ ohm-m. Consequently, a bend of 800 m radius is possible provided that $|Z_s| > 2$ ohms.

Eqn. (39) is significant in that it shows that for a given quality factor ν the maximum permissible curvature is proportional to the *absolute* value of the surface impedance. It thus transpires that a large value of surface reactance definitely improves the performance of the bent waveguide.

(4.1.3) **An Application.**

The important point, yet to be discussed, is how to provide for the necessary surface impedance. This can be done in a number of ways, but in this Section we shall concern ourselves with one method only, namely coating the inner surface of the guide with a thin layer of a suitable dielectric.

It can be shown that coating a metal surface with a thin layer of dielectric is an effective means of enhancing the surface reactance,[9, 11] without appreciably affecting the surface resistance. The resulting surface impedance is with respect to an E-wave; that of a coated surface with respect to an H-wave is different.[9]

This at first gives rise to a difficulty, which can, however, be circumvented by the application of an analysis akin to that indicated in Section 4.2. But, to keep the argument as simple as possible for the purpose of explaining the *modus operandi*, it is permissible to use the expression for the surface impedance as derived for E-waves, leading to results which are a good approximation, particularly in the case of waveguides operated at a frequency much above cut-off.

The surface impedance of a metal surface coated with a thin layer (thickness t) of a dielectric (of relative permittivity ϵ_r and loss factor $\tan\delta$) with respect to an E-wave is[9]

$$Z_s = Z_m + Z_d \quad . \quad . \quad . \quad . \quad . \quad . \quad (40)$$

where Z_m is the surface impedance of the metal surface in the absence of coating, namely

$$Z_m = (1 + j)\sqrt{\left(\frac{\pi f\mu}{\sigma}\right)}\frac{1}{Z_0} \quad . \quad . \quad . \quad . \quad (41)$$

and[9, 10]

$$Z_d = j(k_0 t)\left[\left(\frac{h_1}{k_1}\right)^2 - \left(\frac{h_0}{k_0}\right)^2\right] \quad . \quad . \quad . \quad (42)$$

For waveguides of large diameter, the second term in the square brackets of eqn. (42) is small in comparison with the first and may accordingly be omitted; this results in considerable simplification of all subsequent formulae. Thus, for example, with a 7 cm diameter guide operated at 8·7 mm the error in Z_d on that account is of the order of 2%, which is entirely satisfactory for any applications that we may contemplate. With this approximation in mind we have

$$\left.\begin{aligned} Z_d &= R_d + jX_d \\ &= k_0\frac{\tan\delta}{\epsilon_r}t + jk_0\left(1 - \frac{1}{\epsilon_r}\right)t \end{aligned}\right\} \quad . \quad . \quad (43)$$

Consequently

$$\begin{aligned} R_s &= R_m + R_d \\ &= \frac{1}{Z_0}\sqrt{\left(\frac{\pi f\mu}{\sigma}\right)} + k_0\frac{\tan\delta}{\epsilon_r}t \quad . \quad . \quad . \quad (44) \end{aligned}$$

and

$$\begin{aligned} X_s &= X_m + X_d \\ &= \frac{1}{Z_0}\sqrt{\left(\frac{\pi f\mu}{\sigma}\right)} + k_0\left(1 - \frac{1}{\epsilon_r}\right)t \quad . \quad . \quad (45) \end{aligned}$$

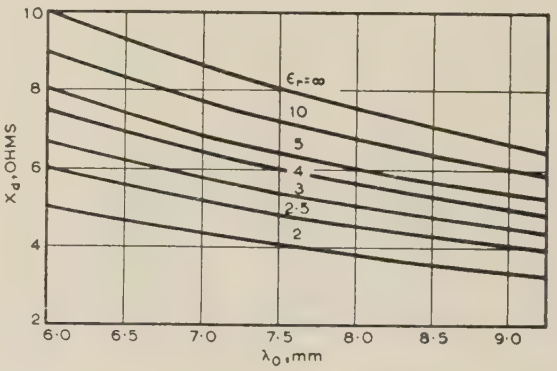

Fig. 8.—Surface reactance X_d of a dielectric-coated surface per 0·001 in thickness of coating.

Fig. 8 shows the variation of X_d as a function of frequency with ϵ_r as parameter. The quantity $X_m = R_m$ is plotted in Fig. 9 for three different metals: copper, aluminium and brass.

For any practical application it is important for the attenuation of a straight waveguide to remain approximately the same; i.e. it is required that R_d shall be small ($R_d \ll X_d$). Whether this condition will be fulfilled or not depends entirely on the relative values of the permittivity and the dielectric loss. The ratio R_d/X_d is given by

$$\frac{R_d}{X_d} = \frac{\tan\delta}{\epsilon_r - 1} \quad . \quad . \quad . \quad . \quad . \quad (46)$$

As an application, consider the following numerical example. What must be the coating thickness of a uniform layer of polythene applied to the inside surface of a copper tube to enable the

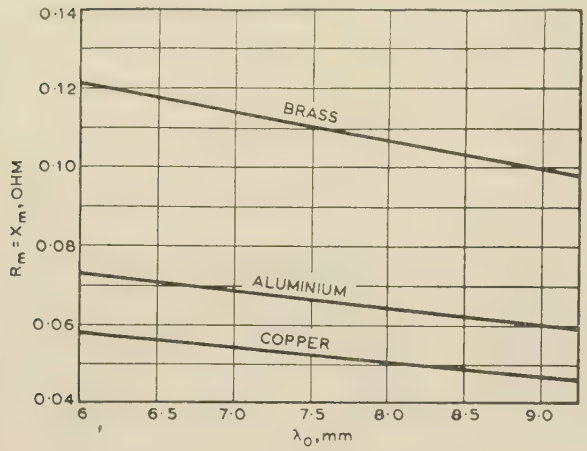

Fig. 9.—Surface impedance of metal surfaces.

guide to follow a bend, whose radius is 400 m, with an increase in attenuation not in excess of 10%?

Using the data contained in Figs. 7–9 we find that if the tube is provided with a 0·001 in thick layer of polythene ($\epsilon_r = 2{\cdot}2$, $\tan\delta = 0{\cdot}0007$), the above requirements will be fulfilled. The tremendous improvement thereby achieved can be seen by contrasting the performance of this guide with that of a plain copper guide: in the latter case a bending radius of less than 20 km could not be tolerated. Fig. 10 shows the relation between the thickness of coating and the radius of bend for three values of ν.

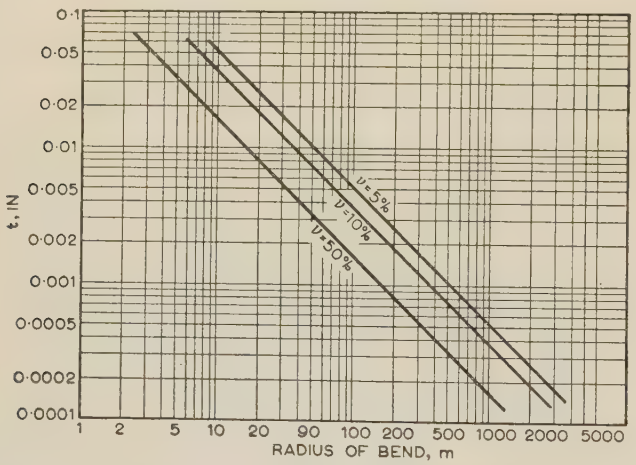

Fig. 10.—Allowable radius of bend for a given quality factor ν as a function of thickness t of polythene ($\epsilon_r = 2{\cdot}2$) coating.
$\lambda_0 = 8{\cdot}7$ mm.
$2s$ = Guide diameter = 7 cm.

Let us view these results in yet a different light. It is not possible to install a waveguide line of any appreciable length in an optically straight path; for a number of reasons, the line will deviate from its straight course in a rather random way. In Fig. 11, the deviation in a span S is denoted by d. If d is small, our previous results can be applied, where R is the radius of curvature of the unintentional bend. We then find that, in the above example, if $S = 10$ m, for a plain copper pipe d must not exceed $\pm 0{\cdot}6$ mm, while in the case of the coated pipe the allowable limits of d are ± 3 cm. It is thus evident that while a pipe cannot be laid to a precision of $\pm 0{\cdot}6$ mm, the tolerances of ± 3 cm are ample.

In the last example eqn. (46) shows a 1% increase in the value of surface resistance, leading to 1% increase in attenuation of

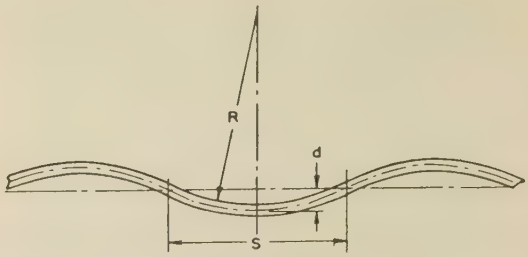

Fig. 11.—The unintentional bend.

the E-wave in a straight pipe, and if the surface impedance for the H-wave were the same, as assumed above, the attenuation of the H-wave would increase by the same amount: in actual fact this is not so and the attenuation of the H-wave increases by much less than this figure.

(4.2) Performance of Anisotropic Waveguides

(4.2.1) General.

A surface is called anisotropic when its surface impedance is, among other factors, dependent on the orientation of the surface with respect to the field components, and a waveguide whose surface is anisotropic is termed an anisotropic waveguide. The theory of anisotropic waveguides has been a subject of separate treatises, and to avoid needless repetition reference to them will be assumed.[9, 13]

The boundary conditions to be imposed in the case of anisotropic waveguides are

$$\left.\begin{aligned} \frac{E_\phi}{H_z}\Big]_s &= Z_\phi \\ \text{and} \qquad -\frac{E_z}{H_\phi}\Big]_s &= Z_z \end{aligned}\right\} \quad . \quad . \quad . \quad . \quad . \quad (47)$$

Where Z_ϕ and Z_z are the circumferential and axial components of the surface impedance, respectively.

The boundary value problem is solved in the manner indicated in Section 4.1.1 leading to eqn. (9), with p given by

$$p = \frac{h_0\beta_0}{k_0^2}\,\frac{R}{s}\,jZ_R \quad . \quad . \quad . \quad . \quad . \quad (48)$$

where

$$Z_R = \left[Z_z - Z_\phi \left(\frac{h_0}{k_0}\right)^2 \right] \quad . \quad . \quad . \quad . \quad (49)$$

Now, it has been shown elsewhere[9] that the propagation of E-waves is influenced by the axial component of surface impedance, Z_z, only, but that the propagation of H_0-waves is unaffected by this impedance; the latter is influenced by the circumferential component of surface impedance, Z_ϕ, only. Consequently, in eqn. (49) we make the following identifications:

$$\left.\begin{aligned} Z_z &= Z_{ZE} \\ Z_\phi &= Z_{ZH} \end{aligned}\right\} \quad . \quad . \quad . \quad . \quad . \quad (50)$$

For large-diameter pipes $|h| \ll k$ and consequently (since we are interested only in cases where Z_ϕ is of the order of Z_z or less) we have substantially

$$Z_R \simeq Z_z = Z_{ZE} \quad . \quad . \quad . \quad . \quad . \quad (51)$$

The wave in an anisotropic waveguide is of the same nature as that in an isotropic one and is given by eqn. (13). The coupling coefficients are as given by eqn. (12), but with p as given by eqn. (48). Again, as with isotropic waveguides, the

case of large p is of particular interest. The perturbation terms of the wave propagation coefficient are given by

$$\begin{bmatrix}\delta(\gamma)_1\\ \delta(\gamma)_2\end{bmatrix}=\begin{bmatrix}\delta(\gamma)_{ZH}+\delta(\gamma)_R\\ \delta(\gamma)_{ZE}\end{bmatrix} \quad . \quad . \quad . \quad (52)$$

where[9]

$$\delta(\gamma)_{ZH}=\frac{Z_\phi}{s}\frac{h_0^2}{k_0\beta_0} \quad . \quad . \quad . \quad . \quad . \quad . \quad . \quad . \quad . \quad (53)$$

$$\delta(\gamma)_{ZE}=\frac{Z_z}{s}\frac{k_0}{\beta_0} \quad . \quad . \quad . \quad . \quad . \quad . \quad . \quad . \quad . \quad (54)$$

$$\delta(\gamma)_R=\frac{1}{2R}\left(\frac{s}{R}\right)\left(\frac{k_0}{\beta_0}\right)^2\frac{k\beta}{h^2}\frac{R_z-jX_z}{|Z_z|^2} \quad . \quad . \quad (55)$$

It will be recognized that $\delta(\gamma)_{ZH}$ and $\delta(\gamma)_{ZE}$ are perturbation terms due to surface impedance (in the absence of curvature) for a guide carrying a pure H_{01}-wave and a pure E_{11}-wave, respectively.

Further, the quality factor, ν, of a bent guide is given by

$$\nu=\frac{\alpha_R}{\alpha_{ZH}}=\frac{1}{2}\left[\frac{s}{R}\left(\frac{k_0}{h_0}\right)^2\frac{1}{|Z_z|}\right]^2\frac{R_z}{R_\phi} \quad . \quad . \quad . \quad . \quad (56)$$

and consequently the chart of Fig. 7 can be used for computations on anisotropic guides provided that allowance is made for the factor R_z/R_ϕ.

At this stage it is instructive to examine eqn. (56) in greater detail. In particular, it will be observed that the quality factor for an anisotropic waveguide depends on the real value of Z_z in addition to its absolute value—in contrast to the isotropic waveguide [eqn. (39)].

There are two cases of practical interest: (*a*) if Z_z is made predominantly resistive ($|Z_z| \simeq R_z$)—this is a case of selective attenuation—then for a given quality factor ν, the maximum permissible curvature will be found proportional to $\sqrt{|Z_z|}$; (*b*) if, on the other hand, Z_z is made predominantly reactive—this is a case of reactive loading—then the curvature will be simply proportional to $|Z_z|$ (i.e. X_z).

It thus transpires that there are two distinct types of anisotropic waveguides suitable for our purposes: (*a*) a waveguide in which a deliberately large amount of attenuation is introduced for the E-waves, leaving the H_{01}-mode unaffected, and (*b*) a waveguide with reactive loading of the E_{11}-wave in order to break up the degeneracy between the E_{11}- and H_{01}-waves. But the choice of the waveguide for any practical application is mainly a matter of engineering convenience.

(4.2.2) An Application.

An anisotropic surface is readily produced. In fact, any surface suitably treated, so as to result in a periodic structure of the surface in a particular dimension only, gives rise to an anisotropic surface impedance, and a corrugated surface is just one of many possible.

As a numerical example consider the following problem.[15] What is the improvement achieved in terms of minimum allowable radius of bend of a 7 cm diameter copper pipe, operated at $\lambda_0 = 8{\cdot}7$ mm, which has been provided with circumferential corrugations, as shown in Fig. 12? Take the dimensions of corrugations to be: $t_1 = 0{\cdot}05$ mm, $t_2 = 0{\cdot}5$ mm, $l = 0{\cdot}2$ mm. Because of the particular proportions chosen for the corrugations in relation to the wavelength, it is permissible to proceed with a number of approximations[9, 14] In particular, we can use eqns. (10) and (11) of Reference 6 and we can assume that the field in

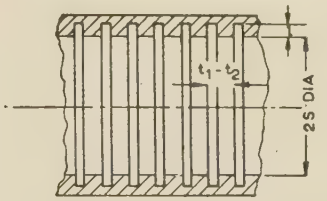

Fig. 12.—Longitudinal section of corrugated pipe.

the corrugations is substantially in the lowest mode of the so-formed short-circuited piece of the radial transmission line (length l). We then find that

$$\left.\begin{aligned}Z_{ZE}Z_0 = Z_zZ_0 &= 0{\cdot}083 + j4{\cdot}95 \text{ ohms}\\ Z_{ZH}Z_0 = Z_\phi Z_0 &= 0{\cdot}057\,5\,(1+j) \text{ ohms}\end{aligned}\right\} \quad . \quad (57)$$

When these values are inserted in the relevant formulae we find that a bending radius as small as 400 m, at the expense of a 10% increase in attenuation due to the bend, is possible. Since attenuation of the pipe itself, when straight, is 10% higher, there is therefore a total 20% degradation. This can be contrasted with the performance of a plain copper pipe, which for a 20% increase in attenuation does not permit bending radii smaller than 14 km. It will be noticed, however, that there is a measurable degradation in the performance of the straight waveguide (10%), which was not the case with the dielectric coated pipe, and it is probably safe to say that all practical forms of anisotropic waveguides are somewhat inferior in their performance in straight runs, but that the degradation can usually be brought to a tolerable figure (say 10%).

(4.2.3) Waveguides of Helical Anisotropy.

Although a corrugated waveguide, as described above, satisfies the need adequately, the structure is not easy to manufacture. A more acceptable form of waveguide is, for example, in the form of a tightly wound helix (of very short pitch) made of a

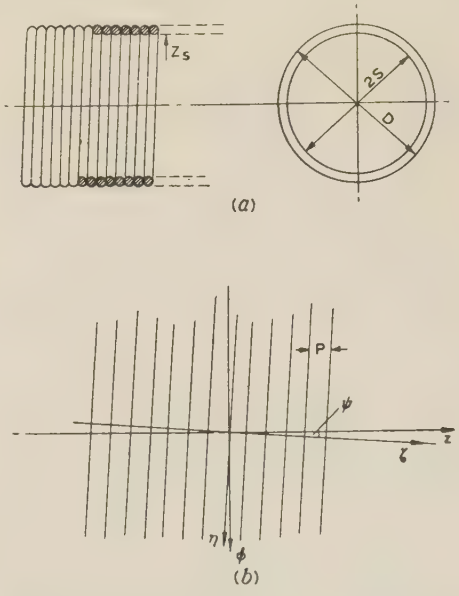

Fig. 13.—The helically anisotropic waveguide.

conducting wire with adjacent turns touching (Fig. 13). Before such a guide is put into commission it is necessary to ascertain whether the wave modes involved (E_{11} and H_{01}) are stable in such structures. This can be shown to be the case,[13] although

under the same circumstances higher-order H-modes are unstable. The case of stable waves will be our concern.

The principal components of the surface impedance (Fig. 13) are related to Z_z and Z_ϕ as follows:[13, 15]

$$\left.\begin{aligned} Z_\phi &= (Z_\eta + Z_\zeta \tan^2\psi)/(1 + \tan^2\psi) \\ \text{and} \quad Z_z &= (Z_\zeta + Z_\eta \tan^2\psi)/(1 + \tan^2\psi) \end{aligned}\right\} \quad . \quad . \quad (58)$$

The performance of waveguides of helical anisotropy (h.a.) when bent can be thus predicted from the formulae given in Section 4.2.1 with Z_ϕ and Z_z given by eqns. (58).

In particular, if the lay angle of the helix, ψ, is small, as it would be in any practical design, eqns. (58) can be approximated by

$$\left.\begin{aligned} Z_\phi &\simeq Z_\eta + Z_\zeta \psi^2 \\ Z_z &\simeq Z_\zeta + Z_\eta \psi^2 \end{aligned}\right\} \quad . \quad . \quad . \quad . \quad (59)$$

Further, since for any practical design we would have $|Z_\zeta| \gg Z_\eta$,

$$\left.\begin{aligned} Z_z &\simeq Z_\zeta \\ Z_\phi &\simeq Z_\eta + Z_\zeta \psi^2 \end{aligned}\right\} \quad . \quad . \quad . \quad . \quad (60)$$

It thus transpires that h.a. waveguides of practical design behave as if Z_z and Z_ϕ components were given by eqn. (60). This equation is of fundamental importance in the design of such waveguides.

There are many significant points contained in eqn. (60). In the first place it will be observed that for a helical waveguide, in contrast to waveguides discussed previously, the attenuation is proportional to $R_\eta + R_\zeta \psi^2$, and consequently, other factors being equal, such a waveguide is inferior by the factor $R_\zeta \psi^2$. Since, for practical waveguides, ψ^2 would be 10^{-4} or even 10^{-6}, in the case of reactive loading ($|Z_\zeta| \simeq X_\zeta \gg |Z_\eta|$) the factor $R_\zeta \psi^2$ would be negligibly small. With a selective attenuation (see Section 4.2.1), however, R_ζ may be $R_\eta \times 10^4$ or larger, leading sometimes to impractical designs.

A possible structure[15] of an h.a. waveguide is shown in Fig. 14(*a*). This waveguide consists of an outer protective cylindrical casing containing a helically wound (copper) wire. For some applications the turns are in mutual contact and for others the wire may be insulated. Another possible construction[15] is as shown in Fig. 14(*b*); here the helix is embedded in a suitable medium, e.g. a dielectric. Further, instead of round wire a conducting tape may be used, while for other applications an anodized aluminium wire gives excellent performance. From the engineering point of view an important feature shared by many h.a. waveguides is that they can be made in long length by a continuous winding process.

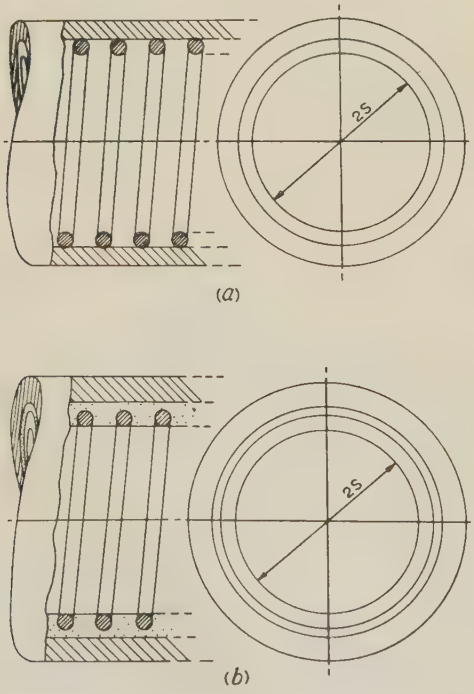

Fig. 14.—Two possible examples of waveguides of helical anisotropy.

(5) CONCLUSIONS

An outline of a long-distance communication system employing waveguides has been presented and various problems peculiar to the system have been briefly discussed. The microwave aspect has been dealt in great detail and in particular the waveguide—the medium of communication—has been closely examined.

Problems associated with the waveguide line have been considered individually and the inadequacy of plain metal waveguides for long-distance application has been stressed. With a view to finding a solution to the pressing problem of unintentional bends an analytical treatment has been developed and criteria for waveguide design have been formulated.

Finally, practical engineering solutions to the problem have been produced and a variety of suitable waveguide designs discussed. The considerable improvement in the waveguide performance thereby achieved has been illustrated by numerical examples.

(6) ACKNOWLEDGMENTS

The author wishes to thank Mr. L. Lewin, of Standard Telecommunication Laboratories Ltd., for a number of interesting discussions.

Acknowledgment is also made to Standard Telecommunication Laboratories Ltd. for facilities granted in the preparation of the manuscript and for permission to publish the paper.

(7) REFERENCES

(1) MILLER, S. E., and BECK, A. C.: 'Low-Loss Waveguide Transmission', *Proceedings of the Institute of Radio Engineers*, 1953, **41**, p. 348.

(2) MILLER, S. E.: 'Waveguide as a Communication Medium', *Bell System Technical Journal*, 1954, **33**, p. 1209.

(3) KARBOWIAK, A. E.: 'Propagation of Transients in Waveguides', *Proceedings I.E.E.*, Monograph No. 224 R, February, 1957 (**104** C, p. 339).

(4) LEWIN, L.: 'Interference in Multi-Channel Circuits', *Wireless Engineer*, 1950, **27**, 294.

(5) MORGAN, S. P.: 'Mode Conversion Losses in Transmission of Circular Electric Waves Through Slightly Non-Circular Guides', *Journal of Applied Physics*, 1916, **21**, p. 329.

(6) ALBERSHEIM, W. O.: U.S. Patent 2649 578: 1953.

(7) JOUGUET, M.: 'Les effets de la courbure sur le propagation des ondes dans les guides à section circulaire', *Câbles et Transmission*, 1947, **2**, p. 133.

(8) ALBERSHEIM, J.: 'Propagation of TE_{01} Waves in Curved Waveguides', *Bell System Technical Journal*, 1949, **28**, p. 1.

(9) KARBOWIAK, A. E.: 'Theory of Imperfect Guides—the Effect of Wall Impedance', *Proceedings I.E.E.*, Paper No. 1841 R, September, 1955 (**102** B, p. 698).

(10) KARBOWIAK, A. E.: 'Approach to Long Haul Waveguide', Technical Memorandum No. 99, Standard Telecommunication Laboratories Ltd., January, 1955.

(11) KARBOWIAK, A. E.: 'Theory of Composite Guides: Stratified Guides for Surface Waves', *Proceedings I.E.E.*, Paper No. 1659 R, July, 1954 (**101**, Part III, p. 238).
(12) KARBOWIAK, A. E.: British Patent No. 751322: 1954.
(13) KARBOWIAK, A. E.: 'Microwave Propagation in Anisotropic Waveguides', *Proceedings I.E.E.*, Monograph No. 147 R, August, 1955 (**103** C, p. 139).
(14) KARBOWIAK, A. E.: 'On the Surface Impedance of a Corrugated Waveguide', *Proceedings I.E.E.*, Paper No. 1882 R, July, 1955 (**102** B, p. 501).
(15) LEWIN, L., and KARBOWIAK, A. E.: British Patent Application No. 34334: 1954.
(16) SIMS, G. D.: 'The Influence of Bends and Ellipticity on the Attenuation and Propagation Characteristics of the H_{01} Circular Waveguide Mode', *Proceedings I.E.E.*, Monograph No. 58 R, January, 1953 (**100**, Part IV, p. 25).

621–52:621.316.71.078

The Institution of Electrical Engineers
Monograph No. 288 M
Feb. 1958
©

THE DETERMINATION OF CONTROL SYSTEM CHARACTERISTICS FROM A TRANSIENT RESPONSE

By J. P. ELLINGTON, B.Sc., A.M.I.Mech.E., and H. McCALLION, B.Sc., Ph.D., A.M.I.Mech.E.

(*The paper was first received 7th May, and in revised form 21st October, 1957. It was published as an* INSTITUTION MONOGRAPH *in February, 1958.*)

SUMMARY

Measured values of the output of a control system are used to form a characteristic equation from which the overall transfer function may be found. To use the method it is necessary to know, or assume, the form of the transfer function, and also to have a knowledge of the input form. In this manner parameters of existing systems may be found either with a view to improving the system or providing data for future designs. A worked example indicates the possible order of accuracy.

LIST OF PRINCIPAL SYMBOLS

θ_i, θ_o = Control system input and output.
$x(t)$ = A measure of the system output.
x_0, x_1, x_2, etc. = Measured values of $x(t)$ at time intervals 0, T, $2T$, etc.
p_i = Characteristic exponential exponent.
A_i = Coefficient of exp $(p_i t)$ in expressions for $x(t)$.
Z_i = Value of exp $(p_i T)$.
X_{ij} = Normalized values of x_0, x_1, etc., from least-squares equation.

(1) INTRODUCTION

In the operation and analysis of existing control systems, one of the most important requirements is a knowledge of the relationships between input and output. This relationship, the overall transfer function, which is of fundamental importance, may then be used for a number of purposes. The response to possible variations of input or external disturbances can be forecast, and further, if this transfer function is known in an analytical form, as opposed to a graphical form, the effect of changes in the system's parameters can be examined with a view to making improvements, without disturbing or interfering with a system already in operation. In addition, the determination and knowledge of the parameters of existing systems could be of great use in the design and synthesis of future systems.

One widely used method of analysis is to determine the frequency response of the system, or the steady-state output and phase difference due to a sinusoidal input. Apart from experimental difficulties, the time required for full analysis may be uneconomic or prohibitive and the information obtained is often of a limited nature. The interpretation of the results may also prove difficult, although approximate methods have been derived[1] whereby transient responses may be estimated from the frequency response.

A rather more fruitful method is to excite the system by means of a pulse or step input and to observe the transient output. This transient may then be analysed by methods such as the Fourier transform or Laplace transform to give the transfer function, but these methods are not suitable for systems which may be subject to uncontrolled disturbances, since they demand integration of the transient over an interval from zero to infinity. Shinbrot[2] gives a résumé of these methods in connection with the motion of aircraft, and also gives a variation of the Fourier transform method for use with observations over a limited time range. However, for systems composed of several components these methods usually require an excessive amount of numerical labour.

The authors' intention is now to restate a method of completely determining the parameters of a linear system from observations of the transient output produced by a known impulsive or step input, the method allowing the system's normal modes and transfer function to be found.

The determinantal form of the characteristic equation given below was first quoted by Sir. J. J. Thomson[3] in connection with the determination of X-ray absorption coefficients, and although he pointed out dynamical applications, his work does not seem to be generally known. This original equation, however, demanded that measurements should be exact and free from errors and noise, and in looking for suitable modifications the authors found that Thomson's work was a special case of a method of Prony[4] for interpolation by means of exponential functions. This latter method has been briefly mentioned by Shinbrot, but despite the necessity for adequate means of analysis it still seems to remain unnoticed. In view of this a new proof of the method suitable for control system work has been prepared, the results being presented in a manner suitable for computation.

(2) DERIVATION

Considering now an actual control system subjected to only one input, it is assumed that mathematical representations of the various system elements are known, the problem being to determine the physical constants involved. In general, if these elements are linear, the relationship between input and output, θ_i and θ_o, is given by the differential equation,

$$\left(a_n\frac{d^n}{dt^n} + a_{n-1}\frac{d^{n-1}}{dt^{n-1}} + \ldots + a_0\right)\theta_o = \left(b_m\frac{d^m}{dt^m} + b_{m-1}\frac{d^{m-1}}{dt^{m-1}} + \ldots + b_0\right)\theta_i \quad . \quad (1)$$

where $n > m$.

Taking the system to be quiescent at time $t = 0$, the Laplace transforms of each side of eqn. (1) may be equated to give

$$\theta_o(p) = \left(\frac{b_m p^m + b_{m-1}p^{m-1} + \ldots + b_0}{a_n p^n + a_{n-1}p^{n-1} + \ldots + a_0}\right)\theta_i(p) = Y(p)\theta_i(p)$$

The overall transfer function $Y(p)$, may then be resolved into partial fractions to give

$$\theta_o(p) = \left(\frac{C_1}{p - p_1} + \frac{C_2}{p - p_2} + \ldots + \frac{C_n}{p - p_n}\right)\theta_i(p) \quad . \quad . \quad . \quad (2)$$

Correspondence on Monographs is invited for consideration with a view to publication.
Mr. Ellington and Dr. McCallion are in the Department of Civil and Mechanical Engineering, University of Nottingham.

The n roots of the characteristic equation, $p_1, p_2 \ldots p_n$, may be real, imaginary or complex, it being assumed that no two roots are equal.

The actual form of the output $\theta_o(t)$ obviously depends upon the type of disturbance which can be applied to the system. For instance, if a unit impulse can be applied then $\theta_i(p) = 1$ and

$$\theta_o(t) = C_1 \exp(p_1 t) + C_2 \exp(p_2 t) + \ldots + C_n \exp(p_n t) \quad (3)$$

If, however, a unit step input, $\theta_i(p) = 1/p$, is used, it is convenient to refer measurements of output to the steady-state output, $\theta_{os} = b_0/a_0$, and write

$$\theta_o(t) - \theta_{os} = (C_1/p_1) \exp(p_1 t) + (C_2/p_2) \exp(p_2 t) + \ldots + (C_n/p_n) \exp(p_n t) \quad . \quad (4)$$

Eqns. (3) and (4) are of the same form, and similar types of expressions can be written for other known forms of impulsive excitation. Thus, in general, some measure of the output, say $x(t)$, can be written as

$$x(t) = A_1 \exp(p_1 t) + A_2 \exp(p_2 t) + \ldots + A_n \exp(p_n t) \quad (5)$$

where the constant terms A_i are related to the transfer function in a known manner through the input transform.

Suppose now that from the output record a total of, say, $(s+1) \geqslant 2n$ measurements of x have been taken at equal time intervals T, at $t = 0$, x being x_0, at $t = T$, x being x_1, etc., then from eqn. (5),

$$\left.\begin{aligned} x_0 &= A_1 + A_2 + \ldots + A_n \\ x_1 &= A_1 Z_1 + A_2 Z_2 + \ldots A_n Z_n \\ x_2 &= A_1 Z_1^2 + A_2 Z_2^2 + \ldots A_n^2 Z_n^2 \end{aligned}\right\} \quad . \quad (6)$$

or $\quad x_k = A_1 Z_1^k + A_2 Z_2^k + \ldots A_n Z_n^k \; (k = 0, 1, 2, \ldots, s)$

where $\quad Z_1 = \exp(p_1 T), Z_2 = \exp(p_2 T)$, etc. $\quad . \quad (7)$

If the set of eqns. (6) are compatible, or self-consistent, then the constants A_1 to A_n can be eliminated from the first $(n+1)$ equations to give the determinant D_1:

$$\mathrm{D}_1 = 0 = \begin{vmatrix} x_0 & 1 & 1 & \ldots \\ x_1 & Z_1 & Z_2 & \ldots \\ \cdot & \cdot & \cdot & \cdot \\ x_n & Z_1^n & Z_2^n & \ldots \end{vmatrix}$$

and generally, eliminating the A_i's from the $(n+1)$ equations commencing with x_j,

$$\mathrm{D}_{j+1} = 0 = \begin{vmatrix} x_j & Z_1^j & Z_2^j & \ldots \\ x_{j+1} & Z_1^{j+1} & Z_2^{j+1} & \ldots \\ & \cdot & \cdot & \cdot \\ x_{j+n} & Z_1^{j+n} & Z_2^{j+n} & \ldots \end{vmatrix} = \begin{vmatrix} x_j & 1 & 1 & \ldots \\ x_{j+1} & Z_1 & Z_2 & \ldots \\ & \cdot & \cdot & \cdot \\ x_{j+n} & Z_1^n & Z_2^n & \ldots \end{vmatrix} \quad . \quad (8)$$

In this way a total number of $(s+1-n)$ determinants may be formed, and if the system under consideration were perfectly linear and free from noise, whilst the measured values were subject to no errors, any n consecutive determinants could be taken and used to form a characteristic equation for the roots Z. In practice, however, noise and slight non-linearities do occur, measurements are not always perfect, and it is necessary to proceed in the following manner.

Taking the $(s+1-n)$ determinants above, each one may be expanded in terms of the elements of its first column to give the following set of equations:

$$\left.\begin{aligned} 0 &= B_0 x_0 + B_1 x_1 + \ldots + B_n x_n \\ 0 &= B_0 x_1 + B_1 x_2 + \ldots + B_n x_{n+1} \\ & \cdot \cdot \cdot \cdot \cdot \\ 0 &= B_0 x_{s-n} + B_1 x_{s-n+1} + \ldots + B_n x_s \end{aligned}\right\} \quad . \quad . \quad (9)$$

The constants, B, in eqn. (9) are functions of the required roots Z, but owing to the errors in x the equations are not consistent, and their number exceeds the number of unknowns. The best estimate of these unknowns can be found by solving eqns. (9) by the method of least squares, the resulting $(n+1)$ normal equations being

$$\left.\begin{aligned} 0 &= B_0 X_{00} + B_1 X_{01} + \ldots + B_n X_{0n} \\ 0 &= B_0 X_{10} + B_1 X_{11} + \ldots + B_n X_{1n} \\ & \cdot \cdot \cdot \cdot \cdot \\ 0 &= B_0 X_{i0} + B_1 X_{i1} + \ldots + B_n X_{in} \end{aligned}\right\} \quad . \quad . \quad (10)$$

$$i = (0, 1, 2, \ldots, n)$$

The coefficients of the unknown B's may be found systematically from the following matrix product:

$$\begin{bmatrix} X_{00} & X_{01} & \ldots & X_{0n} \\ X_{10} & X_{11} & \ldots & X_{1n} \\ & \cdot & \cdot & \cdot \\ X_{n0} & X_{n1} & \ldots & X_{nn} \end{bmatrix} = \begin{bmatrix} x_0 & x_1 & \ldots & x_{s-n} \\ x_1 & x_2 & \ldots & x_{s-n+1} \\ & \cdot & \cdot & \cdot \\ x_n & x_{n+1} & \ldots & x_s \end{bmatrix} \times \begin{bmatrix} x_0 & x_1 & \ldots & x_n \\ x_1 & x_2 & \ldots & x_{n+1} \\ x_2 & x_3 & \ldots & x_{n+2} \\ & \cdot & \cdot & \cdot \\ & \cdot & \cdot & \cdot \\ x_{s-n} & x_{s-n+1} & \ldots & x_s \end{bmatrix} \quad . \quad (11)$$

The symmetry of this matrix should be noticed, $X_{ij} = X_{ji}$, $(i \neq j)$, either as a check, or a means of avoiding arithmetic.

Taking the first n equations in the set above, each one may be rewritten in determinant form, as eqn. (8), and then manipulated in the manner given in the Appendix, to give a characteristic equation, a polynomial of degree n, with real coefficients from which the required roots Z may be found:

$$0 = \begin{vmatrix} 1 & X_{00} & X_{01} & \ldots & X_{0(n-1)} \\ Z & X_{10} & X_{11} & \ldots & X_{1(n-1)} \\ Z^2 & X_{20} & X_{21} & \ldots & X_{2(n-1)} \\ & \cdot & \cdot & \cdot & \cdot \\ Z^n & X_{n0} & X_{n1} & \ldots & X_{n(n-1)} \end{vmatrix} \quad . \quad . \quad . \quad (12)$$

Solving eqn. (12), the required exponents are found from eqn. (7). If the root Z is real

$$p = (1/T) \log_e Z$$

whilst if the root Z is complex, being one of a conjugate pair, say $(\alpha \pm j\beta)$, then

$$p = (1/2T) \log_e (\alpha^2 + \beta^2) \pm j(1/T) \arctan(\beta/\alpha)$$

Having calculated these exponents it is possible to return to eqns. (6), which are now a set of linear equations in the unknown A's, which again may be solved by the method of least squares. Thus, knowing the form of the input, the overall transfer function may be found.

(3) APPLICATION OF METHOD

The use of the above method, and some of its limitations, may best be shown by a fairly simple numerical example.

Taking a system having an overall transfer function

$$Y(p) = \frac{p^3}{(p+1)(p^2 + p/2 + 17/16)}$$

subject to a unit step function $\theta_i(p) = 1/p$, the output transform is

$$\theta_o(p) = \frac{1}{25}\left[\frac{16}{(p+1)} + \frac{9p - 17}{(p+\frac{1}{4})^2 + 1}\right]$$

and the system output to this unit step input is

$$\theta_o(t) = 0{\cdot}64 \exp(-t) + \exp(-t/4)(0{\cdot}36 \cos t - 0{\cdot}77 \sin t)$$

this equation being graphed in Fig. 1.

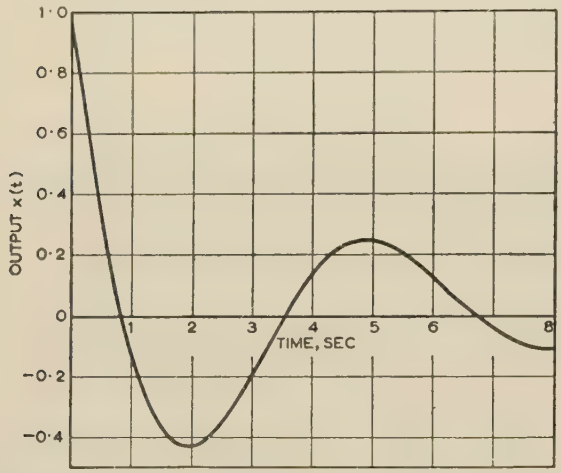

Fig. 1.—Unit step response of system of transfer function $p^3/(p^2 + \frac{1}{2}p + \frac{17}{16})$.

To simulate an actual record, calculated values of response were rounded off to two decimal places and used as measured values. Using a time interval of $T = \frac{1}{2}$ sec over the first 6 sec of the run gives values of $x_0 = 1{\cdot}00$, $x_1 = 0{\cdot}34$, $x_2 = -0{\cdot}12$, etc., at times $t = 0$, $0{\cdot}5$, $1{\cdot}0$, etc., it being taken that the steady-state output is the zero position.

These values substituted in eqn. (11) give the normalized values of the displacement and the resulting characteristic eqn. (12) becomes

$$0 = \begin{vmatrix} 1 & 1{\cdot}6830 & 0{\cdot}8076 & 0{\cdot}0712 \\ Z & 0{\cdot}8076 & 0{\cdot}7406 & 0{\cdot}5156 \\ Z^2 & 0{\cdot}0712 & 0{\cdot}5156 & 0{\cdot}6650 \\ Z^3 & -0{\cdot}4368 & 0{\cdot}2224 & 0{\cdot}5824 \end{vmatrix}$$

Expanding this determinant, or solving otherwise, gives,

$$Z_1 = 0{\cdot}60482 \text{ and } Z_{2,3} = 0{\cdot}76836 \pm j0{\cdot}42044$$

From eqn. (7) the exponents p are given by $Z = \exp(pT)$ or

$$p_1 = 1{\cdot}00576 \text{ and } p_{2,3} = 0{\cdot}26508 \pm j1{\cdot}0012$$

The actual values are $p_1 = 1{\cdot}00$ and $p_{2,3} = 0{\cdot}25 \pm j1{\cdot}00$; it is seen that the major error occurs in the damping factor of the complex delay term.

Returning to eqn. (6),

$$x_k = A_1 \exp(-1{\cdot}00576kT)$$
$$+ \exp(-0{\cdot}26508kT)[A_2 \cos(1{\cdot}0012kT) + A_3 \sin(1{\cdot}0012kT)]$$

the resulting equations, solved by least-squares methods, giving

$$A_1 = 0{\cdot}60569,\ A_2 = 0{\cdot}39760,\ A_3 = -0{\cdot}78750$$

Thus, recalling that the input was a unit step function, the overall transfer function is

$$Y(p) = p\left[\frac{0{\cdot}60569}{(p + 1{\cdot}00576)} + \frac{0{\cdot}39760p - 0{\cdot}68305}{(p + 0{\cdot}26508)^2 + (1{\cdot}0012)^2}\right]$$
$$= p\left[\frac{1{\cdot}00329p^2 + 0{\cdot}03795p - 0{\cdot}03729}{(p + 1{\cdot}00576)(p^2 + 0{\cdot}53016p + 1{\cdot}07267)}\right]$$

Comparing this result with the actual transfer function it will be seen that small terms containing p and p^2 have appeared in the numerator. This is a general feature of the method, and is of course a consequence of using inexact data. However, if the numerical values in the calculated transfer function are now rounded off bearing this point in mind, a good approximation is obtained:

$$Y(p) = \frac{p^3}{(p + 1{\cdot}01)(p^2 + 0{\cdot}53p + 1{\cdot}07)}$$

It is most important not to carry out this rounding-off process until the final solution is obtained, or gross errors may be accumulated throughout the work. Again this is a feature of least-squares methods, and all possible figures should be retained in the calculations.

If the initial data were taken with three-figure accuracy, then over the first 6 sec of the run the characteristic equation becomes

$$0 = \begin{vmatrix} 1 & 1{\cdot}678025 & 0{\cdot}805218 & 0{\cdot}071604 \\ Z & 0{\cdot}805218 & 0{\cdot}738050 & 0{\cdot}514198 \\ Z^2 & 0{\cdot}071604 & 0{\cdot}514198 & 0{\cdot}663385 \\ Z^3 & -0{\cdot}436414 & 0{\cdot}220719 & 0{\cdot}580344 \end{vmatrix}$$

yielding values of the exponents

$$p_1 = 0{\cdot}9990 \text{ and } p_{2,3} = 0{\cdot}2513 \pm j1{\cdot}0000$$

Here the agreement with the original data is very good indeed. In addition, a comparison of this characteristic equation with the previous one demonstrates that rounding-off may introduce errors in the final solution.

Apart from the accuracy of the given data, the choice of time interval T will also influence the accuracy of the solution, but there is no simple rule governing this choice. Obviously a compromise must be made, since too large or too small a time interval can reduce the order of the characteristic equation by failing to resolve the effects of small or large delay terms.

(4) CONCLUSIONS

Measured values, at equally spaced intervals, of the initial response of a control system to a known input are used to form a characteristic equation from which the overall transfer function may be calculated. This characteristic equation, based on Prony's method of exponential interpolation, is formed by a least-square method to obtain a best estimate from measurements subject to noise or errors.

(5) ACKNOWLEDGMENTS

The authors would like to thank Mr. J. V. Parry for the interest he has shown, and for his many suggestions and criticisms.

(6) REFERENCES

(1) KUSTERS, N. L., and MOORE, W. J. M.: 'A Generalization of the Frequency Response Method for the Study of Feed-

back Control Systems', in Symposium on 'Automatic and Manual Control' (Butterworths Scientific Publications), 1952.

(2) SHINBROT, M.: 'On the Analysis of Linear and Non-Linear Dynamical Systems from Transient Response Data', National Advisory Committee for Aeronautics [U.S.A.], Technical Note 3288, 1954.

(3) THOMSON, SIR J. J.: 'A Method of Finding the Coefficients of Absorption of the Different Constituents of a Beam of Heterogeneous Röntgen Rays, or the Periods and Coefficients of Damping of a Vibrating Dynamical System', *Philosophical Magazine*, 1915, **30**, p. 780.

(4) WHITTAKER, E. T., and ROBINSON, G.: 'The Calculus of Observations' (Blackie and Son, Ltd., 1944).

(5) ELLINGTON, J. P., and MCCALLION, H.: 'The Analysis of Transient Vibration Data', *Journal of the Royal Aeronautical Society*, 1956, **60**, p. 659.

(6) VETTIN: 'The Integration of Non-linear Equations', Ministry of Supply, Research and Technical Publications, Translation No. G.D.C. 10/1663T.

(7) APPENDIX

A form of the characteristic equation (12) has been derived previously by the authors,[5] and a similar method has been used by Vettin[6] for the integration of non-linear equations.

Taking the first n normal equations (10), each one may be rewritten in determinant form as eqn. (8):

$$D_1 = 0 = \begin{vmatrix} X_{00} & 1 & 1 & \dots \\ X_{01} & Z_1 & Z_2 & \dots \\ & \dots & \dots & \\ X_{0n} & Z_1^n & Z_2^n & \dots \end{vmatrix}$$

$$D_2 = 0 = \begin{vmatrix} X_{10} & 1 & 1 & \dots \\ X_{11} & Z_1 & Z_2 & \dots \\ & \dots & \dots & \\ X_{1n} & Z_1^n & Z_2^n & \dots \end{vmatrix} \quad \text{etc.}$$

Now multiply determinant D_1 by ξ_1, determinant D_2 by ξ_2, etc., the ξ's remaining undefined, and then take the sum of these determinants to give

$$0 = \begin{vmatrix} (\xi_1 X_{00} + \xi_2 X_{10} + \dots) & 1 & 1 & \dots \\ (\xi_1 X_{01} + \xi_2 X_{11} + \dots) & Z_1 & Z_2 & \dots \\ & \dots & \dots & \\ (\xi_1 X_{0n} + \xi_2 X_{1n} + \dots) & Z_1^n & Z_2^n & \dots \end{vmatrix} \quad . \quad (13)$$

The values of ξ are now to be chosen so that, if possible, the elements of the first column of eqn. (13) each become an integral power of some function or quantity λ. For convenience, use is made of the symmetry of eqn. (11), $X_{ij} = X_{ji}\ (i \neq j)$; then

$$\left.\begin{aligned} \xi_1 X_{00} + \xi_2 X_{10} + \dots &= \lambda^0 \\ \xi_1 X_{10} + \xi_2 X_{11} + \dots &= \lambda^1 \\ \dots & \\ \xi_1 X_{n0} + \xi_2 X_{n1} + \dots &= \lambda^n \end{aligned}\right\} \quad . \quad (14)$$

There are thus $(n-1)$ equations for the n unknown values of ξ, so for these equations to be consistent their eliminant must be zero, or

$$0 = \begin{vmatrix} 1 & X_{00} & X_{01} \dots X_{0(n-1)} \\ \lambda & X_{10} & X_{11} \dots X_{1(n-1)} \\ \lambda^2 & X_{20} & X_{21} \dots X_{2(n-1)} \\ & \dots & \\ \lambda^n & X_{n0} & X_{n1} \dots X_{n(n-1)} \end{vmatrix} \quad . \quad (15)$$

Returning now to eqn. (13) and substituting from eqn. (14),

$$0 = \begin{vmatrix} 1 & 1 & 1 & \dots \\ \lambda & Z_1 & Z_2 & \dots \\ \lambda^2 & Z_1^2 & Z_2^2 & \dots \\ & \dots & \dots & \\ \lambda^n & Z_1^n & Z_2^n & \dots \end{vmatrix} \quad . \quad (16)$$

Eqn. (16) is now an alternant determinant and is a polynomial of degree n in λ. This determinant may be readily evaluated, but it is sufficient merely to determine its factors. It is obvious that $(\lambda - Z_1)$ is a factor, because if $\lambda = Z_1$ two columns are equal and the determinant is zero. $(\lambda - Z_2)$, $(\lambda - Z_3)$, etc., are also seen to be factors, and in a similar manner so also are $(Z_1 - Z_2)$, $(Z_1 - Z_3)$, $(Z_2 - Z_3)$, etc.

Now under the assumption that none of the exponents p are equal, none of the Z are equal, and thus eqn. (16) is only zero when the factors $(\lambda - Z_1)$, $(\lambda - Z_2)$, etc., are zero; thus there are n possible values of λ,

$$\lambda_i = Z_i \quad . \quad (17)$$

These values of λ may now be inserted in eqn. (15), which then becomes a polynomial of degree n in Z:

$$0 = \begin{vmatrix} 1 & X_{00} & X_{01} \dots X_{0(n-1)} \\ Z & X_{10} & X_{11} \dots X_{1(n-1)} \\ Z^2 & X_{20} & X_{21} \dots X_{2(n-1)} \\ & \dots & \\ Z^n & X_{n0} & X_{n1} \dots X_{n(n-1)} \end{vmatrix} \quad . \quad (18)$$

This is then the characteristic equation quoted earlier which yields the required exponents, and hence the overall transfer function.

621.385.032.213.13

The Institution of Electrical Engineers
Monograph No. 289 R
Feb. 1958
©

THE CONDUCTIVITY OF OXIDE CATHODES

Part 5.—Functional Structure of the Cathode

By G. H. METSON, M.C., Ph.D., M.Sc., B.Sc.(Eng.), Member.

(*The paper was first received* 19*th August, and in revised form* 13*th November*, 1957. *It was published as an* INSTITUTION MONOGRAPH *in February*, 1958.)

SUMMARY

In this Part the oxide cathode operating at 1 020° K is shown as a 2-element device—a thin-film cathodic-core thermionic emitter covered by a relatively massive porous oxide matrix. The thin-film emitter determines the total emission available from the cathode, and the porous matrix settles the potential rise experienced by the current before it emerges into the outer vacuum. This potential rise is shown to depend only on the self-generated electron density within the matrix pores and to be largely independent of emission density from the core emitter.

LIST OF PRINCIPAL SYMBOLS

V_A = Potential between cores, volts.
I_A = Electron current through matrix, mA.
R_d = Matrix resistance, ohms.
R_0 = Stable low level of matrix resistance—the 'characteristic resistance', ohms.
R_{max} = Resistance of cold matrix, ohms.
R' = Resistance of unit thickness of matrix, ohms.
ΔV_A = P.D. due to current through cold matrix, volts.
V_{H1}, V_{H2} = Respective heater voltages, volts.
P_{H1}, P_{H2} = Respective heater powers, mW.
T_1, T_2 = Respective cathode temperatures, deg K.
V_{T1}, V_{T2} = Respective thermo-electric correction e.m.f.'s.
$\Delta V_T = V_{T1} - V_{T2}$.

(1) INTRODUCTION

Neglecting the small contribution made by solid semi-conduction to overall conductivity at 1 000° K, it seems well established that the whole cathode current is thermionically emitted at the cathodic core surface and travels vacuum-wise through the oxide matrix overlay. The core surface is thus the essential emitting mechanism which determines the total or temperature-limited current that can be drawn through the matrix. The oxide particles of the overlay itself are, of course, themselves powerful emitters, but they contribute nothing to the main cathode current. The matrix might, in fact, be regarded as a framework supporting a distributed space-charge whose function is to determine the magnitude of potential fall suffered by the electron stream.

It is proposed in the present Part to examine the properties and functional interdependence of the thin-film core emitter and the porous matrix overlay. It will be shown that the two components can be physically separated and will work in isolation, but that their interaction is necessary for long-term cathode operation. Some attention will also be given to the function of the electron-exit boundary of the matrix, i.e. the area of oxide that can be seen by the anode in a conventional diode. It will be shown that the thermionic state of this surface is immaterial to the conductance of the diode.

The experimental valves used in the work were the standard S-type assembly and the 6D15 diode described in previous Parts.* To avoid the complications of gas action, all valves were fitted with active-nickel cores and were well aged before use.

(2) THE THIN-FILM CORE EMITTER

(2.1) Probable Nature of the Emitter

The mechanical structure of the porous matrix at the cathodic core face can be opened to direct visual examination by using the standard $(BaSr)CO_3$ spraying technique on a glass cover slip; the boundary is then available for viewing through the glass. A detailed microscope study of the boundary under suitable arrangements of illumination shows that only a proportion of the glass surface is in physical contact with particles—probably some 50% or more is left bare and uncoated. The carbonate particles on the metal core surface at a typical cathode are presumably arranged in similar fashion. Thermal conversion of carbonate to oxide results in a small overall shrinkage of the matrix, but the shape and relative juxtaposition of individual particles remain unchanged. The core distribution of oxide particles in a fully processed valve is therefore likely to follow the same pattern as the carbonate distribution seen through the glass cover slip, i.e. only a modest proportion of the core surface will be in physical contact with the matrix. During thermal processing, however, the bare areas of cathode core will be subjected to the condensation of barium and strontium oxide vapours arising from nearby (BaSr)O particles. The bare areas therefore become coated with a thin film of mixed alkaline earth oxides and the probable thickness of the film will be a small fraction of a micron. The totality of these thin-film cathode core patches is regarded in the paper as the basic thermionic emitter in the common oxide-cathode system, i.e. the thin-film area determines the total emission available from the cathode at any particular temperature, in contradistinction to the massive porous overlay, which merely determines the potential fall between the core and the electron-exit boundary of the matrix.

(2.2) Emission from Thin Film of Alkaline-Earth Oxides

The thermionic-emission properties of thin films of alkaline-earth oxides on nickel have been thoroughly examined recently by Woods and Wright,† who investigated both single and mixed oxides and compared the total emission measurements with

This paper is a continuation of Monographs Nos. 221 R and 243 R, published in February and June, 1957 (see 104 C, pp. 221 and 243), and Nos. 268 R and 269 R (see pages 183 and 189).
Correspondence on Monographs is invited for consideration with a view to publication.
Dr. Metson is at the Post Office Research Station.

* The dimensions of the S-assembly and the 6D15 type diode are given here for comparison. The 6D15 diode consists of a 2-watt cathode, with a total coated area of 0·45 cm², mounted inside a grid-type anode. This consists of about 73 turns of 28 μ molybdenum wire at about 175 turns/in. The matrix thickness is approximately 60 μ and the distance between the grid plane and the cathode surface is about 110 μ. The S-assembly consists of two of the same 2-watt cathodes clamped together by tungsten springs to form a sandwich of matrix. The sprayed thickness is increased so that the total matrix is about 150 μ thick. Full details, with processing data are set out in Part 1.

† WOODS, J., and WRIGHT, D. A.: 'Thermionic Emission from Thin Films of Barium and Strontium Oxide', *British Journal of Applied Physics*, 1954, 5, p. 74.

Table 1

EMISSION FROM VARIOUS CATHODES

Cathode	Deposition	Thickness	Pulse emission at 1050° K
		microns	amp/cm²
BaO	Evaporation	0·01	0·4
	Evaporation	0·10	1·2
	Evaporation	1·00	0·9
	Spray	100·0	0·6
SrO	Evaporation	0·10	0·1
	Spray	100·0	0·14
SrO on BaO	Evaporation	Both 0·10	3·0
(BaSr)O	Spray	100·0	3·5
BaO on SrO	Evaporation	Both 0·10	0·6

those from the conventional form of sprayed cathode. Some typical results, extracted from the paper, are shown in Table 1.

The results are illuminating, and show that a film of mixed oxides a fraction of a micron thick can give the same total emission as the conventional form of oxide cathode with a sprayed matrix thickness of 100 μ. The higher emission from the film of SrO on BaO compared with that of BaO on SrO is interesting and in line with previous experience on sprayed cathodes.

In comment on these results the author would observe that, when comparing the thin evaporated film with the common thick spray, Woods and Wright are, in effect, comparing the same basic emitter and therefore obtain comparable emission levels.

(2.3) Separation of the Core Emitter

Fig. 1(*a*) shows a schematic of the two core emitters and the matrix of a processed S-type assembly. The thin-film emitters

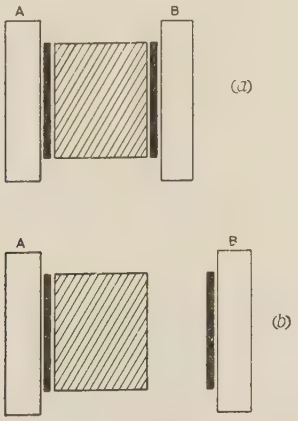

Fig. 1.—Schematic of core emitter and matrix in S-type assembly.

are regarded as adhering strongly to their respective core faces and it can be imagined that the withdrawal of a core, as in Fig. 1(*b*), would take with it the associated thin film. Such an operation would permit comparison of the two conductances of the diode using either the thin film or the normal spray as emitter.

An attempt has been made to realize the schematic of Fig. 1 in a practical way. An active-nickel core was sprayed with mixed carbonates in the usual manner and mounted about 80 μ from a similar core which was bare and free from spray. The system was then processed to the usual S-type schedule and sealed from the pump after firing the getter. After the valve had been activated to minimum impedance in both directions, the cores were set at 1020° K and the two-directional voltage/current

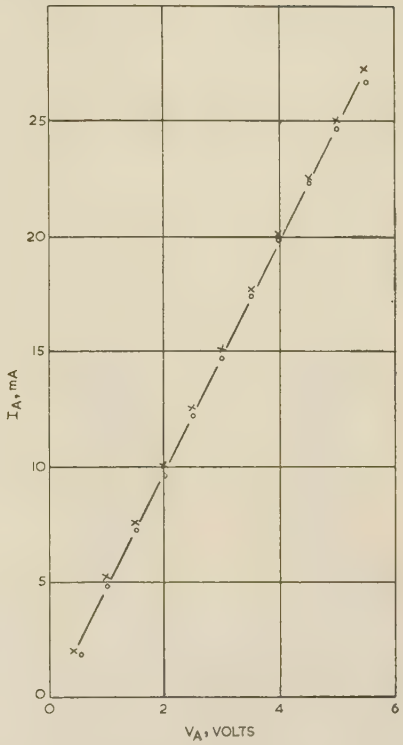

Fig. 2.—Comparison of diode conductance using thin-film and normal sprayed cathodes.

× × × Sprayed cathode.
○ ○ ○ Thin-film cathode.

characteristics were measured. The results are set out in Fig. 2 and show that the device is electrically symmetrical. The following conclusions are drawn:

(*a*) During thermal treatment the bare core B becomes coated with a thin activated film of mixed barium and strontium oxides. The emission from this film at 1020° K is adequate to meet the space-charge requirement of the diode in the direction B–A.

(*b*) The impedances in the A–B and B–A directions of electron flow are identical.

(*c*) The activated block of matrix influences the potential fall through the device but serves no other purpose.

(*d*) The position of the matrix block relative to the core faces has no influence on the impedance of the device, e.g. if the block is suspended midway between the two core faces, the impedance will remain unchanged.

(*e*) The core emitter and the matrix block are separate entities and can function in isolation and independence of each other.

The thickness of the film on core B in the above experiment was estimated from the known rates of evaporation to be about 0·1 μ.

(3) POTENTIAL FALL IN THE MATRIX

(3.1) Limits of Fall

Both conventional and S-type assemblies were used in the experiments, and it will be convenient to express the potential fall between cathode and anode in terms of ohmic resistance in both cases. It was shown in Part 1 that there is a lower limit to the resistance of a standard S-type assembly at 1020° K, and this was described as the characteristic resistance, R_0. In the standard S-type valve R_0 is about 14 ohms at 1020° K, and it is imagined that this limit is set by a space-charge condition arising within the hollow pores of the matrix as a result of thermionic emission from the individual matrix particles. If the emission

from a group of particles is suppressed in some way, e.g. a localized gas action, the matrix will experience a localized increase of resistance. If the thin-film core emitter itself remains functionally unchanged, a gradual suppression of the emission from all the particles of the matrix will result in a steady increase in resistance from R_0 to some upper limit R_{max}. The present Section considers the magnitude of the resistance of such an emission-limited matrix.

(3.2) Resistance of Zero-Emission Matrix

Fig. 3 shows a schematic of the electrodes in an experimental valve. The core pieces A and B, of active nickel, were fitted

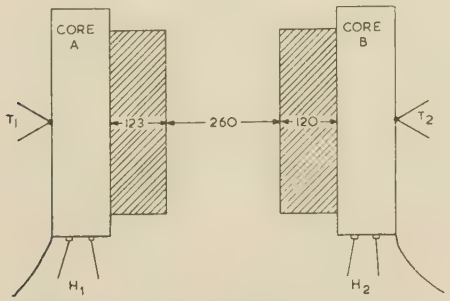

Fig. 3.—Schematic of electrode arrangements in an experimental valve.
Dimensions are in microns.

with internal heaters and were sprayed to a thickness of 120 μ, but were separated by a vacuum gap of 260 μ. The heaters were brought out of the glass envelope separately, so that individual control of core temperature was possible and could be measured using the thermocouples T_1 and T_2. The whole system was vacuum processed in the standard manner for an S-type assembly.

The diode was examined in the following manner: both cores were set accurately at 1 020° K and the voltage/current characteristic of the diode wave measured with core A as cathode and core B as anode. The heater voltage in B was then reduced to zero and that of A readjusted to maintain its temperature at 1 020° K. A second characteristic was measured, and results are set out in Fig. 4. The voltage across the diode was finally reversed and the total emission from the cold B core (540° K) was shown to be less than a microampere. The following conclusions are drawn:

(*a*) The electron stream, I_A, from A passes readily through the matrix covering of B in both hot and cold conditions.
(*b*) At constant I_A the diode voltage, V_A, is increased by ΔV_A when the B matrix is cooled from 1 020° to 540° K.
(*c*) The total emission from the cold matrix is essentially zero and the electron density within its pores is likewise presumed to be zero.

If the resistance of the cold matrix is R_{max}, then

$$\Delta V_A = I_A \,.\, R_{max}$$

and a scrutiny of Fig. 4 will show that R_{max} is approximately 100 ohms and independent of current.

These results can now be applied to a standard S-valve whose matrix has dimensions similar to those of the matrix on the B core shown in Fig. 3. Provided that the cathodic core emitter remains fully operative, the effect of reducing the matrix temperature from 1 020 to 540° K (or, indeed, to room temperature) is only to increase the resistance from $R_0 = 15$ ohms to $R_{max} = 100$ ohms. The S-valve with a cold matrix but a normally functioning core emitter may, in fact, be likened in behaviour to a conventional diode with a vacuum gap equal to the matrix thickness. If the

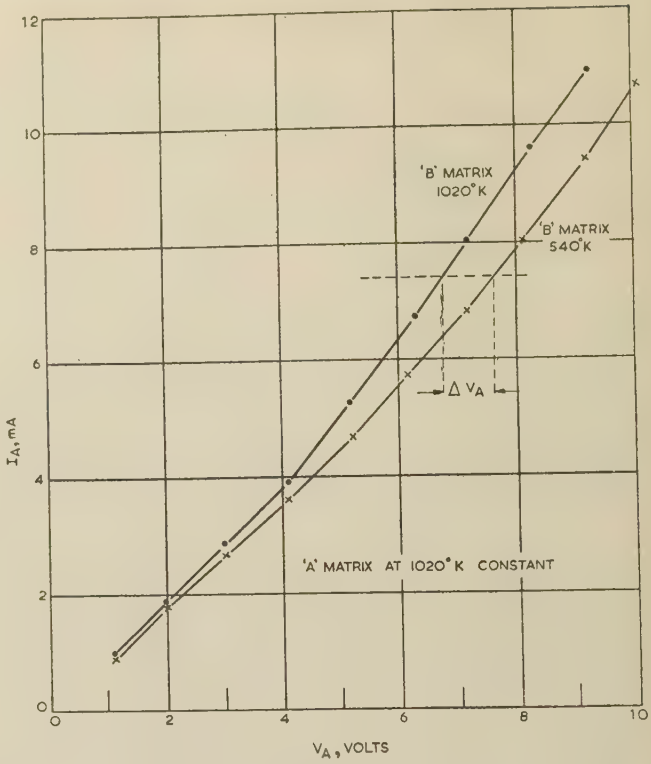

Fig. 4.—Voltage/current characteristic with hot and cold conditions of matrix.

cathodic core emitter is now progressively cooled the diode resistance will change but little from $R_{max} = 100$ ohms until the core emitter approaches temperature limitation of emission, whereafter it will increase abruptly and drastically. This hypothetical picture of S-valve action will be put to test in the next Section.

(3.3) Independence of S-Valve Resistance and Core-Emission Density

Fig. 5(*a*) shows schematically a standard S-assembly. The two cores are of active nickel, and it is assumed that the system has

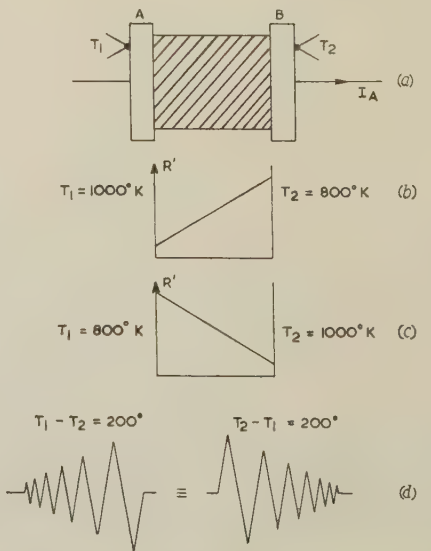

Fig. 5.—Resistance gradients in an S-type assembly.

been vacuum processed to a gas-free condition, i.e. $R_0 = 15$ ohms at 1 020° K. Neglecting the influence of a small testing current on the system, there will be no temperature gradient across the matrix when the core heater voltages are equal. Suppose now that the cathodic core A is maintained at 1 000° K and core B is cooled, by heater-voltage adjustment, to 800° K. The electron density due to particle emission within the matrix pores will now show a gradient through the matrix, and this, in turn, will give rise to an inverse gradient of resistance. Fig. 5(*b*) shows such a gradient, where R' represents the resistance of a small unit thickness of matrix at any point between cores faces; the exact manner in which R' varies with position is immaterial to the argument. Next suppose that A is cooled from 1 000 to 800° K and B is heated from 800 to 1 000° K. This operation will result in gradients of electron density and resistance across the matrix, and R′ is as shown in Fig. 5(*c*). Owing to the essential symmetry of the S-type system and the symmetry of the temperature juxtapositions, it will be clear that the two resistance gradients in Figs. 5(*b*) and 5(*c*) are exact mirror images of each other. In short, the two temperature arrangements leave the *overall* matrix resistance unchanged, as in Fig. 5(*c*), but involve a 200° swing in the temperature of the cathodic core emitter. If, as suggested by Woods and Wright, the work function of the thin-film core emitter is about 1·2 eV, a 200° shift in core-emitter temperature should involve a change in its total emission by a factor of 100. There arises therefore the proposition that the S-assembly resistance is independent of core emission density—providing, of course, that the total emission is greater than any current used to measure to the resistance.

Practical realization of the above condition is simple if certain experimental precautions are taken. Fig. 6 shows a standard

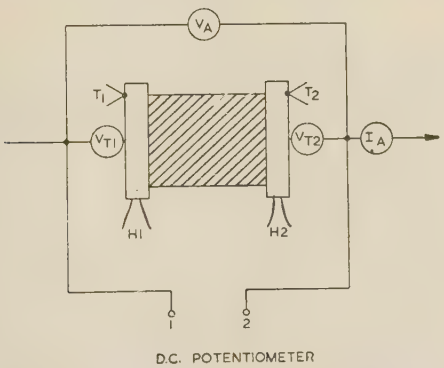

Fig. 6.—Voltage measurements in presence of temperature gradient.

active-nickel-cored S-valve operating in the gas-free condition and carrying a small electron stream, I_A. If the core temperatures T_1 and T_2 are equal, the resistance of the device will be accurately determined by the relationship $R_d = V_A/I_A$, where V_A is the straightforward voltmeter reading across the diode terminals. There are, however, concealed in the relationship two thermo-e.m.f.'s V_{T1} and V_{T2} arising at the core/matrix boundaries, opposing each other in direction and dependent for magnitude on the core-face temperatures. The more correct relationship for resistance is therefore written

$$R_d = \frac{V_A - \Delta V_T}{I_A}$$

where $\Delta V_T = V_{T1} - V_{T2}$ and $\Delta V_T = 0$ for $T_1 = T_2$.

Since the object of the experiment is to vary the relation of the two core temperatures to induce image-wise resistance gradients, it is clear that ΔV_T must be accurately determined by preliminary measurement. Fig. 7 shows the variation of ΔV_T with anodic-

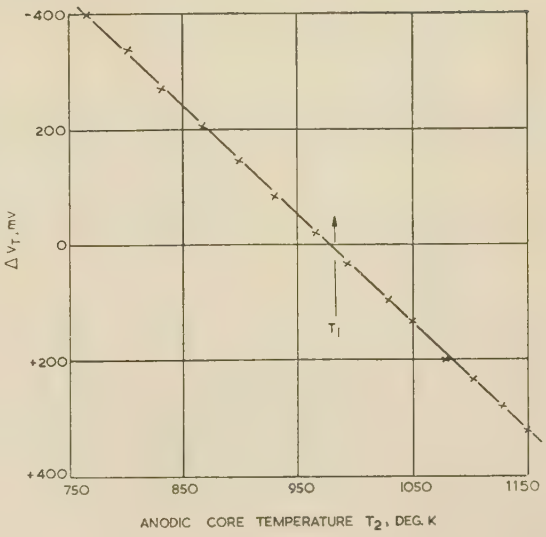

Fig. 7.—Variation of $\Delta V_T/T_2$ at constant T_1 (980° K).

core temperature at constant cathodic-core temperature. The method of measurement is by straightforward d.c. potentiometry —the voltmeter V_A in Fig. 6 is discarded and the potentiometer is set in its place across terminals 1 and 2. The current I_A is reduced to zero by disconnection and ΔV_T is measured over a range of T_2 from 800 to 1 200° K with T_1 constant at 980° K. The identical mirror-image characteristic is obtained by transposing the temperature conditions.

The setting-up of the image-wise resistance gradients can be achieved in three slightly differing ways. Thus, if the core-heater powers are represented by P_{H1} and P_{H2}, core-heater voltages by V_{H1} and V_{H2} and core temperatures by T_1 and T_2, the following arrangements are possible:

(*a*) With T_1 constant, measure R_d/T_2; repeat for image with core temperature transposed.
(*b*) With V_{H1} constant, measure R_d/V_{H2}; repeat for image with core-heater voltages transposed.

The three techniques lead of course to very similar results, and method (*a*) will be used as an example. Four separate characteristic measurements are required, and these are scheduled as follows:

(*c*) Set $I_A = 0$. Measure $\Delta V_T/T_1$, over range 1 150–950° K with $T_2 = 1\,150°$ K constant.
(*d*) Repeat for image with transposed core temperatures.
(*e*) Set $I_A = 20$ mA constant. Measure V_A/T_1 over range 1 150–950° K with $T_2 = 1\,150°$ K constant.
(*f*) Repeat for image with transposed core temperatures.

From these four results are derived the two required variations of R_d/T_1 at constant T_2, and R_d/T_2 at constant T_1, and these are set out in Fig. 8—a single curve being used to cover both characteristics. At every point on the curve the matrix has therefore two resistances of equal magnitude resulting from image temperature gradients but two different cathodic-core emitter temperatures. The resistance of the valve is therefore independent of the core-emitter temperature over a range of some 200°—corresponding to a hundredfold change in core emission.

A second example using method (*b*) is shown in Fig. 9. The technique is exactly the same as for (*a*), except that V_{H1} and V_{H2} are transposed instead of T_1 and T_2. The range of the measurement has been extended, and it will be apparent from the characteristic of variable cathodic-core heater voltage that the two curves

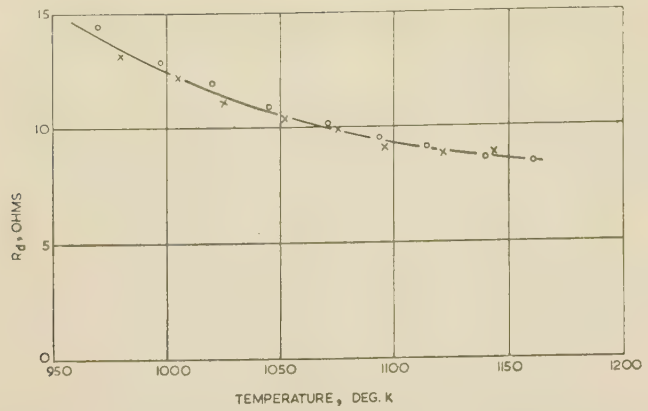

Fig. 8.—Image resistance under image temperature gradients: case A.
× × × T_1 constant; T_2 variable.
○ ○ ○ T_1 variable; T_2 constant.

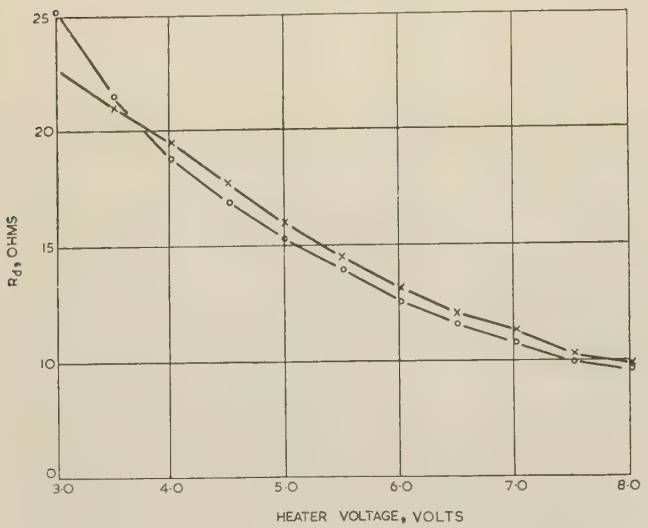

Fig. 9.—Image resistance under image temperature gradients: case *B*.
× × × V_{H1} constant; V_{H2} variable.
○ ○ ○ V_{H1} variable; V_{H2} constant.

diverge when V_{H1} falls to 3·5 volts. This effect is always observed and is probably due to reduction in the space-charge smoothing factor of the cathodic-core emitter.

(3.4) Approach to Maximum-Resistance State

It was concluded in Section 3.2 that the standard S-valve with an effective core emitter but with a zero-emission matrix should have a maximum resistance of about 100 ohms. The approach to this condition can be examined by applying a temperature gradient in such a way that the emission in the matrix adjacent to the anodic core approaches zero. A standard S-assembly is arranged with its cathodic-core emitter temperature, T_1, constant at 980° K while the anodic-core temperature, T_2, is varied between 1 150 and 650° K. The characteristic of R_d/T_2 at constant T_1, derived in the usual way, is set out in Fig. 10. As T_2 falls from 1 150° K, R_d rises at increasing rate up to a maximum rate at 890° K, where it remains constant down to 760° K. Further decrease of T_2 leads to a steady decrease in the rate of rise, and the general appearance of the curve suggests an asymptotic approach to a limiting resistance of 60 ohms. The bulk of this resistance must be in the cold half of the matrix, and it seems reasonable to suggest that the resistance of the whole matrix in a cold state is likely to be about 120 ohms.

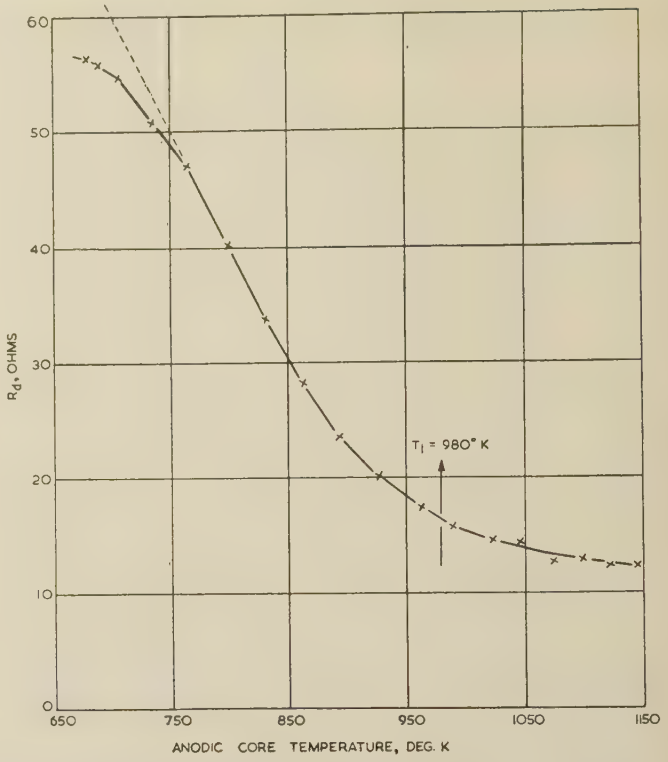

Fig. 10.—Showing approach to constant resistance with decrease of matrix temperature.
T_1 = 980° K constant.

(3.5) Positive Functions of the Matrix

Experiment has shown that the oxide cathode is a combination of two distinct entities—the thin-film core emitter and the bulky porous overlay—each capable of acting in isolation from the other. The core emitter is clearly essential to valve action, but the overlay so far appears to do little but act as the equivalent of a power-absorbing series resistance. In fact, the matrix serves two very necessary purposes, namely maintenance and protection of the core emitter.

The thin-film emitter operating at 1 020° K is vulnerable to wastage by evaporation, and it is perhaps the principal function of the oxide overlay to replace this loss as fast as it occurs by counter-evaporation. The common oxide cathode is thus a dispenser system with its essential thin-film emitter constantly renewed from the massive reserves of the overlay.

The second purpose of the overlay is to protect the film emitter from gas entering the cathode from the surrounding vacuum. To reach the core emitter the gas must work its way through the pore system, and it is reasonable to suppose that a high-density matrix will be more difficult to penetrate than a low-density one. Work by R. W. Lawson at Dollis Hill supports this view, and Fig. 11 shows the response to a common oxygen attack by two similar diodes occupying the same glass envelope—that with a matrix density of 0·61 showing much greater ability to withstand the attack than that with a density of 0·43. A further protective influence arises from the ability of the matrix to convert all gas within its pores to the negative ion state. The passage of a current through the matrix therefore tends to move gas away from the core emitter.

(3.6) Role of the Electron-Exit Boundary of the Matrix

The electron-exit boundary of the matrix appears to play no part in the operation of a conventional diode, apart from the

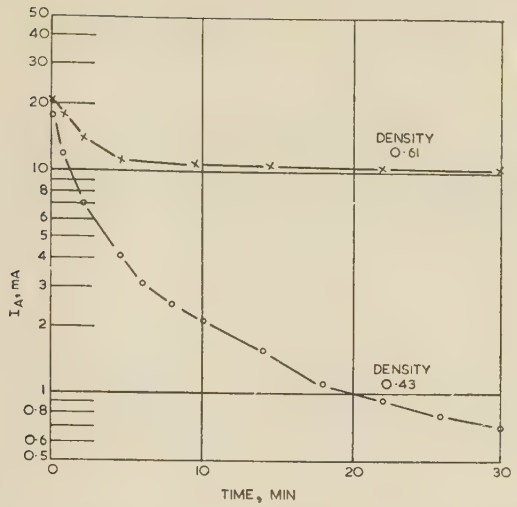

Fig. 11.—Influence of matrix density on resistance of cathode to oxygen attack.

Common pressure = 2×10^{-6} mm Hg.
Common cathode temperature = 1 150° K.

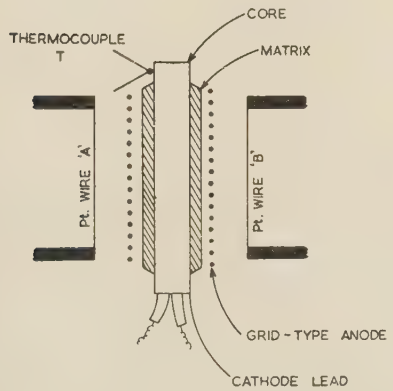

Fig. 12.—Schematic of experimental assembly for surface deposition of platinum.

passive one of providing holes for the escape of electrons from the interior. Complete suppression of electron emission from all visible parts of an oxide cathode should therefore have no influence on the conductance of a conventional valve, and Fig. 12 shows an experimental valve designed to test this assertion. An active-nickel-core cathode with the normal double-oxide matrix was set up as a diode with an open grid-type electron collector. After the usual vacuum processing, a voltage/current characteristic was measured with the cathode core set to 985° K with the aid of the thermocouple T. Two fine platinum wires A and B were then heated electrically to such a temperature and for such a time as to evaporate a grey film of platinum metal on all visible parts of the oxide cathode surface. The platinum wires were then cooled and the oxide cathode was given a brief reactivation treatment to recover it from the gas attack inseparable from the act of bringing the platinum wires close to their melting point. The cathode core was finally set again at 985° K with the aid of the thermocouple, and the voltage/current characteristic was remeasured. The diode conductances before and after platinum deposition are set out in Fig. 13 and seem to be identical.

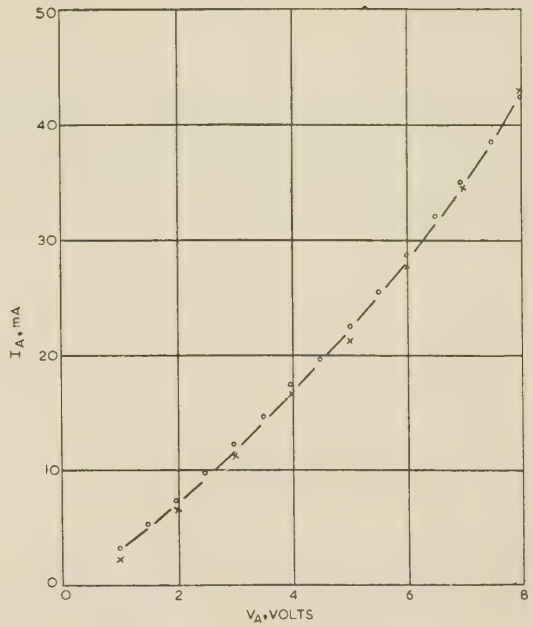

Fig. 13.—Voltage/current characteristic before and after surface deposition of platinum.

Common core temperature = 985° K.
× × × Before.
○ ○ ○ After.

It is assumed that thermionic emission from the surface deposit of platinum at 985° K is negligible. The appearance of the cathode surface before and after deposition is shown in Fig. 14.

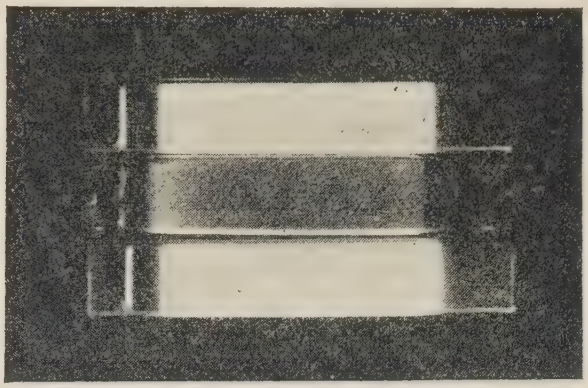

Fig. 14.—Appearance of cathode surface after deposition of platinum.

The outer cathodes are included for comparison, and show cathodes processed normally.

(4) CONCLUSIONS

The present Part may now be summarized in the form of the following conclusions, which are drawn up on the assumption that the whole of the diode current passes vacuum-wise through the hollow pores of the matrix in the temperature range 900–1 100° K.

(*a*) The common oxide cathode has two distinct functional components—the thin-film core emitter and the relatively massive porous matrix overlay. The two components can be physically separated and shown to act independently and in isolation.

(*b*) The core emitter determines the total or temperature-limited emission from the cathode.

(*c*) The matrix overlay determines the voltage rise between core surface and electron-exit-boundary.

(*d*) The voltage gradient through the matrix is determined only by the electron density arising within the matrix as a result of pore-wall thermionic emission. The gradient is largely independent of the level of total emission from the core emitter, provided that this is sensibly larger than the current traversing the matrix.

(*e*) The electron-exit boundary of the matrix plays no active part in the phenomenon of valve conductance, apart from keeping thermal emissivity as low as convenient.

The 5% element of the current which is known to travel the matrix by way of a solid semi-conduction path will, of course, modify these conclusions to some small extent.

(5) ACKNOWLEDGMENT

Acknowledgment is made to the Engineer-in-Chief of the Post Office for permission to make use of the information contained in the paper. The author also wishes to thank Mr. H. Batey for skilled assistance throughout the work.

621.376.223

The Institution of Electrical Engineers
Monograph No. 290 R
Feb. 1958
©

A RECTIFIER MODULATOR WITH STABLE LOW CARRIER-LEAK

By E. HANDS, M.Sc., Graduate.

(*The paper was first received 22nd July, and in revised form 15th November, 1957. It was published as an* INSTITUTION MONOGRAPH *in February, 1958.*)

SUMMARY

The paper is concerned with the development of a modulator capable of giving much lower stable levels of carrier leak than previously obtained. After consideration of various types of modulator, the conclusion is reached that the constant-current modulator, originally proposed by Cooper, is probably capable of giving the highest stable level of carrier rejection. This modulator consists, essentially, of a ring modulator whose input transformer is, ideally, replaced by infinite-impedance valve generators feeding each rectifier input terminal.

The action of the constant-current modulator is analysed in detail on the basis of small differences in the characteristics of the rectifying elements, and associated topics are discussed. Experimental evidence, obtained using a carrier frequency of 3 kc/s, is given which, to a considerable degree, supports the theoretical analysis.

The modulator, thus developed, is capable of giving carrier leak levels more than 90 dB below the carrier current from each source which are stable with temperature and time. Also, the action of the modulator is such that the fundamental component of the carrier leak is not affected by relatively large unbalances in the carrier currents from each source.

(1) INTRODUCTION

The action of any amplitude-modulating system is essentially to produce outputs of additive combinations of carrier and signal frequencies and their harmonics. Thus, if the carrier and signal frequencies are denoted by f_c and f_s respectively, the output is of the form $\Sigma(nf_c \pm mf_s)$, where n and m are zero or integers. In many cases, however, only the sidebands, $f_c \pm f_s$ are required, so that all other output components must be removed. The carrier-frequency harmonics and their associated sidebands are easily removed by simple filters, leaving only the output of carrier frequency to be removed. The complexity of filters for this purpose rapidly increases when the signal extends to low frequencies, owing to the difficulty of separating f_c and $f_c + \delta f$. Thus a modulator circuit which inherently rejects the output of carrier frequency is desirable. Such a device is called a *balanced modulator*.

All balanced-modulator circuits depend for their action on the exact similarity of at least two modulating elements, and since these must be non-linear, such an exact similarity is impossible to achieve in practice so that there is some residual output of carrier frequency. This is termed *carrier leak*.

Many different rectifier-modulator circuits have been proposed and used for obtaining low levels of carrier leak. Most of these are elaborations of the basic series, shunt and ring modulators, mainly the latter. Each of these basic modulators produces approximately the same carrier-leak voltage under given conditions of carrier voltage, rectifier characteristics, etc.,[1] but the ring modulator, having the highest efficiency, is capable of giving a higher ratio of wanted sideband output to carrier leak.

The basic circuit of the ring modulator is shown in Fig. 1. A simple description of the action of the circuit is obtained by assuming that the rectifiers have a finite, constant forward resistance and an infinite reverse resistance, and that the carrier voltage is large compared with that of the signal so that the condition of the rectifying elements is determined solely by the polarity of the carrier. Thus on alternate carrier half-cycles either rectifiers 1 and 3 or 2 and 4 are conducting and the signal in the output transformer alternates in polarity at the carrier frequency. The signal is thus, ideally, multiplied by a perfect square wave, or, more precisely, the modulating function is a square wave. If the circuit resistances in the two possible carrier paths (there will always be two rectifiers with infinite resistance) are equal, the carrier currents in each half of the output transformer will be equal and in antiphase. Thus there will be no output of carrier frequency, and the modulator is therefore balanced.

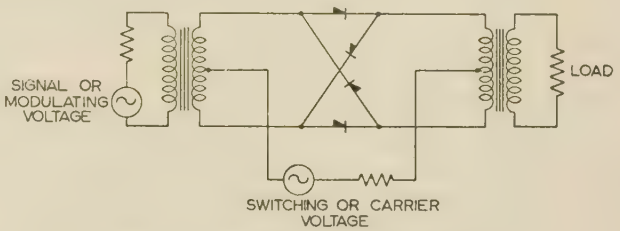

Fig. 1.—Basic ring-modulator circuit.

Owing to the non-ideal characteristics of practical modulating elements, the shape of the modulating function in an actual modulator lies between a square wave and a sine wave (or the waveform of the carrier, if the latter is non-sinusoidal), and, as the characteristics of rectifiers vary from sample to sample, the basic circuit is incapable of giving complete balance to the carrier.

The carrier leak is mainly dependent on the difference in forward resistance of the rectifiers; the only requirement for the reverse resistance is that it should be sufficiently high for its effect to be neglected. If rectifiers are used which have a ratio x between maximum and minimum forward resistance, and if the carrier source resistance is large compared with the rectifier forward resistance, it can be shown that the maximum fundamental component of carrier leak to be expected is given by

$$V_{cl} \simeq \frac{2}{\pi} V_c(x - 1) \quad . \quad . \quad . \quad . \quad . \quad (1)$$

where V_c is the carrier voltage appearing across the rectifiers.[1] For balanced-modulator applications, rectifiers may be obtained which are selected so that their forward resistances lie within a range of $\pm 5\%$, making x equal to 1·1. Using such rectifiers, therefore, it is possible to obtain a fundamental component of leak equal to 0·064 V_c; i.e. the fundamental leak is approximately 24 dB below V_c.

In general, the output which is of interest is that of one first-order sideband, and allowing for a normal overall conversion loss, this output would be approximately 6 dB below the input signal level, which must itself be considerably below the level of V_c owing to the requirements of linearity. Thus, in such a case,

Correspondence on Monographs is invited for consideration with a view to publication.

The paper is based on a thesis submitted for the degree of Master of Science at the University of Birmingham.

Mr. Hands is in the Department of Electrical Engineering, University of Birmingham.

the carrier leak would be less than 18 dB below the level of the sideband output.

There are, however, ways of improving this balance; for example, it is common practice, having sorted rectifiers into groups with $\pm 5\%$ forward resistance, to select further from these groups, by means of trial-and-error substitution, sets of four rectifiers giving low carrier leak. The leak may be further reduced by the interposition of variable voltage-dividers in the ring.[2] These voltage dividers can be adjusted to balance the rectifier forward resistances, thus effectively making x closer to unity and hence reducing the carrier leak. The carrier leak cannot be completely eliminated as the forward resistances can only be balanced at one point in the cycle.

With such processes, it is possible to obtain a fundamental component of carrier leak which is of the order of 60 dB below the level of V_c. However, the dependence of the leak on variations in the rectifier characteristics remains unchanged; i.e. if these variations are such as to cause the rectifiers to have a ratio of maximum to minimum forward resistance of x, eqn. (1) will apply. Considering only temperature effects, it is quite possible for the difference in the temperature coefficients of the four rectifiers to be 1% per deg C, so that a change in temperature of 1° C would suffice to worsen the leak from 60 dB to 45 dB below the level of V_c. It is clear from this example that the stability of highly balanced ring modulators is indeed doubtful. The many variations of the ring modulator which have been developed to reduce the carrier leak all suffer in a similar manner from the effects of variation of forward resistance, and although higher degrees of balance have been obtained, they are only suitable for applications requiring short-term stability.

To obtain a modulator which is capable of a very high degree of carrier balance, with good long-term stability, a method must be used which eliminates, as far as possible, the first-order dependence of the leak upon these variations in forward resistance. A method proposed by Cooper[3] of overcoming this dependence is capable of achieving a large measure of success, and the present paper is a report of a detailed study of it. The circuit is reproduced here for convenience and is shown in Fig. 2. It

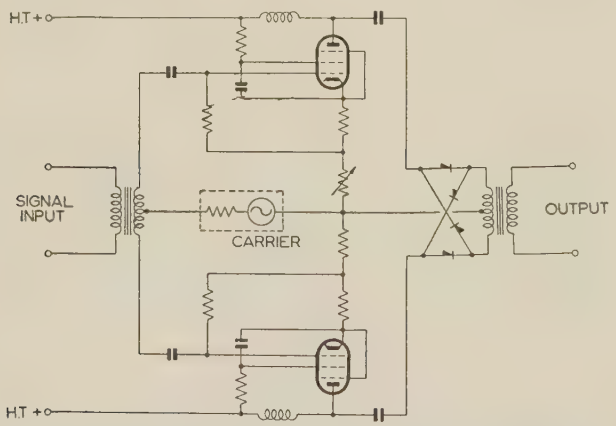

Fig. 2.—Cooper's constant-current modulator circuit.

consists, essentially, of a ring modulator whose input transformer is replaced, ideally, by infinite-impedance valve circuits feeding each rectifier input terminal. Thus, throughout the major part of the cycle, the carrier currents in each half of the primary winding of the output transformer are independently controlled and should therefore be capable of balance by adjustment of the input currents. In the region of the carrier zeros, all four rectifiers become of comparable resistance, and accordingly the constant-current feature is lost for a small fraction of the cycle.

A theoretical analysis of the constant-current modulator is given in the following Section, and experimental results are discussed in Section 3. The latter were obtained at a frequency of 3 kc/s, so that the effects of parasitic capacitances (which are not discussed in the theory) were very small. The capacitances between the output terminals of the drives and earth, owing to their effect on the output impedance of the drives, are more important than the rectifier internal capacitances. It appears that the operation of the circuit would not be greatly affected below frequencies of the order of hundreds of kilocycles per second.

(2) THEORETICAL ANALYSIS

(2.1) Leak at Carrier Peaks

This theoretical analysis is obtained on a basis of small differences in the characteristics of the four rectifiers.

An expression for the instantaneous carrier leak of a constant-current modulator can be obtained by assuming a completely different characteristic for each of the modulating elements. This expression is, however, too complex to have any real value and the case will therefore be considered where three of the rectifiers have exactly similar characteristics and the fourth has a slightly different one. By using the results obtained, the leak waveform in the worst possible case for rectifiers whose characteristics lie within given limits may be evaluated, as will be shown later.

Three main assumptions are made, namely:

(*a*) The impedance of the carrier generators is infinite.
(*b*) The currents from each generator are exactly equal in magnitude and phase.
(*c*) The primary winding of the transformer may be regarded as a short-circuit to the carrier currents.*

If rectifier 1 of Fig. 3 is the one with the odd characteristic, the circuit at any instant can be represented as in Fig. 4. The

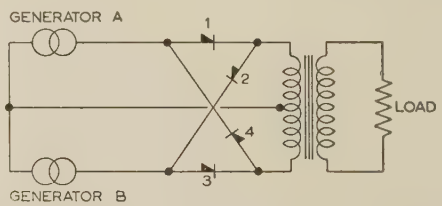

Fig. 3.—Equivalent circuit of constant-current modulator.

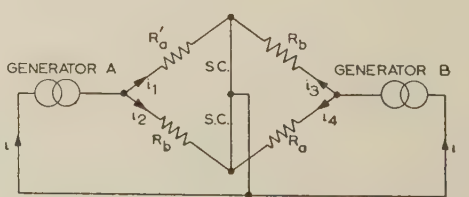

Fig. 4.—Equivalent circuit of constant-current modulator using one rectifier with characteristics different from those of the others.

instantaneous unbalance current in the output transformer is given by

$$i_u = (i_1 - i_2) + (i_3 - i_4)$$

and subsequently, defining the unbalance current ratio, u, as

* The actual impedance seen is dependent upon the ratio of the carrier currents in each half of the primary winding, and if this ratio is not greatly different from unity the assumption of a short-circuit is justifiable. The ratio will be furthest from unity at the carrier zeros, but here the rectifier resistances are large so that any departure from a short-circuit would have negligible effect. A more detailed treatment of the output transformer is given in Appendix 2 of Reference 6.

the ratio i_u/i, where i is the instantaneous carrier current, it can be shown that

$$u = \frac{2R_b(R_a - R_a')}{(R_a + R_b)(R_a' + R_b)} \quad . \quad . \quad . \quad . \quad (2)$$

The unbalance current ratios at the peak values of the carrier current can be expressed in terms of the rectifier forward and reverse resistances, r_f and r_b.

Carrier peak when rectifier 1 *is in its forward condition.*

For this, r_f is substituted for R_a, r_{f1} for R_a', and r_b for R_b.

Hence $$u_f = \frac{2r_b(r_f - r_{f1})}{(r_f + r_b)(r_{f1} + r_b)} \quad . \quad . \quad . \quad . \quad . \quad (3)$$

As r_b is normally very much greater than r_f,

$$u_f \simeq \frac{2(r_f - r_{f1})}{r_b}$$

Or, if there is a small difference $\Delta_f r_f$ between r_f and r_{f1}, the expression becomes

$$u_f \simeq 2\Delta_f \frac{r_f}{r_b} \quad . \quad . \quad . \quad . \quad . \quad . \quad (4)$$

Carrier peak when rectifier 1 *is in its reverse condition.*

Substituting r_b for R_a, r_{b1} for R_a', and r_f for R_b, and using $\Delta_b r_b$ as the difference between r_b and r_{b1},

$$u_b \simeq 2\Delta_b \frac{r_f}{r_b} \quad . \quad . \quad . \quad . \quad . \quad . \quad (5)$$

The results for u_f and u_b illustrate a very important principle, namely that the matching of the reverse resistances of the rectifiers is just as important as that of the forward resistances. In practice, Δ_b is likely to be much greater than Δ_f and will usually be the more important cause of carrier leak. This result, being opposite to that for the ring modulator, is one of the effects of constant-current operation. Furthermore, the results contain a factor r_f/r_b which is absent in the ring-modulator results. As this ratio is normally of the order of 4×10^{-4}, the advantages of the constant-current modulator are already apparent. It should be noted that Δ_f is synonymous with the factor $(x - 1)$ appearing in eqn. (1).

(2.2) Leak near Carrier Zeros

In an experimental constant-current modulator described by Tucker,[1] the output waveform contained narrow peaks of relatively large amplitude in the region of the carrier zeros. These peaks were attributed to the loss of constant-current operation in these regions due to all four rectifiers assuming the same order of resistance, as explained by Cooper.[3] The peaks were also thought to contain the major portion of the leak output energy. This explanation is not entirely satisfactory, as the carrier current in the region of the peaks is very small, so that to produce such peaks the unbalance current ratio would have to be very large.

An approximate idea of the behaviour near the carrier zeros can be obtained by assuming the rectifiers to obey an exponential law of resistance versus voltage. It has been suggested that, at and near cross-over, the rectifier resistance may be very closely represented by

$$r = r_0\varepsilon^{-bV}$$

This law is discussed fully in Reference 4. One of the useful features of the law is that, for most rectifiers of the same type, the index b tends to be constant and differences in rectifier characteristics are caused by variations in r_0.

In order to obtain a theoretical result for the leak, it is assumed that the voltages across all four rectifiers are equal. This is not entirely compatible with the idea of constant-current operation, but if the assumption is not made, V becomes a function of rectifier resistance and current and the expressions become unmanageable. It will be appreciated that the assumption becomes more accurate towards the carrier peak when the odd rectifier is in its reverse condition, and least accurate towards the other carrier peak.

Substituting $r_0\varepsilon^{-bV}$ for R_a, $r_0'\varepsilon^{-bV}$ for R_a', and $r_0\varepsilon^{bV}$ for R_b in eqn. (2), and defining $\Delta_0 r_0$ as $r_0 - r_0'$, then

$$u = \frac{\Delta_0}{\cosh bV(2\cosh bV - \Delta_0\varepsilon^{-bV})} \quad . \quad . \quad . \quad (6)$$

The unbalance current is given by the product of u and i, the instantaneous carrier current. The circuit in each constant-current output consists of two rectifiers back-to-back, whose parallel resistance is given by $r_0/(2\cosh bV)$, neglecting the effect of Δ_0 in this case. Hence the current from each source is approximately given by

$$i = \frac{2V\cosh bV}{r_0} \quad . \quad . \quad . \quad . \quad . \quad . \quad (7)$$

The instantaneous unbalance current is therefore

$$i_u = \frac{2\Delta_0 V}{r_0(2\cosh bV - \Delta_0\varepsilon^{-bV})} \quad . \quad . \quad . \quad (8)$$

Assuming that eqn. (8) cannot be solved for V analytically, the method of obtaining the variation of i_u with i consists in calculating the variation of i_u with V from eqn. (8) and, using eqn. (7), evaluating i for each value of V. Fig. 5 shows the

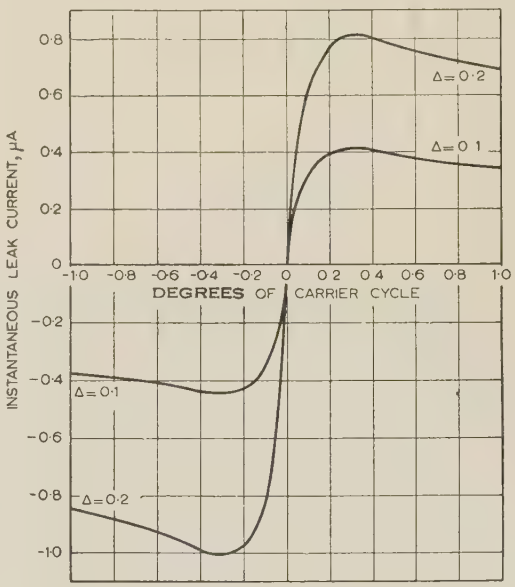

Fig. 5.—Leak waveform near the carrier zero.

Calculated from the theoretical law $r = r_0\varepsilon^{-bV}$, for the case of one unbalanced rectifier and sinusoidal carrier of 5 mA peak.
$b = 16$; $r_0 = 10$ kilohms.

variation of i_u with degrees of cycle for a peak carrier current of 5 mA and with typical values of b and r_0 as 16 and 10 kilohms, respectively. It is apparent from these curves that there is a maximum value of unbalance current which occurs at about 0·3° of the carrier cycle. As Δ_0 is increased further, i.e. above 0·5, there is a tendency for the maximum to occur later in the

cycle, but over the range considered the position of the maximum is practically independent of Δ_0. Also, the term $\Delta_0\varepsilon^{-bV}$ in eqn. (8) is only important at angles below 0·1° for the positive half-cycle, so long as Δ_0 is less than 0·5; hence, for positive carrier,

$$i_u \simeq \frac{\Delta_0 V}{r_0 \cosh bV} \quad . \quad . \quad . \quad . \quad . \quad . \quad (9)$$

On the negative carrier half-cycle, the term $\Delta_0\varepsilon^{-bV}$ becomes $\Delta_0\varepsilon^{bV}$, and as $\cosh(-bV) = \cosh bV$, from eqn. (8),

$$i_u \simeq \frac{2\Delta_0}{r_0(2\cosh bV - \Delta_0\varepsilon^{bV})} \quad . \quad . \quad . \quad (10)$$

Over the range considered, $\Delta_0\varepsilon^{-bV}$ is small, so that $\Delta_0\varepsilon^{bV}$ is effectively equal to $2\Delta_0 \cosh bV$, and hence, from eqn. (10), for negative carrier,

$$i_u \simeq \frac{\Delta_0 V}{r_0(1-\Delta_0)\cosh bV} \quad . \quad . \quad . \quad . \quad (11)$$

By differentiating eqns. (9) and (11), the maximum values of i_u and their positions in the cycle may be obtained. For positive carrier, the peak value of unbalance current is $0{\cdot}663\Delta_0/br_0$ amp and this occurs at a carrier current of $4{\cdot}35/br_0$ amp; for negative carrier, the peak value of unbalance current is $0{\cdot}663\Delta_0/br_0(1-\Delta_0)$ and the position is as for positive carrier.

The magnitudes of these peaks of unbalance current and the carrier current at which they occur are seen to be independent of the peak value of carrier current. This is to be expected, since the effect of increasing carrier current should be to contract, in time, those parts of the leak waveform near the carrier zero and to insert new parts in the region of the carrier peaks.

The results obtained from this exponential analysis can be compared with those obtained for the unbalance currents at the carrier peaks by considering typical values for the various parameters. Typical parameters for germanium rectifiers are: $r_f = 100$ ohms, $r_0 = 10$ kilohms, $r_b = 300$ kilohms, and $b = 16$. Assuming that $\Delta_f = \Delta_b = \Delta_0 = \Delta$, and that the carrier current is 5 mA peak (a normal value), the following results are obtained:

Unbalance current at carrier peaks	$3{\cdot}33\Delta\,\mu$A
Peak unbalance current near carrier zeros ..	$4{\cdot}14\Delta\,\mu$A

As a check on these results, and to investigate the intermediate region between carrier zero and carrier peak, the leak current has been calculated using eqn. (3) and taking the values of r_f and r_b from actual rectifier characteristics. The characteristics used are (*a*) the geometric mean between the 67% sample limits of a batch of germanium rectifiers, and (*b*) the median of the distribution curves of a batch of 50. The resistances at ± 1 volt are respectively (*a*) 100 ohms, 100 kilohms, and (*b*) 180 ohms, 220 kilohms. The unbalance has been achieved, in each case, by using three rectifiers with these characteristics, and subtracting 10% of the resistance at each voltage to obtain the characteristic of the fourth rectifier, thus obtaining a constant value of Δ of 0·1. Compared with the exponential law, this is equivalent to subtracting 10% from the value of r_0. The calculated variations of unbalance current with carrier current are shown in Fig. 6, which also includes, for comparison, the relevant portion of the variation near carrier zero, calculated using the values of b obtained from these characteristics, in the exponential law.

The absence of any definite peaks near the carrier zeros in the waveforms obtained from actual rectifier characteristics is probably due to the variation in the index b. This diminishes rapidly in the reverse direction and has a tendency to rise, initially, in the forward direction. Fig. 7, which shows the

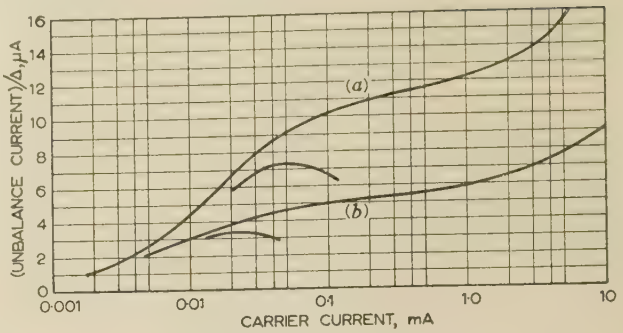

Fig. 6.—Variation of instantaneous unbalance current for the case of three similar rectifiers and one differing by a constant fraction.

The leak near cross-over, calculated using $r = r_0\varepsilon^{-bV}$ is partially shown. (*a*) and (*b*) refer to characteristics given in Section 2.2.

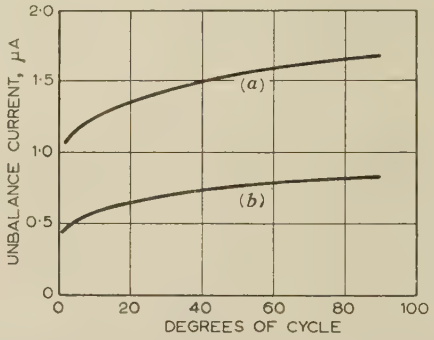

Fig. 7.—Variation of unbalance current over the carrier cycle for a sinusoidal carrier current of 5 mA (r.m.s.).

leak waveform for a carrier current of 5 mA r.m.s., calculated from Fig. 6, indicates that the carrier leak is of fairly constant magnitude throughout the half-cycle.

This analysis of the leak in the region of the carrier zeros indicates that, although peaks in the unbalance current in this region may exist, their magnitude is insufficient to explain the type of waveform obtained in practice.

(2.3) Effect of Unbalance in Carrier Currents

Cooper[3] proposed that it should be possible to balance the modulator by adjusting the magnitude of the current from one driving circuit. Experimental evidence has shown, however, that, although the even harmonics of the carrier leak are altered by such an adjustment, the magnitudes of the fundamental and odd harmonics remain substantially unchanged even with relatively large unbalances—of the order of 10%—of the carrier currents. An approximate idea of this action may be obtained as follows.

Consider, for example, that the resistance of the dissimilar rectifier is low; then, if the carrier currents are equal, too much current will flow through this rectifier and too little through the normal rectifier which is effectively in parallel with it and biased in the opposite direction. If, now, the carrier current from one source is reduced to counteract the excess of current in the dissimilar rectifier, the current flowing through the parallel rectifier will become still less than normal. Thus, there would be an alteration in leak waveform such that the instantaneous leak current would be reduced at one carrier peak and increased at the opposite one.

A more precise analysis is obtained by reconsidering the circuit of Fig. 4 with different carrier currents, i_a and i_b, such

that $i_a - i_b = \delta i_a$. By similar methods of analysis, an equation for the unbalance current ratio is obtained, namely

$$u = \frac{(R_a R_b - R_a' R_b)(2 - \delta) + (R_b^2 - R_a R_a')\delta}{(R_a + R_b)(R_a' + R_b)} \quad . \quad (12)$$

Considering the carrier peak when rectifier 1 is in its forward condition, using the same notation as before and assuming that $r_f \ll r_b$,

$$u \simeq \Delta_f \frac{r_f}{r_b}(2 - \delta) + \delta. \quad . \quad . \quad . \quad . \quad . \quad (13)$$

Considering the opposite carrier peak, the expression for u is found to be

$$u \simeq \Delta_b \frac{r_f}{r_b} \frac{(2 - \delta)}{(1 - \Delta_b)} - \delta \quad . \quad . \quad . \quad . \quad . \quad (14)$$

Thus, if δ is small so that $(2 - \delta)$ is approximately 2, altering δ to reduce u in eqn. (13) will increase u by an equal amount in eqn. (14), and vice versa. Therefore, whilst it is possible to reduce the magnitude of the leak at one carrier peak, its magnitude at the other peak is increased by a similar amount, and the amplitude between these points on the leak waveform remains unchanged. This statement will be true to an extent which depends on the validity of the assumption that $r_f \ll r_b$ at parts of the cycle away from the carrier peaks, so that a waveform is obtained which is quite closely specified by the relationship

$$i_u(\theta) - i_u(\theta + \pi) = C(\theta) \quad . \quad . \quad . \quad . \quad . \quad (15)$$

where $C(\theta)$ is a function of θ, but is constant at a given value of θ, regardless of the value of carrier current. By the use of a Fourier technique it is possible to show (*a*) that the magnitude of the even harmonics does not affect the condition of eqn. (15), and (*b*) that, if the magnitudes of the odd harmonics remain unchanged, the condition of eqn. (15) is satisfied. However, to prove the converse of these results, a further condition specifying the waveform seems to be required. In any event, it is clear from these results that the odd harmonics, if altering at all, will alter much less than the even harmonics.

(2.4) Maximum Leak to be expected in General Case

This Section deals with the case where the characteristics of the four rectifiers in the constant-current modulator lie within a given range. The maximum leak will be obtained with the appropriate combination of rectifiers whose characteristics lie on one or other of the extremes of this range. One such combination is found to be when rectifiers 1 and 2 (Fig. 3) lie on the high extreme, and rectifiers 3 and 4 lie on the low extreme, in both forward and reverse conditions.

For most of the rectifier data studied, it is apparent that the fractional difference between the upper and lower limits of the rectifier characteristics assumes two reasonably constant values, Δ_f and Δ_b. The use of this assumption enables a simple expression to be obtained for the maximum expected leak.

Considering the carrier half-cycle when rectifiers 1 and 3 are in their forward condition, those rectifiers which lie on the lower limit, namely 3 and 4, are fed from different sources but drive the same end of the output transformer. Thus, if rectifiers 1 and 2, whose characteristics lie on the upper limit, are considered to be normal, each low-resistance rectifier, i.e. 3 and 4, can be considered to be a case of one unbalanced rectifier, and the resulting leak will be the sum of two such cases, given by

$$u = 2\frac{r_f}{r_b}(\Delta_f + \Delta_b)$$

On the opposite half-cycle, the leak will be given by the same expression but of opposite sign.

Neglecting, temporarily, any effects near the carrier zeros, it is clear that the leak waveform will lie within a square wave of peak-to-peak amplitude given by

$$4\frac{r_f}{r_b}(\Delta_f + \Delta_b) i_{max}$$

where i_{max} is the peak value of carrier current. Thus the maximum r.m.s. value of the fundamental component of carrier leak using such rectifiers would be given by

$$\frac{8}{\pi}\frac{r_f}{r_b}(\Delta_f + \Delta_b) I \quad . \quad . \quad . \quad . \quad . \quad (16)$$

where I is the r.m.s. carrier current from each source.

(2.5) Evaluation of Δ_f and Δ_b from Rectifier Characteristics

If the regions near the carrier zeros are neglected, the rectifier configuration in the constant-current modulator can, to a first approximation, be divided, as far as currents and voltages internal to the configuration are concerned, into two pairs of parallel back-to-back rectifiers. The voltage across such a pair of rectifiers is determined by their parallel resistance, which will, over most of the carrier cycle, be quite closely equal to the resistance of the rectifier which is in its forward condition. Thus, if the resistance of the latter rectifier is known for any current, the voltage across the rectifier which is in its reverse condition will be known for that current, so that the characteristics required are forward-resistance/current and reverse-resistance/voltage. The value of Δ_f can then be taken as the fractional difference of the forward-resistance/current characteristic. The value of Δ_b, however, is not so easy to determine, as neither the voltages nor the currents are the same for the two rectifiers which are in the reverse condition. It is clear that the voltages across them are more nearly equal than the currents through them, and as the resistance/voltage characteristic of a rectifier usually tends to flatten off in the reverse direction, it should be sufficiently accurate to take Δ_b as the fractional difference of this characteristic.

Rectifier forward characteristics are rarely given in the form of resistance/current, but are often given as resistance/voltage, so that it is of interest to know the relationship between the fractional tolerances of these characteristics. The evaluation of this relationship is facilitated by using the law $R = AI^{-2/3}$, where R is the rectifier resistance, A is a constant for a given rectifier, and I is the current through the rectifier. This law is found to hold quite accurately for forward currents greater than 10 μA, but it cannot be modified or extended to cover the reverse range. Differences in rectifier characteristics are usually due to differences in the constant A, rather than any change in the index. It follows from this law that the forward-resistance/voltage relationship is $R = A^3 V^{-2}$.

Consider two rectifiers obeying these laws, one a normal rectifier and the other low in resistance owing to a lower value of the constant, and assume this new constant is $(1 - \delta)A$. It is evident that, if δ is small so that $(1 - \delta)^3$ is approximately $(1 - 3\delta)$, the difference in the resistance of the two rectifiers, measured at the same voltage, will be approximately three times that measured at the same current. Thus Δ_f will be of the order of one-third of the fractional difference taken from the forward-resistance/voltage characteristic. This is a separate advantage of using constant-current operation; not only does the constant-current modulator give a lower level of carrier leak than a ring modulator using the same rectifiers, but also the forward fractional difference of the rectifiers is effectively improved.

The resistance/voltage characteristics of rectifiers usually show

a much larger fractional difference for the reverse condition than for the forward condition. This effect will be enhanced by the use of resistance/current characteristics, so that, for the constant-current modulator, it should normally be possible to neglect Δ_f in comparison with Δ_b when computing the leak.

A further result arising from the use of this power law is that the voltage across the rectifiers, over the major part of the cycle, will be given by

$$V = A^3 i^{1/3}$$

where i is the instantaneous carrier current. Thus this voltage is considerably more square in waveform than that of the carrier current. This result, coupled with the flattening of the resistance/voltage characteristic, increases the justification of obtaining Δ_b from this characteristic.

(2.6) Driving-Circuit Impedance Requirements

In order to assess the impedance requirements of the driving circuits, it is necessary to consider how the balance is affected by the values of these impedances. The circuit when the impedance of the driving circuits is not infinite is shown in Fig. 8. As before, the case is considered where rectifier number 1

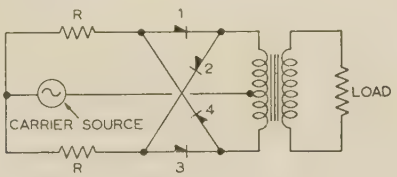

Fig. 8.—Modulator with separate finite-impedance sources.

has a dissimilar characteristic. The voltages applied to each driving circuit are assumed to be equal, and the transformer is considered to act as a short-circuit. The unbalance current is found to be

$$i_u = \frac{R_b(R_a - R_a')(R_b + 2R)\,V}{[R_a'R_b + R(R_a' + R_b)][R_aR_b + R(R_a + R_b)]} \qquad (17)$$

If the unbalance is small and if the driving-circuit impedance is large compared with the resistance of two back-to-back rectifiers, the currents from each source are approximately given by the relationship

$$V = i\left(R + \frac{R_aR_b}{R_a + R_b}\right)$$

Using this expression for V, an expression for u can be obtained:

$$u = \frac{i_u}{i} \simeq \frac{R_b(R_a - R_a')(R_b + 2R)}{[R_a'R_b + R(R_a' + R_b)][R_a + R_b]} \qquad (18)$$

If the driving-circuit impedance is very large so that $R \gg R_b$, eqn. (18) reduces to eqn. (2), where the driving-circuit impedances were considered infinite. Clearly, the requirement $R \gg R_b$ will be most difficult to meet when R_b represents a reverse resistance. Taking this case and assuming that $r_b \gg r_f$ and $R \gg r_f$, u is given by

$$u \simeq \Delta_f \frac{r_f}{r_b}\,\frac{r_b + 2R}{R} \qquad (19)$$

The minimum value of u is clearly obtained when R is infinite. A reasonable compromise might be to have $R = r_b$, when the leak would be 50% above its minimum value.

(3) EXPERIMENTAL RESULTS

(3.1) Modulator Circuit

A modulator constructed according to Cooper's circuit, using pentodes type EF 91, was found to be unsatisfactory owing to non-linearity in the driving circuits. When operated without rectifiers, i.e. with the driving circuits connected direct to the ends of the primary winding of the output transformer, and with a 600-ohm output load, a residual output of irregular waveshape, which, although capable of reduction to a level of 90 dB below the carrier level by resistive and capacitive balancing of the driving circuits, was not stable to 75 dB for more than 30 min. As a final carrier-leak level, when using rectifiers, of better than 90 dB below the carrier level was theoretically indicated, such a circuit was of little use. The use of triodes, instead of pentodes, was found to eliminate these non-linear effects, but unfortunately the use of a single triode in each driving circuit is insufficient to provide the required output impedance as discussed in Section 2.6. The final circuit developed, which is shown in Fig. 9,

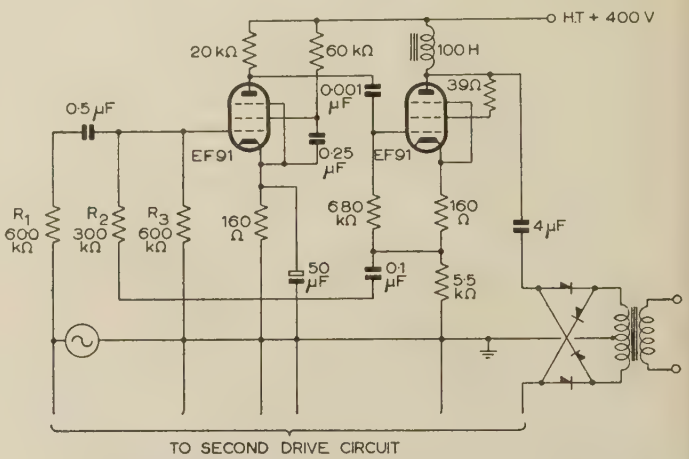

Fig. 9.—Modulator using two-valve drives.

consists of 2-stage driving circuits using triodes in the output stage. Feedback is taken from the cathode resistor of the output valve, via a resistive mixing circuit with phase adjustment, to the control grid of the input pentode. This circuit gave very satisfactory results and was used to obtain the experimental results given in this Section. The output impedance, calculated theoretically, was 28 megohms.

(3.2) Leak near Cross-over

The leak waveform initially obtained was similar to that described by Tucker,[1] in that large peaks occurred in the region of the carrier zeros. As such peaks are not indicated by the theoretical treatment, it is apparent that they are either the result of some reactive effect in the circuit or possibly due to minority-carrier storage in the rectifiers when switched from forward to reverse conditions. The latter effects are readily observed when the type of rectifier used is subjected to a 2-volt peak-to-peak square wave (rise time less than 30 millimicrosec), but are not apparent with sinusoids of frequency up to 250 kc/s. Owing to the one-third power law discussed in Section 2.5, the voltage waveform across the rectifiers of the constant-current modulator, using sinusoidal carrier, would be of the form $\sin^{1/3}\omega t$; thus the conditions at the carrier zero, as regards slope of waveform, may be approximated by using a constant-voltage source at three times the carrier frequency, i.e. 9 kc/s in this case. It is unlikely, therefore, that the cross-over peaks are due to minority-carrier storage.

Reactive effects could be produced either by the final-stage anode inductors or by the output transformer. In order to eliminate one of these unknowns, the output transformer was replaced by a differential amplifier whose input was taken from low-value resistors connected in place of the primary winding of

the output transformer. A differential amplifier for this purpose must be capable of meeting a very rigorous specification. Its rejection ratio, defined as the anti-phase gain divided by the in-phase gain, must be at least 90 dB, as the constant-current modulator was expected to give a possible carrier rejection of this order. The differential amplifier developed by Richards,[5] was modified by the use of valves of higher mutual conductance (EF 91) to extend the bandwidth to 100 kc/s in order to reproduce the cross-over peaks should they occur. By a certain amount of valve selection, a rejection ratio of over 90 dB was obtained, and the anti-phase gain, measured at 3 kc/s was 3 250. Owing to the high anti-phase gain, 15-ohm resistors in the modulator output were found to be sufficient for satisfactory operation. This value of resistance, when compared with the rectifier forward resistance, also approaches quite well the assumption of a short-circuit made in Section 2.

The use of the differential amplifier to replace the output transformer, while not completely eliminating the peaks in the carrier zero region, considerably reduced their magnitude.

A set of oscillograms showing the variation of leak waveform with variation in peak carrier current is reproduced in Fig. 10. The peaks in the carrier zero region increase with increase in carrier current. Now, if no reactive or minority-carrier storage effects were present, the effect of increasing the peak carrier current should be to compress, in time, those parts of the leak waveform near the carrier zeros, and to insert new parts in the region of the carrier peaks; thus the magnitude of the cross-over peaks should be unaffected by changes in peak carrier current. That this is not so again indicates an inductive effect which must now be due to the anode inductors. It is reasonable to suppose that if peaks occur without the output transformer, they would be, effectively, amplified with it. Another interesting feature of the oscillograms, is the 'squareness' of the leak waveform, disregarding the carrier zero regions, which agrees well with the theoretical treatment.

The four rectifiers used in the modulator, to obtain these oscillograms, were not well matched, having forward resistances at 10 mA ranging from 56 to 120 ohms, and reverse resistances at −1 volt ranging from 24 to 280 kilohms. When using selected rectifiers to obtain very low carrier leaks, as discussed later, the magnitude of these peaks relative to that of the mid-cycle leak, was much greater, but as the output leak agreed quite well with that predicted from rectifier characteristics using eqn. (16), it appears that the peaks contribute very little to the magnitudes

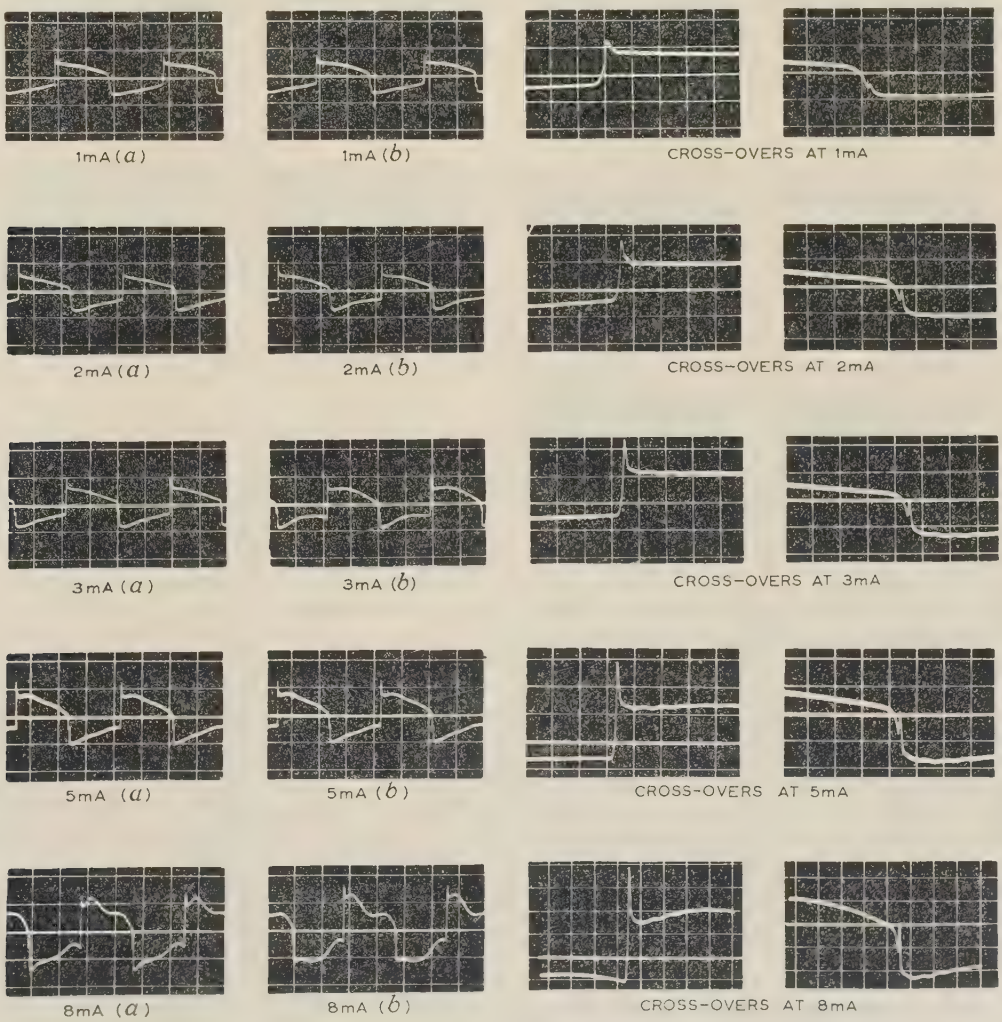

Fig. 10.—Waveform of carrier leak at various values of peak carrier current.

Oscillograms (*a*) and those for the cross-overs are with modulator balanced for minimum second harmonic at the stated current.
Oscillograms (*b*) are with modulator balanced for minimum second harmonic at a peak current of 5 mA.
Oscillograms of cross-overs have deflection sensitivity increased by 70% and time scale expanded ten times.

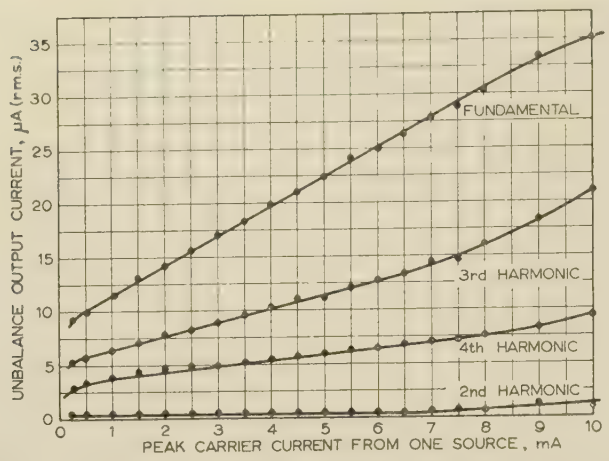

Fig. 11.—Variation of r.m.s. leak output current with peak carrier current.

of the lower harmonics of the leak output. Thus, for most practical purposes, it should be fairly safe to neglect the peaks and consider only the mid-cycle leak.

(3.3) Variation of Leak with Carrier Current

The oscillograms of Fig. 10 indicate that the value of the carrier current does not appreciably affect the setting of the generator balancing controls, as is evidenced by the waveforms (*a*) and (*b*). The variation of the fundamental and harmonic components of the leak when the modulator is balanced for minimum second harmonic at different carrier currents is shown in Fig. 11. From these results it is apparent that the carrier rejection improves slightly with increase of carrier current.

(3.4) Effect of Unbalance in Carrier-Drive Currents

The oscillograms of Fig. 12 show the effects of resistive and capacitive unbalance of the driving-circuit output currents on the leak waveform. The variation of the magnitudes of the d.c., fundamental, and harmonic components of this waveform is given in Fig. 13 as a function of drive-current unbalance. It is apparent from these results that the magnitudes of the d.c. and harmonic components are very sensitive to current unbalance, whilst those of the fundamental and third harmonics remain practically unchanged, even over the relatively large unbalance considered, namely $\pm 10\%$. These latter components do change a small amount, in such a manner that they are proportional to the sum of the carrier currents from each driving circuit. It seems, therefore, that the modulator achieves, inherently, a low value of carrier fundamental leak which is incapable of being reduced or increased by changes in the gains of the driving circuits. Thus the gain stability of these circuits is only important in the rare cases where balance to the second, or higher-order even harmonics, is required.

(3.5) The Use of a Balancing Voltage-Divider in the Output

In the conventional ring modulator, it is normal practice to insert a voltage divider between the two halves of the output-transformer primary winding, as is discussed in the Introduction.

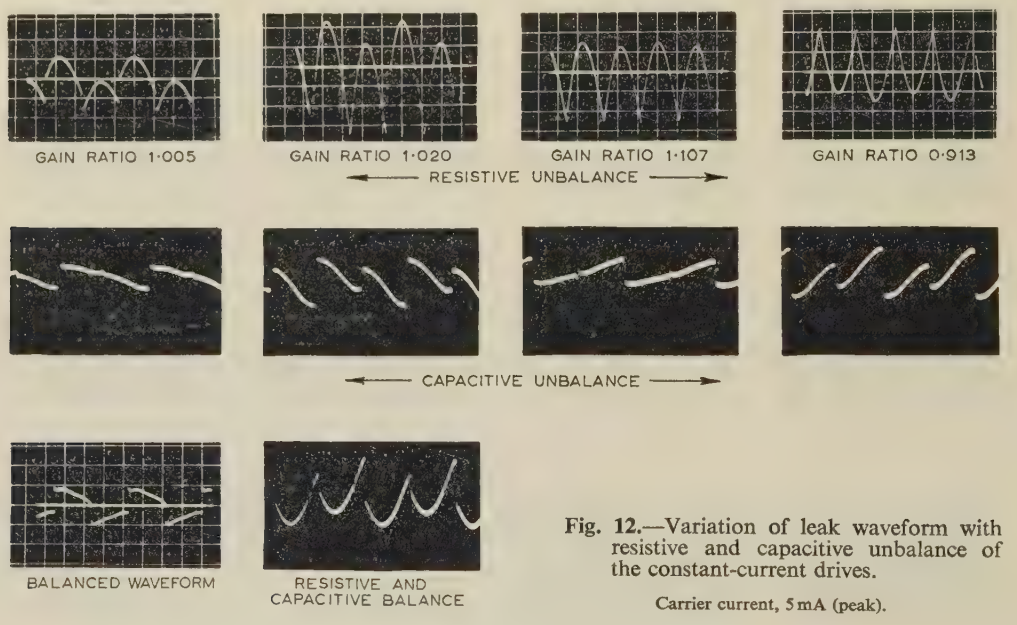

Fig. 12.—Variation of leak waveform with resistive and capacitive unbalance of the constant-current drives.

Carrier current, 5 mA (peak).

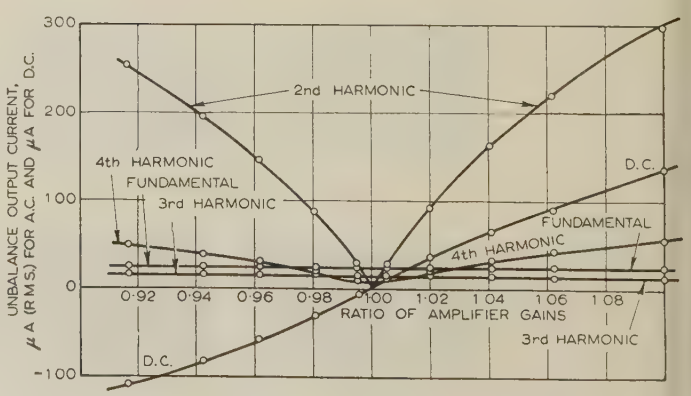

Fig. 13.—Variation of components of leak output current with resistive unbalance of the drives.

Carrier frequency, 2930 c/s; carrier current, 5 mA (peak).

It may be that such a device, if used in the constant-current modulator, would enable the leak to be reduced to an even lower level than that predicted. It would be expected that, if a lower level was achieved, it would not be time stable, as the setting of such a voltage divider would depend on the rectifier characteristics in a similar manner to that of the conventional ring modulator. This idea was tried experimentally by inserting a low-value voltage divider between the terminating resistors, the wiper being connected to the 'earthy' end of the carrier source. As far as could be ascertained, adjustment of this voltage divider was incapable of achieving a lower value of fundamental leak than was obtained with equality of the terminating resistors. The difficulty of measuring the small differences in resistance is considerable, owing to the low value of the total resistance. The fundamental leak obtained with transformer termination did, however, agree with the minimum value obtained with voltage-divider termination, and as the transformer was known to be very accurately balanced, owing to the bifilar method of winding used, it is reasonable to suppose that this minimum does occur with equal terminating resistors. The voltage divider is a useful device, not for reducing the leak below the predicted value, but for adjusting the terminating-resistor equality.

An interesting result obtained from the use of the voltage divider is that its variation within reasonable limits affects the amplitude of only the odd harmonics of the leak, and not that of the even harmonics.

(3.6) The Use of Selected Rectifiers

Groups of four rectifiers were selected, for their low values of Δ , Δ_b and r_f/r_b, from a batch of 20 germanium diodes. These groups were then substituted in the modulator, and, in order to verify the theoretical results for worst leak with rectifiers whose characteristics lie within given limits, all six possible rectifier combinations were investigated.

For the first group, (*a*), the measured parameters were

$$\Delta_f = 0{\cdot}13, \quad \Delta_b = 0{\cdot}3, \quad \text{and } r_f/r_b = 0{\cdot}46 \times 10^{-3}$$

Using eqn. (16), the theoretical maximum value of fundamental leak is obtained as $5{\cdot}12 \times 10^{-4}I$amp, i.e. the fundamental leak is theoretically 66 dB below the carrier level. The worst value of fundamental leak measured was 71 dB below, and one combination gave a leak which was 77 dB below, the carrier level.

The second group, (*b*), investigated had the parameters

$$\Delta_f = 0{\cdot}25, \quad \Delta_b = 0{\cdot}28, \quad \text{and } r_f/r_b = 1{\cdot}75 \times 10^{-4}$$

giving a theoretical worst fundamental leak level of 72·6 dB. In this case, one rectifier combination gave a leak level of 70·5 dB, i.e. 2·1 dB worse than that indicated theoretically, but this discrepancy is not large. One combination of this group gave an output leak whose fundamental component was 92·2 dB below the carrier level.

From these results it is apparent that selection of rectifiers can easily lead to fundamental leak levels in the region of 70 dB below the carrier level and, with rather more care, it is possible to achieve a level of 90 dB.

With any combination of these two groups, the fundamental leak was substantially independent of gain variations in the carrier drive circuits.

(3.7) Stability Tests

The temperature stability of the modulator was checked by enclosing the rectifiers in a temperature-controlled oven. For group (*a*), a warming-up period of 20 min was allowed with the rectifiers at a temperature of 22° C. The temperature was raised to 31·5° C and allowed to remain at that value for 10 min, in order to avoid the effects of uneven temperature distribution, after which time readings of leak were recorded. The temperature was then lowered to 22° C, and after a further period of 10 min, readings were again taken. The following results were obtained:

Leak Current, microamp (r.m.s.)

Temperature	Fundamental	2nd harmonic	3rd harmonic	4th harmonic
deg C				
22	1·87	—	1·87	1·45
31·5	2·72	0·90	2·42	1·57
22	1·90	0·05	1·80	1·51

Thus, increasing the temperature by 9·5° C has raised the fundamental output leak from 65·5 dB to 62·3 dB below the carrier level.

With group (*b*), the fundamental leak at an initial temperature of 21° C was 91 dB below the carrier level. As the temperature was slowly raised the leak current decreased, giving a minimum, which was 97 dB below the carrier level, at 25° C. Further increase in temperature caused the leak current to rise so that at 31° C the level of fundamental leak was 83 dB below the carrier level.

Long-term time-stability tests have not been made, as the temperature-stability tests indicate that the changes in rectifier characteristics which would normally be expected, either due to age or temperature variations, have no great effect upon the level of balance obtained.

(4) CONCLUSIONS

The use of constant-current carrier drives to each half of a split-ring modulator has removed the first-order unbalance effect due to differences of rectifier forward resistance. The ultimate limit to the balance obtainable is now set by the magnitude of the ratio of forward to reverse resistance of the rectifiers multiplied by the magnitudes of the differences in both the forward and the reverse resistances. Due to the effects discussed in Section 2.5, the difference in the reverse resistances is usually the more important.

The important conclusion is reached theoretically, and verified experimentally, that the stability of the fundamental component of the carrier leak is not affected by changes in gain of the constant-current drives, and, for a high balance to this fundamental component, the only requirements of these drives is that they should be linear and have an output impedance which is higher than the maximum reverse resistance of the rectifiers to be used.

In practice, peaks occur in the leak waveform in the region of the carrier zero which are not explained by the circuit theory given here. These peaks are apparently due to inductive effects in the circuit, and although they have large amplitudes relative to the mid-cycle leak, they contribute very little to the magnitudes of the lower harmonics of the leak, and their effect should be negligible for the majority of practical purposes.

The setting of the driving-circuit balancing controls is not greatly affected by the magnitude of the carrier current used, so that the stability of the carrier source is not important.

A useful criterion of temperature stability is the alteration in temperature required to double the leak current. This was found to be of the order of 3 or 4° C for the best levels of balance obtained, and correspondingly greater, as would be expected, for the poorer levels.

As regards the applications of this modulator, it is clearly most directly valuable in communication equipment, and more particularly in measuring instruments. It may be possible to apply it to the chopping of d.c. and low-frequency signals—with great advantages for sensitive 'd.c.' amplification—but this has not yet been fully investigated.

Summarizing: the constant-current modulator is capable of achieving much lower levels of carrier leak—of the order of 90 dB below the carrier level—than have previously been obtained, with the added advantage of good stability.

(5) ACKNOWLEDGMENTS

The author is indebted to Professor D. G. Tucker of the Electrical Engineering Department, University of Birmingham, for his help and guidance throughout the work.

(6) REFERENCES

(1) TUCKER, D. G.: 'Modulators and Frequency Changers' (Macdonald, London, 1953).

(2) TUCKER, D. G.: 'Unbalance Effects in Modulators', *Journal of the British Institution of Radio Engineers*, 1955, **15**, p. 199.

(3) COOPER, W. H. B., *et al.*: Discussion on papers by D. G. Tucker, *Proceedings I.E.E.*, 1949, **96**, Part III, p. 215.

(4) TUCKER, D. G.: 'Rectifier Resistance Laws', *Wireless Engineer*, 1948, **25**, p. 117.

(5) RICHARDS, J. C. S.: 'An Improved Type of Differential-Amplifier', *Electronic Engineering*, 1956, **28**, p. 302.

(6) HANDS, E.: 'A Constant-Current Modulator with Very Low Carrier Leak', M.Sc. Thesis, University of Birmingham, May, 1957.

621.391 : 621.376.56

The Institution of Electrical Engineers
Monograph No. 291 R
Feb. 1958
©

NOISE-REDUCING CODES FOR PULSE-CODE MODULATION

By J. E. FLOOD, Ph.D., Associate Member.

(*The paper was first received* 19*th July, and in revised form* 20*th November*, 1957. *It was published as an* INSTITUTION MONOGRAPH *in February*, 1958.)

SUMMARY

Theory shows that a simple binary pulse-code modulation system does not make the maximum use of a communication channel of given bandwidth and signal/noise ratio. It is suggested that an improvement in output signal/noise ratio can be obtained by modifying the binary code so that errors in its different digits contribute equal amounts of noise power to the output.

The noise contributions of the digits can be equalized by using a greater number of pulses to transmit the more significant digits. However, the resulting increase in bandwidth introduces additional noise which more than offsets the reduced error liability of the digits and so causes a worsening of the output signal/noise ratio. An attempt to equalize the noise contributions of the digits by using a code with a different base for each digit also fails.

It is possible to make the digits of a binary code group contribute equally to the output noise by varying the pulse height or length from digit to digit. An improvement in output signal/noise ratio is then obtained over a range of input signal/noise ratios. The system using pulses of different heights is less complicated than that using different pulse lengths; however, it is more complex than a system using the simple binary code, and it is doubtful if the improvement in signal/noise ratio justifies the additional complexity.

LIST OF SYMBOLS

A = Height of quantizing step, volts.
C = Channel capacity, bits/sec.
f = Cut-off frequency, c/s.
f_b = Bandwidth, c/s.
K = A constant ($\simeq 10$).
k = An integer.
P_n = Noise power, watts.
n = Average number of effective noise bursts per second.
p_r = Probability of error in rth digit.
r = An integer.
P_s = Signal power, watts.
T_r = Duration of rth digit pulse, sec.
V_r = Slicing voltage for rth digit, volts.
V_n = R.M.S. output noise voltage, volts.
V_s = R.M.S. output signal voltage, volts.
Δ = Improvement in signal/noise ratio due to modified code, dB.
μ = Number of digits in code group.
σ = R.M.S. input noise voltage, volts.

(1) INTRODUCTION

In pulse code modulation (p.c.m.), the signal to be transmitted is sampled at regular intervals and the amplitude of each sample is sent by means of a coded group of pulses. The usual method of coding is to represent each sample by a group of pulses, each of which can have only two values: either 'on' or 'off'. A group of n pulses can thus represent 2^n values. Each group represents the sample value in the binary scale of numbers, which uses only two symbols, '0' and '1'.

At the receiving end, the radio-frequency carrier (if any) is amplified and demodulated. The resulting pulses are applied to a slicing circuit, which operates and produces a regenerated pulse whenever the voltage applied to it exceeds a critical value which is chosen to be about half the nominal pulse height. Noise on the transmission path can only affect the output if it is of sufficient amplitude to cause maloperation of the slicing circuit. If the input signal/noise ratio is sufficient for this to happen very infrequently, the output signal is substantially free from interference.

Oliver, Pierce and Shannon[1] have shown that the rate at which a p.c.m. system can transmit information is

$$C = f_b \log_2 \left(1 + \frac{12}{K^2} \frac{P_s}{P_n}\right) \quad . \quad . \quad . \quad . \quad (1)$$

Now, the maximum rate at which the channel can transmit information[2] is

$$C = f_b \log_2 \left(1 + \frac{P_s}{P_n}\right) \quad . \quad . \quad . \quad . \quad (2)$$

Eqns. (1) and (2) are of the same form. Thus, the use of p.c.m. allows bandwidth and signal/noise ratio to be exchanged according to the same logarithmic law as an ideal communication channel. However, the power required by the p.c.m. system is $K^2/12$ times that theoretically required by an ideal system. It should thus be possible to obtain a method of coding which provides the same output signal/noise ratio as binary p.c.m. with only about one-eighth of the transmitted power. Alternatively, for the same transmitted power an improved output signal/noise ratio should be obtainable.

In the simple binary code, each digit is equally liable to error due to noise on the transmission path; however, the amounts of noise which these errors cause at the output of the decoder are unequal. Thus, in a 5-digit code an error in the most significant digit results in an error in the amplitude of the output signal 16 times as great as that caused by an error in the least significant digit. The signal/noise ratio of the system should be improved by making the most significant digits less liable to error than those of less significance, so that they contribute equally to the output noise. Possible methods of doing this are investigated in this paper.

(2) SIGNAL/NOISE RATIO IMPROVEMENT IN P.C.M.

The improvement in signal/noise ratio obtained by the use of simple binary p.c.m. has been investigated by Clavier, Panter and Dite.[3] Their analysis will now be extended to cover the case of a modified code in which the digits are not equally liable to error due to noise on the transmission path.

If a binary code group has μ pulses, the contributions which the pulses make to the decoded output voltage are

$$A, 2A, 2^2A, \ldots, 2^{r-1}A \ldots 2^{\mu-1}A$$

If the probability of an error in the rth pulse of the group is p_r the mean-square noise voltage produced at the output is

$$V_n^2 = A^2 \sum_{r=1}^{\mu} p_r 2^{2(r-1)} \quad . \quad . \quad . \quad . \quad . \quad (3)$$

The probability of error, p_r, depends on the average number of

Correspondence on Monographs is invited for consideration with a view to publication.

Dr. Flood is at the Siemens Edison Swan Research Laboratory.

times per second, $n(V)$, that bursts of noise exceed the voltage, V, at which the pulses are sliced to determine whether they are present. Any positive noise burst which exceeds V and occurs in the absence of a code pulse will cause a spurious pulse to be registered. However, any positive noise burst which occurs during a code pulse merely increases its height and so does not cause any error. If it is assumed that the presence and absence of a code pulse are equally likely, then, on the average, half the positive noise bursts exceeding V will result in errors. In addition, any negative noise burst exceeding V will be assumed to cancel a code pulse which is present, but will not cause error when it is absent. Thus, half the negative noise bursts of amplitude exceeding V also cause errors. Consequently, the average rate at which errors occur (due to both positive and negative bursts of noise) is $n(V)$.

If the noise bursts are independent of each other and have a Poisson distribution, the probability of k bursts occurring in an interval T is

$$p(k) = [n(V)T]^k \frac{\varepsilon^{-n(V)T}}{k!} \quad . \quad . \quad . \quad . \quad (4)$$

If the interval T is that of one digit pulse, only one error can occur ($k = 1$), and if the errors are relatively infrequent $n(V)T \ll 1$.

Eqn. (4) then becomes

$$p_r \simeq n(V_r)T_r \quad . \quad . \quad . \quad . \quad . \quad . \quad . \quad (5)$$

Rice[4] has shown that, if random noise is applied to a circuit with an ideal low-pass frequency characteristic, the number of noise bursts per second which exceed V is

$$n(V) = \frac{f}{\sqrt{3}} \varepsilon^{-V^2/2\sigma^2} \quad . \quad . \quad . \quad . \quad . \quad (6)$$

Substituting for p_r in eqn. (3) by means of eqns. (5) and (6) gives

$$V_n^2 = A^2 \sum_{r=1}^{\mu} \frac{f_r T_r}{\sqrt{3}} 2^{2(r-1)} \varepsilon^{-V_r^2/2\sigma_r^2} \quad . \quad . \quad . \quad (7)$$

This is the output noise voltage for the general case of a binary code group in which the pulses may not be equally liable to error.

If the modulating signal is a sine wave, the greatest possible amplitude is $\frac{1}{2}A(2^\mu - 1)$. The mean-square signal output voltage is then

$$V_s^2 = A^2(2^\mu - 1)^2/8 \quad . \quad . \quad . \quad . \quad . \quad (8)$$

In the simple binary code, all the pulses are of equal height ($2V_b$) and duration (T_b) and equally liable to error. Eqn. (7) then gives

$$V_{nb}^2 = A^2 \frac{f_b T_b}{\sqrt{3}} \varepsilon^{-V_b^2/2\sigma_b^2} \sum_{r=1}^{\mu} 2^{2(r-1)}$$

$$= (4^\mu - 1) \frac{f_b T_b A^2}{3\sqrt{3}} \varepsilon^{-V_b^2/2\sigma_b^2} \quad . \quad . \quad . \quad . \quad . \quad . \quad . \quad (9)$$

From eqns. (8) and (9) the output signal/noise ratio is

$$\frac{V_s^2}{V_{nb}^2} = \frac{3\sqrt{3}(2^\mu - 1)}{8 f_b T_b (2^\mu + 1)} \varepsilon^{V_b^2/2\sigma_b^2} \quad . \quad . \quad . \quad (10)$$

This result was obtained by Clavier, Panter and Dite.[3]

If errors in each of the code pulses are to make equal contributions to the output noise power, then, from eqn. (3), we require

$$p_r = p_1 2^{2(1-r)} \quad . \quad . \quad . \quad . \quad . \quad . \quad . \quad (11)$$

If this condition is satisfied, eqn. (3) becomes

$$V_n^2 = \mu p_1 A^2$$

Substituting for p_1 by means of eqns. (5) and (6),

$$V_n^2 = \frac{\mu f_1 T_1 A^2}{\sqrt{3}} \varepsilon^{-V_1^2/2\sigma^2} \quad . \quad . \quad . \quad . \quad (12)$$

From eqns. (8) and (12) the output signal/noise ratio is

$$\frac{V_s^2}{V_n^2} = \frac{\sqrt{3}(2^\mu - 1)^2}{8\mu f_1 T_1} \varepsilon^{V_1^2/2\sigma_1^2} \quad . \quad . \quad . \quad . \quad (13)$$

Arranging errors in the code pulses to contribute equal amounts to the output noise has changed the output noise power from the value given by eqn. (9) to that given by eqn. (12);

i.e. $$\frac{V_n^2}{V_{nb}^2} = \frac{3\mu f_1 T_1}{(4^\mu - 1) f_b T_b} \exp\left(\frac{V_b^2}{2\sigma_b^2} - \frac{V_1^2}{2\sigma_1^2}\right)$$

The parameters $f_1 T_1$ and $f_b T_b$ determine the shape of the pulses: an acceptable minimum value is 0·5. It will be assumed that the same value is used in each case. Putting $f_1 T_1 = f_b T_b$ and expressing this power ratio in decibels, the improvement in output noise is

$$\Delta = 10 \log_{10}\left(\frac{4^\mu - 1}{3\mu}\right) + 10\left(\frac{V_1^2}{2\sigma_1^2} - \frac{V_b^2}{2\sigma_b^2}\right) \log_{10} \varepsilon \quad \text{decibels} \quad . \quad . \quad (14)$$

(3) CYCLIC PERMUTED CODE

The cyclic permuted code was proposed by Gray[5] in order to reduce errors in the coding process. An example is shown in Table 1.

Table 1

Magnitude of sample	Representation in c.p. code
0	0000
1	0001
2	0011
3	0010
4	0110
5	0111
6	0101
7	0100
8	1100

This code has the advantage for coder operation that a unit change in the value of the sample to be coded can cause only one of the code digits to change its value. However, changing the value of one of the code digits can cause a change of more than one unit in the value of the decoded sample. For example, an error which changes 0100 to 0000 causes an error of 7 units in the decoded output. Thus, the c.p. code provides no advantage over the simple binary code as regards errors caused by noise on the transmission path.

(4) BINARY CODE WITH UNEQUAL NUMBERS OF PULSES PER DIGIT

One method of making the more significant digits less liable to error is to represent them by more than one pulse. If a digit is represented by a single pulse and an effective noise pulse is also present, four possibilities occur, as shown in Table 2. Thus half the possibilities result in an error.

Table 2

Signal pulse present or absent	Polarity of noise pulse	Result	Right or wrong
0	+	1	Wrong
0	−	0	Right
1	+	1	Right
1	−	0	Wrong

If a digit is represented by two pulses, either no noise or one or two noise pulses may be present. If noise is present the possibilities which arise are shown in Table 3. The number of errors which occur is seen to be the same whether a single pulse is accepted as the signal '1' or whether two pulses are required

Table 3

	Signal pulse present or absent	Polarity of noise pulses	Result	Right or wrong (*a*)	Right or wrong (*b*)
1 Noise pulse	00	0+	01	Wrong	Right
	00	0−	00	Right	Right
	11	0+	11	Right	Right
	11	0−	10	Right	Wrong
2 Noise pulses	00	++	11	Wrong	Wrong
	00	−−	00	Right	Right
	00	+−	10	Wrong	Right
	00	−+	01	Wrong	Right
	11	++	11	Right	Right
	11	−−	00	Wrong	Wrong
	11	+−	10	Right	Wrong
	11	−+	01	Right	Wrong

(*a*) If presence of a single pulse is accepted as the signal '1'.
(*b*) If two pulses are required to produce '1' and a single pulse is regarded as '0'.

to produce '1' and a single pulse is regarded as '0'. For both (*a*) and (*b*), only one-quarter of the single noise pulses produce an error in the output and one-half of the noise pulse-pairs produce errors.

If a digit contains three pulses and the presence of two pulses is accepted as the signal '1', a single noise pulse cannot cause error. By drawing up a Table similar to Table 3 it can be shown simply that one-third of the noise pulse-pairs and one-half of noise triple pulses will cause errors. Similarly, if four pulses are used, and two or three pulses are required to produce the signal '1', a single noise pulse cannot cause an error and one-sixth of the noise pulse-pairs will do so. The results obtained for digits containing up to 10 pulses are summarized in Table 4.

This Table shows that a change from an odd number of pulses to the next greater even number halves the rate of error, whereas eqn. (11) requires each digit to be followed by one with one-quarter of the error rate. This suggests that only the odd numbers of pulses should be used. Table 4 also shows that if a group of $2k-1$ pulses is used, k noise pulses are required to produce an error.

If the average number of noise pulses per second is n, the probability of k pulses in time T is given by the Poisson probability distribution [eqn. (4)]. If the duration of each code pulse is T, the probability of k noise pulses occurring during the time of $2k-1$ code pulses is

$$p_k = \frac{[(2k-1)nT]^k}{k!}\varepsilon^{-(2k-1)nT}$$

Table 4

No. of pulses per digit	Effect of noise pulses
1	Single pulses cause error $\frac{1}{2}$ of the time
2	Single pulses cause error $\frac{1}{4}$ of the time 2 pulses cause error $\frac{1}{2}$ of the time
3	Single pulse causes no error 2 pulses cause error $\frac{1}{3}$ of the time
4	Single pulse causes no error 2 pulses cause errors $\frac{1}{8}$ of the time
5	2 pulses cause no error 3 pulses cause error $\frac{1}{4}$ of the time
6	2 pulses cause no error 3 pulses cause error $\frac{1}{8}$ of time
7	3 pulses cause no error 4 pulses cause error $\frac{1}{5}$ of time
8	3 pulses cause no error 4 pulses cause error $\frac{1}{10}$ of time
9	4 pulses cause no error 5 pulses cause error $\frac{1}{6}$ of time
10	4 pulses cause no error 5 pulses cause error $\frac{1}{12}$ of time

Similarly, $$p_{k+1} = \frac{[2(k+1)nT]^{k+1}}{(k+1)!}\varepsilon^{-(2k+1)nT}$$

Therefore $$\frac{p_{k+1}}{p_k} = \frac{[(2k+1)nT]^{k+1}k!}{[(2k-1)nT]^k(k+1)!}\varepsilon^{-2nT}$$

$$\simeq \frac{(2k+1)^{k+1}(nT)}{(2k-1)^k(k+1)} \text{ if } 2nT \ll 1 \quad . \quad . \quad (15)$$

Eqn. (15) shows that if $p_{k+1} = \frac{1}{4}p_k$, the value of nT (i.e. p_1) is determined; moreover, it cannot be the same for each value of k. However, p_1 only varies from 0·055 to 0·044 as k varies from 1 to infinity. Thus, if p_1 is about 0·05, eqn. (11) will be approximately satisfied and the amounts of noise introduced by the different digits will be nearly equal.

If $p_1 = 0{\cdot}05$, from eqns. (5) and (6),

$$\varepsilon^{V_1^2/2\sigma_1^2} = \frac{20}{\sqrt{3}}f_1T_1 \quad . \quad . \quad . \quad . \quad . \quad (16)$$

The different digits thus only contribute equal amounts to the output noise power when the input signal/noise ratio is that given by eqn. (16). The mean-square output noise voltage is then given by eqn. (12).

The modified code requires μ times as many pulses per code group as the simple binary code; for example, a 7-digit code requires no less than 49 pulses. Consequently, the bandwidth of the system must be increased μ times ($f_1 = \mu f_b$), and the input noise power increases in the same proportion ($\sigma_1^2 = \mu\sigma_b^2$). The probability of receiving noise pulses is thus increased, and this offsets their reduced effect when they do occur. If both systems use pulses of the same amplitude ($V_1 = V_b$), the ratio of the output noise powers, from eqns. (9) and (12),

$$\frac{V_n^2}{V_{nb}^2} = \frac{3\mu f_1T_1}{(4^\mu - 1)f_bT_b}\exp\frac{V_1^2}{2\sigma_1^2}\left(\frac{\sigma_1^2}{\sigma_b^2} - 1\right)$$

$$= \frac{3\mu}{(4^\mu - 1)}\exp\frac{V_1^2}{2\sigma_1^2}(\mu - 1) \text{ if } f_1T_1 = f_bT_b$$

Substituting for $V_1^2/2\sigma_1^2$ from eqn. (16) gives

$$\frac{V_n^2}{V_{nb}^2} = \frac{3\mu}{4^\mu - 1}\left(\frac{20}{\sqrt{3}}f_1T_1\right)^{(\mu-1)}$$

Consequently, an improvement in the output signal/noise ratio is only obtained if

$$\frac{4^{\mu}-1}{3\mu} > \left(\frac{20}{\sqrt{3}} f_1 T_1\right)^{(\mu-1)}$$

The minimum value for $f_1 T_1$ is 0·5, so we require

$$\frac{4^{\mu}-1}{3\mu} > \left(\frac{10}{\sqrt{3}}\right)^{(\mu-1)}$$

which is not satisfied by any positive integral value of $\mu - 1$. The increase in the number of effective noise pulses thus outweighs the reduced effect of the noise pulses and the signal/noise ratio at the output is actually worsened. It is clear that very inefficient use is being made of the additional pulses transmitted. If it is permissible to use more pulses than the simple binary code requires, it is clearly better to abandon binary coding completely and adopt some form of error-correcting code[6] for the group of code pulses rather than digit by digit.

(5) CODE WITH DIGITS OF UNEQUAL BASE

A possible method of equalizing the amount of noise power introduced by errors in the different digits is to make the less significant more liable to error than in the case of the simple binary code. If this enables the code to be sent over a channel of smaller bandwidth an improvement in output signal/noise ratio may result. In a group of code pulses, the first pulse could have only two values (on and off), the second could have three (full amplitude, half amplitude and off), the next four, and so on. Alternatively, the first pulse could have two values, the second four, the third eight, etc. In general, the pulse representing the rth digit can have n_r values. The values for the various pulses in the code group and the signal amplitudes they represent are shown in Table 5.

Table 5

Digit	Pulse values	Signal amplitude values
1	0, 1	0, $\frac{1}{2}$
2	0, $1/(n_2-1)$, $2/(n_2-1)$ ... $(n_2-2)/(n_2-1)$, 1	0, $1/2n_2$, $2/2n_2$, ..., $(n-1)/2n_2$
3	0, $1/(n_3-1)$, $2/(n_3-1)$ ... 1	0, $1/2n_2n_3$, $2/2n_2n_3$, ..., $(n_3-1)/2n_2n_3$
μ	0, $1/(n_\mu-1)$, $2/(n_\mu-1)$ ... 1	0, $1/2n_2n_3 \ldots n_\mu$, $2/2n_2n_3 \ldots n_\mu$, ..., $(n_\mu-1)/2n_2n_3 \ldots n_\mu$

A noise pulse which coincides with the first digit will introduce an error if its height exceeds half the pulse voltage and the error voltage will be of value one-half. A noise pulse which coincides with the second digit will introduce an error voltage of $1/2n_2$ if its height exceeds $1/(n_2-1)$, an error of $2/2n_2$ if its height exceeds $2/(n_2-1)$, and so on. Similarly for the subsequent digits as shown in Table 6.

Let the probability of a noise pulse exceeding amplitude x be $p(x)$. Provided that the input signal/noise ratio is adequate (i.e. $\exp V^2/2\sigma^2 \gg 1$), we can assume that

$$p\left[\frac{1}{2(n_r-1)}\right] \gg p\left[\frac{3}{2(n_r-1)}\right],\ p\left[\frac{5}{2(n_r-1)}\right] \ldots p\left[\frac{2n_r-3}{2(n_r-1)}\right]$$

Table 6

Digit	Amplitude exceeded by noise pulse	Resultant error voltage
1	$\frac{1}{2}$	$\frac{1}{2}$
2	$1/2(n_2-1)$ $3/2(n_2-1)$ . . . $(2n_2-3)/2(n_2-1)$	$1/2n_2$ $2/2n_2$ . . . $(n_2-1)/2n_2$
3	$1/2(n_3-1)$ $3/2(n_3-1)$ . . . $(2n_3-3)/2(n_3-1)$	$1/2n_2n_3$ $2/2n_2n_3$ . . . $(n_3-1)/2n_2n_3$
μ	$1/2(n_\mu-1)$ $3/2(n_\mu-1)$ . . . $(2n_\mu-3)/2(n_\mu-1)$	$1/2n_2n_3 \ldots n_\mu$ $2/2n_2n_3 \ldots n_\mu$ . . . $(n_\mu-1)/2n_2n_3 \ldots n_\mu$

The mean-square noise voltage at the output is thus

$$V_n^2 \simeq \frac{1}{\mu}\left\{\frac{p(\frac{1}{2})}{2^2} + \frac{p[1/2(n_2-1)]}{2^2 n_2^2} + \frac{p[1/2(n_3-1)]}{2^2 n_2^2 n_3^2} + \ldots + \frac{p[1/2(n_\mu-1)]}{2^2 n_2^2 n_3^2 \ldots n_\mu^2}\right\}$$

To equalize the noise power contributed by errors in the different digits we therefore require

$$p[1/2(n_2-1)] = n_2^2\, p(\tfrac{1}{2})$$
$$p[1/2(n_3-1)] = n_3^2\, p[1/2(n_2-1)]$$
$$\ldots\ldots\ldots\ldots$$
$$p[1/2(n_\mu-1)] = n_\mu^2\, p[1/2(n_{\mu-1}-1)]$$

Now, from eqn. (6),

$$p[1/2(n_2-1)] = p(\tfrac{1}{2}) \exp\left[1 - \frac{1}{(n_2-1)^2}\right]\frac{V^2}{2\sigma^2}$$

$$p[1/2(n_3-1)] = p[1/2(n_2-1)] \exp\left[\frac{1}{(n_2-1)^2} - \frac{1}{(n_3-1)^2}\right]\frac{V^2}{2\sigma^2}$$

$$\ldots\ldots\ldots\ldots\ldots\ldots\ldots\ldots$$

$$p[1/2(n_\mu-1)] = p[1/2(n_{\mu-1}-1)] \exp\left[\frac{1}{(n_{\mu-1}-1)^2} - \frac{1}{(n_\mu-1)^2}\right]\frac{V^2}{2\sigma^2}$$

Therefore

$$\log n_2^2 = \left[1 - \frac{1}{(n_2-1)^2}\right]\frac{V^2}{2\sigma^2}$$

$$\log n_3^2 = \left[\frac{1}{(n_2-1)^2} - \frac{1}{(n_3-1)^2}\right]\frac{V^2}{2\sigma^2}$$

$$\ldots\ldots\ldots\ldots$$

$$\log n_\mu^2 = \left[\frac{1}{(n_{\mu-1}-1)^2} - \frac{1}{(n_\mu-1)^2}\right]\frac{V^2}{2\sigma^2}$$

hence $n_2, n_3, \ldots, n_\mu$ can be evaluated.

It is seen that the values of $n_2, n_3, \ldots, n_\mu$ depend on $V^2/2\sigma^2$; moreover, they are not integers. It is therefore impossible to equalize the noise contributions of the different digits if these can have only an integral number of values.

(6) BINARY CODE WITH PULSES OF UNEQUAL HEIGHT

Another method of equalizing the noise power introduced by errors in the different digits is to transmit the digits by pulses of equal duration T but different height ($2V_r$). The more significant digits are sent by larger-amplitude pulses than the less significant digits, so the former can be made less liable to error than the latter. At the receiving end of the modified system, the pulse corresponding to each digit must be sliced by a discriminator circuit set to the appropriate level. This may be done, as shown in Fig. 1, by using a separate discriminator for each digit and

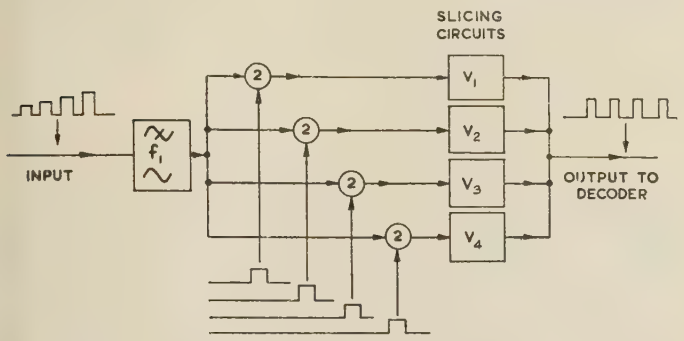

Fig. 1.—Receiving end of p.c.m. system using pulses of unequal height.

gating each pulse to the appropriate circuit. Alternatively, a single discriminator may be used (e.g. a Schmitt trigger circuit) whose reference voltage is changed for each digit to be received. The amplitudes of the more significant pulses can be larger than that of the pulses in a simple binary p.c.m. system which uses the same mean transmitter power. It should thus be possible to obtain a better signal/noise ratio by using the modified system.*

The probability of error in each code pulse is given by eqn. (5). For the errors in the code pulses to make equal contributions to the output noise, the ratios of their error probabilities to that of the least significant pulse is given by eqn. (11). From these two equations

$$\frac{fT}{\sqrt{3}}[\exp(-V_r^2/2\sigma^2)]4^{r-1} = \frac{fT}{\sqrt{3}}\exp(-V_1^2/2\sigma^2)$$

Therefore
$$V_r^2 = V_1^2 + 2(\log_\varepsilon 4)(r-1)\sigma^2$$
$$= V_1^2[1 + 2{\cdot}772(r-1)\sigma^2/V_1^2] \quad . \quad . \quad . \quad (17)$$

The relationship between the pulse heights thus depends on the noise level. If the pulse heights are adjusted for one particular value of σ, at other noise levels errors in the pulses will no longer contribute equal amounts of noise to the output.

If the amplitude of each pulse in the group is $2V_r$, $r = 1, \ldots, \mu$, the mean-square voltage of the group of code pulses is $4V^2$, where

$$V^2 = \frac{1}{\mu}\sum_{r=1}^{\mu} V_r^2 = V_1^2[1 + 1{\cdot}386(\mu-1)\sigma^2/V_1^2] \qquad (18)$$

This is equivalent to the mean-square voltage ($4V_b^2$) of each pulse in a simple binary p.c.m. system which uses the same transmitted power as the modified system.

By substituting from eqn. (18) in eqn. (14), the improvement Δ in signal/noise ratio obtained by using the modified code is

$$\Delta = 10\log_{10}\left(\frac{4^\mu - 1}{3\mu}\right) - 3{\cdot}01(\mu-1) \text{ decibels} \qquad (19)$$

The improvement obtained for various numbers of digits in the code group is shown in Table 7.

* If the rating of the transmitter is limited by peak power rather than mean power, it will not be possible to obtain an improved signal/noise ratio by means of the modified code, but merely a reduction of mean transmitted power.

Table 7

No. of digits, μ	Improvement, Δ dB
1	0
2	1
3	2·5
4	4·3
5	6·3
6	8·4
7	10·8
8	13·3

The improvement shown in the Table is obtained only for the noise level for which the modification is made. If the noise level changes, the improvement will be less. If the system is adjusted for a noise voltage σ_0, the relationship between the pulse heights is given by eqn. (17) with $\sigma = \sigma_0$. At other input noise levels the output noise level is given by eqn. (7). With an r.m.s. input noise voltage σ' the mean-square output noise voltage is thus

$$V_n'^2 = \frac{A^2 f_1 T_1}{\sqrt{3}}\sum_1^\mu 2^{2(r-1)}\exp(-V_r^2/2\sigma'^2)$$
$$= \frac{A^2 f_1 T_1}{\sqrt{3}}[\exp(-V_1^2/2\sigma'^2)]\sum_1^\mu 2^{2(r-1)}[\exp -1{\cdot}386(r-1)] \qquad (\sigma_0^2/\sigma'^2)$$
$$= \frac{A^2 f_1 T_1}{\sqrt{3}}[\exp(-V_1^2/2\sigma'^2)]\frac{1 - 4^{\mu(1-\sigma_0^2/\sigma'^2)}}{1 - 4^{1-\sigma_0^2/\sigma'^2}}$$

The mean-square output voltage with the simple binary code, V_{nb}^2, is given by eqn. (9), and V_b^2 is given by eqn. (18).

Therefore
$$\frac{V_n'^2}{V_{nb}^2} = \frac{1 - 4^{\mu(1-\sigma_0^2/\sigma'^2)}}{1 - 4^{1-\sigma_0^2/\sigma'^2}}\,\frac{3 \times 4^{(\mu-1)\sigma_0^2/2\sigma'^2}}{4^\mu - 1}$$

Expressing this ratio in decibels gives as the improvement in output signal/noise ratio

$$\Delta = 10\log_{10}\frac{(4^\mu - 1)(1 - 4^{1-\sigma_0^2/\sigma'^2})}{3[1 - 4^{\mu(1-\sigma_0^2/\sigma'^2)}]} - 3{\cdot}01(\mu-1)\sigma_0^2/\sigma'^2 \text{ decibels} \qquad (20)$$

For input noise voltages exceeding σ_0 the improvement, Δ, obtained, although smaller, is still positive. For input noise voltages less than σ_0 the improvement is again less than the maximum and vanishes when the noise power is approximately halved. At still smaller input noise powers the simple binary code is better than the modified code. In Fig. 2, curve (*a*) shows how the output signal/noise ratio varies with input signal/noise ratio for a simple binary code system using 5 digits. Curves (*b*) and (*c*) are for the modified system adjusted to provide maximum improvement in output signal/noise ratio at input signal/noise ratios of 10 dB and 13 dB respectively.

(7) BINARY CODE WITH PULSES OF UNEQUAL LENGTH

If the digits are transmitted by pulses of different duration, they can be received by circuits of different bandwidth and so be subject to different amounts of noise. The more significant digits can be sent by longer pulses than the less significant digits: they can therefore be received by circuits of smaller bandwidth, which thus receive less noise than the shorter pulses of the less significant digits. The different pulses can be of equal height and applied to the same slicing circuit as shown in Fig. 3.

The probability of error in each code pulse is given by eqn. (5). For the errors in the code pulses to make equal contributions to

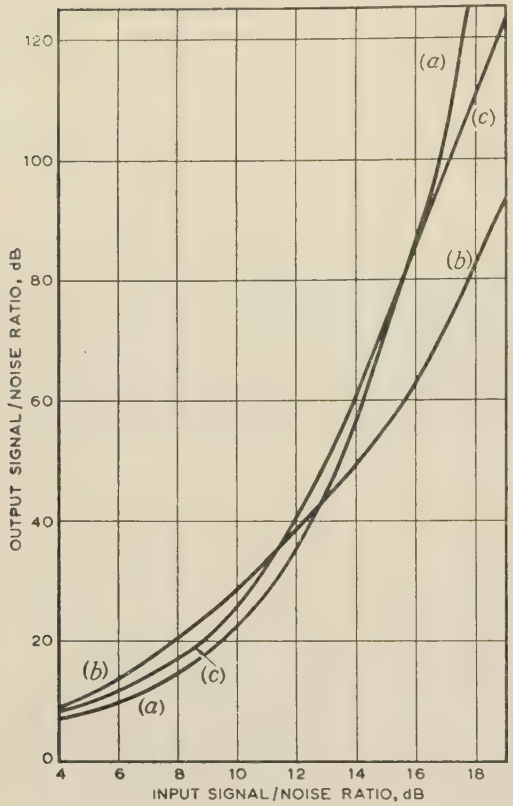

Fig. 2.—Signal/noise ratio improvement in p.c.m. systems.

(*a*) Using simple binary code.
(*b*) Code modified to give maximum improvement at 10 dB input signal/noise ratio.
(*c*) Code modified to give maximum improvement at 13 dB input signal/noise ratio.

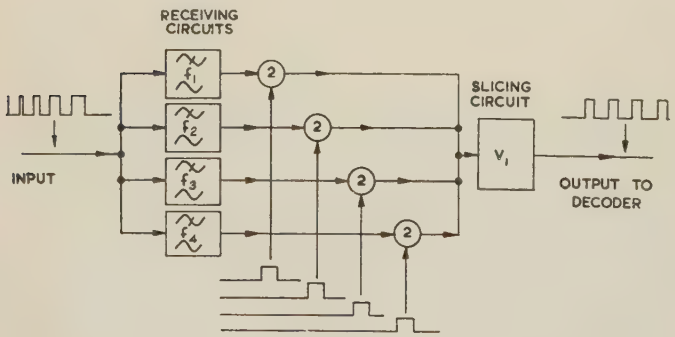

Fig. 3.—Receiving end of p.c.m. system using pulses of unequal length.

the output noise, the ratios of their error probabilities to that of the least significant pulse is given by eqn. (11). From these two equations

$$4^{r-1} f_r T_r \varepsilon^{-V^2/2\sigma_r^2} = f_1 T_1 \varepsilon^{-V^2/2\sigma_1^2}$$

The noise power for each digit is proportional to the bandwidth of its receiver, and it will be assumed that $f_r T_r = f_1 T_1$;

i.e.
$$\frac{\sigma_r^2}{\sigma_1^2} = \frac{f_r}{f_1} = \frac{T_1}{T}$$

Therefore

$$4^{r-1} \exp(-V^2 T_r / 2\sigma_1^2 T_1) = \exp(-V^2/2\sigma_1^2)$$

$$\frac{V^2}{2\sigma_1^2}\left(\frac{T_r}{T_1} - 1\right) = (r-1)\log_\varepsilon 4$$

$$T_r = T_1 [1 + 2{\cdot}772(r-1)\sigma_1^2/V^2] \quad . \quad . \quad . \quad (21)$$

The similarity between eqns. (21) and (17) should be noted. As in the system with variable pulse height, the relation between the pulses depends on the noise level. If the pulse lengths are adjusted for one particular value of σ_1, at other noise levels errors in the pulses will no longer contribute equal amounts of noise to the output. From eqn. (21), the mean pulse duration is

$$T_b = \frac{1}{\mu}\sum_1^\mu T_r$$

$$= T_1[1 + 1{\cdot}386(\mu - 1)\sigma_1^2/V^2]$$

This is the duration of each pulse in a simple binary p.c.m. system which uses the same transmitted power as the modified system. The bandwidth required by the simple binary p.c.m. system is $f_b = f_1 T_1 / T_b$, and the mean-square input noise voltage is

$$\sigma_b^2 = \sigma_1^2 f_b / f_1 = \sigma_1^2 T_1 / T_b$$

$$= \sigma_1^2 / [1 + 1{\cdot}386(\mu - 1)\sigma_1^2/V^2] \quad . \quad . \quad (22)$$

The improvement in signal/noise ratio due to the modified code is obtained by substituting from eqn. (22) in eqn. (14), which gives

$$\Delta = 10 \log_{10}\left(\frac{4^\mu - 1}{3}\right) - 3{\cdot}01(\mu - 1) \text{ decibels}$$

This result is identical with eqn. (19). The improvement in signal/noise ratio which can be obtained by varying the pulse length is thus equal to that obtainable by varying the pulse height and is given by Table 7.

(8) CONCLUSIONS

It is possible to obtain a better output signal/noise ratio than that provided by simple binary p.c.m. by making the more significant digits less liable to error than the less significant ones so that they contribute equally to the output noise. This can be done by using a greater number of pulses to transmit the more significant digits. However, the resulting increase in bandwidth introduces additional noise which more than offsets the reduced error liability of the digits and so causes a worsening of the output signal/noise ratio. An attempt to equalize the noise contributions of the digits by making each use a code with a different base also fails.

It is possible to make the digits of a binary code group contribute equally to the output noise by varying the pulse height or length from digit to digit. An improvement in output signal/noise ratio is obtained over a range of input signal/noise ratios. At high input signal/noise ratios, however, the modified system gives more output noise than the simple binary code system, but the output noise is then usually so low that the deterioration is not important. The system using pulses of unequal height is less complicated than that using pulses of unequal length, which requires separate receivers of different bandwidth for the different digits. However, the system using pulses of different height is more complicated than a simple binary system, and it is doubtful if the improvement in signal/noise ratio obtained justifies the additional complexity, particularly in view of the already excellent noise performance of simple binary p.c.m.

(9) ACKNOWLEDGMENTS

Acknowledgment is made to Siemens Edison Swan Ltd. for permission to publish the paper. Thanks are due to Mr. J. E. Halder for calculating the results shown in Fig. 2.

(10) REFERENCES

(1) OLIVER, B. M., PIERCE, J. R., and SHANNON, C. E.: 'The Philosophy of P.C.M.', *Proceedings of the Institute of Radio Engineers*, 1948, **36**, p. 1324.

(2) SHANNON, C. E.: 'The Mathematical Theory of Communication', *Bell System Technical Journal*, 1948, **27**, pp. 379 and 623.

(3) CLAVIER, A. G., PANTER, P. F., and DITE, W.: 'Signal to Noise Improvement in a Pulse-Count Modulation System', *Proceedings of the Institute of Radio Engineers*, 1949, **37**, p. 355.

(4) RICE, S. O.: 'Mathematical Analysis of Random Noise', *Bell System Technical Journal*, 1944, **23**, p. 282.

(5) GRAY, F.: 'Pulse Code Communications', U.S. Patent No. 2632058, March, 1953.

(6) HAMMING, R. W.: 'Error Detecting and Correcting Codes', *Bell System Technical Journal*, 1950, **29**, p. 147.

DISCUSSION ON THE ABOVE MONOGRAPH

Dr. D. A. Bell (*communicated*): The unequal significance of digits is the weakness of p.c.m., but its strength is the fact that it is quantized; an approach to channel capacity in the Shannon sense depends on the receiver being able to make a choice out of a finite collection of possible messages. A difficulty is that the Shannon formula $C = f_b \log_2 (1 + P_s/P_n)$ refers to a rate of communication with negligible risk of error; which in the p.c.m. case would mean communication with 'noise' consisting only of quantizing noise. The communication rate for p.c.m. suggested by Oliver, Pierce and Shannon is based on the assumption of a finite but tolerable error-rate, so that it is not strictly comparable with the channel-capacity formula until a correction has been made for this accepted error-rate.

It is interesting to compare Dr. Flood's Table 4 with the theoretical minimum number of digits required for an error-correcting binary code to replace each single digit. If the code group is regarded as one information digit plus c check digits, the requirement is $2^c \geqslant F$, where F is the number of different kinds of error which may occur, inclusive of the no-error case. If there are just k interfering noise pulses amongst $c + 1$ digits, the number of possible faults (kinds of error) is

$$(c + 1)!/k!(c + 1 - k)!$$

But if the number of interfering pulses may be anything from 0 to k inclusive,

$$F = \sum_{r=0}^{k} \frac{(c + 1)!}{r!(c + 1 - r)!} \quad . \quad . \quad . \quad . \quad (A)$$

Table A shows the values of F for values of $c + 1$ from 1 to 10 and k from 1 to 6, together with the values of 2^c. The terms in the summation in eqn. (A) are binomial coefficients, so that if k were equal to $c + 1$ we should have $F = (1 + 1)^{c+1} = 2^{c+1}$. Since the c additional digits can cover only cases up to $F = 2^c$, k must be less than $c + 1$ in such a way that F is halved. This is possible if the binomial series has an even number of terms, i.e. if $c + 1$ is odd and there is then a number k such that $F = 2^c$ exactly. This is why an odd number of pulses per digit is more satisfactory than an even number.

The major difference between the author's approach and Hamming's is that the former uses a logical test on an arbitrary code, while the latter has constructed codes in such a way that the location of error is indicated by a set of parity checks. In either case the additional digits must be sufficiently numerous to contain the exact information required to correct the error.

Table A

No. of pulses per digit, $c + 1$	k						2^c
	1	2	3	4	5	6	
1	—	—	—	—	—	—	—
2	3	4	—	—	—	—	2
3	4	7	8	—	—	—	4
4	5	11	15	16	—	—	8
5	6	16	26	31	32	—	16
6	7	22	42	57	63	64	32
7	8	29	64	99	120	127	64
8	9	37	93	163	219	247	128
9	10	46	130	256	386	470	256
10	11	56	176	386	638	848	512

Table 3 shows for the case of two pulses per digit an error rate of $\frac{1}{4}$ if one pulse is mutilated by noise, and an error rate of $\frac{1}{2}$ if both pulses are mutilated. An error rate of $\frac{1}{2}$ in a binary system represents zero information, but in a realistic assessment one should presumably weight the occurrence of one and two noise pulses respectively according to the Poisson formula, or if p_1 is small one might put $p_2 \simeq p_1^2$ and $p_0 \simeq 1 - p_1 - p_2$. For example, with $p_1 = 10\%$ the system using two pulses per digit would produce $2\frac{1}{2}\%$ false digits due to single noise pulses and $\frac{1}{2}\%$ due to pairs of noise pulses, making 3% overall error rate.

The fact that the use of an error-correcting code group for individual digits does not improve the communication rate is consistent with the basic philosophy of communication theory. The rate for a given signalling power can always be increased by increasing the bandwidth, but only if the resulting signals are interpreted by a probability estimate of the whole, not by seeking certainty for each element of the code group. In the multi-dimensional geometric analogue, one must look at the resultant distance between different message points, not at the differences in individual co-ordinates which correspond with the individual elements of the code group.

Dr. J. E. Flood (*in reply*): I am grateful to Dr. Bell for providing a useful addition to Section 4 of the paper. His discussion of an error-correcting code for a single information digit provides an interesting explanation of the results in Table 4. The paper points out that it is better to use an error-correcting code for the whole group of pulses rather than for each separate digit. Dr. Bell has correctly stated the reason for this.

621.372.5

The Institution of Electrical Engineers
Monograph No. 292 R
Feb. 1958
©

SOME OPTIMUM FOUR-TERMINAL NETWORKS HAVING GIVEN INPUT AND OUTPUT SHUNT CAPACITANCES

By O. P. D. CUTTERIDGE, M.Sc.(Eng.), Ph.D., Associate Member.

(*The paper was first received 28th May, and in revised form 16th September, 1957. It was published as an* INSTITUTION MONOGRAPH *in February, 1958.*)

SUMMARY

The paper deals with the open-circuit transfer impedances of low-pass 4-terminal networks having given parasitic capacitances shunted across both input and output terminals. The discussion, in the first instance, is in terms of the poles and zeros of the transfer function, although physical realizations of optimum networks are also derived.

The first part of the paper deals with the adjustment of the driving-point impedances to produce a transfer impedance having a maximum d.c. gain consistent with given pole and zero positions; various cases having two and three poles are considered. In the remainder of the paper optimum pole-zero patterns yielding maximum-gain/rise-time quotients consistent with monotonic response are obtained.

LIST OF SYMBOLS

ω = Angular frequency.
$p = j\omega$ = Complex frequency.
$z_{11}, z_{12}, z_{21}, z_{22}$ = Open-circuit impedance functions of a 4-terminal network (4-pole).
Δ = Nodal determinant of a 4-pole system.
$\Delta_{11}, \Delta_{12}, \Delta_{22}$ Various cofactors of Δ.
$\mathscr{R}z_{11}, \mathscr{R}z_{12}, \mathscr{R}z_{22}$ = Real parts of z_{11}, z_{12} and z_{22}.
C_1, C_2 = Shunt capacitances at ends 1 and 2, respectively, of a 4-pole system.
C = Shunt capacitance at either end of a symmetrical 4-pole system.
a, b = Parameters used in Sections 2.1, 2.2, and 2.3.
k = Parameter used in Sections 2.1, 2.2 and 2.4.
x = Parameter used in Sections 2.1 and 2.2.
y = Parameter used in Section 2.2.
k_1, k_2 = Parameters used in Sections 2.3 and 2.5.
x_1, x_2 = Parameters used in Sections 2.3, 2.4 and 2.5.
$Z_a = z_{11} - z_{12}$.
$Z_b = z_{11} + z_{12}$.
α, β, γ = Parameters used in Sections 2.4 and 2.5.
T_R = Rise-time using Elmore's definition.
Φ = Figure of merit of network using Elmore's rise-time definition.
Φ_{max} = Maximum value of Φ obtainable with monotonic response.
$f_n(t)$ = Transient response to a step-function drive, normalized to unity at infinite time.
G = Direct-current gain of network.
A, B = Real and either of the imaginary parts, respectively, of a pair of conjugate complex poles.
$D = B/A$.

(1) INTRODUCTION

The methods used here are basically the same as those adopted by the author in a previous paper[1] on 2-terminal networks. Thus no particular form of network is assumed at the outset and the discussion is conducted in terms of the poles and zeros of the network functions. The maximum obtainable d.c. gain of the open-circuit transfer impedance of a passive 4-terminal network is, for given poles and zeros, limited by the passive restrictions and the parasitic shunt capacitances. In the following Section maximum possible d.c. gains are derived for some networks containing up to three poles.

(2) OPEN-CIRCUIT TRANSFER IMPEDANCES HAVING MAXIMUM POSSIBLE D.C. GAIN

As is well known,[2] the external behaviour of a linear 4-terminal network (4-pole) is completely determined by four independent functions of frequency (or functions of p, the complex frequency), e.g. the open-circuit impedance functions z_{11}, z_{12}, z_{21} and z_{22}. For a passive 4-pole composed exclusively of reciprocal elements, such as that being considered here, $z_{12} = z_{21}$. If, in addition, the 4-pole is symmetrical, $z_{11} = z_{22}$. The expressions for the open-circuit impedance functions in terms of the nodal determinant, Δ, of the 4-pole and its various cofactors are

$$\left.\begin{aligned} z_{11} &= \frac{\Delta_{11}}{\Delta} \\ z_{12} &= \frac{\Delta_{12}}{\Delta} \\ z_{22} &= \frac{\Delta_{22}}{\Delta} \end{aligned}\right\} \quad \ldots\ldots\ldots \quad (1)$$

Thus, for a 4-pole composed of lumped linear elements, the z's are ratios of polynomials in p with real coefficients, and stability considerations confine the poles of the z's to the left-half p-plane. The zeros of z_{11} and z_{22} are also confined to the left-half p-plane, as are those of z_{12} in the case of a minimum-phase 4-pole, but in general the zeros of z_{12} can lie anywhere in the plane.

The fact that the 4-pole is passive means that the following restrictions are placed upon the real parts of the z's at real frequencies:

$$\left.\begin{aligned} \mathscr{R}z_{11} &\geqslant 0 \\ \mathscr{R}z_{11}\mathscr{R}z_{22} - (\mathscr{R}z_{12})^2 &\geqslant 0 \\ \mathscr{R}z_{22} &\geqslant 0 \end{aligned}\right\} \quad \ldots\ldots \quad (2)$$

These restrictions were first derived by Vaulot[3] and later by Gewertz,[4] who also gave a general synthesis procedure for a linear passive 4-pole. A much simpler derivation of these restrictions was given by Tellegen.[5]

If a 4-pole has parasitic shunt capacitances across both ends, various additional restrictions are imposed on the open-circuit impedance functions. For the transfer impedance z_{12}, the number of zeros cannot be greater than one less than the number of poles, and for the driving-point functions z_{11} and z_{22}, the number of zeros must be equal to one less than the number of

Correspondence on Monographs is invited for consideration with a view to publication.
Dr. Cutteridge is in the Electrical Engineering Department, Faculty of Technology, University of Manchester.

poles; this is to ensure correct behaviour at infinite frequency. If the number of zeros of z_{12} is less than the number of poles by at least two,* then, at infinite frequency, z_{11} and z_{22} tend to $1/pC_1$ and $1/pC_2$, respectively, where C_1 and C_2 are the shunt capacitances at ends 1 and 2, respectively,† and $p = j\omega$. By substituting these restrictions in eqns. (2), one can obtain an upper limit to the d.c. gain of z_{12}. The exact form for the optimum z_{12} functions will depend on the particular pole-zero combinations, and some of the simpler cases are now considered.

(2.1) Symmetrical 4-Pole with Transfer Impedance z_{12} having Two Poles and no Zeros

Let the parasitic shunt capacitance at both ends of the 4-pole be C. The open-circuit impedance functions can be written

$$\left.\begin{aligned} z_{12}(p) &= \frac{k}{p^2 + 2ap + b} \\ z_{11}(p) &= \frac{1}{C}\,\frac{p + x}{p^2 + 2ap + b} \end{aligned}\right\} \quad . \quad . \quad . \quad . \quad (3)$$

where $a > 0$, $b > 0$, $x > 0$.

$$\left.\begin{aligned} \text{Hence} \qquad \mathscr{R}z_{12}(j\omega) &= \frac{k(b - \omega^2)}{(b - \omega^2)^2 + 4a^2\omega^2} \\ \text{and} \qquad \mathscr{R}z_{11}(j\omega) &= \frac{1}{C}\,\frac{xb + \omega^2(2a - x)}{(b - \omega^2)^2 + 4a^2\omega^2} \end{aligned}\right\} \quad . \quad . \quad . \quad (4)$$

Substituting eqns. (4) into the passive restrictions (2), we have

$$2a \geqslant x \quad . \quad . \quad . \quad . \quad . \quad . \quad . \quad . \quad (5)$$

and $$[xb + \omega^2(2a - x)]^2 - C^2k^2[b - \omega^2]^2 \geqslant 0$$

which finally reduces to

$$(x^2 - C^2k^2)(b^2) + 2(\omega^2 b)[x(2a - x) + C^2k^2] + \omega^4[(2a - x)^2 - C^2k^2] \geqslant 0 \quad (6)$$

For condition (6) to be satisfied by all $\omega^2 \geqslant 0$, we must have

$$\left.\begin{aligned} x^2 &\geqslant C^2k^2 \\ (2a - x)^2 &\geqslant C^2k^2 \end{aligned}\right\} \quad . \quad . \quad . \quad . \quad . \quad . \quad (7)$$

Thus

$$\left.\begin{aligned} (C^2k^2)_{max} &= a^2 \\ \text{given by} \qquad x &= a \end{aligned}\right\} \quad . \quad . \quad . \quad . \quad . \quad . \quad (8)$$

$$\left.\begin{aligned} \text{giving} \qquad (z_{12})_{opt} &= \pm\,\frac{a}{C(p^2 + 2ap + b)} \\ \text{with corresponding} \quad z_{11} &= \frac{1}{C}\,\frac{(p + a)}{(p^2 + 2ap + b)} \end{aligned}\right\} \quad . \quad . \quad . \quad (9)$$

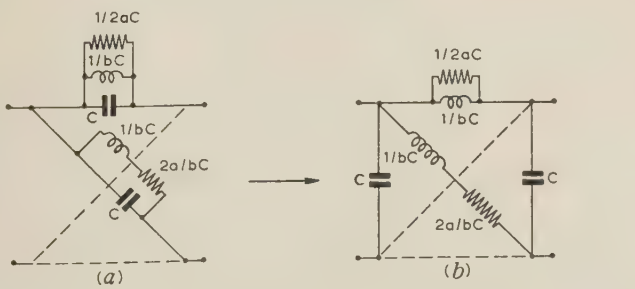

Fig. 1.—Lattice realization of optimum network for symmetrical 4-pole with transfer impedance z_{12} having two poles and no zeros.

* If the number of zeros of z_{12} is one less than the number of poles, the position is different; such a case is considered in Section 2.3.

† C_1 and C_2 will have this significance throughout the paper; C will be written for C_1 and C_2 in the case of a symmetrical 4-pole.

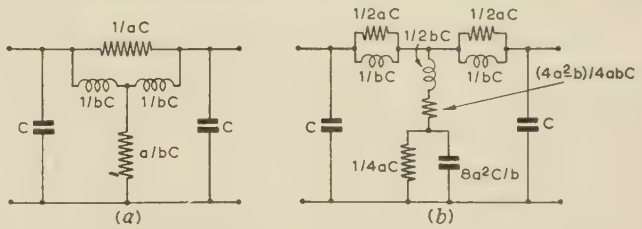

Fig. 2.—Unbalanced networks equivalent to lattice network of Fig. 1.
(*a*) Bridged-T network.
(*b*) π-network, realizable for $4a^2 \geqslant b$.

The corresponding physical network can be realized as a symmetrical lattice in the usual manner;[6] the realization for z_{12} with the positive sign is shown in Fig. 1. Fig. 2 shows two unbalanced networks developed from the lattice of Fig. 1.

(2.2) Asymmetrical 4-Pole with Transfer Impedance z_{12} having Two Poles and no Zeros

Let C_1 and C_2 be the parasitic shunt capacitances across ends 1 and 2 of the 4-pole. The open-circuit impedance functions then take the following forms:

$$\left.\begin{aligned} z_{12}(p) &= \frac{k}{p^2 + 2ap + b} \\ z_{11}(p) &= \frac{1}{C_1}\,\frac{p + x}{p^2 + 2ap + b} \\ z_{22}(p) &= \frac{1}{C_2}\,\frac{p + y}{p^2 + 2ap + b} \end{aligned}\right\} \quad . \quad . \quad . \quad (10)$$

where $a > 0$, $b > 0$, $x > 0$, $y > 0$.

$$\left.\begin{aligned} \text{Hence} \qquad \mathscr{R}z_{12}(j\omega) &= \frac{k(b - \omega^2)}{(b - \omega^2)^2 + 4a^2\omega^2} \\ \mathscr{R}z_{11}(j\omega) &= \frac{1}{C_1}\,\frac{xb + \omega^2(2a - x)}{(b - \omega^2)^2 + 4a^2\omega^2} \\ \text{and} \qquad \mathscr{R}z_{22}(j\omega) &= \frac{1}{C_2}\,\frac{yb + \omega^2(2a - y)}{(b - \omega^2)^2 + 4a^2\omega^2} \end{aligned}\right\} \quad . \quad . \quad (11)$$

Thus $\mathscr{R}z_{11} \geqslant 0$ and $\mathscr{R}z_{22} \geqslant 0$ imply, respectively,

$$\left.\begin{aligned} 2a &\geqslant x \\ \text{and} \qquad 2a &\geqslant y \end{aligned}\right\} \quad . \quad . \quad . \quad . \quad . \quad . \quad . \quad (12)$$

and the restriction $\mathscr{R}z_{11}\mathscr{R}z_{22} - (\mathscr{R}z_{12})^2 \geqslant 0$ yields

$$b^2(xy - C_1C_2k^2) + b\omega^2[x(2a - y) + y(2a - x) + 2C_1C_2k^2] + \omega^4[(2a - x)(2a - y) - k^2C_1C_2] \geqslant 0 \quad (13)$$

For condition (13) to be satisfied for all $\omega^2 \geqslant 0$, we must have

$$\left.\begin{aligned} xy &\geqslant C_1C_2k^2 \\ (2a - x)(2a - y) &\geqslant C_1C_2k^2 \end{aligned}\right\} \quad . \quad . \quad . \quad (14)$$

From conditions (14) it is easily seen that

$$\left.\begin{aligned} (C_1C_2k^2)_{max} &= a^2 \\ \text{given by} \qquad x &= y = a \end{aligned}\right\} \quad . \quad . \quad . \quad . \quad (15)$$

Thus

$$\left.\begin{aligned} (z_{12})_{opt} &= \pm\,\frac{a}{(p^2 + 2ap + b)\sqrt{(C_1C_2)}} \\ \text{with corresponding} \\ z_{11} &= \frac{1}{C_1}\,\frac{p + a}{p^2 + 2ap + b} \\ \text{and} \qquad z_{22} &= \frac{1}{C_2}\,\frac{p + a}{p^2 + 2ap + b} \end{aligned}\right\} \quad . \quad . \quad (16)$$

One possible physical realization of the network corresponding to eqns. (16) is easily obtained by examining the form of the z-matrix of a 4-pole preceded by an ideal transformer (see, for example, Reference 2). It is then seen that, by preceding one of the optimum 4-poles derived in Section 2.1 by an ideal transformer of turns ratio $1 : \sqrt{(C_1/C_2)}$ [or, equally well, by following the 4-pole by an ideal transformer of ratio $1 : \sqrt{(C_2/C_1)}$], a realization corresponding to eqns. (16) is obtained.

(2.3) Symmetrical 4-Pole with Transfer Impedance z_{12} having Two Poles and One Zero

The open-circuit impedance functions can be written:

$$\left.\begin{aligned} z_{12}(p) &= \frac{k_2 p + k_1}{p^2 + 2ap + b} \\ \text{and} \quad z_{11}(p) &= \frac{x_2 p + x_1}{p^2 + 2ap + b} \end{aligned}\right\} \quad . \quad . \quad . \quad . \quad (17)$$

where $a > 0$, $b > 0$, $x_1 > 0$, $x_2 > 0$.

Owing to the form of the transfer function in this case, the driving-point function no longer tends to $1/pC$ at infinity, where C is the parasitic shunt capacitance at each end of the 4-pole. The effect of the shunt capacitance can be introduced as follows:

$$\left.\begin{aligned} z_{11} - z_{12} = Z_a, \text{ say} &= \frac{(x_2 - k_2)p + (x_1 - k_1)}{p^2 + 2ap + b} \\ \text{and} \quad z_{11} + z_{12} = Z_b, \text{ say} &= \frac{(x_2 + k_2)p + (x_1 + k_1)}{p^2 + 2ap + b} \end{aligned}\right\} \quad (18)$$

Hence, at infinite frequency, Z_a becomes a capacitance of $1/(x_2 - k_2)$ and Z_b becomes a capacitance of $1/(x_2 + k_2)$. Thus, equating the smaller of these capacitances to C and making the larger capacitance positive,

$$\left.\begin{aligned} & x_2 + k_2 = 1/C \\ \text{and} \quad & x_2 - k_2 > 0 \end{aligned}\right\} \text{ for } k_2 > 0 \quad . \quad . \quad . \quad (19)$$

$$\left.\begin{aligned} \text{or} \quad & x_2 - k_2 = 1/C \\ \text{and} \quad & x_2 + k_2 > 0 \end{aligned}\right\} \text{ for } k_2 < 0 \quad . \quad . \quad . \quad (20)$$

The real parts of z_{11} and z_{12} are easily obtained as

$$\left.\begin{aligned} \mathscr{R}z_{11}(j\omega) &= \frac{bx_1 + \omega^2(2ax_2 - x_1)}{(b - \omega^2)^2 + 4a^2\omega^2} \\ \text{and} \quad \mathscr{R}z_{12}(j\omega) &= \frac{bk_1 + \omega^2(2ak_2 - k_1)}{(b - \omega^2)^2 + 4a^2\omega^2} \end{aligned}\right\} \quad . \quad . \quad (21)$$

Thus $\mathscr{R}z_{11} \geqslant 0$ and $(\mathscr{R}z_{11})^2 - (\mathscr{R}z_{12})^2 \geqslant 0$ imply, respectively,

$$2ax_2 - x_1 \geqslant 0 \quad . \quad . \quad . \quad . \quad . \quad . \quad (22)$$

and

$$b^2(x_1^2 - k_1^2) + 2b\omega^2[x_1(2ax_2 - x_1) - k_1(2ak_2 - k_1)] + \omega^4[(2ax_2 - x_1)^2 - (2ak_2 - k_1)^2] \geqslant 0 \quad (23)$$

For condition (23) to be satisfied it is necessary that

$$x_1^2 \geqslant k_1^2 \quad . \quad . \quad . \quad . \quad . \quad . \quad (24)$$

and

$$(2ax_2 - x_1)^2 \geqslant (2ak_2 - k_1)^2 \quad . \quad . \quad . \quad (25)$$

On substituting conditions (19) and (20) in (25) and optimizing k_1 in accordance with (22) and (24), the optimum z_{12} is finally given by

$$(z_{12})_{opt} = \pm \frac{1}{C} \frac{(k_2 C)p + a}{p^2 + 2ap + b} \quad . \quad . \quad . \quad (26)$$

with corresponding

$$z_{11} = \frac{1}{C} \frac{(x_2 C)p + a}{p^2 + 2ap + b} \quad . \quad . \quad . \quad . \quad (27)$$

$$\left.\begin{aligned} \text{where} \quad & 0 < k_2 C < 1/2 \\ \text{and} \quad & 1 > x_2 C > 1/2 \end{aligned}\right\} \quad . \quad . \quad . \quad . \quad . \quad (28)$$

$$\left.\begin{aligned} \text{and such that} \quad & x_2 C + k_2 C = 1 \\ \text{and} \quad & x_2 C > k_2 C \end{aligned}\right\} \quad . \quad . \quad . \quad . \quad . \quad (29)$$

Eqn. (26) was obtained on the basis of k_1 and k_2 having the same sign. If k_1 and k_2 are of opposite sign, the optimum value of k_1 is found to occur when $k_2 = 0$, which means eliminating the zero of z_{12} initially assumed to be present. This case then reduces to that considered in Section 2.1, with identical results.

Inserting eqns. (26) and (27) in (18), and taking the positive sign in eqn. (26) for concreteness,* we have

$$z_{11} - z_{12} = Z_a = \frac{1}{C} \frac{(x_2 C - k_2 C)p}{p^2 + 2ap + b} \quad . \quad . \quad (30)$$

and

$$z_{11} + z_{12} = Z_b = \frac{1}{C} \frac{p + 2a}{p^2 + 2ap + b} \quad . \quad . \quad . \quad (31)$$

Since

$$\frac{1}{Z_a} = \frac{p}{x_2 - k_2} + \frac{2a}{x_2 - k_2} + \frac{b}{x_2 - k_2} \frac{1}{p} \quad . \quad . \quad (32)$$

and

$$\frac{1}{Z_b} = pC + \frac{1}{(p + 2a)/bC} \quad . \quad . \quad . \quad . \quad (33)$$

one possible physical realization of the 4-pole is as shown in Fig. 3.

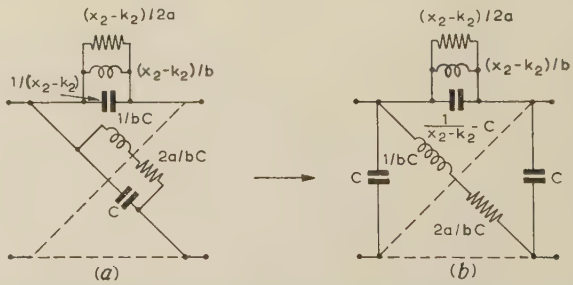

Fig. 3.—Lattice realization of optimum network for symmetrical 4-pole with transfer impedance z_{12} having two poles and one zero.

(2.4) Symmetrical 4-Pole with Transfer Impedance z_{12} having Three Poles and no Zeros

The open-circuit impedance functions can be written:

$$\left.\begin{aligned} z_{12}(p) &= \frac{k}{p^3 + \alpha p^2 + \beta p + \gamma} \\ \text{and} \quad z_{11}(p) &= \frac{1}{C} \frac{p^2 + x_2 p + x_1}{p^3 + \alpha p^2 + \beta p + \gamma} \end{aligned}\right\} \quad . \quad . \quad . \quad (34)$$

where $x_1 > 0, x_2 > 0, \alpha > 0, \beta > 0, \gamma > 0$

and, in addition, $\alpha\beta > \gamma \quad . \quad . \quad . \quad . \quad . \quad . \quad . \quad (35)$

which is obtained by applying the Hurwitz stability criteria to the cubic polynomial, whose zeros must be confined to the left half-plane.

* The negative sign in eqn. (26) would only interchange Z_a and Z_b in eqns. (30) and (31).

Hence

$$\mathscr{R}z_{12}(j\omega) = \frac{k(\gamma - \alpha\omega^2)}{(\gamma - \alpha\omega^2)^2 + \omega^2(\beta - \omega^2)^2}$$

and

$$\mathscr{R}z_{11}(j\omega) = \frac{1}{C}\,\frac{x_1\gamma + \omega^2(x_2\beta - x_1\alpha - \gamma) + \omega^4(\alpha - x_2)}{(\gamma - \alpha\omega^2)^2 + \omega^2(\beta - \omega^2)^2} \qquad (36)$$

Substituting eqns. (36) into the passive restrictions (2), we have

$$x_1\gamma + \omega^2(x_2\beta - x_1\alpha - \gamma) + \omega^4(\alpha - x_2) \geqslant 0 \qquad (37)$$

and

$$[x_1\gamma + \omega^2(x_2\beta - x_1\alpha - \gamma) + \omega^4(\alpha - x_2)]^2 - C^2k^2(\gamma - \alpha\omega^2)^2 \geqslant 0 \qquad (38)$$

Now, for $k > 0$, condition (38) reduces to

$$x_1\gamma + \omega^2(x_2\beta - x_1\alpha - \gamma) + \omega^4(\alpha - x_2) - Ck(\gamma - \alpha\omega^2) \geqslant 0$$

for $$0 < \alpha\omega^2 < \gamma \qquad (39)$$

and

$$x_1\gamma + \omega^2(x_2\beta - x_1\alpha - \gamma) + \omega^4(\alpha - x_2) + Ck(\gamma - \alpha\omega^2) \geqslant 0$$

for $$\gamma < \alpha\omega^2 < \infty \qquad (40)$$

Some immediate consequences from conditions (37)–(40) are

$$\alpha - x_2 \geqslant 0 \qquad (41)$$

$$x_1 - Ck \geqslant 0 \qquad (42)$$

Assuming* that $(Ck)_{max}$ is obtained when $x_1 = Ck$, and substituting this in condition (40),

$$2\gamma Ck + \omega^2(x_2\beta - \gamma - 2\alpha Ck) + \omega^4(\alpha - x_2) \geqslant 0$$

for $$\gamma < \alpha\omega^2 < \infty \qquad (43)$$

The limiting value of Ck from (43) is obtained when the left-hand side is a perfect square, the condition for which is

$$(x_2\beta - \gamma - 2\alpha Ck)^2 = 8\gamma Ck(\alpha - x_2) \qquad (44)$$

If both sides of eqn. (44) are differentiated with respect to x_2 and $d(Ck)/dx_2$ is put equal to zero, $(Ck)_{max}$ is finally obtained as

$$(Ck)_{max} = \tfrac{1}{2}\beta \qquad (45)$$

given by $$x_2 = \frac{\alpha\beta - \gamma}{\beta} \qquad (46)$$

It will be found that these values satisfy (37) and that (38) reduces to

$$(\gamma/\beta^2)\omega^2(\omega^2 - \beta)^2[\gamma\omega^2 + \beta(\alpha\beta - 2\gamma)] \geqslant 0 \qquad (47)$$

Thus $(Ck)_{max}$ will be given by eqn. (45) only provided that $\alpha\beta \geqslant 2\gamma$, since otherwise (47) will not be satisfied at very low frequencies.

Hence $$(z_{12})_{opt} = \pm\frac{\beta/2}{C(p^3 + \alpha p^2 + \beta p + \gamma)}$$

with corresponding $$z_{11} = \frac{p^2 + (\alpha\beta - \gamma)p/\beta + \beta/2}{C(p^3 + \alpha p^2 + \beta p + \gamma)} \qquad (48)$$

provided that $$\alpha\beta \geqslant 2\gamma \qquad (49)$$

A possible lattice realization of the corresponding 4-pole is shown in Fig. 4 for z_{12} with positive sign.

* It can easily be verified that this does, in fact, yield the maximum value of Ck.

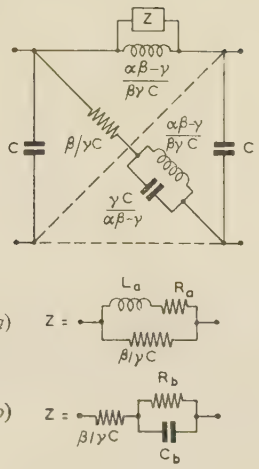

Fig. 4.—Lattice realization of optimum network for symmetrical 4-pole with transfer impedance z_{12} having three poles and no zeros.

(*a*) For $\beta^3(\alpha\beta - 2\gamma) > \gamma(\alpha\beta - \gamma)^2$

$$L_a = \frac{\beta^2(\alpha\beta - \gamma)}{\beta^3C(\alpha\beta - 2\gamma) - \gamma C(\alpha\beta - \gamma)^2}$$

$$R_a = \frac{\beta(\alpha\beta - \gamma)^2}{\beta^3C(\alpha\beta - 2\gamma) - \gamma C(\alpha\beta - \gamma)^2}$$

(*b*) For $\beta^3(\alpha\beta - 2\gamma) < \gamma(\alpha\beta - \gamma)^2$

$$R_b = \frac{\gamma(\alpha\beta - \gamma)^2 - \beta^3(\alpha\beta - 2\gamma)}{\beta^2\gamma C(\alpha\beta - 2\gamma)}$$

$$C_b = \frac{\gamma^2C(\alpha\beta - \gamma)}{\gamma(\alpha\beta - \gamma)^2 - \beta^3(\alpha\beta - 2\gamma)}$$

(2.5) Symmetrical 4-Pole with Transfer Impedance z_{12} having Three Poles and One Zero

The open-circuit impedance functions are here

$$z_{12}(p) = \frac{k_2p + k_1}{p^3 + \alpha p^2 + \beta p + \gamma}$$

and

$$z_{11}(p) = \frac{1}{C}\,\frac{p^2 + x_2p + x_1}{p^3 + \alpha p^2 + \beta p + \gamma} \qquad (50)$$

where, as in Section 2.4, $\alpha > 0$, $\beta > 0$, $\gamma > 0$, $x_1 > 0$, $x_2 > 0$ and $\alpha\beta > \gamma$. Further, in the first instance, take $k_1 > 0$. Then $(\mathscr{R}z_{11})^2 - (\mathscr{R}z_{12})^2 \geqslant 0$ finally reduces to

$$[x_1\gamma + \omega^2(x_2\beta - x_1\alpha - \gamma) + \omega^4(\alpha - x_2)]^2 - C^2[k_1\gamma + \omega^2(k_2\beta - k_1\alpha) - k_2\omega^4]^2 \geqslant 0 \qquad (51)$$

Proceeding as in Section 2.4, we finally obtain

$$(Ck_1)_{max} = \tfrac{1}{2}\beta \qquad (52)$$

given by $$x_2 + Ck_2 = \frac{\alpha\beta - \gamma}{\beta} \qquad (53)$$

Substituting these values in condition (51) yields

$$(\gamma/\beta)(\omega^2 - \beta)^2[\omega^2(x_2\beta - Ck_2\beta - \gamma) + \omega^4(\alpha - x_2 + Ck_2)] \geqslant 0 \qquad (54)$$

Thus $(Ck_1)_{max}$ will be given by eqn. (52) only provided that

$$x_2\beta - Ck_2\beta \geqslant \gamma \qquad (55)$$

and $$x_2\beta - Ck_2\beta \leqslant \alpha\beta \qquad (56)$$

otherwise (54) will not be satisfied at very low and very high frequencies. Eqn. (53) and conditions (55) and (56) together

determine the following ranges of values of x_2 and Ck_2 consistent with $Ck_1 = \frac{1}{2}\beta$:

$$\alpha - \frac{\gamma}{2\beta} > x_2 > \frac{\alpha}{2} \quad . \quad . \quad . \quad . \quad . \quad . \quad (57)$$

$$-\frac{\gamma}{2\beta} < Ck_2 < \frac{\alpha\beta - 2\gamma}{2\beta} \quad . \quad . \quad . \quad . \quad (58)$$

Thus k_2 will be negative (indicating a non-minimum-phase transfer impedance) over the whole range indicated by condition (58) unless $\alpha\beta > 2\gamma$.

It will be found that the pair of values $x_2 = \frac{1}{2}\alpha$ and $Ck_2 = (\alpha\beta - 2\gamma)/2\beta$ satisfy the equation $\mathscr{R}z_{11} \geqslant 0$ provided that the Hurwitz condition, $\alpha\beta > \gamma$, is satisfied. Other pairs of values of x_2 and Ck_2 from conditions (57) and (58) will satisfy $\mathscr{R}z_{11} \geqslant 0$ only if an additional restriction exists on the values of α, β and γ.

For example, it is easily verified that

$$\left.\begin{aligned} x_2 = \alpha - \frac{\gamma}{2\beta},\ Ck_2 = -\frac{\gamma}{2\beta} \\ \text{are possible only provided that} \\ 5\gamma > \alpha\beta > \gamma \end{aligned}\right\} \quad . \quad . \quad . \quad (59)$$

and

$$\left.\begin{aligned} x_2 = \frac{\alpha\beta - \gamma}{\beta},\ Ck_2 = 0 \\ \text{are possible only provided that} \\ \alpha\beta > 2\gamma \end{aligned}\right\} \quad . \quad . \quad . \quad . \quad (60)$$

which latter result checks with that obtained in Section 2.4.

To summarize:

$$\left.\begin{aligned} (z_{12})_{opt} = \pm \frac{Ck_2 p + \beta/2}{C(p^3 + \alpha p^2 + \beta p + \gamma)} \\ \text{with corresponding} \\ z_{11} = \frac{p^2 + x_2 p + \beta/2}{C(p^3 + \alpha p^2 + \beta p + \gamma)} \end{aligned}\right\} \quad . \quad . \quad (61)$$

where Ck_2 lies within the range given by (58) and the corresponding value of x_2 is obtained from eqn. (53). In general, an additional restriction exists on the values of α, β and γ, its exact nature depending on the value of Ck_2 selected. Two examples of this are given in eqns. (59) and (60) and no extra restriction is, in fact, necessary when Ck_2 has its maximum possible value of $(\alpha\beta - 2\gamma)/2\beta$.

(3) MAXIMUM-GAIN/RISE-TIME QUOTIENTS CONSISTENT WITH MONOTONIC RESPONSE

In this Section, various transfer-impedance functions having maximum gain, derived in Section 2, are taken in turn and their poles and zeros adjusted so as to produce a monotonically increasing output having minimum rise-time when a step-function input is applied.

In order to obtain a measure of the relative efficiencies of networks in this respect, it is convenient to define the figure of merit of a network as

$$\frac{\text{Gain/rise-time of network}}{\text{Gain/rise-time of parallel } RC \text{ network}^*}$$

Its value for a particular network will depend somewhat on the definition of rise-time adopted. Two definitions will be used here; one is the time taken for the response to a step-function drive to rise from 10% to 90% of its final value, and the other is Elmore's[6] definition. The latter is applicable only in the case of monotonic response but has the advantage of being easily derived from the Laplace transform of the output. Thus, if F(p) is the p-multiplied Laplace transform of the response, normalized to unity at infinite time, to a step-function drive

and

$$F(p) = \frac{1 + a_1 p + a_2 p^2 + \ldots + a_m p^m}{1 + b_1 p + b_2 p^2 + \ldots + b_n p^n} \quad . \quad . \quad (62)$$

then T_R, Elmore's definition of rise-time, is given by

$$\frac{T_R^2}{2\pi} = b_1^2 - a_1^2 + 2(a_2 - b_2) \quad . \quad . \quad . \quad . \quad (63)$$

(3.1) Maximum Figure of Merit Obtainable with Two Poles and no Zeros

The optimum function z_{12} is given in eqn. (16) as

$$(z_{12})_{opt} = \pm \frac{a}{(p^2 + 2ap + b)\sqrt{(C_1 C_2)}}$$

For this function, T_R is easily shown to be given by

$$\frac{T_R^2}{2\pi} = \frac{2(2a^2 - b)}{b^2} \quad . \quad . \quad . \quad . \quad . \quad (64)$$

and hence, if Φ is the figure of merit using Elmore's rise-time definition,

$$\Phi = \frac{\frac{1}{2}(C_1 + C_2)}{\sqrt{(C_1 C_2)}} \sqrt{\left(\frac{2a^2}{2a^2 - b}\right)} \quad . \quad . \quad . \quad (65)$$

The maximum possible value of b consistent with monotonic response is $b = a^2$, which corresponds to the critically damped condition of two coincident real poles. Writing Φ_{max} for the maximum Φ obtainable with monotonic response, we have

$$\Phi_{max} = \frac{\frac{1}{2}(C_1 + C_2)}{\sqrt{(C_1 C_2)}} \sqrt{2} \quad . \quad . \quad . \quad . \quad (66)$$

which reduces to $\sqrt{2}$ for equal input and output capacitances. If these capacitances are unequal, the figure of merit would be somewhat greater, e.g. 6% and 15% larger for capacitance ratios of 2 : 1 and 3 : 1, respectively.

If $f_n(t)$ is the transient response normalized to unity at infinite time in the critically damped case, then

$$f_n(t) = 1 - [1 + t/G\sqrt{(C_1 C_2)}] \exp [-t/G\sqrt{(C_1 C_2)}] \quad (67)$$

where G is the d.c. gain,* from which the 10%–90% rise-time is found to be $3{\cdot}36\ G\sqrt{(C_1 C_2)}$, corresponding to a figure of merit, using the 10%–90% rise-time definitions, of $0{\cdot}654\ (C_1 + C_2)/\sqrt{(C_1 C_2)}$ or 1·31 for equal input and output capacitances.

(3.2) Maximum Value of Figure of Merit Obtainable with Two Poles and One Zero

The optimum relations are derived in eqns. (26) and (28), namely

$$(z_{12})_{opt} = \pm \frac{1}{C} \frac{(k_2 C)p + a}{p^2 + 2ap + b}$$

with $0 < k_2 C < 0{\cdot}5$.

Eqn. (26) gives

$$\frac{T_R^2}{2\pi} = \frac{4a^2}{b^2} - \frac{(k_2 C)^2}{a^2} - \frac{2}{b} \quad . \quad . \quad . \quad . \quad (68)$$

and hence

$$\Phi = \frac{2a^2}{\sqrt{[4a^4 - (k_2 C)^2 b^2 - 2a^2 b]}} \quad . \quad . \quad . \quad (69)$$

Inserting the maximum value of b consistent with monotonic response ($=a^2$) and the maximum of $k_2 C (=0{\cdot}5)$ in eqn. (69), we have

$$\Phi_{max} = \frac{4}{\sqrt{7}} = 1{\cdot}51 \quad . \quad . \quad . \quad . \quad . \quad (70)$$

* The shunt capacitance of this network should be equal to the sum of the input and output shunt capacitances of the 4-pole system under consideration.

* G has this significance throughout the remainder of the paper.

By taking k_2C slightly less than 0·5 a figure of merit slightly less than $4/\sqrt{7}$ could be obtained without degeneracy in the corresponding network, realized in Fig. 3.

The normalized transient response in the limiting case, $f_n(t)$, is given by

$$f_n(t) = 1 - (1 + t/2GC)\varepsilon^{-t/GC} \quad . \quad . \quad . \quad (71)$$

from which the 10%–90% rise-time and the 10%–90% figure of merit are found to be $3{\cdot}07GC$ and 1·43, respectively.

(3.3) Maximum Value of Figure of Merit Obtainable with Three Poles and no Zeros

Here the appropriate maximum gain function, given by eqn. (48), is

$$(z_{12})_{opt} = \pm \frac{\beta/2}{C(p^3 + \alpha p^2 + \beta p + \gamma)}$$

provided that $\alpha\beta \geqslant 2\gamma$.

For this function,

$$\frac{T_R^2}{2\pi} = \frac{\beta^2 - 2\alpha\gamma}{\gamma^2} \quad . \quad . \quad . \quad . \quad . \quad (72)$$

and hence

$$\Phi = \frac{1}{\sqrt{(1 - 2\alpha\gamma/\beta^2)}} \quad . \quad . \quad . \quad . \quad (73)$$

and the maximum value of $2\alpha\gamma/\beta^2$ consistent with monotonic response will yield Φ_{max}.

Consider first the case of z_{12} having three real poles; this will always result in monotonic response. The function $2\alpha\gamma/\beta^2$ will have its maximum value, $\frac{2}{3}$, when the three real poles are coincident.

Thus
$$\Phi_{max} = \sqrt{3} \quad . \quad . \quad . \quad . \quad . \quad . \quad (74)$$

for three real poles.

The other case to consider is that in which z_{12} has one real pole and the other two are conjugate complex. The limiting condition for monotonic response then is that the real parts of the poles should be equal, giving

$$\frac{2\alpha\gamma}{\beta^2} = 6\frac{(1 + B^2/A^2)}{(3 + B^2/A^2)^2} \quad . \quad . \quad . \quad . \quad (75)$$

where A is the real part of the poles and B is the imaginary part of either of the conjugate complex pair. The maximum of the function $2\alpha\gamma/\beta^2$ is now $\frac{3}{4}$, given by $B = A$, and hence

$$\Phi_{max} = 2 \quad . \quad . \quad . \quad . \quad . \quad . \quad (76)$$

for one pole real and two conjugate complex.

The corresponding normalized transient responses are

$$f_n(t) = 1 - \varepsilon^{-3t/2GC}[1 + 3t/2GC + \tfrac{1}{2}(3t/2GC)^2] \; . \quad (77)$$

and
$$f_n(t) = 1 - \varepsilon^{-t/GC}[2 - \cos(t/GC) + \sin(t/GC)] \; . \quad (78)$$

from which the 10% — 90% rise-times are, respectively, $2{\cdot}81GC$ and $2{\cdot}51GC$, yielding corresponding figures of merit, calculated using the 10% — 90% rise-time definition, of 1·56 and 1·75, respectively.

It is of interest to consider whether the value of B/A giving the maximum figure of merit calculated on an Elmore rise-time basis also yields the optimum figure of merit using 10% — 90% rise-time. For general values of B/A the normalized transient response to a step-function drive, $f_n(t)$, is given by

$$f_n(t) = 1 - \frac{1}{D^2}\exp\left(-\frac{3 + D^2}{1 + D^2}\frac{t}{2GC}\right)$$
$$\left[(1 + D^2) - \cos\left(\frac{3 + D^2}{1 + D^2}\frac{Dt}{2GC}\right) + D\sin\left(\frac{3 + D^2}{1 + D^2}\frac{Dt}{2GC}\right)\right] \quad (79)$$

where $D = B/A$.

From this the 10% — 90% rise-time and corresponding figure of merit can be calculated for various values of B/A. Fig. 5 shows the variation in figure of merit over the range $1 < B/A < 10$; the maximum is 1·96, given by $B/A = 2{\cdot}1$. This represents an 11% increase over the value obtained by assuming that the value of B/A which optimized the figure-of-merit on the basis of Elmore's rise-time also optimized that calculated on the 10% — 90% rise-time definition. Fig. 6 compares the transient response for coincident real poles with that for $B/A = 2$.

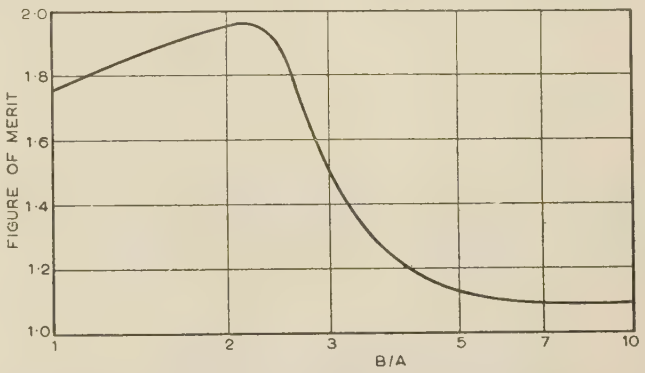

Fig. 5.—Variation of 10%–90% figure of merit with the parameter B/A.

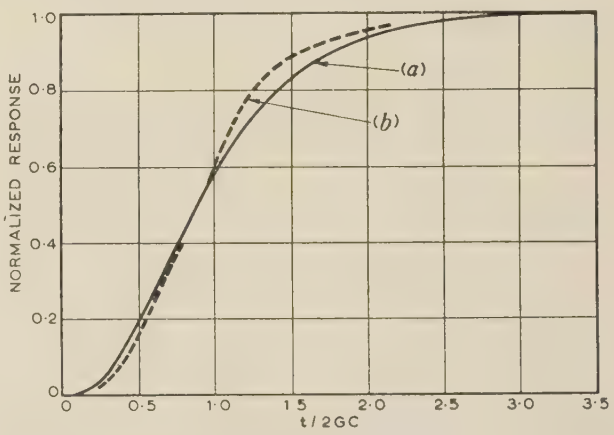

Fig. 6.—Two transient responses with three poles and no zeros.
(*a*) Coincident real poles.
(*b*) Collinear complex poles, $B/A = 2$.

(4) REFERENCES

(1) CUTTERIDGE, O. P. D.: 'Transient Response of Two-Terminal Networks', *Proceedings I.E.E.*, Monograph No. 212 R, December, 1956 (**104** C, p. 234).

(2) GUILLEMIN, E. A.: 'Communication Networks' (John Wiley, New York, 1935), Vol. 2, Chapter 4.

(3) VAULOT, A. E.: 'Sur les constantes du quadripôle passif', *Revue Générale de l'Électricité*, 1927, **22**, p. 493.

(4) GEWERTZ, C. M.: 'Synthesis of a Finite Four-Terminal Network from its Prescribed Driving-Point Functions and Transfer Function', *Journal of Mathematics and Physics*, 1933, **12**, p. 1.

(5) TELLEGEN, B. D. H.: 'Sur les constantes du quadripôle passif', *Revue Générale de l'Électricité*, 1928, **24**, p. 211.

(6) ELMORE, W. C.: 'The Transient Response of Damped Linear Networks with Particular Regard to Wide-Band Amplifiers', *Journal of Applied Physics*, 1948, **19**, p. 55.

621.317.333.82

The Institution of Electrical Engineers
Monograph No. 293 M
Feb. 1958
©

THE INTERPRETATION OF THE RESULTS OF IMPULSE BREAKDOWN TESTS

By R. HANCOX, B.Sc.(Eng.), Ph.D., Graduate.

(*The paper was first received* 23rd *September, and in revised form* 9th *December*, 1957. *It was published as an* INSTITUTION MONOGRAPH *in February*, 1958.)

SUMMARY

The paper considers a high-voltage impulse-breakdown test procedure consisting of a series of impulses of increasing magnitude leading to breakdown. The results expected from such a test are compared with the variation with voltage of the probability of breakdown for a single pulse.

LIST OF PRINCIPAL SYMBOLS

$P(V)$ = Probability of breakdown occurring as the result of the application of a single impulse of peak value V.
V_1 = Mean breakdown voltage, i.e. that voltage for which $P(V) = 0{\cdot}5$.
S_1 = Standard deviation of the distribution of $P(V)$ with voltage.
$Q(V)$ = Probability of breakdown occurring for the first time as the result of the application of the last impulse of a series of impulses increasing in regular steps to a voltage V.
V_s = Incremental voltage difference between successive impulses in an increasing series.
V_2 = Estimate of the mean breakdown voltage obtained from tests with series of increasing impulses.
S_2 = Standard deviation of the distribution of $Q(V)$ with voltage.

(1) INTRODUCTION

When a high-voltage impulse is applied to an insulating gap there is a certain probability that failure, or breakdown, of the dielectric will occur. This probability increases from zero to unity as the voltage is raised, and the mean breakdown voltage of the gap is defined as that voltage for which the probability of breakdown is one-half. If the mean breakdown voltage is to be measured experimentally, it is sometimes convenient to use a test procedure in which series of impulses of a given waveform and of regularly increasing magnitude are applied to the gap until failure occurs, since in this way the maximum information may be obtained from a limited number of breakdowns. Tests on the impulse breakdown strength of transformer oil or other liquid dielectrics are often made in this way. The results obtained with such a procedure, however, can be shown to be dependent on the value chosen for the incremental voltage difference between successive impulses in the series, and thus must be interpreted with care.* The paper considers the relationship between the results to be expected from experiments of this type and the variation with voltage of the probability of breakdown occurring as the result of the application of a single impulse.

(2) GENERAL ANALYSIS

The probability, $P(V)$, that breakdown of a gap will occur as the result of the application of a single impulse of peak value V has a distribution similar to that shown in Fig. 1(*a*), and the mean breakdown voltage, V_1, is defined as the voltage for which $P(V) = 0{\cdot}5$. However, when a series of impulses of increasing magnitude are applied to a gap, the probability that breakdown will occur for the first time at a particular voltage level is dependent on whether or not breakdown occurs at the lower levels. Thus the probability, $Q(V)$, of breakdown occurring for the first time at a voltage V under these conditions is equal to the probability of breakdown occurring as the result of the application of a single impulse of magnitude V multiplied by the product of the probabilities of breakdown not occurring for each of the preceding impulses. Thus if the peak values of successive impulses in the series are increased in regular steps equal to V_s from an initial value V_a, the probability that the first breakdown will occur as the result of the application of the Nth impulse is

$$Q(V) = P(V) \prod_{n=0}^{n=N-2} [1 - P(V_a + nV_s)] \quad . \quad . \quad (1)$$

where

$$V = V_a + (N-1)V_s \quad . \quad . \quad . \quad . \quad (2)$$

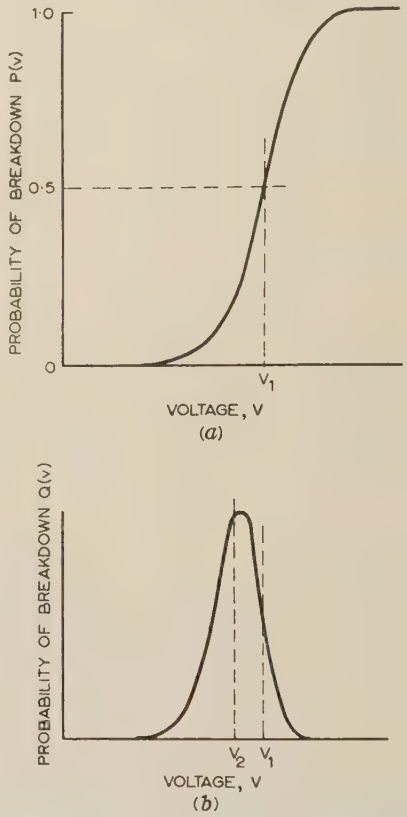

Fig. 1.—Variation of the probability of breakdown with voltage.
(*a*) For a single impulse.
(*b*) For a series of increasing impulses.

* LEWIS, T. J.: 'The Statistical Basis of Impulse Testing', *Proceedings I.E.E.*, Monograph No. 249 M, July, 1957 (105 C, p. 27).

Correspondence on Monographs is invited for consideration with a view to publication
Dr. Hancox is at the U.K.A.E.A. Atomic Energy Research Establishment.

Since $P(V)$ varies from zero to unity as the voltage is increased, $1 - P(V)$ must fall to zero for large voltages, and $Q(V)$ as defined by eqn. (1) must tend to zero for voltages which are considerably below or above the mean breakdown voltage. If $Q(V)$ is evaluated for any given incremental voltage V_s and a range of initial voltages $0 \leqslant V_a < V_s$, a continuous distribution is obtained similar to that shown in Fig. 1(*b*). This curve represents the results that would be obtained from an infinite series of tests under these conditions using series of increasing impulses leading to a breakdown. The mean voltage of the distribution, V_2, is the estimate of the mean breakdown voltage obtained in this manner, and does not necessarily coincide with V_1; it is given by

$$V_2 = \frac{\int_0^\infty Q(V)V\,dV}{\int_0^\infty Q(V)\,dV} \quad . \quad . \quad . \quad . \quad . \quad (3)$$

The variance (square of the standard deviation S_2) of the distribution is given by

$$S_2^2 = \frac{\int_0^\infty Q(V)(V - V_2)^2 dV}{\int_0^\infty Q(V)\,dV} \quad . \quad . \quad . \quad . \quad (4)$$

The relationship between V_1, V_2 and V_s is given by eqns. (1)–(3), and may be evaluated for any given distribution of $P(V)$.

(3) RESULTS WITH P(V) NORMALLY DISTRIBUTED

The variation of $P(V)$ with voltage obtained in breakdown tests often approximates to the normal distribution function, or integrated Gaussian distribution, given by

$$P(V) = \frac{1}{S_1\sqrt{(2\pi)}} \int_0^V \exp -\frac{(v - V_1)^2}{2S_1^2} dv \quad . \quad . \quad (5)$$

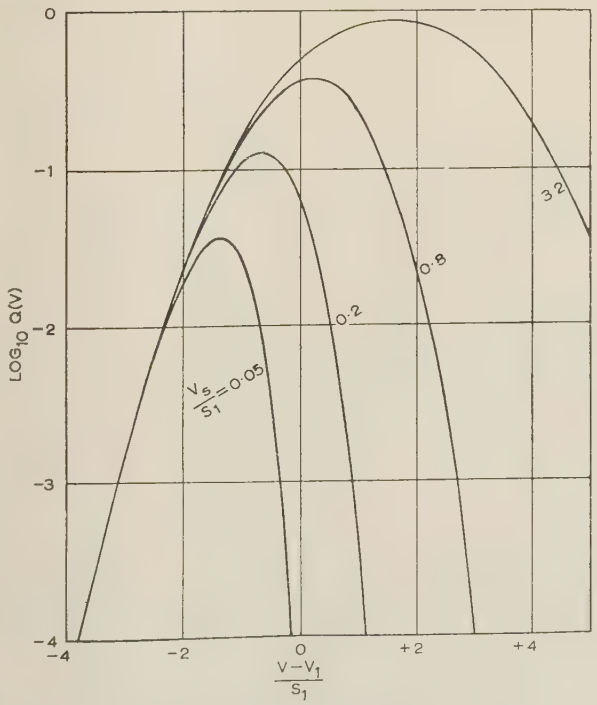

Fig. 2.—Variation of $Q(V)$ with voltage.

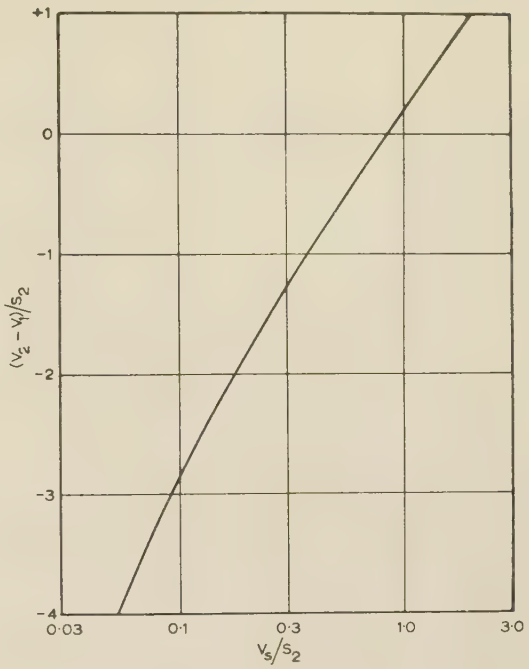

Fig. 3.—Difference in means of the distributions of $Q(V)$ and $P(V)$.

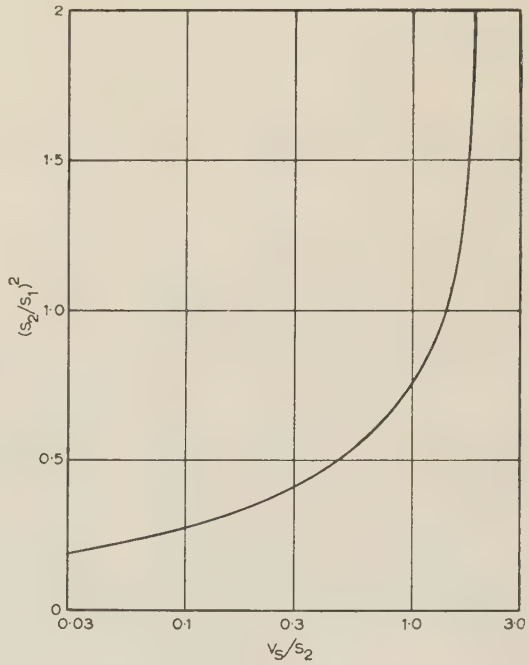

Fig. 4.—Ratio of the variances of the distributions of $Q(V)$ and $P(V)$.

provided that $P(V) = 1$ when $V \to \infty$, where V_1 is the mean breakdown voltage as previously defined and S_1 is the standard deviation of the distribution.

With this distribution of $P(V)$ assumed, several plots of $Q(V)$ have been computed from eqn. (1) using published values for the normal distribution function.* Some of these are shown in Fig. 2, from which it is possible to obtain the relationship between

* LINDLEY, D. V., and MILLER, J. C. P.: 'Cambridge Elementary Statistical Tables' (University Press, Cambridge, 1953).

V_1 and V_2 in terms of either S_1 or S_2. In Fig. 3 the difference between V_1 and V_2 is plotted against the incremental voltage, V_s, where both are expressed in terms of S_2. In Fig. 4 the ratio of the variances of the distributions of $Q(V)$ and $P(V)$ are plotted for various incremental voltages.

These curves have been calculated on the assumption that the values of the initial impulse, V_a, in each series are distributed uniformly in the range $0 \leqslant V_a < V_s$. If the initial voltage is not controlled in any test, the results obtained may differ from those plotted in Figs. 3 and 4, although the difference will not exceed a few per cent over the range of incremental voltages given by $V_s < S_2$, provided that $V_1 - V_a > 4S_1$. In any particular experiment an error may also arise from the limited number of results obtained; furthermore, the theory does not take into account the scatter introduced by inhomogeneities in the test specimens.

The results summarized in Fig. 3 show that the estimate of the mean breakdown voltage, V_2, may differ considerably from the mean breakdown voltage V_1. If, for example, in a test which consisted of the application of series of increasing impulses, the voltage was raised in steps equal to 2% of the estimate obtained for the mean breakdown voltage and the standard deviation of the results was 10% of this voltage, the estimate of the mean breakdown voltage would be 18% below the voltage which would give a probability of breakdown for a single impulse of one-half. The standard deviation of the probability of breakdown for a single impulse would be 16% in this example, which is 60% greater than the value given by the experiment.

(4) CONCLUSION

It is seen that the estimate of the mean breakdown voltage, V_2, obtained by means of a test procedure employing series of increasing impulses may differ from the mean breakdown voltage defined in Section 1. Furthermore, the variance of the results obtained in such tests is seen to differ from the variance of the distribution of the probability of breakdown with a single impulse. It is therefore obvious that the results from impulse breakdown tests of this type must be interpreted with care. Moreover, when comparing the results of tests it may be desirable to take into account the effect of the test procedure. The relationship between these parameters has been calculated for the case where the probability of breakdown with a single impulse follows the integrated Gaussian distribution.

It should be noted that, when the incremental voltage is approximately equal to the standard deviation of the results obtained, the differences between V_2 and V_1, and between S_2 and S_1, are small. If, therefore, the incremental voltage is not predetermined by other considerations, the best estimate of the mean breakdown voltage will be obtained by the use of impulses increasing in steps equal to the expected standard deviation of the results.

(5) ACKNOWLEDGMENTS

The author wishes to acknowledge the assistance of Mr. J. W. Gould with the many numerical calculations upon which the figures in this paper are based.

621.311.153:621.315.09

The Institution of Electrical Engineers
Monograph No. 294 S
Mar. 1958
©

THE ECONOMIC LOADING OF TRANSMISSION SYSTEMS

By H. NICHOLSON, M.Eng., A.M.I.Mech.E., and J. W. LYNN, M.Sc., Associate Members.

(*The paper was first received* 15*th May, and in revised form* 22*nd November*, 1957. *It was published as an* INSTITUTION MONOGRAPH *in March*, 1958.)

SUMMARY

In several publications Kron, Kirchmayer and others have outlined methods for transforming power-system operating data in terms of complex voltages and currents into information concerning real generator powers and transmission losses. These losses are related to the individual generator loadings by a set of constants which are dependent only upon operating conditions at normal load.

In the present paper Kron's methods for establishing a transmission loss equation for a hypothetical 3-generator, 2-load system are described and the analysis is extended for application to an actual section of the British network.

The coefficients of the loss equation are obtained from the basic impedance matrix of the system and various transformation matrices, which transform the basic matrix to the final loss matrix, based on certain operating assumptions.

A method is developed for combining the loss formula with station fuel costs for economic system operation. The resulting loading equations are illustrated in nomograph form as an aid to system load dispatching.

In the paper, owing to certain limitations of the required information regarding system loads, certain of the load-flow conditions have been estimated by calculation, and the accuracy of the loss analysis is correspondingly limited. However, the purpose of the paper is to illustrate available methods and not to formulate an accurate set of loading equations.

LIST OF PRINCIPAL SYMBOLS

I^{L1}, I^{L2}, etc. = Load currents.
I^{L} = Total system (or hypothetical) load current.
l_1, l_2, etc. = Ratios of individual to hypothetical load currents.
Z_{11}, Z_{22}, etc. = Impedance matrices for reference frames 1, 2, etc.
C_2^1, C_3^2, etc. = Transformation matrices between quantities in reference frames 1 and 2, 2 and 3, etc.
V_1, V_2, etc. = Terminal voltages of generators 1, 2, etc.
V_{L1}, V_{L2}, etc. = Voltages at loads L_1, L_2, etc.
$Z_{n.K}$ = Measured leakage impedance of system network between generator or load n and generator or load K.
$Z_{G.G}$ = A matrix of measured network self impedances seen from generating points of entry.
$Z_{L.L}$ = A matrix of measured network self impedances seen from load points of entry.
$Z_{L.G}$ = Measured mutual impedances with generator points energized.
$Z_{G.L}$ = Measured mutual impedances with load points energized.
I^1, I^2, etc. = Generator currents.
Z_{n-K} = Complex impedance components for impedance matrix Z_{33}.
θ_1, θ_2, etc. = Angles by which generator terminal voltages V_1, V_2, etc., are referred to a common axis.
V_{d_n}, V_{q_n} = Direct and quadrature components respectively of voltage vector V_4.
I^{dK}, I^{qK} = Direct and quadrature components respectively of current vector I^4.
$I^{d'K}$ = Components of current vector I^5.
Λ_n = Ratio of reactive to active power for generator n at normal load.
$\lvert V_n \rvert_0$ = Terminal voltage of generator n at normal load.
M_{nK} = General term of loss matrix Z_{66}.
B_{nK} = General term of loss matrix using simplified analysis.
R_{n-K} = Real components of impedance matrix Z_{33} used in final loss matrix.
L_n = Incremental transmission loss at generator n.
P_K, Q_K = Active and reactive power supplied by generator K.
P_L = Total system transmission losses $= \sum_n \sum_K P_n \cdot B_{nK} \cdot P_K$.
S_n = Cost of fuel input to station n, £/hour.
λ = Incremental cost of received power, £/MWh.

(1) INTRODUCTION

For optimum operating efficiency of large power systems it is necessary to co-ordinate generation on an equal incremental fuel-cost basis with the incremental cost of the transmission line losses. Extensive research has taken place in America into methods of combining these costs by the application of transmission-loss formulae. These express the transmission-line losses as functions of the generator and interconnector power and a set of constants. The loss equations, once obtained, are applicable for any condition of generation and load, if the simplifying assumptions made in deriving the equations are valid for all system conditions.

Following the Steinberg and Smith[1] publication in 1943 on the economic loading of power plants, a method for expressing total transmission losses in terms of generator power was pioneered by George[2] in the same year. Ward, Eaton and Hale[4] extended George's original methods, and provided a more generalized and analytical approach to the derivation of a loss formula, by use of the a.c. network analyser. George, Page and Ward[3] co-ordinated transmission losses and fuel costs by the application of a loss equation containing constants derived from a network analyser study.

Kron,[5] in 1951, derived a loss-equation using tensorial methods, requiring considerably fewer measurements and calculations. Kirchmayer and Stagg,[6] using Kron's methods, obtained a transmission-loss formula for the American Gas and Electric system and investigated the effects of Kron's simplifying assumptions on the accuracy of the loss formula. Kron,[9] in a second paper, considered the existence of off-nominal turn ratios and their representation on an a.c. network analyser with auto-transformers. He followed this by two further publications,[10,13] in which he considered the study and co-ordination of several interconnected transmission systems, by combining the solutions of small components by a series of transformations.

Correspondence on Monographs is invited for consideration with a view to publication.
Mr. Nicholson is with Lever Bros., Port Sunlight, Ltd., and Mr. Lynn is in the Electrical Engineering Department, University of Liverpool.

Imburgia, Kirchmayer, and Stagg[16] have described a computer for use in system load dispatching. The computer calculates, from the loss constants of a system, transmission loss penalty factors which are used in conjunction with an incremental fuel cost slide-rule for obtaining economic balance between generating stations. Operation of the slide-rule and the computer provides a method of combining transmission losses and generation costs, and of applying them to the loading of a system under rapidly changing conditions.

In Part 1 of Kron's work, six basic reference frames are established for solving steady-state power-system problems, and, in particular, for determining total and incremental transmission losses.

The transmission-loss formula to be derived, as in other methods, involves the generated power of all sources and a set of constants. These constants (self- and mutual-impedances) once established are suitable for use under any operating conditions, within the limits of the operating assumptions, unless a physical change in the system takes place. The constants are obtained from a.c. network-analyser data or by analytical methods. The use of tensor algebra provides a method of transforming operating data (complex voltages and currents) into information concerning real powers, losses and a set of constants by means of a series of operations called 'transformations of reference frames'.

The object of the present paper is to relate the performance of power systems to a set of linear equations, containing real generator powers P and incremental losses L incurred in the transmission system. These equations are of the form $L = M \,.\, P$, where M in matrix form represents a set of real constants which are dependent only upon operating conditions at normal load.

(2) STUDY OF KRON'S ANALYSIS

(2.1) System Operating Assumptions

The methods outlined by Kron for determining a transmission-loss formula involve certain fundamental concepts of tensor analysis, and a number of assumptions concerning the operation of a power system. These assumptions are as follows:

(*a*) The ratio of each load current to the total load current of a system, at normal load, remains constant as the loads vary.

(*b*) The generator currents remain fixed in phase angle relative to each other as the generator loads vary.

(*c*) The generator voltage magnitudes remain constant.

(*d*) The ratio of reactive power to active power of each source remains constant.

(2.2) Reference Frames

This present power system study will involve the introduction of the following reference frames:

1. Measurement of leakage impedances Z_{11}.
2. Introduction of one hypothetical load I^L which replaces all system load currents, where $I^L = \sum_1^n I^{L_n}$.
3. Elimination of I^L, leaving generator currents only.
4. Generator currents and voltages are transformed into axes, in phase and in quadrature with the respective generator voltages. Matrices of complex quantities are changed into larger matrices containing only real quantities.
5. Using the assumption of constant ratio of generator active/reactive power, each generator current is replaced by its projection upon the terminal voltage existing at normal load.
6. Active components of generator currents are transformed into generator powers. Since voltage differences have been used in the previous reference frames, the transformation matrix in frame 6 yields generator power loss.

(2.2.1) Reference Frame 1.

Consider a hypothetical power system consisting of generators G_1, G_2, G_3 supplying loads L_1, L_2 via a transmission network as in Fig. 1.

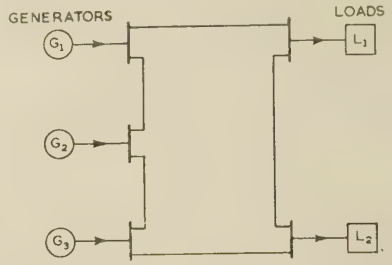

Fig. 1.—Hypothetical 3-generator 2-load power system.

The self and mutual leakage impedances of the system network are measured, usually from a network-analyser study, by:

(i) Disconnecting the generating plant and loads from the network.

(ii) Injecting unit current between each generator and a reference point in the system.

(iii) Measuring voltage differences between all generating and load points and the reference point.

This is repeated for measurement of load self-impedances by injecting unit current into the network at L_1 and L_2.

The impedances of the network from a generator point of entry are called generator self-impedances, and transfer or mutual impedances to other points. Impedances measured from load points are termed load self- and mutual impedances. The actual self-impedances of the generators and loads do not enter explicitly into the analysis.

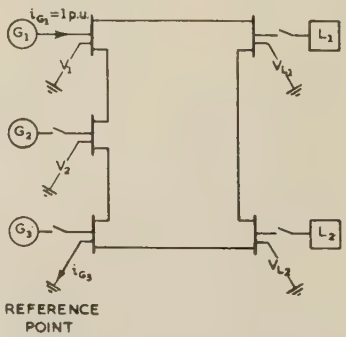

Fig. 2.—Reference frame 1: basic measurements.

Thus in Fig. 2, with unit current injected at G_1,

$$\left.\begin{aligned} \text{the generator self impedance, } Z_{1.1} &= V_1 \\ \text{and the mutual impedances, } Z_{2.1} &= V_2 \\ Z_{3.1} &= V_{L1} \\ Z_{4.1} &= V_{L2} \end{aligned}\right\} \quad \ldots\ldots \quad (1)$$

The impedance matrix for the system is therefore

$$Z_{11} = \begin{array}{c|cccc} & G_1 & G_2 & L_1 & L_2 \\ \hline G_1 & Z_{1.1} & Z_{1.2} & Z_{1.3} & Z_{1.4} \\ G_2 & Z_{2.1} & Z_{2.2} & Z_{2.3} & Z_{2.4} \\ L_1 & Z_{3.1} & Z_{3.2} & Z_{3.3} & Z_{3.4} \\ L_2 & Z_{4.1} & Z_{4.2} & Z_{4.3} & Z_{4.4} \end{array} = \begin{array}{c|cc} & G & L \\ \hline G & Z_{G.G} & Z_{G.L} \\ L & Z_{L.G} & Z_{L.L} \end{array} \quad (2)$$

Since the network mutual impedances form a symmetrical system,

$$Z_{G.L} = (Z_{L.G})_t$$

where $(Z_{L.G})_t$ is the transpose of matrix $(Z_{L.G})$.

That is, the mutual impedances with load points energized are equal to those with respect to the generator sources.

The equations for the system now take the form

$$\left.\begin{aligned} V_1 - V_R &= Z_{1.1}I^1 + Z_{1.2}I^2 + Z_{1.3}I^{L1} + Z_{1.4}I^{L2} \\ V_2 - V_R &= Z_{2.1}I^1 + Z_{2.2}I^2 + Z_{2.3}I^{L1} + Z_{2.4}I^{L2} \\ V_{L1} - V_R &= Z_{3.1}I^1 + Z_{3.2}I^2 + Z_{3.3}I^{L1} + Z_{3.4}I^{L2} \\ V_{L2} - V_R &= Z_{4.1}I^1 + Z_{4.2}I^2 + Z_{4.3}I^{L1} + Z_{4.4}I^{L2} \end{aligned}\right\} \quad . \quad (3)$$

If these system equations are solved by inverting the impedance matrix, the equivalent circuit will then be as shown in Fig. 3.

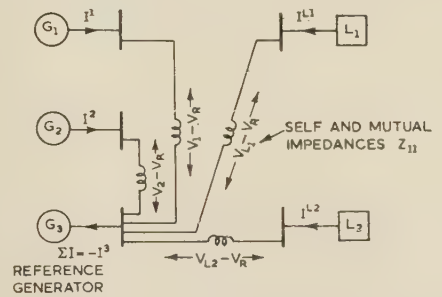

Fig. 3.—Equivalent circuit for measurement reference frame 1.

(2.2.2) **Reference Frame 2.**

Let the total system load current, during a normal load period, be given by

$$I^L = I^{L1} + I^{L2} \ (= \text{hypothetical load}) \quad . \quad . \quad . \quad (4)$$

Then, from assumption (*a*),

$$\frac{I^{L1}}{I^L} = l_1, \quad \frac{I^{L2}}{I^L} = l_2 \quad . \quad . \quad . \quad . \quad . \quad (5)$$

where l_1, l_2 are constant complex ratios.

Thus

$$\left.\begin{aligned} I^{L1} &= l_1 I^L \\ I^{L2} &= l_2 I^L \end{aligned}\right\} \quad . \quad . \quad . \quad . \quad . \quad . \quad (6)$$

or

$$I^{L_n} = C_L^{L_n} I^L \text{ where } C_L^{L_n} = \begin{array}{c|c} & L \\ \hline 1 & l_1 \\ \hline 2 & l_2 \end{array} \quad . \quad . \quad . \quad (7)$$

The system with individual load currents may therefore be transformed into one which contains only the hypothetical total current I^L by the transformation matrix

$$C_2^1 = \begin{array}{c|ccc} & 1 & 2 & L \\ \hline 1 & 1 & & \\ 2 & & 1 & \\ \hline L_1 & & & l_1 \\ \hline L_2 & & & l_2 \end{array} \quad . \quad . \quad . \quad . \quad . \quad (8)$$

(Note that the generator currents remain constant.)

and the currents and voltages in reference frame 2 are given by

$$I^1 = C_2^1 I^2 \quad . \quad . \quad . \quad . \quad . \quad . \quad (9)$$

$$V_2 = (C_2^1)_t^* V_1 \quad . \quad . \quad . \quad . \quad . \quad . \quad (10)$$

where $(C_2^1)_t^*$ is the conjugate of the matrix (C_2^1) transposed.

The system impedances in frame 2 are given by

$$Z_{22} = (C_2^1)_t^* Z_{11} C_2^1$$

$$= \begin{array}{c|ccc} & 1 & 2 & L \\ \hline 1 & Z_{1.1} & Z_{1.2} & \begin{matrix} Z_{1.3}l_1 \\ +Z_{1.4}l_2 \\ =(a_1) \end{matrix} \\ \hline 2 & Z_{2.1} & Z_{2.2} & \begin{matrix} Z_{2.3}l_1 \\ +Z_{2.4}l_2 \\ =(a_2) \end{matrix} \\ \hline L & \begin{matrix} Z_{3.1}l_1^* \\ +Z_{4.1}l_2^* \\ =(b_1) \end{matrix} & \begin{matrix} Z_{3.2}l_1^* \\ +Z_{4.2}l_2^* \\ =(b_2) \end{matrix} & \begin{matrix} Z_{3.3}l_1l_1^* \\ +Z_{3.4}l_2l_1^* \\ +Z_{4.3}l_1l_2^* \\ +Z_{4.4}l_2l_2^* \\ =(w) \end{matrix} \end{array} \quad . \quad (11)$$

The system performance is now represented by the equation

$$V_2 = Z_{22}I^2$$

i.e.

$$\left.\begin{aligned} V_1 - V_R &= Z_{1.1}I^1 + Z_{1.2}I^2 + a_1 I^L \\ V_2 - V_R &= Z_{2.1}I^1 + Z_{2.2}I^2 + a_2 I^L \\ V_L - V_R &= b_1 I^1 \quad + b_2 I^2 \quad + w I^L \end{aligned}\right\} \quad . \quad . \quad (12)$$

where in this example V_L, the hypothetical load voltage, is the weighted average of the 2-load voltages;

i.e.

$$V_L = l_1^* V_{L1} + l_2^* V_{L2} \quad . \quad . \quad . \quad . \quad . \quad (13)$$

and

$$\left.\begin{aligned} a_1 &= \sum_{K=3}^{4}\sum_{n=1}^{2} Z_{1.K} l_n a_2 = \sum_{K=3}^{4}\sum_{n=1}^{2} Z_{2.K} l_n \\ b_1 &= \sum_{K=3}^{4}\sum_{n=1}^{2} Z_{K.1} l_n^* b_2 = \sum_{K=3}^{4}\sum_{n=1}^{2} Z_{K.2} l_n^* \\ w &= \sum\sum\sum Z_{ll} \text{ as given above} \end{aligned}\right\} \quad . \quad . \quad (14)$$

The system may now be represented as in Fig. 4.

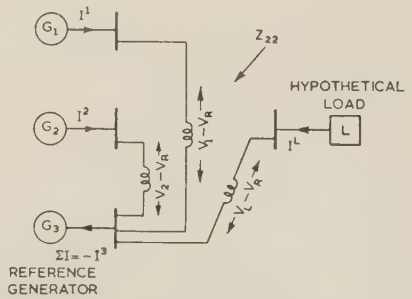

Fig. 4.—Equivalent circuit for reference frame 2 with one hypothetical load.

The system losses are now given by $I^{2*}Z_{22}I^2 = I^{2*}V_2$. However, this method of determining losses is not desirable since it involves the difference between large quantities, namely between generator and load powers.

(2.2.3) **Reference Frame 3.**

In this reference frame, the hypothetical load current is eliminated by introducing a transformation tensor C from a known equation of constraint. Now

$$I^1 + I^2 + I^3 + I^L = 0$$

Therefore $$I^L = -I^1 - I^2 - I^3 \; (= -\Sigma I^G) \quad . \quad . \quad . \quad (15)$$

Since the generator currents I^1 and I^2 remain unchanged in this reference frame, the required transformation matrix to replace the equation of constraint is

$$C_3^2 = \begin{array}{c|ccc} & 1 & 2 & 3 \\ \hline 1 & 1 & & \\ 2 & & 1 & \\ L & -1 & -1 & -1 \end{array} \quad . \quad . \quad . \quad . \quad (16)$$

The currents and voltages in this reference frame are now given by

$$I^2 = C_3^2 I^3 \quad . \quad . \quad . \quad . \quad . \quad . \quad . \quad (17)$$

$$V_3 = (C_3^2)_t^* V_2 \quad . \quad . \quad . \quad . \quad . \quad . \quad . \quad (18)$$

and the system impedances by

$$Z_{33} = (C_3^2)_t^* Z_{22} C_3^2 \quad . \quad . \quad . \quad . \quad . \quad (19)$$

The impedance matrix Z_{33} is asymmetrical and complex.

The performance equations obtained from $V_3 = Z_{33} I^3$ are

$$\left.\begin{aligned} V_1 - V_L &= (Z_{1.1} - b_1 - a_1 + w)I^1 \\ &\quad + (Z_{1.2} - b_2 - a_1 + w)I^2 + (w - a_1)I^3 \\ V_2 - V_L &= (Z_{2.1} - b_1 - a_2 + w)I^1 \\ &\quad + (Z_{2.2} - b_2 - a_2 + w)I^2 + (w - a_2)I^3 \\ V_3 - V_L &= (w - b_1)I^1 + (w - b_2)I^2 + wI^3 \end{aligned}\right\} \quad . \quad (20)$$

The voltages V_3 represent the potential differences between generators and hypothetical load with currents I^3 entering and leaving at these points.

The components of the system equations are represented in Fig. 5. It is evident from this Figure that the load voltages and currents do not now exist in this reference frame 3.

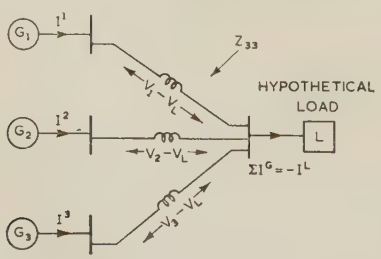

Fig. 5.—Equivalent circuit for reference frame 3.

The equation $I^{3*} \cdot V_3$ represents the various losses in the system with reference to the generator currents and the voltage drops between the generators and hypothetical load. It does not involve the difference of large quantities.

(2.2.4) **Reference Frame 4—Change of Axes.**

For the hypothetical system under consideration, the generator and load terminal voltages and currents for a normal load period are illustrated in Fig. 6(*a*) and 6(*b*).

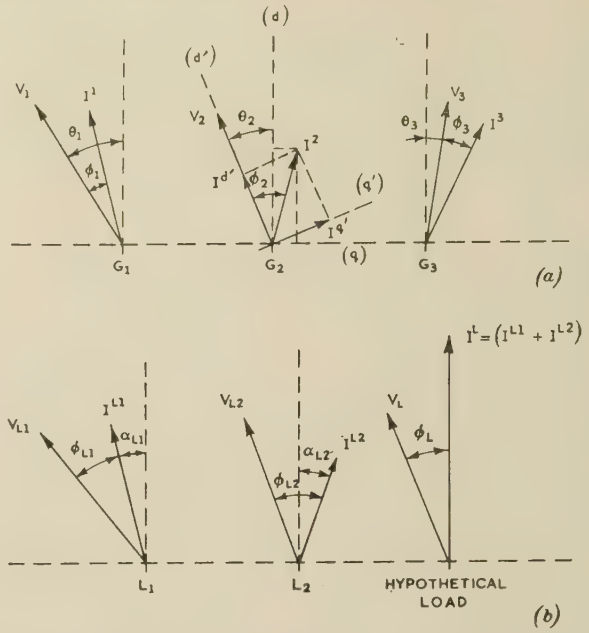

Fig. 6.—Vector diagrams for the hypothetical system at normal load.

(*a*) Normal load generator voltages and currents.
(*b*) Load voltages and currents at normal load.

The generator terminal voltages V_1, V_2 and V_3 are referred to a direct axis along the direction of the total load current, by angles θ_1, θ_2 and θ_3, respectively. The generator currents lag behind the terminal voltages by the respective angles ϕ_1, ϕ_2 and ϕ_3. The load voltage and current conditions at normal load are illustrated in Fig. 6(*b*).

A set of axes d' and q' is now introduced, along and at right angles to the generator terminal voltages. The generator currents projected upon the respective normal load terminal voltages will then represent the generator powers.

In this new reference frame, the active and reactive power components of each generator current I, will be given by,

$$I' = I^{d'} + jI^{q'} \quad . \quad . \quad . \quad . \quad . \quad . \quad (21)$$

The effect of rotating the axes d and q to new axes d' and q' is obtained by rotating the current vectors in the opposite direction, through an angle $-\theta$, so that

$$I = \varepsilon^{-j\theta} I' \quad . \quad . \quad . \quad . \quad . \quad . \quad . \quad (22)$$

Thus, for all generator currents, the transformation matrix required for quantities in reference frame 4 is

$$C_4^3 = \begin{array}{c|ccc} & 1 & 2 & 3 \\ \hline 1 & \varepsilon^{-j\theta_1} & & \\ 2 & & \varepsilon^{-j\theta_2} & \\ 3 & & & \varepsilon^{-j\theta_3} \end{array} \quad . \quad . \quad (23)$$

The new impedance matrix is now given by

$$Z_{44} = (C_4^3)_t^* Z_{33} C_4^3 \quad . \quad . \quad . \quad . \quad . \quad (24)$$

and the system equations take the form

$$V_4 = Z_{44} I^4$$

or
$$|V_n| - V_L\varepsilon^{j\theta_n} = \sum_{K=1}^{3} Z_{n-K}\varepsilon^{j(\theta_n-\theta_k)}(I^K\varepsilon^{-j\theta_K}) \quad . \quad (25)$$
$(n = 1, 2, 3)$

where Z_{n-K} is the general term of Z_{33};

or

$$|V_n| - V_L\varepsilon^{j\theta_n} = \sum_{K=1}^{3} \{[R_{n-K}\cos(\theta_n-\theta_K) - X_{n-K}\sin(\theta_n-\theta_K)] + j[X_{n-K}\cos(\theta_n-\theta_K) + R_{n-K}\sin(\theta_n-\theta_K)]\}(I^K\varepsilon^{-j\theta_K}) \quad . \quad (26)$$

where $(R_{n-K} + jX_{n-K})$ represents the components of Z_{n-K}. The voltage vector V_4 represents the voltage drop from generators to hypothetical load.

Any complex impedance, say $Z = R + jX$, may be replaced by a matrix containing only real numbers of the form

$$Z = \begin{array}{c|cc} & d & q \\ \hline d & R & -X \\ q & X & R \end{array} \quad . \quad (27)$$

This introduces direct and quadrature axes d and q, in which the voltage and current vectors are represented by in-phase and quadrature components.

Thus if $I = I^d + jI^q$ and $V = V_d + jV_q$, then, in matrix form,

$$I = \begin{array}{c|c} & d \\ \hline d & I^d \\ \hline q & I^q \end{array} \quad \text{and} \quad V = \begin{array}{c|c} & d \\ \hline d & V_d \\ \hline q & V_q \end{array} \quad . \quad (28)$$

Thus the complex equation $V_4 = Z_{44}I^4$ may be expressed in terms of real quantities by replacing the respective matrices by others containing twice as many equations and variables, but containing all real components.

For the 3-generator system, with the impedance Z_{44} expressed in real numbers, the general equations for system performance will take the form

$$\left.\begin{aligned} V_{d_n} &= \sum_{K=1}^{3}[R_{n-K}\cos(\theta_n-\theta_K) - X_{n-K}\sin(\theta_n-\theta_K)]I^{dK} \\ &\quad - \sum_{K=1}^{3}[X_{n-K}\cos(\theta_n-\theta_K) + R_{n-K}\sin(\theta_n-\theta_K)]I^{qK} \\ V_{q_n} &= \sum_{K=1}^{3}[X_{n-K}\cos(\theta_n-\theta_K) + R_{n-K}\sin(\theta_n-\theta_K)]I^{dK} \\ &\quad + \sum_{K=1}^{3}[R_{n-K}\cos(\theta_n-\theta_K) - X_{n-K}\sin(\theta_n-\theta_K)]I^{qK} \end{aligned}\right\} \quad . \quad (29)$$
$(n = 1, 2, 3)$

(2.2.5) **Reference Frame 5.**

In this frame the reactive components of the generator currents are expressed in terms of the active components in phase with the normal load terminal voltages.

Using assumption (d) of Section 2.1, the components of the various generator currents may be expressed in the form

$$\left.\begin{aligned} I^d &= I^d \\ I^q &= \Lambda I^d \end{aligned}\right\} \quad . \quad (30)$$

where the constant Λ is given by the ratio of the normal load measurements, $I^{q'}/I^{d'} = \tan\phi_n$ (in Fig. 6a) $= Q/P$, Q and P being the reactive and active power components respectively, of each generator at normal load.

Such a set of equations for the components of all generator currents in the 3-generator system will produce the transformation matrix

$$C_5^4 = \begin{array}{c|ccc|ccc} & d_1 & d_2 & d_3 & q_1 & q_2 & q_3 \\ \hline d_1 & 1 & & & & & \\ d_2 & & 1 & & & & \\ d_3 & & & 1 & & & \\ \hline q_1 & \Lambda_1 & & & & & \\ q_2 & & \Lambda_2 & & & & \\ q_3 & & & \Lambda_3 & & & \end{array}$$

i.e.
$$I^4 = C_5^4 I^5 \quad . \quad (31)$$

The new impedance matrix, containing only real numbers, is now given by $(C_5^4)_t Z_{44} C_5^4$, and the system equations are given by the general term

$$(V_{d_n} + \Lambda_n V_{q_n}) = \sum_{K=1}^{3}\{[R_{n-K}\cos(\theta_n-\theta_K) - X_{n-K}\sin(\theta_n-\theta_K)](1+\Lambda_n\Lambda_K) + [X_{n-K}\cos(\theta_n-\theta_K) + R_{n-K}\sin(\theta_n-\theta_K)](\Lambda_n-\Lambda_K)\} \times (I^{dK} + \Lambda_K I^{qK}) \quad . \quad (32)$$
$(n = 1, 2, 3)$

(2.2.6) **Reference Frame 6—Transformation of Generator Current into Power.**

By assuming that the generator terminal voltages remain practically constant in the region of the normal load values, the active power of each generator will be given by

$$\left.\begin{aligned} P_1 &= I^{d1'}|V_1|_0 \quad I^{d1'} = 1/|V_1|_0 \quad P_1 \\ P_2 &= I^{d2'}|V_2|_0 \text{ or } I^{d2'} = 1/|V_2|_0 \quad P_2 \\ P_3 &= I^{d3'}|V_3|_0 \quad I^{d3'} = 1/|V_3|_0 \quad P_3 \end{aligned}\right\} \quad . \quad (33)$$

Thus the required transformation matrix for quantities in this reference frame is

$$C_6^5 = \begin{array}{c|ccc} & 1 & 2 & 3 \\ \hline 1 & \dfrac{1}{|V_1|_0} & & \\ 2 & & \dfrac{1}{|V_2|_0} & \\ 3 & & & \dfrac{1}{|V_3|_0} \end{array} \quad . \quad (34)$$

The final impedance matrix is given by

$$Z_{66} = (C_6^5)_t Z_{55} C_6^5 \quad . \quad (35)$$

and the system equations are given by

$$\frac{V_{dn}+\Lambda_n V_{qn}}{|V_n|_0}=\sum_{K=1}^{3}\frac{1}{|V_n|_0|V_K|_0}\{[R_{n-K}\cos(\theta_n-\theta_K)-X_{n-K}\sin(\theta_n-\theta_K)](1+\Lambda_n\Lambda_K)+[X_{n-K}\cos(\theta_n-\theta_K)+R_{n-K}\sin(\theta_n-\theta_K)](\Lambda_n-\Lambda_K)\}P_K$$

or

$$=\sum_{K=1}^{3}M_{nK}P_K \quad . \quad . \quad . \quad . \quad . \quad . \quad (36)$$

where $P_K=(I^{dK}+\Lambda_K I^{qK})|V_K|_0$

is the real power supplied by generator K and M_{nK} represents a set of real constants.

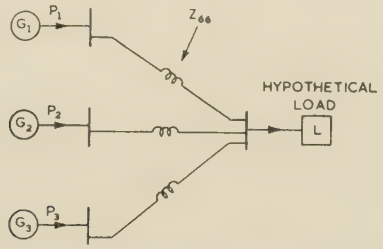

Fig. 7.—Equivalent circuit for the final reference frame 6 with active generator powers.

Fig. 7 illustrates the equivalent circuit with real impressed generator powers.

The final loss equation is now of the form

$$V_6=Z_{66}I^6 \quad . \quad . \quad . \quad . \quad . \quad . \quad (37)$$

The dimension of I^6 is that of power, and it represents the active power P supplied by each generator.

The term $V_6=(C_6^5)_t V_5$ is dimensionless owing to the inverse voltage form of C_6^5. Its components are fractions, say L, and represent the incremental I^2R transmission losses of the system, ∂ loss/∂P.

Z_{66} represents the final 'loss' matrix containing real components M_{nK} of inverse power form Z/V^2.

Thus, in terms of generator powers and incremental I^2R losses, the system equations take the form

$$L_n=\sum_K M_{nK}P_K \quad . \quad . \quad . \quad . \quad . \quad (38)$$

which is equal to the incremental transmission loss at generator n, ∂ losses/∂P_n.

The total I^2R losses in the system are thus given by

$$P_{\text{losses}}=\sum_n\sum_K P_n M_{nK}P_K \quad . \quad . \quad . \quad . \quad (39)$$

(2.3) Simplification of the Analysis for Total and Incremental Loss Studies

For incremental loss calculations only the real parts of the differences of potential existing in the basic measurement reference frame 1 need to be measured. It is also sufficient to use only the real components of the matrix C_L for transformation from reference frame 1 to 2. This latter simplification will produce a symmetrical impedance matrix Z_{22} containing only real components, and the former a and b components change to $d=(a+b)/2$.

The total I^2R losses in the system may be found by using only the symmetrical part of Z_{66} containing coefficients R_{66}, say B. In this case, the total transmission losses are given by

$$P_{\text{losses}}=\sum_n\sum_K P_n B_{nK}P_K \text{ and } B_{nK}=B_{Kn} \quad . \quad (40)$$

Thus, for the 3-generator system,

$$P_{\text{losses}}=B_{11}P_1^2+B_{22}P_2^2+B_{33}P_3^2+2B_{12}P_1P_2+2B_{13}P_1P_3+2B_{23}P_2P_3 \quad . \quad (41)$$

The same result is also obtained if only the symmetrical part of R_{33} and the skew-symmetric part of X_{33} are used when transforming Z_{33} to Z_{66}, assuming Z_{33} has the form $R_{33}+jX_{33}$.

Using the above simplifications, the general loss coefficient takes the form

$$B_{nK}=\frac{R_{n-K}}{|V_n|_0|V_K|_0}[\cos(\theta_n-\theta_K)(1+\Lambda_n\Lambda_K)+\sin(\theta_n-\theta_K)(\Lambda_n-\Lambda_K)] \quad . \quad (42)$$

(3) STUDY OF THE LOADING CONDITIONS ON A SECTION OF THE BRITISH NETWORK

The Grid system for which a transmission-loss formula is to be determined consists of the 132 kV Warrington section of the North West, Merseyside and North Wales Divisional Network.

This section comprises steam generating stations at Warrington, Percival Lane and Ince, and 33 kV Area Board load points at Warrington, Percival Lane, Ince, Crewe and Knutsford. Fig. 8

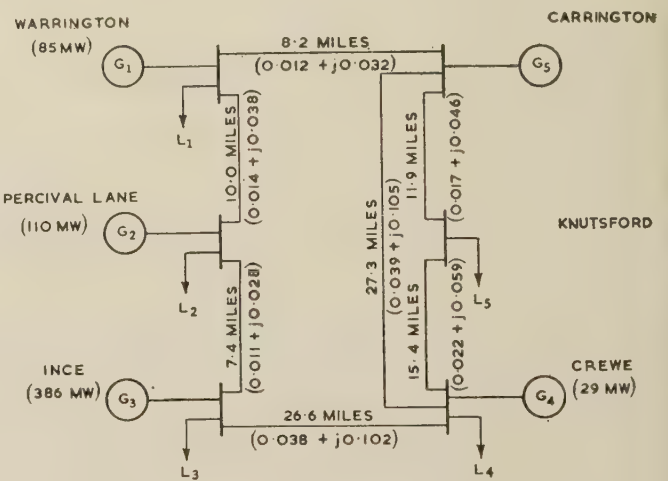

Fig. 8.—System diagram—Warrington Section.
Base apparent power—100 MVA.
Base voltage—132 kV.

illustrates a simplified diagram of this system with the main generating, load and interconnection points. The available active-power generation exported at each busbar is given in this diagram, which also shows the contribution from Marchwiel and part of Maentwrog at the Crewe station. The diagram also illustrates the route length of each overhead line forming the network, and the per-unit impedances for a 100 MVA base at 132 kV.

(3.1) Load Flow Study

The study was carried out analytically in the absence of network-analyser facilities. The first part consisted in determining the approximate system load flows from the known generator loadings and the active-power demands at the load points. It was assumed that there was a normal 12% outage of the available generation at all stations, and the load demands used were those that existed in January, 1955, during the normal peak periods of 0700–1300 hours (see Fig. 10).

The power equations for a short line were then used for calculating the various terminal voltages and angles in the given system. Reactive line flows were also determined from these

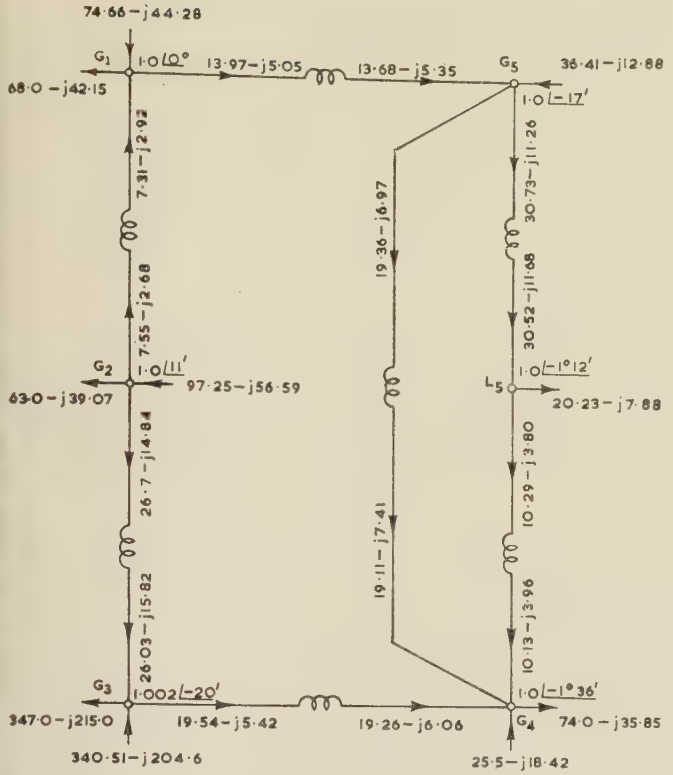

Fig. 9.—Load-flow data for a weekday peak period, including line flows, generator loadings, load demands and bus voltages.

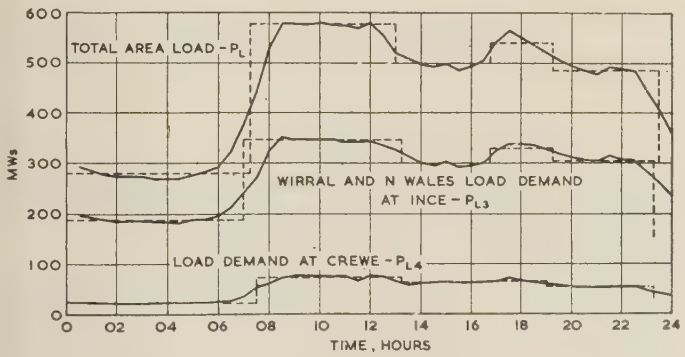

Fig. 10—System load demands—17th January, 1955.

(*a*) Total area load, P_L.
(*b*) Wirral and North Wales load demand at Ince, P_{L3}.
(*c*) Load demand at Crewe, P_{L4}.

equations, and balance of busbar conditions in the system loop was obtained by a series of successive approximations.

The results of the final approximation to system load flows to give the desired system balance and realistic generator and load reactive demands are illustrated in the load-flow diagram of Fig. 9.

(4) STUDY OF THE APPLICATION OF KRON'S METHODS TO A SECTION OF THE BRITISH NETWORK

(4.1) Reference Frame 1

For the measurement of the basic impedance matrix of the Warrington section network, illustrated in Fig. 8, the Carrington tie-line connection G_5 was chosen as reference point and was earthed.

With unit current impressed at the generator G_1 the various leakage impedances are given by

$$Z_{n,K} = \frac{V_{Gn}}{i_{GK}} \quad . \quad . \quad . \quad . \quad . \quad . \quad . \quad (43)$$

and in this case reference generator current I_{GR} = impressed current I_{GK}.

Thus for generator points of entry,

$$\left.\begin{aligned} Z_{1.1} &= \frac{V_{G1}}{i_{G1}} = 0{\cdot}0105 + j0{\cdot}0280 \\ Z_{2.1} &= \frac{V_{G2}}{i_{G1}} = 0{\cdot}0087 + j0{\cdot}0231 \\ Z_{3.1} &= \frac{V_{G3}}{i_{G1}} = 0{\cdot}0073 + j0{\cdot}0195 \\ Z_{4.1} &= \frac{V_{G4}}{i_{G1}} = 0{\cdot}0025 + j0{\cdot}0067 \end{aligned}\right\} \quad . \quad . \quad (44)$$

and for load points of entry,

$$\left.\begin{aligned} Z_{5.1} &= Z_{1.1} = 0{\cdot}0105 + j0{\cdot}0280 \\ Z_{6.1} &= Z_{2.1} = 0{\cdot}0087 + j0{\cdot}0231 \\ Z_{7.1} &= Z_{3.1} = 0{\cdot}0073 + j0{\cdot}0195 \\ Z_{8.1} &= Z_{4.1} = 0{\cdot}0025 + j0{\cdot}0067 \\ Z_{9.1} &= \frac{V_{L5}}{i_{G1}} = 0{\cdot}0011 + j0{\cdot}0029 \end{aligned}\right\}$$

With unit current impressed at generator G_2,

$$\left.\begin{aligned} Z_{1.2} &= 0{\cdot}0087 + j0{\cdot}0231 = Z_{5.2} \\ Z_{2.2} &= 0{\cdot}0188 + j0{\cdot}0507 = Z_{6.2} \\ Z_{3.2} &= 0{\cdot}0160 + j0{\cdot}0428 = Z_{7.2} \\ Z_{4.2} &= 0{\cdot}0055 + j0{\cdot}0146 = Z_{8.2} \\ Z_{9.2} &= 0{\cdot}0023 + j0{\cdot}0063 \end{aligned}\right\} \quad . \quad . \quad (45)$$

With unit current impressed at generator G_3,

$$\left.\begin{aligned} Z_{1.3} &= 0{\cdot}0073 + j0{\cdot}0195 = Z_{5.3} \\ Z_{2.3} &= 0{\cdot}0160 + j0{\cdot}0428 = Z_{6.3} \\ Z_{3.3} &= 0{\cdot}0226 + j0{\cdot}0600 = Z_{7.3} \\ Z_{4.3} &= 0{\cdot}0078 + j0{\cdot}0206 = Z_{8.3} \\ Z_{9.3} &= 0{\cdot}0033 + j0{\cdot}0089 \end{aligned}\right\} \quad . \quad . \quad (46)$$

With unit current impressed at generator G_4,

$$\left.\begin{aligned} Z_{1.4} &= 0{\cdot}0025 + j0{\cdot}0067 = Z_{5.4} \\ Z_{2.4} &= 0{\cdot}0055 + j0{\cdot}0146 = Z_{6.4} \\ Z_{3.4} &= 0{\cdot}0078 + j0{\cdot}0206 = Z_{7.4} \\ Z_{4.4} &= 0{\cdot}0158 + j0{\cdot}0419 = Z_{8.4} \\ Z_{9.4} &= 0{\cdot}0067 + j0{\cdot}0182 \end{aligned}\right\} \quad . \quad . \quad (47)$$

With unit current impressed at the load L_1 the leakage impedances are equal to those obtained with unit current impressed at the generator G_1. Similarly, with impressed currents at L_2, L_3 and L_4 the leakage impedances are equal to those obtained with impressed currents at G_2, G_3 and G_4, respectively.

With unit current impressed at the load point L_5,

$$\left.\begin{aligned} Z_{1.9} &= 0{\cdot}0011 + j0{\cdot}0029 = Z_{5.9} \\ Z_{2.9} &= 0{\cdot}0023 + j0{\cdot}0063 = Z_{6.9} \\ Z_{3.9} &= 0{\cdot}0033 + j0{\cdot}0089 = Z_{7.9} \\ Z_{4.9} &= 0{\cdot}0067 + j0{\cdot}0182 = Z_{8.9} \\ Z_{9.9} &= 0{\cdot}0125 + j0{\cdot}0339 \end{aligned}\right\} \quad . \quad . \quad (48)$$

The above impedances now form the components of the basic symmetrical leakage-impedance matrix Z_{11}.

(4.2) Reference Frame 2

In this analysis the hypothetical load for a normal load period will be given by

$$I^L = I^{L1} + I^{L2} + I^{L3} + I^{L4} + I^{L5} \quad . \quad . \quad . \quad (49)$$

and the components of the C_L matrix by

$$l_1 = \frac{I^{L1}}{I^L}, \quad l_2 = \frac{I^{L2}}{I^L}, \quad l_3 = \frac{I^{L3}}{I^L}, \quad l_4 = \frac{I^{L4}}{I^L}, \quad l_5 = \frac{I^{L5}}{I^L} \quad . \quad (50)$$

However, since available information for the given load points consists of the half-hourly active-power loading only, it is not possible to obtain the constant complex ratios, l_1, l_2, etc., in the above form. An assumption is thus made that the ratio of the active-power loading at the load points to the total active-power load remains constant, and approximates to the corresponding current ratios, as given above. Such an approximation assumes that all load voltages and power factors are equal, and that all load currents are displaced equally from the total load current. These assumptions are valid for the system under consideration owing to the small phase displacements between the terminal voltages, the previously assumed constant load power factors and the approximate nominal system voltages at the load points.

A similar assumption is made by George,[2] in which the average line voltage and average power factor for the heavily loaded portions of the systems are used in the analysis.

Fig. 10 illustrates the half-hourly integrated loadings on 17th January, 1955, for two of the five load points, and the total area load for the Warrington section network. To compare the general trend of each load to that of the total system load, the ratio of each half-hourly load to that of the total was calculated.

It was apparent from these ratios that the trend of the total load was reflected at all load points; that is, the pattern of demand was the same at all load points, as stated in assumption (*a*).

The loading ratios to be used in this analysis have been obtained by averaging the individual half hourly ratios, and are

$$l_1 = 0{\cdot}110, \; l_2 = 0{\cdot}108, \; l_3 = 0{\cdot}633, \; l_4 = 0{\cdot}111, \; l_5 = 0{\cdot}038 \quad . \quad . \quad . \quad . \quad (51)$$

The absence of reactive metering data at the load points prevented the use of complex ratios in this analysis. The leakage-impedance matrix for reference frame 2 is now given by

$$Z_{22} = (C_2^1)_t^* Z_{11} (C_2^1)$$

In this analysis $(C_2^1)^* = (C_2^1)$ and only the real components of Z_{11} are considered.

The components of Z_{22} are given and calculated as follows:

$$\left.\begin{aligned}
&Z_{1.1} = 0{\cdot}0105, Z_{1.2} = 0{\cdot}0087, Z_{1.3} = 0{\cdot}0073, \\
&\qquad\qquad Z_{1.4} = 0{\cdot}0025 \\
&Z_{2.1} = 0{\cdot}0087, Z_{2.2} = 0{\cdot}0188, Z_{2.3} = 0{\cdot}0160, \\
&\qquad\qquad Z_{2.4} = 0{\cdot}0055 \\
&Z_{3.1} = 0{\cdot}0073, Z_{3.2} = 0{\cdot}0160, Z_{3.3} = 0{\cdot}0226, \\
&\qquad\qquad Z_{3.4} = 0{\cdot}0078 \\
&Z_{4.1} = 0{\cdot}0025, Z_{4.2} = 0{\cdot}0055, Z_{4.3} = 0{\cdot}0078, \\
&\qquad\qquad Z_{4.4} = 0{\cdot}0158 \\
&d_1 = Z_{1.5}l_1 + Z_{1.6}l_2 + Z_{1.7}l_3 + Z_{1.8}l_4 + Z_{1.9}l_5 \\
&\qquad\qquad = 0{\cdot}00703 \\
&d_2 = Z_{2.5}l_1 + Z_{2.6}l_2 + Z_{2.7}l_3 + Z_{2.8}l_4 + Z_{2.9}l_5 \\
&\qquad\qquad = 0{\cdot}01381 \\
&d_3 = Z_{3.5}l_1 + Z_{3.6}l_2 + Z_{3.7}l_3 + Z_{3.8}l_4 + Z_{3.9}l_5 \\
&\qquad\qquad = 0{\cdot}01783 \\
&d_4 = Z_{4.5}l_1 + Z_{4.6}l_2 + Z_{4.7}l_3 + Z_{4.8}l_4 + Z_{4.9}l_5 \\
&\qquad\qquad = 0{\cdot}00781
\end{aligned}\right\} \quad . \quad (52)$$

and w is given by,

$$\begin{aligned}
&Z_{5.5}l_1l_1^* + Z_{5.6}l_2l_1^* + Z_{5.7}l_3l_1^* \\
&\qquad + Z_{5.8}l_4l_1^* + Z_{5.9}l_5l_1^* = 0{\cdot}000774 \\
&Z_{6.5}l_1l_2^* + Z_{6.6}l_2l_2^* + Z_{6.7}l_3l_2^* \\
&\qquad + Z_{6.8}l_4l_2^* + Z_{6.9}l_5l_2^* = 0{\cdot}001492 \\
&Z_{7.5}l_1l_3^* + Z_{7.6}l_2l_3^* + Z_{7.7}l_3l_3^* \\
&\qquad + Z_{7.8}l_4l_3^* + Z_{7.9}l_5l_3^* = 0{\cdot}011285 \\
&Z_{8.5}l_1l_4^* + Z_{8.6}l_2l_4^* + Z_{8.7}l_3l_4^* \\
&\qquad + Z_{8.8}l_4l_4^* + Z_{8.9}l_5l_4^* = 0{\cdot}000867 \\
&Z_{9.5}l_1l_5^* + Z_{9.6}l_2l_5^* + Z_{9.7}l_3l_5^* \\
&\qquad + Z_{9.8}l_4l_5^* + Z_{9.9}l_5l_5^* = 0{\cdot}000140 \\
&\qquad\qquad\qquad\qquad\qquad\qquad\qquad\qquad 0{\cdot}014558 = w
\end{aligned}$$

(4.3) Reference Frame 3

In frame 3 the hypothetical load current I^L is replaced by the reference generator current $I^R = I^5$, using the equation of constraint given by

$$I^L = -I^1 - I^2 - I^3 - I^4 - I^5, \text{ i.e. } = -\Sigma I^G \quad . \quad (53)$$

The impedance matrix is given by

$$Z_{33} = (C_3^2)_t^* Z_{22} (C_3^2)$$

and its components (R_{n-K}) are

$Z_{1.1} - 2d_1 + w$ $= +0{\cdot}011$	$Z_{1.2} - d_1 - d_2 + w$ $= +0{\cdot}00242$	$Z_{1.3} - d_1 - d_3 + w$ $= -0{\cdot}003$	$Z_{1.4} - d_1 - d_4 + w$ $= +0{\cdot}00222$	$w - d_1$ $= +0{\cdot}00753$
$Z_{2.1} - d_2 - d_1 + w$ $= +0{\cdot}00242$	$Z_{2.2} - 2d_2 + w$ $= +0{\cdot}00574$	$Z_{2.3} - d_2 - d_3 + w$ $= -0{\cdot}00108$	$Z_{2.4} - d_2 - d_4 + w$ $= -0{\cdot}00156$	$w - d_2$ $= +0{\cdot}00075$
$Z_{3.1} - d_3 - d_1 + w$ $= -0{\cdot}003$	$Z_{3.2} - d_3 - d_2 + w$ $= -0{\cdot}00108$	$Z_{3.3} - 2d_3 + w$ $= +0{\cdot}00150$	$Z_{3.4} - d_3 - d_4 + w$ $= -0{\cdot}00328$	$w - d_3$ $= -0{\cdot}00327$
$Z_{4.1} - d_4 - d_1 + w$ $= +0{\cdot}00222$	$Z_{4.2} - d_4 - d_2 + w$ $= -0{\cdot}00156$	$Z_{4.3} - d_4 - d_3 + w$ $= -0{\cdot}00328$	$Z_{4.4} - 2d_4 + w$ $= +0{\cdot}01474$	$w - d_4$ $= +0{\cdot}00675$
$w - d_1$ $= +0{\cdot}00753$	$w - d_2$ $= +0{\cdot}00075$	$w - d_3$ $= -0{\cdot}00327$	$w - d_4$ $= +0{\cdot}00675$	w $= +0{\cdot}01456$

. (54)

It will be noted that the components of Z_{33} are symmetric, and contain only real quantities similar to the real symmetrical components R_{33} of Kron's analysis,[5] and the *Kmn* coefficients of Ward, Eaton and Hale [Reference 4 eqn. (6)].

(4.4) Calculation of Loss Constants

The general term of the loss matrix is given by

$$B_{nK} = \frac{R_{n-K}}{|V_n|_0 |V_K|_0} [\cos(\theta_n - \theta_K)(1 + \Lambda_n\Lambda_K) + \sin(\theta_n - \theta_K)(\Lambda_n - \Lambda_K)] \quad . \quad . \quad . \quad . \quad (55)$$

The generator terminal voltage angles, θ, may be referred to any reference axis, and in the present study this has been taken along the terminal voltage of generator G_1.

The constant ratio ($\Lambda = Q/P$) for each generator, and the generator terminal voltages are those obtained from the normal load-flow study, and are illustrated in Table 1.

Table 1

GENERATOR DATA FROM LOAD-FLOW STUDY

Generator G_n	Generator output		Generator terminal voltage angle w.r.t. $G_1\theta$	Q/P ratio Λ_n	Per-unit bus voltage V_n
	P (MW)	Q (MVAr)			
G_1	74·66	44·28	0	0·593 1	1·0
G_2	97·25	56·59	+11′	0·581 9	1·0
G_3	340·51	204·6	−20′	0·600 9	1·001 5
G_4	25·5	18·42	−1° 36′	0·722 4	1·0
G_5	36·41	12·88	−17′	0·353 7	1·0

From the foregoing general term,

$$B_{11} = \frac{1}{|V_1|_0^2} R_{1-1}(1 + \Lambda_1^2)$$
$$= 0{\cdot}011(1 + 0{\cdot}593\,1^2) = 0{\cdot}014\,87 \quad . \quad . \quad . \quad . \quad . \quad . \quad (56)$$

$$B_{12} = \frac{R_{1-2}}{|V_1|_0 |V_2|_0} [\cos(\theta_1 - \theta_2)(1 + \Lambda_1\Lambda_2) + \sin(\theta_1 - \theta_2)(\Lambda_1 - \Lambda_2)]$$
$$= 0{\cdot}002\,42\,[\cos(-11')(1 + 0{\cdot}593\,1 \times 0{\cdot}581\,9) + \sin(-11')(0{\cdot}593\,1 - 0{\cdot}581\,9)] = 0{\cdot}003\,255 \quad . \quad (57)$$

All the B_{nK} coefficients obtained from the foregoing general term are given in Table 2.

Thus, for the 5-generator system, the total system per-unit loss is given by

$$P_L = 0{\cdot}014\,9P_1^2 + 0{\cdot}007\,7P_2^2 + 0{\cdot}002P_3^2 + 0{\cdot}022\,4P_4^2 + 0{\cdot}016\,4P_5^2 + 0{\cdot}006\,5P_1P_2 - 0{\cdot}008\,1P_1P_3 + 0{\cdot}006\,3P_1P_4 + 0{\cdot}018\,2P_1P_5 - 0{\cdot}002\,9P_2P_3 - 0{\cdot}004\,4P_2P_4 + 0{\cdot}001\,8P_2P_5 - 0{\cdot}009\,4P_3P_4 - 0{\cdot}007\,9P_3P_5 + 0{\cdot}016\,8P_4P_5 \quad . \quad . \quad . \quad . \quad . \quad (58)$$

where P_1, P_2, etc., are the per-unit station loadings.

For the station loadings obtained from the load-flow study, i.e. for

$P_1 = 74{\cdot}66$ MW, $P_2 = 97{\cdot}25$ MW, $P_3 = 340{\cdot}51$ MW, $P_4 = 25{\cdot}5$ MW, and $P_5 = 36{\cdot}41$ MW

the total system loss is, $P_L = 0{\cdot}006\,227$ per unit or $0{\cdot}623$ MW.

These losses do not compare favourably with those obtained from the load-flow study, the results of which are illustrated in Fig. 9. However, the main purpose of the flow study was for the determination of voltages, angles and Q/P ratios. Excessive errors in the losses estimated from Fig. 9 are the results of finding differences of large quantities.

(5) CO-ORDINATION OF INCREMENTAL FUEL COSTS AND TRANSMISSION LOSSES

In this Section the previously determined transmission losses of the system are combined with the incremental fuel costs of the generating stations, and a loading schedule is obtained which will give minimum operating costs for given total generation.

In the case of a number of generating stations supplying a power system and loaded on an equal incremental fuel cost basis, power will be transmitted from low- to high-cost regions due to the variation of fuel costs at different stations. For economic division of load between the stations it is thus necessary to consider the resulting transmission losses, and to amend the station operating costs accordingly.

(5.1) Methods of Co-ordination

The mathematical analysis for co-ordinating incremental fuel costs and transmission losses is based on the methods for determining the maxima and minima of a function of two variables, the latter also being related by an equation of constraint.

Using the methods of Lagrange's undetermined multipliers (Courant,[32] Kirchmayer and Stagg[8]), the condition for minimum fuel input is given by

$$\frac{dS_n}{dP_n} + \lambda\frac{\partial P_L}{\partial P_n} = \lambda \quad . \quad . \quad . \quad . \quad . \quad . \quad (59)$$

where dS_n/dP_n = incremental fuel cost (£/MWh) of station n.

and $\partial P_L/\partial P_n$ = incremental transmission loss (MW) for a megawatt change in generation (MW/MW) at station n.

Solution of the non-linear simultaneous equations obtained from eqn. (59) for each station, by variation of λ, will yield the plant schedules for different total system loadings.

If, in the general case, the fuel cost input curve for station n is assumed to be of the form

$$S_n = m_nP_n^2 + C_nP_n(\text{£/hr.}) \quad . \quad . \quad . \quad . \quad (60)$$

then

$$\frac{dS_n}{dP_n} = (2m_n)P_n + C_n = m_n'P_n + C_n \quad . \quad . \quad (61)$$

Table 2

COMPONENTS OF FINAL LOSS MATRIX

nK	11	22	33	44	55
B_{nK}	+0·014 87	+0·007 68	+0·002 04	+0·022 43	+0·016 38
nK	12	13	14	15	23
B_{nK}	+0·003 26	−0·004 06	+0·003 16	+0·009 12	−0·001 46
nK	24	25	34	35	45
B_{nK}	−0·002 21	+0·000 91	−0·004 69	−0·003 96	+0·008 42

where m_n' = slope of incremental cost curve (£/MWh/MW).

and C_n = intercept on incremental cost scale (£/MWh).

Also $$\frac{\partial P_L}{\partial P_n} = \sum_K 2B_{nK}P_K$$

Thus eqn. (59) becomes

$$(m_n'P_n + C_n) + \lambda \sum_K 2B_{nK}P_K = \lambda \quad . \quad . \quad . \quad (62)$$

For the five generator system under consideration, the co-ordination equations are

$$\left.\begin{aligned} m_1'P_1 + \lambda(2B_{11}P_1 + 2B_{12}P_2 + 2B_{13}P_3 + 2B_{14}P_4 \\ + 2B_{15}P_5) = \lambda - C_1 \\ m_2'P_2 + \lambda(2B_{12}P_1 + 2B_{22}P_2 + 2B_{23}P_3 + 2B_{24}P_4 \\ + 2B_{25}P_5) = \lambda - C_2 \\ \text{etc.} \end{aligned}\right\} \quad . \quad (63)$$

Available information, however, concerning station fuel costs will take the form

$$S_n = m_nP_n + C_n \quad . \quad . \quad . \quad . \quad . \quad (64)$$

where m_n and C_n now relate to the slope and intercept of the input/output curves.

Thus $$\frac{dS_n}{dP_n} = m_n$$

In this case it is now possible to charge the system losses at the incremental rate of received power λ, and to obtain a loading schedule from the solution of linear equations.

(5.1.1) Co-ordination Equations for a Five-Generator System.

In terms of the actual B_{nK} constants and linear input-output curves, the co-ordination equations simplify to

$$\left.\begin{aligned} 0{\cdot}0298P_1 + 0{\cdot}0065P_2 - 0{\cdot}0081P_3 + 0{\cdot}0063P_4 \\ + 0{\cdot}0182P_5 = \frac{1}{100}\left(1 - \frac{m_1}{\lambda}\right) \\ 0{\cdot}0065P_1 + 0{\cdot}0154P_2 - 0{\cdot}0029P_3 - 0{\cdot}0044P_4 \\ + 0{\cdot}0018P_5 = \frac{1}{100}\left(1 - \frac{m_2}{\lambda}\right) \\ -0{\cdot}0081P_1 - 0{\cdot}0029P_2 + 0{\cdot}004P_3 - 0{\cdot}0094P_4 \\ - 0{\cdot}0079P_5 = \frac{1}{100}\left(1 - \frac{m_3}{\lambda}\right) \\ 0{\cdot}0063P_1 - 0{\cdot}0044P_2 - 0{\cdot}0094P_3 + 0{\cdot}0448P_4 \\ + 0{\cdot}0168P_5 = \frac{1}{100}\left(1 - \frac{m_4}{\lambda}\right) \\ 0{\cdot}0182P_1 + 0{\cdot}0018P_2 - 0{\cdot}0079P_3 + 0{\cdot}0168P_4 \\ + 0{\cdot}0328P_5 = \frac{1}{100}\left(1 - \frac{m_5}{\lambda}\right) \end{aligned}\right\} \quad (65)$$

(P_1, P_2, etc., are per-unit station loadings.)

or, in matrix form, $$BP = \left(1 - \frac{m}{\lambda}\right)$$

The solution for the station loadings will now be obtained by inversion of the $5 \times 5B$ matrix. This is calculated using the methods of Kron,[25], p. 258, for the inverse of a two-row compound matrix.

Such an inversion yields the matrix equation

$$P = B^{-1}\left(1 - \frac{m}{\lambda}\right)$$

This gives the respective per-unit loadings for minimum total fuel cost as follows:

$$\left.\begin{aligned} P_1 = 46{\cdot}922 - \frac{1}{\lambda}(5{\cdot}699m_1 + 4{\cdot}730m_2 + 29{\cdot}965m_3 \\ + 5{\cdot}600m_4 + 0{\cdot}928m_5) \\ P_2 = 45{\cdot}635 - \frac{1}{\lambda}(4{\cdot}730m_1 + 5{\cdot}486m_2 + 28{\cdot}758m_3 \\ + 5{\cdot}452m_4 + 1{\cdot}209m_5) \\ P_3 = 273{\cdot}446 - \frac{1}{\lambda}(29{\cdot}965m_1 + 28{\cdot}758m_2 + 174{\cdot}902m_3 \\ + 32{\cdot}583m_4 + 7{\cdot}238m_5 \\ P_4 = 51{\cdot}181 - \frac{1}{\lambda}(5{\cdot}600m_1 + 5{\cdot}452m_2 + 32{\cdot}583m_3 \\ + 6{\cdot}362m_4 + 1{\cdot}184m_5) \\ P_5 = 11{\cdot}420 - \frac{1}{\lambda}(0{\cdot}928m_1 + 1{\cdot}209m_2 + 7{\cdot}238m_3 \\ + 1{\cdot}184m_4 + 0{\cdot}861m_5) \\ \Sigma P = 428{\cdot}604 - \frac{1}{\lambda}(46{\cdot}922m_1 + 45{\cdot}635m_2 \\ + 273{\cdot}446m_3 + 51{\cdot}181m_4 + 11{\cdot}420m_5) \end{aligned}\right\} \quad . \quad (66)$$

Loading Schedule.

From the weekly return of fuel costs at steam stations contained in Form CEA/G.S.-15 of the Central Electricity Authority, the following incremental costs were estimated, and they are used for illustrating the application of the above loading equations. These are assumed figures only, based on average fuel costs and existing orders of merit.

m_1	m_2	m_3	m_4	m_5
0·5	0·6	0·4	0·8	0·35 pence/kWh
2·08	2·50	1·67	3·33	1·46 £/MWh

Under these conditions the loading equations reduce to the following form:

$$\left.\begin{aligned} P_1 = \ 46{\cdot}922 - \frac{93{\cdot}723}{\lambda} \\ P_2 = \ 45{\cdot}635 - \frac{91{\cdot}500}{\lambda} \\ P_3 = 273{\cdot}446 - \frac{545{\cdot}377}{\lambda} \\ P_4 = \ 51{\cdot}181 - \frac{102{\cdot}606}{\lambda} \\ P_5 = \ 11{\cdot}420 - \frac{22{\cdot}240}{\lambda} \\ \Sigma P = 428{\cdot}604 - \frac{855{\cdot}446}{\lambda} \end{aligned}\right\} \quad . \quad . \quad . \quad (67)$$

The respective station loadings are now obtained by determining the value of λ for a summated generation (ΣP), and applying this same value of λ to each remaining equation.

For per-unit values of ΣP in excess of 4·316, corresponding to a value of λ equal to 2·0162£/MWh, it becomes necessary to base-load the available generation at G_4, say equal to the maximum per-unit value of 0·29.

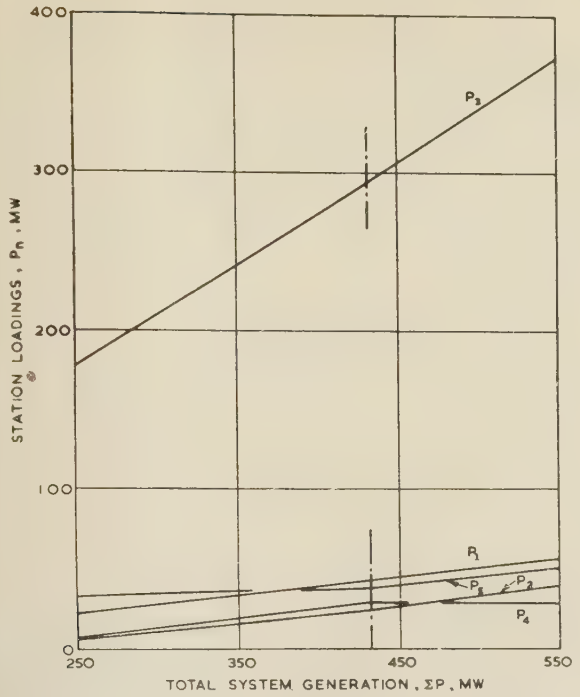

Fig. 11.—Generator loading schedule for optimum system economy.
G_4 base-loaded at $\Sigma P = 4 \cdot 316$.

(5.1.2) Co-ordination Equations with Generating Station G_4 (Crewe) Base-Loaded at its Maximum Available Generation of 29 MW.

With G_4 base-loaded at 29 MW, the co-ordination equations (65) can be reduced. Inversion of the B matrix will again give the solutions for generator loadings in the form

$$P = B^{-1}\left(C - \frac{m}{\lambda}\right)$$

Loading Schedule.

Using the previously assumed incremental fuel costs, and for values of ΣP in excess of 4·316, the loading equations now take the form

$$\left.\begin{aligned} P_1 &= 2 \cdot 1181 - \frac{3 \cdot 3918}{\lambda} \\ P_2 &= 2 \cdot 0178 - \frac{3 \cdot 5599}{\lambda} \\ P_3 &= 12 \cdot 7805 - \frac{19 \cdot 8330}{\lambda} \\ P_5 &= 1 \cdot 9493 - \frac{3 \cdot 1455}{\lambda} \\ \Sigma P \text{ (including } P_4 = 0 \cdot 29) &= 19 \cdot 1557 - \frac{29 \cdot 9302}{\lambda} \end{aligned}\right\} \quad . \quad (68)$$

A complete loading schedule obtained from these equations for system loads, ranging between 250 and 550 MW, is illustrated in Fig. 11.

The accuracy of the generator loading equations has been studied by checking the inversion of the B matrix, eqn. (65), from the product BB^{-1}. This was found to be of approximate unit matrix form, thus indicating that the inversion of B is correct.

An investigation has also been carried out to check the scaling of this matrix. From the study, which consisted of checking each step in the inversion of B, it is apparent that the expression $(B_{44}B_{55} - B_{45}^2)$ which appears throughout the inversion is having a powerful effect on the expressions for generator loadings, and in particular on the term $174 \cdot 902 m_3$ in eqn. (66).

$$\left.\begin{aligned} \text{Now} \quad B_{44} &= \frac{R_{4-4}}{|V_4|_0^2}(1 + \Lambda_4^2) \\ \text{and} \quad B_{55} &= \frac{R_{5-5}}{|V_5|_0^2}(1 + \Lambda_5^2) \end{aligned}\right\} \quad . \quad . \quad . \quad . \quad (69)$$

Also, from the Z_{33} matrix, eqn. (54),

$$\left.\begin{aligned} R_{4-4} &= Z_{4.4} - 2d_4 + w \\ \text{and} \quad R_{5-5} &= w \end{aligned}\right\} \quad . \quad . \quad . \quad . \quad (70)$$

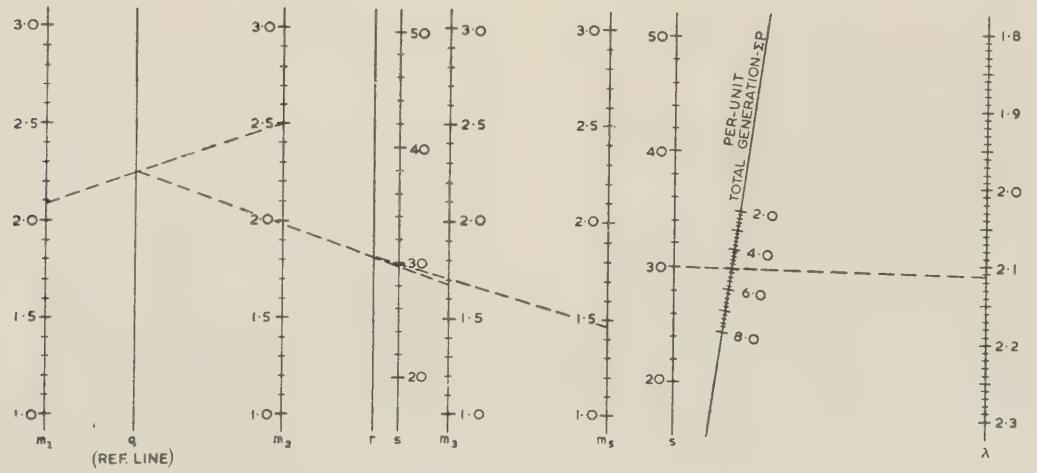

Fig. 12.—Nomogram for total generation $\sum_1^5 P$.

Examples.
Left-hand Nomogram.
$m_1 = 2 \cdot 08$ £/MWh to $m_2 = 2 \cdot 50$ £/MWh gives q.
q to $m_3 = 1 \cdot 67$ £/MWh gives r.
r to $m_5 = 1 \cdot 46$ £/MWh gives s.
Right-hand Nomogram.
$s = 29 \cdot 8$ £/MWh to required total generation of 500 MW gives λ.

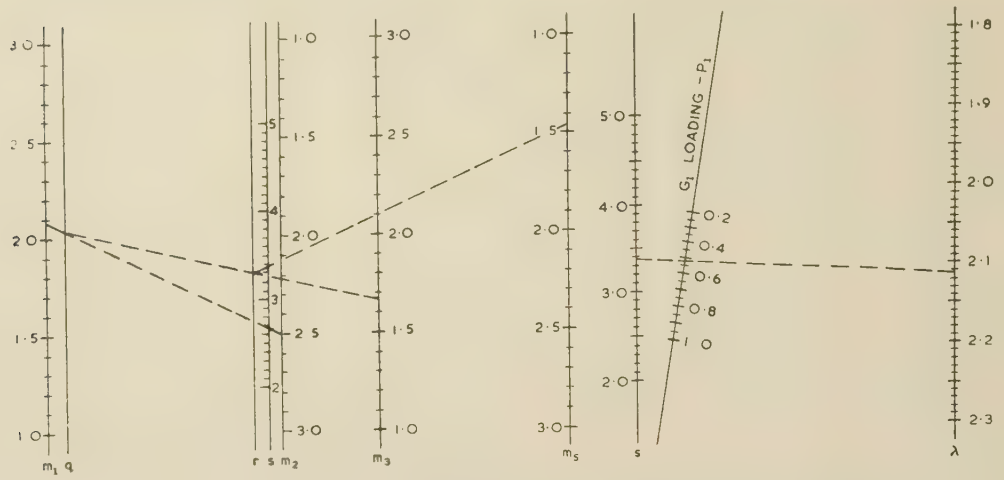

Fig. 13.—Nomogram for generator G_1 of loading P_1.

Example.
As in Fig. 12 to give *new* value of s.
$s = 3{\cdot}36$ £/MWh to $\lambda = 2{\cdot}113$ £/MWh (from Fig. 12) gives $P_1 = 52$ MW.

Now $$Z_{4.4} \simeq 2d_4 \quad . \quad . \quad . \quad . \quad . \quad . \quad (71)$$

Therefore the value of w appears to be influencing the components of B^{-1}.

From a study of the components of w (=0·014 558), it is found that the term $Z_{7.7}l_3l_3^* = Z_{3.3}l_3l_3^*$ (=0·009 056) is excessive in relation to all other quantities.

It can thus be concluded that the generator self-impedance $Z_{3.3}$ (with unit current injected at generator G_3), the loading ratio l_3 (i.e. load at Ince as a proportion of total load) and the ratio Λ_4 of reactive to active power for generator G_4 (Crewe), at normal load, are having powerful effects on individual generator loadings.

This investigation illustrates the fact that, in practice, considerable accuracy in computation will be required when the magnitudes of the system parameters and load ratios have wide differences.

(5.2) Loading Schedule Nomograms

The form of the final co-ordination equations enables a set of nomograms to be constructed to represent the various generator loadings for optimum operating efficiency.

The methods given in Reference 34 have been used for the five loading equations, including the one for total generation, and give rise to five nomograms, two of which are illustrated in Figs. 12 and 13.

Each diagram represents the respective loading equation and each variable is represented by a graduated line. Index lines drawn across the diagrams according to the values of the variables, in this case the station costs, will give a direct solution of the equations they represent. The various generator loadings are obtained by the use of the respective nomograms, using the known m values and the values of λ found from the total generation nomogram of Fig. 12.

The example given on the nomograms illustrates a loading schedule for a total system generation of 500 MW, and the various generator loadings compare with those obtained by calculation from the loading equations.

(6) CONCLUSION

In this present analysis, fuel costs and losses have been co-ordinated using the exact equations in conjunction with linear input-output characteristics for each station. With this assumption, the solutions obtained from one matrix inversion are valid for all variations in fuel costs, and the linear loading equations may be adapted for nomographic representation as illustrated in the paper. These charts will provide a method of developing rapidly the economic loading schedules as functions of total generation.

If the incremental fuel costs are assumed as functions of the station loadings, then each variation in station costs will necessitate a matrix inversion. In this case the rapid calculation of incremental transmission losses combined with generating costs, and the immediate application of these results to the system, will require the use of simplified network analysers or digital computers for the solution of the linear equations.

Comparing the economic loading schedule of Fig. 11 with the loadings obtained from the load flow study, it is apparent that for greater operating economy the generation at Percival Lane, G_2, and to a lesser extent that at Warrington, G_1, must be reduced and transferred to the more economic sources at Ince, G_3, and the Carrington interconnection, G_5—provided that adequate tie-line capacity is available.

A schedule for minimum loss can be obtained from the foregoing analysis, and if compared with that obtained by considering the effects of fuel costs, it becomes apparent that the value of the low-cost import at G_5 is much reduced due to the greater effects of line losses. Station loadings at G_1 and G_2 under these conditions are greater than the corresponding loadings obtained when considering fuel costs. Plant availability, provision for security of supplies and relative generation costs usually prevent the loading of stations on a minimum-transmission-loss basis. Such a condition, however, is of value in the planning of transmission systems and in comparing delivered costs from stations having equal incremental generation costs.

This analysis has been restricted to the determination of loading schedules for a small section of the North West, Merseyside and North Wales divisional network. The effects of incremental transmission losses on the selective loading of generating plant will become more apparent when the analysis is applied under light load conditions on this particular network, such as those obtaining at night and during the summer months, and when applied under more general conditions to larger sections of the Grid system.

(7) ACKNOWLEDGMENTS

The authors wish to express their thanks to Professor J. M. Meek, D.Eng., of Liverpool University, for his support and for the interest he has shown in the work. They are grateful to the Divisional Controller of the North West, Merseyside and North Wales Division of the Central Electricity Authority, for providing and giving permission to use technical data and for helpful discussions held with members of his staff.

One of the authors (H. N.) wishes to thank Lever Brothers, Port Sunlight, Ltd., for granting him permission to undertake these investigations.

(8) BIBLIOGRAPHY

(1) STEINBERG, M. S., and SMITH, T. H.: 'Economy Loading of Power Plants and Electric Systems' (John Wiley, New York, 1943).

(2) GEORGE, E. E.: 'Intrasystem Transmission Losses', *Transactions of the American I.E.E.*, 1943, **62**, p. 153.

(3) GEORGE, E. E., PAGE, H. W., and WARD, J. B.: 'Co-ordination of Fuel Cost and Transmission Loss by Use of the Network Analyser to Determine Plant Loading Schedules', *ibid.*, 1949, **68**, Part II, p. 1152.

(4) WARD, J. B., EATON, J. R., and HALE, H. W.: 'Total and Incremental Losses in Power Transmission Networks', *ibid.*, 1950, **69**, Part I, p. 626.

(5) KRON, G.: 'Tensorial Analysis of Integrated Transmission Systems, Part I—The Six Basic Reference Frames', *ibid.*, 1951, **70**, Part II, p. 1239.

(6) KIRCHMAYER, L. K., and STAGG, G. W.: 'Analysis of Total and Incremental Losses in Transmission Systems', *ibid.*, 1951, **70**, Part II, p. 1197.

(7) KIRCHMAYER, L. K., and MCDANIEL, G. H.: 'Transmission Losses and Economic Loading of Power Systems', *G.E.C. Review*, Oct., 1951, p. 39.

(8) KIRCHMAYER, L. K., and STAGG, G. W.: 'Evaluation of Methods of Co-ordinating Incremental Fuel Costs and Incremental Transmission Losses', *Transactions of the American I.E.E.*, 1952, **71**, Part III, p. 513.

(9) KRON, G.: 'Tensorial Analysis of Integrated Transmission Systems, Part II—Off-Nominal Turn Ratios', *ibid.*, 1952, **71**, Part III, p. 505.

(10) KRON, G.: 'Tensorial Analysis of Integrated Transmission Systems, Part III—The Primitive Division', *ibid.*, 1952, **71**, Part III, p. 814.

(11) GLIMN, A. F., KIRCHMAYER, L. K., and STAGG, G. W.: 'Analysis of Losses in Interconnected Systems', *ibid.*, 1952, **71**, Part III, p. 796.

(12) GLIMN, A. F., HABERMANN, R., KIRCHMAYER, L. K., and STAGG, G. W.: 'Loss Formulae Made Easy', *ibid.*, 1953, **72**, Part III, p. 730.

(13) KRON, G.: 'Tensorial Analysis of Integrated Transmission Systems, Part IV—The Interconnection of Transmission Systems', *ibid.*, 1953, **72**, Part III, p. 827.

(14) KIRCHMAYER, L. K., GLIMN, A. F., and STAGG, G. W.: 'Analysis of Losses in Loop-Interconnected Systems', *ibid.*, 1953, **72**, Part III, p. 944.

(15) BROWNLEE, W. R.: 'Co-ordination of Incremental Fuel Costs and Incremental Transmission Losses by Functions of Voltage Phase Angles', *ibid.*, 1954, **73**, Part III, p. 65.

(16) IMBURGIA, C. A., KIRCHMAYER, L. K., and STAGG, G. W.: 'A Transmission-Loss Penalty Factor Computer', *ibid.*, 1954, **73**, Part III, p. 567.

(17) HARKER, D. C., JACOBS, W. E., FERGUSON, R. W., and HARDER, E. L.: 'Loss Evaluation, Part I—Losses Associated with Sale Power—In-Phase Method', *ibid.*, 1954, **73**, Part III, p. 709.

(18) HARDER, E. L., FERGUSON, R. W., JACOBS, W. E., and HARKER, D. C.: 'Loss Evaluation, Part II—Current—and Power—Form Loss Formulae', *ibid.*, 1954, **73**, Part III, p. 716.

(19) TRAVERS, R. H., HARKER, D. C., LONG, R. W., and HARDER, E. L.: 'Loss Evaluation, Part III—Economic Dispatch Studies of Steam-Electric Generating Systems', *ibid.*, 1954, **73**, Part III, p. 1091.

(20) HARDER, E. L.: 'Economic Load Dispatching', *Westinghouse Engineering*, 1954, **6**, p. 194.

(21) GEORGE, E. E., and PIERCE, R. E.: 'Economics of Long-Distance Energy Transmission', *Transactions of the American I.E.E.*, 1948, **67**, Part III, p. 195.

(22) GEORGE, E. E.: 'Principles of Load Allocation Among Generating Units', *ibid.*, 1953, **72**, Part III, p. 49.

(23) WARD, J. B.: 'Economy Loading Simplified', *ibid.*, 1953, **73**, Part III, p. 1306.

(24) HALE, H. W.: 'Power Losses in Interconnected Transmission Networks', *ibid.*, 1952, **71**, Part III, p. 993.

(25) KRON, G.: 'Tensor Analysis of Networks' (John Wiley, New York, 1939).

(26) ZABORSZKY, J., and RITTENHOUSE, J. W.: 'Electric Power Transmission' (The Ronald Press Company, New York, 1954), p. 581.

(27) COOPER, A. R.: 'Load Dispatching and the Reasons for it, with Special Reference to the British Grid System', *Journal I.E.E.*, 1948, **95**, Part II, p. 713.

(28) OLDROYD, G.: 'Economy Loading of Generating Plant', *Electrical Review*, 9th December, 1949, p. 1095.

(29) DON, N.: 'Economical Loading', *ibid.*, 19th January, 1951, p. 112.

(30) TOMBS, F. L.: 'Economic Loading', *ibid.*, 23rd March, 1951, p. 581.

(31) PARSONS, L. J., and MARTENS, C.: 'Computer Matches Incremental Rates', *Power*, August, 1950, p. 114.

(32) COURANT, R.: 'Differential and Integral Calculus' (Interscience Publishers, New York, 1936), Vol. II, p. 188–211.

(33) LACOPO, M. J.: 'Interconnected System Energy Accounting Procedure and Related Operating Practices', *Transactions of the American I.E.E.*, 1953, **72**, Part III, p. 1196.

(34) ALLCOCK, H. J., and JONES, J. R.: 'The Nomogram' (Pitman, 1941).

(35) SEREBRENNIKOV, V. N.: 'Determination of Data for the Load Dispatcher's Selection of the Order of Loading Turbo-generator Sets', *Elektricheskie Stantsii*, 1954, **12**, p. 6.

(36) BILLAM, P. M.: 'Some Impressions of Electric Utility Practices in the U.S.A., *I.E.E. Student's Quarterly Journal*, 1954, **25**, p. 15.

621.313.1

The Institution of Electrical Engineers
Monograph No. 295 S
Mar. 1958
©

TENSOR ANALYSIS OF ELECTRICAL MACHINE HUNTING

By J. W. LYNN, M.Sc., Associate Member.

(*The paper was first received 6th August, and in revised form 25th November*, 1957. *It was published as an* INSTITUTION MONOGRAPH *in March*, 1958.)

SUMMARY

The paper gives first a brief résumé of previous work on tensor analysis of electrical machines. The steady-state equations of the synchronous machine are written in Park's reference axes, and from these the hunting equations are derived. It is then shown that these equations are part of a general group of transformations of reference axes of the synchronous machines, all of which are embraced by the general tensor equations. The hunting equations are then derived in a freely-rotating reference system. These equations are rewritten in tensor form and the significance of the grouping of terms into tensors is discussed. The latter equations are shown to give a more realistic interpretation of the hunting equations and the equivalent circuit.

LIST OF PRINCIPAL SYMBOLS

Indices.

a, b, c = Quantities in axes fixed to the machine stator and rotor windings.
k, n, m = Quantities in axes all relatively stationary.
α, β, γ = Quantities in axes fixed or free on the stator and rotating freely on the rotor.
s, t = Quantities associated with the mechanical rotational effects in the machine (e.g. generated voltages and torque).
u, v, w = Quantities in a general equation.

Electrical parts of the equations.

V_m, V_α, etc. = Electrical voltage vectors in axes denoted by indices.
x^k, x^α, etc. = Electric variables. The electrical charges in machine windings, referred to axes denoted by indices.
$\dot{x}^\alpha$ ($\equiv i^\alpha$) = Electric current vector, in axes denoted by indices.
$R_{\gamma\alpha}$ = Resistance matrix, in axes denoted by indices.
$L_{\gamma\alpha}$ = Inductance matrix, in axes denoted by indices.
$G_{\gamma\alpha}$ = Generated voltage coefficients, in axes denoted by indices.

Mechanical part of the equations.

f_s = Mechanical force.
x^s = Mechanical variable θ, the angular position of the machine rotor during rotation.
$\dot{x}^s$ ($\equiv i^s \equiv p\theta$) = Angular velocity of machine rotor.
R_{ss} = Mechanical friction coefficients.
L_{ss} ($\equiv J$) = Moment of inertia of machine rotor.

General symbols.

$\boldsymbol{v}$ = Generalized force vector (voltage or mechanical force).
$\boldsymbol{R}$ = Generalized dissipation matrix (resistance or friction).
$\boldsymbol{L}$ = Generalized inductance matrix (inductance or inertia).
$\boldsymbol{i}$ = Generalized current vector (electric current or angular velocity).
C^k_α = Connection matrix between quantities in axes denoted by indices.
$\boldsymbol{C}$ = Direct notation for C^k_α, etc.
$\boldsymbol{C}_{(t)}$ = Transpose of matrix $\boldsymbol{C}$.
$\Omega^\delta_{\alpha\beta}$ = 'Non-holonomic object' containing functions of C, in axes denoted by indices.
$[\alpha\beta, \gamma]$ = A 'connection' term containing functions of $L_{\gamma\alpha}$ in axes denoted by indices.
$\Gamma_{\alpha\beta,\gamma}$ = A 'connection' term containing both $[\alpha\beta, \gamma]$ and $\Omega_{\alpha\beta,\gamma}$ in axes denoted by indices.
$S_{\alpha\beta\gamma}$ = Tensor giving the terms $G_{\gamma\alpha}$.

(1) INTRODUCTION

With rapid expansion in the field of control systems a fuller understanding of the dynamical behaviour of rotating electrical machines has become of increasing importance. For this reason, and also because of general developments in electrotechnics, the teaching of electrical machine theory from a generalized dynamical viewpoint is now being considered in universities and colleges. Brown, Kusko and White[1] give details of a laboratory machine for teaching purposes, the windings of which can be interconnected in a variety of ways to give the characteristics of a range of d.c. and a.c. machines.

One of the pioneers of this approach to electrical machine analysis was Gabriel Kron.[2, 3, 4] The matrix and tensor methods which he has developed since 1934 have led to a better understanding of the fundamental concepts underlying all machine systems. A survey of these methods is given in Reference 5. The above References show that the analysis of most types of electrical machines can be expressed by a single set of dynamical equations.

Recently the behaviour of oscillating-machine systems has been receiving a great deal of attention.[6, 7, 8] Transient and hunting conditions have been the subject of investigation throughout the history of machine analysis. The development of hunting analysis of synchronous machines can be indicated briefly by selection of one or two representative publications, as follows.

In 1929 Wennerberg[9] extended the early work of Kapp and Rosenberg. Starting with the design details of a 3-phase salient-pole machine he resolved the armature magnetomotive-force and flux waves into two axes in quadrature on the armature (stator). During hunting the field rotates and oscillates with respect to these axes. Wennerberg then derived equations for voltages, currents and torque during small oscillations of the rotor. The expressions are complicated because of the fixed armature axes chosen. All steady-state currents and voltages are functions of sin ωt and cos ωt (where ω is the synchronous angular velocity of the rotor), and the hunting equations are, of course, obtained by making small changes in steady-state values. In his expressions for hunting torque the trigonometrical terms of synchronous frequency ultimately disappear and the torque is expressed as

$$\Delta T = A'X \sin(h\omega)t + A''(h\omega)X \cos(h\omega)t$$

where $h\omega$ is the angular velocity of hunting. Inspection of this

Correspondence on Monographs is invited for consideration with a view to publication.
Mr Lynn is in the Department of Electrical Engineering, University of Liverpool.

expression yields the synchronizing and damping torque coefficients, A' and A''.

Prescott and Richardson,[10] using implicitly the same reference system as Wennerberg, derived a comprehensive set of equations giving the damping and synchronizing torque coefficients of a salient-pole alternator. They examined, in particular, the effects of armature resistance and armortisseur parameters on hunting. Curves are then given showing calculated and experimental results for a laboratory machine.

About this time the two-reaction theory of the salient-pole synchronous machine was developed. In 1926 Doherty and Nickle,[11] following Blondel, resolved the armature resultant m.m.f. and flux-linkage waves into axes along the field pole and in quadrature with it. These axes were considered to rotate synchronously along with the field structure. Both the armature and field quantities are therefore constant along these axes in the steady state, trigonometrical terms at synchronous frequency having been eliminated by transformation of the phase quantities into these axes. During hunting the reference axes rotate and oscillate with the field structure. In 1929 Park[12] expressed this theory in terms of transient or 'operational' impedances in these axes, which could be measured directly by tests on the machine. Park then extended his theory to include hunting conditions. His equations of hunting are physically the same as those of earlier investigators, but in terms of machine parameters they are more explicit. They are also more comprehensive in that the operational impedances incorporate the effects of the rotor (field) circuit parameters as well as those of armortisseurs. Park's equations have now become generally accepted in synchronous-machine theory.

Liwschitz,[13] using the latter reference axes, has analysed the hunting of a synchronous machine as a special case of the general problem of a doubly-fed machine. Concordia[14] has given a very comprehensive set of results of the application of Park's analysis to a particular machine.

In 1942 a.c. machines, including the salient-pole synchronous machine were described by a general theory of equivalent circuits, by Kron,[15] for both steady-state and hunting conditions. These circuits were subsequently used by Concordia, Kron and Crary.[16, 17]

The above work is confined to analysis of behaviour of a single machine synchronized with a large system. Kron[15] indicated that the analysis and equivalent circuits in Park's reference frame become complicated when external circuits are connected to the machine terminals. The synchronous-machine axes rotate and oscillate with the field structure, and the external network must also be analysed along oscillating axes. He then selected axes which are identical with those of Park in the steady state but which rotate uniformly and do not oscillate.[18] Equivalent hunting circuits were derived along these uniformly rotating axes, which could be interconnected to build up complete systems.[7, 19] These circuits are such that the resistance power loss in each mesh gives the damping torque. Synchronizing torque can also be read from the circuit.

The physical concepts arising in the new reference frame have been examined in detail.[19] In order to generalize his work on machines, Kron uses the methods of tensor calculus. Heffron, Rosenberry and Rothe[6, 7] have given an alternative, more conventional, analysis in which they compare hunting equations of an interconnected system in the reference frames of both Park and Kron, and point out the advantages of the uniformly rotating axes.

In the theory of relativity, Einstein's quest was for laws of nature that would hold irrespective of the reference frame chosen. Kron's approach to machine analysis has been from the same viewpoint. He looked for basic concepts which exist in all machines regardless of the reference axes and for equations expressing these concepts. He formulated these for his primitive machine and used already existing tensor analysis to deal with the transformation of these equations, to give those of any required machine with any chosen reference axes. As in relativity, it was found that the fundamental machine concepts having physical significance in steady-state, transient or hunting operation were all tensors.[18] Equivalent-circuit meshes were seen to yield groups of terms which constitute tensors. Conversely, if equivalent circuits were to be set up, the terms of the equations should be grouped into tensor quantities. Apart from equivalent circuits, this tensor grouping of the equations appears to give a better physical picture of the correlation of different forms of energy in any physical system. Prof. Kondo[20] has used tensor equations, identical in form with the machine equations, for the analysis of aircraft oscillations in which aerodynamic and other forces are considered.

The present paper shows how these tensor terms arise in hunting analysis of a synchronous machine and how the tensor grouping of terms is associated with the equivalent hunting circuit. The equations are particular cases of the general machine equations, and the same analysis is therefore directly applicable to many other types of d.c. and a.c. machines.

(2) TENSOR EQUATIONS OF ELECTRICAL MACHINES

(2.1) Matrix Equations

The voltage equations of the stationary-axis primitive machine shown in Fig. 1, with axes *ds*, *dr*, *qr* and *qs*, can be written down by inspection. Written in matrix form these are as follows:

$$\begin{array}{c|c} & \\ ds & v_{ds} \\ dr & v_{dr} \\ qr & v_{qr} \\ qs & v_{qs} \end{array} = \begin{array}{c|cccc} & ds & dr & qr & qs \\ ds & r_{ds} + L_{ds}p & M_d p & & \\ dr & M_d p & r_{dr} + L_{dr}p & L_{qr}p\theta & M_q p\theta \\ qr & -M_d p\theta & -L_{dr}p\theta & r_{qr} + L_{qr}p & M_q p \\ qs & & & M_q p & r_{qs} + L_{qs}p \end{array} \cdot \begin{array}{c|c} & \\ ds & i^{ds} \\ dr & i^{dr} \\ qr & i^{qr} \\ qs & i^{qs} \end{array} \quad . \quad . \quad . \quad (1)$$

These are seen to include those derived by Park[12] in 1926 for the synchronous machine along direct and quadrature axes, usually written[21] as follows

Impressed field voltage.

$$v_{fd} = R_{fd}i^{fd} + L_{fd}pi^{fd} + M_d pi^{dr} \quad . \quad . \quad . \quad (2)$$

Generated voltage.

$$v_{dr} = -M_d pi^{fd} - R_{dr}i^{dr} - L_{dr}pi^{dr} + L_{qr}i^{qr}p\theta \quad . \quad (3)$$

$$v_{qr} = -M_d i^{fd}p\theta - L_{dr}i^{dr}p\theta - R_{qr}i^{qr} - L_{qr}pi^{qr} \quad . \quad (4)$$

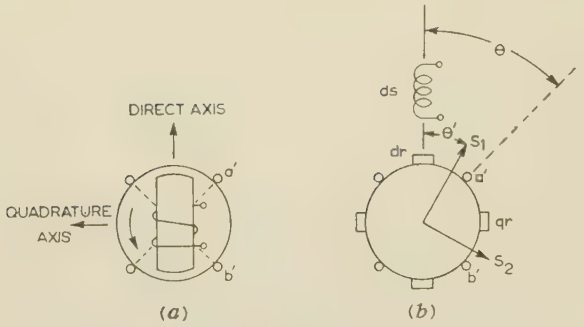

Fig. 1.—The primitive machine.
(*a*) 2-phase synchronous-machine field structure rotating.
(*b*) Primitive machine with armature rotating.

Generated electrical torque.

$$F = \psi_d i^{qr} - \psi_q i^{dr} \quad . \quad . \quad . \quad . \quad . \quad . \quad (5)$$

where $$\psi_d = -M_d i^{fd} - L_{dr} i^{dr} \quad . \quad . \quad . \quad . \quad . \quad (6)$$

and $$\psi_q = -L_{qr} i^{qr} \quad . \quad . \quad . \quad . \quad . \quad . \quad (7)$$

In eqns. (3) and (4) the quadrature field axis has been omitted for simplicity.

Equivalent circuits for the synchronous machine have been developed by Kron[15] and studied by Ku[22] by resolving the set of eqns. (1) into forward- and backward-rotating instantaneous symmetrical components.

Eqns. (1) are of the form

$$\boldsymbol{v} = \boldsymbol{Ri} + \boldsymbol{Lpi} + \boldsymbol{Gip\theta} \quad . \quad . \quad . \quad . \quad (8)$$

or $$\boldsymbol{v} = \boldsymbol{Z} \,.\, \boldsymbol{i} \quad . \quad . \quad . \quad . \quad . \quad . \quad . \quad (9)$$

where $$\boldsymbol{Z} = (\boldsymbol{R} + \boldsymbol{Lp} + \boldsymbol{Gp\theta}) \quad . \quad . \quad . \quad . \quad (10)$$

The torque is given by

$$f = \boldsymbol{i}^* \,.\, \boldsymbol{G} \,.\, \boldsymbol{i} \quad . \quad . \quad . \quad . \quad . \quad . \quad (11)$$

(the asterisk denoting conjugate values), the 'torque matrix' G being

	ds	*dr*	*qr*	*qs*
ds				
dr			L_{qr}	M_q
qr	$-M_d$	$-L_{dr}$		
qs				

. (12)

It is shown in Reference 3 that the impedance matrix of eqn. (1) can be transformed to give that for any other commutator machine, by the simple transformation

$$\boldsymbol{Z}' = \boldsymbol{C}_{(t)} \,.\, \boldsymbol{Z} \,.\, \boldsymbol{C} \quad . \quad . \quad . \quad . \quad . \quad . \quad (13)$$

where C is the matrix connecting mesh currents in the derived machine windings with the branch currents of the primitive machine coils. If the transformation is to be carried out to any reference axes which are rotating relative to the direct and quadrature axes, then, as shown in Reference 3, the transformation law is

$$\boldsymbol{Z}' = \boldsymbol{C}_{(t)} \,.\, \boldsymbol{Z} \,.\, \boldsymbol{C} + \boldsymbol{C}_{(t)} \,.\, \boldsymbol{L} \,.\, \frac{\partial \boldsymbol{C}}{\partial \theta'} p\theta' \quad . \quad . \quad . \quad (14)$$

where $p\theta'$ is the angular velocity of the reference frame with respect to the direct and quadrature axes system. This leads to an equation of the form

$$\boldsymbol{v}' = \boldsymbol{R'i'} + \boldsymbol{L'pi'} + \boldsymbol{G'i'p\theta} + \boldsymbol{V'i'p\theta'} \quad . \quad . \quad (15)$$

or $$\boldsymbol{v}' = \boldsymbol{Z}' \,.\, \boldsymbol{i}' \quad . \quad . \quad . \quad . \quad . \quad . \quad . \quad (16)$$

where $$\boldsymbol{Z}' = (\boldsymbol{R}' + \boldsymbol{L'p} + \boldsymbol{G'p\theta} + \boldsymbol{V'p\theta'}) \quad . \quad . \quad . \quad (17)$$

If the direct- and quadrature-axis quantities are transformed to uniformly rotating axes S_1 and S_2, the connection matrix C is given by the relation between the currents in the two systems as shown in Fig. 1.

$$\begin{aligned} i^{ds} &= i^{ds} \\ i^{dr} &= i^{S1} \cos\theta' - i^{S2} \sin\theta' \\ i^{qr} &= i^{S1} \sin\theta' + i^{S2} \cos\theta' \\ i^{qs} &= i^{qs} \end{aligned} \quad . \quad . \quad . \quad . \quad . \quad . \quad . \quad . \quad (18)$$

and

$C =$

	dr	S_1	S_2	*qs*
ds	1			
dr		$\cos\theta'$	$-\sin\theta'$	
qr		$\sin\theta'$	$\cos\theta'$	
qs				1

. (19)

The terms of expression (17) are given in full in Reference 5.

If the angle θ' is, in fact, the load angle λ, the axes S_1 and S_2 coincide with the voltage axes of the machine. The angle λ is constant in the steady state and the last term in eqn. (15) is zero. The impedance matrix is then given by the transformation (13), which gives (neglecting axis *qs*)

$$\boldsymbol{Z}' = \boldsymbol{C}_{(t)} \,.\, \boldsymbol{Z} \,.\, \boldsymbol{C} \quad . \quad . \quad . \quad . \quad . \quad (20)$$

$Z' =$

	ds	S_1	S_2
ds	$r_{ds} + L_{ds}p$	$M_d \cos\lambda p$	$-M_d \sin\lambda p$
S_1	$M_d \cos\lambda p$ $-M_d \sin\lambda p\theta$	$r_{dr} + L_{dr}\cos^2\lambda p$ $+ L_{qr}\sin^2\lambda p$ $+(L_{qr} - L_{dr})\sin\lambda\cos\lambda p\theta$	$(L_{qr} - L_{dr})\sin\lambda\cos\lambda p$ $+ L_{dr}\sin^2\lambda p\theta$ $+ L_{qr}\cos^2\lambda p\theta$
S_2	$-M_d \sin\lambda p$ $-M_d \cos\lambda p\theta$	$(L_{qr} - L_{dr})\sin\lambda\cos\lambda p$ $- L_{dr}\cos^2\lambda p\theta$ $- L_{qr}\sin^2\lambda p\theta$	$r_{qr} + L_{qr}\cos^2\lambda p$ $+ L_{dr}\sin^2\lambda p$ $-(L_{qr} - L_{dr})\cos\lambda\sin\lambda p\theta$

. . (21)

The matrix multiplication shown above, to give a change of reference frame, is extremely simple, and the obvious question that arises is whether any knowledge of tensors is required and whether there is any advantage in learning a new mathematical technique involving, among other things, a complicated index notation. The answer begins to appear when one looks at the general law of transformation of impedance during small disturbances of the machine voltages, currents and speed.[3] If the hunting impedance in Park's reference system is $\mathscr{Z}$, the hunting impedance matrix in a free frame is given by

$$\mathscr{Z}' = \left[C_{(t)} \cdot \mathscr{Z} \cdot C + C_{(t)} \cdot L \cdot \frac{\partial C}{\partial \theta'} p\theta' \right] (\Delta i' + \Delta\theta') + \left[C_{(t)} \cdot \mathscr{Z} \cdot \frac{\partial C}{\partial \theta'} i' + C_{(t)} \cdot L \cdot \frac{\partial C^2}{(\partial\theta')^2} (p\theta') + C_{(t)} \cdot L \cdot \frac{\partial C}{\partial \theta'} pi' + \frac{\partial C_{(t)}}{\partial \theta'} \cdot Z \cdot C \cdot i' - \frac{\partial V'}{\partial \theta'} \right] \Delta\theta' \quad . \quad (22)$$

The purpose of tensor analysis is to present all the transformations of machine reference frames in a consistent dynamical theory for steady-state and hunting analysis of all types of machines. The fundamental ideas underlying the tensor approach as developed by Kron have been examined in Reference 5. The salient points are now summarized.

(2.2) General Tensor Equations of Electrical Machines

In Reference 24 the different concepts of flux linkage and generated voltages arising under different transformations of machine reference axes have been classified. These components change with the angular velocity of the reference frames and some arise in one system of measurement and disappear in others. When machine equations are expressed in tensor form these various voltage components are part of a total 'tensor' voltage which includes both flux linkage and flux density. A tensor voltage cannot disappear under any transformation, and it is this, whatever its components, that is associated with the invariant power and stored electromagnetic energy in the machine. Resistance drop is also a tensor voltage.

Another advantage of using tensor equations is that there are available general routine laws covering all possible transformations of reference axes, the machine power remaining invariant with each change of reference system.

The tensor equation of the rotating electrical machine is an equation which has the same basic terms for all machines, these having different components for each machine or with each reference system chosen. The motion of the rotor is included in the form of rate of change of self and mutual coupling of the rotor and stator coils with changing rotor angle.

The voltage equation of a single coil having resistance and inductance is written

$$v = Ri + L\frac{di}{dt} \quad . \quad . \quad . \quad . \quad . \quad . \quad . \quad (23)$$

The equation for a set of coils, some of which rotate with respect to the others, becomes

$$v_w = R_{wu} i^u + L_{wu} \frac{\delta i^u}{dt} \quad . \quad . \quad . \quad . \quad . \quad (24)$$

where $\dfrac{\delta i^u}{dt}$ is the 'absolute' derivative of the current with respect to time. Every term is then a tensor. As shown in Reference 5,

$$\frac{\delta i^u}{dt} = \frac{di^u}{dt} + \Gamma^u_{vw} i^v i^w \quad . \quad . \quad . \quad . \quad . \quad (25)$$

where Γ^u_{vw} contains functions of the matrix C which relates the currents in two different systems,

$$i^u = C^u_\alpha i^\alpha \quad . \quad . \quad . \quad . \quad . \quad . \quad . \quad (26)$$

and

$$\frac{\delta i^u}{dt} = \frac{\delta i^\alpha}{dt} C^u_\alpha \quad . \quad . \quad . \quad . \quad . \quad . \quad . \quad (27)$$

The indices range over the different machine variables, namely the electrical charges in each coil and the angle of rotation of the rotor. The coil currents and angular velocity of the rotor are then written, for example,

$$i^u = \frac{dq^u}{dt} \quad . \quad . \quad . \quad . \quad . \quad . \quad . \quad (28)$$

and

$$i^s = \frac{d\theta}{dt} = p\theta \quad . \quad . \quad . \quad . \quad . \quad . \quad . \quad (29)$$

The index s is used to denote the mechanical variable, the angle θ.

Also

$$L_{wu} \frac{\delta i^u}{dt} = L_{wu} \frac{di^u}{dt} + \Gamma_{uv,w} i^u i^v \quad . \quad . \quad . \quad . \quad (30)$$

The machine equation in its general form therefore becomes

$$v_w = R_{wu} i^u + L_{wu} p i^u + \Gamma_{uv,w} i^u i^v \quad . \quad . \quad . \quad (31)$$

The whole of tensor analysis of rotating electrical machinery is based on a knowledge of the components of the term $\Gamma_{uv,w} i^u i^v$ in eqn. (31). When these are understood and facility in manipulating the index notation has been attained, the group properties of electrical machines become clear and analysis of a wide range of machines under many different operating conditions becomes a matter of routine procedure. The study of the Γ terms and their expansion have been carried out in detail in Reference 5.

(2.3) Synchronous-Machine Systems

The analysis of synchronous machines can be carried out using any one of three reference systems shown in Fig. 1, namely

(*a*) Actual phase quantities, or 2-phase co-ordinates of these.
(*b*) The reference frame of Park. This is much more suitable for most cases, and is in general use for synchronous-machine studies at constant speed.
(*c*) The free frame. In this system the field quantities are referred to axes fixed on the field as in reference systems (*a*) and (*b*). Armature quantities are referred to axes which rotate uniformly with respect to the armature as in reference frame 2, but these can be chosen to have any uniform velocity, they can have any fixed position relative to the field structure, and the angular velocity of the reference frame is independent of any oscillations of the field structure. The simplest case is that in which the free frame coincides with that of Park under steady-state constant-speed conditions.

The machine equations in each frame have the same form and are identified by different systems of indices as follows:

Frame (a) $$v_c = R_{ca} i^a + L_{ca} p i^a + \Gamma_{ab,c} i^a i^b \quad . \quad . \quad . \quad (32)$$

Frame (b) $$v_m = R_{mk} i^k + L_{mk} p i^k + \Gamma_{kn,m} i^k i^n \quad . \quad . \quad . \quad (33)$$

Frame (c) $$v_\gamma = R_{\gamma\alpha} i^\alpha + L_{\gamma\alpha} p i^\alpha + \Gamma_{\alpha\beta,\gamma} i^\alpha i^\beta \quad . \quad . \quad . \quad (34)$$

where $$v_m = C^c_m v_c \quad . \quad . \quad . \quad . \quad . \quad . \quad . \quad . \quad . \quad (35)$$

$$L_{\gamma\alpha} = L_{mk} C^m_\gamma C^k_\alpha \quad . \quad . \quad . \quad . \quad . \quad . \quad . \quad . \quad (36)$$

etc.

The most general form of the term $\Gamma_{uv,w}$ in eqn. (31) is, as shown in Reference 5,

$$\Gamma_{uv,w} \equiv \frac{1}{2}\left(\frac{\partial L_{wv}}{\partial x_u} + \frac{\partial L_{wu}}{\partial x_v} - \frac{\partial L_{uv}}{\partial x_w} \right) - S_{wvu} - S_{wuv} + S_{uvw} + \Omega_{wv,u} + \Omega_{wu,v} - \Omega_{uv,w} \quad . \quad (37)$$

In the voltage equation

$$x^v = \theta \quad \text{and} \quad i^v = p\theta \quad . \quad . \quad . \quad . \quad . \quad (38)$$

In the steady state

$$\Gamma_{uv,w} i^u i^v \equiv \left(\frac{\partial L_{wu}}{\partial x^v} - 2S_{wvu} + 2\Omega_{wv,u} \right) i^u i^v \quad . \quad . \quad (39)$$

$$-2S_{wvu} \equiv C_{(t)} \,.\, \boldsymbol{G} \,.\, \boldsymbol{C} \equiv \boldsymbol{G}' \quad . \quad . \quad . \quad (40)$$

and the torque matrix in the new frame is

$$2\Omega_{wv,u} = \frac{\partial C_t^{-1}}{\partial \theta'} C_{(t)} L' = \rho L' \quad . \quad . \quad . \quad . \quad (41)$$

where L' is the inductance matrix in the new frame

and

$$\rho = \begin{array}{c|cccc} w \backslash u & & & & \\ \hline & & & & \\ & & & -1 & \\ & & 1 & & \\ & & & & \end{array} \quad . \quad . \quad . \quad . \quad (42)$$

Thus $\Gamma_{uv,w} i^u i^v$ becomes, in the steady-state equations,

$$\frac{\partial \boldsymbol{L}'}{\partial \theta'} \,.\, p\theta' \,.\, \boldsymbol{i}' + \boldsymbol{G}' \,.\, \boldsymbol{i}' \,.\, \rho\boldsymbol{\theta} + \rho \boldsymbol{L}' \,.\, \boldsymbol{i}' \,.\, p\boldsymbol{\theta}' \quad . \quad . \quad (43)$$

where $p\theta$ is the angular velocity of the rotor and $p\theta'$ is the angular velocity of the reference frame with respect to the rotor.

In reference frame (*a*) the second and third terms of expression (43) do not arise. They appear only in transformations from reference frame (*a*) to any other reference frame.

In reference frame (*b*) the first and third terms are zero.

In reference frame (*c*) all three terms arise. An important point is that, while inductances along reference frame (*c*) can be constant in the steady state (if the axes rotate at synchronous speed or coincide with Park's axes), they are subject to incremental changes when the field structure oscillates. This means that a term such as $(\partial L'/\partial\theta')p\theta'$, which arises in the general equations, may be zero in the steady state, but under hunting conditions it becomes $(\partial L'/\partial\lambda)p(\Delta\lambda)$ and must be retained. The use of the general form of the term $\Gamma_{uv,w}$ in hunting equations ensures that all possible interactions of currents, fluxes and speed, together with their increments, are included in the final equations.

The disadvantage of Park's equations [frame (*b*)] for hunting analysis is that the armature reference frame is fixed along the field structure and oscillates with it. This means that circuits connected to the armature must also be analysed along the same oscillating reference system.[19] It is simpler and more realistic to analyse the machine in the first place along reference frame (*c*). External networks can then be more easily included. It is reference frame (*c*) that leads to the new equivalent circuit in which the system damping torque is given by the network mesh-resistance power loss.

(3) SYNCHRONOUS-MACHINE HUNTING EQUATIONS. PARK'S REFERENCE FRAME

The machine is that shown in Fig. 1, with armature axes *dr* and *qr*, stationary with respect to the field. The quadrature field circuit has been omitted in the following equations. The resistance, inductance, torque and impedance matrices are as follows:

$$\boldsymbol{v} = \boldsymbol{Ri} + \boldsymbol{Lpi} + \boldsymbol{Gip\theta}$$

or

$$\boldsymbol{v} = \boldsymbol{Z} \,.\, \boldsymbol{i}$$

where

$$\boldsymbol{Z} = \begin{array}{c|ccc} & ds & dr & qr \\ \hline ds & r_{ds} + L_{ds}p & M_d p & \\ dr & M_d p & r_{dr} + L_{dr}p & L_{qr}p\theta \\ qr & -M_d p\theta & -L_{dr}p\theta & r_{qr} + L_{qr}p \end{array} \quad . \quad (44)$$

$$\boldsymbol{R} = \begin{array}{c|ccc} & ds & dr & qr \\ \hline ds & r_{ds} & & \\ dr & & r_{dr} & \\ qr & & & r_{qr} \end{array} \quad . \quad (45)$$

$$\boldsymbol{L} = \begin{array}{c|ccc} & ds & dr & qr \\ \hline ds & L_{ds} & M_d & \\ dr & M_d & L_{dr} & \\ qr & & & L_{qr} \end{array} \quad . \quad (46)$$

$$\boldsymbol{G} = \begin{array}{c|ccc} & ds & dr & qr \\ \hline ds & & & \\ dr & & & L_{qr} \\ qr & -M_d & -L_{dr} & \end{array} \quad . \quad . \quad . \quad (47)$$

The hunting equation may be found as in dynamics by considering small increments of the quantities in the steady-state equations (8) and (11).

Thus

$$(\boldsymbol{v} + \Delta\boldsymbol{v}) = (\boldsymbol{Z} + \Delta\boldsymbol{Z})(\boldsymbol{i} + \Delta\boldsymbol{i}) \quad . \quad . \quad . \quad (48)$$

or

$$(\boldsymbol{v} + \Delta\boldsymbol{v}) = (\boldsymbol{R} + \Delta\boldsymbol{R})(\boldsymbol{i} + \Delta\boldsymbol{i}) + (\boldsymbol{L} + \Delta\boldsymbol{L})\boldsymbol{p}(\boldsymbol{i} + \Delta\boldsymbol{i}) + (\boldsymbol{G} + \Delta\boldsymbol{G})(\boldsymbol{i} + \Delta\boldsymbol{i})(\boldsymbol{p\theta} + \Delta\boldsymbol{p\theta}) \quad . \quad (49)$$

Multiplying out and subtracting the original equation the hunting equation of voltage is found:

$$\Delta\boldsymbol{v} = (\boldsymbol{R} + \boldsymbol{Lp} + \boldsymbol{Gp\theta})\Delta\boldsymbol{i} + \boldsymbol{Gi}(\Delta\boldsymbol{p\theta}) \quad . \quad . \quad (50)$$

The torque equation becomes

$$\Delta\boldsymbol{f} = \boldsymbol{i}^* \,.\, \boldsymbol{G} \,.\, \Delta\boldsymbol{i} + \Delta\boldsymbol{i}^* \,.\, \boldsymbol{G} \,.\, \boldsymbol{i} \quad . \quad . \quad . \quad (51)$$

The matrix form of eqns. (50) and (51) can now be written, including a mechanical row and column involving the mechanical variables.

The equation has the form

$$\Delta\boldsymbol{v} = \mathscr{Z} \,.\, \Delta\boldsymbol{i} \quad . \quad . \quad . \quad . \quad . \quad . \quad (52)$$

which, when written in full, expands to

$$\begin{array}{c|c} & \\ \hline ds & \Delta v_{ds} \\ dr & \Delta v_{dr} \\ qr & \Delta v_{qr} \\ s & \Delta f \end{array} = \begin{array}{c|cccc} & ds & dr & qr & s \\ \hline ds & r_{ds} + L_{ds}p & M_d p & & \\ dr & M_d p & r_{dr} + L_{dr}p & L_{qr}p\theta & i^{qr}L_{qr}p \\ qr & -M_d p\theta & -L_{dr}p\theta & r_{qr} + L_{qr}p & -i^{ds}M_d p - i^{dr}L_{dr}p \\ s & i^{qr}M_d & 2i^{qr}L_D & 2i^{dr}L_D + i^{ds}M_d & Jp^2 \end{array} \cdot \begin{array}{c|c} & \\ \hline ds & \Delta i^{ds} \\ dr & \Delta i^{dr} \\ qr & \Delta i^{qr} \\ s & \Delta\theta \end{array} \quad . \quad . \quad . \quad (53)$$

where $$L_D = (L_{dr} - L_{qr})/2$$

and J is the rotor inertia constant.

These equations have been studied in detail both analytically and by means of equivalent circuits,[6, 22] and they will now be used only as a starting-point for the study of the hunting equations expressed in the free reference frame.

(4) HUNTING EQUATIONS IN THE FREE FRAME

In the free frame the reference axes do not oscillate with the rotor. The equations are first expressed along the axes d' and q' of Fig. 2, rotating synchronously with the terminal voltage vector position.

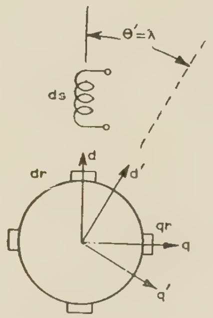

Fig. 2.—Free reference axes.
Axes d' and q' along terminal voltage axes.
Axes d and q coinciding with Park's axes.

This may be done in either of two ways:

(i) The hunting equations (53) can be transformed directly to those in the free frame using the law of transformation given by eqn. (22). In this equation the p-operator in $\mathscr{L}$ refers only to $\Delta i'$ or $\Delta\theta'$ and not to C; and in Z, p refers only to C and i' and not to $\Delta\theta'$.

(ii) The more elegant method is to set up the steady-state equations in the new frame and from these to derive the hunting equation.

The steady-state equation is eqn. (34). Taking small increments of this as before, the hunting equations, as shown in detail in Appendix 11.1, are as follows:

Voltage equation.

$$\Delta v_\alpha + \frac{\partial v_\alpha}{\partial x^\beta}\Delta x^\beta =$$

$$(R_{\alpha\beta}\Delta i^\beta + L_{\alpha\beta}p\Delta i^\beta + \Gamma_{\beta s,\alpha}p\theta\Delta i^\beta + \Gamma_{s\gamma,\alpha}p\theta\Delta i^\gamma)$$

$$+ \left[\Gamma_{\beta s,\alpha}i^\beta p + \Gamma_{s\gamma,\alpha}i^\gamma p + \frac{\partial\Gamma_{\beta s,\alpha}}{\partial\lambda}i^\beta p\theta + \frac{\partial\Gamma_{s\gamma,\alpha}}{\partial\lambda}i^\gamma p\theta + \frac{\partial L_{\alpha\beta}}{\partial\lambda}(pi^\beta)\right]\Delta\lambda \quad . \quad (54)$$

which becomes, for the synchronous machine,

$$\Delta \boldsymbol{v}' = (\boldsymbol{R}' + \boldsymbol{L}'p + \boldsymbol{G}'p\theta)\Delta\boldsymbol{i}' + \left(\frac{\partial \boldsymbol{L}'}{\partial\lambda}\boldsymbol{i}'p + \frac{\partial \boldsymbol{G}'}{\partial\lambda}\boldsymbol{i}'p\theta\right)\Delta\lambda \quad . \quad (55)$$

The torque equation is

$$\Delta f = \Delta \boldsymbol{i}'^* . \boldsymbol{G}' . \boldsymbol{i}' + \boldsymbol{i}'^* . \boldsymbol{G}' . \Delta\boldsymbol{i}' + \frac{\partial \boldsymbol{G}'}{\partial\lambda}\boldsymbol{i}'^* . \boldsymbol{i}' . \Delta\lambda + Jp^2\Delta\lambda \quad . \quad . \quad . \quad . \quad . \quad (56)$$

In matrix form these expand to

$$\begin{array}{c} ds \\ d' \\ q' \\ s \end{array}\begin{bmatrix} \Delta v_{ds} \\ \Delta v_{d'} \\ \Delta v_{q'} \\ \Delta f \end{bmatrix} = \begin{array}{c|c|c|c|c} & ds & d' & q' & s \\ \hline ds & r_{ds} + L_{ds}p & M_d \cos\lambda p & -M_d \sin\lambda p & \begin{matrix} -M_d \sin\lambda i^d p \\ -M_d \cos\lambda i^q p \end{matrix} \\ \hline d' & \begin{matrix} M_d\cos\lambda p \\ -M_d \sin\lambda p\theta \end{matrix} & \begin{matrix} r_{dr} + L_{dr}\cos^2\lambda p \\ +L_{qr}\sin^2\lambda p \\ +(L_{qr}-L_{dr})\sin\lambda\cos\lambda p\theta \end{matrix} & \begin{matrix} (L_{qr}-L_{dr})\sin\lambda\cos\lambda p \\ +L_{dr}\sin^2\lambda p\theta \\ +L_{qr}\cos^2\lambda p\theta \end{matrix} & \begin{matrix} 2(L_{qr}-L_{dr})\cos\lambda\sin\lambda i^d p \\ +(L_{qr}-L_{dr})(\cos^2\lambda - \sin^2\lambda)i^q p \\ -i^{ds}M_d\sin\lambda p \\ -2(L_{qr}-L_{dr})\cos\lambda\sin\lambda i^q p\theta \\ +(L_{qr}-L_{dr})(\cos^2\lambda-\sin^2\lambda)i^d p\theta \\ -M_d\cos\lambda i^{ds}p\theta \end{matrix} \\ \hline q' & \begin{matrix} -M_d\sin\lambda p \\ -M_d\cos\lambda p\theta \end{matrix} & \begin{matrix} (L_{qr}-L_{dr})\sin\lambda\cos\lambda p \\ -L_{dr}\cos^2\lambda p\theta \\ -L_{qr}\sin^2\lambda p\theta \end{matrix} & \begin{matrix} r_{qr} + L_{qr}\cos^2\lambda p \\ +L_{dr}\sin^2\lambda p \\ -(L_{qr}-L_{dr})\cos\lambda\sin\lambda p\theta \end{matrix} & \begin{matrix} -2(L_{qr}-L_{dr})\cos\lambda\sin\lambda i^q p \\ +(L_{qr}-L_{dr})(\cos^2\lambda-\sin^2\lambda)i^d p \\ -i^{ds}M_d\cos\lambda p \\ -2(L_{qr}-L_{dr})\cos\lambda\sin\lambda i^d p\theta \\ -(L_{qr}-L_{dr})(\cos^2\lambda-\sin^2\lambda)i^q p\theta \\ +M_d i^{ds}\sin\lambda p\theta \end{matrix} \\ \hline s & \begin{matrix} M_d\sin\lambda i^d \\ +M_d\cos\lambda i^q \end{matrix} & \begin{matrix} i^{ds}M_d\sin\lambda \\ -(L_{qr}-L_{dr})(\cos^2\lambda-\sin^2\lambda)i^q \\ -2(L_{qr}-L_{dr})\cos\lambda\sin\lambda i^d \end{matrix} & \begin{matrix} i^{ds}M_d\cos\lambda \\ -(L_{qr}-L_{dr})(\cos^2\lambda-\sin^2\lambda)i^d \\ +2(L_{qr}-L_{dr})\sin\lambda\cos\lambda i^q \end{matrix} & \begin{matrix} Jp^2 + M_d\cos\lambda i^{ds}i^d \\ -M_d\sin\lambda i^{ds}i^q \\ -(L_{qr}-L_{dr})(\cos^2\lambda-\sin^2\lambda)i^d i^d \\ +(L_{qr}-L_{dr})(\cos^2\lambda-\sin^2\lambda)i^q i^q \\ +4(L_{qr}-L_{dr})\sin\lambda\cos\lambda i^d i^q \end{matrix} \end{array} \cdot \begin{array}{c} ds \\ d' \\ q' \\ s \end{array}\begin{bmatrix} \Delta i^{ds} \\ \Delta i^{d'} \\ \Delta i^{q'} \\ \Delta\lambda \end{bmatrix} \quad . \quad . \quad . \quad (57)$$

These equations are very much simplified when the free axes are considered to coincide with Park's reference axes in the steady state. The angle λ then becomes zero. This does not imply that the machine load angle is zero, but only that the reference frame has been rotated. The load angle λ is still inherent in the equations in the computation of the steady-state currents involved in the hunting equations.

In the free frame along the field axes the machine-impedance matrix becomes

	ds	*d*	*q*	*s*
ds	$r_{ds} + L_{ds}p$	$M_d p$	.	$-M_d i^q p$
d	$M_d p$	$r_r + L_{dr}p$	$L_{qr}p\theta$	$(L_{qr} - L_{dr})i^q p$ $+(L_{qr} - L_{dr})i^d p\theta$ $-M_d i^{ds} p\theta$
q	$-M_d p\theta$	$-L_{qr}p\theta$	$r_r + L_{qr}p$	$(L_{qr} - L_{dr})i^d p$ $-(L_{qr} - L_{dr})i^q p\theta$ $-M_d i^{ds} p$
s	$M_d i^q$	$-(L_{qr} - L_{dr})i^q$	$M_d i^{ds}$ $-(L_{qr} - L_{dr})i^d$	$Jp^2 + M_d i^{ds} i^d$ $-(L_{qr} - L_{dr})i^d i^d$ $+(L_{qr} - L_{dr})i^q i^q$

. (58)

(5) THE TENSOR EQUATIONS OF HUNTING

The time rate of change of a vector with respect to axes fixed on the vector is written di^α/dt, where the components of the vector in the given reference frame are i^α. With respect to another co-ordinate system, e.g. one that rotates with respect to the original vector position, the time rate of change becomes the absolute derivative $\delta i^\alpha/dt$, where, in general terms,

$$\frac{\delta i^\alpha}{dt} = \frac{di^\alpha}{dt} + \Gamma^\alpha_{\beta\gamma} i^\beta \frac{dx^\gamma}{dt} \quad . \quad . \quad . \quad . \quad . \quad (60)$$

The absolute differential is written

$$\delta i^\alpha = di^\alpha + \Gamma^\alpha_{\beta\gamma} i^\beta dx^\gamma \quad . \quad . \quad . \quad . \quad (61)$$

In setting up the conventional equations of hunting, small changes Δi^α, etc., were considered in each of the terms of the steady-state equations. No consideration was given as to whether the resulting equations were tensor equations. In fact, as stated in Section 2.2, in general the ordinary differential of a tensor is not a tensor. The absolute differential shown in eqn. (61) is a tensor. The tensor equation of hunting has been developed by Kron in Reference 2, by taking absolute increments δi^α, etc., in each of the terms of the tensor steady-state equation.

Taking absolute increments of the steady-state eqn. (34) gives

$$(v_\gamma + \Delta v_\gamma) = (R_{\gamma\alpha} + \delta R_{\gamma\alpha})(i^\alpha + \delta i^\alpha) + (\delta L_{\gamma\alpha})\frac{\delta i^\alpha}{dt} + L_{\gamma\alpha}\delta\left(\frac{\delta i^\alpha}{dt}\right) \quad . \quad . \quad . \quad . \quad (62)$$

and the tensor equation of small oscillation becomes

$$\delta v_\gamma = R_{\gamma\alpha}\delta i^\alpha + L_{\gamma\alpha}\delta\left(\frac{\delta i^\alpha}{dt}\right) \quad . \quad . \quad . \quad . \quad (63)$$

It is now necessary to express this equation in terms of δi^α. This change introduces a new tensor which in geometry is called the Riemannian–Christoffel curvature tensor, because it gives a measure of the intrinsic curvature of any given space in Riemannian geometry. It arises from the fact that, as shown in Appendix 11.2,

$$\delta\left(\frac{\delta i^\alpha}{dt}\right) - \frac{\delta}{dt}(\delta i^\alpha) = K^{\cdot\cdot\cdot\alpha}_{\delta\gamma\beta} i^\beta i^\delta dx^\gamma \quad . \quad . \quad . \quad (64)$$

where the term on the right-hand side is the new tensor. Eqn. (63) now becomes

$$\delta v_\gamma = R_{\gamma\alpha}\delta i^\alpha + L_{\gamma\alpha}\frac{\delta}{dt}(\delta i^\alpha) + K_{\delta\pi\alpha\gamma} i^\alpha i^\delta dx^\pi \quad . \quad . \quad (65)$$

Appendix 11.2 shows how this equation is expanded to give the machine voltage and torque equations of hunting in tensor form. These are written by Kron in Reference 19 as follows:

Voltage equation.

$$\delta v_\gamma = \left\{R_{\gamma\alpha}\delta i^\alpha + L_{\gamma\alpha}\frac{\delta}{dt}(\delta i^\alpha)\right\} + K_{st\alpha\gamma} i^\alpha (p\theta)\Delta\lambda \quad . \quad (66)$$

or

$$\Delta \boldsymbol{v}' = \left\{[\boldsymbol{R}' + \boldsymbol{L}'p + \boldsymbol{G}'p\boldsymbol{\theta}]\Delta \boldsymbol{i}' + \frac{\partial \boldsymbol{L}'}{\partial \boldsymbol{\lambda}} \boldsymbol{i}' p(\boldsymbol{\Delta\lambda}) + \boldsymbol{G}' \,.\, \boldsymbol{\rho i}' \,.\, p\boldsymbol{\theta} \,.\, \boldsymbol{\Delta\lambda}\right\} + \left[\frac{\partial \boldsymbol{G}'}{\partial \boldsymbol{\lambda}} \boldsymbol{i}' - \boldsymbol{G}' \,.\, \boldsymbol{\rho i}'\right] p\boldsymbol{\theta} \,.\, \boldsymbol{\Delta\lambda} \quad . \quad (67)$$

Torque equation (neglecting the friction tensor $R_{\gamma\alpha}\delta i^\alpha$).

$$\delta f = \left\{J\frac{\delta}{dt}(\delta i^t)\right\} + K_{\delta t\alpha s} i^\delta i^\alpha \Delta\lambda \quad . \quad . \quad . \quad (68)$$

or

$$\Delta f = \left\{J\frac{d}{dt}(\Delta\omega) - [\Delta \boldsymbol{i}'^* \,.\, \boldsymbol{G}' \,.\, \boldsymbol{i}' + \boldsymbol{i}'^* \,.\, \boldsymbol{G}' \,.\, \boldsymbol{\Delta i}' + \boldsymbol{i}'^* \,.\, \boldsymbol{G}' \,.\, \boldsymbol{\rho i}' \,.\, \boldsymbol{\Delta\lambda}]\right\} + \left[\boldsymbol{i}'^* \,.\, \frac{\partial \boldsymbol{G}'}{\partial \boldsymbol{\lambda}} \,.\, \boldsymbol{i}' - \boldsymbol{i}'^* \,.\, \boldsymbol{G}' \,.\, \boldsymbol{\rho i}'\right]\boldsymbol{\Delta\lambda} \quad . \quad (69)$$

The first set of terms in square brackets in eqn. (69) is part of the second term on the right-hand side of eqn. (65). It gives a complex quantity. The real part is in phase with the increment of angular velocity $\Delta\omega$, and is therefore in time quadrature with the displacement angle $\Delta\lambda$ and gives the damping torque. The imaginary part is in anti-phase with the displacement angle, and is counted a negative synchronizing torque. The second square-bracketed set of terms in eqn. (69), which is given by the new tensor term, is seen on inspection of its components to have only a positive real value, in phase with the displacement

angle. It gives the machine positive synchronizing torque. The matrix components of these equations are examined in the following Section. Eqns. (67) and (69) are seen to consist of the non-tensor equations (55) and (56) with a term added and subtracted. Thus the tensor equations of hunting give the conventional equations, with an important difference, namely a regrouping of terms which leads to a change in interpretation.[7, 19] The mathematical implication of the regrouping, from non-tensor to tensor form, has been explained by Hoffmann.[25]

(6) EQUIVALENT CIRCUIT FOR HUNTING EQUATIONS IN THE FREE REFERENCE FRAME

Equivalent circuits for a.c. electrical machines can be obtained by operating upon the impedance matrices in such a way as to make them symmetrical.[4, 22] The primitive machine is an equivalent 2-phase machine, and resolution of the direct and quadrature quantities into 2-phase symmetrical co-ordinates leads to the required symmetry of the impedance matrix.

In the free frame the transformation is

$$\left.\begin{aligned} i^{ds} &= i^{ds} \\ i^{d} &= (i^{f} + i^{b})/\sqrt{2} \\ i^{q} &= -j(i^{f} - i^{b})/\sqrt{2} \end{aligned}\right\} \quad . \quad . \quad . \quad . \quad . \quad (70)$$

and

$$\left.\begin{aligned} i^{ds} &= i^{ds} \\ i^{f} &= (i^{d} + ji^{q})/\sqrt{2} \\ i^{b} &= (i^{d} - ji^{q})/\sqrt{2} \end{aligned}\right\} \quad . \quad . \quad . \quad . \quad . \quad (71)$$

and

$$\left.\begin{aligned} \mathbf{Z}'' &= \boldsymbol{C}'^{*}_{(t)} \,.\, \mathbf{Z}' \,.\, \boldsymbol{C}' \\ \boldsymbol{v}'' &= \boldsymbol{C}'_{(t)} \,.\, \boldsymbol{v}' \\ \boldsymbol{i}' &= \boldsymbol{C}' \,.\, \boldsymbol{i}'' \end{aligned}\right\} \quad . \quad . \quad . \quad . \quad . \quad (72)$$

the asterisk denoting conjugate values.

$$C' = \frac{1}{\sqrt{2}}$$

	ds	*f*	*b*	*s*
ds	$\sqrt{2}$			
d		1	1	
q		$-j$	j	
s				$\sqrt{2}$

. . (73)

The impedance matrix (59) now becomes

	ds	*f*	*b*	*s*
ds	$r_{ds} + L_{ds}p$	$\frac{1}{\sqrt{2}}M_d p$	$\frac{1}{\sqrt{2}}M_d p$	$\frac{1}{\sqrt{2}}jM_d(i^f - i^b)$
f	$\frac{1}{\sqrt{2}}M_d(p - jp\theta)$	$r_r + L_S(p - jp\theta)$	$L_D(p - jp\theta)$	$b_f(p - jp\theta)$
b	$\frac{1}{\sqrt{2}}M_d(p + jp\theta)$	$L_D(p + jp\theta)$	$r_r + L_S(p + jp\theta)$	$b_b(p + jp\theta)$
s	$-\frac{1}{\sqrt{2}}jM_d(i^f - i^b)$	$-b_b$	$-b_f$	$Jp^2 + jb_f i^b - jb_b i^f$

. (74)

where $L_S = \dfrac{L_{dr} + L_{qr}}{2}$ and $L_D = \dfrac{L_{dr} - L_{qr}}{2}$

In this matrix,

$$\left.\begin{aligned} b_f &= (b_d + jb_q)/\sqrt{2} \\ b_b &= (b_d - jb_q)/\sqrt{2} \end{aligned}\right\} \quad . \quad . \quad . \quad . \quad (75)$$

where b_d and b_q are defined from matrix (58):

$$\left.\begin{aligned} b_d &= -B_d - L_{dr}i^q \\ b_q &= -B_q - L_{qr}i^d \end{aligned}\right\} \quad . \quad . \quad . \quad . \quad (76)$$

$$\left.\begin{aligned} B_d &= -L_{qr}i^q \\ B_q &= L_{dr}i^d + M_d i^{ds} \end{aligned}\right\} \quad . \quad . \quad . \quad . \quad (77)$$

$$\left.\begin{aligned} B_f = .(B_d + jB_q)/\sqrt{2} &= j\left(\frac{1}{\sqrt{2}}M_d i^{ds} + i^f L_S + i^b L_D\right) \\ B_b = (B_d - jB_q)/\sqrt{2} &= -j\left(\frac{1}{\sqrt{2}}M_d i^{ds} + i^f L_D + i^b L_S\right) \end{aligned}\right\} \quad . \quad (78)$$

and

$$b_f = -(B_f - i^f jL_S + i^b jL_D)$$

$$= -j\left(\frac{1}{\sqrt{2}}M_d i^{ds} + 2i^b L_D\right) \quad . \quad . \quad . \quad (79)$$

$$b_b = -(B_b + i^b jL_S - i^f jL_D)$$

$$= j\left(\frac{1}{\sqrt{2}}M_d i^{ds} + 2i^f L_D\right) \quad . \quad . \quad . \quad . \quad (80)$$

The additional term in eqn. (67) which is added and subtracted is

$$\boldsymbol{G}' \,.\, \rho \boldsymbol{i}' \,.\, p\theta \,.\, \Delta\boldsymbol{\lambda} \quad . \quad . \quad . \quad . \quad . \quad (81)$$

This set of terms arises only in the last column of the voltage part of matrix (74). Thus the last column of this part of the matrix can be written

$$\frac{\partial \boldsymbol{L}''}{\partial \boldsymbol{\lambda}} \boldsymbol{i}'' p(\Delta\boldsymbol{\lambda}) + \left\{[\boldsymbol{G}'' \,.\, \rho \boldsymbol{i}''] + \left[\frac{\partial \boldsymbol{G}''}{\partial \boldsymbol{\lambda}} \boldsymbol{i}'' - \boldsymbol{G}'' \,.\, \rho \boldsymbol{i}''\right]\right\} p\theta\Delta\boldsymbol{\lambda} \,. \quad (82)$$

where $\boldsymbol{G}''$ is now the 'symmetrical component' form of the matrix $\boldsymbol{G}$. The terms of expression (82) in square brackets expand in matrix form to

$$\frac{\partial \boldsymbol{G}''}{\partial \boldsymbol{\lambda}} =$$

	ds	*f*	*b*
ds			
f	$-\frac{M_d}{\sqrt{2}}$		$-2L_D$
b	$-\frac{M_d}{\sqrt{2}}$	$-2L_D$	

. (83)

$$G''\rho = \begin{array}{c|ccc} & ds & f & b \\ ds & & & \\ f & & L_S & -L_D \\ b & & -L_D & L_S \end{array} \quad . \quad (84)$$

$$K = \left(\frac{\partial G''}{\partial \lambda} - G''\rho\right) = \begin{array}{c|ccc} & ds & f & b \\ ds & & & \\ f & -\frac{M_d}{\sqrt{2}} & -L_S & -L_D \\ b & -\frac{M_d}{\sqrt{2}} & -L_D & -L_S \end{array} \quad . \quad (85)$$

Matrix (85) given by the tensor $\boldsymbol{K}$ is seen to comprise the quantities B_f and B_b, and expression (82) therefore divides the quantities b_f and b_b into two significant parts:

$$b_f = -B_f + (i^f jL_S - i^b jL_D) \quad . \quad . \quad . \quad . \quad (86)$$

$$b_b = -B_b - (i^b jL_S - i^f jL_D) \quad . \quad . \quad . \quad . \quad (87)$$

The equivalent circuit can now be drawn for steady hunting conditions at the hunting frequency $h\omega$. This is shown in Fig. 3.

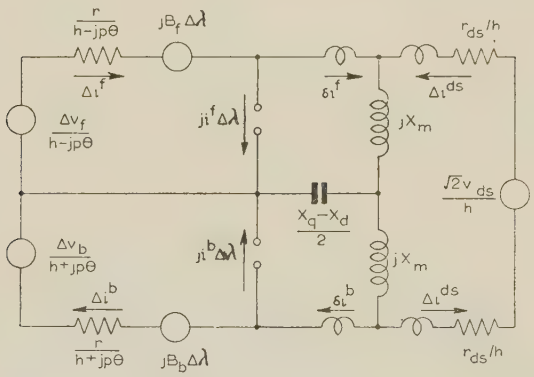

Fig. 3.—Equivalent circuit for salient-pole synchronous-machine hunting.

The addition of injected voltages and currents is indicated *a priori* by the grouping of terms shown in eqns. (86) and (87).

When the circuit is drawn in this manner the effects of increments of current Δi and the absolute changes δi become apparent.[19] In the symmetrical component form,

$$\delta i^\alpha = \Delta i^\alpha + \Gamma^\alpha_{\beta\gamma} i^\beta i^\gamma \quad . \quad . \quad . \quad . \quad . \quad (88)$$

becomes

$$\delta i^f = \Delta i^f - j i^f \Delta\lambda \quad . \quad . \quad . \quad . \quad . \quad (89)$$

and

$$\delta i^b = \Delta i^b + j i^b \Delta\lambda \quad . \quad . \quad . \quad . \quad . \quad (90)$$

(These are the 'absolute changes' used by Ku[22].)

The significance of active and reactive power in the equivalent circuit is discussed in the following Section.

(7) THE TORQUE EQUATION AND THE EQUIVALENT CIRCUIT

The machine torque equation can be written down from matrix (74), using the grouping of terms indicated by the tensor equation of torque [eqn. (69)],

$$\Delta f = \left\{\left[-j\frac{M_d}{\sqrt{2}}(i^f - i^b)\Delta i^{ds*} - b_f \Delta i^{f*} - b_b \Delta i^{b*}\right] + [i''^* \,.\, G''\rho \,.\, i''\Delta\lambda]\right\} + \left[i''^* \,.\, \frac{\partial G''}{\partial \lambda} \,.\, i'' - i''^* \,.\, G''\rho \,.\, i''\right]\Delta\lambda \quad . \quad (91)$$

Examination of the equivalent circuit meshes shows that the active and reactive power measured at the points indicated, namely ΔiV, give real and imaginary parts of the first set of terms in square brackets in eqn. (91), with a time-quadrature difference. Under steady hunting conditions the total torque expression can be written, as in Park's reference frame, by

$$\Delta f = (T_{synch} + jT_{damp})\Delta\lambda \quad . \quad . \quad . \quad . \quad (92)$$

and the real component of power as measured from the equivalent circuit of Fig. 3, namely the resistance loss in each mesh, corresponds to the damping torque given by eqn. (92). The imaginary part gives the corresponding component of (negative) synchronizing torque.

The additional components of negative and positive synchronizing torque are given by the remaining two sets of terms in square brackets in eqn. (91). Components of these terms are included in the equivalent circuit, but they cannot be read off the circuit directly since the injected voltages and currents are already associated with the displacement angle $\Delta\lambda$. Fig. 4 shows

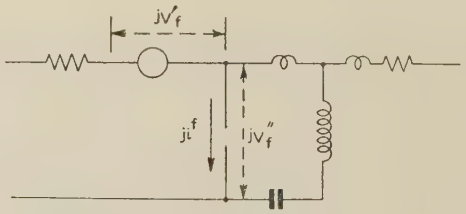

Fig. 4.—Contribution of forward armature mesh to synchronizing torque.
$if V_f'$ gives positive (impressed) synchronizing torque.
$if V_f''$ gives negative synchronizing torque.

how the circuit can be interpreted to indicate the contribution of each mesh to synchronizing torque.

Positive synchronizing torque given by the tensor $\boldsymbol{K}$ expands to

$$(-B_f i^f + B_b i^b)\Delta\lambda \quad . \quad . \quad . \quad . \quad . \quad (93)$$

This can be compared with the machine power output equation[22]

$$-B_f i^b + B_b i^f \quad . \quad . \quad . \quad . \quad . \quad (94)$$

and it is seen that the positive synchronizing torque at any load angle is, in fact, given by the reactive component of the machine power output. The simple equation for synchronizing power of a round-rotor machine given in textbooks[26] is usually written

$$\left(\frac{Ev}{x}\cos\lambda\right)\Delta\lambda \quad . \quad . \quad . \quad . \quad . \quad (95)$$

and the expression in brackets is again the reactive component of the steady-state vector power output.

(8) CONCLUSION

The equations of performance of any conventional electrical machine can be derived by an automatic tensor transformation of those of the primitive machine. A similar type of transformation can be used to express the equations of a given machine in any one of several sets of reference axes. The transformation of Park's equations for the synchronous machine to those in Kron's freely rotating axes leads to simple overall equations for an interconnected system.

The complex interaction of currents and fluxes in a machine during hunting can be more easily followed in different reference systems when the corresponding transformation of equations is carried out using matrices and the routine methods of tensor analysis. The tensor form of the equations of hunting of a machine in the free frame has two advantages:

(*a*) Synchronizing torque terms are inherently grouped together in terms of the angle of oscillation $\Delta\lambda$. Positive and negative damping terms are inherently grouped in terms of the increment of angular velocity $\Delta\omega$ and give this component of torque as the real part of a complex expression. Damping torque is thus directly associated with the resistances in the electrical system.

(*b*) The terms of the tensor equations in symmetrical component form give, directly, the meshes in an equivalent circuit. This form of equivalent circuit can be interconnected with corresponding circuits for an external network and additional machines. The resistance power loss in each mesh gives the damping torque contributed by that part of the system.

The significance of tensor groups of terms in the steady-state equations of electrical machines has already been noted.[5] The tensor form of the hunting equations gives a physical picture of the hunting phenomena as represented by the equivalent circuit. It would appear that this method of formulating dynamical equations could be used to advantage in the analogue study of complex devices in which interchange of different forms of energy takes place, for example, aircraft, missiles and nuclear reactors.

(9) ACKNOWLEDGMENTS

The author wishes to express his appreciation of the support and encouragement of Prof. J. M. Meek of the University of Liverpool. He wishes to thank Mr. Gabriel Kron for his interest and valuable comments in correspondence during the preparation of the paper. The author is also indebted to his colleagues, Messrs. A. S. Aldred and C. V. Jones, for many stimulating discussions.

(10) REFERENCES

(1) Brown, G. S., Kusko, A., and White, D. C.: 'A New Educational Programme in Energy Conversion', *Electrical Engineering*, 1956, **75**, p. 180.

(2) Kron, G.: 'Non-Riemannian Dynamics of Rotating Electrical Machinery', *Journal of Mathematics and Physics*, 1934, **13**, p. 103.

(3) Kron, G.: 'The Application of Tensor to the Analysis of Rotating Electrical Machinery', *General Electrical Review*, 1935–38. Published in book form 1938 and 1942.

(4) Kron, G.: 'Equivalent Circuits of Electric Machinery' (John Wiley, 1951).

(5) Lynn, J. W.: 'The Tensor Equations of Electrical Machines', *Proceedings I.E.E.*, Monograph No. 117 S, January, 1955 (**102** C, p. 149).

(6) Heffron, W. G., Rosenberry, G. M., and Rothe, F. S.: 'Generalized Hunting Equations of Power Systems', *Transactions of the American I.E.E.*, 1952, **71**, Part III, p. 1095.

(7) Kron, G.: 'A New Theory of Hunting', *ibid.*, 1952, **71**, Part III, p. 859. (See also contribution to discussion by Heffron.)

(8) Messerle, H. K., and Bruck, R. W.: 'Steady-State Stability of Synchronous Generators as Affected by Regulators and Governors', *Proceedings I.E.E.*, Monograph No. 134 S, June, 1955 (**103** C, p. 24).

(9) Wennerberg, J.: 'Hunting Constants of Synchronous Machines for Oscillations of Small Amplitude', *Asea Journal*, 1929, **4**, p. 61.

(10) Prescott, J. C., and Richardson, J. E.: 'The Inherent Instability of Synchronous Machinery', *Journal I.E.E.*, 1934, **75**, p. 497.

(11) Doherty, R. E., and Nickle, C. A.: 'Synchronous Machines', *Transactions of the American I.E.E.*, 1926, **45**, p. 912.

(12) Park, R. H.: 'Two-Reaction Theory of Synchronous Machines', *ibid.*, 1929, **48**, p. 716, and 1933, **52**, p. 352.

(13) Liwschitz, M. M.: 'Positive and Negative Damping in Synchronous Machines', *ibid.*, 1941, **60**, p. 210.

(14) Concordia, C.: 'Synchronous Machine Damping and Synchronizing Torques', *ibid.*, 1951, **70**, Part I, p. 731.

(15) Kron, G.: 'Equivalent Circuits for the Hunting of Electrical Machinery', *ibid.*, 1942, **61**, p. 290.

(16) Concordia, C., and Kron, G.: 'Damping and Synchronising Torques of Power Selsyns', *ibid.*, 1945, **64**, p. 367.

(17) Kron, G., Concordia, C., and Crary, S. B.: 'The Doubly Fed Machine', *ibid.*, 1942, **61**, p. 286.

(18) Kron, G.: 'Equivalent Circuits for Oscillating Systems and the Riemann–Christoffel Curvature Tensor', *ibid.*, 1943, **62**, p. 25.

(19) Kron, G.: 'A Physical Interpretation of the Riemann–Christoffel Curvature Tensor', *The Tensor* (New Series), 1955, **4**, p. 150.

(20) Kondo, K.: 'On the Dynamics of the Aeroplane and Non-Riemannian Geometry', Parts I and II, *Journal of the Japan Society of Aeronautical Engineering*, 1954, pp. 161–166 and pp. 193–196.

(21) Concordia, C.: 'Synchronous Machines' (John Wiley, 1951).

(22) Ku, Y. H.: 'Rotating-Field Theory and General Analysis of Synchronous and Induction Machines', *Proceedings I.E.E.*, Monograph No. 54 U, June, 1952 (**99**, Part IV, p. 410).

(23) Gibbs, W. J.: 'Tensors in Electrical Machine Theory' (Chapman and Hall, 1952).

(24) Kron, G.: 'Classification of the Reference Frames of a Synchronous Machine', *Transactions of the American I.E.E.*, 1950, **69**, Part II, p. 720.

(25) Hoffmann, B.: 'Tensors and Equivalent Circuits', *Journal of Mathematics and Physics*, 1946, **25**, p. 21.

(26) Say, M. G.: 'Performance and Design of Alternating Current Machines', 2nd Edition (Pitman, 1948).

(27) Schouten, J. A.: 'Ricci Calculus', 2nd Edition (Springer, Berlin, 1954).

(28) Synge, J. L.: 'On the Geometry of Dynamics', *Philosophical Transactions of the Royal Society*, A, 1927, **266**, p. 31.

(11) APPENDIX

(11.1) Small Oscillation Equation

The free-frame steady-state equation is

$$v_\alpha = R_{\alpha\beta} i^\beta + L_{\alpha\beta} p i^\beta + \Gamma_{\beta\gamma,\alpha} i^\beta i^\gamma \quad . \quad . \quad . \quad (96)$$

This is divided into voltage and torque equations.

Voltage equation.

The index α is electrical. The indices β and γ are electrical, indicating currents i^β or i^γ, or mechanical values s, indicating angular velocity $i^s \equiv p\theta$.

$$v_\alpha = R_{\alpha\beta}i^\beta + L_{\alpha\beta}pi^\beta + \Gamma_{s\gamma,\alpha}i^\gamma p\theta + \Gamma_{\beta s,\alpha}i^\beta p\theta \quad . \quad (97)$$

Torque equation.

The index α takes the mechanical part of the range. The indices β and γ have electrical values.

$$v_s = R_{ss}i^s + L_{ss}pi^s + \Gamma_{\beta\gamma,s}i^\beta i^\gamma \quad . \quad . \quad . \quad (98)$$

or
$$v_s = R_{ss}p\theta + Jp^2\theta + \Gamma_{\beta\gamma,s}i^\beta i^\gamma \quad . \quad . \quad . \quad (99)$$

The small-oscillation equation is obtained by taking small increments of values in eqn. (96). This gives

$$\Delta v_\alpha + \frac{\partial v_\alpha}{\partial x^\pi}\Delta x^\pi = R_{\alpha\beta}\Delta i^\beta + L_{\alpha\beta}p(\Delta i^\beta) + \Delta L_{\alpha\beta}pi^\beta + \Gamma_{\beta\gamma,\alpha}i^\beta\Delta i^\gamma + \Gamma_{\beta\gamma,\alpha}\Delta i^\beta i^\gamma + \Delta\Gamma_{\beta\gamma,\alpha}i^\beta i^\gamma \quad . \quad (100)$$

The corresponding voltage and torque equations are as follows:

Voltage equation.

$$\Delta v_\alpha + \frac{\partial v_\alpha}{\partial x^t}\Delta x^t = R_{\alpha\beta}\Delta i^\beta + L_{\alpha\beta}p(\Delta i^\beta) + \Gamma_{t\gamma,\alpha}\Delta(p\theta)i^\gamma + \Gamma_{\beta s,\alpha}\Delta i^\beta p\theta + \Gamma_{s\gamma,\alpha}\Delta i^\gamma p\theta + \Gamma_{\beta t,\alpha}i^\beta\Delta(p\theta) + \frac{\partial L_\beta}{\partial x^t}(pi^\beta)\Delta x^t + \frac{\partial\Gamma_{s\gamma,\alpha}}{\partial x^t}(p\theta)i^\gamma\Delta x^t + \frac{\partial\Gamma_{\beta s,\alpha}}{\partial x^t}i^\beta(p\theta)\Delta x^t \quad . \quad (101)$$

The index t denotes excursions of the rotor over the increment of speed,

$$\Delta(p\theta) = p(\Delta\theta) = p(\Delta\lambda)$$

The terms of the voltage equation are expanded in a manner indicated by the following example:[5]

$$\Gamma_{t\gamma,\alpha}i^\gamma\Delta i^t = \{[t\gamma,\alpha] - S_{\alpha\gamma t} - S_{\alpha t\gamma} + S_{t\gamma\alpha} + \Omega_{\alpha\gamma,t} + \Omega_{\alpha t,\gamma} - \Omega_{t\gamma,\alpha}\}i^\gamma\Delta i^t = \{[t\gamma,\alpha] - S_{\alpha t\gamma} + \Omega_{\alpha t,\gamma}\}i^\gamma\Delta x^t \quad . \quad (102)$$

Other terms are zero as shown in Sections 4 and 5 of Reference 5.

Now
$$-2S_{\alpha t,\gamma} = G' = C_{(t)} \,.\, G \,.\, C \quad . \quad . \quad . \quad (103)$$

where G' is the free-frame torque matrix and G is the torque matrix in Park's equations.

$$2\Omega_{\alpha t,\gamma} = \frac{\partial C^{-1}_{(t)}}{\partial\lambda} \,.\, C_{(t)} \,.\, L' = \rho L' = 2S_{\alpha t\gamma} \,. \quad . \quad (104)$$

Also
$$[t\gamma,\alpha] \equiv \frac{1}{2}\left(\frac{\partial L_{\alpha\gamma}}{\partial x^t} + \frac{\partial L_{\alpha t}}{\partial x^\gamma} - \frac{\partial L_{t\gamma}}{\partial x^\alpha}\right) = \frac{1}{2}\frac{\partial L_{\alpha\gamma}}{\partial x^t} \quad . \quad (105)$$

The index s denotes the mechanical variable θ, and

$$\frac{\partial\Gamma_{\beta s,\alpha}}{\partial x^\pi}i^s i^\gamma\Delta x^\pi = \frac{\partial}{\partial x^\pi}\left(\frac{1}{2}\frac{\partial L_{\alpha\beta}}{\partial x^s} - S_{\alpha s\beta} + \Omega_{\alpha s,\beta}\right)i^s i^\beta\Delta x^\pi \quad . \quad (106)$$

$$\frac{\partial L_{\alpha\beta}}{\partial x^s}i^s \equiv \frac{\partial L_{\alpha\beta}}{\partial\theta}p\theta = 0 \quad . \quad . \quad . \quad . \quad (107)$$

$$\Omega_{\alpha s,\beta}i^s = \frac{\partial C^{-1}_{(t)}}{\partial\theta} \,.\, C_{(t)} \,.\, L' \,.\, p\theta = 0 \quad . \quad . \quad (108)$$

$$S_{\alpha s\beta}i^s = \tfrac{1}{2}G'p\theta \quad . \quad . \quad . \quad . \quad . \quad (109)$$

Thus
$$\frac{\partial\Gamma_{s\gamma,\alpha}}{\partial x^t}i^s i^\gamma\Delta x^t + \frac{\partial\Gamma_{\beta s,\alpha}}{\partial x^t}i^s i^\beta\Delta x^t = \frac{\partial G'}{\partial\lambda}i' \,.\, p\theta \,.\, \Delta\lambda \quad . \quad (110)$$

Therefore eqn. (101) becomes

$$\Delta v' + \frac{\partial v'}{\partial\lambda}\Delta\lambda = [R' + L'p + G'p\theta]\Delta i' + \left[\frac{\partial L'}{\partial\lambda}i'p + \frac{\partial G'}{\partial\lambda}i'p\theta\right]\Delta\lambda \quad . \quad (111)$$

Torque equation.

$$\Delta F = Jp^2(\Delta\lambda) + \Gamma_{\beta\gamma,s}i^\beta\Delta i^\gamma + \Gamma_{\beta\gamma,s}\Delta i^\beta i^\gamma + \frac{\partial\Gamma_{\beta\gamma,s}}{\partial\lambda}i^\beta i^\gamma\Delta\lambda \quad . \quad . \quad . \quad . \quad (112)$$

$$\Gamma_{\beta\gamma,s}i^\beta\Delta i^\gamma = \{[\beta\gamma,s] - S_{s\gamma\beta} - S_{s\beta\gamma} + S_{\beta\gamma s} + \Omega_{s\gamma,\beta} + \Omega_{s\beta,\gamma} - \Omega_{\beta\gamma,s}\}i^\beta\Delta i^\gamma \quad . \quad (113)$$

$$[\beta\gamma,s]i^\beta\Delta i^\gamma = \frac{1}{2}\frac{\partial L'}{\partial\theta}i'\Delta i' = 0 \quad . \quad . \quad . \quad (114)$$

$$(\Omega_{s\gamma,\beta} + \Omega_{s\beta,\gamma} - \Omega_{\beta\gamma,s})i^\beta\Delta i^\gamma = \frac{\partial C^{-1}_{(t)}}{\partial\theta} \,.\, C_{(t)} \,.\, L' \,.\, i' \,.\, \Delta i' = 0 \quad . \quad . \quad . \quad . \quad (115)$$

$$(-S_{s\gamma\beta} - S_{s\beta\gamma} + S_{\beta\gamma s})i^\beta\Delta i^\gamma \text{ becomes}^5 \quad . \quad . \quad (116)$$

$$(-S_{s\gamma\beta} - S_{s\beta\gamma})i^\beta\Delta i^\gamma = \tfrac{1}{2}(i' \,.\, G' \,.\, \Delta i' + \Delta i' \,.\, G' \,.\, i') \quad . \quad (117)$$

Thus

$$\Gamma_{\beta\gamma,s}i^\beta\Delta i^\gamma + \Gamma_{\beta\gamma,s}\Delta i^\beta i^\gamma = \Delta i' \,.\, G' \,.\, i' + i' \,.\, G' \,.\, \Delta i' \,. \quad (118)$$

$$\frac{\partial\Gamma_{\beta\gamma,s}}{\partial x^t}i^\beta i^\gamma\Delta x^t = i' \,.\, \frac{\partial G'}{\partial\lambda} \,.\, i' \,.\, \Delta\lambda \quad . \quad . \quad . \quad (119)$$

Therefore eqn. (98) becomes $\left(\text{neglecting the friction term } R\frac{d\theta}{dt}\right)$

$$\Delta f = \Delta i'^* \,.\, G' \,.\, i' + i'^* \,.\, G' \,.\, \Delta i' + i'^* \,.\, \frac{\partial G'}{\partial\lambda} \,.\, i' \,.\, \Delta\lambda + Jp^2(\Delta\lambda) \quad . \quad . \quad . \quad . \quad (120)$$

(11.2) The Tensor $K_{\delta\gamma\beta\alpha}$

The absolute differential of a contravariant vector is

$$\delta\phi^i = d\phi^i + \Gamma^h_{kj}\phi^k dx^j \quad . \quad . \quad . \quad . \quad (121)$$

Therefore
$$\frac{\delta}{dt}(\delta i^h) = \frac{\delta}{dt}(di^h + \Gamma^h_{kj}i^k dx^j) \quad . \quad . \quad (122)$$

$$= \frac{d}{dt}(di^h + \Gamma^h_{kj}i^k dx^j) + \Gamma^h_{mn}(di^m + \Gamma^m_{pq}i^p dx^q)\frac{dx^n}{dt}$$

$$= \frac{d}{dt}(di^h) + \frac{d\Gamma^h_{kj}}{dt}i^k dx^j + \Gamma^h_{kj}\frac{di^k}{dt}dx^j + \Gamma^h_{kj}i^k\frac{d}{dt}(dx^j) + \Gamma^h_{mn}di^m i^n + \Gamma^h_{mn}\Gamma^m_{pq}i^p i^n dx^q \quad . \quad (123)$$

Similarly
$$\delta\left(\frac{\delta i^\beta}{dt}\right) = \delta\left(\frac{di^\beta}{dt} + \Gamma^\beta_{\gamma\delta}i^\gamma\frac{dx^\delta}{dt}\right) \quad . \quad . \quad (124)$$

$$= d\left(\frac{di^\beta}{dt}\right) + d\Gamma^\beta_{\gamma\delta}i^\gamma i^\delta + \Gamma^\beta_{\gamma\delta}di^\gamma i^\delta + \Gamma^\beta_{\gamma\delta}i^\gamma dx^\delta + \Gamma^\beta_{\pi\sigma}\frac{di^\pi}{dt}dx^\sigma + \Gamma^\beta_{\pi\sigma}\Gamma^\pi_{\alpha\beta}i^\alpha i^\beta dx^\sigma \quad . \quad (125)$$

Therefore $\delta\left(\frac{\delta i^\beta}{dt}\right) - \frac{\delta}{dt}(\delta i^\beta)$

$$= -\frac{\partial \Gamma^\beta_{\gamma\delta}}{\partial x^\alpha} i^\gamma i^\delta dx^\alpha - \frac{\partial \Gamma^\beta_{\pi\sigma}}{dx^\lambda} i^\pi i^\lambda dx^\sigma + \Gamma^\beta_{\sigma\pi}\Gamma^\sigma_{\alpha\beta} i^\alpha i^\beta dx^\pi$$

$$- \Gamma^\beta_{\lambda\epsilon}\Gamma^\lambda_{\eta\theta} i^\eta i^\epsilon dx^\theta + \Gamma^\beta_{\gamma\delta}\left[d\left(\frac{dx^\delta}{dt}\right) - \frac{d}{dt}(dx^\delta)\right] i^\gamma \quad . \quad (126)$$

The bracketed difference in expression (126) is not zero because the electrical variables are non-holonomic, i.e. they are related only through non-integrable differentials,[5] and

$$\frac{\partial^2 x^\delta}{\partial x^\gamma \partial x^\beta} \neq \frac{\partial^2 x^\delta}{\partial x^\beta \partial x^\gamma} \quad . \quad . \quad . \quad . \quad . \quad . \quad (127)$$

This is shown in Reference 27, as follows:

$$\frac{\partial^2 P}{\partial x^i \partial x^j} - \frac{\partial^2 P}{\partial x^j \partial x^i} = C^\mu_j \frac{\partial C^\lambda_i}{\partial x^\mu}\frac{\partial P}{\partial x^\lambda} - C^\mu_i \frac{\partial C^\lambda_j}{\partial x^\mu}\frac{\partial P}{\partial x^\lambda}$$

$$= \frac{\partial P}{\partial x^h}\left(C^\mu_j C^h_\lambda \frac{\partial C^\lambda_i}{\partial x^\mu} - C^\mu_i C^h_\lambda \frac{\partial C^\lambda_j}{\partial x^\mu}\right)$$

$$= \frac{\partial P}{\partial x^h}\left[C^{j'}_j C^{i'}_i \left(\frac{\partial C^h_{i'}}{\partial x^{j'}} - \frac{\partial C^h_{j'}}{\partial x^{i'}}\right)\right]$$

$$= \frac{\partial P}{\partial x^h} \cdot 2\Omega^h_{ij} = -\frac{\partial P}{\partial x^h} \cdot 2\Omega^h_{ji} \quad . \quad . \quad . \quad . \quad . \quad (128)$$

where $$\Omega^h_{ij} = \tfrac{1}{2} C^{j'}_j C^{i'}_i \left(\frac{\partial C^h_{i'}}{\partial x^{j'}} - \frac{\partial C^h_{j'}}{\partial x^{i'}}\right) \quad . \quad . \quad . \quad (129)$$

and in expression (126)

$$\Gamma^\beta_{\gamma\delta}\left[d\left(\frac{dx^\beta}{dt}\right) - \frac{d}{dt}(dx^\delta)\right] i^\gamma = -\Gamma^\beta_{\gamma\delta} i^\gamma \cdot 2\Omega^\delta_{\pi\sigma} i^\pi dx^\sigma \quad . \quad (130)$$

With appropriate rearrangement of indices

$$K^\alpha_{\delta\gamma\beta} i^\delta i^\beta dx^\gamma = \delta\left(\frac{\delta i^\alpha}{dt}\right) - \frac{\delta}{dt}(\delta i^\alpha) \quad . \quad . \quad (131)$$

where

$$K^\alpha_{\delta\gamma\beta} = \frac{\partial \Gamma^\alpha_{\beta\delta}}{\partial x^\gamma} - \frac{\partial \Gamma^\alpha_{\beta\gamma}}{\partial x^\delta} + \Gamma^\alpha_{\lambda\gamma}\Gamma^\lambda_{\beta\delta} - \Gamma^\alpha_{\lambda\delta}\Gamma^\lambda_{\beta\gamma} + 2\Gamma^\alpha_{\beta\lambda}\Omega^\lambda_{\delta\gamma} \quad . \quad (132)$$

The tensor equation of small oscillations now becomes, as given by Kron,[18]

$$\Delta v_\alpha + \delta v_\alpha = \delta(R_{\alpha\beta} i^\beta) + L_{\alpha\beta}\frac{\delta}{\delta t}(\delta i^\beta) + K_{\delta\gamma\beta\alpha} i^\beta i^\delta dx^\gamma \quad . \quad (133)$$

which expands, as shown in References 2 and 18, giving

$$\Delta v_\alpha + \frac{\partial v_\alpha}{\partial x^\beta}\Delta x^\beta = -\Gamma_{\gamma\delta,\alpha}\frac{di^\gamma}{dt}\Delta x^\delta + R_{\alpha\beta}\Delta i^\beta + \Gamma_{\gamma\delta,\alpha}\frac{di^\gamma}{dt}\Delta x^\delta$$

$$+ L_{\alpha\beta}\frac{d}{dt}(\Delta i^\beta) - \frac{\partial L_{\alpha\beta}}{\partial x^\gamma}\frac{di^\beta}{dt}\Delta x^\gamma + \Gamma_{\beta\gamma,\alpha}\Delta i^\beta i^\gamma + \Gamma_{\beta\gamma,\alpha} i^\beta \Delta i^\gamma$$

$$+ \left(\frac{\partial \Gamma_{\beta\gamma,\alpha}}{\partial x^\delta} + \Gamma_{\lambda\delta,\alpha}\Gamma^\lambda_{\beta\gamma} - \Gamma_{\lambda\gamma,\alpha}\Gamma^\lambda_{\beta\delta} - 2\Gamma_{\beta\lambda,\alpha}\Omega^\lambda_{\delta\gamma}\right) i^\beta i^\delta \Delta x^\gamma$$

$$+ \left(\frac{\partial \Gamma_{\beta\delta,\alpha}}{\partial x^\gamma} - \frac{\partial \Gamma_{\beta\gamma,\alpha}}{\partial x^\delta} + \Gamma_{\lambda\gamma,\alpha}\Gamma^\lambda_{\beta\delta} - \Gamma_{\lambda\delta,\alpha}\Gamma^\lambda_{\beta\gamma} + 2\Gamma_{\beta\lambda,\alpha}\Omega^\lambda_{\delta\gamma}\right) i^\beta i^\delta \Delta x^\gamma$$

. . . . (134)

This is seen to be the same as the conventional equation with the following terms added and subtracted:

$$\Gamma_{\beta\gamma,\alpha}\frac{di^\beta}{dt}\Delta x^\gamma + \left(\Gamma_{\lambda\delta,\alpha}\Gamma^\lambda_{\beta\gamma} + 2\Gamma_{\beta\lambda,\alpha}\Omega^\lambda_{\delta\gamma} + \frac{\partial \Gamma_{\beta\gamma,\alpha}}{\partial x^\delta}\right) \quad . \quad (135)$$

In the synchronous-machine equations in the free frame the steady-state current is constant and

$$\Gamma_{\beta\gamma,\alpha}\frac{di^\beta}{dt}\Delta x^\gamma = 0 \quad . \quad . \quad . \quad . \quad . \quad (136)$$

The remaining terms expand in the voltage equation to

$$\left(\Gamma_{\lambda s,\alpha}\Gamma^\lambda_{\beta t} + 2\Gamma_{\beta\lambda,\alpha}\Omega^\lambda_{st} + \frac{\partial \Gamma_{\beta\gamma,\alpha}}{\partial x^s}\right) i^\beta i^s \Delta x^\gamma$$

$$+ \left(\Gamma_{\lambda\delta,\alpha}\Gamma^\lambda_{st} + 2\Gamma_{s\lambda,\alpha}\Omega^\lambda_{\delta t} + \frac{\partial \Gamma_{s\gamma,\alpha}}{\partial x^\delta}\right) i^s i^\delta \Delta x^\gamma \quad . \quad (137)$$

The index γ takes the value t indicating the mechanical variable which undergoes incremental changes, namely the load angle λ. The index s as usual denotes the holonomic variable, the angular position θ, of the rotor. Only the first and fifth terms have non-zero values. The additional terms in the voltage equation are therefore

$$(\Gamma_{\lambda s,\alpha}\Gamma^\lambda_{\delta t} + 2\Gamma_{s\lambda,\alpha}\Omega^\lambda_{\delta t}) i^\delta i^s \Delta\lambda \quad . \quad . \quad . \quad (138)$$

$$= (\Gamma_{\lambda s,\alpha} + \Gamma_{s\lambda,\alpha})\rho^\lambda_\delta i^\delta p\theta\Delta\lambda \quad . \quad . \quad . \quad (139)$$

$$= \boldsymbol{G' \cdot \rho i' p\theta \Delta\lambda} \quad . \quad . \quad . \quad . \quad . \quad . \quad . \quad (140)$$

The corresponding term in the torque equation is

$$(\Gamma_{\lambda\delta,s} + \Gamma_{\beta\lambda,s})\rho^\lambda_\delta i^\beta i^\gamma \Delta\lambda \quad . \quad . \quad . \quad . \quad (141)$$

$$= \boldsymbol{-i' \cdot G' \cdot \rho i' \cdot \Delta\lambda} \quad . \quad . \quad . \quad . \quad (142)$$

The small oscillation equations are therefore as given by Kron in Reference 19, namely

Voltage equation.

$$\boldsymbol{\Delta v' = [R' + L'p + G'p\theta]\Delta i' + \frac{\partial L'}{\partial \lambda} i' p(\Delta\lambda) + G' \cdot \rho i' \cdot p\theta \cdot \Delta\lambda}$$

$$\boldsymbol{+ \left[\frac{\partial G'}{\partial \lambda} i' - G' \cdot \rho i'\right] p\theta \cdot \Delta\lambda} \quad . \quad (67)$$

Torque equation.

$$\boldsymbol{\Delta f = J\frac{d}{dt}(\Delta\omega) - [\Delta i'^* \cdot G' \cdot i' + i'^* \cdot G' \cdot \Delta i' + i'^* \cdot G' \cdot \rho i' \Delta\lambda]}$$

$$\boldsymbol{+ \left[i'^* \cdot \frac{\partial G'}{\partial \lambda} \cdot i' - i'^* \cdot G' \cdot \rho i'\right] \Delta\lambda} \quad . \quad (69)$$

where $\Delta\lambda$ is the displacement angle and $\Delta\omega = p(\Delta\lambda)$ is the angular velocity of displacement.

621.372.832.43

The Institution of Electrical Engineers
Monograph No. 296 R
Mar. 1958
©

INTRINSIC DIRECTIONAL COUPLER USING ELLIPTICAL COUPLING APERTURES

By J. FIGANIER, B.Sc., and E. A. ASH, Ph.D., Graduate.

(*The paper was first received 9th October, and in revised form 28th November*, 1957. *It was published as an* INSTITUTION MONOGRAPH *in March*, 1958.)

SUMMARY

The use of elliptical coupling apertures between two rectangular parallel waveguides for the realization of intrinsic directional couplers is investigated. It is found that both codirectional and contradirectional characteristics can be obtained. The possibilities of using the intrinsic directional property to improve the characteristics of multi-element couplers or to construct filter couplers are examined.

LIST OF PRINCIPAL SYMBOLS

$x, y, z; a, b, d, p, q$ = Co-ordinates and dimensions relating to waveguides and coupling apertures, explained in Fig. 1.
ϵ = Eccentricity of the elliptical aperture.
λ_0 = Free-space wavelength.
λ_g = Guide wavelength (H_{01}-mode).
λ_c = Cut-off wavelength (H_{01}-mode).
λ_{0m} = Wavelength for maximum directivity.
k = Free-space wave number.
$\boldsymbol{E}$ = Electric field strength.
$\boldsymbol{H}$ = Magnetic field strength.
E_A = Peak value of the electric field in the secondary guide travelling in the positive z-direction.
E_B = Peak value of the electric field in the secondary guide travelling in the negative z-direction.
P = Electric polarizability of the coupling aperture.
M = Magnetic polarizability of the coupling aperture.
ρ = Directivity, defined by the ratio of E_A/E_B.
n = Subscript denoting direction normal to the plane of the coupling aperture.
l = Subscript denoting direction in the plane of the aperture, normal to the direction of propagation.
E, F = Complete elliptic integrals of the first and second kinds respectively.
f_b = Bandwidth of the directional coupler.

(1) INTRODUCTION

Directional coupling between two waveguides may arise as a result of interference effects between several coupling apertures (interference coupler), or may be the consequence of an inherent asymmetry in the coupling provided by a single aperture (intrinsic coupler). It is possible to combine these two principles in a single coupler by using a series of interfering apertures, each one of which is itself inherently directional. Such a coupler can, for a given length, be designed to give a higher directivity or maintain a specified directivity over a larger bandwidth, than either the purely intrinsic or purely interference type. It does not appear that such a coupler has been described, although the principle is of course frequently used in connection with antenna arrays. Another possibility is to use the intrinsic directional properties to couple a signal in one direction at one frequency, and to use the interference properties to couple a signal in the opposite direction at a different frequency. In this way, two frequency bands can be extracted from one waveguide and sent along two different paths, using only a single coupler. This is a type of 'filter coupler', examples of which, using microwave strip line, have recently been described.[1]

The first requirement for the practical realization of such devices is an intrinsic directional coupler, in which the two guides are parallel. Now, interference couplers are necessarily of the forward type, in that the signal in the secondary guide is travelling in the same direction as that in the primary guide (codirectional coupler). Thus to realize a coupler with enhanced directivity or bandwidth, we must use a coupling element intrinsically directional in the forward sense, whereas the filter coupler will require an element directional in the backward sense (contra-directional coupler). In rectangular guides, a forward element can be obtained by the use of two crossed slots in the broad common wall, as shown by Surdin,[2] or by the use of a separate pair of slots, one series and the other shunt, as shown by Riblet and Saad.[3] Crossed slots can also provide a backward element, but in this case it is necessary to offset the two guides laterally.[2] A simpler contradirectional coupler is the well known Bethe coupler,[4] which consists of a single circular hole placed on the centre-line of the common broad wall. Unfortunately the directional property can be obtained at a single frequency only, if the two guides are to remain parallel. It seemed, however, that a small modification to the shape of the hole might well allow an extension of the use of such a coupler to other frequencies. In fact, it was found that, if the aperture is made elliptical, dimensions can be specified to produce a reverse coupler, with theoretically infinite directivity at any given frequency above the cut-off frequency of the waveguides. Furthermore, if the elliptical hole is moved off the centre-line, it is again possible to obtain an intrinsic forward element which, by a suitable choice of dimensions, can be made to operate at any given frequency. The main part of this paper is devoted to an examination, both theoretical and experimental, of some of these properties of the elliptical-hole coupling element. A calculation illustrating the use of two such elements for the realization of a filter coupler is presented in Section 2.4.

(2) THEORETICAL ANALYSIS

The general theory of coupling between two guides through a small aperture has been developed by Bethe.[5] For a wave of unit amplitude, travelling in the positive z-direction in the primary guide, he finds waves of amplitudes E_A and E_B travelling in the positive and negative z-directions respectively in the secondary guide, where, for identical guides supporting the same mode,[6]

Correspondence on Monographs is invited for consideration with a view to publication.
The authors were formerly at Queen Mary College, University of London; Mr. Figanier is now in the Portuguese Scientific Civil Service, and Dr. Ash is now with Standard Telecommunication Laboratories Ltd.

$$E_A = -\frac{jk}{2S}(PE_n^2 - M_lH_l^2 - M_zH_z^2) \quad . \quad . \quad (1)$$

$$E_B = -\frac{jk}{2S}(PE_n^2 + M_lH_l^2 - M_zH_z^2) \quad . \quad . \quad (2)$$

with $$S = \int\int E_t \times H_t dxdy$$

the integration extending over the complete cross-section of the guide, where E_n, H_l, H_z are the magnitudes of the (unperturbed) normal mode components at the centre of the aperture, and E_t, H_t are the real magnitudes of the transverse components of the fields in the primary guide.

Eqns. (1) and (2) are valid for apertures which are sufficiently small compared with the wavelength, so that the variation of the magnitudes and phases of the fields over the aperture can be neglected. A further requirement is that the aperture shall be sufficiently far from the corners of the guide. For rectangular

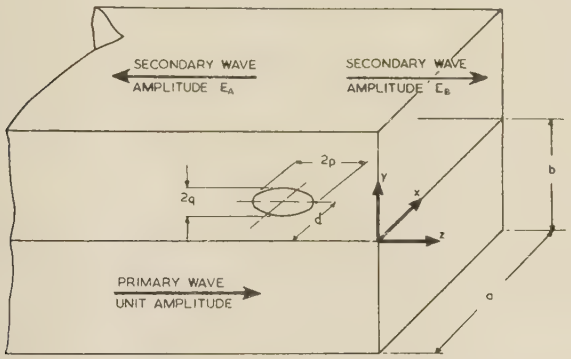

Fig. 1.—Geometrical parameters of the elliptical-hole coupler.

guides with an aperture in the broad face as shown in Fig. 1, eqns. (1) and (2) become

$$E_A = -\frac{jk}{2S}(PE_y^2 - M_xH_x^2 - M_zH_z^2) \quad . \quad . \quad (3)$$

$$E_B = -\frac{jk}{2S}(PE_y^2 + M_xH_x^2 - M_zH_z^2) \quad . \quad . \quad (4)$$

For an elliptical aperture, the polarizabilities are:[7]

$$\left.\begin{aligned} P &= \tfrac{1}{3}\pi pq^2\left(\frac{1}{\mathrm{E}}\right) = \tfrac{1}{3}\pi pq^2P' \\ M_1 &= \tfrac{1}{3}\pi pq^2\frac{\epsilon^2}{\mathrm{E}-(1-\epsilon^2)\mathrm{F}} = \tfrac{1}{3}\pi pq^2M_1' \\ M_2 &= \tfrac{1}{3}\pi pq^2\frac{\epsilon^2}{(1-\epsilon^2)(\mathrm{F}-\mathrm{E})} = \tfrac{1}{3}\pi pq^2M_2' \end{aligned}\right\} \quad . \quad . \quad (5)$$

M_1 and M_2 are the components of the magnetic polarizability directed along the major and minor axes of the ellipse respectively. The functions P', M_1', M_2' are defined by the eqns. (5).

For rectangular guides supporting H_{01}-modes, there is only a single field component, H_z, at the side walls, so that, as may be seen from eqns. (1) and (2), a coupling aperture would show no directive properties. On the other hand, for an elliptical hole positioned as shown in Fig. 1,

$$E_A = R\left[P' - \left(\frac{\lambda_0}{\lambda_g}\right)^2 M_x' - \left(\frac{\lambda_0}{\lambda_c}\right)^2 \cot^2\left(\frac{\pi d}{a}\right)M_z'\right] \quad (6)$$

$$E_B = R\left[P' + \left(\frac{\lambda_0}{\lambda_g}\right)^2 M_x' - \left(\frac{\lambda_0}{\lambda_c}\right)^2 \cot^2\left(\frac{\pi d}{a}\right)M_z'\right] \quad (7)$$

where $$R = -j\frac{\pi}{3}\left(\frac{\lambda_g}{\lambda_0}\right)\frac{kpq^2}{ab}\sin^2\left(\frac{\pi d}{a}\right)$$

In these equations M_x' is equal to M_1' if the major axis of the ellipse is in the x-direction, and is equal to M_2' if it is in the z-direction, and similarly for M_z'. The behaviour of the functions P', M_1', and M_2' is shown as functions of ϵ in Fig. 2.

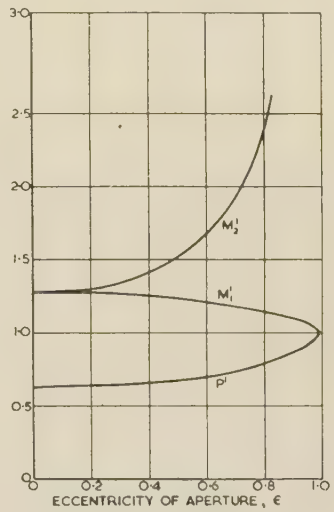

Fig. 2.—The functions P', M_1' and M_2' as a function of ϵ.

(2.1) Conditions for Infinite Directivity

The conditions for an ideal contradirectional coupler is that E_B should be zero, for a codirectional coupler that E_A should be zero. From eqns. (6) and (7) it is easily shown that, for either of these conditions to be satisfied,

$$\left(\frac{\lambda_0}{\lambda_c}\right)^2 = \frac{M_x' \pm P'}{M_x' \pm M_z' \cot^2(\pi d/a)} \quad . \quad . \quad . \quad (8)$$

where the negative signs apply to the case $E_A = 0$, and the positive signs apply to the case $E_B = 0$. The right-hand side of eqn. (8) is a function of d and ϵ only. These two variables must be restricted to values which make λ_0 real, and also less than the cut-off wavelength, λ_c. Hence we require that

$$1 > \frac{M_x' \pm P'}{M_x' \pm M_z' \cot^2(\pi d/a)} > 0 \quad . \quad . \quad . \quad (9)$$

Inspection of Fig. 2 reveals that the value of P' never exceeds that of either M_1' or M_2'. This permits the condition of eqn. (9) to be expressed in the form

$$P' \gtrless M_z' \cot^2\left(\frac{\pi d}{a}\right) \quad . \quad . \quad . \quad . \quad . \quad (10)$$

where the top and bottom inequalities refer to the cases $E_A = 0$ and $E_B = 0$ respectively. The limits on the possible choice of d and ϵ imposed by eqn. (10) can readily be shown to lead to the results presented in Table 1.

In this Table, the critical value of the eccentricity, ϵ_1, satisfies the following equation:

$$P' \cot^2\left(\frac{\pi d}{a}\right) = M_2' \quad . \quad . \quad . \quad . \quad (11)$$

Table 1

CONDITIONS FOR CODIRECTIONAL AND CONTRADIRECTIONAL DIRECTIVITY

Position of hole	Conditions for $E_A = 0$		Conditions for $E_B = 0$	
	Major axis *z*-oriented	Minor axis *z*-oriented	Major axis *z*-oriented	Minor axis *z*-oriented
$0 < d/a < 0{\cdot}250$	impossible	impossible	arbitrary	arbitrary
$0{\cdot}250 < d/a < 0{\cdot}304$	impossible	$\epsilon_2 < \epsilon < 1$	arbitrary	$0 < \epsilon < \epsilon_2$
$0{\cdot}304 < d/a < 0{\cdot}500$	$0 < \epsilon < \epsilon_1$	arbitrary	$\epsilon_1 < \epsilon < 1$	impossible
$d/a = 0{\cdot}500$	arbitrary	arbitrary	impossible	impossible

and the critical value, ϵ_2, satisfies

$$P' \cot^2 \left(\frac{\pi d}{a}\right) = M_1' \quad . \quad . \quad . \quad . \quad (12)$$

The Table shows the possible choice of ϵ for a given position and orientation of the elliptical aperture to make either E_A or E_B equal to zero. A number of significant facts can be deduced from this Table in conjunction with eqn. (9):

(*a*) Any pair of values (d, ϵ) will make either E_A or E_B equal to zero at some frequency.

(*b*) At all frequencies above cut-off, both E_A and E_B can be made zero by two suitable (different) choices of the variables (d, ϵ).

(*c*) No pair of values (d, ϵ) will make E_A zero at one frequency and E_B zero at another.

The last condition is interesting in that it implies that, in the case considered, it is not possible to realize a filter coupler with a single aperture. Nevertheless it may well prove possible to construct such a coupler with a differently shaped or oriented aperture.

Some computations of eqn. (8) have been carried out for the case $E_A = 0$ (contradirectional coupler). These are presented in Fig. 3, which shows λ_0/λ_c as a function of ϵ, with d/a as a

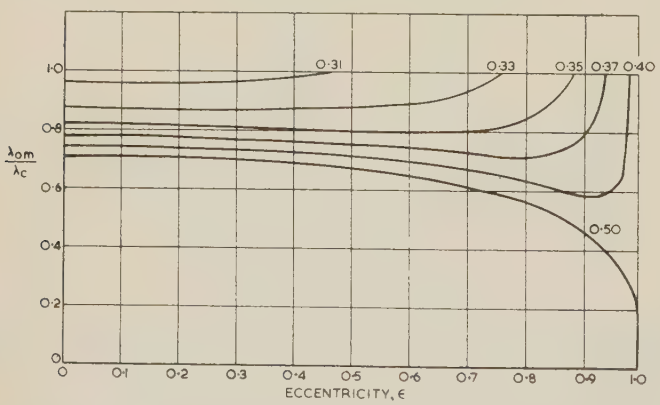

Fig. 3.—Wavelength for maximum directivity of the contradirectional coupler as a function of the eccentricity of the coupling aperture, for a number of values of d/a.

parameter. It is noted that, for any wavelength and $d/a < 0{\cdot}5$, there are two values of the eccentricity which can be used. It can be shown that the design with the smaller value of ϵ will in general be less sensitive to constructional errors in either d or ϵ.

(2.2) Bandwidth

The bandwidth of a directional coupler may be defined in terms of λ_{0m}, λ_{01} and λ_{02}, the wavelengths at the two points where the directivity falls to a specified value ρ, according to the relation

$$f_b(\rho) = \frac{\lambda_{01} - \lambda_{02}}{\lambda_{0m}} \quad . \quad . \quad . \quad . \quad . \quad (13)$$

The two extreme wavelengths are readily found from eqns. (6) and (7). For the contradirectional coupler,

$$\left(\frac{\lambda_0}{\lambda_c}\right)^2 = \frac{(P' - M_1') \pm \rho(P' + M_1')}{[M_2' \cot^2 (\pi d/a) - M_1'] \pm \rho[M_2' \cot^2 (\pi d/a) + M_1']} \quad . \quad . \quad . \quad . \quad (14)$$

where $\lambda_0 = \lambda_{01}$ for the positive sign, and $\lambda_0 = \lambda_{02}$ for the negative sign.

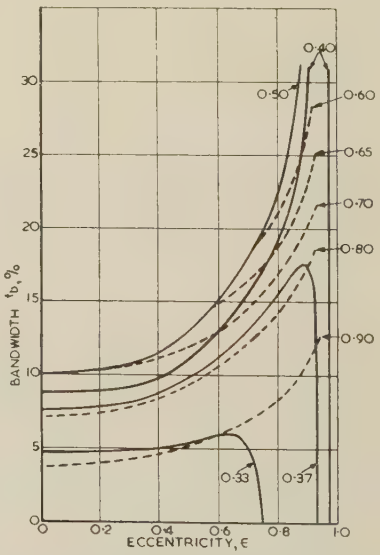

Fig. 4.—Percentage bandwidth over which the contradirectional coupler maintains a directivity in excess of 26 dB, for a number of values of d/a.

The dotted lines are contours of constant λ_0/λ_c.

Fig. 4 shows some results computed from eqn. (14), for the contradirectional coupler, choosing $\rho = 26$ dB. It is seen that, at a given frequency, a suitable choice of d and ϵ allows considerable latitude in the choice of bandwidth. The dotted lines in Fig. 4 are contours of constant λ_0. It can be shown that the bandwidth of a Bethe coupler, for a given value of λ_0, is given by the intersection of the appropriate contour with the $d/a = 0{\cdot}5$ line. The elliptical-hole coupler can therefore always be designed to give a greater bandwidth than the equivalent Bethe coupler. The significance of this fact in practice is in some doubt because, for coupling apertures sufficiently large to give coupling losses less than 30 dB, the theoretical predictions of bandwidth are subject to large errors.

Table 2

Coupling Factors, Bandwidths and Wavelengths for Maximum Directivity, for Different Holes

$2p$	ϵ	d/a	Coupling factor	f_b Theory	f_b Measured	λ_{0m} Theory	λ_{0m} Theory (modified)	λ_{0m} Measured
cm			dB	%	%			
1·35	0·550	0·50	21	14	5·3	9·50	9·60	9·60
1·64	0·647	0·50	24	—	—	9·10	9·27	9·62
1·49	0·652	0·50	22	16·5	6·1	9·09	9·24	9·33
1·66	0·730	0·50	22	18·5	6·4	8·63	8·84	9·10
1·88	0·777	0·50	25	21·8	—	8·22	8·52	9·22
1·87	0·794	0·50	25	22	6·5	8·14	8·38	8·82
1·85	0·820	0·50	24	24	5·2	7·87	8·10	8·55
1·87	0·794	0·43	24	20·3	6·9	8·38	8·85	9·20

(2.3) Coupling Factor

The coupling factor is numerically equal to E_B for the contradirectional coupler, to E_A for the codirectional coupler. It is proportional to pq^2 and, for small values of the eccentricity, it will be comparable with the coupling factor of a Bethe coupler having an aperture of radius $(pq^2)^{1/3}$. The theoretical value of the coupling factor for the particular couplers investigated experimentally, calculated from eqn. (7), is indicated in Table 2.

(2.4) Design of a Filter Coupler

As one example of the use of an elliptical-aperture contradirectional coupler, one may take the simplest type of filter coupler with only two apertures. The results of a numerical example are shown in Fig. 5. This coupler has been so designed

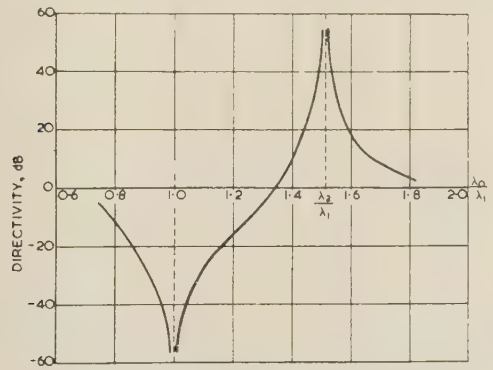

Fig. 5.—Directivity of a coupler with two apertures spaced L apart, each intrinsically codirectional at $\lambda_0 = \lambda_2$, and together contradirectional (interference) at $\lambda_0 = \lambda_1$.
$L = \frac{1}{4}\lambda_g$ at $\lambda_0 = \lambda_1 \searrow d/a = 0{\cdot}5$
$L = \frac{1}{2}\lambda_g$ at $\lambda_0 = \lambda_2 \int \lambda_1/\lambda_e = 0{\cdot}5$

that the apertures are separated by $\frac{1}{2}\lambda_g$ at the frequency for which $E_A = 0$, and by $\frac{1}{4}\lambda_g$ at the frequency for which $E_B = 0$. This ensures that there is no deterioration of the intrinsic performance as a result of interference effects, but is not, of course, a necessary design condition. The performance shown in Fig. 5 could be modified to give greater or less bandwidth by the addition of further apertures.

(3) EXPERIMENTS

(3.1) Experimental Apparatus and Method

The main purpose of the experimental work was to gain some idea of the limitations of the theory arising out of the assumptions made. The experiments were largely confined to the determination of the frequency for maximum directivity for the contradirectional coupler. Measurements were made between 3·0 Gc/s and 3·75 Gc/s, using standard WG10 waveguide (2·84 in × 1·34 in internal dimensions). Both the primary and the secondary guides were machined out of the solid. The common wall was a sheet of copper, 0·030 in thick, clamped between the primary and secondary guides. This method of construction allows the rapid interchange of coupling apertures, and permits the use of a very thin common wall without the danger of distorting the guides. The elliptical apertures were cut by hand; dimensional errors did not exceed 3% of the major axis. A difficulty is to ensure that the transition to normal waveguide at the ends of the copper sheet does not produce excessive reflections. Preliminary calculations indicated that, if the inevitable gap could be reduced to less than 0·010 in, the reflections would not be significant. Measurements on the primary guide, using a copper sheet without any coupling apertures, showed that the voltage standing-wave ratio (v.s.w.r.) never exceeded 1·11. Since it is only the reflection at the far end of the coupler which can affect the measurement of directivity it may be concluded that an error due to this cause would not be significant for directivities less than 50 dB. A somewhat greater difficulty was the need to accommodate a load with a sufficiently low v.s.w.r. in the restricted length available in the secondary guide. Using four staggered resistance-card attenuators, the v.s.w.r. could be kept below 1·1 over the complete experimental bandwidth.

Fig. 6 shows a block diagram of the measurement system. The

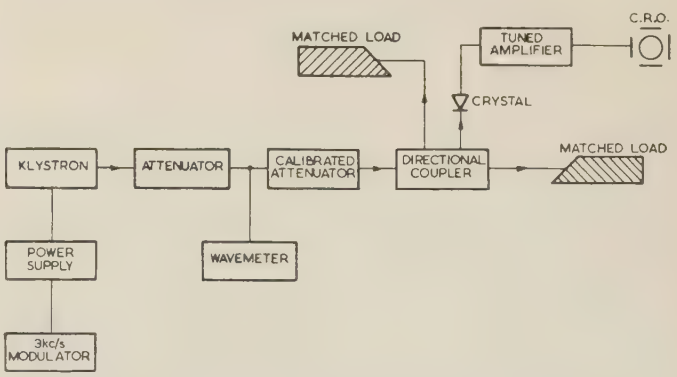

Fig. 6.—Block diagram of the experimental apparatus.

directivity was determined by a substitution method, using a calibrated variable attenuator. The change in attenuation in the primary guide, required to keep the signal level detected in the secondary guide constant on reversing the coupler, was measured. The klystron was square-wave modulated at 3 kc/s, and the rectified signal from the crystal detector in the secondary guide was amplified by a selective amplifier (bandwidth 30 c/s) and displayed on a cathode-ray oscilloscope. After eliminating

various sources of microwave and audio-frequency leakage, the detector sensitivity was limited by noise at a power level of about 70 dB below that fed into the primary guide. Coupling factors of the order of 30–40 dB were used in the experiments, so that the maximum measurable directivity, as limited by signal/noise ratio, was not less than 30 dB.

(3.2) Experimental Results

The directivity was measured as a function of wavelength for each aperture. A typical experimental curve is shown in Fig. 7.

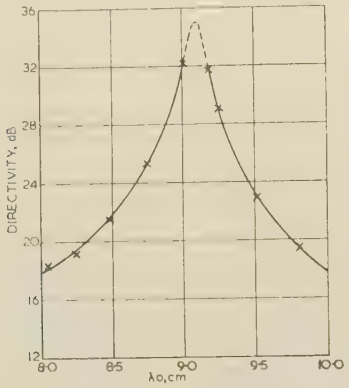

Fig. 7.—Experimental curve of directivity as a function of wavelength for an aperture with $d/a = 0{\cdot}5$.
$\epsilon = 0{\cdot}730$. $2p = 1{\cdot}66$ cm.

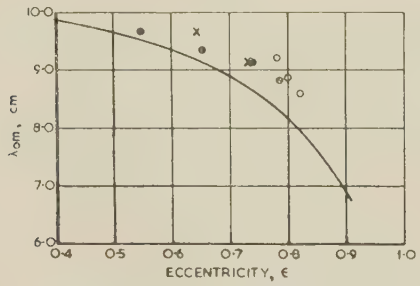

Fig. 8.—Measured wavelength for maximum directivity compared with the theoretical curve.
● $2 = 1{\cdot}13$ cm.
× $2p = 1{\cdot}65$ cm.
○ $2p = 1{\cdot}87$ cm.

In this, as in all other cases, the maximum directivity was too great to be measured, but the wavelength for maximum directivity could be deduced with an uncertainty less than $\pm\frac{1}{2}\%$.

Fig. 8 shows the results obtained for a series of apertures with constant minor axis, and for a series with constant major axis, compared with the theoretical curve. As may be seen in Table 2, the coupling factor does not vary over very wide limits for the apertures in one series. A single experiment was performed in which the wavelength for maximum directivity was measured for an aperture off the centre-line, and subsequently for an identical aperture on the centre-line. The result is shown in Fig. 9. Table 2 lists the geometrical parameters of the apertures investigated, and compares the experimental results with the theoretical results for the frequency at which the directivity has its maximum value.

(4) DISCUSSION

Comparison with theory shows a general shift of the experimental points to higher wavelengths. This shift is attributed to

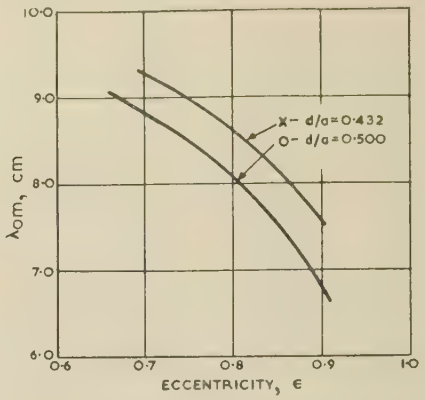

Fig. 9.—Measured λ_{0m} for two positions of similar holes compared with the theoretical curves.
$\times$ $d/a = 0{\cdot}432$
$\bigcirc$ $d/a = 0{\cdot}500$
$\Big\}$ $2p = 1{\cdot}87$ cm.

the finite size of the holes, and indicates that the effect of the variation of the magnitude and the phase of the fields over the aperture, neglected in Bethe's theory, is in fact not insignificant. The unperturbed field has a phase variation proportional to the length of the aperture, and a magnitude variation which is a function of the width. Although it is of course the variation of the perturbed fields which is relevant, one can form some tentative impression of the relative importance of the two effects from Fig. 8. Since the experimental results do not run parallel to the theoretical curve with either p or q constant, it would appear that, for the range of apertures used, both effects are significant and lead to deviations of the same order of magnitude.

A qualitative explanation for the discrepancies revealed is not hard to find. For an aperture on the centre-line, the coupling produced by the z-component of the magnetic field is entirely neglected by the theory since its mean value over the aperture is zero. Yet for apertures of the dimensions used, the value of H_z at the edge of the aperture may amount to as much as 25% of the value of H_x. Since the coupling is proportional to the square of the amplitudes of the normal mode components, the effect of H_z will, for the contradirectional coupler, be such as to reinforce that due to H_x. Inspection of eqn. (8) will show that this would indeed result in a shift of the wavelength for maximum directivity to longer wavelengths. One might expect that the order of magnitude of this effect would be predicted by using the r.m.s. value of H_z over the aperture in eqn. (8). The eighth column in Table 2 has been calculated in this way. It is seen that the correction is somewhat less than, but of the same order of magnitude as, the discrepancy. A more accurate estimate of the effect of the H_z-component would require an extension of Bethe's theory to fields which are not constant over the aperture.

A further departure from the theoretical assumptions is the phase change along the length of the aperture, where this is an appreciable fraction of the guide wavelength. The sense of the error incurred can again be deduced by a qualitative argument: the field radiated into the secondary guide by various sub-areas of the aperture will have different phases. This will result in a directional effect of the interference type, in the opposite sense to that produced by the intrinsic action of the elliptical aperture. Thus the backward wave is weakened, the forward wave remaining substantially unchanged. This effect clearly could not alter the frequency at which the directivity reaches its maximum value, in the idealized case where this maximum is infinitely large. In practice, the presence of losses ensure a finite directivity and the reduction of the amplitude of the backward wave will result in a further loss of directivity, an effect that will increase rapidly with

frequency. In consequence one observes a reduction in the frequency at which the maximum directivity is obtained.

The coupling factors were not measured accurately, but were always 5–10 dB higher than the theoretical values listed in Table 2. This again is undoubtedly due to the limitations of the theory for large apertures, as is the large discrepancy between predicted and measured bandwidths. These discrepancies are also encountered in the design of conventional Bethe couplers.

(5) CONCLUSIONS

It has been shown that, by suitable choice of the position and eccentricity of an elliptical coupling aperture in the common broad wall of two parallel rectangular waveguides, an intrinsically directive coupling can be obtained. This coupling may be either codirectional or contradirectional. The frequency at which the directivity has its maximum value is restricted only by the cut-off frequency of the guides. Within certain rather wide limits the bandwidth may be specified separately.

Experiments with contradirectional elliptical apertures has shown that the frequency of maximum directivity, for apertures with coupling factors of the order of 30 dB, can in most cases be predicted from theory with an accuracy of about 5%. The frequency at which the directivity has its maximum value as predicted by theory always exceeds the measured values, a discrepancy which is readily explicable in sign, and order of magnitude, by the variation of the field quantities over the aperture, which is neglected by the theory.

Considerable discrepancies are noted between measurements of the coupling factor and bandwidth, and predicted values based on the small-aperture theory, and are attributed to the inaccuracy of the latter for the comparatively large apertures used in the experiments.

An example is given of a two-aperture coupler, using elliptical apertures, which is contradirectional at one frequency and codirectional at another, and its performance is calculated.

(6) ACKNOWLEDGMENTS

The authors are greatly indebted to Dr. G. B. Walker for encouragement and help throughout the work. One of the authors (J. F.) is also indebted to the Instituto de Alta Cultura of Portugal, for having extended his grant in order to bring the work to completion.

(7) REFERENCES

(1) Coale, F. S.: 'A Travelling-Wave Directional Filter', *Transactions of the Institute of Radio Engineers*, 1956, **MTT–4**, p. 256.

(2) Surdin, M.: 'Directive Couplers in Wave Guides', *Journal I.E.E.*, 1946, **93**, Part IIIA, p. 725.

(3) Riblet, H. J., and Saad, T. S.: 'A New Type of Waveguide Directional Coupler', *Proceedings of the Institute of Radio Engineers*, 1948, **36**, p. 61.

(4) Montgomery, C. G.: 'Technique of Microwave Measurements', Radiation Laboratory Series (McGraw-Hill, 1948), p. 858.

(5) Bethe, H. A.: 'Theory of Diffraction by Small Holes,' *Physical Review*, 1944, **66**, p. 163.

(6) Bethe, H. A.: 'Theory of Side Windows in Wave Guides', *Massachusetts Institute of Technology, Radiation Laboratory Report* 43–27.

(7) Montgomery, C. G., *et al.* (Ed.): 'Principles of Microwave Circuits', Radiation Laboratory Series (McGraw-Hill, 1948), p. 178.

621.391:621.372.542.4

The Institution of Electrical Engineers
Monograph No. 297 R
Mar. 1958
©

OPTIMUM NETWORK FUNCTIONS FOR THE SAMPLING OF SIGNALS IN NOISE

By H. S. HEAPS, B.Sc., M.A., and M. R. McKAY, B.E.

(*The paper was first received* 12*th June, and in revised form* 22*nd November*, 1957. *It was published as an* INSTITUTION MONOGRAPH *in March*, 1958.)

SUMMARY

The paper examines the detection of a signal received upon a noise background, and determines the transfer functions of the networks which maximize (*a*) the ratio between the average amplitude of n successive samples of the output signal and the r.m.s. output noise, and (*b*) a continuous sample of the output. The optimum ratio is calculated when the input is a rectangular pulse upon white noise or a cosine pulse upon non-white noise.

(1) INTRODUCTION

The detection of a signal in the presence of noise is achieved by observing some quantity whose value in the absence of the signal is measurably different from that when the signal is present. In many instances it is convenient to choose as the observed quantity some function of the amplitude of the signal plus noise at the output of the detector. In the absence of the signal the observed quantity fluctuates with the noise background. Thus, for a weak signal the detection efficiency depends upon the amount of change in the observed quantity which constitutes, with reasonable probability, an indication of the presence of the signal. The inclusion of a further network to increase the ratio between the observed quantity when the signal is present and its value when the signal is absent may facilitate detection; the consideration of such a network is the purpose of the paper.

Dwork[1] obtained an expression for the transfer function required to produce at the output the greatest possible value of instantaneous peak signal amplitude consistent with a fixed mean output noise power. The resulting ratio between the peak signal and the r.m.s. noise is

$$\frac{P_S^2}{P_N^2} = \frac{1}{2\pi}\int_{-\infty}^{\infty} \frac{|F(\omega)|^2}{|\sigma(\omega)|^2} d\omega \quad . \quad . \quad . \quad . \quad (1)$$

where $|F(\omega)|^2$ and $|\sigma(\omega)|^2$ are the power spectra of the signal and the noise respectively. The transfer function which leads to the above value of P_S/P_N is

$$H(\omega) = \frac{F^*(\omega)\varepsilon^{-j\omega T}}{\lambda|\sigma(\omega)|^2} \quad . \quad . \quad . \quad . \quad . \quad (2)$$

where λ is an arbitrary constant, T is the time of occurrence of the peak, and the asterisk denotes the complex conjugate.

Dwork's transfer function is not always realizable by a physical network.

With white noise the condition for physical realizability of Dwork's optimum transfer function is that the entire input signal must have entered the circuit prior to the sampling time at which the peak signal is to be produced. This condition is also obvious intuitively, since it is equivalent to the statement that the processing circuit in the receiver output cannot make the best use of the signal until the entire signal has been received. It follows that, for a signal of finite duration received upon white noise, the realizability condition may always be satisfied by the choice of a sufficiently large sampling time.

When the signal is not of finite duration the realizability condition implies that the sampling time must be chosen at infinity. If the signal amplitude tends to zero with increasing time, a circuit designed to process a sufficiently large time sample of the signal will lead to a value of P_S/P_N sufficiently close to the optimum value given by eqn. (1). In practice, the necessity of evaluating the receiver output at a finite time implies that the processing circuit must be designed to deal with a finite sample of signal and hence with an input whose amplitude may be supposed to be zero after the lapse of a sufficiently long time.

Zadeh and Ragazzini[2] have shown that a physically realizable transfer function to produce a maximum ratio between the peak signal and the r.m.s. noise at a chosen time T is given by

$$H(\omega) = \frac{1}{2\pi\sigma_1(\omega)}\int_0^{\infty}\varepsilon^{-j\omega t}dt\int_{-\infty}^{\infty}\frac{F^*(\omega_1)}{\lambda\sigma_1^*(\omega_1)}\varepsilon^{j\omega_1(t-T)}d\omega_1 \quad . \quad (3)$$

The function $\sigma_1(\omega)$ must be chosen so that $|\sigma_1(\omega)| = |\sigma(\omega)|$ and $\sigma_1(\omega)$ has no poles or zeros when $\mathscr{I}\omega > 0$.

Since eqn. (3) is more cumbersome to evaluate explicitly than eqn. (2), it is desirable to make direct use of eqn. (2), and hence eqn. (1), whenever possible. It is accordingly desirable to know the least restrictions that must be placed upon the signal and the noise in order to permit physical realizability of the transfer function (2). However, a discussion of the condition for physical realizability of Dwork's transfer function when the noise is not white is not at present available in the literature.

The theories of Dwork and of Zadeh and Ragazzini concern the production of a single signal peak that is instantaneously as large as possible in comparison with the r.m.s. noise. In many instances a more efficient method of detection results if the output is sampled over a continuous interval. It may then be desirable to include a network whose function is to produce an extended signal peak whose value averaged over a given finite time is as large as possible in comparison with the r.m.s. noise.

An alternative method of detection is in terms of the average value of n successive samples of the output chosen at equal intervals. The theory in the paper is illustrated by the determination of a transfer function to maximize the ratio between the average of n successive samples of the output signal and the r.m.s. output noise. As the number of samples is increased and the time interval between them is decreased, the average of the discrete samples approximates to that of a continuous sample. The problem of deciding whether or not a given sequence of samples indicates the presence of a signal has been discussed by Slattery.[3]

(2) OPTIMUM TRANSFER FUNCTION

Adapting the notation of Dwork,[1] the signal input, $V_i(t)$, and output, $V_0(t)$, of the network at time t may be represented in the forms

$$V_i(t) = (1/2\pi)\int_{-\infty}^{\infty} F(\omega)\varepsilon^{j\omega t}d\omega \quad . \quad . \quad . \quad . \quad (4)$$

Correspondence on Monographs is invited for consideration with a view to publication.

Mr. Heaps is Associate Professor of Engineering Mathematics, Nova Scotia Technical College. Mr. McKay is with the Maritime Telegraph and Telephone Company, Halifax, Canada.

For republication in the *Proceedings*, sundry corrections have been made at the suggestion of Mr. E. L. R. Webb and with the assistance of Mr. A. Mahommed.

$$V_0(t) = (1/2\pi)\int_{-\infty}^{\infty} F(\omega)H(\omega)\varepsilon^{j\omega t}d\omega \quad . \quad . \quad . \quad (5)$$

where

$$F(\omega) = \int_{-\infty}^{\infty} V_i(t)\varepsilon^{-j\omega t}dt \quad . \quad . \quad . \quad . \quad . \quad (6)$$

and $H(\omega)$ is the transfer function of a network chosen to process the pulse in a manner to facilitate detection. If the power spectrum of the input noise is $|\sigma(\omega)|^2$, the mean square noise output is given by

$$P_N^2 = (1/2\pi)\int_{-\infty}^{\infty} |\sigma(\omega)H(\omega)|^2 d\omega \quad . \quad . \quad . \quad . \quad (7)$$

Suppose that the transfer function $H(\omega)$ is to be chosen such that, for some specified function $G(\omega)$, the quantity

$$P_S(T) = (1/2\pi)\int_{-\infty}^{\infty} F(\omega)H(\omega)G(\omega)\varepsilon^{j\omega T}d\omega \quad . \quad . \quad (8)$$

is as large as possible compared with P_N^2. Then H must be chosen such that $\partial Q/\partial H = 0$, where

$$Q = (1/2\pi)[F(\omega)H(\omega)G(\omega)\varepsilon^{j\omega T} - \lambda|\sigma(\omega)H(\omega)|^2] \quad . \quad (9)$$

and λ is a Lagrangian multiplier.[4] The condition $\partial Q/\partial H = 0$ is fulfilled when

$$F(\omega)G(\omega)\varepsilon^{j\omega T} - \lambda|\sigma(\omega)|^2 H^*(\omega) = 0 \quad . \quad . \quad (10)$$

Thus

$$H(\omega) = \frac{F^*(\omega)G^*(\omega)\varepsilon^{-j\omega T}}{\lambda|\sigma(\omega)|^2} \quad . \quad . \quad . \quad . \quad (11)$$

leads to a stationary value of Q.

When $H(\omega)$ is chosen according to eqn. (11), then $P_S(T)$ of eqn. (8) has a value, P_S, given by

$$P_S = (1/2\pi)\int_{-\infty}^{\infty} \frac{|F(\omega)|^2|G(\omega)|^2}{\lambda|\sigma(\omega)|^2}d\omega \quad . \quad . \quad . \quad (12)$$

and so the value of $P_S(T)^2/P_N^2$ is

$$P_S^2/P_N^2 = (1/2\pi)\int_{-\infty}^{\infty} \frac{|F(\omega)|^2|G(\omega)|^2}{|\sigma(\omega)|^2}d\omega \quad . \quad . \quad (13)$$

It will now be shown that the stationary value of P_S^2/P_N^2 according to eqn. (13) is indeed the maximum value of $P_S(T)^2/P_N^2$. It follows from eqn. (8) that

$$|P_S(T)| \leqslant (1/2\pi)\int_{-\infty}^{\infty} |F(\omega)H(\omega)G(\omega)|d\omega \quad . \quad . \quad (14)$$

Hence

$$|P_S(T)/P_N|^2 \leqslant (1/2\pi)\frac{[\int |F(\omega)H(\omega)G(\omega)|d\omega]^2}{\int |\sigma(\omega)H(\omega)|^2 d\omega} \quad . \quad (15)$$

Now by Schwartz's inequality[4] for any functions $x(\omega)$ and $y(\omega)$,

$$\frac{[\int x(\omega)y(\omega)d\omega]^2}{\int |x(\omega)|^2 d\omega} \leqslant \int |y(\omega)|^2 d\omega \quad . \quad . \quad . \quad (16)$$

Putting $x(\omega) = \sigma(\omega)H(\omega)$ and $y(\omega) = F(\omega)G(\omega)/\sigma(\omega)$, eqns. (15) and (16) show that

$$|P_S(T)/P_N|^2 \leqslant (1/2\pi)\int_{-\infty}^{\infty} \frac{|F(\omega)|^2|G(\omega)|^2 d\omega}{|\sigma(\omega)|^2} \quad . \quad (17)$$

and hence P_S^2/P_N^2 as given by eqn. (13) is indeed the maximum value of $P_S(T)^2/P_N^2$.

In order that the transfer function $H(\omega)$ of eqn. (11) should correspond to a physically realizable network it is necessary that the output response, $V_0(t)$, to a unit impulse input, $V_1(t)$, at time $t = 0$ should be zero for $t < 0$. Now, with $H(\omega)$ chosen as in eqn. (11), the output resulting from a unit impulse input is

$$V_0(t) = (1/2\pi)\int_{-\infty}^{\infty} \frac{F^*(\omega)G^*(\omega)\varepsilon^{j\omega(t-T)}}{\lambda|\sigma(\omega)|^2}d\omega \quad . \quad (18)$$

Substitution of $F(\omega)$ from eqn. (6) enables eqn. (18) to be written in the form

$$V_0(t) = \int_{-\infty}^{\infty} g^*(t_1)h^*(T - t - t_1)dt_1 \quad . \quad . \quad . \quad (19)$$

where

$$h(t) = \int_{-\infty}^{\infty} \frac{F(\omega)}{\lambda|\sigma(\omega)|^2}\varepsilon^{j\omega t}d\omega \quad . \quad . \quad . \quad . \quad (20)$$

and

$$g(t) = (1/2\pi)\int_{-\infty}^{\infty} G(\omega)\varepsilon^{j\omega t}d\omega \quad . \quad . \quad . \quad . \quad (21)$$

The condition that $V_0(t) = 0$ for $t < 0$ is thus equivalent to the condition

$$\int_{-\infty}^{\infty} g(t_1)h(t - t_1)dt_1 = 0 \quad \text{for} \quad t > T \quad . \quad . \quad . \quad (22)$$

The function $g(t)$ represents the response $P_S(t)$ to an impulsive input in the absence of the processing network. The left-hand side of eqn. (22) is the mutual correlation function of $g(t)$ and the Fourier transform of $F(\omega)/\lambda|\sigma(\omega)|^2$. The condition for physical realizability of the transfer function (11) is thus that the mutual correlation function is zero for $t > T$.

In many instances the specified function $G(\omega)$ is the transfer function of a filter of finite memory, so that $g(t)$ is zero for sufficiently large values of t. Suppose, in fact, that there exists a t_0 such that $g(t) = 0$ for $t > t_0$. The condition (22) is then satisfied by any function $h(t)$ for which $h(t) = 0$ when $t > T - t_0$, and hence is satisfied whenever

$$\int_{-\infty}^{\infty} \frac{F(\omega)}{|\sigma(\omega)|^2}\varepsilon^{j\omega t}d\omega = 0 \quad \text{for} \quad t > T - t_0 \quad . \quad . \quad (23)$$

By a theorem of Wiener[5] the condition for the existence of a finite time T for which eqn. (23) may be satisfied is equivalent to the condition

$$\int_{-\infty}^{\infty} \frac{1}{1 + \omega^2} \log\left[\frac{|F(\omega)|}{|\sigma(\omega)|^2}\right]d\omega < \infty \quad . \quad . \quad . \quad (24)$$

The form (24) of the realizability condition is a precise formulation which includes the intuitively obvious condition that there must be no frequency band over which the noise vanishes but the signal does not. The existence of such a frequency band would imply that P_S/P_N could be made infinite by the use of an ideal rectangular band-pass filter. The problem discussed in the paper would then be replaced by that of approximating the ideal rectangular filter by a realizable one with a finite number of circuit elements. P_S/P_N could be made as large as required by the choice of a sufficiently close approximation.

To illustrate the above remarks, consider the case of an input rectangular pulse of duration t_a received upon a noise background for which $|\sigma(\omega)|^2 = \omega^2/(\omega^2 + \omega_b^2)$ where ω_b is a constant. With the time origin chosen at the centre of the pulse, $F(\omega) = 2A(\sin \frac{1}{2}\omega t_a)/\omega$, where A is the height of the pulse. The functions $|\sigma(\omega)|^2$ and $F(\omega)$ are shown in Fig. 1. The condition (24) is not fulfilled, because of the infinite behaviour of the integrand at $\omega = 0$. However, P_S/P_N may be made as large as desired by the use of a sufficiently narrow low-pass filter.

Likewise, if a rectangular pulse is received upon a noise background for which $|\sigma(\omega)|^2 = \omega_b^2/(\omega^2 + \omega_b^2)$, eqn. (24) is not true because of the behaviour of the integrand at $\omega = \infty$. In this

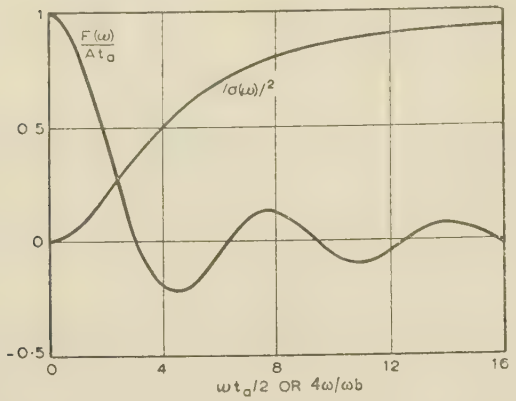

Fig. 1.—Graph of $F(\omega) = 2A\ (\sin \frac{1}{2}\omega t_a)/\omega$ and $|\sigma(\omega)|^2 = \omega^2/(\omega^2 + \omega_b^2)$.

instance P_S/P_N may be made as large as required by the use of a sufficiently high-pass filter. However, if a cosine pulse of shape $V(t) = \cos(\pi t/t_a)$ of duration $-\frac{1}{2}t_a < t < \frac{1}{2}t_a$ is received upon a noise background for which $|\sigma(\omega)|^2 = \omega_b^2/(\omega^2 + \omega_b^2)$, then

$$F(\omega) = \frac{(2\pi/t_a)\cos\frac{1}{2}\omega t_a}{(\pi/t_a)^2 - \omega^2}$$

and the condition (24) is fulfilled. The graphs of $|\sigma(\omega)|^2$ and $F(\omega)$ are shown in Fig. 2.

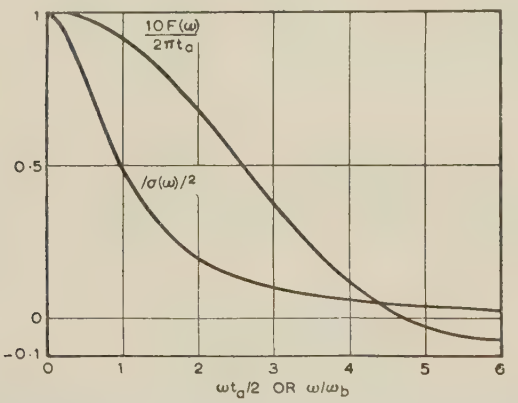

Fig. 2.—Graph of $F(\omega) = (2\pi t_a)[(\pi/t_a)^2 - \omega^2]^{-1}\cos\frac{1}{2}\omega t_a$ and $|\sigma(\omega)|^2 = \omega_b^2/(\omega^2 + \omega_b^2)$.

If $G(\omega)$ is chosen as

$$G(\omega) = 1 + \varepsilon^{-j\omega\tau} + \varepsilon^{-2j\omega\tau} + \ldots + \varepsilon^{-(n-1)j\omega\tau}$$

$$= \frac{\sin\frac{1}{2}n\omega\tau}{\sin\frac{1}{2}\omega\tau}\varepsilon^{-\frac{1}{2}(n-1)j\omega\tau} \quad . \quad . \quad . \quad . \quad . \quad . \quad . \quad . \quad (25)$$

then $P_S(T)$ represents the sum of n samples of the output chosen successively at intervals τ. Also

$$g(t) = V_1(t) + V_1(t-\tau) + V_1(t-2\tau) + \ldots + V_1[t-(n-1)\tau]$$

and eqn. (22) takes the form

$$h(t) + h(t-\tau) + h(t-2\tau) + \ldots + h[t-(n-1)\tau] = 0 \quad \text{for } t > T \quad . \quad (26)$$

which implies that T must be chosen such that $h(t) = 0$ for $t > T - (n-1)\tau$. Putting $n\tau = t_d$, and letting $\tau \to 0$, then for fixed values of t_d

$$\tau G(\omega) = \frac{2\sin\frac{1}{2}\omega t_d}{\omega}\varepsilon^{-\frac{1}{2}j\omega t_d} \quad . \quad . \quad . \quad . \quad (27)$$

and $\tau P_S(T)$ represents the output integrated over the time t_d.

For white noise $|\sigma(\omega)|^2 = 1$, $h(t) = \dfrac{2\pi}{\lambda}V_i(t)$, and the condition (26) implies that the entire signal must have entered the network before the first sample is chosen.

If the noise is not white and it is impossible to choose a finite T to satisfy eqn. (22), the method of Zadeh and Ragazzini[2] may be applied to show that the optimum realizable transfer function for a given T is

$$H(\omega) = \frac{1}{2\pi\lambda\sigma_1(\omega)}\int_0^\infty \varepsilon^{-j\omega t}dt \int_{-\infty}^{\infty} \frac{F^*(\omega_1)G^*(\omega_1)}{\sigma_1^*(\omega_1)}\varepsilon^{j\omega_1(t-T)}d\omega_1 \quad . \quad (28)$$

where $\sigma_1(\omega)$ is chosen as in eqn. (3). It is to be noted that the transfer function (28) is, in general, optimum only for a fixed value of T, while the function (11) is optimum over all values of T.

(3) SAMPLES OF RECTANGULAR PULSE UPON WHITE NOISE

If the input signal consists of a rectangular pulse of duration t_a then, with suitable choice of the origin of time,

$$V_i(t) = \begin{cases} A & \text{for } |t| < \frac{1}{2}t_a \\ 0 & \text{for } |t| > \frac{1}{2}t_a \end{cases} \quad . \quad . \quad . \quad (29)$$

Therefore $$F(\omega) = 2A\ (\sin\frac{1}{2}\omega t_a)/\omega \quad . \quad . \quad . \quad . \quad . \quad (30)$$

and the total energy contained in the pulse is $w = A^2 t_a$.

To determine the network function which maximizes the sum of n samples of the output at intervals τ, put

$$G(\omega) = \frac{\sin\frac{1}{2}n\omega\tau}{\sin\frac{1}{2}\omega\tau}\varepsilon^{-\frac{1}{2}(n-1)j\omega\tau} \quad . \quad . \quad . \quad . \quad (31)$$

The quantity $P_S(T)\tau$ represents an approximation to the time integral of the output amplitude over a time $n\tau$. The similar integral of the r.m.s. noise is $n\tau P_N$, and so $P_S(T)$ should be compared with nP_N. For a fixed n the maximum value of $P_S(T)/nP_N$ is P_S/nP_N, where, according to eqn. (13),

$$M_n(\tau) = P_S^2/n^2P_N^2 = \frac{A^2t_a^2}{2\pi n^2}\int_{-\infty}^{\infty}\frac{\sin^2\frac{1}{2}\omega t_a}{(\frac{1}{2}\omega t_a)^2}\frac{\sin^2\frac{1}{2}n\omega\tau}{\sin^2\frac{1}{2}\omega\tau}d\omega \quad . \quad (32)$$

$$= \frac{2w}{\pi n^2}\int_0^\infty \frac{\sin^2 x}{x^2}\frac{\sin^2(n\tau x/t_a)}{\sin^2(\tau x/t_a)}dx \quad . \quad . \quad (33)$$

where x denotes $\frac{1}{2}\omega t_a$. In eqn. (32) it is assumed that $|\sigma(\omega)|^2 = 1$; thus w denotes the ratio between the input signal energy and input mean square noise amplitude per unit bandwidth.

Evaluation of the integral (33) leads to the following formula for $M_n(\tau)$ (see Section 6.1):

$$M_n(\tau) = (w/n^2)[3 + \tfrac{1}{2}(n-2)(n+3) - (1/6)n(n-1)(n+1)(\tau/t_a) + \sum_{k=1}^{n-1} k|1-(n-k)(\tau/t_a)|] \quad . \quad (34)$$

which is plotted as a function of τ in Fig. 3 for several values of n.

The maximum signal/noise ratio that can result after integra-

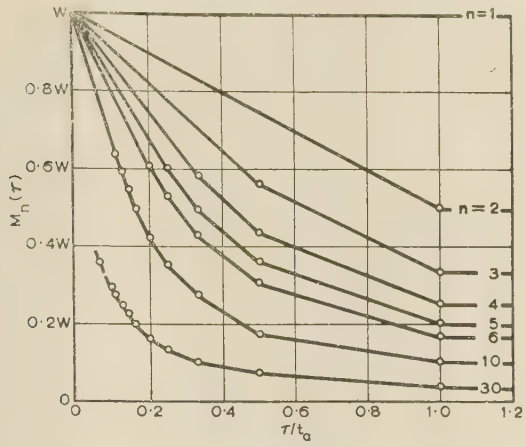

Fig. 3.—Optimum ratio between the average of n successive samples of the output signal amplitude and the r.m.s. noise amplitude when the input is a rectangular pulse upon white noise.

tion of the output over a time t_d is obtained by use of eqn. (27). The resulting ratio is

$$M(t_d) = \frac{P_S^2}{t_d^2 P_N^2} = \frac{2A^2 t_a^3}{\pi d^2} \int_0^\infty \frac{\sin^2 x}{x^2} \frac{\sin^2 (x t_d/t_a)}{x^2} dx \quad . \quad (35)$$

which has the values (see Section 6.2)

$$\left.\begin{aligned} & w\left(1 - \frac{1}{3}\frac{t_d}{t_a}\right) \text{ if } t_d < t_a \\ \text{and} \quad & w\left[\frac{t_a}{t_d} - \frac{1}{3}\left(\frac{t_a}{t_d}\right)^2\right] \text{ if } t_d > t_a \end{aligned}\right\} \quad . \quad . \quad . \quad (36)$$

The function $M(t_d)$ is shown by a broken curve in Fig. 4; the continuous curves show $M_n(\tau) = M_n(t_d/t_a)$ for $n = 2$–5 and are included for comparison. Examination of Fig. 4 shows

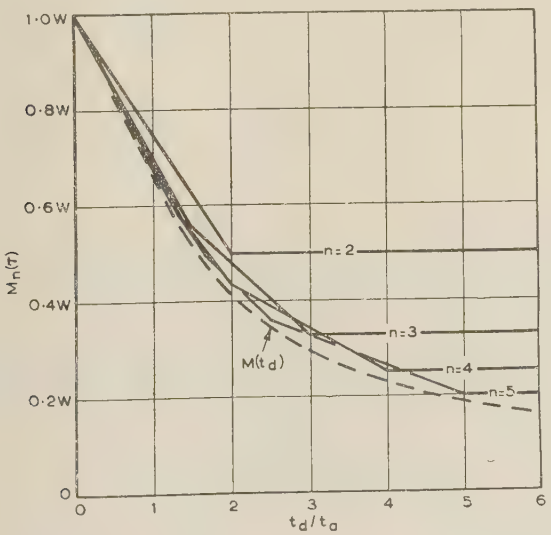

Fig. 4.—Optimum ratio between the average output signal amplitude and the r.m.s. noise amplitude when the input is a rectangular pulse upon white noise.

that the average of a series of discrete samples of the output is approximately equivalent to a continuous average, provided that the time interval between successive samples is less than the length of the input pulse.

(4) CONTINUOUS SAMPLE OF COSINE PULSE UPON NON-WHITE NOISE

If the input signal is a finite pulse of cosine shape given by

$$\left.\begin{aligned} V_i(t) = A\cos(\pi t/t_a) \quad & \text{for } |t| < \tfrac{1}{2}t_a \\ 0 \quad & \text{for } |t| > \tfrac{1}{2}t_a \end{aligned}\right\} \quad . \quad . \quad (37)$$

then

$$F(\omega) = \frac{2\pi A}{t_a} \frac{\cos \tfrac{1}{2}\omega t_a}{(\pi/t_a)^2 - \omega^2} \quad . \quad . \quad . \quad . \quad (38)$$

and the total energy contained in the pulse is $w = \frac{1}{2}A^2 t_a$.

The cosine pulse may be regarded as approximating to the shape of an originally rectangular pulse which has been transmitted through a propagating medium and has suffered distortion in the form of a rounding of the discontinuities at the beginning and the end.

Suppose that the pulse is received upon a noise background for which $|\sigma(\omega)|^2 = \omega_b^2/(\omega_b^2 + \omega^2)$, where ω_b is the value of ω at which the mean square noise per unit bandwidth of ω is equal to one-half of the d.c. component.

By eqns. (27) and (13) the maximum signal/noise ratio for a continuous sample of the output integrated over a time t_d is

$$M(t_d) = \frac{P_S^2}{t_d^2 P_N^2} = \frac{8A^2\pi}{t_a^2 t_d^2} \int_{-\infty}^{\infty} \frac{\cos^2 \tfrac{1}{2}\omega t_a}{[\omega^2 - (\pi/t_a)^2]^2} \frac{\sin^2 \tfrac{1}{2}\omega t_d}{\omega^2} \frac{\omega_b^2 + \omega^2}{\omega_b^2} d\omega$$

$$. \quad . \quad . \quad (39)$$

Thus (see Section 6.3)

$$M(t_d) = \frac{4w}{\pi^2}\frac{t_a}{t_d}\left[1 + \frac{(\omega_b^2 + \pi^2/t_a^2)}{2\omega_b^2}\cos(\pi t_d/t_a) + \frac{t_a}{t_d}\frac{(\omega_b^2 + \pi^2/t_a^2)}{\omega_b^2}\sin^2(\pi t_d/2t_a) - \frac{t_a}{t_d}\frac{(3\omega_b^2 + \pi^2/t_a^2)}{2\pi\omega_b^2}\sin(\pi t_d/t_a)\right]$$

if $t_d < t_a$, and

$$M(t_d) = \frac{4w}{\pi^2}\frac{t_a}{t_d}\left[2 - \frac{t_a}{t_d} + \frac{t_a}{2t_d}\left(\frac{\omega_b^2 + \pi^2/t_a^2}{\omega_b^2}\right)\right] \quad . \quad (40)$$

if $t_d > t_a$.

The function $M(t_d)$ is plotted as a function of t_d for various values of ω_b in Fig. 5, the appropriate value of $\omega_b/(\pi/t_a)$ being

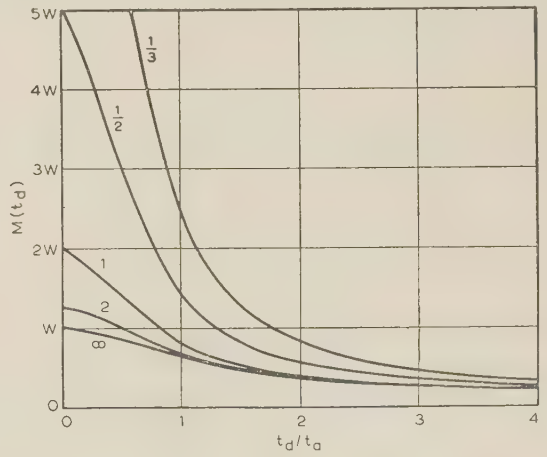

Fig. 5.—Optimum ratio between the average output signal amplitude and the r.m.s. noise amplitude when the input is a cosine pulse upon non-white noise.

indicated on each curve. The curve for which $\omega_b/(\pi/t_a) = \infty$ applies when the input noise is white. The value of W indicates the ratio between the input signal energy and the input d.c. noise power. This definition of W is consistent with that adopted

in Figs. 3 and 4. It may be noted that for Figs. 3 and 4 the total input noise power is infinite, while for Fig. 5 the total input noise power is equal to $\frac{1}{2}\omega_b$.

Comparison of Figs. 4 and 5 indicates that, when the continuous sample of the output extends over a time less than the duration of the input pulse, it is possible to design a much more efficient optimum network to deal with a cosine pulse than with a rectangular pulse. For a cosine pulse the optimum signal/noise ratio is approximately the same as for white noise when $\omega_b/(\pi/t_a) > 2$ but is significantly higher for smaller values.

(5) REFERENCES

(1) DWORK, B. M.: 'Detection of a Pulse Superposed on Fluctuation Noise', *Proceedings of the Institute of Radio Engineers*, 1950, **38**, p. 771.

(2) ZADEH, L. A., and RAGAZZINI, J. R.: 'Optimum Filters for the Detection of Signals in Noise', *ibid.*, 1952, **40**, p. 1223.

(3) SLATTERY, T. G.: 'The Detection of a Sine-Wave in the Presence of Noise by the Use of a Nonlinear Filter', *ibid.*, p. 1232.

(4) WEINSTOCK, R.: 'Calculus of Variations' (McGraw-Hill, New York, 1952), pp. 48 and 44.

(5) PALEY, R. E. A. C., and WIENER, N.: 'Fourier Transforms in the Complex Domain' (American Mathematical Society Colloquium Publications, Vol. XIX, New York, 1934), p. 16.

(6) DWIGHT, H. B.: 'Tables of Integrals and Other Mathematical Data' (MacMillan, New York, 1947).

(7) SNEDDON, I. N.: 'Fourier Transforms' (McGraw-Hill, New York, 1951), p. 24.

(8) ERDÉLYI, A., MAGNUS, W., OBERHETTINGER, F., and TRICOMI, F. G.: 'Tables of Integral Transforms', Vol. I (McGraw-Hill, New York, 1954), p. 19.

(6) APPENDICES

(6.1) Proof of Eqn. (34)

The integral in eqn. (33) may be evaluated by the following procedure. First divide $\sin(\tau x/t_a)$ into $\sin(n\tau x/t_a)$ by means of formulae (403.11) or (403.13) of Reference 6. Then express the integrand of eqn. (33) as a sum of terms of type $(\sin^2 kx)/x^2$ and integrate according to the formula

$$\int_0^\infty \frac{\sin^2 kx}{x^2}dx = |k|\pi/2 \quad . \quad . \quad . \quad . \quad (41)$$

Proof of the general formula (34) is very tedious and is outlined below for the specific instance in which $n = 3$. Since

$$\frac{\sin^2(3\tau x/t_a)}{\sin^2(\tau x/t_a)} = [3 - 4\sin^2(\tau x/t_a)]^2$$

then

$$\begin{aligned}\frac{\sin^2 x}{x^2}\frac{\sin^2(3\tau x/t_a)}{\sin^2(\tau x/t_a)} &= \frac{[3\sin x - 4\sin x\sin^2(\tau x/t_a)]^2}{x^2}\\ &= \frac{[\sin x + \sin(1+2\tau/t_a)x + \sin(1-2\tau/t_a)x]^2}{x^2}\\ &= \frac{3\sin^2 x}{x^2} - \frac{4\sin^2(\tau/t_a)x}{x^2} + \frac{\sin^2(1+2\tau/t_a)x}{x^2}\\ &+ \frac{2\sin^2(1+\tau/t_a)x}{x^2} + \frac{\sin^2(1-2\tau/t_a)x}{x^2}\\ &+ \frac{2\sin^2(1-\tau/t_a)x}{x^2} - \frac{2\sin^2(2\tau/t_a)x}{x^2} \quad . \quad (42)\end{aligned}$$

Thus, by eqn. (41),

$$\int_0^\infty \frac{\sin^2 x}{x^2}\frac{\sin^2(3\tau x/t_a)}{\sin^2(\tau x/t_a)}dx = \tfrac{1}{2}\pi\left(6 - \frac{4\tau}{t_a} + \left|1 - \frac{2\tau}{t_a}\right| + 2\left|1 - \frac{\tau}{t_a}\right|\right)$$

and hence

$$M_3(\tau) = \frac{w}{9}\left(6 - \frac{4\tau}{t_a}\right) + \left|1 - \frac{2\tau}{t_a}\right| + 2\left|1 - \frac{\tau}{t_a}\right|\right) \quad (43)$$

in agreement with eqn. (34).

(6.2) Proof of Eqn. (36)

The integral in eqn. (35) is

$$I = \int_0^\infty \frac{\sin^2 x}{x^2}\frac{\sin^2(xt_d/t_a)}{x^2}dx \quad . \quad . \quad . \quad . \quad (44)$$

By the convolution theorem for the Fourier cosine transform[7] eqn. (44) may also be written in the form

$$I = \int_0^\infty u(y)v(y)dy \quad . \quad . \quad . \quad . \quad . \quad (45)$$

where $$u(y) = (2/\pi)^{1/2}\int_0^\infty \frac{\sin^2 x}{x^2}\cos xydx$$

and $$v(y) = (2/\pi)^{1/2}\int_0^\infty \frac{\sin^2(xt_d/t_a)}{x^2}\cos xydx$$

The explicit values of $u(y)$ and $v(y)$ are respectively[8]

$$u(y) = \left\{\begin{array}{ll}\left(\frac{\pi}{2}\right)^{1/2}(1-\frac{1}{2}y) & \text{if } y<2\\ 0 & \text{if } y>2\end{array}\right\} \quad . \quad . \quad (46)$$

and

$$v(y) = \left\{\begin{array}{ll}\left(\frac{\pi}{2}\right)^{1/2}[(t_d/t_a) - \frac{1}{2}y] & \text{if } y<2t_d/t_a\\ 0 & \text{if } y>2t_d/t_a\end{array}\right\} \quad . \quad (47)$$

If expressions (46) and (47) are substituted into eqn. (45) the integration is trivial and leads to

$$I = \left\{\begin{array}{ll}\frac{\pi}{2}\frac{t_d^2}{t_a^2}\left(1 - \frac{t_d}{3t_a}\right) & \text{if } t_d < t_a\\ \frac{\pi}{2}\left(\frac{t_d}{t_a} - \frac{1}{3}\right) & \text{if } t_d > t_a\end{array}\right\} \quad . \quad . \quad (48)$$

(6.3) Proof of Eqn. (40)

For real values of ω the integrand of eqn. (39) is the real part of the function

$$\tfrac{1}{4}z(\omega) = \frac{f(\omega)(\omega_b^2 + \omega^2)}{[\omega^2 - (\pi/t_a)^2]^2\omega^2\omega_b^2} \quad . \quad . \quad . \quad (49)$$

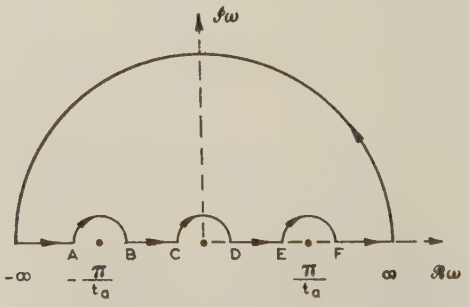

Fig. 6.—Path of integration of $z(\omega)$.

where

$$f(\omega) = 1 + \varepsilon^{jt_a\omega} - \varepsilon^{jt_a\omega} - \tfrac{1}{2}\varepsilon^{j(t_a+t_d)\omega} - \tfrac{1}{2}\varepsilon^{\pm j(t_a-t_d)\omega} \quad (50)$$

In the above definition of $f(\omega)$ the plus sign is to be used if $t_d < t_a$ and the minus sign if $t_d > t_a$.

For complex values of ω the function $z(\omega)$ has no singularities inside the contour shown in Fig. 6. The integral of $z(\omega)$ around the large semicircle tends to zero as the radius of the semicircle tends to infinity. The integrals around the small semicircles tend to the following values as the radii tend to zero:

$$\int_C^D = \left\{ \begin{array}{ll} \dfrac{-t_a^4 t_d}{\pi^3} & \text{if } t_a < t_a \\ \dfrac{-t_a^4(2t_d - t_a)}{\pi^3} & \text{if } t_d > t_a \end{array} \right\} \quad . \quad . \quad . \quad (51)$$

$$\int_A^B + \int_E^F = \left\{ \begin{array}{ll} \dfrac{-t_a^4}{2\pi^3}\dfrac{(\omega_b^2 + \pi^2/t_a^2)}{\omega_b^2}[t_a - (t_a - t_d)\cos(\pi t_d/t_a) & \\ \quad - \dfrac{t_a}{\pi}\dfrac{(3\omega_b^2 + \pi^2/t_a^2)}{(\omega_b^2 + \pi)/t_a^2}\sin(\pi t_d/t_a)] & \text{if } t_d < t_a \\ \dfrac{-t_a^5}{2\pi^3}\dfrac{(\omega_b^2 + \pi^2/t_a^2)}{\omega_b^2} & \text{if } t_d > t_a \end{array} \right\} (52)$$

Integration of $z(\omega)$ around the contour in Fig. 6 shows that

$$\int_{-\infty}^{\infty} \frac{\cos^2 \tfrac{1}{2}\omega t_a}{[\omega^2 - (\pi/t_a)^2]^2} \frac{\sin^2 \tfrac{1}{2}\omega t_d}{\omega^2} \frac{\omega_b^2 + \omega^2}{\omega_b^2} d\omega = -\int_C^D - \int_A^B - \int_E^F \quad (53)$$

Substitution of integrals (51) and (52) into eqn. (53) leads to the result (40).

DISCUSSION ON THE ABOVE MONOGRAPH

Mr. E. L. R. Webb (*Canada: communicated*): During the course of correspondence with Prof. Heaps it became apparent that there was a subtle but definite point of difference in the presentation of radar and sonar signals on type 'A' scans. Whereas in radar, the observer's reaction bandwidth is almost invariably (Moon radars excepted) the narrowest in the system, in sonar it may occur that the observer is relatively wideband. In other words, the radar observer integrates over a number of sweeps, whereas a sonar observer may make several 'partial' judgments during the course of a single sweep. The result is a tendency for a radar man to use a different definition of Prof. Heap and Mr. McKay's function $G(\omega)$. Specifically, if $G(\omega)$ were instrumented by a network which behaved like a 'tapped delay line adder' the signal would still be given by eqn. (12).

$$P_S = \int_{-\infty}^{\infty} \frac{|F(\omega)|^2 |G(\omega)|^2}{\lambda |\sigma(\omega)|^2} \frac{d\omega}{2\pi}$$

but the noise output would become

$$N_{out}^2 = \int_{-\infty}^{\infty} \frac{|F(\omega)|^2 |G(\omega)|^4}{\lambda^2 |\sigma(\omega)|^2} \frac{d\omega}{2\pi}$$

and eqn. (13) would be replaced by

$$\text{Signal/noise (power ratio)} = \frac{\left(\int \dfrac{|F|^2|G|^2}{|\sigma|^2} \dfrac{d\omega}{2\pi}\right)^2}{\int \dfrac{|F|^2|G|^4}{|\sigma|^2} \dfrac{d\omega}{2\pi}}$$

For the case of rectangular pulse, white noise and integration over time t_d this expression takes the form

$$A^2 t_a^2 \frac{(\int \operatorname{sinc}^2 x \operatorname{sinc}^2 y df)^2}{\int \operatorname{sinc}^2 x \operatorname{sinc}^4 y df}$$

where $\operatorname{sinc} \theta = \dfrac{\sin\theta}{\theta}$; $x = \pi f t_a$; $y = \pi f t_d$; which obviously reduces to the same form as would eqn. (13) for $t_d = 0$.

Similar (and even more unwieldy) expressions result for other pulse shapes and non-white noise. It is a general result, however, that for vanishingly small values of t_d (instantaneous sampling) all signal/noise ratios remain finite.

Prof. H. S. Heaps and **Mr. M. R. McKay** (*in reply*): We are grateful for Mr. Webb's remarks concerning the differences in the presentation of radar and sonar signals.

Throughout the paper it is supposed that the signal and noise are passed through a single filter of transfer function $H(\omega)$ and that $G(\omega)/n$ represents the process of averaging n samples of the output signal amplitude. The average of the n samples is compared to the r.m.s. output noise, and the resulting ratio is found to have a maximum value given by P_S/nP_N.

In Mr. Webb's communication it is supposed that the signal and noise are passed through a filter followed by a tapped delay line adder of transfer function $G(\omega)$. The quantity P_S/N_{out} represents the ratio of the signal output of the adder at a single instant to the r.m.s. noise output of the adder. It should be noted that since Mr. Webb assumes $H(\omega)$ to be chosen according to eqn. (11), then $H(\omega)$ maximizes the ratio of the signal output of the adder to the r.m.s. noise input of the adder. The maximum value of P_S/N_{out} occurs when $\partial Q'/\partial H = 0$, where

$$Q' = (1/2\pi)[F(\omega)H(\omega)G(\omega)e^{j\omega T} - \lambda|\sigma(\omega)|^2|H(\omega)|^2|G(\omega)|^2]$$

The condition $\partial Q'/\partial H = 0$ implies that

$$H(\omega) = \frac{F^*(\omega)G^*(\omega)e^{-j\omega T}}{\lambda|\sigma(\omega)|^2|G(\omega)|^2}$$

and hence the maximum value of $(P_S/N_{out})^2$ is given by

$$\frac{P_S^2}{N_{out}^2} = (1/2\pi)\int \frac{|F(\omega)|^2}{|\sigma(\omega)|^2} d\omega$$

621.376.56

The Institution of Electrical Engineers
Monograph No. 298 R
Mar. 1958
©

THE RATE OF TRANSMISSION OF INFORMATION IN PULSE-CODE-MODULATION SYSTEMS

By A. R. BILLINGS, B.Sc., Ph.D., Graduate.

(*The paper was first received 30th August, and in revised form 19th December, 1957. It was published as an* INSTITUTION MONOGRAPH *in March, 1958.*)

SUMMARY

A general expression is obtained for the maximum rate of communication of information in pulse-code modulation systems using any scale of numbers, when the interfering noise has a Gaussian amplitude distribution. The particular cases of binary and tertiary coding are dealt with in more detail, and a comparison is made between the communication rate R and the ideal channel capacity C. It is shown that for both systems the communication efficiency R/C reaches a maximum of the order of 80% at particular signal/noise ratios. It is also shown that in all systems, regardless of the scale of numbers used, the communication efficiency tends to 63·6% as the signal/noise ratio tends to zero.

(1) INTRODUCTION

Any communication system in which a signal is sampled regularly and the sample amplitudes are quantized and transmitted as numbers is a pulse-code modulation (p.c.m.) system. The effect of noise is to introduce errors when decoding at the receiver, and previous assessments of the performance of p.c.m. systems[1] have been based on the signal/noise ratio required to keep errors down to a specified minimum. Whilst this is a good criterion to use with the simple practical systems at present in use, it is not a true measure of the potential capacity of systems for transmitting information if an error-correcting code is used. Without in any way suggesting how this error correction is to be achieved, the paper is concerned with the calculation of the true maximum rate of communication of information in p.c.m. systems, from a knowledge of the *a priori* and *a posteriori* uncertainties of the transmitted symbols or numbers.

(2) CODING AND DECODING

To simplify the exposition, all voltages in p.c.m. systems, both transmitted and received, will be referred to unit resistance. Also, the interfering noise will be assumed to have a Gaussian amplitude distribution, in which case, when the noise has power σ^2, the amplitude distribution is

$$P(v) = \frac{1}{\sigma\sqrt{(2\pi)}} \exp\left(\frac{-v^2}{2\sigma^2}\right) \quad . \quad . \quad . \quad . \quad (1)$$

In the general p.c.m. system a continuous message of bandwidth Δf is sampled at a frequency $2\Delta f$ and the amplitude of the samples is quantized into Q levels. If coding is to be in scale of n numbers, then Q is chosen such that

$$n^X = Q \quad . \quad . \quad . \quad . \quad . \quad . \quad . \quad (2)$$

where X is an integer. It is then possible to specify the message by a succession of scale-of-n numbers transmitted at a frequency $2X\Delta f$. In all that follows a simple p.c.m. system in which $X = 1$ will be assumed. This restriction is imposed solely to provide a simplicity of description, and the arguments can very easily be extended to systems where $X \neq 1$. Thus the following arguments are only strictly true for what are termed one-to-one coding systems but can easily be modified for other systems.

These simple p.c.m. systems operate as follows. A continuous message of bandwidth Δf is sampled at a frequency $2\Delta f$ and quantized into n levels, and pulses of short duration with respect to $1/\Delta f$ are transmitted to identify the quantized level. The coding system is such that when the rth level in the series 0, 1, 2 . . . r . . . $(n-1)$ is selected a pulse of amplitude $(2r - n + 1)K$ is transmitted, where K is a constant. It is convenient to introduce another parameter k which relates K to the interfering noise. If σ is the r.m.s. noise voltage, k is defined as K/σ. Thus the transmitted signal consists of narrow pulses spaced $1/2\Delta f$ seconds apart, having amplitudes selected from a group of amplitudes spaced $2k\sigma$ apart and ranging from $(n-1)k\sigma$ to $(1-n)k\sigma$. The pulses thus produced are passed through the transmission path which, for the present, will be assumed to have a rectangular pass characteristic with cut-off frequency Δf. The output from this transmission system no longer consists of pulses, but is a smooth time function with random noise superimposed on it. This signal + noise is sampled at the receiver at times corresponding to the transmitted pulses, and an assessment is made of the probable sequence of transmitted numbers, using the decoding method described below. Again, in the interests of simplicity, the overall transmission system, including amplifiers, will be specified as such that in the absence of noise the amplitudes of transmitted and received samples shall be equal.

The decoding technique is the simplest possible. The amplitudes of the received samples, including noise, are compared with the quantizing levels at the transmitter, and any particular received sample is decoded as specifying the number associated with the quantizing level to which its amplitude is nearest. Owing to the presence of noise, decoding errors will occur and there will always be some residual uncertainty about what was transmitted. It is this residual uncertainty which must be evaluated.

Having decoded the received samples, a quantized version of the original continuous message can be regenerated, either by passing the pulses through a perfect low-pass filter of bandwidth Δf or by using a step detector and appropriate equalizer. In this context a step detector is defined as a device which, when supplied with a sequence of pulses of amplitudes A_1, A_2, A_3, etc., will produce an output of amplitude A_1 between the arrivals of the first and second pulses and an output of amplitude A_2 between the arrivals of the second and third pulses, and so on.

(3) CHANNEL CAPACITY

Shannon[2] has derived an expression for the capacity of a channel for transmitting information in the presence of Gaussian noise. If the noise power is P_n, the mean signal power is P_s and the transmission bandwidth is Δf, the channel capacity is

$$C = \Delta f \log_2 (1 + P_s/P_n) \quad . \quad . \quad . \quad . \quad (3)$$

Correspondence on Monographs is invited for consideration with a view to publication.
Dr. Billings is at the University of Bristol.

In any practical system subjected to restrictions on mean power, bandwidth and noise, the rate of transmission of information, R, is always less than C, the rate at which information is transmitted by an ideal system subjected to the same restrictions. A convenient measure of the performance of a practical system is given by the ratio R/C, which is here termed the communication efficiency. In computing C it is necessary to calculate P_s, which will involve the parameters of the practical system. This does not imply that C is dependent upon the coding system but rather that P_s is so dependent. For the simple system described above the mean signal power is easily calculated in terms of received noise power σ^2, for if all the n numbers have equal probabilities of selection

$$P_s = (1/n)\sum_{r=0}^{n-1} k^2\sigma^2(2r - n + 1)^2 \quad . \quad . \quad . \quad (4)$$

whence

$$P_s/P_n = \frac{(n^2 - 1)k^2}{3} \quad . \quad . \quad . \quad . \quad . \quad (5)$$

and the channel capacity of the ideal system subjected to the same restrictions is

$$C = \Delta f\{\log_2 [3 + (n^2 - 1)k^2] - \log_2 3\} \quad . \quad . \quad (6)$$

(4) RATE OF TRANSMISSION OF INFORMATION

If $x_1, x_2 \ldots$, etc., are the transmitted numbers and $y_1, y_2 \ldots$, etc., are the decoded versions of these numbers, it is possible to specify the uncertainty of the transmitted sequence as $H(x)$, that of the received sequence as $H(y)$, and the uncertainty of the sequence $x_1y_1, x_2y_2 \ldots$, etc., as $H(x, y)$. It can be shown[3, 4] that the rate of transmission of information is

$$R = H(x) + H(y) - H(x, y) \text{ bits/sec} \quad . \quad . \quad . \quad (7)$$

and therefore the problem is simply that of determining $H(x)$, $H(y)$ and $H(x, y)$, the coding and decoding techniques and the properties of the interfering noise being known.

(4.1) The Uncertainty $H(x)$

It is well known[3] that the uncertainty of numbers selected independently at a frequency $2\Delta f$ from n possible numbers is

$$H(x) = -2\Delta f \sum_{i=0}^{n-1} p(i)\log_2 p(i) \text{ bits/sec} \quad . \quad . \quad (8)$$

where $p(i)$ is the probability of occurrence of symbol i. Further, if, as assumed here, all n symbols have equal probabilities of selection

$$H(x) = 2\Delta f \log_2 (n) \text{ bits/sec} \quad . \quad . \quad . \quad . \quad (9)$$

Thus the problem of calculating $H(x)$ is simple.

(4.2) The Uncertainty $H(x, y)$

To determine $H(x, y)$ the decoding technique must be known in order to calculate the probabilities $p(i, j)$ for i and j between 0 and $(n - 1)$, where $p(i, j)$ is the probability that i is transmitted and that j is received. The probabilities can be stated under four different conditions:

(i) *When* $i = j \neq 0$ *or* $(n - 1)$.

$$p(i, j) = \frac{1}{n\sigma\sqrt{(2\pi)}}\int_{-k\sigma}^{k\sigma} \exp\left(\frac{-v^2}{2\sigma^2}\right)dv \quad . \quad . \quad . \quad . \quad (10)$$

$$= \frac{1}{n}\operatorname{erf}\left(\frac{k}{\sqrt{2}}\right) \quad . \quad . \quad . \quad . \quad . \quad . \quad . \quad . \quad (11)$$

(ii) *When* $i = j = 0$ *or* $(n - 1)$.

$$p(i, j) = \frac{1}{n\sigma\sqrt{(2\pi)}}\int_{-k\sigma}^{\infty} \exp\left(\frac{-v^2}{2\sigma^2}\right)dv \quad . \quad . \quad . \quad . \quad (12)$$

$$= \frac{1}{2n}\left[1 + \operatorname{erf}\left(\frac{k}{\sqrt{2}}\right)\right] \quad . \quad . \quad . \quad . \quad . \quad (13)$$

(iii) *When* $i = j + m$ *and* $j \neq 0$ *or* $(n - 1)$.

$$p(i, j) = \frac{1}{n\sigma\sqrt{(2\pi)}}\int_{(|2m|-1)k\sigma}^{(|2m|+1)k\sigma} \exp\left(\frac{-v^2}{2\sigma^2}\right)dv \quad . \quad . \quad . \quad . \quad . \quad (14)$$

$$= \frac{1}{2n}\left\{\operatorname{erf}\left[\frac{(|2m| + 1)k}{\sqrt{2}}\right] - \operatorname{erf}\left[\frac{(|2m| - 1)k}{\sqrt{2}}\right]\right\} \quad . \quad (15)$$

(iv) *When* $i = j + m$, *and* $j = 0$ *or* $(n - 1)$.

$$p(i, j) = \frac{1}{n\sigma\sqrt{(2\pi)}}\int_{(|2m|-1)k\sigma}^{\infty} \exp\left(\frac{-v^2}{2\sigma^2}\right)dv \quad . \quad . \quad . \quad (16)$$

$$= \frac{1}{2n}\left\{1 - \operatorname{erf}\left[\frac{(2m - 1)k}{\sqrt{2}}\right]\right\} \quad . \quad . \quad . \quad (17)$$

Now

$$H(x, y) = \sum_{i=0, j=0}^{n-1, n-1} p(i, j)\log_2 p(i, j) \quad . \quad . \quad . \quad (18)$$

From which

$$H(x, y) = -\frac{2\Delta f}{n}\left\{\left[(n - 2)\operatorname{erf}\left(\frac{k}{\sqrt{2}}\right)\right]\log_2\left[\frac{1}{n}\operatorname{erf}\left(\frac{k}{\sqrt{2}}\right)\right] + \left[1 + \operatorname{erf}\left(\frac{k}{\sqrt{2}}\right)\right]\log_2\left\{\frac{1}{2n}\left[1 + \operatorname{erf}\left(\frac{k}{\sqrt{2}}\right)\right]\right\}\right.$$

$$+\sum_{m=1}^{n-2}(n - m - 1)\left\{\operatorname{erf}\left[\frac{(2m + 1)k}{\sqrt{2}}\right] - \operatorname{erf}\left[\frac{(2m - 1)k}{\sqrt{2}}\right]\right\}\log_2\left(\frac{1}{2n}\left\{\operatorname{erf}\left[\frac{(2m + 1)k}{\sqrt{2}}\right] - \operatorname{erf}\left[\frac{(2m - 1)k}{\sqrt{2}}\right]\right\}\right)$$

$$\left.+\sum_{m=1}^{n-1}\left\{1 - \operatorname{erf}\left[\frac{(2m - 1)k}{\sqrt{2}}\right]\right\}\log_2\left(\frac{1}{2n}\left\{1 - \operatorname{erf}\left[\frac{(2m - 1)k}{\sqrt{2}}\right]\right\}\right)\right\} \quad . \quad . \quad . \quad . \quad (19)$$

(4.3) The Uncertainty $H(y)$

To calculate $H(y)$ the probabilities $p'(0) \ldots p'(j) \ldots p'(n - 1)$ must be computed, where $p'(j)$ is the probability that at any instant the received waveform lies within the limits $(2j - n + 1 \pm 1)k\sigma$. These probabilities can be obtained in two sets, with the knowledge that $p'(j) = p'(n - 1 - j)$.

First, when $j = 0$

$$p'(j) = \frac{1}{n\sigma\sqrt{(2\pi)}}\sum_{r=0}^{n-1}\int_{(2r-1)k\sigma}^{\infty} \exp\left(\frac{-v^2}{2\sigma^2}\right)dv \quad . \quad . \quad (20)$$

$$= \frac{1}{2}\left\{1 - \frac{1}{n}\sum_{r=2}^{n-1}\operatorname{erf}\left[\frac{(2r - 1)k}{\sqrt{2}}\right]\right\} \quad . \quad . \quad (21)$$

Secondly, when $0 < j \leqslant \dfrac{n-1}{2}$

$$p'(j) = \frac{1}{n\sigma\sqrt{(2\pi)}}\left[\int_{-k\sigma}^{k\sigma} \exp\left(\frac{-v^2}{2\sigma^2}\right)dv + 2\sum_{r=1}^{j}\int_{(2r-1)k\sigma}^{(2r+1)k\sigma} \exp\left(\frac{-v^2}{2\sigma^2}\right)dv + \sum_{r=j+1}^{n-j-1}\int_{(2r-1)k\sigma}^{(2r+1)k\sigma} \exp\left(\frac{-v^2}{2\sigma^2}\right)dv\right] \quad . \quad (22)$$

From the above, when n is even

$$H_e(y) = -2\Delta f\left[\left\{1 - \frac{1}{n}\sum_{r=2}^{n-1}\operatorname{erf}\left[\frac{(2r-1)k}{\sqrt{2}}\right]\right\} \times \log_2\left(\frac{1}{2}\left\{1 - \frac{1}{n}\sum_{r=2}^{n-1}\operatorname{erf}\left[\frac{(2r-1)k}{\sqrt{2}}\right]\right\}\right) + \sum_{m=1}^{M}\frac{1}{n}\left\{\operatorname{erf}\left[\frac{(2m+1)k}{\sqrt{2}}\right] + \operatorname{erf}\left[\frac{(2n-2m-1)k}{\sqrt{2}}\right]\right\} \times \log_2\left(\frac{1}{2n}\left\{\operatorname{erf}\left[\frac{(2m+1)k}{\sqrt{2}}\right] + \operatorname{erf}\left[\frac{(2n-2m-1)k}{\sqrt{2}}\right]\right\}\right)\right] \quad . \quad . \quad . \quad . \quad (23)$$

where M is the next integer below $(n-1)/2$.

When n is odd an additional term arises and

$$H_0(y) = H_e(y) - \frac{2\Delta f}{n}\left\{\operatorname{erf}\left(\frac{nk}{\sqrt{2}}\right)\log_2\left[\frac{1}{n}\operatorname{erf}\left(\frac{nk}{\sqrt{2}}\right)\right]\right\} \quad . \quad (24)$$

The expressions for $H(y)$ and $H(x, y)$ are rather complicated but simplify considerably for low values of n. The solutions for $n = 2$ and $n = 3$ will now be considered as special cases.

(5) BINARY P.C.M.

With binary p.c.m. the quantizing levels are $+k\sigma$ and $-k\sigma$. The probabilities $p(i)$, $p(i, j)$ and $p'(j)$ are easily calculated, thus

$$p(0) = p(1) = 0{\cdot}5$$
$$p'(0) = p'(1) = 0{\cdot}5$$
$$p(0, 0) = p(1, 1) = \frac{1}{4}\left[1 + \operatorname{erf}\left(\frac{k}{\sqrt{2}}\right)\right]$$
$$p(0, 1) = p(1, 0) = \frac{1}{4}\left[1 - \operatorname{erf}\left(\frac{k}{\sqrt{2}}\right)\right]$$

whence

$$R = \Delta f\left\{\left[1 + \operatorname{erf}\left(\frac{k}{\sqrt{2}}\right)\right]\log_2\left[1 + \operatorname{erf}\left(\frac{k}{\sqrt{2}}\right)\right] + \left[1 - \operatorname{erf}\left(\frac{k}{\sqrt{2}}\right)\right]\log_2\left[1 - \operatorname{erf}\left(\frac{k}{\sqrt{2}}\right)\right]\right\} \quad . \quad (25)$$

and it is already known, from eqn. (6), that

$$C = \Delta f \log_2(1 + k^2)$$

Calculations of the communication efficiency R/C have been made for several values of k and are plotted in Fig. 1. It will be seen that the efficiency is a maximum for a signal/noise power ratio of about 2 and the value of this maximum is about 76%.

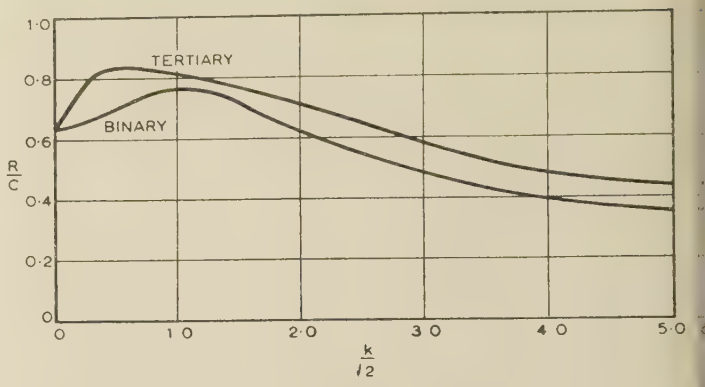

Fig. 1.—Variation of communication efficiency with size of quantizing steps.

(6) TERTIARY P.C.M.

For tertiary p.c.m. the probabilities $p(i)$, $p'(j)$ and $p(i, j)$ are still fairly easy to calculate. We have

$$p(0) = p(1) = p(2) = \tfrac{1}{3}$$

and probabilities $p(i, j)$ and $p'(j)$ are given in Tables 1 and 2.

Table 1

PROBABILITIES $p(i, j)$

i \ j	0	1	2
0	$\frac{1}{6}\left[1 + \operatorname{erf}\left(\frac{k}{\sqrt{2}}\right)\right]$	$\frac{1}{6}\left[\operatorname{erf}\left(\frac{3k}{\sqrt{2}}\right) - \operatorname{erf}\left(\frac{k}{\sqrt{2}}\right)\right]$	$\frac{1}{6}\left[1 - \operatorname{erf}\left(\frac{k}{\sqrt{2}}\right)\right]$
1	$\frac{1}{6}\left[1 - \operatorname{erf}\left(\frac{k}{\sqrt{2}}\right)\right]$	$\frac{1}{3}\operatorname{erf}\left(\frac{k}{\sqrt{2}}\right)$	$\frac{1}{6}\left[1 - \operatorname{erf}\left(\frac{k}{\sqrt{2}}\right)\right]$
2	$\frac{1}{6}\left[1 - \operatorname{erf}\left(\frac{k}{\sqrt{2}}\right)\right]$	$\frac{1}{6}\left[\operatorname{erf}\left(\frac{3k}{\sqrt{2}}\right) - \operatorname{erf}\left(\frac{k}{\sqrt{2}}\right)\right]$	$\frac{1}{6}\left[1 + \operatorname{erf}\left(\frac{k}{\sqrt{2}}\right)\right]$

Table 2

PROBABILITIES $p'(j)$

j	0	1	2
$p'(j)$	$\frac{1}{2} - \frac{1}{6}\operatorname{erf}\left(\frac{3k}{\sqrt{2}}\right)$	$\frac{1}{3}\operatorname{erf}\left(\frac{3k}{\sqrt{2}}\right)$	$\frac{1}{2} - \frac{1}{6}\operatorname{erf}\left(\frac{3k}{\sqrt{2}}\right)$

whence

$$R = \frac{2\Delta f}{3}\left\{\left[1 + \operatorname{erf}\left(\frac{k}{\sqrt{2}}\right)\right]\log_2\left[1 + \operatorname{erf}\left(\frac{k}{\sqrt{2}}\right)\right] + \left[1 - \operatorname{erf}\left(\frac{k}{\sqrt{2}}\right)\right]\log_2\left[1 - \operatorname{erf}\left(\frac{k}{\sqrt{2}}\right)\right] + \operatorname{erf}\left(\frac{k}{\sqrt{2}}\right)\log_2\left[2\operatorname{erf}\left(\frac{k}{\sqrt{2}}\right)\right] + \left[\operatorname{erf}\left(\frac{3k}{\sqrt{2}}\right) - \operatorname{erf}\left(\frac{k}{\sqrt{2}}\right)\right]\log_2\left[\operatorname{erf}\left(\frac{3k}{\sqrt{2}}\right) - \operatorname{erf}\left(\frac{k}{\sqrt{2}}\right)\right] + \left[1 - \operatorname{erf}\left(\frac{3k}{\sqrt{2}}\right)\right]\log_2\left[1 - \operatorname{erf}\left(\frac{3k}{\sqrt{2}}\right)\right] - \operatorname{erf}\left(\frac{3k}{\sqrt{2}}\right)\log_2\left[\frac{2}{3}\operatorname{erf}\left(\frac{3k}{\sqrt{2}}\right)\right] - 3\left[1 - \frac{1}{3}\operatorname{erf}\left(\frac{3k}{\sqrt{2}}\right)\right]\log_2\left[1 - \frac{1}{3}\operatorname{erf}\left(\frac{3k}{\sqrt{2}}\right)\right]\right\} \quad . \quad (26)$$

whilst
$$C = \Delta f \log_2 \left(1 + \frac{8}{3}k^2\right) \quad . \quad . \quad . \quad . \quad (27)$$

Again R/C has been plotted as a function of k, and it will be seen that the peak efficiency occurs when the signal/noise power ratio is about 0·5 and that the maximum efficiency is about 82%.

(7) GENERAL P.C.M. SYSTEM AT LOW SIGNAL/NOISE RATIOS

Although the expression for R becomes complicated and clumsy when n is greater than two, it does simplify if k is made very small, i.e. if the signal/noise ratio is low. The approximations which are useful in these conditions are that when k is small

$$\operatorname{erf} \frac{k}{\sqrt{2}} \simeq \alpha k \quad . \quad . \quad . \quad . \quad . \quad . \quad (28)$$

where
$$\alpha = \sqrt{\frac{2}{\pi}} \quad . \quad . \quad . \quad . \quad . \quad . \quad (29)$$

and that when z is small

$$\log_e (1 + z) \simeq z - \frac{z^2}{2} \quad . \quad . \quad . \quad . \quad (30)$$

Inserting these approximations into the expression for R gives

$$R = \frac{2\Delta f}{n \log_e 2}\left\{(1 + \alpha k)\left(\alpha k - \frac{\alpha^2 k^2}{2}\right) + n[1 - (n-2)\alpha k]\left[(n-2)\alpha k + \frac{(n-2)^2}{2}\alpha^2 k^2\right] - \sum_{r=1}^{n-1}[1 - (2r-1)\alpha k]\left[(2r-1)\alpha k + \frac{(2r-1)^2}{2}\alpha^2 k^2\right]\right\} \quad . \quad . \quad . \quad . \quad . \quad (31)$$

It can be demonstrated that the terms in αk are zero; thus when k is very small, ignoring third-order powers of αk and above,

$$R = \frac{2\Delta f \alpha^2 k^2}{n \log_e 2}\left[\frac{1}{2} - \frac{n(n-2)^2}{2} + \sum_{r=1}^{n-2}\frac{(2r-1)^2}{2}\right] \quad . \quad (32)$$

$$= \frac{2\Delta f (n^2 - 1)\alpha^2 k^2}{6 \log_e 2} \quad . \quad . \quad . \quad . \quad . \quad . \quad . \quad (33)$$

From eqn. (6), $C = \Delta f \log_2 \left[1 + \frac{(n^2-1)k^2}{3}\right]$

which, when k is very small, becomes

$$C = \frac{2\Delta f k^2}{\log_e 2}\left(\frac{n^2 - 1}{6}\right)$$

whence
$$\lim_{k \to 0}\left(\frac{R}{C}\right) = \alpha^2 = \frac{2}{\pi} \quad . \quad . \quad . \quad . \quad . \quad (34)$$

Thus the communication efficiency in all p.c.m. systems of the type described above is 63·6% at low signal/noise ratios.

(8) EXTENSION TO SITUATION WHERE THE TRANSMISSION PATH DOES NOT HAVE A PERFECT LOW-PASS CHARACTERISTIC

If the transmission system has a pass characteristic which is not rectangular, then at the time corresponding to a particular received sample there will be a residual error due to the after effects of previous transmitted pulses. In order to evaluate $H(y)$ and $H(x, y)$ in these circumstances, the distribution of the residual error must be calculated for each of the received levels, and must be taken into account when calculating the probabilities $p'(j)$ and $p(i, j)$. If the impulse response of the transmission system is known, such a computation is straightforward, but very tedious.

(9) CONCLUSIONS

It can be seen that over a wide range of signal/noise ratios the communication efficiency of p.c.m. systems can be in the range 70–80%, and that even at very low signal/noise ratios the efficiency is greater than 60%. In existing p.c.m. systems, without error correction, the signal/noise ratios that are used are such that the communication efficiency is less than 33%. This suggests the need for the investigation of error-correcting codes which will permit the higher efficiencies quoted above to be achieved.

(10) ACKNOWLEDGMENTS

The author wishes to acknowledge the help of his wife, Dr. J. G. Billings, in the computation of the communication efficiencies.

(11) REFERENCES

(1) Oliver, B. M., Pierce, J. R., and Shannon, C. E.: 'The Philosophy of P.C.M.', *Proceedings of the Institute of Radio Engineers*, 1948, **36**, p. 1324.
(2) Shannon, C. E.: 'Communication in the presence of Noise', *ibid.*, 1949, **37**, p. 10.
(3) Shannon, C. E., and Weaver, W.: 'Mathematical Theory of Communication' (University of Illinois Press, 1949).
(4) Jelonek, Z.: 'A Comparison of Transmission Systems', Second Symposium on Information Theory, p. 44 (Butterworths Scientific Publications, 1953).

621.396.8

The Institution of Electrical Engineers
Monograph No. 299 R
Apr. 1958
©

THE USE OF EQUIVALENT SECONDARY SOURCES IN THE THEORY OF GROUND-WAVE PROPAGATION OVER AN INHOMOGENEOUS EARTH

By Z. GODZIŃSKI.

(*The paper was first received* 20*th February, and in revised form* 3*rd December*, 1957. *It was published as an* INSTITUTION MONOGRAPH *in April*, 1958.)

SUMMARY

The paper deals with the propagation of a vertically polarized ground-wave over an inhomogeneous spherical earth. On the basis of approximate boundary conditions and a specially chosen auxiliary function in Green's theorem, the integral equation for the attenuation function is derived. A general method of solving this integral equation by numerical techniques for paths composed of a number of homogeneous sections is discussed. It is proved that the result is in agreement with the reciprocity theorem.

The actual field is shown to be the superposition of the fields generated by the primary source and by secondary sources distributed along the path. It is demonstrated that the distributed secondary sources may be approximately replaced by a number of suitably chosen equivalent secondary sources. An approximate method of calculation based on this property is introduced. The method is discussed in some detail in two cases: when the paths may be regarded plane and when they extend into the diffraction zone. The proposed method makes possible a simple and rapid calculation of field strength in many practical cases. It may be used for any phase characteristic of the complex permittivity of the soil.

The paper confirms the important conclusion that placing the transmitting or receiving antenna over a well-conducting soil may considerably improve the reception. It is shown further that the electrical properties of the earth in the neighbourhood of the transmitter also have an influence on the phase of the field.

LIST OF PRINCIPAL SYMBOLS

E = Electric force, volts/m.
E = Effective value of normal component of electric field intensity, mV/m.
P' = Power radiated by a given dipole over a perfectly conducting plane, kW.
$p_0 = 300\sqrt{P'}$ = Primary source.
D = Length of the path, m or km.
x = Distance from the transmitter to the considered point of the path, m or km.
x_{j-1}, x_j = Distances from the transmitter to the ends of jth section ($x_0 = 0$), m or km.
a = Earth's radius, m.
λ = Wavelength, m.
$k = 2\pi/\lambda$ = Propagation coefficient in free space, m^{-1}.
σ = Conductivity of the ground, mhos/m.
ϵ = Relative permittivity of the ground.
ϵ' = Complex relative permittivity of the ground.
ρ = Sommerfeld's numerical distance.
$y(\rho)$ = Sommerfeld's attenuation function for plane earth.
s = Factor transforming geometrical distance into numerical distance.
s_0 = Parameter s for auxiliary homogeneous earth.
w = Attenuation function.
Subscripts of w denote the method of calculation:
t = Theoretical (correct) value.
ss = Value computed by means of secondary sources.
$\tau_0 = \alpha_0 - i\beta_0, \delta$ = Parameters in residue series [see eqns. (78), (79) and (83)].

Correspondence on Monographs is invited for consideration with a view to publication.
Mr. Godziński is at the Instytut Łączności, Wrocław, Poland.

(1) INTRODUCTION

The growing importance of modern means of telecommunication and radio-navigation has increased the interest of theoreticians as well as practical engineers in the problem of radio-wave propagation over an inhomogeneous earth. There exist at present a considerable number of theoretical investigations of this problem.[1–20] In some of them comparatively simple formulae are presented, but these are based on considerable simplifications or are valid only in certain special cases. No final formulae are available for the general case and the computations become very, and sometimes prohibitively, laborious. Furutsu[10, 11, 13, 14] and Wait[16] have performed such calculations for certain simple mixed-path problems and have shown the results in the form of plots of attenuation function. This procedure seems impossible in the general case, however, because of the large number of independent parameters: the lengths of the sections, their electrical characteristics and the frequency. There is therefore a need for practical methods of computation, sufficiently accurate and general, and at the same time rapid in application; the purpose of the paper is to meet this need.

An approximate method of calculating the propagation over mixed paths is discussed, according to which the particular parts of the path are replaced by certain equivalent secondary sources. The physical content of the method is the process of the multiple scattering of waves, except that the distributed secondary sources are replaced by appropriate discrete ones. In simpler cases the method makes possible a rapid calculation of field strength or attenuation function. If complicated paths are considered, however, the interaction between all parts of the path obviously increases the laboriousness of the method. For this reason, in another paper the two most important semi-empirical methods, namely Millington's method and the equivalent numerical-distance method, will be compared with the theory and discussed as to their practical applicability.

(2) INTEGRAL EQUATION FOR THE ATTENUATION FUNCTION

(2.1) Formulation of the Problem

The analysis in the present paper is carried out for the case in which short vertical transmitting and receiving antennas (dipoles) are situated at the points A (transmitter) and B (receiver) close to the surface of a horizontally inhomogeneous spherical earth of radius a. In the vertical direction the ground is assumed homogeneous; the atmosphere is assumed homogeneous, of relative permittivity 1. The complex relative permittivity of the ground is denoted by ϵ', and the permittivity and propagation

oefficient of free space are respectively denoted by ϵ_0 and k. The time factor is taken to be exp $(i\omega t)$.

2.2) Derivation of the Integral Equation for the Attenuation Function

As for a homogeneous spherical earth, we introduce the adial Hertzian vector, $r\Pi$, and determine the electric and nagnetic field intensities in the atmosphere outside the sources f the field from the relations

$$E = \text{curl curl } (r\Pi); \quad H = i\omega\epsilon_0 \text{ curl } (r\Pi) \quad . \quad . \quad . \quad (1)$$

The vectors E and H satisfy Maxwell's equations if the scalar unction Π satisfies the wave equation

$$\nabla^2\Pi + k^2\Pi = 0 \quad . \quad . \quad . \quad . \quad . \quad (2)$$

Eqns. (1) may be used to determine the components of E and H n spherical co-ordinates; because of the lack of complete axial ymmetry the expressions are now not as simple as for the omogeneous earth. This fact is important as regards the con-ection between the radial component of electric field intensity nd the function Π. It is easy to show that the differences etween the homogeneous-earth expressions and the present nes are generally negligible; in fact, they are connected with he change in direction of the wavefront caused by the inhomo-eneity of the ground. The most pronounced perturbations ccur on passing a land-sea boundary, giving rise to the 'coastal efraction' phenomenon. As the coastal refraction angles sually amount only to a few degrees,[2, 5, 10, 14] it may be shown hat the homogeneous-earth expressions for the components of E and H constitute generally a very good approximation in the ase of the inhomogeneous earth as well.

Of fundamental importance for the proposed theory is the ntroduction of the so-called approximate boundary conditions. These are based on the assumption that the wave propagating nside the earth has approximately the character of a plane-wave. The fact that the electrical properties of the soil are not constant in the horizontal direction may change the character of the wave propagating inside the earth and thus change also he boundary conditions; this effect will depend on the rate of variation of the earth constants.[3] Consequently the approximate oundary conditions for a homogeneous spherical earth,[21, 22, 3, 5]

$$\frac{\partial\Pi}{\partial r} = \frac{ik}{\sqrt{(\epsilon' + 1)}}\Pi \quad . \quad . \quad . \quad . \quad . \quad (3)$$

are approximately valid also for the inhomogeneous spherical earth, except at places with very rapid changes of ϵ'.[3, 5] This circumstance, important for a spherical as well as for a flat earth, has been generally disregarded in existing researches. Some investigations of Feinberg[2, 3, 5] have shown that in most practical cases such simplification is admissible. In the imme-diate neighbourhood of a boundary between different sections of a path the deviation from eqn. (3) may, however, be con-siderable, but the influence they can exert on the field charac-teristics still awaits clarification. In the present analysis we will assume boundary conditions as given by eqn. (3).

Further analysis is carried out on the basis of Green's theorem, i.e.

$$\int_V (v_g\nabla^2\Pi - \Pi\nabla^2 v_g)dV = \int_S \left(v_g\frac{\partial\Pi}{\partial n} - \Pi\frac{\partial v_g}{\partial n}\right)dS \quad . \quad (4)$$

The surface S bounding the volume V is shown in Fig. 1. It is formed by the infinitely distant surface S_∞, two very small hemi-spheres containing the sources of the field (S_A) and the point of reception (S_B), and the surface of the earth except in the immediate vicinity of points A and B (S_E). For the function v_g

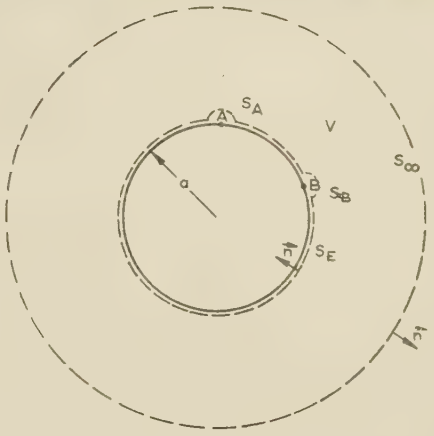

Fig. 1.—Volume and surfaces of integration in eqn. (4).

we assume, like Π, the scalar Hertzian function for a spherical earth, and only for the case when a vertical dipole is situated at the point B and the earth is homogeneous with arbitrary electrical parameters. Taking into account the singularities of the functions Π and v_g near the points A and B, applying approxi-mate boundary conditions, and using the principle of stationary phase, eqn. (4) may be reduced[15] to a one-dimensional integral equation for the attenuation function:

$$w(D) = w_{s_0}(D) - i\sqrt{\frac{D}{\pi}}\int_0^D \frac{w(x)w_{s_0}(D-x)}{\sqrt{[x(D-x)]}}(\sqrt{s} - \sqrt{s_0})dx \quad . \quad (5)$$

The path of integration in eqn. (5) is that along the great circle joining the points A and B, x and D being the distances measured from the point A along this great circle to the point of inte-gration and to the point B respectively. The parameter s is the factor transforming the geometrical distance, d, into Sommer-feld's numerical distance ρ, i.e.

$$\rho = sd; \; s = -i\frac{k}{2(\epsilon' + 1)} \quad . \quad . \quad . \quad . \quad (6)$$

This parameter changes along the path, i.e. it is a function of x. The parameter s_0 is the one for our auxiliary homogeneous earth; it is constant and quite arbitrary. The attenuation functions w are taken with respect to twice the field in free space; accordingly, at very short distances they approach unity. The arguments in parenthesis are the distances, and the subscript s_0 denotes the attenuation function over a homogeneous earth of parameter s_0. Similarly $w(x)$ and $w(D)$ denote those over the inhomogeneous earth considered at distances x and D from the transmitter; $w_{s_0}(D)$ is the attenuation function over the homogeneous earth s_0 at a distance D; and $w_{s_0}(D - x)$ is that over the homogeneous earth s_0 at a distance $D - x$, i.e. either when the transmitter is at the point B and the receiver at the point x, or when the transmitter is at the point x and the receiver at the point B.

For the path composed of several (n) homogeneous sections, eqn. (5) becomes

$$w(D) = w_{s_0}(D) - i\sqrt{\frac{D}{\pi}}\sum_{j=1}^{n}(\sqrt{s_j} - \sqrt{s_0})\int_{x_{j-1}}^{x_j}\frac{w(x)w_{s_0}(D-x)}{\sqrt{[x(D-x)]}}dx \quad . \quad . \quad . \quad . \quad (7)$$

where x_{j-1}, x_j denote the ends of the jth section with the parameter $s = s_j$.

Eqn. (7) is the fundamental integral equation of the proposed theory. In the plane-earth approximation it gives the integ-

ral equation of Feinberg's theory[2, 3, 5] and is equivalent to the 2- and 3-section plane-earth formulae of Clemmow,[6, 7] Bremmer[9] and Wait.[16] For the spherical earth also there is a good agreement with other theories. It will be shown later that for a path composed of very long sections eqn. (7) gives the same result as Furutsu obtained previously by a different method.[12–14] Wait, in his investigations,[19] obtained for 2-section paths the same formula as eqn. (7), and Bremmer very recently[20] derived an expression essentially equivalent to it.

The approximations used in the derivation of eqn. (7) are twofold. First, there is the adoption of the stationary-phase principle, which means *inter alia* that no great changes of electrical earth parameters occur in the direction perpendicular to the path within the first few Fresnel zones. In conditions where considerable lateral inhomogeneities may be found, deviations from eqn. (7) must be expected. Secondly, there is the approximation which gives, as Fresnel zones, ellipses with a major axis equal to D instead of a somewhat greater value. This approximation is also to be found in other theoretical investigations and may be of some influence for the points of the path lying in the immediate vicinity of the boundary between two different sections. This is another justification for a more thorough investigation of the transition regions.

(2.3) Evaluation of the Attenuation Function

The great advantage of the integral equation (7) is the ease with which it makes possible the calculation of propagation characteristics for every multi-section path. To this end we make use of the arbitrariness of s_0, which is a direct consequence of the auxiliary homogeneous earth previously introduced of arbitrary parameter s_0; this ingenious method of attack is due to Feinberg.[2, 3, 5]

The attenuation function over the first section is the same as over a homogeneous ground with the parameter $s = s_1$. In order to compute the attenuation function over the second section, $s_0 = s_2$ is assumed. The integral in eqn. (7) then vanishes along the second section and the remaining integral can be calculated. Having computed in this way the course of the attenuation function along the second section, we assume $s_0 = s_3$; thus the integral along the third section vanishes and the remaining integrals along the first and second sections can be computed, etc.

In practical calculations a convenient unit of length is 1 km; eqn. (6) for s then becomes

$$s = \frac{\pi \times 10^3}{\lambda[60\sigma\lambda + i(\epsilon + 1)]} \quad . \quad . \quad . \quad . \quad . \quad (8)$$

where the wavelength λ is given in metres and the conductivity of the ground σ in M.K.S. units; s is then given in (kilometres)$^{-1}$. Curves of $|s|$ as a function of λ for typical soils are plotted in Fig. 2.

The calculation of the attenuation function according to eqn. (7) is in principle very simple; in practice, however, the computations are generally very laborious. In subsequent Sections an approximate method of calculation will be presented based on the concept of equivalent secondary sources. Some formulae will also be given which have been derived in simpler cases directly from eqn. (7).

(3) EQUIVALENT SECONDARY SOURCES

(3.1) Introduction of Secondary Sources

The electric field intensity depends on the electric moment of the radiating dipole. If, instead, we characterize the source by the radiated power, we obtain for the normal component of electric field intensity the well-known formula

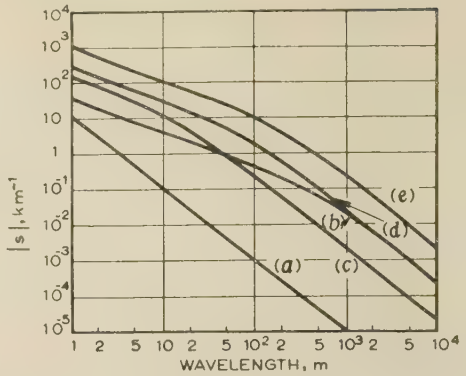

Fig. 2.—Variation of $|s|$ with wavelength for typical soils.
(*a*) Sea ($\epsilon = 80$; $\sigma = 4{\cdot}5$ mhos/m).
(*b*) Fresh water ($\epsilon = 80$; $\sigma = 2 \times 10^{-3}$ mho/m).
(*c*) Wet soil ($\epsilon = 20$; $\sigma = 2 \times 10^{-2}$ mho/m).
(*d*) Average soil ($\epsilon = 10$; $\sigma = 2 \times 10^{-3}$ mho/m).
(*e*) Dry soil ($\epsilon = 2$; $\sigma = 2 \times 10^{-4}$ mho/m).

$$E(D) = 300 \frac{\sqrt{P'}}{D} w(D) \quad . \quad . \quad . \quad . \quad . \quad (9)$$

In this formula E is the effective value of the field strength in millivolts per metre, D is the distance in kilometres, and P' is the power, in kilowatts, which the dipole of a given electric moment would radiate over a perfectly conducting plane. In eqn. (9) the rapidly varying factor $\exp(-ikD)$ has been omitted as it has no influence on the subsequent discussion. To simplify the notation we will call $300\sqrt{P'}$ the primary source p_0, i.e.

$$p_0 = 300\sqrt{P'} \quad . \quad . \quad . \quad . \quad . \quad . \quad (10)$$

Eqn. (9) then becomes $E(D) = \frac{p_0}{D} w(D)$ . . . . . (11)

Multiplying both sides of eqn. (7) by p_0/D, we obtain

$$E(D) = E_{s_0}(D) - \frac{i}{\sqrt{\pi}} \sum_{j=1}^{n} (\sqrt{s_j} - \sqrt{s_0}) \int_{x_{j-1}}^{x_j} \left[E(x) \sqrt{\left(x \frac{D-x}{D} \right)} dx \right] \frac{w_{s_0}(D-x)}{D-x} \quad . \quad (12)$$

In this formula $E_{s_0}(D)$ denotes the field which would be produced by the given sources at a distance D over a homogeneous earth of $s = s_0$, and $E(x)$ denotes the field existing at the point x over the inhomogeneous earth under consideration. Eqn. (12) may be interpreted as follows:

For the calculation of the electric field over an inhomogeneous earth we may formally assume the earth to be homogeneous with a certain (arbitrary) parameter $s = s_0$. The electric field $E(D)$ is then the superposition of the field $E_{s_0}(D)$ produced by the primary source p_0 and the fields produced by the secondary sources dp distributed along the path given by

$$dp = -\frac{i}{\sqrt{\pi}} (\sqrt{s} - \sqrt{s_0}) E(x) \sqrt{\left(x \frac{D-x}{D} \right)} dx \quad . \quad (13)$$

Eqn. (12) thus becomes

$$E(D) = E_{s_0}(D) + \int_0^D dp \frac{w_{s_0}(D-x)}{D-x} \quad . \quad . \quad . \quad (14)$$

The intensity of the secondary sources is not constant but

depends on the distance D by the factor $[x(D-x)/D]^{1/2}$. It may be shown[15] that this factor is related to the width of the area within the few first Fresnel zones, which, according to Feinberg,[2,3] may be regarded as the effective path of the radio waves.

(3.2) Agreement with the Reciprocity Theorem

One general problem of great importance must be mentioned at this point; it is the question whether eqn. (7) satisfies the reciprocity theorem. When discussing this problem we may formally assume the earth to be homogeneous of some parameter $s = s_0$ and calculate the field as the superposition of the fields of the primary source and the secondary sources distributed along the path. The secondary sources are, however, proportional to the field intensity at the point considered, and this field in turn is the result of the superposition of the fields of the primary source and all secondary sources preceding this point. Consequently, the field at the point of reception represents the superposition of the fields, being the result of the interaction of all elements of the path in all combinations of successive elements; the transmitting antenna is regarded here as the first element. Considering one of such combinations of successive elements, it is easy to prove[15] that the partial field thus produced satisfies the reciprocity theorem. Consequently, the total field, being the sum of such partial ones, will also satisfy the reciprocity theorem.

The agreement with the reciprocity theorem is of great importance, not only because it ensures that in the course of the analysis no inadmissible simplifications have been made, but also since it makes it possible during the calculation to place the primary source at this end of the path, which is more convenient as regards the errors or the laboriousness of computations.

The above discussion is important also in another respect, i.e. it has shown that mixed-path propagation is in fact a process of multiple scattering.

(3.3) Introduction of Equivalent Secondary Sources

As mentioned before, secondary sources dp depend on distance; it proves convenient to introduce secondary sources dp_∞, calculated for $D = \infty$ and therefore independent of D:

$$dp_\infty = -\frac{i}{\sqrt{\pi}}(\sqrt{s}-\sqrt{s_0})E(x)(\sqrt{x})dx; \quad dp = dp_\infty\sqrt{\frac{D-x}{D}} \quad . \quad (15)$$

Eqn. (14) then becomes

$$E(D) = E_{s_0}(D) + \int_0^D dp_\infty \sqrt{\left(\frac{D-x}{D}\right)}\ \frac{w_{s_0}(D-x)}{D-x} \quad (16)$$

Let us consider the partial field $E_{d_1d_2}$ produced by secondary sources placed over the section $d_1 < x < d_2$; it is given by

$$E_{d_1d_2} = \int_{d_1}^{d_2} dp_\infty \sqrt{\left(\frac{D-x}{D}\right)}\ \frac{w_{s_0}(D-x)}{D-x} \quad . \quad . \quad (17)$$

For simplicity we put

$$\sqrt{\left(\frac{D-x}{D}\right)}\ \frac{w_{s_0}(D-x)}{D-x} = \mathrm{F}(x)$$

Expanding $\mathrm{F}(x)$ in a Taylor series about a certain point $x = \xi$, we obtain

$$E_{d_1d_2} = \mathrm{F}(\xi)\int_{d_1}^{d_2} dp_\infty + \mathrm{F}'(\xi)\int_{d_1}^{d_2}(x-\xi)dp_\infty + \tfrac{1}{2}\mathrm{F}''(\xi)\int_{d_1}^{d_2}(x-\xi)^2 dp_\infty + \ldots \quad . \quad (18)$$

For not too large distances $(x-\xi)$ the third term in eqn. (18) is very small. If we demand that the second term be equal to zero, we obtain

$$\xi = \frac{\int_{d_1}^{d_2} x dp_\infty}{\int_{d_1}^{d_2} dp_\infty} \quad . \quad . \quad . \quad . \quad . \quad . \quad . \quad (19)$$

Because of the complex character of dp_∞, eqn. (19) in general cannot be satisfied; consequently we modify it and demand that*

$$\xi = \frac{\int_{d_1}^{d_2} |x dp_\infty|}{\left|\int_{d_1}^{d_2} dp_\infty\right|} \quad . \quad . \quad . \quad . \quad . \quad . \quad . \quad (20)$$

Denoting

$$p_{d_1d_{2\infty}} = \int_{d_1}^{d_2} dp_\infty; \quad p_{d_1d_2} = p_{d_1d_{2\infty}}\sqrt{\frac{D-\xi}{D}} \quad . \quad . \quad (21)$$

we obtain finally

$$E_{d_1d_2} \simeq p_{d_1d_2}\frac{w_{s_0}(D-\xi)}{D-\xi} = p_{d_1d_{2\infty}}\sqrt{\left(\frac{D-\xi}{D}\right)}\ \frac{w_{s_0}(D-\xi)}{D-\xi} \quad (22)$$

The result just obtained may also be formulated in terms of the attenuation function. From eqns. (22) and (11) we may regard the attenuation function $w(D)$ as the superposition of the contributions from the primary source and the secondary sources. The contribution from the part of the path considered is then

$$\Delta w_{d_1d_2} = \frac{D}{p_0}E_{d_1d_2} = \frac{p_{d_1d_{2\infty}}}{p_0}\sqrt{\left(\frac{D}{D-\xi}\right)}w_{s_0}(D-\xi) \quad (23)$$

Eqn. (23) states that the secondary sources distributed over the section of the path $d_1 < x < d_2$ may be replaced by a single equivalent secondary source p_{d1d2} placed at their 'centre of gravity' at the point $x = \xi$. The site of this equivalent secondary source does not depend on the distance D; its magnitude does depend, however, on distance in the same manner as do the elementary secondary sources dp.

An important property of the equivalent secondary sources is the ease with which they can be calculated for any value of s_0. In fact, if, for a certain $s_0 = s_0'$, they are equal to p', then according to eqns. (15) and (21) their value p'' for another $s_0 = s_0''$ is given by

$$p'' = \frac{\sqrt{s}-\sqrt{s_0''}}{\sqrt{s}-\sqrt{s_0'}}p' \quad . \quad . \quad . \quad . \quad . \quad (24)$$

The introduction of equivalent secondary sources is important not only because it leads to an approximate method of computation but also because it helps to provide a clearer picture of the phenomena occurring. We will illustrate this by one general conclusion regarding the errors of computation. In some cases the primary source and the secondary sources may cancel one another almost completely. In such cases the calculations—by all methods—must be performed especially carefully if excessive errors are to be avoided.

(4) INFLUENCE ON THE FIELD OF A SMALL INHOMOGENEITY OF THE PATH

The investigation of the change of the field due to an inhomogeneity on an otherwise homogeneous path can give a valuable insight into the mechanism of the influence of particular parts

* The consideration of the way in which the contributions from the elements of the path are added together to form the field $E_{d_1d_2}$ has led to the conclusion that it would be more suitable to accept eqn. (20) than to assume for ξ simply the modulus of the right-hand side of eqn. (19).

of the path on the field. The analysis can be made very simple under the assumption that the inhomogeneity is constituted by a very short section of length dx, placed at the point x and characterized by the parameter s' different from s for the rest of the path. The 'primary' field which would exist at the point of reception over the homogeneous path s would be equal to

$$E_{pr} = \frac{p_0}{D} w_s(D) \quad . \quad . \quad . \quad . \quad . \quad . \quad (25)$$

In order to compute the field in the presence of the inhomogeneity, we assume $s_0 = s$ and sum the fields from the primary source p_0 and the secondary source dp. The change of the field dE with respect to the primary field E_{pr} will be produced by the secondary source dp:

$$dE = \frac{dp}{D-x} w_s(D-x)$$

$$= -\frac{i}{\sqrt{\pi}}(\sqrt{s'} - \sqrt{s}) E(x) \sqrt{\left[\frac{x}{D(D-x)}\right]} w_s(D-x)dx \quad . \quad (26)$$

The assumption of a very small length of the section s' enables us to take for the field $E(x)$ approximately the value which would exist at the point x on a homogeneous path s. The relative change of the field is thus

$$\frac{dE}{E_{pr}} = -\frac{i}{\sqrt{\pi}}(\sqrt{s'} - \sqrt{s}) \frac{\sqrt{D}}{\sqrt{[x(D-x)]}} \frac{w_s(x) w_s(D-x)}{w_s(D)} dx \quad . \quad (27)$$

Eqn. (27) shows clearly that the influence of the inhomogeneity depends strongly on its location over the path. It is greatest for small distances from the transmitter or receiver, and least for locations in the middle of the path.

As an example we will consider eqn. (27) for not too great distances, i.e. we will use the plane-earth approximation; eqn. (27) then becomes

$$\frac{dE}{E_{pr}} = i\frac{\sqrt{s} - \sqrt{s'}}{\sqrt{s}} \left\{ \sqrt{\frac{\rho}{\pi}} \frac{y\left(\frac{x}{D}\rho\right) y\left[\left(1 - \frac{x}{D}\right)\rho\right]}{y(\rho)\sqrt{\left[\frac{x}{D}\left(1 - \frac{x}{D}\right)\right]}} \right\} \frac{dx}{D}$$

$$= i\frac{\sqrt{s} - \sqrt{s'}}{\sqrt{s}} \eta \frac{dx}{D} \quad . \quad . \quad . \quad . \quad . \quad . \quad . \quad . \quad . \quad (28)$$

where $\rho = sD$. The function η has been computed for a few values of ρ; the corresponding curves are shown in Fig. 3. For small numerical distances the influence of the inhomogeneity is also very small, since the attenuation of the wave is then insignificant. As ρ increases, this influence increases at first and then begins to diminish rapidly.

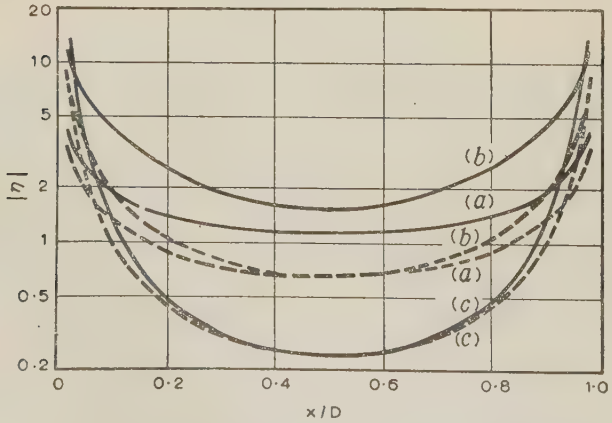

Fig. 3.—Curves of the function $|\eta|$ from eqn. (28).
(*a*) $|\rho| = 1$. (*b*) $|\rho| = 10$. (*c*) $|\rho| = 100$.
——— $\psi = 0°$; — — $\psi = 90°$. $\psi = \arctan \frac{\epsilon + 1}{60\sigma\lambda}$.

The results given here are valid in principle only for infinitely small inhomogeneities. They present, however, a possibility of ascertaining in practical cases whether an exact calculation of the influence of a given inhomogeneity is indispensable, or if it is sufficient to estimate it, or, finally, if it may even be completely disregarded. These results are also of great importance as regards the understanding of the phenomena occurring.

(5) CALCULATION OF SHORT MIXED PATHS IN THE PLANE-EARTH APPROXIMATION BY MEANS OF EQUIVALENT SECONDARY SOURCES

(5.1) General Formulae

Assuming a plane earth, eqn. (7) takes the form

$$w(D) = y(s_0 D) - i\sqrt{\frac{D}{\pi}} \sum_{j=1}^{n} (\sqrt{s_j} - \sqrt{s_0}) \int_{x_{j-1}}^{x_j} \frac{w(x) y[s_0(D-x)]}{\sqrt{[x(D-x)]}} dx$$

. . . . (29)

where y is Sommerfeld's attenuation function for a plane earth, and $s_0 D$, $s_0(D-x)$ are numerical distances [see eqn. (6)].

We will consider first the equivalent secondary sources over the first section of the path for the part lying between the points d_1 and d_2 (where $d_1 < x < d_2$). According to eqns. (11), (15) and (21),

$$p_{d_1 d_2 \infty} = -\frac{i}{\sqrt{\pi}}(\sqrt{s} - \sqrt{s_0}) p_0 \int_{d_1}^{d_2} \frac{y(sx)}{\sqrt{x}} dx \quad . \quad . \quad (30)$$

Denoting the numerical distance by ρ and using the relation given by Bremmer,[9]

$$\frac{1}{n!}\int_0^{\rho_1} y(\rho)\rho^{n-\frac{1}{2}} d\rho = -i(\sqrt{\pi}) - \sum_{m=0}^{n} \frac{\rho_1^{m-\frac{1}{2}}}{m!}\left[y(\rho_1) + \frac{1}{2m-1}\right] \quad . \quad (31)$$

we introduce a new function $v(\rho)$, where

$$v(\rho_1) = -\frac{i}{\sqrt{\pi}} \int_0^{\rho_1} \frac{y(\rho)}{\sqrt{\rho}} d\rho = -1 - i\frac{1 - y(\rho_1)}{\sqrt{(\pi\rho_1)}} \quad . \quad (32)$$

Eqn. (30) then takes the form

$$p_{d_1 d_2 \infty} = p_0 \frac{\sqrt{s} - \sqrt{s_0}}{\sqrt{s}} [v(sd_2) - v(sd_1)] \quad . \quad . \quad (33)$$

Polar diagrams of the function $v(\rho)$ for five phase angles of the parameter s are shown in Fig. 4; they have been computed by means of Karpov's tables.[23] The asymptotic formulae for $v(\rho)$ are:

For small ρ ($|\rho| \ll 1$),

$$v(\rho) = -i\frac{2}{\sqrt{\pi}}\rho^{1/2} - \rho + i\frac{4}{3\sqrt{\pi}}\rho^{3/2} + \ldots \quad . \quad (34)$$

For large ρ ($|\rho| \geqslant 10$),

$$v(\rho) \simeq -1 - \frac{i}{\sqrt{(\pi\rho)}} \quad . \quad . \quad . \quad . \quad (35)$$

In order to compute the position of the centre of gravity ξ of the secondary sources, we use eqn. (20), which gives

$$|\bar{\rho}| = |s\bar{\xi}| = \frac{\int_0^{\rho_2} |\rho dv(\rho)| - \int_0^{\rho_1} |\rho dv(\rho)|}{|v(\rho_2) - v(\rho_1)|} \quad . \quad . \quad (36)$$

where $\rho_1 = sd_1$ and $\rho_2 = sd_2$.

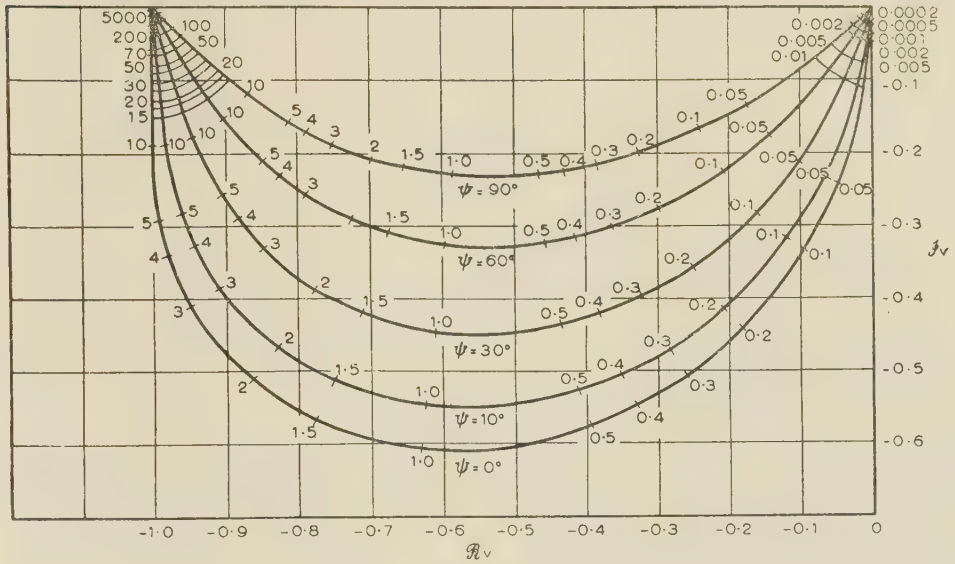

Fig. 4.—Polar diagrams of function $v(\rho)$ for the parameter $\psi = \arctan \frac{\epsilon + 1}{60\sigma\lambda}$.

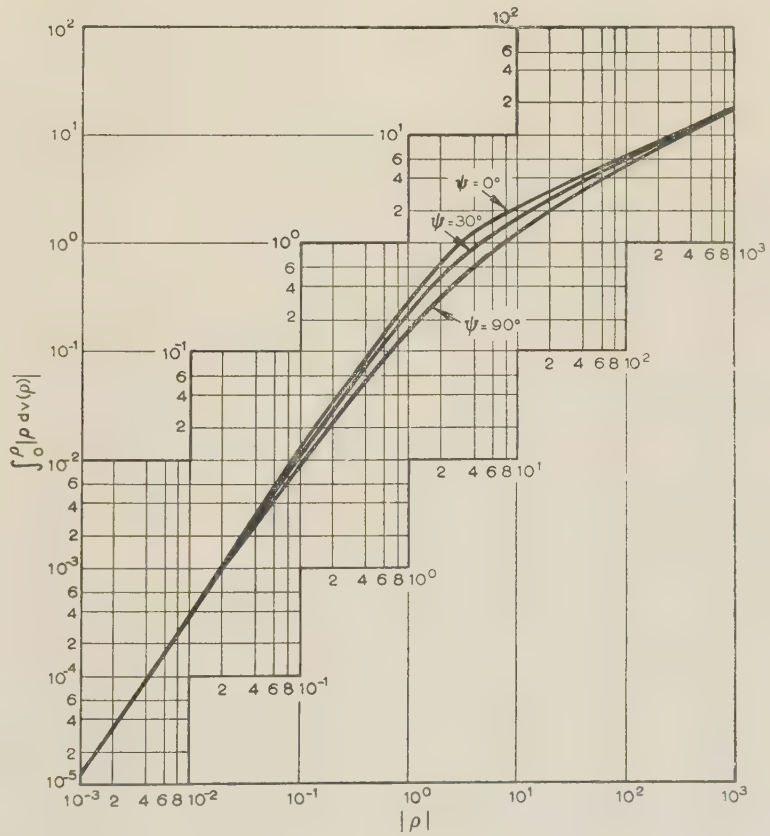

Fig. 5.—$\int_0^\rho |\rho dv(\rho)| = f(|\rho|)$ for the parameter $\psi = \arctan \frac{\epsilon + 1}{60\sigma\lambda}$.

The integrals occurring in eqn. (36) have been computed for three phase angles of the parameter s; corresponding curves are shown in Fig. 5. For very large and very small numerical distances eqn. (36) can be evaluated analytically, giving

For very large ρ, $\xi \simeq \sqrt{(d_1 d_2)}$ . . . . . (37)

For very small ρ, $\xi \simeq \frac{1}{3}[d_1 + \sqrt{(d_1 d_2)} + d_2]$. (38)

For $d_1 = 0$, $d_2 = d$, eqn. (38) gives

$$\xi \simeq \tfrac{1}{3} d \quad . \quad . \quad . \quad . \quad . \quad . \quad (39)$$

In Fig. 6 are shown curves of ξ/d for the section at the antenna ($d_1 = 0$, $d_2 = d$). It follows from them that the larger the numerical distance $\rho = sd$, the smaller the ratio ξ/d.

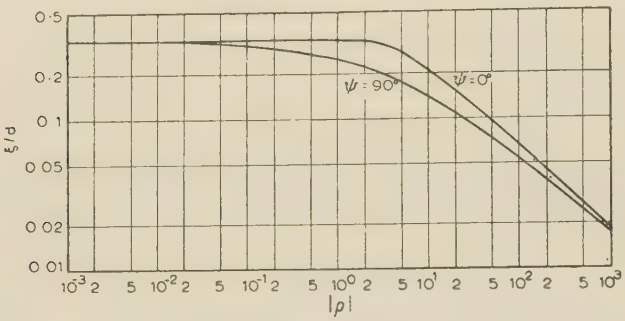

Fig. 6.—Variation of ξ/d with $|\rho|$ for section at the antenna; $\psi = \arctan \frac{\epsilon}{60\sigma\lambda}$.

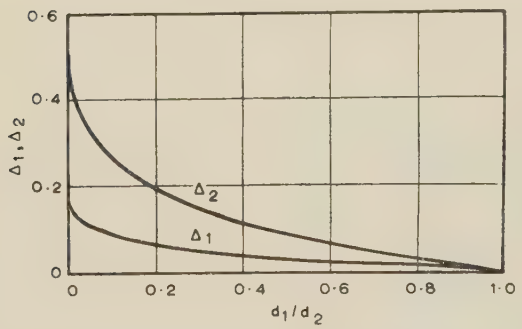

Fig. 7.—Relative differences between the arithmetic mean and values calculated according to eqns. (37) and (38).

$$\Delta_1 = \frac{\frac{1}{2}(d_1 + d_2) - \frac{1}{3}[d_1 + \sqrt{(d_1 d_2)} + d_2]}{d_2 - d_1}; \quad \Delta_2 = \frac{\frac{1}{2}(d_1 + d_2) - \sqrt{(d_1 d_2)}}{d_2 - d_1}$$

Where the ratio d_2/d_1 is not too large, we may take for ξ instead of eqns. (37) and (38) simply the arithmetical mean, $\xi = \frac{1}{2}(d_1 + d_2)$; the relative deviations from the correct values are shown in Fig. 7.

Where the first section of the path is sea, we may often assume it to be perfectly conducting, which gives $s = 0$. By virtue of expansion (34), eqn. (33) then takes the form

$$p_{d_1 d_2 \infty} = i\frac{2}{\sqrt{\pi}} p_0[\sqrt{(s_0 d_2)} - \sqrt{(s_0 d_1)}] \quad . \quad . \quad (40)$$

For the calculation of ξ we use in such cases eqns. (38) and (39).

The equivalent secondary sources over the farther sections of the path may be calculated in an essentially similar way as for the first section.[15] Because of the practical applications we will consider only the equivalent secondary sources for the second section of the path when it is relatively short. Analysing this problem we make use of the reciprocity theorem and of the results just obtained for the first section of the path. After an easy but somewhat lengthy calculation it may be shown[15] that the equivalent secondary sources $p_{2\infty}$ for a short second section are given by

$$p_{2\infty} = p_{2\infty}^{(0)} + p_{2\infty}^{(1)} \quad . \quad . \quad . \quad . \quad . \quad (41)$$

where $$p_{2\infty}^{(0)} = p_0 \frac{\sqrt{s_2} - \sqrt{s_0}}{\sqrt{s_1}}[v(s_1 x_2) - v(s_1 x_1)] \quad . \quad . \quad (42)$$

$$p_{2\infty}^{(1)} = p_0 \frac{\sqrt{s_2} - \sqrt{s_0}}{\sqrt{s_2}} \frac{\sqrt{s_2} - \sqrt{s_1}}{\sqrt{s_2}} \frac{y[s_1(\xi_2 - \xi_2')]}{\sqrt{[s_2(\xi_2 - \xi_2')]}} u[s_2(x_2 - x_1)]$$
$$. \quad . \quad . \quad . \quad (43)$$

The notations used in eqns. (42) and (43) are partly illustrated by Fig. 8. ξ_2 denotes the position of the centre of gravity of

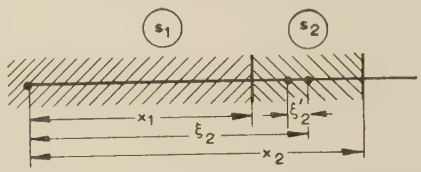

Fig. 8.—Notations used in eqns. (42) and (43).

secondary sources over the second section of the path. An examination of eqns. (20) and (41) shows that for practical purposes the centre of gravity may be placed in the middle of the section, i.e.

$$\xi_2 \simeq \tfrac{1}{2}(x_1 + x_2) \quad . \quad . \quad . \quad . \quad . \quad . \quad (44)$$

ξ_2' denotes the position of the centre of gravity of the first section of a path, which would be created by placing the transmitting antenna at the point ξ_2 (see Fig. 8). In other words, ξ_2' is the position of the centre of gravity of the first section, having the length $\frac{1}{2}(x_2 - x_1)$ and parameter $s = s_2$.

In eqn. (43) there has been introduced also a new function, $u(\rho)$, defined by

$$u(\rho_1) = -\frac{i}{\sqrt{\pi}} \int_0^{\rho_1} v(\rho) d\rho = \frac{i}{\sqrt{\pi}} \left[v(\rho_1) + \rho_1 + i\frac{2}{\sqrt{\pi}} \sqrt{\rho_1} \right] . \quad (45)$$

The polar diagrams of the function $u(\rho)$ for five phase angles of the parameter s are shown in Figs. 9 and 10. The asymptotic formulae for $u(\rho)$ are as follows:

For small ρ ($|\rho| \ll 1$),

$$u(\rho) = -\frac{4}{3\pi}\rho^{3/2} + \frac{i}{2\sqrt{\pi}}\rho^2 + \frac{8}{15\pi}\rho^{5/2} - \ldots \quad . \quad (46)$$

For large ρ ($|\rho| \geqslant 10$),

$$u(\rho) \simeq \frac{i}{\sqrt{\pi}}\rho - \frac{2}{\pi}\sqrt{\rho} - \frac{i}{\sqrt{\pi}} \quad . \quad . \quad . \quad (47)$$

In cases of land-sea paths we may often assume $s = 0$ for sea sections; eqns. (42) and (43) then take the form:

(*a*) $s_1 = 0$ (first section sea, second section land)

$$p_{2\infty}^{(0)} = -i\frac{2}{\sqrt{\pi}} p_0(\sqrt{s_2} - \sqrt{s_0})(\sqrt{x_2} - \sqrt{x_1}) \quad . \quad (48)$$

$$p_{2\infty}^{(1)} = p_0 \frac{\sqrt{s_2} - \sqrt{s_0}}{\sqrt{s_2}} \frac{u[s_2(x_2 - x_1)]}{\sqrt{[s_2(\xi_2 - \xi_2')]}} \quad . \quad . \quad (49)$$

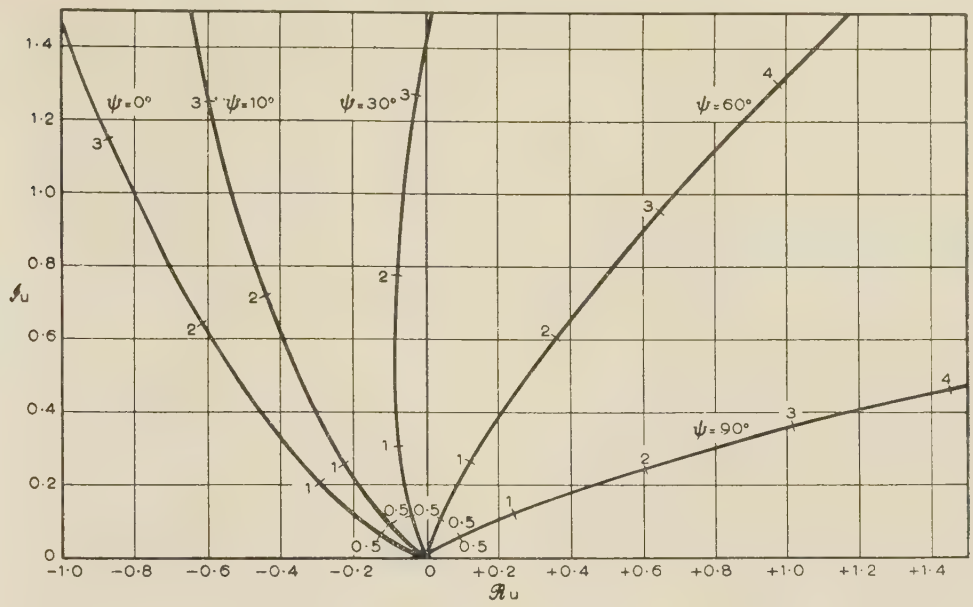

Fig. 9.—Polar diagrams of function $u(\rho)$ for small numerical distances; $\psi = \arctan \frac{\epsilon + 1}{60\sigma\lambda}$.

(*b*) $s_2 = 0$ (first section land, second section sea)

$$p_{2\infty}^{(0)} = -p_0\left(\sqrt{\frac{s_0}{s_1}}\right)[v(s_1x_2) - v(s_1x_1)] \quad . \quad . \quad (50)$$

$$p_{2\infty}^{(1)} = -\frac{4}{3\pi}p_0\sqrt{\left[s_0s_1\frac{(x_2 - x_1)^3}{\xi_2 - \xi_2'}\right]}y[s_1(\xi_2 - \xi_2')] \quad . \quad (51)$$

(5.2) Two-Section Paths

The results so far obtained make possible a simple calculation of the field in some important mixed-path problems. As a first example we will consider a 2-section path with a comparatively short first section (Fig. 11). Since, according to the reciprocity theorem, we may interchange transmitter and receiver, the above assumption means that we discuss, in fact, the more general problem of a 2-section path with one section short as compared with the other. We assume $s_0 = s_2$ and replace the first section by one equivalent secondary source p_1, placed at the point ξ_1. From eqns. (33) and (21),

$$p_1 = p_0\frac{\sqrt{s_1} - \sqrt{s_2}}{\sqrt{s_1}}v(s_1x_1)\sqrt{\frac{D - \xi_1}{D}} \quad . \quad . \quad (52)$$

The field strength $E(D)$ at the point B is then

$$E(D) = p_0\frac{y(s_2D)}{D} + p_1\frac{y[s_2(D - \xi_1)]}{D - \xi_1}$$

$$= \frac{p_0}{D}\left\{y(s_2D) + \frac{\sqrt{s_1} - \sqrt{s_2}}{\sqrt{s_1}}v(s_1x_1)\sqrt{\left(\frac{D}{D - \xi_1}\right)}y[s_2(D - \xi_1)]\right\}$$

. . . . . (53)

and the attenuation function for the path is

$$w(D) = y(s_2D) + \frac{\sqrt{s_1} - \sqrt{s_2}}{\sqrt{s_1}}v(s_1x_1)\sqrt{\left(\frac{D}{D - \xi_1}\right)}y[s_2(D - \xi_1)]$$

. . . . . (54)

If $x_1 \ll D$, we may consider $\xi_1 \simeq 0$; then

$$w(D) \simeq y(s_2D)\left[1 + \frac{\sqrt{s_1} - \sqrt{s_2}}{\sqrt{s_1}}v(s_1x_1)\right] \quad . \quad . \quad (55)$$

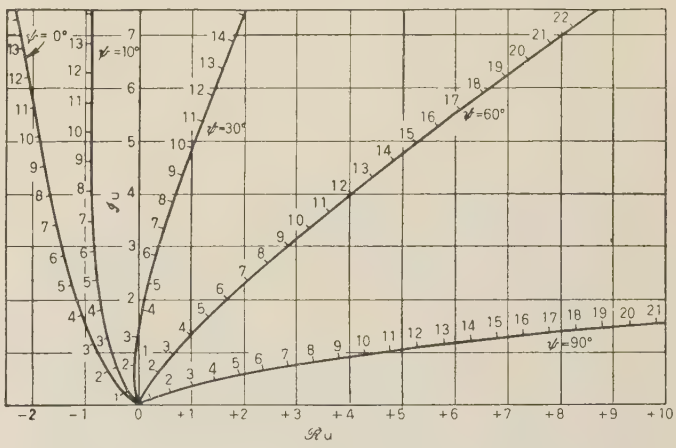

Fig. 10.—Polar diagrams of function $u(\rho)$ for large numerical distances; $\psi = \arctan \frac{\epsilon + 1}{60\sigma\lambda}$.

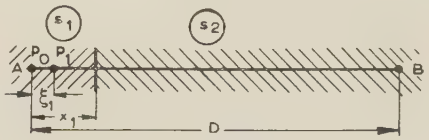

Fig. 11.—Two-section path with a comparatively short first section.

An example is given in Fig. 12, which shows clearly that a considerable increase of field strength can be achieved by suitably locating the transmitting antenna.

On the basis of the reciprocity theorem we may also use eqn. (55) when computing the field on the second section at points near the boundary of the first section. After an obvious change of notation, we obtain for the path (from Fig. 13)

$$w(D) \simeq y(s_1D)\left[1 + \frac{\sqrt{s_2} - \sqrt{s_1}}{\sqrt{s_2}}v(s_2\delta)\right] \quad . \quad . \quad (56)$$

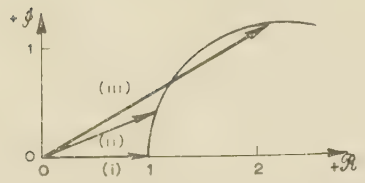

Fig. 12.—Increase of the field strength due to the presence of a well-conducting section near the transmitting antenna.

Diagram of the factor $\left[1 + \frac{\sqrt{s_1} - \sqrt{s_2}}{\sqrt{s_1}} v(s_1 x_1)\right]$ from eqn. (55). Parameters s_1 and s_2 real; $s_1 \ll s_2$. Vectors (i), (ii) and (iii) correspond successively to an increasing length of a well-conducting section.

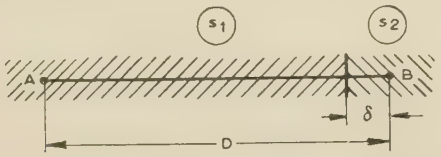

Fig. 13.—Two-section path with a very short second section.

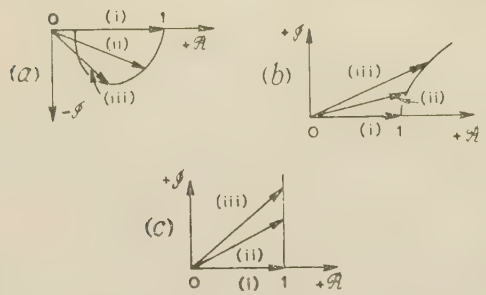

Fig. 14.—Field changes on passing the boundary.

Diagrams of the factor $\left[1 + \frac{\sqrt{s_2} - \sqrt{s_1}}{\sqrt{s_2}} v(s_2\delta)\right]$ from eqn. (56). Parameters s_1 and s_2 real. Vectors (i), (ii) and (iii) correspond successively to an increasing distance from the boundary.

(*a*) $s_2 \gg s_1$. (*b*) $s_2 \ll s_1$. (*c*) $s_2 = 0$.

Some examples of field changes on passing the boundary of the first section are shown in Fig. 14. It is interesting to note that in the transition to a much better-conducting ground a considerable increase of field strength can take place; this is a well-known 'recovery effect'.

So far we have discussed the field intensity; it is interesting, however, to consider also the phase of the wave. According to eqn. (55) and Fig. 12, the properties of the ground near the transmitting antenna will influence not only the amplitude of the field but also its phase. This can perhaps give some explanation of the recent experiments of Pressey, Ashwell and Fowler on radio aids to navigation.[24, 25]

For similar reasons the phase of the wave changes after transition to a differently conducting ground. Eqn. (56) and Fig. 14 show that, on passing to a better-conducting soil, the phase velocity of the wave should increase; on passing the boundary in the reverse direction the phase velocity should diminish. This conclusion is essentially in agreement with the results of measurements made by Pressey, Ashwell and Fowler.[26, 24, 25]

Where the sections of a 2-section path have comparable lengths, it may be necessary to use more than one equivalent secondary source. How many secondary sources are to be used depends on the ratio between the geometrical lengths of the sections, on the numerical distances they represent, and finally on the degree of inhomogeneity of the path. The first circumstance is obvious. The second arises from the fact that for

Table 1

RATIO $w(D)_{ss}/w(D)_t$ FOR A NUMBER OF LAND-SEA PATHS

$\lvert s_l/l_l \rvert$	ψ_l	l_l/D	$w(D)_t$	$w(D)_{ss}/w(D)_t$								
				Number of secondary sources (on land)					Number of secondary sources (on sea)			
				1		2	3	1		2	3	
				$\xi_1 = 0$	$\xi_1 \neq 0$			$\xi_1 = 0$	$\xi_1 \neq 0$			
1·5	0°	$\frac{1}{3}$	$0{\cdot}59 \angle -73°$	$1{\cdot}03 \angle 5°$	$1{\cdot}06 \angle 0°$	$1{\cdot}02 \angle 0°$		$0{\cdot}69 \angle -31°$	$0{\cdot}95 \angle -12°$	$0{\cdot}99 \angle -3°$		
		$\frac{2}{3}$	$0{\cdot}58 \angle -77°$	$1{\cdot}05 \angle 9°$	$1{\cdot}10 \angle 1°$	$1{\cdot}03 \angle -1°$		$0{\cdot}89 \angle -18°$	$1{\cdot}01 \angle -4°$			
		1	$0{\cdot}57 \angle -82°$	$1{\cdot}06 \angle 14°$	$1{\cdot}14 \angle 3°$	$1{\cdot}03 \angle 0°$		$0{\cdot}98 \angle -9°$	$1{\cdot}01 \angle -1°$			
	90°	$\frac{1}{3}$	$0{\cdot}39 \angle -34°$	$1{\cdot}06 \angle 2°$	$1{\cdot}02 \angle -1°$			$0{\cdot}72 \angle -9°$	$0{\cdot}91 \angle -3°$	$0{\cdot}97 \angle 0°$		
		$\frac{2}{3}$	$0{\cdot}37 \angle -36°$	$1{\cdot}11 \angle 4°$	$1{\cdot}04 \angle -1°$			$0{\cdot}84 \angle -4°$	$0{\cdot}97 \angle 0°$			
		1	$0{\cdot}35 \angle -39°$	$1{\cdot}18 \angle 7°$	$1{\cdot}08 \angle -1°$	$1{\cdot}01 \angle -1°$		$0{\cdot}93 \angle -3°$	$0{\cdot}99 \angle 0°$			
10	0°	$\frac{1}{3}$	$0{\cdot}16 \angle -95°$	$1{\cdot}16 \angle 5°$	$1{\cdot}22 \angle -6°$	$1{\cdot}04 \angle -3°$		$0{\cdot}55 \angle -7°$	$0{\cdot}81 \angle -3°$	$0{\cdot}94 \angle -2°$	$0{\cdot}96 \angle -1°$	
		$\frac{2}{3}$	$0{\cdot}15 \angle -101°$	$1{\cdot}29 \angle 11°$	$1{\cdot}41 \angle -5°$	$1{\cdot}09 \angle -1°$	$1{\cdot}04 \angle 0°$	$0{\cdot}68 \angle -5°$	$0{\cdot}90 \angle -1°$	$0{\cdot}96 \angle 0°$		
		1	$0{\cdot}12 \angle -108°$	$1{\cdot}54 \angle 18°$	$1{\cdot}77 \angle -3°$	$1{\cdot}21 \angle 0°$	$1{\cdot}11 \angle 1°$	$0{\cdot}83 \angle -4°$	$0{\cdot}98 \angle 0°$	$1{\cdot}00 \angle 0°$		
	90°	$\frac{1}{3}$	$0{\cdot}16 \angle -45°$	$1{\cdot}11 \angle 3°$	$1{\cdot}02 \angle -3°$	$0{\cdot}99 \angle 0°$		$0{\cdot}61 \angle -4°$	$0{\cdot}84 \angle -2°$	$0{\cdot}93 \angle 0°$	$0{\cdot}97 \angle 0°$	
		$\frac{2}{3}$	$0{\cdot}145 \angle -47°$	$1{\cdot}22 \angle 5°$	$1{\cdot}09 \angle -4°$	$1{\cdot}02 \angle -1°$		$0{\cdot}75 \angle -3°$	$0{\cdot}93 \angle 0°$	$0{\cdot}97 \angle 1°$		
		1	$0{\cdot}125 \angle -49°$	$1{\cdot}41 \angle 7°$	$1{\cdot}21 \angle -7°$	$1{\cdot}08 \angle -2°$	$1{\cdot}05 \angle -1°$	$0{\cdot}87 \angle -2°$	$0{\cdot}99 \angle 0°$	$1{\cdot}00 \angle 0°$		

D, l_l are the lengths of the whole path and of the land section, respectively; ξ_1 is the distance from the equivalent secondary source to the transmitter; s_l, s_s are the parameters s for land and sea sections, respectively; $s_s = 0$; ψ_l is the phase angle of s_l [$s_l = |s_l| \exp(-i\psi_l)$].

great numerical distances the $v(\rho)$ curve (Fig. 4) shows marked curvature and consequently can no longer be approximated by a single straight line. The last circumstance applies in connection with the intensity of the secondary sources. According to eqn. (13) the secondary sources are proportional to the difference $(\sqrt{s} - \sqrt{s_0})$. Consequently, where this difference is small, the intensity of the secondary sources is also small and may be calculated less precisely. However, when this difference is large, e.g. for land-sea paths, the influence of the secondary sources is great and a more elaborate procedure must be adopted.

Because of the great variety of parameters (lengths of the sections and magnitudes and phase angles of the parameters s), it is not possible to give any general rule as to the choice of the number of equivalent secondary sources. In order to obtain some indication, several land-sea paths have been considered; the results of the calculations are summarized in Table 1. Here $w(D)_{ss}$ denotes the value of the attenuation function calculated by means of the secondary sources, and $w(D)_t$ the theoretical (correct) value computed in the cases considered by numerical integration of eqn. (7); this notation will also be used in the subsequent analysis. As mentioned before, the inhomogeneity of the ground is most pronounced for land-sea paths, and the examples given in Table 1 may therefore be regarded as being in some sense extreme. In Table 2 are given the results of calculations for some paths of varying degrees of inhomogeneity, but of constant overall numerical distance. Table 2 shows clearly that, as expected, the errors of the method rapidly diminish when the inhomogeneity of the path becomes small.

Table 2

RATIO $w(D)_{ss}/w(D)_t$ FOR SOME PATHS OF VARYING INHOMOGENEITY

$\frac{s_2}{s_1}$	$w(D)_t$	$w(D)_{ss}/w(D)_t$	
		Secondary source on section	
		s_1	s_2
0	$0{\cdot}15 \angle -101°$	$1{\cdot}41 \angle -5°$	$0{\cdot}90 \angle -1°$
0·1	$0{\cdot}115 \angle -152°$	$1{\cdot}36 \angle -16°$	$0{\cdot}86 \angle 5°$
0·2	$0{\cdot}091 \angle -168°$	$1{\cdot}21 \angle -6°$	$0{\cdot}92 \angle 9°$
0·5	$0{\cdot}065 \angle -178°$	$1{\cdot}00 \angle -9°$	$1{\cdot}01 \angle 6°$

l_1, l_2, s_1, s_2 are the lengths and parameters s of the first and second sections, respectively; $l_1 = l_2$; s_1 and s_2 are real; $s_1 l_1 + s_2 l_2 = 10$. When computing $w(D)_{ss}$ one secondary source has been used.

For land-sea paths with a land section representing a large numerical distance ($|s_l l_l| \gg 1$), the method of equivalent secondary sources could be checked against the formula derived by Feinberg,[3, 5]

$$w(D) = -\frac{1}{2s_l D}\left[1 + \frac{2i}{\sqrt{\pi}}\sqrt{\left(s_l D\frac{D-l_l}{l_l}\right)}\right] . \quad . \quad (57)$$

The results of calculations have shown that only for $x_1 \ll D$ may the first section of the path be replaced by a single secondary source. If x_1 is not very much smaller than D, two or three secondary sources must be used. When secondary sources are placed on the sea, the sea section may be replaced by two sources even if it constitutes about 80% of the whole path; in such an extreme case the errors amount to about 10%. When secondary sources are placed on land, the errors are much bigger and a finer subdivision of the land section is necessary. Some indication as to the proper division could be obtained from the calculations of the attenuation function for land-sea paths with land and sea sections of equal length. The most difficult case has proved to be when the parameter s_l was real and $s_l l_l \simeq 50$; it was then necessary to use three secondary sources in order to reduce the errors to about 10%. When s_l was real and $s_l l_l$ was very great (say, some hundreds), and also for imaginary s_l and any great value of $|s_l l_l|$, two secondary sources could be used and the errors did not exceed about 5%.

The explanation of this behaviour seems obvious: the errors depend upon the curvature of the $v(\rho)$-curve, the distribution of the secondary sources along the path and the changes of the attenuation function with distance. Consequently, with growing numerical distance, a more elaborate procedure must be adopted, unless the numerical distance is so great that the influence of the parts of the section lying far from the transmitter may be disregarded.

Essential for success is the way of subdividing a section into parts. Useful experience has been obtained with the division as shown in Table 3.

Table 3

THE DIVISION OF THE FIRST SECTION OF A PATH INTO PARTS

	Two parts	Three parts	
	$x_1^{(1)}/x_1$	$x_1^{(1)}/x_1$	$x_1^{(2)}/x_1$
Land			
$\lvert s_l l_l\rvert = 1{\cdot}5$	$0{\cdot}\dot{3}$	—	—
10	0·2	0·1/0·15	0·4/0·5
50	0·2	0·06	0·2
very great	$s_1 x_1^{(1)} = 20$	—	—
Sea ($s \simeq 0$)	0·6	0·3	0·7

x_1, $x_1^{(1)}$, $x_1^{(2)}$ are the distances from the transmitter to the end of the first section and to the end of the first and second parts of the first section, respectively; l_l is the length of the land section.

Interesting results are obtained when both sections of the path represent very great numerical distances $[|s_1 x_1| \gg 1, |s_2(D - x_1)| \gg 1]$. As mentioned before, the first section of such a path can be replaced by one secondary source only when the first section is comparatively short; in the general case more secondary sources, placed at appropriate points $\xi_1^{(1)}, \xi_1^{(2)}, \ldots$ are necessary. Nevertheless, we will replace the first section by one secondary source p_1 which we will situate at the same point as the transmitting antenna. From eqn. (33),

$$p_1 = p_0\frac{\sqrt{s_1} - \sqrt{s_2}}{\sqrt{s_1}}v(s_1 x_1) \quad . \quad . \quad . \quad . \quad (58)$$

For large numerical distances we may, from eqn. (35), make $v(s_1 x_1) \simeq -1$, which means another approximation, sometimes also quite rough. Instead of p_0 we now have the effective source p_{ef}, given by

$$p_{ef} = p_0 + p_1 = p_0\sqrt{\frac{s_2}{s_1}} \quad . \quad . \quad . \quad . \quad (59)$$

The field at the point of reception is then

$$E(D) = \frac{p_{ef}}{D}y(s_2 D) = \frac{p_0}{D}\frac{-1}{2\sqrt{(s_1 s_2)}D} \quad . \quad . \quad (60)$$

since $y(s_2 D) \simeq -1/(2s_2 D)$. This gives, for the attenuation function,

$$w(D) = -\frac{1}{2\sqrt{(s_1 s_2)}D} \quad . \quad . \quad . \quad . \quad (61)$$

which is independent of the lengths of particular sections. The same result has been obtained by other methods by Feinberg[3, 5] and Bremmer.[9]

The argument used is apparently independent of the numerical distance of the second section of the path; it therefore seems possible to assume $s_2 = 0$. Proceeding as before, and taking for $v(s_1x_1)$ only a better approximation,

$$v(s_1x_1) = -1 - \frac{i}{\sqrt{(\pi s_1 x_1)}} \quad . \quad . \quad . \quad . \quad (62)$$

we obtain finally

$$w(D) = -\frac{i}{\sqrt{(\pi s_1 x_1)}} \quad . \quad . \quad . \quad . \quad (63)$$

Comparison of eqn. (63) with the rigorous formula (57) shows that the result obtained is correct only in the case of comparatively short land sections, representing very great numerical distances.

It may be instructive to explain why eqn. (61) gives comparatively small errors while eqn. (63) can be sometimes of no practical value. As follows from the method of deriving eqn. (22), the concept of equivalent secondary sources is especially suitable when the length of the section is small compared with the distance to the receiver. In the cases just considered this condition is fulfilled only when the first section is comparatively short ($x_1 \ll D$); the method of equivalent secondary sources then gives strictly correct results. When the lengths of both sections are comparable, the secondary sources on the parts of the first section near the boundary are much nearer the receiver and have therefore a much stronger influence on the field than when $x_1 \ll D$. However, if in these cases also we use the same procedure as before, the errors of the method must increase. If the second section is sea ($s_2 = 0$), then $p_1 \simeq -p_0$ and the secondary sources cancel almost completely the primary source p_0; the errors which are introduced when replacing the distributed secondary sources by a single equivalent secondary source are then the most pronounced. If the second section is land, the cancellation is not so complete and the relative errors are then much smaller.

Because of the practical importance of eqn. (61), we will discuss it now from a somewhat different point of view. As mentioned before, eqn. (61) states that the attenuation function $\Delta w(D)$ of the corresponding attenuation functions. According to eqn. (7) we obtain

$$\Delta w(D) = -i\sqrt{\frac{D}{\pi}}(\sqrt{s_1} - \sqrt{s_2})\int_{l_1}^{l_2} \frac{y(s_1x)y[s_2(D-x)]}{\sqrt{[x(D-x)]}}dx \quad . \quad (64)$$

For attenuation functions $y(s_1x)$ and $y[s_2(D-x)]$ we use the asymptotic expressions valid for large numerical distances

$$y(s_1x) = -\frac{1}{2s_1x}; \quad y[s_2(D-x)] = -\frac{1}{2s_2(D-x)} \quad . \quad (65)$$

which give

$$\Delta w(D) = \frac{i}{2\sqrt{\pi}} \frac{\sqrt{s_2} - \sqrt{s_1}}{s_1 s_2 D^{3/2}} \left\{ \frac{2l_2 - D}{\sqrt{[l_2(D-l_2)]}} + \frac{D - 2l_1}{\sqrt{[l_1(D-l_1)]}} \right\} \quad . \quad . \quad . \quad . \quad (66)$$

To simplify the formulae we assume $l_2 = D - l_1$ and compare $\Delta w(D)$ with $w(D)$ as given by eqn. (61); we then obtain

$$\frac{\Delta w(D)}{w(D)} = \frac{2i}{\sqrt{\pi}} \frac{\sqrt{s_1} - \sqrt{s_2}}{\sqrt{(s_1 s_2 D)}} \frac{D - 2l_1}{\sqrt{[l_1(D-l_1)]}} \quad . \quad . \quad (67)$$

Eqn. (67) illustrates the influence on the field of the middle parts of a path composed of sections representing great numerical distances. It also gives a useful indication as to the errors of eqn. (61).

(5.3) Three-Section Paths

The general problem of a 3-section path may be solved in two ways: by assuming either $s_0 = s_3$ or $s_0 = s_2$. In the first case the secondary sources over the first and second sections of the path must be calculated, and this is in principle always possible.[15] In practice, however, computation of the secondary sources over the second section is fairly laborious except when the second section is comparatively short. This is why such a case only was previously considered [eqns. (41)–(51)].

According to Fig. 3 the influence of the middle parts of the path is least when the path represents a great numerical distance. If we consider two paths, land–sea–land and sea–land–sea, the second section of the path will have a much smaller influence in the first case than in the second case. Consequently, if we replace the second section by one secondary source, the errors will be much smaller and the applicability of the method much wider for land–sea–land paths than for sea–land–sea paths. Table 4 confirms these conclusions. It also gives indications as to the limits of application of the method discussed. The examples in Table 4 have been chosen so as to make possible the comparison with two approximate formulae derived by

Table 4

THE RATIO $w(D)_{ss}/w(D)_t$ FOR CERTAIN LAND–SEA 3-SECTION PATHS

x_1	x_2	D	s_1	s_2	s_3	$w(D)_t$	$w(D)_{ss} : w(D)_t$
km			km^{-1}				
30	40	70	1 (land)	0 (sea)	1 (land)	$0{\cdot}0079 \angle -182°$	$1{\cdot}03 \angle 0°$
20	80	100				$0{\cdot}0131 \angle -184°$	$0{\cdot}84 \angle -1°$
40	60	100	0 (sea)	1 (land)	0 (sea)	$0{\cdot}47 \angle -11°$	$0{\cdot}90 \angle 1°$
40	80	120				$0{\cdot}336 \angle -12°$	$0{\cdot}75 \angle 1°$

All parameters s are real. The second section of the path is replaced by one secondary source. x_1, x_2, D are the distances from the transmitter to the end of the first, second and third sections, respectively.

is independent of the lengths of particular sections; this can constitute surely only an approximation. In order to explain this we will consider a path of length D, composed of two sections (with parameters s_1 and s_2) representing great numerical distances. We will consider two cases, namely when the first section has the lengths l_1 and l_2, and will calculate the difference

Feinberg.[3, 5] In the cases considered the errors of Feinberg's formulae [$w(D)_t$ in Table 4] should probably not exceed a few per cent.

In the second case ($s_0 = s_2$), the first and third sections of the path must be replaced by suitable secondary sources. Another procedure, however, is also possible. If we replace the first section by a number of secondary sources $p_1^{(1)}, p_1^{(2)}, \ldots$ we may then formally regard the path as consisting of two sections with parameters s_2 and s_3 and compute the field as the superposition of the fields of all the sources $p_0, p_1^{(1)}, p_1^{(2)}, \ldots$ These partial fields we can calculate according to the reciprocity theorem, i.e. by placing all these sources at B and calculating the fields at points A, $\xi_1^{(1)}, \xi_1^{(2)}, \ldots$ (Fig. 15). We therefore

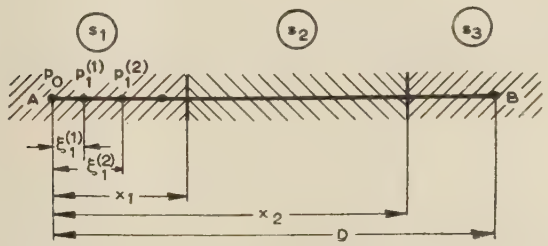

Fig. 15.—Computation of attenuation function for 3-section paths when $s_0 = s_2$.

replace the third section of the path by suitable secondary sources, as was done in the corresponding 2-section problem. The procedure described is in principle quite general. It is especially suitable when the number of secondary sources used is small. This occurs either when the first and third sections are comparatively short, or when they represent very great numerical distances.

We will first consider the case when the first and third sections are comparatively very short, i.e. when $x_1 \ll D$ and $D - x_2 \ll D$. According to eqn. (33), we replace the first section by an equivalent secondary source p_1, which we place at A (see Fig. 15):

$$p_1 = p_0 \frac{\sqrt{s_1} - \sqrt{s_2}}{\sqrt{s_1}} v(s_1 x_1) \quad . \quad . \quad . \quad . \quad (68)$$

At A we have now an effective source p'_{ef}, given by

$$p'_{ef} = p_0 + p_1 = p_0 \left[1 + \frac{\sqrt{s_1} - \sqrt{s_2}}{\sqrt{s_1}} v(s_1 x_1) \right] \quad . \quad (69)$$

To compute the field at B we use the reciprocity theorem, i.e. we place p'_{ef} at B and calculate the field at A. The third section we replace by an equivalent secondary source placed at B, and so obtain at B an effective source p''_{ef}, given by

$$p''_{ef} = p_0 \left[1 + \frac{\sqrt{s_1} - \sqrt{s_2}}{\sqrt{s_1}} v(s_1 x_1) \right] \left\{ 1 + \frac{\sqrt{s_3} - \sqrt{s_2}}{\sqrt{s_3}} v[s_3(D - x_2)] \right\} \quad . \quad . \quad . \quad . \quad (70)$$

This gives, for the attenuation function over the path considered, the final expression

$$w(D) = y(s_2 D) \left[1 + \frac{\sqrt{s_1} - \sqrt{s_2}}{\sqrt{s_1}} v(s_1 x_1) \right] \left\{ 1 + \frac{\sqrt{s_3} - \sqrt{s_2}}{\sqrt{s_3}} v[s_3(D - x_2)] \right\} \quad . \quad (71)$$

We will now consider the condition when all three sections of the path represent very great numerical distances. According to the discussion in Section 5.2 we may, in this case also, replace the first and third sections approximately by single secondary sources, placed at A and B. Putting in eqn. (71) $v(s_1 x_1) \simeq -1$, $v[s_3(D - x_2)] \simeq -1$ and $y(s_2 D) = -1/(2s_2 D)$, we obtain

$$w(D) \simeq -\frac{1}{2\sqrt{(s_1 s_3)} D} \quad . \quad . \quad . \quad . \quad (72)$$

Like eqn. (61) this formula has also been derived by other methods by Feinberg[3, 5] and Bremmer.[9]

From eqn. (72) it is seen that the field does not depend on the length of the second section of the path. As follows from the comparison of eqn. (72) with eqn. (61), the attenuation function would be the same even in the absence of the second section. This means that the influence of the secondary sources from the second section of the path has been completely disregarded; this has, in fact, resulted from the assumptions $v(s_1 x_1) = -1$ and $v[s_3(D - x_2)] = -1$.

Summarizing the discussion of the 3-section problem, we see that in all cases the attenuation function may be computed by means of equivalent secondary sources; in some cases the calculations may be, however, somewhat laborious. Of great advantage for the calculations is the fact that the middle parts of the path have a comparatively small influence on the field. Thus, the secondary sources over those parts of the path need not be calculated especially precisely.

(5.4) Multi-Section Paths

The secondary sources may in principle be used also for the computation of the attenuation function for multi-section paths.[15] The calculation then becomes laborious and somewhat complicated and generally offers no serious advantage as compared with the numerical integration of eqn. (7). In two special cases, however, a simple and interesting discussion is possible.

As the first example we will consider an overland path composed of n sections, of which the first and the nth represent great numerical distances. The middle parts of such a path have only a small influence on the field; accordingly we may approximately replace the sections 2, 3, . . ., $n - 1$ by a single homogeneous section of some appropriately chosen parameter $s_{n'}$. From eqn. (72) the attenuation function is then

$$w(D) \simeq -\frac{1}{2\sqrt{(s_1 s_n)} D} \quad . \quad . \quad . \quad . \quad (73)$$

which represents a direct generalization of eqns. (61) and (72). The parameter s_{ef} has dropped out of the final formula (73); this means, however, that we have in fact completely disregarded the influence of all sections of the path except the first and the last. This conclusion is supported also by comparison of eqn. (73) with eqn. (61) for 2-section paths.

As the second example we will consider a path composed of n sections, of which the last one of length δ is comparatively very short. We will assume $s_0 = s_{n-1}$ and replace the sections $1, 2, \ldots, n - 2$ by appropriate equivalent secondary sources. We have thus transformed our problem into a 2-section one with a number of sources of radiation; the field at the point of reception we find as the superposition of fields of the primary source and of all secondary sources. Further analysis is quite similar to the case of eqn. (56): the presence of a short section s_n may be taken into account by introducing a factor

$$1 + \frac{\sqrt{s_n} - \sqrt{s_{n-1}}}{\sqrt{s_n}} v(s_n \delta)$$

As this factor appears in the formulae for all partial fields, it may consequently be used also for the total field. The attenua-

tion function for the case considered, i.e. for the points near the boundary, thus takes the form

$$w(D) = w(D)_{s_n \to s_{n-1}}\left[1 + \frac{\sqrt{s_n} - \sqrt{s_{n-1}}}{\sqrt{s_n}} v(s_n\delta)\right] \quad . \quad (74)$$

where $w(D)_{s_n \to s_{n-1}}$ denotes the attenuation function when the section $n-1$ would reach to the end of the path, i.e. when s_n would be equal to s_{n-1}. On the basis of the reciprocity theorem, eqn. (74) may also be used, with obvious changes in notation, in the cases when the first section of the path, i.e. the section lying close to the transmitter, is very short. This result could also be derived directly by replacing the first section by an appropriate secondary source and calculating p_{ef} similarly as in eqn. (69). The analysis in this case must be, however, more careful, because it is necessary to discuss the influence of the secondary sources from the parts of the second section near the boundary with the first section. As we have already obtained the desired result, we will not consider the problem any more from this point of view.

Eqn. (74) represents a generalization of the results obtained in Section 5.2 for 2-section paths. The limits of application of eqn. (74), as well as its errors, can be estimated on the basis of the remarks in Section 5.2. We thus obtain the condition that the length δ should be much less than the distance from the point of reception to each of the sources. In practice, however, near but weak sources often need not be taken into account, and this means a wider application of eqn. (74). The amplitude and phase changes of the wave on passing the boundary are discussed in Section 5.2.

(6) LONG MIXED PATHS

(6.1) General Considerations

For longer distances the plane-earth approximation is not satisfactory and the influence of earth curvature must be taken into account. The distances d up to which the earth may be considered plane are as follows:

Reference 27: $d \leqslant 12(\lambda)^{1/3}$ . . . . . (75*a*)

Reference 28: $d \leqslant 5(\lambda)^{1/3}$ . . . . . (75*b*)

Reference 29: $d \leqslant 7(\lambda)^{1/3}$ . . . . . (75*c*)

In these formulae d is in kilometres and λ in metres.

For a homogeneous spherical earth we have at present three formulae[28, 30, 20] for the attenuation function $w(D)$:

For small numerical distances ρ,

$$w(D) = 1 - i(\sqrt{\pi})\rho^{1/2} - 2\rho + i(\sqrt{\pi})(1 - \tfrac{1}{2}\delta^3)\rho^{3/2} + \tfrac{4}{3}(1 - \delta^3)\rho^2 - i\frac{\sqrt{\pi}}{2}(1 - \tfrac{3}{2}\delta^3)\rho^{5/2} - \ldots \quad . \quad (76)$$

For any numerical distances ρ,

$$w(D) = y(\rho) + \tfrac{1}{2}[(1 + 2\rho)y(\rho) - 1 + i(\sqrt{\pi})\rho^{1/2}]\delta^3 + [(\tfrac{1}{2}\rho^2 - 1)y(\rho) - i(\sqrt{\pi})\rho^{1/2}(1 - \rho) + 1 - 2\rho + \tfrac{5}{6}\rho^2]\delta^6 + \ldots \quad . \quad (77)$$

The residue series

$$w(D) = D^{1/2}\left(-\frac{2\pi i}{a}\right)^{1/2}(ka)^{1/6}\sum_{q=0}^{\infty}\frac{\exp\left[-i\tau_q(ka)^{1/3}D/a\right]}{2\tau_q - 1/\delta^2} \quad . \quad (78)$$

where $\delta = -i\dfrac{\epsilon'}{(ka)^{1/3}(\epsilon' - 1)^{1/2}} = \dfrac{(ka)^{1/6}}{(2as)^{1/2}}\exp(-i\tfrac{3}{4}\pi)$. (79)

and τ_q denotes certain complex values depending on δ.

The series (76) is useful for small numerical distances, as then only a few terms of it need be considered; in such cases eqn. (76) differs, however, insignificantly from the corresponding plane-earth formula. In subsequent analysis we will therefore not take eqn. (76) into account. Similarly we will disregard eqn. (77) because of its very complicated form.

As regards the residue series, it may be easily used in mixed-path problems because of its convenient analytical form; Wait's research[19] of 2-section paths may serve here as an example. However, in a general case, when many terms of the series must be used, the calculations become laborious because of the many complex parameters appearing in the formulae. In the subsequent analysis we will discuss explicitly only those cases in which it is sufficient to consider merely the first term of the residue series, i.e. when the distances are so great that the receiver is in the diffraction zone. According to Millington[31] these distances are

For errors $\leqslant$ 3 dB $\quad d \geqslant 20(\lambda)^{1/3}$ . . . . . (80*a*)

For errors $\leqslant$ 1 dB $\quad d \geqslant 30(\lambda)^{1/3}$ . . . . . (80*b*)

where, again, d is in kilometres and λ in metres. In such cases

$$w(D) = \sqrt{(D)}C\exp(tD) \quad . \quad . \quad . \quad . \quad (81)$$

with

$$C = \frac{\left(-\dfrac{2\pi i}{a}\right)^{1/2}(ka)^{1/6}}{2\tau_0 - 1/\delta^2} \quad . \quad . \quad . \quad . \quad (82)$$

$$\tau_0 = \alpha_0 - i\beta_0 \quad . \quad . \quad . \quad . \quad . \quad . \quad (83)$$

$$t = -i[(ka)^{1/3}/a]\tau_0 = -ik(ka)^{-2/3}\tau_0 = k(ka)^{-2/3}(-i\alpha_0 - \beta_0) \quad . \quad . \quad . \quad . \quad . \quad . \quad (84)$$

Values of α_0 and β_0 have been given by Norton.[27]

(6.2) Two-Section Paths

As follows from the remarks in Section 6.1, the general case of a 2-section path with arbitrary lengths of the sections will present very great analytical difficulties. A comparatively simple analysis is possible in two instances: first, when one section (say the first) may be regarded as plane and is, at the same time, very much shorter than the other, and secondly, when at least one of the sections is very long.

In the first case, i.e. for $x_1 \ll D$, a seemingly obvious generalization of eqn. (55) gives

$$w(D) = w_{s_2}(D)\left[1 + \frac{\sqrt{s_1} - \sqrt{s_2}}{\sqrt{s_1}} v(s_1 x_1)\right] \quad . \quad . \quad (85)$$

Closer examination shows, however, that eqn. (85) is valid only when $w_{s_2}(D - x)$ is approximately constant over the first section; this problem will be discussed in more detail in the subsequent analysis.

In the second case we will assume the second section to be so long that the attenuation function $w_{s_2}(D - x)$ over the first may be calculated from eqn. (81); consequently the length of the second section $(D - x_1)$ must be at least that given by eqns. (80). The parameters referring to the first section will be denoted by the subscript 1, and those for the second section by the subscript 2. Similarly as in Section 5.1 we will calculate the contributions to the attenuation function, and to the field, originating from the part of the first section lying between the

points d_1 and d_2. Assuming $s_0 = s_2$, we obtain, by virtue of eqn. (7),

$$\Delta w_{d_1 d_2} = -i\sqrt{\frac{D}{\pi}}(\sqrt{s_1} - \sqrt{s_2})\int_{d_1}^{d_2} \frac{w_{s_1}(x) w_{s_2}(D-x)}{\sqrt{[x(D-x)]}}dx$$

$$= w_{s_2}(D)\frac{-i}{\sqrt{\pi}}(\sqrt{s_1} - \sqrt{s_2})\int_{d_1}^{d_2} \frac{w_{s_1}(x)}{\sqrt{x}} \exp(-t_2 x)dx \quad . \quad (86)$$

and $$E_{d_1 d_2} = \frac{p_0}{D}\Delta w_{d_1 d_2}$$

$$= \frac{w_{s_2}(D)}{D} p_0 \frac{-i}{\sqrt{\pi}}(\sqrt{s_1} - \sqrt{s_2})\int_{d_1}^{d_2} \frac{w_{s_1}(x)}{\sqrt{x}} \exp(-t_2 x)dx \quad . \quad (87)$$

According to eqn. (87) the part of the first section considered may be replaced by an equivalent secondary source $p_{d_1 d_2}$, placed at the same point as the transmitting antenna, given by

$$p_{d_1 d_2} = p_0 \frac{-i}{\sqrt{\pi}}(\sqrt{s_1} - \sqrt{s_2})\int_{d_1}^{d_2} \frac{w_{s_1}(x)}{\sqrt{x}} \exp(-t_2 x)dx \quad . \quad (88)$$

As the distances d_1 and d_2 are quite arbitrary, we may conclude that when the second section of a 2-section path is very long the first may always be replaced by one equivalent secondary source placed at the same point as the transmitting antenna. This property may be generalized in an obvious way for all paths having very long last sections. In such cases all sections preceding the last one may be replaced by a suitable secondary source placed at the beginning of the path.

When the first section of a path may be regarded as approximately plane we may replace $w_{s_1}(x)$ by $v(s_1 x)$. As in Section 3.3 we may expand $\exp(-t_2 x)$ in series and then obtain, as a generalization of eqn. (33),

$$p_{d_1 d_2} = p_0 \frac{\sqrt{s_1} - \sqrt{s_2}}{\sqrt{s_1}} \varepsilon^{-t_2 \xi}[v(s_1 d_2) - v(s_1 d_1)] \quad . \quad (89)$$

where ξ is the position of the 'centre of gravity' of the part of the path considered; the secondary source itself is, however, placed as before at the beginning of the path. According to eqn. (89) the simple formula (85) may be applied only if $\varepsilon^{-t_2 x_1} \simeq 1$; if this condition is not fulfilled the first section must be subdivided, even if $x_1 \ll D$.

We consider now the case when both sections of the path are very long, as in Fig. 16. When calculating the attenuation

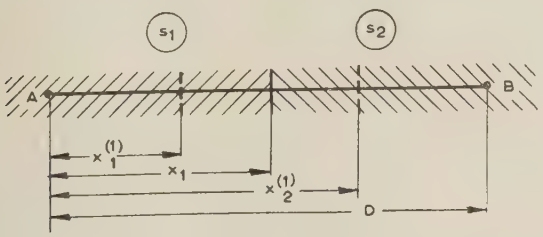

Fig. 16.—Path composed of two very long sections.

function we first place the transmitter at the point A, assume $s_0 = s_2$ and divide the first section into two parts. The first part we choose so long that for $x > x_1^{(1)}$ the attenuation function $w_1(x)$ may be found from eqn. (81). As $w_{s_2}(D-x)$ also has the same form, we obtain, after easy reductions,

$$w(D)' = \sqrt{(D)}C_2 \exp(t_2 D)$$

$$\left\{A_{1,2} - \frac{i}{\sqrt{\pi}} C_1 \frac{\sqrt{s_1} - \sqrt{s_2}}{t_1 - t_2} \exp[(t_1 - t_2)x_1]\right\} \quad . \quad (90)$$

with

$$A_{1,2} = 1 - \frac{i}{\sqrt{\pi}}(\sqrt{s_1} - \sqrt{s_2})\left\{\int_0^{x_1^{(1)}} \frac{w_{s_1}(x)}{\sqrt{x}} \exp(-t_2 x)dx - \frac{C_1}{t_1 - t_2} \exp[(t_1 - t_2)x_1^{(1)}]\right\} \quad . \quad (91)$$

If instead of $s_0 = s_2$ we assume $s_0 = s_1$ and place the transmitter at B, we obtain similarly

$$w(D)'' = (\sqrt{D})C_1 \exp(t_1 D)$$

$$\left\{A_{2,1} - \frac{i}{\sqrt{\pi}} C_2 \frac{\sqrt{s_2} - \sqrt{s_1}}{t_2 - t_1} \exp[(t_2 - t_1)(D - x_1)]\right\} \quad . \quad (92)$$

with

$$A_{2,1} = 1 - \frac{i}{\sqrt{\pi}}(\sqrt{s_2} - \sqrt{s_1})\left\{\int_0^{D - x_2^{(1)}} \frac{w_{s_2}(x)}{\sqrt{x}} \exp(-t_1 x)dx - \frac{C_2}{t_2 - t_1} \exp[(t_2 - t_1)(D - x_2^{(1)})]\right\} \quad . \quad (93)$$

According to the reciprocity theorem (see Section 3.2) $w(D)' = w(D)''$. As the term $A_{1,2}$ is a function of $x_1^{(1)}$ and $A_{2,1}$ is a function of $D - x_2^{(1)}$, they are independent of each other; as a consequence of the condition $w(D)' = w(D)''$ they both must be equal to zero. We thus obtain the interesting result that for a path composed of two very long sections the attenuation function is given by a simple formula

$$w(D) = (\sqrt{D})C_1 C_2 \frac{-i}{\sqrt{\pi}} \frac{\sqrt{s_1} - \sqrt{s_2}}{t_1 - t_2} \exp[t_1 x_1 + t_2(D - x_1)] \quad . \quad (94)$$

For further discussion we shall write eqn. (94) once more in a somewhat modified form:

$$w(D) = w_{s_2}(D) \frac{-i}{\sqrt{\pi}} C_1 \frac{\sqrt{s_1} - \sqrt{s_2}}{t_1 - t_2} \exp[(t_1 - t_2)x_1] \quad . \quad (95)$$

According to eqn. (95) the path composed of two very long sections may be reduced to a homogeneous path of parameter $s = s_2$, but instead of p_0 the primary source is then $p_{ef}^{(1)}$, given by

$$p_{ef}^{(1)} = p_0 \frac{-i}{\sqrt{\pi}} C_1 \frac{\sqrt{s_1} - \sqrt{s_2}}{t_1 - t_2} \exp[(t_1 - t_2)x_1] \quad . \quad (96)$$

Eqns. (85), (89), (88) and (95) describe the influence of the first section of the path on the field. The influence of short sections is the same as for a plane earth. When the length of the first section increases, there appear increasing deviations from plane-earth relations. For very long first sections eqns. (94) and (95) are valid, and, when considered as functions of x_1, represent a logarithmic spiral winding around the point O. The influence of the first section of the path on the field may be plotted as a function of x_1 in the plane of complex variables. We thus obtain interesting curves of different shapes depending on the relations between the electrical parameters of both sections; Fig. 17 shows an example.

(6.3) Multi-Section Paths

First we will consider the case when all sections of the path, except possibly the first and the last, are very long. As previously, x_{j-1}, x_j will denote the ends of the jth section. The parameters referring to the jth section will be given the subscript j.

When computing the field over the second section very far from the boundary with the first, we may, according to the discussion in Section 6.2, replace the first section by some appro-

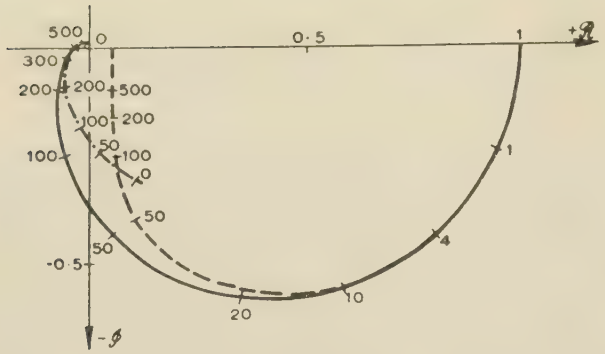

Fig. 17.—The influence of the first section of a very long path on the field: $w(D)/w_{s2}(D) = f(x_1)$.

First section: land ($\epsilon = 4$; $\sigma = 10^{-2}$ mho/m). Second section: sea ($\epsilon = 80$; $\sigma = 4$ mhos/m). Frequency: 1 Mc/s. Numbers denote the length of the first section in kilometres.

——— Correct result; — — According to eqn. (85); —·— According to eqn. (95).

priate equivalent secondary source p_1. We may then consider the path as homogeneous of parameter $s = s_2$, with the effective primary source $p_{ef}^{(1)}$ given by

$$p_{ef}^{(1)} = p_0 + p_1 \quad . \quad . \quad . \quad . \quad . \quad . \quad (97)$$

For very short first sections eqn. (85) gives $p_{ef}^{(1)}$ directly:

$$p_{ef}^{(1)} = p_0\left[1 + \frac{\sqrt{s_1} - \sqrt{s_2}}{\sqrt{s_1}} v(s_1 x_1)\right] . \quad . \quad . \quad (98)$$

For longer first sections p_1 must be calculated according to eqns. (89) and (88), and then $p_{ef}^{(1)}$ according to eqn. (97). For very long first sections $p_{ef}^{(1)}$ is given by eqn. (96).

When calculating the field over the third section we may assume $s_0 = s_2$ and evaluate the influence of secondary sources from the first and third. As mentioned before, the field of the primary source p_0 and of the secondary sources from the first section may be reduced to the field of an effective primary source $p_{ef}^{(1)}$. The secondary sources over the third section, and consequently the field over that section, will thus be the same as in the case of a 2-section path with first section of length x_2 and parameter $s = s_2$, the second of parameter $s = s_3$, and primary source $p_{ef}^{(1)}$.

When the third section is shorter than the lengths given by eqns. (80), the field may be calculated according to the reciprocity theorem by placing $p_{ef}^{(1)}$ at the end of the path and computing the field at its beginning. Again, the influence of the third section may be taken into account by replacing $p_{ef}^{(1)}$ by an appropriate $p_{ef}^{(1,3)}$, which gives

$$E(D) = \frac{p_{ef}^{(1,3)}}{D} w_{s_2}(D) \quad . \quad . \quad . \quad . \quad . \quad (99)$$

and

$$w(D) = w_{s_2}(D)\frac{p_{ef}^{(1,3)}}{p_0} = w_{s_2}(D)\frac{p_{ef}^{(1)}}{p_0}\frac{p_{ef}^{(1,3)}}{p_{ef}^{(1)}} \quad . \quad . \quad (100)$$

When the third section is very long we may use directly eqn. (95), which gives

$$w(D) = w_{s_3}(D)\frac{p_{ef}^{(1)}}{p_0}\frac{-i}{\sqrt{\pi}} C_2 \frac{\sqrt{s_2} - \sqrt{s_3}}{t_2 - t_3} \exp\left[(t_2 - t_3)x_2\right] . \quad (101)$$

It follows from eqn. (101) that the 3-section path considered has been thus reduced to a homogeneous path with parameter $s = s_3$ and with a primary source $p_{ef}^{(2)}$ given by

$$p_{ef}^{(2)} = p_0\frac{p_{ef}^{(1)}}{p_0}\frac{-i}{\sqrt{\pi}} C_2 \frac{\sqrt{s_2} - \sqrt{s_3}}{t_2 - t_3} \exp\left[(t_2 - t_3)x_2\right] . \quad (102)$$

From the above discussion it follows by induction that in the general case also of a path composed of many very long sections, except possibly the first and last, the field may be calculated as over a homogeneous earth, while the influence of subsequent sections of the path appears in the form of certain factors in the expression for the effective primary source.

When the path consists of n sections, all very long except possibly the first one, the path may be reduced to a homogeneous earth s_n with an effective primary source $p_{ef}^{(n-1)}$ given by

$$p_{ef}^{(n-1)} = p_0\frac{p_{ef}^{(1)}}{p_0}\frac{-i}{\sqrt{\pi}} C_2 \frac{\sqrt{s_2} - \sqrt{s_3}}{t_2 - t_3}\frac{-i}{\sqrt{\pi}} C_3 \frac{\sqrt{s_3} - \sqrt{s_4}}{t_3 - t_4} \times \ldots$$
$$\ldots \times \frac{-i}{\sqrt{\pi}} C_{n-1}\frac{\sqrt{s_{n-1}} - \sqrt{s_n}}{t_{n-1} - t_n} \exp\left[t_2 x_2 + t_3(x_3 - x_2) + \ldots\right.$$
$$\left.\ldots + t_{n-1}(x_{n-1} - x_{n-2}) - t_n x_{n-1}\right] \quad . \quad . \quad (103)$$

The attenuation function over the path considered will therefore be

$$w(D) = w_{s_n}(D)\frac{p_{ef}^{(n-1)}}{p_0} = (\sqrt{D})C_n\frac{p_{ef}^{(1)}}{p_0}\frac{-i}{\sqrt{\pi}} C_2 \frac{\sqrt{s_2} - \sqrt{s_3}}{t_2 - t_3}$$
$$\frac{-i}{\sqrt{\pi}} C_3 \frac{\sqrt{s_3} - \sqrt{s_4}}{t_3 - t_4} \times \ldots \times \frac{-i}{\sqrt{\pi}} C_{n-1}\frac{\sqrt{s_{n-1}} - \sqrt{s_n}}{t_{n-1} - t_n}$$
$$\exp\left[t_2 x_2 + t_3(x_3 - x_2) + \ldots + t_n(D - x_{n-1})\right] . \quad (104)$$

We will now consider a path which differs from the one just discussed only by the presence of a not very long $(n + 1)$th section. The situation is quite similar to that discussed for 3-section paths [see eqns. (99) and (100)], and consequently the attenuation function for the path will differ from eqn. (104) only by a factor accounting for the presence of the $(n + 1)$th section.

When all n sections of the path are very long we substitute in eqn. (104) for $p_{ef}^{(1)}/p_0$ the formula (96) and obtain for $w(D)$ a simple expression,

$$w(D) = (\sqrt{D})C_n\frac{-i}{\sqrt{\pi}} C_1 \frac{\sqrt{s_1} - \sqrt{s_2}}{t_1 - t_2}\frac{-i}{\sqrt{\pi}} C_2 \frac{\sqrt{s_2} - \sqrt{s_3}}{t_2 - t_3} \times \ldots$$
$$\ldots \times \frac{-i}{\sqrt{\pi}} C_{n-1}\frac{\sqrt{s_{n-1}} - \sqrt{s_n}}{t_{n-1} - t_n}$$
$$\exp\left[t_1 x_1 + t_2(x_2 - x_1) + \ldots + t_n(D - x_{n-1})\right] . \quad (105)$$

For practical computations it is convenient to change the notation to that used in the homogeneous-spherical-earth theory [see eqns. (79), (82), (83) and (84)]. We thus obtain

$$(\sqrt{D})C_n = \varepsilon^{-i(\pi/4)}(2\pi k D)^{1/2}(ka)^{-1/3}(2\tau_{0n} - 1/\delta_n^2)^{-1} \quad . \quad (106)$$

$$\frac{-i}{\sqrt{\pi}} C_i \frac{\sqrt{s_i} - \sqrt{s_k}}{t_i - t_k} = -\frac{1/\delta_i - 1/\delta_k}{(2\tau_{0i} - 1/\delta_i^2)(\tau_{0i} - \tau_{0k})} \quad . \quad (107)$$

$$\exp(t_i x) = \exp\left[-ik(ka)^{-2/3}\alpha_{0i}x\right]\exp\left[-k(ka)^{-2/3}\beta_{0i}x\right] . \quad (108)$$

Eqn. (105), in the notation according to eqns. (106)–(108), has been obtained by Furutsu[12-14] by another method. Eqn. (94) previously obtained represents a specialization of eqn. (105) for 2-section paths.

Finally, we will discuss the influence on the field of a comparatively short section which is neither the first nor the last. We will consider first a 3-section path with very long first and third sections and a comparatively short second section. From eqn. (7) the contribution of the second section to the attenuation function for $s_0 = s_3$ amounts to

$$\Delta w_{x_1 x_2} = -i\sqrt{\frac{D}{\pi}}(\sqrt{s_2} - \sqrt{s_3})\int_{x_1}^{x_2} \frac{w(x)w_{s_3}(D - x)}{\sqrt{[x(D - x)]}} dx \quad . \quad (109)$$

On the basis of the reciprocity theorem we may use eqn. (85) for $w(x)$; after an obvious change of notation we obtain

$$w(x) \simeq w_{s_1}(x)\left\{1 + \frac{\sqrt{s_2} - \sqrt{s_1}}{\sqrt{s_2}} v[s_2(x - x_1)]\right\} \quad . \quad (110)$$

The limits of application of eqn. (110) as well as its error should be clear from the discussion in Section 6.2. After substituting for $w_{s_3}(D - x)$ from eqn. (81), eqn. (109) may be reduced to

$$\Delta w_{x_1 x_2} = w_{s_3}(D) C_1 \frac{\sqrt{s_2} - \sqrt{s_3}}{s_2} \exp\left[(t_1 - t_3)\xi_2\right] \times \left\{-\frac{i}{\sqrt{\pi}} s_2(x_2 - x_1) + \frac{\sqrt{s_2} - \sqrt{s_1}}{\sqrt{s_2}} u[s_2(x_2 - x_1)]\right\} . \quad (111)$$

where ξ_2 denotes the position of the 'centre of gravity' of the second section, and u is the function determined by eqn. (45). Similarly, as in the case of the plane earth [see eqn. (44)], we may assume $\xi_2 = \frac{1}{2}(x_1 + x_2)$. It follows from eqn. (111) that a comparatively short second section may be replaced by the equivalent secondary source p_2, placed at the beginning of the path, given by

$$p_2 = p_0 C_1 \frac{\sqrt{s_2} - \sqrt{s_3}}{s_2} \exp\left[(t_1 - t_3)\xi_2\right] \times \left\{-\frac{i}{\sqrt{\pi}} s_2(x_2 - x_1) + \frac{\sqrt{s_2} - \sqrt{s_1}}{\sqrt{s_2}} u[s_2(x_2 - x_1)]\right\} . \quad (112)$$

This makes possible an easy calculation of the field over the third section at points lying very far from the boundary ($x - x_2$ very large). We therefore assume $s_0 = s_3$, replace the first and second sections by suitable equivalent sources p_1 and p_2, and calculate the effective primary source $p_{ef}^{(1+2)}$ given by

$$p_{ef}^{(1+2)} = p_0 + p_1 + p_2 \quad . \quad . \quad . \quad . \quad . \quad (113)$$

The path may then be regarded as homogeneous with a parameter $s = s_3$ and a primary source $p_{ef}^{(1+2)}$. For source p_2 we substitute in eqn. (113) from eqn. (112). To find the influence of the first section, we may calculate directly $p_0 + p_1$ from eqn. (96), only changing the subscripts 2 into 3, i.e.

$$p_0 + p_1 = p_0 \frac{-i}{\sqrt{\pi}} C_1 \frac{\sqrt{s_1} - \sqrt{s_3}}{t_1 - t_3} \exp\left[(t_1 - t_3)x_1\right] \quad . \quad (114)$$

The generalization of this procedure is very simple. In fact the only important assumptions have been that the section considered is comparatively short; that the preceding and the following sections are very long; and that we can replace the influence of all preceding sections by a single source of radiation placed at the beginning of the path. The calculation of the field over the paths satisfying these conditions (e.g. those composed of successively very long and comparatively short sections) is carried out step by step by subsequent reduction of the path to a suitable homogeneous earth and the computation of the corresponding effective primary sources.

(7) CONCLUSIONS

The discussion presented in the paper is based on the integral equation (7); its physical background is the interaction of secondary sources distributed over the surface of the earth. The problem is, physically and mathematically, complicated. Some simplification is possible through replacing the distributed secondary sources by equivalent secondary sources; for complicated mixed paths, however, this method also proves unsatisfactory. As mentioned in the Introduction, Furutsu and Wait have performed rigorous calculations for some cases and have presented the results in the form of graphs. This method of attack seems impossible in the general case because of the large number of independent parameters. Even in the simplest case of plane 2-section paths the consideration of the complex character of numerical distances increases the number of parameters by two, as compared with the set of graphs computed by Wait[16] under the assumption of real numerical distances. In this respect the method of equivalent secondary sources is of advantage, since it is valid for every phase characteristic of the parameter s. Another advantage of this method is the clear physical picture it gives of the phenomena occurring; this may sometimes be a real help in practical computations.

Summing up the discussion, we must regard the problem of practical mixed-path calculations as only partially solved so far and needing further investigation. In this respect an interesting suggestion has been made by Senior,[17] but further studies are necessary to decide whether his method will be suitable for practical computations.

In view of the laboriousness of the theoretical computations, the so-called semi-empirical methods can be of great practical importance. In another paper the two most important of them, namely Millington's method and the equivalent numerical-distance method, will be compared with theory in order to determine their errors and to find the limits of their application.

(8) ACKNOWLEDGMENTS

The author wishes to thank Mr. G. Millington for his many valuable remarks and very great and kind help in preparing the manuscript for publication. The author is indebted to Dr. T. Tomankiewicz for his friendly support during the course of the work and to the Director of the Institute of Telecommunication, Docent T. Rzymkowski, for his kind permission to publish the paper. The author is also grateful to Dr. J. R. Wait for his valuable remarks.

(9) REFERENCES

(1) Grünberg, G. A., and Fock, V. A.: 'On the Theory of Coastal Refraction of Electromagnetic Waves', from 'Investigations of Propagation of Radio Waves' edited by B. A. Vvedensky (Academy of Sciences, U.S.S.R., Moscow, 1948), p. 69.

(2) Feinberg, E. L.: 'Propagation of Radio Waves along a Real Surface', *ibid.*, p. 97.

(3) Alpert, J. L., Ginzburg, V. L., and Feinberg, E. L.: 'Propagation of Radio Waves' (GITTL, Moscow, 1953), Chapter IX, p. 184.

(4) 'Ground-Wave Propagation over Mixed Paths—a Brief Review of the Present Situation', C.C.I.R., Warsaw, 1956, Document 501.

(5) Feinberg, E. L.: 'Theory of Mixed Path Propagation of Radiowaves and Engineering Methods of Calculation', *ibid.*, Document 563.

(6) Clemmow, P. C.: 'Ground-Wave Propagation across a Land/Sea Boundary', *Nature*, 1950, **165**, p. 107.

(7) Clemmow, P. C.: 'Radio Propagation over a Flat Earth across a Boundary separating Two Different Media', *Philosophical Transactions of the Royal Society*, A, 1953, **246**, p. 1.

(8) 'New Method of Calculating Ground-Wave Field Strength over Mixed Paths', C.C.I.R., London, 1953, Document 141.

(9) Bremmer, H.: 'The Extension of Sommerfeld's Formula for the Propagation of Radio Waves over a Flat Earth to Different Conductivities of the Soil', *Physica*, 1954, **20**, p. 441.

(10) FURUTSU, K.: 'Propagation of Electro-Magnetic Waves over a Flat Earth across a Boundary Separating Different Media and Coastal Refraction', *Journal of the Radio Research Laboratories* (Tokyo), 1955, **2**, p. 1.

(11) FURUTSU, K.: 'Propagation of Electro-Magnetic Waves over a Flat Earth across Two Boundaries separating Three Different Media', *ibid.*, 1955, **2**, p. 239.

(12) FURUTSU, K.: 'Propagation of Electro-Magnetic Waves over the Spherical Earth across Boundaries separating Different Earth Media', *ibid.*, 1955, **2**, p. 345.

(13) FURUTSU, K., and KOIMAI, S.: 'The Calculation of Field Strength over Mixed Paths on a Spherical Earth', *ibid.*, 1956, **3**, p. 391.

(14) FURUTSU, K.: 'Ground-Wave Propagation over Mixed Paths—Calculation of Ground-Wave Field Strengths and Phases in Propagation over Mixed Paths', C.C.I.R., Warsaw, 1956, Document 322.

(15) GODZIŃSKI, Z.: 'Extension of Feinberg's Theory to the Case of Electromagnetic Wave Propagation over an Inhomogeneous Spherical Earth and Introduction of an Approximate Method of Computation based on Equivalent Secondary Sources', *ibid.*, Document 454.

(16) WAIT, J. R.: 'Mixed Path Ground Wave Propagation: 1. Short Distances', *Journal of Research of the National Bureau of Standards*, 1956, **57**, p. 1.

(17) SENIOR, T. B. A.: 'Radio Propagation over a Discontinuity in the Earth's Electrical Properties—I', *Proceedings I.E.E.*, Monograph No. 192 R, August, 1956 (**104** C, p. 43).

(18) SENIOR, T. B. A.: 'Radio Propagation over a Discontinuity in the Earth's Electrical Properties—II. Coastal Refraction', *ibid.*, Monograph No. 210 R, October, 1956 (**104** C, p. 139).

(19) WAIT, J. R.: 'On the Theory of Propagation along a Curved Surface', *Transactions of the Institute of Radio Engineers*, Vol. AP (to be published).

(20) BREMMER, H.: 'Applications of Operational Calculus to Ground-Wave Propagation, in particular for Long Waves', *Proceedings of the Institute of Radio Engineers* (to be published).

(21) LEONTOVICH, M. A.: 'On the Approximate Boundary Conditions for Electromagnetic Field on the Surface of Well-Conducting Bodies', Reference 1, p. 5.

(22) LEONTOVICH, M. A., and FOCK, V. A.: 'Solution of the Problem of Electromagnetic Wave Propagation along the Earth's Surface by the Parabolic Equation Method', Reference 1, p. 13.

(23) KARPOV, K. A.: 'Tables of Function $w(z) = e^{-z^2}\int_0^z e^x dx$ in the Complex Plane' (Academy of Sciences, U.S.S.R., Moscow, 1954).

(24) PRESSEY, B. G., ASHWELL, G. E., and FOWLER, C. S.: 'Change of Phase with Distance of a Low-Frequency Ground Wave propagated across a Coast-Line', *Proceedings I.E.E.*, Paper No. 2082 R, July, 1956 (**103** B, p. 527).

(25) PRESSEY, B. G., and ASHWELL, G. E.: 'The Deviation of Low-Frequency Ground Waves at a Coast-Line', *ibid.*, Paper No. 2083 R, July, 1956 (**103** B, p. 535).

(26) PRESSEY, B. G., ASHWELL, G. E., and FOWLER, C. S.: 'The Measurement of the Phase Velocity of Ground-Wave Propagation over a Land Path', *ibid.*, Paper No. 1438 R, March, 1953 (**100**, Part III, p. 73).

(27) NORTON, K. A.: 'The Calculation of Ground-Wave Field Intensity over a Finitely Conducting Spherical Earth', *Proceedings of the Institute of Radio Engineers*, 1941, **29**, p. 623.

(28) BREMMER, H.: 'Terrestrial Radio Waves' (Elsevier Publishing Co., New York, 1949), p. 85.

(29) ALPERT, J. L., GINZBURG, V. L., and FEINBERG, E. L.: Reference 3, p. 234.

(30) BREMMER, H.: 'The Evaluation of Ground-Wave Fields for Short Distances', C.C.I.R., London, 1953, Document 162.

(31) MILLINGTON, G.: 'Ground-Wave Propagation over an Inhomogeneous Smooth Earth', *Proceedings I.E.E.*, Paper No. 794 R, January, 1949 (**96**, Part III, p. 53).

621.371 : 621.396.677.85

The Institution of Electrical Engineers
Monograph No. 300 R
Apr. 1958
©

THE FIELDS ASSOCIATED WITH AN INTERFACE BETWEEN FREE SPACE AND AN ARTIFICIAL DIELECTRIC

By J. BROWN, M.A., Ph.D., Associate Member, and J. S. SEELEY, B.Sc.(Eng.), Ph.D.

(*The paper was first received* 20*th December*, 1957, *and in revised form* 28*th January*, 1958. *It was published as an* INSTITUTION MONOGRAPH *in April*, 1958.)

SUMMARY

In most respects artificial dielectrics behave in a similar way to normal solid dielectrics. A complication is sometimes observed in that apparent phase discontinuities occur at the interface between free space and an artificial dielectric, such discontinuities arising from the excitation of reactive fields near the interface. It is shown that the behaviour can be analysed in terms of evanescent waves inside the dielectric and in free space, and detailed calculations are given for the metal-strip type of delay dielectric. Measured values of the parameters of an equivalent circuit representing the free-space/artificial-dielectric interface are shown to agree with calculated values within the limits of experimental error.

LIST OF PRINCIPAL SYMBOLS

λ_0 = Free-space wavelength.
λ = Wavelength of a plane wave in a dielectric of permittivity ϵ.
a, c, d = Dimensions defined in Fig. 1.
β_n = Attenuation coefficient for nth mode.
$a_1, a_2, \ldots$ = Incident-mode amplitudes.
$b_1, b_2, \ldots$ = Reflected-mode amplitudes.
$t = \mathrm{Sin}^2(\pi d/2a)$.
$p = [1 - j(a/\lambda)\log_\epsilon t]^{-1}$.
Z_1, Z_2 = Mode wave impedances.
$\boldsymbol{L}, \boldsymbol{M}, \boldsymbol{N}, \boldsymbol{B}, \boldsymbol{T}$ = 2×2 square matrices.
v_1, v_2 = Mode voltages.
i_1, i_2 = Mode currents.
γ_1, γ_2 = Propagation coefficients of modes in delay structure.
α_{ij}, β_{ij} = Mode constants as defined in eqns. (24) and (25).

Square matrices are indicated by upper-case bold-face type; column matrices by lower-case bold-face type.

(1) INTRODUCTION

In a previous discussion[1] of the properties of artificial dielectrics it was pointed out that reactive fields are established near an interface between free space and the dielectric. These fields modify the reflection properties of the interface by introducing apparent phase discontinuities in the transmitted and reflected waves. The only example so far discussed in detail concerns the artificial dielectric formed by a stack of equi-spaced parallel conducting plates. An exact solution for the fields excited by a plane wave incident on this medium from free space has been provided by Carlson and Heins[2] and from this an equivalent circuit can be deduced to represent the behaviour of the propagating waves. In the present paper an approximate solution will be obtained for the metal-strip dielectric,[3] which is one of the most useful artificial dielectrics for the construction of microwave lenses.

Correspondence on Monographs is invited for consideration with a view to publication.
Dr. Brown is Reader in Electrical Engineering, University College, London.
Dr. Seeley was in the Department of Electrical Engineering, Imperial College, London, and is now at the Royal Aircraft Establishment.

The metal-strip dielectric consists of a two-dimensional array of conducting strips positioned perpendicular to the electric field of the incident wave [Fig. 1(*a*)]. A good approximation to the properties of this material is obtained by representing each plane of strips by a shunt reactance, and to this order of approximation the reactive fields at the interface between the dielectric and free space can be neglected. If the successive planes of strips are close together, interaction occurs between the reactive fields associated with each plane and the equivalent circuit must be modified. A valid representation is a set of transmission lines corresponding to the plane wave and the possible evanescent waves which are coupled together at the positions of the planes of strips [Fig. 1(*b*)]. A general theory[4] for the behaviour of such a coupled system shows that it can be replaced by a continuous region capable of supporting a number of independent modes, each typified by a propagation coefficient and a transverse field distribution in a similar way to the modes of a waveguide. These modes are excited at the interface between the material and free space. When only one mode can propagate freely, the effects of the remaining evanescent modes can be lumped together to give any of the possible representations discussed in Reference 1. In Section 2 the theory will be developed on the assumption that only the least attenuated of the evanescent modes need be considered, and this development will be used to give an equivalent circuit for the junction between free space and the artificial dielectric.

(2) CALCULATION OF AN EQUIVALENT CIRCUIT FOR A FREE-SPACE/DIELECTRIC INTERFACE

The calculation is divided into three stages:

(*a*) The fields associated with one plane of strips are examined in detail, and particular attention is paid to the behaviour when an evanescent wave is incident on the strips owing to excitation from an adjacent plane. This represents a straightforward extension of the calculations used to determine the equivalent reactance of a plane of strips.

(*b*) The results of (*a*) give the representation of the medium in the form of Fig. 1(*b*), and the second stage is to obtain from this the possible modes of propagation within the medium. This is effected by applying the results of Reference 4.

(*c*) The final stage is the calculation of the reflection and transmission coefficients at the interface between free space and the medium, and leads directly to the desired equivalent circuit.

To facilitate comparison with the experimental results described in Section 3, it is assumed that the metal strips are embedded in a dielectric of permittivity ϵ. The dimensions of the strips are shown in Fig. 1.

(2.1) The Fields associated with a Single Plane of Strips

Conducting planes can be introduced in planes of symmetry to reduce the problem to that of a capacitive iris in a strip transmission line, Fig. 2(*a*). With the co-ordinate system shown, the only non-zero field components are E_x, E_z and H_y. The field can be expanded as a set of modes, consisting of the TEM

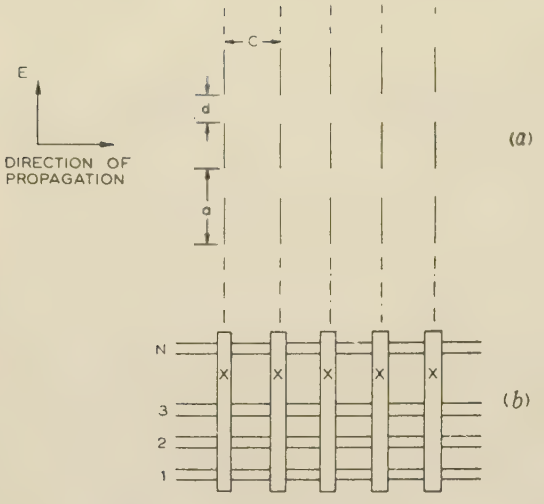

Fig. 1.—Metal-strip dielectric.

(*a*) Cross-section.
(*b*) Equivalent circuit.

The transmission lines 1, 2, ... N represent the possible waves in the dielectric supporting the strips. At each plane of strips the waves are coupled together, this coupling being represented by the reactive networks X.

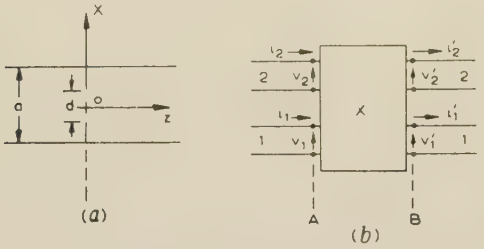

Fig. 2.—Parallel-plate line with capacitive iris in the plane $z = 0$.

(*a*) Cross-section.
(*b*) Equivalent circuit.
Line 1 represents the TEM wave.
Line 2 represents the least attenuated E mode.

At the terminals A and B, the voltages and currents correspond to the transverse electric and magnetic fields immediately to the left and right respectively of the iris.

mode and a set of E modes, all of which are evanescent provided that a is less than $\lambda/2$, λ being the wavelength of a plane wave in the dielectric base. The problem of calculating the equivalent reactance of the strip depends upon determining the field excited by an incident TEM mode. For the present analysis, a more general incident field, consisting of a plane wave plus the first E-mode, is assumed. This excites a reflected field and a transmitted field, so that

$$E_x = a_1\varepsilon^{-jkz} + a_2\varepsilon^{-\beta_2 z}\cos(2\pi x/a) + \sum_{n=1}^{\infty} b_n\varepsilon^{\beta_n z}\cos[2(n-1)\pi x/a] \quad \text{when } z \leqslant 0$$

$$= (a_1 + b_1)\varepsilon^{-jkz} + (a_2 + b_2)\varepsilon^{-\beta_2 z}\cos(2\pi x/a) + \sum_{n=3}^{\infty} b_n\varepsilon^{-\beta_n z}\cos[2\pi(n-1)x/a] \text{ when } z \geqslant 0 \quad (1)$$

where a_1, a_2 are respectively the amplitudes of the incident TEM- and E-mode fields, b_n is the amplitude of the nth reflected mode, and

$$jk = \beta_1 = j\omega(\epsilon\mu_0)^{1/2} \quad . \quad . \quad . \quad . \quad . \quad . \quad . \quad . \quad . \quad (2)$$

$$\beta_n^2 = 4(n-1)^2\pi^2/a^2 - k^2 \qquad n \geqslant 2 \quad . \quad . \quad . \quad . \quad (3)$$

Eqn. (1) is written in such a way that the continuity of E_x across the plane $z = 0$, where the strip is located, is automatically satisfied. The component H_y must be continuous in the gap between the strips, and this enables the amplitudes b_n to be calculated in terms of the incident amplitudes a_1 and a_2. Under quasi-static conditions, i.e. if a is much less than λ, the term k^2 can be neglected in eqn. (3), and the calculation of the values of b_1, b_2, etc., can be made by a simple extension of the method used by Schwinger[5] for the capacitive iris. The details of the calculation are given in Reference 6, the result being

$$\begin{bmatrix} b_1 \\ b_2 \end{bmatrix} = \begin{bmatrix} p-1 & jp(1-t)a/\lambda \\ 2p(1-t) & 2j(a/\lambda)(1-t)^2p + t^2 - 1 \end{bmatrix}\begin{bmatrix} a_1 \\ a_2 \end{bmatrix} \quad (4)$$

where $$t = \sin^2(\pi d/2a) \quad . \quad . \quad . \quad . \quad . \quad . \quad . \quad . \quad (5)$$

$$p = [1 - j(a/\lambda)\log_\varepsilon t]^{-1} \quad . \quad . \quad . \quad . \quad (6)$$

The values for the remaining amplitudes b_n are not required.

The matrix equation, eqn. (4), is now used to determine the form of the coupling networks in Fig. 1(*b*). The condition investigated in this Section is illustrated by Fig. 2(*b*), where transmission lines are used to represent the TEM and first E modes. The propagation coefficients for these lines are jk and β_2 respectively and the impedances are taken as Z_1 and Z_2, the wave impedances for the TEM and first E modes respectively. The voltages and currents, as defined in Fig. 2(*b*), are related by a reactance matrix, which can be used to give an equation[4] of the form

$$\begin{bmatrix} v_1 \\ v_2 \\ i_1 \\ i_2 \end{bmatrix} = \begin{bmatrix} \boldsymbol{L} & \boldsymbol{M} \\ \boldsymbol{N} & \tilde{\boldsymbol{L}} \end{bmatrix}\begin{bmatrix} v_1^1 \\ v_2^1 \\ i_1^1 \\ i_2^1 \end{bmatrix} \quad . \quad . \quad . \quad . \quad (7)$$

where $\boldsymbol{L}$, $\boldsymbol{M}$, $\boldsymbol{N}$ are 2×2 square matrices and $\tilde{\boldsymbol{L}}$ is the transpose of $\boldsymbol{L}$. $\boldsymbol{L}$ is a real matrix and $\boldsymbol{M}$, $\boldsymbol{N}$ are imaginary symmetric matrices. For the present problem, this equation can be simplified, since the field component E_x is continuous in the plane of the strips, implying that

$$\begin{bmatrix} v_1 \\ v_2 \end{bmatrix} = \begin{bmatrix} v_1^1 \\ v_2^1 \end{bmatrix} \quad . \quad . \quad . \quad . \quad . \quad . \quad . \quad (8)$$

from which it follows that

$$\boldsymbol{L} = \tilde{\boldsymbol{L}} = \boldsymbol{I} \quad . \quad . \quad . \quad . \quad . \quad . \quad . \quad (9)$$

$$\boldsymbol{M} = \boldsymbol{O} \quad . \quad . \quad . \quad . \quad . \quad . \quad . \quad (10)$$

$\boldsymbol{I}$ being the 2×2 unit matrix and $\boldsymbol{O}$ the 2×2 zero matrix.

The normal procedure relating voltages and currents on transmission lines to the complex amplitudes of the incident and reflected waves gives

$$\begin{bmatrix} v_1 \\ v_2 \end{bmatrix} = \begin{bmatrix} v_1^1 \\ v_2^1 \end{bmatrix} = \begin{bmatrix} a_1 + b_1 \\ a_2 + b_2 \end{bmatrix} \quad . \quad . \quad . \quad . \quad (11)$$

$$\begin{bmatrix} i_1 \\ i_2 \end{bmatrix} = \begin{bmatrix} 1/Z_1 & 0 \\ 0 & 1/Z_2 \end{bmatrix}\begin{bmatrix} a_1 - b_1 \\ a_2 - b_2 \end{bmatrix} \quad . \quad . \quad (12)$$

$$\begin{bmatrix} i_1^1 \\ i_2^1 \end{bmatrix} = \begin{bmatrix} 1/Z_1 & 0 \\ 0 & 1/Z_2 \end{bmatrix}\begin{bmatrix} a_1 + b_1 \\ a_2 + b_2 \end{bmatrix} \quad . \quad . \quad (13)$$

From eqns. (7)–(9),

$$\begin{bmatrix} i_1 \\ i_2 \end{bmatrix} = \boldsymbol{N}\begin{bmatrix} v_1 \\ v_2 \end{bmatrix} + \begin{bmatrix} i_1^1 \\ i_2^1 \end{bmatrix} \quad . \quad . \quad . \quad . \quad (14)$$

and substitution from eqns. (11)–(13) gives

$$\boldsymbol{Z}^{-1}\begin{bmatrix} a_1 - b_1 \\ a_2 - b_2 \end{bmatrix} = \boldsymbol{N}\begin{bmatrix} a_1 + b_1 \\ a_2 + b_2 \end{bmatrix} + \boldsymbol{Z}^{-1}\begin{bmatrix} a_1 + b_1 \\ a_2 + b_2 \end{bmatrix} \quad (15)$$

where $\boldsymbol{Z}$ is the matrix $\begin{bmatrix} Z_1 & 0 \\ 0 & Z_2 \end{bmatrix}$

Eqn. (15) simplifies to

$$[\boldsymbol{N} + 2\boldsymbol{Z}^{-1}]\begin{bmatrix} b_1 \\ b_2 \end{bmatrix} = -\boldsymbol{N}\begin{bmatrix} a_1 \\ a_2 \end{bmatrix} \quad . \quad . \quad . \quad (16)$$

which, when compared with eqn. (4), shows that

$$[\boldsymbol{I} + 2\boldsymbol{N}^{-1}\boldsymbol{Z}^{-1}]^{-1} = -\begin{bmatrix} p - 1 & jp(1-t)a/\lambda \\ 2p(1-t) & 2j(a/\lambda)(1-t)^2 + t^2 - 1 \end{bmatrix} \quad . \quad . \quad . \quad . \quad (17)$$

from which $\boldsymbol{N}$ can be obtained. The matrix in eqn. (7) which specifies the properties of the reactive coupling network is then determined in terms of the strip dimensions and the operating wavelength.

(2.2) Possible Modes of Propagation in a Strip Dielectric

When a number of transmission lines are coupled together at regular intervals by identical networks, a set of independent modes of propagation can be found equal in number to the number of transmission lines. The voltages and currents at the points midway between the coupling networks can be expressed as a sum of these modes, each of which has a particular propagation coefficient and a definite relation between the voltages and currents in the individual lines. This approach is an obvious extension of the simple transmission-line analysis already referred to, and represents a basic section of the medium of length c [Fig. 3(*a*)] as a set of independent lines [Fig. 3(*b*)]. From a general study of such coupled systems,[4] it can be shown that the mode propagation coefficients are given by the latent roots of a matrix, which in the present problem becomes

$$\boldsymbol{T} = \boldsymbol{C}^2 + \boldsymbol{S}^2 + \boldsymbol{SZNC} \quad . \quad . \quad . \quad . \quad . \quad . \quad (18)$$

where

$$\boldsymbol{C} = \begin{bmatrix} \cos(kc/2) & 0 \\ 0 & \cosh(\beta_2 c/2) \end{bmatrix} \quad . \quad . \quad . \quad (19)$$

$$\boldsymbol{S} = \begin{bmatrix} j\sin(kc/2) & 0 \\ 0 & \sinh(\beta_2 c/2) \end{bmatrix} \quad . \quad . \quad . \quad (20)$$

The latent roots of $\boldsymbol{T}$ are obtained to a sufficient degree of approximation in Section 6.1, and, from them, the propagation coefficients of the two possible modes in the metal delay structure[4] are given by

$$\cosh(\gamma_1 c) = \left[\cos(kc) + \left(\frac{a}{\lambda}\right)\log_\varepsilon t \sin(kc)\right]\left[1 + \frac{4a}{\lambda}(1-t)^2 \sin(kc)\varepsilon^{-\beta_2 c}\right] \quad (21)$$

$$\cosh(\gamma_2 c) = \varepsilon^{\beta_2 c}/2t^2 \quad . \quad . \quad . \quad . \quad . \quad . \quad . \quad . \quad . \quad . \quad (22)$$

The first of these differs from the expression obtained from the simple transmission-line theory[3] only in the presence of the second factor. This factor tends rapidly to unity as c increases, confirming that the simple theory is valid when the separation between adjacent planes of strips is sufficiently large. Substitution from eqn. (5) for t and the use of the quasi-static approximation for β_2 shows that this factor cannot exceed $1 + (4a/\lambda)\exp(-2\pi c/a)]$. It is easily verified that this differs from unity by less than 1% if a/λ is less than 0·25 and c/a exceeds 0·75, conditions which are often satisfied in practice. Eqn. (21) will give more accurate values for the propagation coefficient γ_1 when the strip dimensions do not satisfy these restrictions.

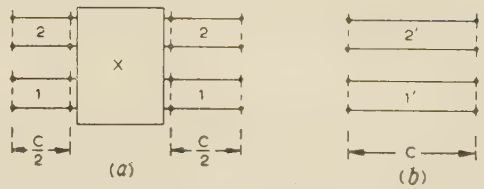

Fig. 3.—Metal-strip dielectric.
(*a*) Basic section of equivalent circuit. The elements are those defined in Fig. 2(*b*).
(*b*) Representation of basic section by two independent lines corresponding to the two modes of propagation in the strip dielectric.

In the applications of interest, the first-mode propagation coefficient, i.e. γ_1, is imaginary and $\cosh(\gamma_1 c)$ is less than unity. The second mode is evanescent, and when approximations are made in eqn. (22) by neglecting the other evanescent modes it is found that

$$\gamma_2 = 2\pi/a + \frac{4}{c}\log_\varepsilon\left(\operatorname{cosec}\frac{\pi d}{a}\right) \quad . \quad . \quad . \quad (23)$$

Each of the two modes is associated with a particular transverse field distribution and this can be specified by the relative amplitudes of the waves on the two lines of Fig. 3(*b*). These relative amplitudes are obtained from the latent vectors of the matrix $\boldsymbol{T}$ and also give the transverse field distribution in the structure at points midway between adjacent planes of strips.[4] These fields can be written

$$E_x = \alpha_{1i} + \alpha_{2i}\cos(2\pi x/a) \quad . \quad . \quad . \quad . \quad (24)$$

$$H_y = \beta_{1i} + \beta_{2i}\cos(2\pi x/a) \quad . \quad . \quad . \quad . \quad (25)$$

where the suffix i indicates which mode is being considered.

The calculation of the values of the constants associated with the two modes is carried out in Section 6.2. For the present purpose the general expressions can be simplified by assuming that the strip spacings are much less than the operating wavelength, and then

$$\alpha_{21} = 4\alpha_{11}(1-t)\exp(-\tfrac{1}{2}\beta_2 c) \quad . \quad . \quad . \quad . \quad (26)$$

$$\alpha_{12} = 0 \quad . \quad . \quad . \quad . \quad . \quad . \quad . \quad . \quad . \quad . \quad . \quad (27)$$

$$Z_1\beta_{11} = k_1\alpha_{11}/k \quad . \quad . \quad . \quad . \quad . \quad . \quad . \quad . \quad (28)$$

$$Z_1\beta_{12} = -2j\alpha_{22}(a/\lambda)(1-t)\exp(-\tfrac{1}{2}\beta_2 c) \quad . \quad (29)$$

$$Z_2\beta_{21} = 2j\alpha_{11}k_1 c(1-t)\exp(-\tfrac{1}{2}\beta_2 c) \quad . \quad . \quad (30)$$

$$Z_2\beta_{22} = \alpha_{22} \quad . \quad . \quad . \quad . \quad . \quad . \quad . \quad . \quad . \quad . \quad (31)$$

in which γ_1 has been replaced by jk_1.

The remaining two constants, α_{11} and α_{22}, can be regarded as the amplitudes of the first and second modes respectively in the artificial dielectric. They are determined in order to satisfy the continuity of the fields at the free-space/dielectric interface when a plane wave is incident from free space.

(2.3) Behaviour at a Free-Space/Dielectric Interface

The interface between free space and the dielectric is defined to be a distance $c/2$ from the first plane of strips. In this plane the fields excited within the dielectric consist of the two modes defined by letting i equal 1 and 2 in eqns. (24) and (25). The dielectric supporting the strips is also presumed to terminate at this plane, the discontinuity resulting from this being taken into

account by the choice of Z_1 and Z_2 as wave impedances within the dielectric. Suppose that the incident plane wave is given at the interface plane by

$$E_x = 1;\ H_y = 1/Z_0 \quad . \quad . \quad . \quad . \quad . \quad (32)$$

where Z_0 is the free-space plane-wave impedance. There is also a reflected plane wave of amplitude R_1, and inspection of eqn. (24) shows that the continuity of E_x across the interface plane requires a 'reflected' evanescent wave in the free-space region. If this has amplitude R_2, the fields on the free-space side of the interface are

$$E_x = 1 + R_1 + R_2 \cos(2\pi x/a) \quad . \quad . \quad . \quad . \quad (33)$$

$$H_y = (1 - R_1)/Z_0 - (R_2/Z_{02}) \cos(2\pi x/a) \quad . \quad (34)$$

where Z_{02} is the wave impedance for the evanescent wave in free space. For the plane waves in free space and in the supporting dielectric

$$Z_0/Z_1 = (\epsilon/\epsilon_0)^{1/2} \quad . \quad . \quad . \quad . \quad . \quad (35)$$

and for the evanescent waves

$$Z_{02}/Z_2 = (\epsilon/\epsilon_0)^{1/2} \quad . \quad . \quad . \quad . \quad . \quad (36)$$

to the degree of approximation being considered.

Inspection of eqns. (24), (25), (33) and (34) shows that continuity across the interface requires that

$$1 + R_1 = \alpha_{11} + \alpha_{12} \quad . \quad . \quad . \quad . \quad . \quad . \quad (37)$$

$$R_2 = \alpha_{21} + \alpha_{22} \quad . \quad . \quad . \quad . \quad . \quad . \quad (38)$$

$$1 - R_1 = (\epsilon/\epsilon_0)^{1/2} Z_1(\beta_{11} + \beta_{12}) \quad . \quad . \quad . \quad (39)$$

$$-R_2 = (\epsilon/\epsilon_0)^{1/2} Z_2(\beta_{21} + \beta_{22}) \quad . \quad . \quad . \quad (40)$$

Only the values of R_1 and α_{11}, corresponding respectively to the amplitudes of the reflected plane wave and the transmitted wave in the dielectric, are needed, and they can be found by eliminating the other unknowns from eqns. (26)–(31) and (37)–(40). The results are

$$R_1 = \frac{k_0 - k_1}{k_0 + k_1} - \frac{16jk_0^2}{(k_0 + k_1)^2} \frac{a}{\lambda} \frac{\cos^4(\pi d/2a)}{1 + (\epsilon/\epsilon_0)^{1/2}} \exp(-2\pi c/a) \quad (41)$$

and

$$\alpha_{11} = 1 + R_1 = \frac{2k_0}{k_0 + k_1} \left[1 - \frac{8jk_0}{k_0 + k_1} \frac{a}{\lambda} \frac{\cos^4(\pi d/2a)}{1 + (\epsilon/\epsilon_0)^{1/2}} \exp(-2\pi c/a)\right] \quad (42)$$

in which k_0 is the free-space plane-wave phase-change coefficient, and t has been replaced by its value from eqn. (5).

From these results the parameters of the equivalent circuit of Fig. 4 can be calculated. A convenient choice for the impedance of the line representing the incident plane wave is Z_0, and Z must then be calculated to give the correct magnitude of R_1, as given by eqn. (41). To the order of approximation retained in the present analysis

$$R_1 = |1 - n|/(1 + n) \quad . \quad . \quad . \quad . \quad (43)$$

where $n = k_1/k_0$ is the refractive index of the artificial dielectric.

Hence, Z can be selected as Z_0/n or nZ_0; the former is preferred as being identical to the value for a continuous dielectric of the same refractive index.

No fresh information is yielded by considering the magnitude of α_{11}, because conservation of power requires that the incident energy be shared between the reflected and transmitted waves. The amplitudes of these waves are therefore not independent.

The extra lengths of line in Fig. 4 are selected to give the correct value for the phases of the reflected and transmitted waves, so that

$$2k_0 l_1 = \pi - \arg R_1 \quad . \quad . \quad . \quad (44)$$

$$k_0 l_1 + k_1 l_2 = -\arg \alpha_{11} \quad . \quad . \quad . \quad . \quad (45)$$

The π in eqn. (44) arises because Z is less than Z_0 (n exceeds unity), giving a phase change of π on reflection at the junction between the two lines in Fig. 4. The arguments of R_1 and α_{11} are both small, and to an adequate degree of approximation

$$k_0 l_1 = -\frac{8a \cos^4(\pi d/2a) \exp(-2\pi c/a)}{\lambda(n^2 - 1)[1 + (\epsilon/\epsilon_0)^{1/2}]} \quad . \quad . \quad (46)$$

$$l_2 = -l_1 \quad . \quad . \quad . \quad . \quad . \quad . \quad . \quad . \quad . \quad . \quad (47)$$

Two points of interest arise in this result. First, the lengths are independent of the wavelength, and secondly, since they are numerically equal but of opposite sign, the net result is equivalent to supposing that the dielectric extends into free space a distance l_2 beyond the physical interface. Kharadly[7] has already suggested that this is a possible method of allowing for the reactive fields at the interface and has given experimental evidence of its validity.

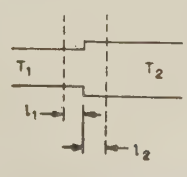

Fig. 4.—Equivalent circuit for free-space/artificial-dielectric interface.

T_1 is a line of phase-constant k_0 and impedance Z_0, representing the free-space plane wave.

T_2 is a line of phase-constant k_1 and impedance Z representing the principal mode in the artificial dielectric.

Terminals A and B correspond to planes on the free-space and dielectric sides of the interface, respectively.

(3) EXPERIMENTAL VERIFICATION OF THEORETICAL RESULTS

Detailed measurements on a strip dielectric have been carried out to verify the predictions of the theory given in the preceding Sections. Miles[8] has shown that there is a very close correspondence between free-space propagation at normal incidence on the type of structure considered and free-space propagation obliquely incident. His argument has been extended to show that experiments on artificial dielectrics of the strip type can be carried out in a rectangular waveguide, provided that all wavelengths are interpreted as guide wavelengths.[9] The strip dielectric was therefore made from tin-foil 0·002 in thick supported by expanded polystyrene of relative permittivity 1·035, the whole assembly being contained in waveguide No. 10. The dimensions of the strips [see Fig. 1(*a*)] were

$$a = 3{\cdot}40\,\text{cm}$$

$$c = 0{\cdot}508\,\text{cm}$$

$$d = a/2 = 1{\cdot}70\,\text{cm}$$

The operating frequency was such that the wavelength in the empty guide was 15·55 cm (i.e. $k_0 = 2\pi/15{\cdot}55$) and in a guide filled with expanded polystyrene the wavelength was 15·00 cm ($k = 2\pi/15{\cdot}00$). In the application of the theory, the effective relative permittivity of the supporting dielectric is therefore to be taken as

$$\epsilon/\epsilon_0 = (15{\cdot}55/15{\cdot}00)^2 = 1{\cdot}075 \quad . \quad . \quad . \quad (48)$$

(3.1) Measurement Technique

Considerable difficulties arise in making measurements on a single interface, and a method was developed by which results could be obtained using sections of finite length. For each such section the magnitude of the reflection coefficient, $|\rho|$, and its phase, ψ, referred to the input interface can be obtained very accurately by the Weissfloch or tangent method.[10] The problem then reduces to finding a method of extracting the parameters of the equivalent circuit (Fig. 5) from the measured values of $|\rho|$ and ψ taken for a series of different lengths, l.

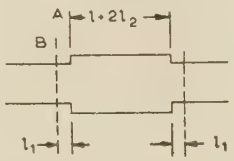

Fig. 5.—Equivalent circuit for section of artificial dielectric of length l.

From Fig. 5 the impedance looking to the right at A is

$$Z_A = Z\frac{Z_0 + jZ\tan\phi}{Z + jZ_0\tan\phi} \quad . \quad . \quad . \quad . \quad (49)$$

where $$\phi = k_1(l + 2l_2) \quad . \quad . \quad . \quad . \quad . \quad (50)$$

The corresponding reflection coefficient is

$$\rho_A = \frac{Z_0 - Z_A}{Z_0 + Z_A} = \frac{j(Z_0^2 - Z^2)\tan\phi}{2ZZ_0 + j(Z_0^2 + Z^2)\tan\phi} \quad . \quad (51)$$

and the reflection coefficient at B, which corresponds to the free-space side of the interface, is

$$\rho_B = |\rho|\varepsilon^{j\psi} = \frac{j(Z_0^2 - Z^2)\tan\phi}{2ZZ_0 + j(Z_0^2 + Z^2)\tan\phi}\exp(2jk_0l) \quad (52)$$

Hence $$|\rho| = \frac{(Z_0^2 - Z^2)\,|\tan\phi|}{[4Z^2Z_0^2 + (Z_0^2 + Z^2)^2\tan^2\phi]^{1/2}} \quad . \quad . \quad (53)$$

from which it can be shown that

$$\frac{2|\rho|}{(1 - |\rho|^2)^{1/2}} = \left(\frac{Z_0}{Z} - \frac{Z}{Z_0}\right)|\sin\phi|$$

$$= \left(\frac{Z_0}{Z} - \frac{Z}{Z_0}\right)|\sin[k_1(l + 2l_2)]| \quad (54)$$

It is assumed in eqns. (52) to (54) that Z is less than Z_0. Eqn. (54) shows that if $2|\rho|/(1 - |\rho|^2)^{1/2}$ is plotted against l a sinusoidal curve will result. Further, the zeros of this curve occur for

$$k_1(l + 2l_2) = \text{a multiple of } \pi \quad . \quad . \quad . \quad (55)$$

so that observations of the positions of two zeros will give both k_1 and l_2. The maximum value of $2|\rho|/(1 - |\rho|^2)^{1/2}$ occurs when the sine function is unity and is equal to $(Z_0^2 - Z^2)/ZZ_0$, from which Z/Z_0 can be calculated.

The experimental curve for the specimens tested is shown in Fig. 6, $2|\rho|/(1 - |\rho|^2)^{1/2}$ being plotted against the number of strips in the section. From this curve, using the above argument, it is found that

$$k_1 = \frac{\pi}{11 \cdot 1c} = \frac{\pi}{5 \cdot 63} \text{ whence } n = k_1/k_0 = 1 \cdot 38$$

$$k_1l_2 = 0 \cdot 14, \text{ i.e. } l_2 = 0 \cdot 023\lambda_0/n = 0 \cdot 017\lambda_0$$
$$(Z_0^2 - Z^2)/ZZ_0 = 0 \cdot 70, \text{ i.e. } Z/Z_0 = 0 \cdot 71.$$

The only remaining parameter is l_1, and to obtain this the

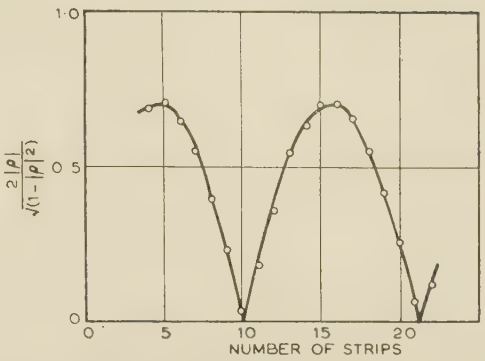

Fig. 6.—Curve plotted from measured values of reflection-coefficient magnitude for different numbers of strips in section.

phase of the reflection coefficient must be considered. From eqn. (52),

$$|\rho|\cos\psi = \frac{(Z_0^2 - Z^2)\tan\phi[(Z_0^2 + Z^2)\tan\phi\cos(2k_0l_1) - 2ZZ_0\sin(2k_0l_1)]}{[4Z^2Z_0^2 + (Z_0^2 + Z^2)^2\tan^2\phi]^{1/2}} \quad . \quad . \quad . \quad . \quad (56)$$

which, together with eqn. (53), leads after some algebraic manipulation to

$$\frac{2\cos\psi}{(1 - |\rho|^2)^{1/2}} = \left[4\sin^2(2k_0l_1) + \cos^2(2k_0l_1)\left(\frac{Z_0}{Z} + \frac{Z}{Z_0}\right)^2\right]^{1/2} \times \left|\sin\left[\phi + \tan^{-1}\left(\frac{2ZZ_0\tan 2k_0l_1}{Z^2 + Z_0^2}\right)\right]\right| \quad (57)$$

which shows that if $2\cos\psi/(1 - |\rho|^2)^{1/2}$ is plotted against the length of the section a sinusoidal curve again results. The zeros differ from those of the previous curve by the angle $\text{arc tan}\left(\frac{2\tan 2k_0l_1}{\frac{Z}{Z_0} + \frac{Z_0}{Z}}\right)$ and can therefore be used to determine l_1.

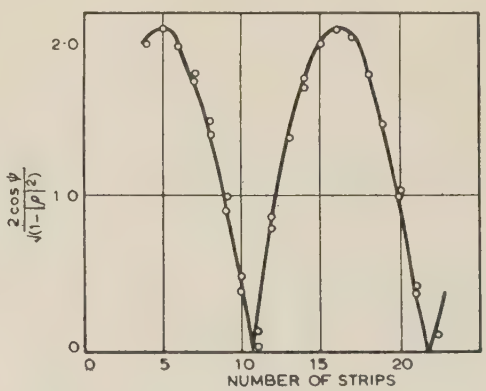

Fig. 7.—Curve plotted from measured values of reflection-coefficient magnitude and phase for different numbers of strips in section.

The experimental curve is shown in Fig. 7, from which it is found that

$$k_0l_1 = -0 \cdot 081 \quad \text{i.e. } l_1 = -0 \cdot 013\lambda_0$$

The properties of the strip dielectric are now completely specified.

(3.2) Comparison of Theoretical and Experimental Results

The theoretical values for the parameters of the strip dielectric are easily obtained by substituting the values of the dimensions,

wavelength and effective relative permittivity of the supporting material in the appropriate equations of Section 2. The results are collected in Table 1.

Table 1

THEORETICAL AND MEASURED VALUES OF METAL-STRIP-DIELECTRIC PARAMETERS

Quantity	Theoretical value	Measured value	Estimated maximum error
			%
Refractive index, n ..	1·37	1·38	±1
Relative impedance, Z/Z_0	0·73	0·71	±3
Length, l_1	$-0{\cdot}014\lambda_0$	$-0{\cdot}013\lambda_0$	±25
Length, l_2	$+0{\cdot}014\lambda_0$	$0{\cdot}017\lambda_0$	±25

In each case the difference between the experimental and theoretical values is within the limits of experimental error.

(4) CONCLUSION

It has been shown that the effects of reactive fields at the interface between free space and an artificial dielectric may be predicted by considering the excitation of evanescent modes.

$$\boldsymbol{T} = \begin{bmatrix} \exp(-jkc) + j\sin(kc)\left[\frac{1}{p} + \frac{2ja(1-t)^2}{\lambda t^2}\right] & \frac{2a(1-t)}{\lambda t^2}\sin\left(\frac{kc}{2}\right)\cosh\left(\frac{\beta_2 c}{2}\right) \\ -\frac{4(1-t)}{t^2}\sinh\left(\frac{\beta_2 c}{2}\right)\cos\left(\frac{kc}{2}\right) & \exp(-\beta_2 c) + \frac{1}{t^2}\sinh(\beta_2 c) \end{bmatrix} \quad . \quad . \quad . \quad . \quad . \quad (63)$$

Reasonable approximations to the phase shifts which occur at the interface can be obtained by making allowance for the excitation of the first of these evanescent modes. The method described in the paper is general and can be applied in principle to any form of artificial dielectric.

(5) REFERENCES

(1) BROWN, J., and JACKSON, W.: 'The Properties of Artificial Dielectrics at Centimetre Wavelengths', *Proceedings I.E.E.*, Paper No. 1699 R, January, 1955 (**102** B, p. 11).

(2) CARLSON, J. F., and HEINS, A. E.: 'Reflection of an Electromagnetic Wave by an Infinite Set of Plates', *Quarterly Journal of Applied Mathematics*, 1947, **4**, p. 313.

(3) BROWN, J.: 'Design of Metallic Delay Dielectrics', *Proceedings I.E.E.*, Paper No. 915 R, January, 1950 (**97**, Part III, p. 45).

(4) BROWN, J.: 'Propagation in Coupled Transmission Line Systems', *Quarterly Journal of Mechanics and Applied Mathematics*. To be published.

(5) SCHWINGER, J.: 'Discontinuities in Waveguides' (M.I.T. Lecture Notes. D. S. Saxon, Ed.)

(6) BROWN, J.: 'A Theoretical Study of Some Artificial Dielectrics', Ph.D. Thesis, University of London, December, 1954.

(7) EL-KHARADLY, M. M. Z.: 'Some Experiments on Artificial Dielectrics at Centimetric Wavelengths', *Proceedings I.E.E.*, Paper No. 1700 R, January, 1955 (**102** B, p. 17).

(8) MILES, J. W.: 'The Reduction of Three Dimensional Electromagnetic Problems', *Journal of Applied Physics*, 1952, **23**, p. 372.

(9) BROWN, J., and CARNE, A.: Paper in preparation.

(10) BARLOW, H. M., and CULLEN, A. L.: 'Microwave Measurements' (Constable, 1950).

(6) APPENDIX

(6.1) Calculation of the Latent Roots of the Matrix T

The matrix $\boldsymbol{T}$ is defined by eqn. (18), which can be rewritten thus

$$\boldsymbol{T} = [\boldsymbol{C} - \boldsymbol{S}]^2 + 2\boldsymbol{S}[\boldsymbol{I} + \tfrac{1}{2}\boldsymbol{Z}\boldsymbol{N}]\boldsymbol{C} \quad . \quad . \quad . \quad (58)$$

From eqn. (17)

$$[\boldsymbol{N} + 2\boldsymbol{Z}^{-1}]^{-1}\boldsymbol{N} = \boldsymbol{I} - \begin{bmatrix} p & jp(1-t)(a/\lambda) \\ 2p(1-t) & t^2 + 2jp(1-t)^2(a/\lambda) \end{bmatrix} \quad (59)$$

i.e. $$[\boldsymbol{N} + 2\boldsymbol{Z}^{-1}]^{-1}[\boldsymbol{N} - \boldsymbol{N} - 2\boldsymbol{Z}^{-1}] = -\begin{bmatrix} p & jp(1-t)(a/\lambda) \\ 2p(1-t) & t^2 + 2jp(1-t)^2(a/\lambda) \end{bmatrix} \quad (60)$$

giving

$$\tfrac{1}{2}\boldsymbol{Z}[\boldsymbol{N} + 2\boldsymbol{Z}^{-1}] = \begin{bmatrix} p & jp(1-t)(a/\lambda) \\ 2p(1-t) & t^2 + 2jp(1-t)(a/\lambda) \end{bmatrix} \quad (61)$$

$$\boldsymbol{I} + \tfrac{1}{2}\boldsymbol{Z}\boldsymbol{N} = \begin{bmatrix} \frac{1}{p} + \frac{2ja(1-t)^2}{\lambda t^2} & -\frac{ja(1-t)}{\lambda t^2} \\ -\frac{2(1-t)}{\lambda t^2} & \frac{1}{t^2} \end{bmatrix} . \quad (62)$$

Substitution into eqn. (58) gives

The latent roots of $\boldsymbol{T}$ are the roots of the equation

$$\left\{\exp(-jkc) + j\sin(kc)\left[\frac{1}{p} + \frac{2ja(1-t)^2}{\lambda t^2}\right] - \xi\right\}\left[\exp(-\beta_2 c) + \frac{1}{t^2}\sinh(\beta_2 c) - \xi\right] + \frac{2a(1-t)^2}{\lambda t^4}\sin(kc)\sinh(\beta_2 c) = 0 \quad . \quad . \quad . \quad (64)$$

The analysis is based on the neglect of coupling by evanescent modes other than the least attenuated, and approximations to the same degree of accuracy can be made in calculating the latent roots. The values are

$$\xi_1 = \left[\cos(kc) + \frac{a}{\lambda}\log_\varepsilon t\sin(kc)\right]\left[1 + \frac{4a}{\lambda}(1-t)^2\sin(kc)\exp(-\beta_2 c)\right] \quad (65)$$

$$\xi_2 = \exp(\beta_2 c)/2t^2 \quad . \quad . \quad . \quad . \quad (66)$$

From the general theory for coupled transmission lines, the propagation coefficients of the possible modes are given by

$$\cosh(\gamma_1 c) = \xi_1 \quad . \quad . \quad . \quad . \quad . \quad (67)$$

$$\cosh(\gamma_2 c) = \xi_2 \quad . \quad . \quad . \quad . \quad . \quad (68)$$

(6.2) Calculation of the Mode Distributions

The fields corresponding to the two modes have the form given by eqns. (24) and (25). The elements $[\alpha_{1i}, \alpha_{2i}]$ come from the latent vector of $\boldsymbol{T}$ corresponding to the root ξi, so that

$$\frac{\alpha_{21}}{\alpha_{11}} = -\frac{\exp(-jkc) + j\left[\frac{1}{p} + \frac{2ja}{\lambda t^2}(1-t)^2\right]\sin(kc) - \xi_1}{2\left(\frac{a}{\lambda t^2}\right)(1-t)\sin\left(\frac{kc}{2}\right)\cosh\left(\frac{\beta_2 c}{2}\right)} \quad (69)$$

$$\frac{\alpha_{12}}{\alpha_{22}} = -\frac{2\left(\frac{a}{\lambda t^2}\right)(1-t)\sin\left(\frac{kc}{2}\right)\cosh\left(\frac{\beta_2 c}{2}\right)}{\exp(-jkc) + j\left[\frac{1}{p} + \frac{2ja}{\lambda t^2}(1-t)^2\right]\sin(kc) - \xi_2} \quad (70)$$

To the required degree of approximation these equations become

$$\alpha_{21} = 4\alpha_{11}(1-t)\cos(\tfrac{1}{2}kc)\exp(-\tfrac{1}{2}\beta_2 c) \quad . \quad . \quad (71)$$

$$\alpha_{21} = 2\alpha_{22}(1-t)\sin(\tfrac{1}{2}kc)\exp(-\tfrac{1}{2}\beta_2 c) \quad . \quad . \quad (72)$$

The elements β_{ij} which determine the current (magnetic-field) distributions are obtained[4, 6] from the general relation

$$Z\beta = \boldsymbol{S}^{-1}\boldsymbol{C}\alpha\boldsymbol{W} \quad . \quad . \quad . \quad . \quad . \quad . \quad (73)$$

where $\boldsymbol{W}$ is a diagonal matrix with elements $\tanh(\frac{1}{2}\gamma_s c)$; $s = 1, 2$.

Hence

$$Z_1\beta_{11} = \alpha_{11}\tan(\tfrac{1}{2}k_1 c)/\tan(\tfrac{1}{2}kc) \quad . \quad . \quad . \quad (74)$$

$$Z_1\beta_{12} = -j\alpha_{12}\cot(\tfrac{1}{2}kc) \quad . \quad . \quad . \quad . \quad . \quad (75)$$

$$Z_2\beta_{21} = j\alpha_{21}\tan(\tfrac{1}{2}k_1 c) \quad . \quad . \quad . \quad . \quad . \quad (76)$$

$$Z_2\beta_{22} = \beta_{22} \quad . \quad . \quad . \quad . \quad . \quad . \quad . \quad . \quad . \quad (77)$$

to the same degree of approximation as before.

A further simplification can be made when the spacings a, c are much less than the wavelength, by replacing the trigonometric functions by their first approximations. This leads to the set of eqns. (26) to (31), which are accurate to the first powers of (a/λ) and (c/λ).

621.371: 621.396.67

The Institution of Electrical Engineers
Monograph No. 301[R
Apr. 1958

A GENERALIZED FORM OF THE AERIAL RECIPROCITY THEOREM

By J. BROWN, M.A., Ph.D., Associate Member.

(*The paper was first received* 10*th December*, 1957, *and in revised form* 28*th January*, 1958. *It was published as an* INSTITUTION MONOGRAPH *in April* 1958.)

SUMMARY

The reciprocity theorem which relates the transmission and reception properties of an aerial is extended to give information on the phase and amplitude of the signal received by the aerial for an incident plane wave of any polarization. The paper includes a rigorous proof based on the Lorentz reciprocity theorem for electromagnetic fields.

LIST OF SYMBOLS

r, θ, ϕ = Spherical polar co-ordinates.
θ', ϕ' = Polar angles defining direction of incoming plane wave.
ξ, η, ζ = Co-ordinates in feeder.
k = Phase-change coefficient for free-space plane wave.
β = Phase-change coefficient for mode in feeder.
Y_0 = Wave admittance for free-space plane wave.
Y_w = Wave admittance for mode in feeder.
$\boldsymbol{n}, \boldsymbol{v}, \boldsymbol{i}_r, \boldsymbol{p}$ = Unit vectors.
$\boldsymbol{E}$ = Electric field strength with suffixes as defined in text.
$\boldsymbol{H}$ = Magnetic field strength with suffixes as defined in text.
F, F' = Radiation patterns.
A, B = Complex amplitude constants.
S_1, S_2, S_3 = Surfaces of integration.
R = Radius of spherical surface S_3.
G = Power gain.
A_{eff} = Effective receiving area.
λ = Wavelength of free-space plane wave.

(1) INTRODUCTION

The usual proof of the reciprocity theorem relating the transmission and reception properties of an aerial is based on circuit theory,[1,2,3] and yields information only about signal powers. In some recent work by the author, it was necessary to extend the theorem to give information on the phases of the signals as well as their amplitudes, and this has led to a proof of the theorem based on electromagnetic field theory. Further, this proof considers only the fields radiated by the aerial under consideration, and the signal received when the aerial is illuminated by an incident plane wave. There is no need, as in the proof based on circuits, to introduce a second aerial.

The situation considered is shown in Fig. 1. L is a feeder, which may be either a transmission line or a waveguide, connected to the aerial, which is contained in the region V. The precise type of aerial is immaterial and has no bearing on the analysis.

A reference plane, P, is selected in the feeder and the phases of all the fields can be related to the phase at this plane. The only restriction on the position of P is that it should be sufficiently far from the aerial to ensure that the only field at P is that corresponding to the dominant mode in the feeder.

When the aerial is used as a transmitter, power is supplied to the feeder and a radiation field is established outside the region of the aerial. The position of any point can be specified by spherical polar co-ordinates r, θ, ϕ referred to an origin, O, within the region occupied by the aerial. The transmitting radiation pattern of the aerial is then the function of θ and ϕ which describes the variation of the radiated field for a large fixed value of the co-ordinate r. If the region V, occupied by the aerial, is of finite size, it is clear that in the limit, as r tends to infinity, the precise position of O is immaterial so long as it lies within V.

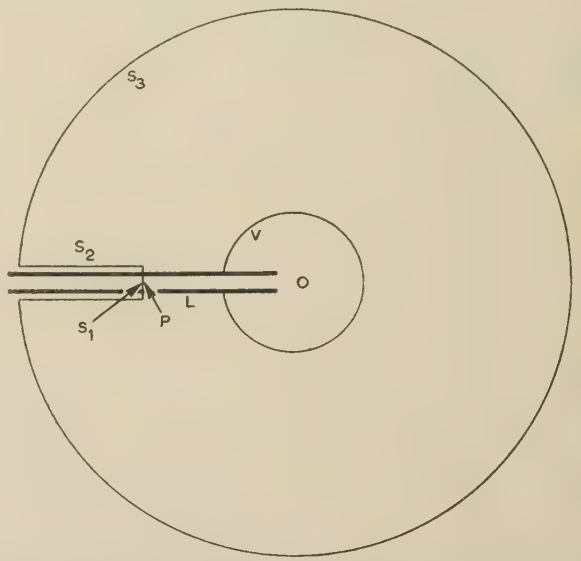

Fig. 1.—Diagram showing the physical arrangement discussed.

The aerial can have any form and lies within the region V. It is fed by the transmission line or waveguide L, in which P is a plane to which the phases of the transmitted and received signals are referred. S_1, S_2, S_3 are surfaces over which integrations are carried out.

When the aerial is used as a receiver, a plane wave is incident upon it and a signal is established within the feeder travelling away from the aerial. It will be assumed that the feeder is terminated in a matched load so that there is no wave in the feeder travelling towards the aerial. The plane wave will also be scattered by the aerial, giving rise to a reradiation field. The amplitude of the signal received in the feeder will depend on the direction of the incident plane wave, which can be specified by the spherical polar angles θ, ϕ. The functional dependence of the received amplitude on the angles θ and ϕ is the receiving radiation pattern of the aerial. It will be shown that the transmitting and receiving radiation patterns are given by the same function of θ and ϕ, in accordance with the circuit-theory version of the reciprocity theorem. Further, the proportionality constant between the patterns will be obtained in such a way that information on phases as well as on amplitudes can be obtained.

(2) PROOF OF THE RECIPROCITY THEOREM

(2.1) The Aerial as a Transmitter

It is assumed that the feeder is matched to the aerial, so that

Correspondence on Monographs is invited for consideration with a view to publication.
Dr. Brown is Reader in Electrical Engineering, University College, London.

there is no reflected wave in the feeder. The transmitting radiation pattern is defined for unit power flow in the feeder, to simplify later calculations of power gain. Expressions are wanted for the fields in the feeder and the fields radiated by the aerial.

(2.1.1) The Fields in the Feeder.

For any waveguide or transmission line, the transverse fields for a single mode are given by

$$\boldsymbol{E}_t(\xi, \eta, \zeta) = A\boldsymbol{E}(\xi, \eta) \exp(-j\beta\zeta) \quad . \quad . \quad . \quad (1)$$

$$\boldsymbol{H}_t(\xi, \eta, \zeta) = Y_w \boldsymbol{n} \times \boldsymbol{E}_t(\xi, \eta, \zeta) \quad . \quad . \quad . \quad . \quad (2)$$

where ξ, η = Co-ordinates in a plane transverse to the axis of the feeder.

ζ = Co-ordinate in the direction of the feeder axis. In the present case ζ is measured from the reference plane P towards the aerial. Eqns. (1) and (2) therefore represent a wave travelling towards the aerial.

$\boldsymbol{n}$ = Unit vector in the positive ζ-direction.

$\boldsymbol{E}(\xi, \eta)$ = Vector function of ξ, η, defining the transverse electric field of the mode. $\boldsymbol{E}(\xi, \eta)$ can always be selected to be a real function and this will be assumed here.

β = Phase-change coefficient for the mode.

Y_w = Wave admittance for the mode.

A = Complex coefficient giving the amplitude and phase of the wave at $\zeta = 0$, i.e. the reference plane P.

Since all phases are being referred to the plane P, A can be assumed real without loss of generality. The amplitude of A is given by the condition that there is unit power flow towards the aerial, so that from Poynting's theorem

$$\tfrac{1}{2}A^2 Y_w \iint_{S1} |\boldsymbol{E}(\xi, \eta)|^2 d\xi d\eta = 1 \quad . \quad . \quad . \quad . \quad (3)$$

where S_1 is the feeder cross-section.

(2.1.2) The Radiated Field.

The radiated field need be defined only for a very large value of the co-ordinate r and at any point appears as if it were a plane wave travelling in the positive r direction. The radiated field can therefore be expressed as

$$\boldsymbol{E}_{rad}(r, \theta, \phi) = \frac{\boldsymbol{F}(\theta, \phi)}{r} \exp(-jkr) \quad . \quad . \quad . \quad (4)$$

$$\boldsymbol{H}_{rad}(r, \theta, \phi) = (Y_0/r)\boldsymbol{i}_r \times \boldsymbol{F}(\theta, \phi) \exp(-jkr) \quad . \quad . \quad (5)$$

where Y_0 = Wave admittance of a plane wave in free space.

$\boldsymbol{F}(\theta, \phi)$ = Transmitting radiation pattern, expressed in vector form to define the direction as well as the magnitude of the radiated field.

and $\boldsymbol{i}_r$ = Unit vector in the direction of increasing r.

Since the radiation field behaves locally as a plane wave, both the electric and magnetic fields are perpendicular to the direction of $\boldsymbol{i}_r$. This is satisfied by eqns. (4) and (5), provided that

$$\boldsymbol{i}_r \cdot \boldsymbol{F}(\theta, \phi) = 0 \quad . \quad . \quad . \quad . \quad . \quad . \quad (6)$$

The factor r which appears in the denominators of eqns. (4) and (5) ensures that the inverse-square law for power is satisfied.

(2.2) The Aerial as a Receiver

Let the direction of the incoming plane wave be specified by the spherical polar angles (θ', ϕ'). The most general expression for a plane wave from this direction is

$$\boldsymbol{E}_{inc}(r, \theta, \phi) = \boldsymbol{E}_0 \exp\{jkr[\sin\theta' \sin\theta \cos(\phi' - \phi) + \cos\theta' \cos\theta]\} \quad . \quad (7)$$

$$\boldsymbol{H}_{inc}(r, \theta, \phi) = Y_0 \boldsymbol{p} \times \boldsymbol{E}_{inc} \quad . \quad . \quad . \quad . \quad . \quad (8)$$

where $\boldsymbol{p}$ is a unit vector in the direction of propagation defined by the angles (θ', ϕ')

and $\boldsymbol{E}_0$ is a constant vector giving the direction and magnitude of the electric field. Since the directions of the electric fields and of propagation are orthogonal for a plane wave,

$$\boldsymbol{E}_0 \cdot \boldsymbol{p} = 0 \quad . \quad . \quad . \quad . \quad . \quad . \quad . \quad (9)$$

This incident field establishes a wave in the feeder travelling away from the aerial. From the results of the previous solution, this wave can be expressed as

$$\boldsymbol{E}'_t(\xi, \eta, \zeta) = B\boldsymbol{E}(\xi, \eta) \exp(j\beta\zeta) \quad . \quad . \quad . \quad . \quad . \quad (10)$$

$$\boldsymbol{H}'_t(\xi, \eta, \zeta) = -Y_w B\boldsymbol{n} \times \boldsymbol{E}(\xi, \eta) \exp(j\beta\zeta) \quad . \quad . \quad (11)$$

where B is a complex constant giving the amplitude and phase of the wave at the reference plane, P. The value of B will depend on the values of $\boldsymbol{E}_0$, θ' and ϕ'.

The incident field also causes reradiation by the aerial and the resulting fields can be expressed as:

$$\boldsymbol{E}'_{rad}(r, \theta, \phi) = \frac{1}{r}\boldsymbol{F}'(\theta, \phi) \exp(-jkr) \quad . \quad . \quad (12)$$

$$\boldsymbol{H}'_{rad}(r, \theta, \phi) = \frac{1}{r} Y_0 \boldsymbol{i}_r \times \boldsymbol{F}'(\theta, \phi) \exp(-jkr) \quad . \quad (13)$$

where $\boldsymbol{F}'(\theta, \phi)$ is the reradiation pattern and depends also on the values of $\boldsymbol{E}_0$, θ' and ϕ'. $\boldsymbol{F}'(\theta, \phi)$ will not in general resemble $\boldsymbol{F}(\theta, \phi)$.

(2.3) Application of the Lorentz Reciprocity Theorem

A general theorem which applies to any electromagnetic fields in a source-free region bounded by a closed surface S, is[4]

$$\int_S (\boldsymbol{E}_1 \times \boldsymbol{H}_2) - (\boldsymbol{E}_2 \times \boldsymbol{H}_1) \cdot \boldsymbol{v} dS = 0 \quad . \quad . \quad (14)$$

where $\boldsymbol{E}_1$, $\boldsymbol{H}_1$ and $\boldsymbol{E}_2$, $\boldsymbol{H}_2$ = Two solutions for the electromagnetic fields within the region,

$\boldsymbol{v}$ = Unit vector in the direction of the outward normal to S.

This theorem will be applied to the present problem by taking $\boldsymbol{E}_1$, $\boldsymbol{H}_1$ as the fields when the aerial transmits (Section 2.1) and $\boldsymbol{E}_2$, $\boldsymbol{H}_2$ as the fields when a plane wave is incident on the aerial (Section 2.2). The surface S is shown in Fig. 1 and consists of three parts:

S_1 = The cross-section of the feeder at the reference plane P.

S_2 = The outer conducting surface of the feeder.

S_3 = A sphere of radius R centred on 0.

On S_2, any electric field must be normal to the surface and any magnetic field must be tangential to it. All products of the type $E \times H$ must therefore vanish, so that there is no contribu-

tion to the integral in eqn. (14) from S_2. Substitution of the appropriate values for E_1, etc., in eqn. (14) then gives

$$-\int_{S_1}\Big\{-ABY_w\boldsymbol{E}(\xi,\eta)\times[\boldsymbol{n}\times\boldsymbol{E}(\xi,\eta)]-ABY_w\boldsymbol{E}(\xi,\eta)\times[\boldsymbol{n}\times\boldsymbol{E}(\xi,\eta)]\Big\}.\boldsymbol{n}d\xi d\eta+\int_{S_3}\Big\{\frac{1}{R}\exp(-jkR)\boldsymbol{F}(\theta,\phi)\times\Big[\boldsymbol{H}_{inc}(R,\theta,\phi)+\frac{1}{R}Y_0\boldsymbol{i}_r\times\boldsymbol{F}'(\theta,\phi)\exp(-jkR)\Big]-\Big[\boldsymbol{E}_{inc}(R,\theta,\phi)+\frac{1}{R}\exp(-jkR)\boldsymbol{F}'(\theta,\phi)\Big]\times\Big[\frac{Y_0}{R}\boldsymbol{i}_r\times\boldsymbol{F}(\theta,\phi)\exp(-jkR)\Big]\Big\}\boldsymbol{i}_rR^2\sin\theta d\theta d\phi=0 \quad . \quad (15)$$

Since $\boldsymbol{n}$ and $\boldsymbol{E}(\xi,\eta)$ are orthogonal

$$\boldsymbol{E}(\xi,\eta)\times[\boldsymbol{n}\times\boldsymbol{E}(\xi,\eta)]=|\boldsymbol{E}(\xi,\eta)|^2\boldsymbol{n} \quad . \quad . \quad (16)$$

so that the first integral in eqn. (15) reduces to

$$I_1=2ABY_w\int_{S_1}|\boldsymbol{E}(\xi,\eta)|^2d\xi d\eta \quad . \quad . \quad . \quad (17)$$

Further, the integral has been evaluated in eqn. (3), so that

$$I_1=4B/A \quad . \quad . \quad . \quad . \quad . \quad . \quad (18)$$

In the second integral, both $\boldsymbol{F}(\theta,\phi)$ and $\boldsymbol{F}'(\theta,\phi)$ are normal to $\boldsymbol{i}_r$ and from this it follows that the terms involving $\boldsymbol{F}'(\theta,\phi)$ cancel, leaving

$$I_2=R\exp(-jkR)\int_{S_3}\Big\{\boldsymbol{F}(\theta,\phi)\times\boldsymbol{H}_{inc}(R,\theta,\phi)-Y_0\boldsymbol{E}_{inc}(R,\theta,\phi)\times[\boldsymbol{i}_r\times\boldsymbol{F}(\theta,\phi)]\Big\}.\boldsymbol{i}_r\sin\theta d\theta d\phi \quad (19)$$

The final term also simplifies since $\boldsymbol{F}(\theta,\phi)$ is normal to $\boldsymbol{i}_r$, giving

$$I_2=R\exp(-jkR)\int_{S_3}\Big\{[\boldsymbol{F}(\theta,\phi)\times\boldsymbol{H}_{inc}(R,\theta,\phi)].\boldsymbol{i}_r-Y_0\boldsymbol{E}_{inc}(R,\theta,\phi).\boldsymbol{F}(\theta,\phi)\Big\}\sin\theta d\theta d\phi \quad . \quad (20)$$

Substitution from eqns. (7) and (8) gives

$$I_2=Y_0R\exp(-jkR)\int_0^{2\pi}\int_{-\pi/2}^{\pi/2}\Big\{[\boldsymbol{F}(\theta,\phi)\times(\boldsymbol{p}\times\boldsymbol{E}_0)].\boldsymbol{i}_r-\boldsymbol{E}_0.\boldsymbol{F}(\theta,\phi)\Big\}\times\exp\Big\{jkR[\sin\theta'\sin\theta\cos(\phi'-\phi)+\cos\theta'\cos\theta]\Big\}\times\sin\theta d\theta d\phi \quad . \quad (21)$$

In the integrand the argument of the exponential varies rapidly with θ and ϕ and the method of stationary phase[5] can be used. This gives an asymptotic expansion for the integral, and in the limit, as R tends to infinity, only the first term of this expansion is needed. The stationary-phase point occurs at

$$\theta=\theta';\ \phi=\phi' \quad . \quad . \quad . \quad . \quad . \quad . \quad (22)$$

so that eqn. (21) becomes

$$I_2=Y_0R\exp(-jkR)\Big\{[\boldsymbol{F}(\theta',\phi')\times(\boldsymbol{p}\times\boldsymbol{E}_0)].\boldsymbol{i}_r-\boldsymbol{E}_0.\boldsymbol{F}(\theta',\phi')\Big\}I \quad . \quad (23)$$

where

$$I=\int_0^{2\pi}\int_{-\pi/2}^{\pi/2}\exp\Big\{jkR[\sin\theta'\sin\theta\cos(\theta'-\phi)+\cos\theta'\cos\theta]\Big\}\sin\theta d\theta d\phi \quad . \quad (24)$$

Further, in eqn. (23), the unit vector $\boldsymbol{i}_r$ is defined at $\theta=\theta'$, $\phi=\phi'$ and is therefore equal to $-\boldsymbol{p}$, so that

$$I_2=-2Y_0R\exp(-jkR)\boldsymbol{E}_0.\boldsymbol{F}(\theta',\phi')I \quad . \quad . \quad (25)$$

The double integral I can be evaluated directly by the method described by Silver,* giving

$$I=\frac{2\pi}{kR}\exp(jkR-j\pi/2) \quad . \quad . \quad . \quad . \quad (26)$$

The results for I_1 and I_2 can now be substituted in eqn. (15) and an expression obtained for the complex amplitude, B, of the wave in the feeder when the aerial acts as a receiver. This expression is

$$B=\frac{Y_0A}{k}\exp(-j\pi/2)\boldsymbol{E}_0.\boldsymbol{F}(\theta',\phi') \quad . \quad . \quad (27)$$

It will be noticed that this result is independent of the radius R for which the integrations were performed. The results for these integrations are exact as the radius R tends to infinity.

(3) DISCUSSION

Eqn. (27) can be regarded as an extended form of the aerial reciprocity theorem and gives in a convenient form the behaviour of the aerial as a receiver in terms of its properties as a transmitter. The extension over previous statements of the reciprocity theorem is twofold:

(*a*) the phase of the signal received by the aerial feeder is determined as well as its amplitude, and

(*b*) there are no restrictions on the direction of polarization of the plane wave incident upon the aerial.

The derivation of the result is completely rigorous and full account is taken of the reradiation from the aerial when it acts as a receiver. The extension of the result to incident fields which are not plane waves has already been discussed.[6]

A convenient way of expressing the amplitude reciprocity relation is to state the effective receiving area of the aerial in terms of its power gain. It will be shown that eqn. (27) gives the same result as obtained by other methods.

The power gain of the aerial at any point is the ratio of the power flux per unit area at that point when the aerial is radiating to the power flux per unit area at the same point when the same total power is uniformly radiated in all directions. It follows from the definition of the transmitting radiation pattern in Section 2.1 that the power gain for the direction defined by the angles (θ,ϕ) is

$$G(\theta,\phi)=Y_0|\boldsymbol{F}(\theta,\phi)|^2 \quad . \quad . \quad . \quad . \quad (28)$$

The effective receiving area of the aerial when a plane wave is incident from the direction (θ,ϕ) is the ratio of the power delivered to the feeder to the power flux per unit area in the incident wave. Hence, from Section 2.2,

$$A_{eff}(\theta,\phi)=\frac{\frac{1}{2}|B|^2Y_w\int\int_{s1}|\boldsymbol{E}(\xi,\eta)|^2d\xi d\eta}{\frac{1}{2}Y_0|\boldsymbol{E}_0|^2} \quad . \quad . \quad (29)$$

When eqns. (27) and (3) are used, this becomes

$$A_{eff}(\theta,\phi)=\frac{(\pi Y_0k)^2[\boldsymbol{E}_0.\boldsymbol{F}(\theta,\phi)]^2}{\frac{1}{2}Y_0|\boldsymbol{E}_0|^2} \quad . \quad . \quad . \quad (30)$$

It is obvious that the receiving area has a maximum value when $\boldsymbol{E}_0$ is parallel to $\boldsymbol{F}(\theta,\phi)$, a result to be expected on physical grounds. For this case

$$A_{eff}(\theta,\phi)=\tfrac{1}{2}\lambda^2Y_0|\boldsymbol{F}(\theta,\phi)|^2 \quad . \quad . \quad . \quad (31)$$

where λ is the free-space wavelength, equal to $2\pi/k$.

* Reference 1, p. 121.

Finally, if $|F(\theta, \phi)|^2$ is eliminated from eqns. (28) and (31), there results

$$A_{eff}(\theta, \phi) = \lambda^2 G(\theta, \phi)/4\pi \quad . \quad . \quad . \quad . \quad (32)$$

a well-known formula.

(4) REFERENCES

(1) SILVER, S.: 'Microwave Antenna Theory and Design' (McGraw-Hill, New York, 1949).

(2) SCHELKUNOFF, S. A., and FRIIS, H. T.: 'Antennas: Theory and Practice' (Wiley, New York, 1952).

(3) JORDAN, E. C.: 'Electromagnetic Waves and Radiating Systems' (Prentice-Hall, New York, 1950).

(4) STRATTON, J. A.: 'Electromagnetic Theory' (McGraw-Hill, New York, 1952).

(5) JEFFREYS, H., and JEFFREYS, B. S.: 'Methods of Mathematical Physics' (Cambridge University Press, Second Edition 1950).

(6) BROWN, J.: 'A Theoretical Analysis of Some Errors in Aerial Measurements' (see page 343).

621.313.1.013.4

The Institution of Electrical Engineers
Monograph No. 302 U
Apr. 1958
©

AN ANALYSIS OF COMMUTATION FOR THE UNIFIED-MACHINE THEORY

By C. V. JONES, M.Eng., B.Sc., Associate Member.

(*The paper was first received* 11*th October*, 1957, *and in revised form* 11*th February*, 1958. *It was published as an* INSTITUTION MONOGRAPH *in April*, 1958.)

SUMMARY

The logical treatment of the unified-machine theory is of such merit that it seems likely eventually to supersede the classical treatment entirely. The unified theory is, however, at present deficient in two respects. It requires two primitive machines, a slip-ring primitive and a commutator primitive, as the bases for analysis, and it tacitly assumes the existence of a perfect commutator. The mechanism of commutation is entirely neglected.

The paper gives a new theory of commutation, which not only elucidates this mechanism but enables the performance of any machine or machine system to be developed from one basis only, namely the simplest case of two coils with relative angular movement.

Each stage of the analysis is supported with a comprehensive series of experimental results. The tests involved introduce some interesting problems, and a new method for the measurement of the coefficient of self-inductance to direct currents is developed.

(1) INTRODUCTION

The great merit possessed by the unified-machine theory is that of a continuous logical development from first principles to complex machine systems. To make clear the object of the paper, a brief recapitulation of this development is necessary.

The simplest form of electrical machine is a solenoid or electromagnet, in which the inductance varies with the position of the armature, and hence with time. The voltage equation is

$$V = RI + L\frac{dI}{dt} + I\frac{dL}{dt} \quad . \quad . \quad . \quad . \quad . \quad (1)$$

and the power equation becomes

$$P = RI^2 + \frac{d(\frac{1}{2}LI^2)}{dt} + \frac{1}{2}I^2\frac{dL}{dt}$$

The final term in this equation denotes the electrical power converted into mechanical power by the movement of the armature; it must therefore equal Fdx/dt, where F is the force upon, and x the displacement of, the armature. It follows that

$$F = \frac{1}{2}I^2\frac{dL}{dx}$$

Alternatively, the variation of L may be caused by a variation in angular position θ, so that, similarly, if T is the torque,

$$T = \frac{1}{2}I^2\frac{dL}{d\theta} \quad . \quad . \quad . \quad . \quad . \quad . \quad . \quad (2)$$

Eqns. (1) and (2) are the voltage and torque equations of the simplest machine.

For two or more coils, the concept of mutual inductance is required. For two coils with mutual inductance the voltage equations are

$$\left.\begin{aligned} V_1 &= R_1I_1 + \frac{d(L_1I_1)}{dt} + \frac{d(M_{12}I_2)}{dt} \\ V_2 &= R_2I_2 + \frac{d(L_2I_2)}{dt} + \frac{d(M_{21}I_1)}{dt} \end{aligned}\right\} \quad . \quad . \quad . \quad (3)$$

and consideration of the power equation gives for the torque

$$T = \frac{1}{2}I_1^2\frac{dL_1}{d\theta} + \frac{1}{2}I_2^2\frac{dL_2}{d\theta} + I_1I_2\frac{dM_{12}}{d\theta} \quad . \quad . \quad . \quad (4)$$

In obtaining the torque equation, the assumption has been made that $M_{12} = M_{21}$. This equality is well established for linear (air-cored) inductors, and is capable of theoretical proof from energy considerations. For saturable iron-cored inductors, however, it is considered that the equality can only be established by experiment. A wide range of experiments by the author has shown that, provided the saturation conditions are carefully reproduced, the equality is always confirmed. It is therefore assumed throughout the paper, and there results a certain symmetry in the voltage equations, which is seen later to be of great importance.

Eqns. (3) and (4) are adequate for the analysis of all electrical machines not fitted with commutators. Such 'slip-ring' machines include not only alternators and wound-rotor induction motors, but also machines without any connections to the rotor, such as squirrel-cage motors and inductor alternators. Commutator machines require a different method of analysis, which introduces fundamental difficulties. These difficulties will be investigated in detail later.

Although the equations of any slip-ring machine may be written down immediately by comparison with eqns. (3) and (4), yet the solution of these differential equations for any particular type of machine has constituted historically the major problem of machine analysis. In the case of the alternator, the problem was finally resolved by Park,[1] after valuable preliminary work by Blondel[2, 3] and by Doherty and Nickle.[4] The corresponding induction-motor problem was solved by Fortescue.[5] The equations are to-day most satisfactorily treated by the methods of tensor analysis, which were first applied to machine problems by Kron. The subject has been given an exhaustive analysis by Kron himself,[6, 7, 8] and also by Gibbs,[9] Lynn[10] and others.

In matrix form the basic equations given above may be written

$$\boldsymbol{V} = \boldsymbol{RI} + p\boldsymbol{LI} \quad . \quad . \quad . \quad . \quad . \quad . \quad . \quad (3a)$$

$$T = \frac{1}{2}\boldsymbol{I}_t\frac{d\boldsymbol{L}}{d\theta}\boldsymbol{I} \quad . \quad . \quad . \quad . \quad . \quad . \quad . \quad . \quad (4a)$$

where the voltage and current matrices $\boldsymbol{V}$ and $\boldsymbol{I}$ have as many rows as there are different windings on the machine. The symbol $\boldsymbol{I}_t$ denotes the transpose of the current matrix, while $\boldsymbol{R}$ and $\boldsymbol{L}$ are the resistance and inductance matrices, $\boldsymbol{R}$ being diagonal and $\boldsymbol{L}$ symmetric. The operator p (= d/dt) acts on the product of $\boldsymbol{L}$ and $\boldsymbol{I}$.

(2) THE SLIP-RING PRIMITIVE MACHINE

Kron's slip-ring primitive machine consists, as shown in Fig. 1, of two stator windings and two independent rotor windings, whose ends are connected to pairs of slip rings. Eqn. (3) is readily extended to the case of four windings, and the

Correspondence on Monographs is invited for consideration with a view to publication.

Mr. Jones is in the Department of Electrical Engineering, University of Liverpool.

voltage equation of the machine is given in its most general form by

$$\begin{vmatrix} V_1 \\ V_2 \\ V_3 \\ V_4 \end{vmatrix} = \begin{vmatrix} R_1+pL_1 & pM_{12} & pM_{13} & pM_{14} \\ pM_{21} & R_2+pL_2 & pM_{23} & pM_{24} \\ pM_{31} & pM_{32} & R_3+pL_3 & pM_{34} \\ pM_{41} & pM_{42} & pM_{43} & R_4+pL_4 \end{vmatrix} \times \begin{vmatrix} I_1 \\ I_2 \\ I_3 \\ I_4 \end{vmatrix} \quad (5)$$

For further progress a knowledge of the variation of the inductance coefficients with θ is necessary.

For alternators and induction motors, the following assumptions may legitimately be made:

(*a*) that the stator windings are in electrical space quadrature;
(*b*) that the rotor windings are in electrical space quadrature;
(*c*) that the rotor windings are similar;
(*d*) that the rotor has a smooth cylindrical surface; and
(*e*) that space harmonics higher than the second may be neglected.

The impedance matrix then assumes the more concrete form of eqn. (6),[6, 7, 8, 9, 10] thus

$$Z = \begin{vmatrix} R_1+L_1p & & -M_1p\sin\theta & M_1p\cos\theta \\ & R_2+L_2p & M_2p\cos\theta & M_2p\sin\theta \\ -M_1p\sin\theta & M_2p\cos\theta & R_3+L_ap-L_bp\cos 2\theta & -L_bp\sin 2\theta \\ M_1p\cos\theta & M_2p\sin\theta & -L_bp\sin 2\theta & R_3+L_ap+L_bp\cos 2\theta \end{vmatrix} \quad (6)$$

Here the operator p acts in general on products of functions of θ and time-varying currents.

The difficulties of solution of the above equations are primarily due to the fact that not only are the inductance coefficients non-linear functions of the currents, owing to saturation, but the saturation of the rotor windings also varies with the rotor position. Although the first stages in the solution of this alternator problem were developed by Blondel from physical considerations, it is possible to consider it as the purely mathematical problem of finding a passive transformation which will eliminate θ from the impedance matrix. The required transformation is

$$I = \begin{vmatrix} I_1 \\ I_2 \\ I_3 \\ I_4 \end{vmatrix} = CI' = \begin{vmatrix} 1 & & & \\ & 1 & & \\ & & \cos\theta & -\sin\theta \\ & & \sin\theta & \cos\theta \end{vmatrix} \times \begin{vmatrix} I_1 \\ I_2 \\ I_q \\ I_d \end{vmatrix} \quad (7)$$

From the tensor point of view, this transformation is non-holonomic, and the use of advanced concepts of analytical dynamics and tensor analysis is required for its successful application. The correct result may, however, be readily obtained by direct matrix methods. This matrix analysis is considered to be important, and since it does not appear to have been given elsewhere, it is given in full in Section 11. The transformed voltage equation has the form

$$V' = Z'I'$$

where

$$V' = \begin{vmatrix} V_1 \\ V_2 \\ V_q \\ V_d \end{vmatrix} = \begin{vmatrix} V_1 \\ V_2 \\ V_3\cos\theta + V_4\sin\theta \\ -V_3\sin\theta + V_4\cos\theta \end{vmatrix}$$

$$I' = \begin{vmatrix} I_1 \\ I_2 \\ I_q \\ I_d \end{vmatrix} = \begin{vmatrix} I_1 \\ I_2 \\ I_3\cos\theta + I_4\sin\theta \\ -I_3\sin\theta + I_4\cos\theta \end{vmatrix} \quad \ldots\ldots (8)$$

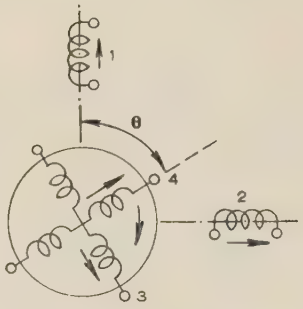

Fig. 1.—Slip-ring primitive machine.

and

$$Z' = \begin{vmatrix} R_1+L_1p & & & M_1p \\ & R_2+L_2p & M_2p & \\ -\omega M_1 & M_2p & R_3+L_qp & -\omega L_d \\ M_1p & \omega M_2 & \omega L_q & R_3+L_dp \end{vmatrix} \quad (9)$$

where $\omega = d\theta/dt$, $L_d = L_a + L_b$ and $L_q = L_a - L_b$.

The torque is given by the expression

$$T = I_t' G' I' \quad . \quad . \quad . \quad . \quad . \quad . \quad (10)$$

where G' is the coefficient of ω in Z'.

Certain points of great importance arise in connection with eqns. (8), (9) and (10).

First, it is clear that the transformation has in fact resulted in the elimination of θ from the alternator equations. Not only does it now become possible to solve the equations by normal methods, but, equally important, saturation curves of L_d and L_q may be determined uniquely by experiment, since the values of these quantities are no longer influenced by rotor position. The new equations, unlike eqn. (6), are therefore of direct practical application. Whilst no great attention is paid to the point here, it must be stressed that such phenomena as saturation and iron losses can be treated at least as easily with the unified theory as with classical methods. This is essential, because a theory which neglected these phenomena, however mathematically elegant it may be, would be of little practical value.

Secondly, the transformed impedance matrix is no longer symmetric. Whilst the self-inductances on the leading diagonal and the mutual inductances on the trailing diagonal are symmetric, the rotational inductances, which appear on the rotor rows only, are not. The original impedance matrix of the machine [eqn. (6)] was derived from physical considerations and is symmetric. The asymmetric matrix [eqn. (9)] followed as the result of a mathematical transformation. It need not be symmetric, since it no longer has a direct physical significance.

Thirdly, the torque equation (10) now has a different form from that of the original equation (4*a*).

The second and third points arise again in the next Section, and will be discussed fully later.

(3) THE COMMUTATOR PRIMITIVE MACHINE

The derivation of the equations of the slip-ring machine from first principles, considered in the previous Section, was perfectly straightforward. This is not the case with the primitive commutator machine to be considered now.

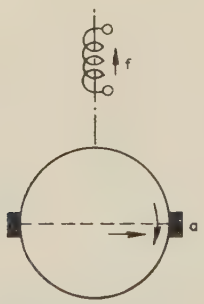

Fig. 2.—Simplest form of commutator machine.

If the simplest form of commutator machine of Fig. 2 be considered, it is possible, by means of a series of simple experiments at the field and armature terminals and at the shaft, to establish the familiar equations

$$\left.\begin{aligned} V_f &= R_f I_f + L_f p I_f \\ V_a &= R_a I_a + L_a p I_a + M' \omega I_f \end{aligned}\right\} \quad . \quad . \quad . \quad (11)$$

$$T = M' I_f I_a \quad . \quad . \quad . \quad . \quad . \quad . \quad (12)$$

Consideration of the armature voltage equation shows that the units of the product $M'\omega$ are ohms or henrys per second. Since ω is the angular velocity of the rotor in electrical radians per second it follows that the units of M' must be henrys per electrical radian. It will be confirmed later that M' is in fact of the nature of a space rate of change of inductance. Such inductance quantities are of frequent occurrence and will be referred to as *rotational inductance coefficients*.

If the cross-field machine in Fig. 3, which has two stator and

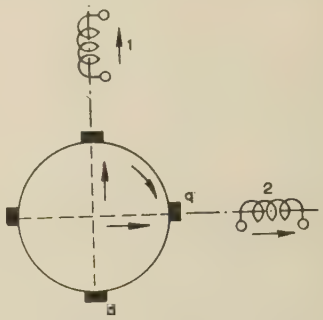

Fig. 3.—Commutator primitive machine.

two rotor windings, is investigated in a similar manner, its equations, conveniently written in matrix form, are found to be as follows:

$$\begin{vmatrix} V_1 \\ V_2 \\ V_q \\ V_d \end{vmatrix} = \begin{vmatrix} R_1 + L_1 p & & & M_1 p \\ & R_2 + L_2 p & M_2 p & \\ -\omega M_1' & M_2 p & R_q + L_q p & -\omega L_d' \\ M_1 p & \omega M_2' & \omega L_q' & R_d + L_d p \end{vmatrix} \times \begin{vmatrix} I_1 \\ I_2 \\ I_q \\ I_d \end{vmatrix}$$

$$. \quad . \quad . \quad . \quad (13)$$

If the two rotor windings are similar, this impedance matrix becomes identical in form with that of eqn. (9). This result is made even more remarkable by the fact that if the rotor of the slip-ring primitive machine (Section 2) carries balanced 2-phase currents, the transformed currents and voltages of eqn. (8) become direct currents and voltages. It follows that the p terms disappear from eqn. (9) and that the transformed equations of the alternator become identical with those of a d.c. commutator machine. The discovery of such mathematical analogies between the equations of types of machines that are physically quite distinct forms one of the main attractions of Kron's unified-machine theory.

Unfortunately, the existence of this remarkable analogy does not eliminate the severe difficulties presented by the equations of the commutator machine, as they appear above. These difficulties may be specified as follows:

(*a*) The equations of the machine are not symmetric. It is true that the equations of the transformed slip-ring machine were not symmetric. But in that case the initial equations, which represented directly the physical performance of the machine, were symmetric, and the asymmetry only arose as the result of a mathematical operation. Since the mathematical process was correct, the result must be correct and no difficulty arises. The commutator-machine equations, on the other hand, were derived as the result of experiments at the machine terminals, and must therefore be looked upon as giving a true physical picture of the performance of the machine. But the equations of any linear static network and any slip-ring machine are known to be symmetric, and in nature, in general, action and reaction are equal and opposite. The precise mechanism

whereby the asymmetry of the commutator machine arises may therefore properly be looked upon as a difficulty that requires further investigation.

(*b*) The equations of the machine give no explicit evidence whatsoever of the existence of any commutator, nor of any interpole windings. From design and frequently from operational considerations, as well as in the classical theory of d.c. machines, the study of commutation plays a fundamental role. It follows that the complete disregard of this vital phenomenon may properly be considered as a difficulty in eqns. (11)–(13).

(*c*) The equations of the machine ignore completely the presence of two windings, the short-circuited turns and the interpoles. These windings introduce two phenomena at least which, it would seem, cannot be neglected without justification. First, in the simple commutator machine in Fig. 2 there is a fixed position in space at which the current in the armature windings is continually being reversed. Since this position is on the direct axis of the field, it might be anticipated that a very high voltage would be induced thereby in the field winding. This voltage was measured for a particular machine and found to be ten times the rated voltage of the armature. Secondly, since the output voltage of the machine is produced by the rotation of the armature winding through the flux of the field winding, it is to be expected that a much higher voltage would be generated in the field by the rotation past it of the flux of armature reaction. Measurements of this voltage show that it also has a very high value. The apparent neglect of such important phenomena constitutes a third difficulty.

The point is not that the equations above are incorrect; they are in fact derived from the results of direct experiments. It is simply that the terminal quantities are only the end-product of a complex process, and whilst it may be legitimate to utilize this end-product for further analysis, a study of the underlying processes is essential if the equations are to be convincing and if the unified theory is to be considered wholly satisfactory. This study is carried out in the remaining part of the paper.

(4) DERIVATION OF THE COMMUTATOR MACHINE WITH INTERPOLES

Further consideration of the simple commutator machine in Fig. 2 shows that it has in effect four distinct windings, of which only two appear in the diagram and in eqn. (11). There are in fact two stator windings set in electrical space quadrature, namely the field and the interpoles, and there are two rotor windings also set in electrical space quadrature, namely the main armature winding and the short-circuited turns. Although these two rotor windings are actually part of one closed symmetrical armature winding, yet they must be treated separately, because the action of the commutator is such that the currents in the short-circuited turns are different from those in the main armature.

The following analysis begins with the 4-winding slip-ring primitive machine shown diagrammatically in Fig. 1. The intention is to convert this machine into the (nominally) 2-winding commutator machine in Fig. 2 by converting one stator winding (1) into the field winding, the other (2) into the interpole winding, one rotor winding (3) into the main armature winding and the other (4) into the short-circuited armature turns. The conversion, however, is to be a physical and not a mathematical one.

The general equations of the machine in Fig. 1, which no longer has similar rotor windings, are as given in eqn. (5). The torque is given by eqn. (4*a*). The only simplifying assumption that it is legitimate to make is that the rotor is cylindrical, from which it follows that the self-inductances of the stator windings are independent of the angular position of the rotor, and their mutual inductance is zero. With these exceptions, the inductance coefficients in the impedance matrix are all functions of rotor position. These coefficients have been measured for a particular machine and are as shown in Fig. 4. The curves, which are discussed in detail later, are considered to be typical. Normal assumptions about the symmetries of the iron circuit and windings enable the general form of the inductance coefficients to be expressed as Fourier series of θ as follows:

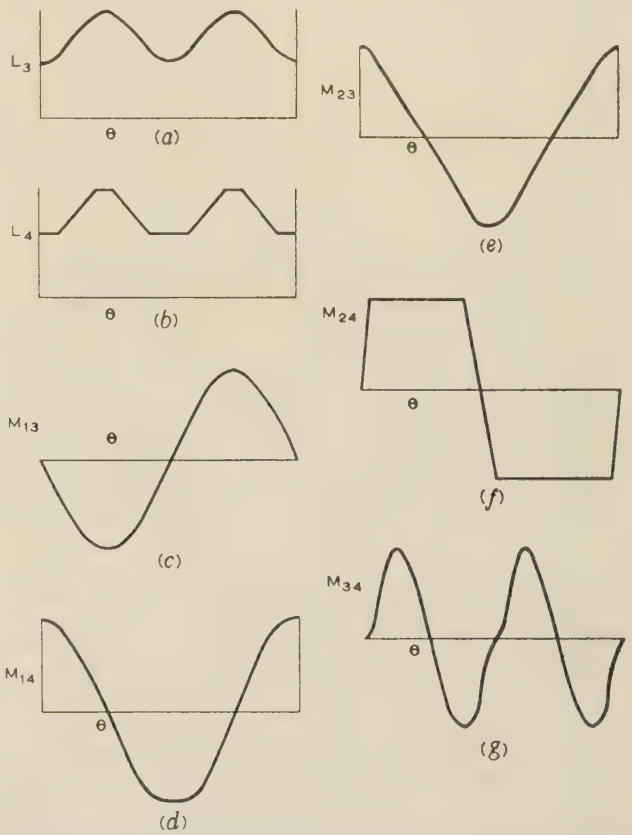

Fig. 4.—Variation with rotor position of the coefficients of self- and mutual inductance.

L_1 and L_2 are independent of θ

$$\left.\begin{aligned}
L_3 &= L_{30} + \sum_{n=1}^{\infty} L_{3n} \cos(2n\theta) \\
M_{12} &= 0 \\
M_{13} &= \sum_{n=1}^{\infty} M_{13n} \sin[(2n-1)\theta] \\
M_{14} &= \sum_{n=1}^{\infty} M_{14n} \cos[(2n-1)\theta] \\
L_4 &= L_{40} + \sum_{n=1}^{\infty} L_{4n} \cos(2n\theta) \\
M_{23} &= \sum_{n=1}^{\infty} M_{23n} \cos[(2n-1)\theta] \\
M_{24} &= \sum_{n=1}^{\infty} M_{24n} \sin[(2n-1)\theta] \\
M_{34} &= \sum_{n=1}^{\infty} M_{34n} \sin(2n\theta)
\end{aligned}\right\} \quad . \quad . \quad (14)$$

The voltage generated in the windings of a normal d.c. commutator machine is alternating, and the purpose of the commutator is to reverse the connections to the coils at the instant when the voltage generated in them changes sign. As far as currents in the armature are concerned, reversals occur twice in a cycle and the time of reversal is relatively short. As far as position in space is concerned, however, the process of current reversal is continuously repetitive. Whilst the current in a particular coil reverses but seldom, there is always some coil in which a reversal is taking place. From this point of view the time of a cycle of operations is clearly the time taken by the rotor to move through the thickness of a brush. (This is on the assumption, for the moment, that the thickness of a brush is equal to the thickness of one commutator segment pitch.)

During the time of commutation, the connections to the armature of the machine are not changed, so that during this short interval the machine must behave in exactly the same manner as a slip-ring machine. At the end of the interval the connections are suddenly changed, and an identical cycle of events begins. The point of the argument, therefore, is that the behaviour of the commutator primitive machine may be determined completely simply by analysing the behaviour of an appropriate slip-ring primitive machine whose equations are known, during the time of commutation of one coil.

This method of analysis overcomes the difficulties referred to in Section 3; for the impedance matrix is symmetric, the interpoles and short-circuited turns are taken into account, and all the induced voltages in the machine are considered.

Let the interval of commutation be δ. Then, since the axis of the coils being commutated is the direct axis of the field, it follows that the limits of θ during the time of commutation will be from $-\frac{1}{2}\delta$ to $+\frac{1}{2}\delta$, $2\pi/\delta$ being the number of commutator segments per pair of poles. In practice, the value of δ is small, and it is a reasonable assumption, so far as the values of the inductance coefficients given in eqn. (14) are concerned, that $\sin 2\theta = \sin \delta = 0$ and that $\cos \delta = 1$. When these assumptions are made, θ disappears explicitly from the impedance matrix and an appreciable simplification occurs. The general term in the voltage equations $p(MI)$ may be expanded thus

$$p(MI) = MpI + \omega M'I$$

where $M' = dM/d\theta$ (a rotational inductance coefficient) and ω is written for $d\theta/dt$, so that wherever p appears in the impedance matrix it operates upon current only. Using eqns. (14) with the above assumptions, the impedance matrix of eqn. (5) becomes

$$Z = \begin{array}{|c|c|c|c|} \hline R_1 + L_1p & . & \omega M'_{13} & M_{14}p \\ \hline . & R_2 + L_2p & M_{23}p & \omega M'_{24} \\ \hline \omega M'_{13} & M_{23}p & R_3 + L_3p & \omega M'_{34} \\ \hline M_{14}p & \omega M'_{24} & \omega M'_{34} & R_4 + L_4p \\ \hline \end{array} \quad . \quad (15)$$

This impedance matrix applies to the machine in Fig. 5, wherein the two sets of brushes shown are in reality the same

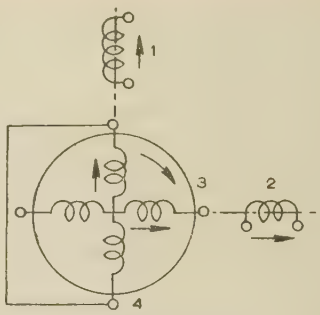

Fig. 5.—Diagram showing the double action of brushes in providing an external connection to the armature (3) and a short-circuit path for the coils undergoing commutation (4).

set. The brushes, in fact, may be considered as having two purposes; the first, corresponding to (3), of supplying current to the armature, and the second, corresponding to (4), of reversing or short-circuiting the armature current. It will be noted that the method of deriving the matrix is such that it remains symmetric.

In practice, the armature and interpoles are connected in series so that their magnetomotive forces oppose. This connection may be accomplished by means of an active transformation of standard type,[7, 8, 9] thus

$$Z' = C_tZC$$

where Z is the old and Z' the new impedance matrix. C is the connection matrix given in this case by the relationship

$$C = \begin{array}{|c|c|c|} \hline 1 & & \\ \hline & -1 & \\ \hline & 1 & \\ \hline & & 1 \\ \hline \end{array}$$

It follows that the new voltage equation is given by

$$\begin{array}{|c|} \hline V_1 \\ \hline V_{23} \\ \hline V_4 \\ \hline \end{array} = \begin{array}{|c|c|c|} \hline R_1 + L_1p & \omega M'_{13} & M_{14}p \\ \hline \omega M'_{13} & (R_2 + R_3) + (L_2 - 2M_{23} + L_3)p & -\omega(M'_{24} - M'_{34}) \\ \hline M_{14}p & -\omega(M'_{24} - M'_{34}) & R_4 + L_4p \\ \hline \end{array} \times \begin{array}{|c|} \hline I_1 \\ \hline I_{23} \\ \hline I_4 \\ \hline \end{array} \quad . \quad . \quad . \quad . \quad (16)$$

where V_{23} is the voltage applied to the armature and interpoles in series, and I_{23} is their common current.

The impedance matrix is naturally still symmetric.

(5) ELIMINATION OF THE SHORT-CIRCUITED TURNS

From one point of view the voltage equation just given is final. It gives the relation between the voltages and currents in the four different windings of the machine over a particular interval of time representative of the complete operation. On the other hand, it is a basic principle of the tensor analysis of the performance of machines that there can be only as many sets of equations as there are sets of terminals on the machine. Since the commutator machine considered (Fig. 2) has terminals

only for the field and for the armature, it is necessary before the equations can be regarded as wholly satisfactory to eliminate from the impedance matrix the row and column corresponding to the short-circuited turns, since there are no external connections to these turns. There is a standard procedure for the elimination of unwanted rows and columns of a matrix,[7, 8] but owing to the unusual nature of the present problem it is more satisfactory to use a different method.

First of all, let eqn. (16) be expanded out of its matrix form. This gives

$$V_1 = (R_1 + L_1 p)I_1 + \omega M'_{13} I_{23} + M_{14} p I_4 \quad . \quad (17)$$

$$V_{23} = \omega M'_{13} I_1 + [(R_2 + R_3) + (L_2 - 2M_{23} + L_3)p]I_{23} - \omega(M'_{24} - M'_{34})I_4 \quad . \quad (18)$$

$$V_4 = M_{14} p I_1 - \omega(M'_{24} - M'_{34})I_{23} + (R_4 + L_4 p)I_4 \quad . \quad (19)$$

It is now proposed to consider these equations one by one.

(5.1) The Short-Circuited-Turns Equation

The voltage equation of the short-circuited turns just given is

$$V_4 = M_{14} p I_1 - \omega(M'_{24} - M'_{34})I_{23} + (R_4 + L_4 p)I_4$$

Each term of this equation will be studied in turn. The first term, V_4, represents the voltage applied to the short-circuited turns from an external source, and is clearly zero. The second term, $M_{14}pI_1$, represents physically the voltage that would be induced in the turns by simple mutual induction if the field current was changing. For a d.c. machine, the field current may be assumed to be constant so this term will disappear. For an a.c. commutator machine, however, the term will be important unless the interval of commutation is very small compared with the period of the supply. For the moment, a d.c. machine will be assumed and this term may therefore be neglected.

Eqn. (17) thus reduces to

$$(R_4 + L_4 p)I_4 - \omega(M'_{24} - M'_{34})I_{23} = 0 \quad . \quad . \quad . \quad (20)$$

The significance of the components of these terms is as follows. $R_4 I_4$ is the resistive voltage drop in the turns; the value of R_4 depends not only upon the resistance of the conductors, but also upon the resistance of the brushes which complete the short-circuit, and upon their contact resistance. Furthermore, this latter resistance is known not to be constant. The term $L_4 p I_4$ is the voltage due to the self-inductance of the turns, and $\omega M'_{34} I_3$ is the voltage that would be generated in the turns by their rotation in the field of the armature (armature reaction) if the interpoles were omitted or unexcited. Finally, since $I_{23} = -I_2 = +I_3$, the term $-\omega M'_{24} I_{23}$ is the voltage that would be generated in the turns by their rotation in the field of the interpoles, if the armature were unexcited. M'_{24} is not normally constant during the interval of commutation, since the interpole shoes are in general bevelled to improve commutation.

If the interpole winding were arbitrary, the above equation could be used to determine the variation of the current I_4 during commutation. But, in fact, the interpole winding is not arbitrary. It is designed with the specific object of ensuring that the armature current shall be precisely reversed during commutation. It follows that eqn. (20) must only be another form, albeit an unfamiliar one, of the equation used by the designer to determine the number of turns and the dimensions of the magnetic circuit of the interpoles. It expresses the familiar fact that the ampere-turns on the interpoles must first counteract armature reaction and then set up a flux sufficient to produce a voltage equal and opposite to the resistive and self-inductive voltages in the turns.

From the point of view of operation as distinct from design, it is of interest to solve eqn. (20) on the assumption that the parameters are constant. The solution will be only approximate, since R_4 varies with current and M'_{24} with position. The solution is

$$I_4 = A\varepsilon^{-(R_4/L_4)t} + (M'_{24} - M'_{34})\omega I_{23}/R_4 \quad . \quad . \quad (21)$$

The value of the constant of integration A is found from the fact that at the beginning of commutation, when $t = -\frac{1}{2}T_c$, $I_4 = -I_{23}$. Substitution of the value of A thus found gives

$$I_4 = (M'_{24} - M'_{34})\omega I_{23}/R_4 - [1 + (M'_{24} - M'_{34})(\omega/R_4)]I_{23}\varepsilon^{-(R_4/L_4)(t+\frac{1}{2}T_c)} \quad . \quad (22)$$

For ideal commutation I_4 must equal $+I_{23}$ at the end of commutation, i.e. when $t = +\frac{1}{2}T_c$. Making this substitution and solving for M'_{24} gives

$$M'_{24} = M'_{34} + (R_4/\omega)(1 + \varepsilon^{-R_4 T_c/L_4})/(1 - \varepsilon^{-R_4 T_c/L_4}) \quad . \quad (23)$$

It is clear that this may be looked upon as an alternative formula for the design of the interpoles. If the value of the index of the exponential is small, a simpler formula may be found by expanding only as far as the first order of small quantities, giving

$$M'_{24} = M'_{34} + 2L_4/\delta \quad . \quad . \quad . \quad . \quad . \quad (24)$$

where $\delta = \omega T_c$ is the electrical angle of commutation, which is constant. On this approximate basis the equation of I_4 reduces to

$$I_4 = (t/\tfrac{1}{2}T_c)I_{23}$$

and commutation is linear.

In general it is found that the effect of the non-linearity of R_4 is to tend to make commutation linear, even when the expansion of the exponential is not legitimate.

For a well-designed machine, therefore, eqn. (19) for V_4 simply gives a correct description of the process of commutation. Since it otherwise contributes no information about the performance of the machine, it may be omitted from further consideration. Two important points remain to be mentioned. First, for a.c. operation the mutual inductance between the short-circuited turns and the field winding would appear to make perfect commutation impossible. Secondly, the analysis made above for the particular case when the brush thickness is equal to the commutator pitch may be extended directly to the more general case. The voltage of the short-circuited turns will now be given by a more complex equation, but it will still be this equation that determines the design of the interpoles.

(5.2) The Armature Equation

The armature equation has been given as eqn. (18):

$$V_{23} = \omega M'_{13} I_1 + [(R_2 + R_3) + (L_2 - 2M_{23} + L_3)p]I_{23} - \omega(M'_{24} - M'_{34})I_4$$

Here, V_{23} is the externally applied armature voltage, and $\omega M'_{13} I_1$ is the voltage generated in the armature by its rotation in the flux of the main field. The term $(R_2 + R_3) + (L_2 - 2M_{23} + L_3)$ simply represents the self-impedance of the armature and interpoles in series. The negative sign of the mutual inductance arises from the fact that the ampere-turns of the two windings are opposed. Each of these terms is straightforward and none requires further consideration.

There remains the final term $-\omega(M'_{24} - M'_{34})I_4$, which repre-

sents the voltage generated in the armature and interpoles in series by the rotation past them of the flux produced by the currents in the short-circuited turns. During the interval of commutation this voltage changes sign with I_4. For a d.c. machine, the other quantities in the equation are essentially constant, so the importance of the term under consideration lies in its mean value rather than in its instantaneous value during the interval of commutation. The continuous change in I_4 will produce a ripple in the armature voltage, but this is usually unimportant. So far as the mean value of the term is concerned, it is clear that for linear commutation the mean value of I_4 is zero and therefore the term will have no net effect upon the armature voltage.

Should the interpoles be too weak, however, then towards the end of the interval of commutation the current in the short-circuited turns will not be approaching its correct reversed value. Sparking does not necessarily follow, because the brush resistance may be sufficient to force the current rapidly to its correct value by the end of commutation. Nevertheless, the mean value of the current in the short-circuited turns will no longer be zero, and the effect will be to accentuate the normal falling of the load characteristic of the machine. Similarly, overwound interpoles tend to give the machine a rising characteristic. These phenomena are both known but not perhaps well known. The effect of the repetitive change of current in the short-circuited turns is therefore to produce a ripple in the armature voltage, but for linear commutation the net effect is zero. On the assumption of linear commutation the effect of the I_4 term is thus negligible and it may be omitted from the equation. Eqn. (18) therefore assumes the simpler form

$$V_{23} = \omega M'_{13} I_1 + (R_{23} + L_{23}p)I_{23} \quad . \quad . \quad (25)$$

where R_{23} and L_{23} are written for the resistance and inductance respectively of the armature and interpoles in series.

(5.3) The Field Equation

The remaining equation is eqn. (17), namely

$$V_1 = (R_1 + L_1 p)I_1 + \omega M'_{13} I_{23} + M_{14} p I_4$$

where V_1 is the voltage applied to the field and $(R_1 + L_1 p)I_1$ is the voltage drop due to the field's self-impedance. Both these terms are straightforward and need not be considered further.

The last two terms are the most interesting in the analysis. The term $M_{14}pI_4$ represents the voltage induced in the field by the change of current in the short-circuited turns, which lie on the same axis, and $\omega M'_{13}I_{23}$ is the voltage generated in the field by the rotation of the current-carrying armature. A little consideration shows that both these terms are relatively large, and cannot be neglected as second-order effects. For, in the term $M_{14}pI_4$ the component pI_4 is due to the reversal of the full armature current in the short interval of commutation, whilst M_{14} depends upon the number of turns of the field winding, which is large. The main generated voltage is given by $\omega M'_{13}I_1$, and since I_{23} is normally much greater than I_1, it follows that the term here, namely $\omega M'_{13}I_{23}$, must also be very large. As mentioned earlier, neither of these terms appears in the normal form of the equations of the machine.

The solution to the difficulty lies in the fact that although both terms are large they are at all times equal and opposite. Their net effect is zero. This result, which is of fundamental importance, may be demonstrated as follows.

Consider a full-pitch armature coil connected to slip rings. Its mutual inductance with the field winding over a cycle is shown in Fig. 6(*a*). This quantity will be unaffected if the ends

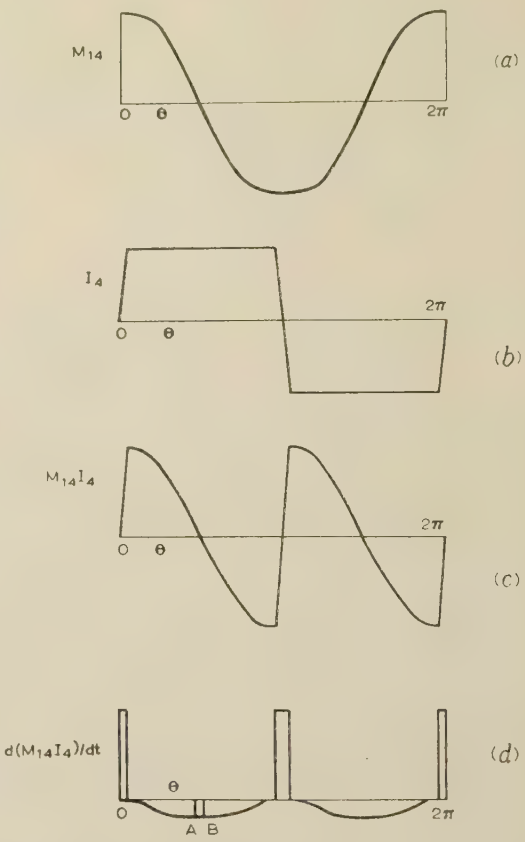

Fig. 6.—Reaction on the field of a rotating current-carrying armature coil.

(*a*) Mutual inductance.
(*b*) Current.
(*c*) Flux linkage.
(*d*) Induced voltage.

of the coil are connected to commutator segments instead of slip rings. Suppose that the turn is, in fact, part of the armature of the commutator machine. Then, assuming linear commutation, the current in the turn over the same interval will be as shown in Fig. 6(*b*). The voltage induced in the field by rotation of this turn will be given by $d(MI)/dt$. The product MI is shown in Fig. 6(*c*), and its differential, giving the voltage, in Fig. 6(*d*). Consideration of this curve shows that the positive peaks are produced by direct mutual induction, since they occur when M is constant and therefore represent MdI/dt. The integral of the induced voltage curve [Fig. 6(*d*)] is the curve MI in Fig. 6(*c*), and the average value of the induced voltage over a cycle is therefore zero. Nevertheless, if the armature winding of the machine did consist of a single coil only, the reaction on the field given by the voltage waveform [Fig. 6(*d*)] would be appreciable. The reactions of a uniformly wound armature may be determined from the following considerations.

The voltage *induced* in the field at any time by the reversal of current in the coils being short-circuited is given by the positive peaks of the curve in Fig. 6(*d*). The voltage being *generated* in the field at the same time by the rotation of any other set of armature coils depends upon the position of that set. For one particular set of coils, for example, the voltage might be given by the ordinate A in Fig. 6(*d*), and for the neighbouring set by the ordinate B. It follows that if the curve in Fig. 6(*d*) is divided up into equal strips of width δ, the mean voltage generated in the field at a particular time by the whole armature (less the short-

circuited turns) is the sum of the mean ordinates of all the strips. If these voltages are now multiplied by δ, the result is equal to the area of the negative parts of the curve. But the total area of Fig. 6(d) is zero, so the net voltage induced in the field by the currents in both armature and the short-circuited turns is zero. Fig. 6(d) now applies at all times.

Returning now to eqn. (17), the term $M_{14}pI_4$ corresponds to the positive peaks in Fig. 6(d); the term $\omega M'_{13}I_{23}$ corresponds to the negative parts. It follows that the sum of the two terms is zero at all times.

Eqn. (17) therefore reduces to

$$V_1 = (R_1 + L_1 p)I_1 \quad . \quad . \quad . \quad . \quad . \quad (26)$$

Thus the short-circuited-turn equation gives valuable information about the process of commutation, but makes no other contribution to the performance of the machine, and may therefore be omitted. The mean value of the short-circuited-turns term in the armature equation is zero, so it also may be omitted. Finally, the short-circuited-turns term in the field equation above is cancelled by another term. The object of eliminating the short-circuit row and column has therefore been achieved. There remain only eqns. (25) and (26), namely

$$V_{23} = \omega M'_{13}I_1 + (R_{23} + L_{23}p)I_{23}$$
$$V_1 = (R_1 + L_1 p)I_1$$

which are identical with eqns. (11), the equations determined experimentally at the terminals.

It is now possible to see whence the asymmetry of these equations has arisen. The non-zero asymmetric term $\omega M'_{13}I_1$ has as its reciprocal the non-zero term $\omega M'_{13}I_{23}$ in the field equation. Although this is a large term it is compensated by the term $M_{14}pI_4$. The reciprocal of this is the term $M_{14}pI_1$ in the short-circuited-turns equation. This, however, disappears because I_1 is constant. The result is therefore asymmetric because the currents in the windings have been considered and not simply the impedances.

To make this clear, consider the simple case of a two-winding transformer whose impedance matrix is symmetric, and suppose that the terminal voltages are manipulated in such a way that the current in the primary winding is sinusoidal with angular frequency ω, whilst the secondary current is direct. Then the term $M_{12}pI_1$ becomes $j\omega M_{12}I_1$ whilst the reciprocal term becomes zero, and the symmetry is lost.

(6) TORQUE OF THE COMMUTATOR MACHINE

Since the equations of the commutator machine in Sections 5.2 and 5.3 have been derived from those of a slip-ring machine, it follows that the torque is given by eqn. (4a). When this equation is applied to the voltage equations (16) it can be seen that $dL/d\theta$ is simply the set of coefficients of ω in the matrix, that is

$$dL/d\theta = \begin{array}{|c|c|c|} \hline . & M'_{13} & . \\ \hline M'_{13} & . & -(M'_{24} - M'_{34}) \\ \hline . & -(M'_{24} - M'_{34}) & . \\ \hline \end{array}$$

This matrix is symmetric, so the following mathematical manipulation becomes possible. The torque is given by

$$T = \tfrac{1}{2}I_t dL/d\theta I = I_{t\frac{1}{2}}(G + G_t)I + I_{t\frac{1}{2}}(G - G_t)I$$

where

$$G = \begin{array}{|c|c|c|} \hline . & . & . \\ \hline M'_{13} & . & -(M'_{24} - M'_{34}) \\ \hline . & . & . \\ \hline \end{array}$$

and G_t is its transpose. It will be seen that $G + G_t$ is equal to $dL/d\theta$, whilst $G - G_t$ is a skew-symmetric matrix, and its quadratic form with the matrix I is identically zero.[8]

Evaluating the expression for T gives

$$T = I_t GI \quad . \quad . \quad . \quad . \quad . \quad . \quad . \quad (27)$$

The short-circuited-turns row is here zero, and the component of torque due to the term on the short-circuited-turns column, when evaluated, is found to be $-I_{23}(M'_{24} - M'_{34})I_4$. For correctly wound interpoles the mean value of I_4, and hence also of this component of torque, is zero. Under these conditions the term may be omitted. It must be appreciated, however, that underwound or overwound interpoles affect the net torque of a motor just as they affect the output characteristic of a generator. On the assumption of linear commutation, however, the term has no significance, so the short-circuited-turns row and column may be omitted from the matrix for G, giving

$$G = \begin{array}{|c|c|} \hline . & . \\ \hline M'_{13} & . \\ \hline \end{array} \quad . \quad . \quad . \quad . \quad . \quad . \quad . \quad (28)$$

which is in agreement with the experimentally determined eqn. (12), and also with the accepted commutator-primitive equations.

This completes the derivation of the true commutator primitive machine from the slip-ring machine. The equations have been derived upon the basis of a study of conditions during one interval of commutation only. But none of the quantities remaining in the equations depends upon this fact, and since events during one cycle of commutation are identically repeated in all other intervals, it follows that the resulting equations must be of general application.

It is a simple matter to extend the analysis to cover the more general case of two stator and two rotor windings, and thus obtain eqns. (13). It may be mentioned that these four windings do not include the interpole and short-circuited turns of the main analysis.

(7) EXPERIMENTAL RESULTS

The comprehensive series of tests which was carried out to verify the analytical work served also to illustrate some of the problems associated with the measurement of the tensor quantities of machines. In classical machine tests it is normally only mutual inductances, short-circuit inductances and rotational inductances that are measured and the methods of measurement are well known and accurate. Tensor analysis requires the measurement of self-inductances and also the rate of change of inductance with position.

The measurements must be carried out under conditions approaching as closely as possible those obtaining in the normal operation of the machine. For this reason, a.c. methods of inductance measurement are not likely to be of value on a d.c. machine with solid poles. High-frequency methods are almost certainly valueless, and experience has shown that it is difficult

(though not impossible) to obtain good results with normal 50 c/s methods. Ballistic methods were therefore adopted throughout.

(7.1) Experimental Techniques

Almost all the tests were carried out with the machine stationary. The brush-gear was removed and leads were soldered directly to appropriate commutator segments.

(7.1.1) Mutual Inductance Measurement.

The measurement of mutual inductance using a ballistic voltmeter is straightforward. The voltage induced in an open-circuit secondary winding by a changing primary current is given by $V_2 = MdI_1/dt$. If a steady direct current be reversed, integration gives, for the flux linkage,

$$\Psi = \int_0^\infty V_2 dt = M \int_{-I_1}^{+I_1} dI_1 = 2MI_1$$

The ballistic voltmeter reading is directly proportional to Ψ, giving

$$M = \tfrac{1}{2}\Psi/I$$

It is necessary for accurate results that the period of the voltmeter should be long compared with the time-constant of the coil. A ballistic galvanometer with a period of 8 sec was used, and the time-constant of the coils reduced by using high voltages in series with high resistances.

One of the chief difficulties is with the main field and is due to the damping effects of eddy currents in the solid parts of the magnet structure. A preliminary series of tests with increasing voltage (i.e. diminishing time-constants) enabled a satisfactory final arrangement to be obtained.

(7.1.2) Self-Inductance Measurement.

The following method, which is believed to be original, was used for the measurement of self-inductance. The inductor was connected with three non-inductive resistors in the Wheatstone-bridge circuit shown in Fig. 7. Using a d.c. supply, the

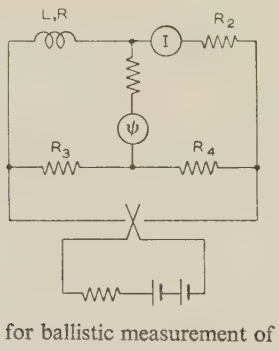

Fig. 7.—Circuit for ballistic measurement of self-inductance.

bridge was balanced and the supply connections were then reversed. The final steady-state condition is again balance, but there is a transient disturbance due to the inductance concerned. Simple analysis shows that the inductance is given by

$$L = \frac{\frac{1}{2}\Psi}{I} \frac{R_3 + R_4}{R_4}$$

For equal ratio arms, the simpler formula $L = \Psi/I$ is applicable. Some numerical results confirming the method are given in Section 7.3.2.

(7.1.3) Circuits for Ballistic Inductance Measurement.

One further point of technique must be mentioned. It was decided not to disconnect the armature conductors from their

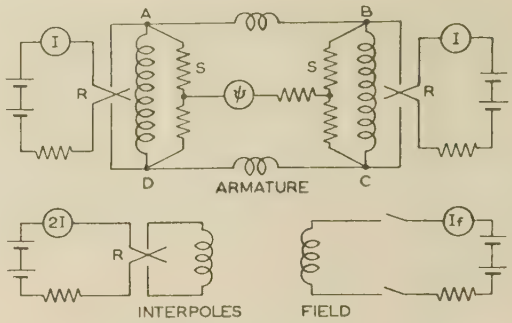

Fig. 8.—Circuit for measurement of mutual inductance between the armature-with-interpoles and the short-circuited turns.

risers. Tests had therefore to be carried out between different parts of a closed armature. Fig. 8 shows a circuit typical of those used. It is for the measurement of the mutual inductance between the armature-with-interpoles and the short-circuited turns. ABCDA represents the armature winding, shown for simplicity as a ring winding. The two parallel paths, AD and BC, of the main armature were supplied in parallel from independent sources with equal currents. The interpole winding carried a current of twice this value. The three supply connections were simultaneously reversed through ganged reversing switches R, and the flux linkage in the parallel pairs of short-circuited turns AB and CD read on the galvanometer, which was connected across the centre taps of two similar resistors S. To simulate normal conditions of operation, the field winding carried its rated current, which was not reversed.

(7.2) Variation of Inductance with Rotor Position

The machine tested was a 2-pole, 230-volt, 3 kW, 1 400 r.p.m. d.c. generator with an interpole winding.

The commutator segment thickness was 0·155 in and the mica thickness 0·031 in. The brush thickness was 0·375 in, and the number of armature coils short-circuited by each brush set was therefore very closely two.

The first series of tests was carried out to determine the variations with rotor position of the sixteen inductance coefficients of eqn. (5). The experimental results have already been given in Fig. 4. One modification to the actual results obtained has been made in plotting the curves of this Figure. This was thought to be desirable because the width of the interpole shoe (0·75 in) was only slightly different from that of the rotor teeth (0·625 in), and with 18 rotor teeth a pronounced 18th harmonic therefore appeared in the waveforms of all interpole inductance coefficients. This harmonic has been smoothed out from the curves in Fig. 4.

Full notes on this series of tests cannot be given, but the following points are of interest.

(*a*) The self-inductance of the short-circuited turns has the expected trapezoidal form, but the maximum value occurs when the turns lie on the interpole axis and not the field axis. It would appear that the leakage reluctance of the pole faces is less than the direct reluctance of the poles and yoke [Fig. 4(*b*)].

(*b*) When numbers of such turns are connected in series to form the main armature winding, the trapezoidal form disappears, and the self-inductance of the main armature differs from a pure sine wave only by the limits of experimental error [Fig. 4(*a*)].

(*c*) The five curves of mutual inductance shown in Fig. 4 were all measured in both directions. In every case it was found that, provided the currents were so adjusted that similar saturation conditions obtained, the two values of mutual inductance were the same. Most interesting perhaps is the mutual inductance between the armature and the interpoles. In Fig. 4(*e*) the 18th harmonic has been smoothed out. Fig. 9 gives the actual results in both

directions. It will be seen that the difference between the two sets of results is very slight. The test is a severe one for the thesis that mutual inductance is always reciprocal, since the interpole winding is lumped whilst the armature winding is distributed and the interpole permeance is lumped whilst the armature permeance is distributed. A further complication is the 18th harmonic. The reciprocity shown in this stringent test is considered conclusive.

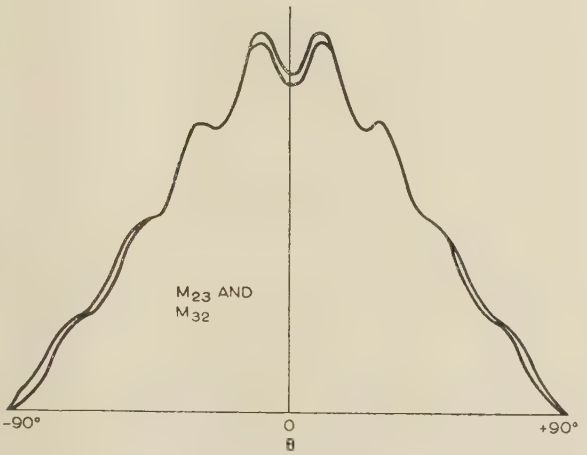

Fig. 9.—Comparison between the two curves of mutual inductance for armature and interpoles obtained from measurements in opposite directions.

(7.3) Variation of Inductance with Current

The second series of tests was carried out to measure the saturation curves of inductance at the fixed rotor position $\theta = 0°$. The inductances concerned are those given in eqn. (16). It is convenient to discuss the results in the same order as that in which the theory appears in Section 5.

(7.3.1) The Short-Circuited-Turns Inductances.

The most important terms in the short-circuited-turns equation are the self-impedance of the turns and their rotational inductance with the armature and interpoles.

It was found that the self-inductance of the turns was independent of their own current and of the interpole-winding current, but was reduced by 63% when normal current flowed in the field winding. This latter value, which represents normal operating conditions, is the value required.

It should be pointed out that the reduction in the self-inductance is attributed entirely to saturation effects. If the inductance had been measured by normal a.c. methods the presence of the closed coupled circuit, which the energized field windings provide, would naturally lead to a reduction in the apparent inductance. The ballistic method used, however, depends in effect only upon the initial and final steady-state d.c. conditions and not at all upon the nature of the intervening transient.

The inductance varied according to whether the two turns were in the same or different slots. A mean value considered to be adequate is

$$L_4 = 1{\cdot}71 \times 10^{-4}\text{H}$$

It is difficult to predict the effective value of the turns resistance, since this includes the brush and contact resistances. It will shortly be shown that the value adopted is fortunately not critical. The resistance of the coils alone was found to be 0·0586 ohm. In the calculations below a value of 0·06 ohm (almost certainly too low) was first taken and then a second value of 0·120 ohm (likely to be too high). In spite of the arbitrary factor of 2 in these values, there is very little difference in the results.

The values of the rotational inductance between the turns and (*a*) the armature, (*b*) the interpoles, and (*c*) both interpoles and armature, were then measured for the three cases in which the coil sides lie in different positions in the same slots, and for the fourth case, in which they are in different slots. The effect of the field ampere-turns was again appreciable, and the tests were carried out with normal field current. In this test also the rotational inductance was found to be much lower when the coil sides were in different slots. The following mean value for the rotational inductance for the armature-with-interpoles and the short-circuited turns was obtained:

$$M'_{24} - M'_{34} = 2{\cdot}12 \times 10^{-3}\text{H/rad}$$

With these values, it becomes possible to estimate the variation of current in the short-circuited turns during commutation and hence to determine the efficiency of interpole compensation. At a speed of 1 500 r.p.m. the value of ω is 157 rad/s. The brush short-circuits two of the 72 commutator segments, so the time of commutation is $1{\cdot}111 \times 10^{-3}$ sec. When these numerical values are substituted in eqn. (22), the following equations are obtained:

$$I_4 = [5{\cdot}55 - 6{\cdot}55\varepsilon^{-0{\cdot}390(\frac{1}{2}+t/T_c)}]I_{23}$$
$$I_4 = [2{\cdot}775 - 3{\cdot}775\varepsilon^{-0{\cdot}780(\frac{1}{2}+t/T_c)}]I_{23}$$

corresponding to the two arbitrary values of R_4 discussed above. Graphs of these curves over the interval of commutation are given in Fig. 10, from which it can be seen that the effect of R_4 is slight.

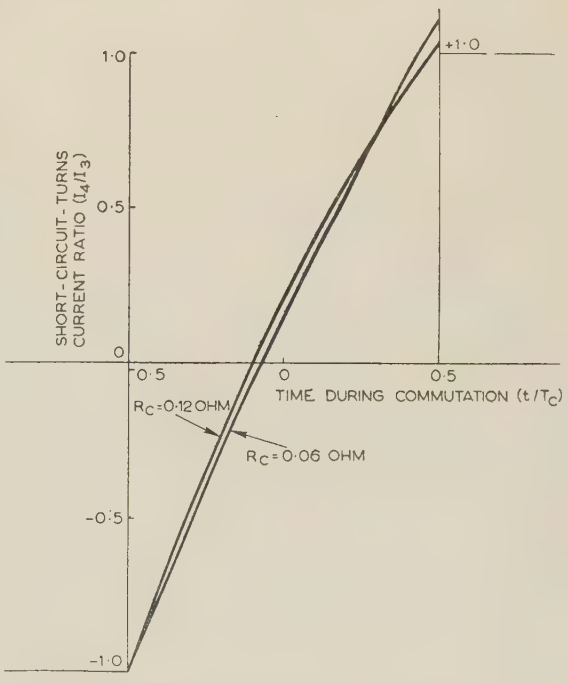

Fig. 10.—Calculated current during commutation for two values of effective short-circuit-turns resistance.

The ideal value of $M'_{24} - M'_{34}$ as given by eqn. (23) is $1{\cdot}99 \times 10^{-3}$ H/rad for $R_4 = 0{\cdot}06$ ohm, and $2{\cdot}06 \times 10^{-3}$ H/rad for $R_4 = 0{\cdot}12$ ohm. The approximate value from eqn. (24) is $1{\cdot}96 \times 10^{-3}$ H/rad. These values compare with the measured value of $2{\cdot}12 \times 10^{-3}$ H/rad.

These results show that the both the experimental techniques and the theoretical analysis are sound.

(7.3.2) **The Armature and Interpole Inductances.**

The rotational inductance coefficient between the field and the armature is important because it is the only one of the sixteen which appears in the operational impedance matrix of a simple d.c. machine. From the standstill ballistic measurements of this quantity the open-circuit characteristic of the machine

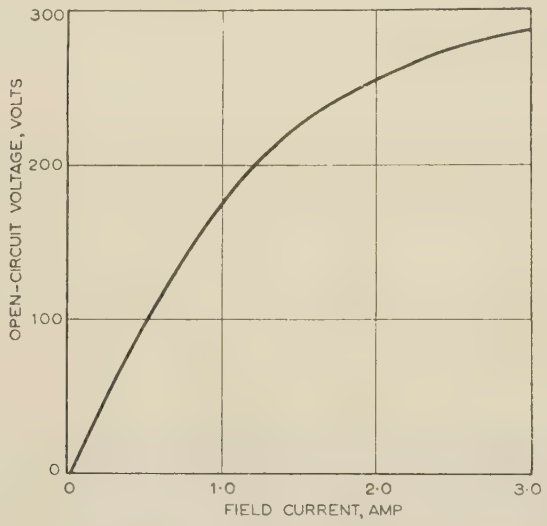

Fig. 11.—Predicted and measured open-circuit characteristic.

shown in Fig. 11 was calculated. The same curve was obtained by an open-circuit test at normal speed.

The following results obtained for the self-inductance of the armature and interpoles are of interest:

Self-inductance of the armature alone, L_3	0·042 3 H.
Self-inductance of the interpoles alone, L_2	0·020 2 H.
Mutual inductance of armature with interpoles, M_{23}	0·011 9 H.
Mutual inductance of interpoles with armature, M_{32}	0·011 5 H.
Predicted value, $L_2 + L_3 - M_{23} - M_{32}$	0·039 1 H.
Self-inductance of the armature-interpoles, measured	0·039 1 H.

The agreement between the predicted and measured values confirms the validity of the bridge method developed for the measurement of self-inductance. The reciprocity of the mutual inductance is again noticeable. It will be noticed also that, although the interpoles overcome armature reaction in the commutation zone, yet this action is local. The inductance of the armature is greater than that of the interpoles, and the latter do not form a compensating winding.

An important point arose in connection with these tests. Although the interpoles and main armature both lie on the quadrature axis, and although their self-inductance was independent of the currents they carried, it was found to depend critically upon the direct-axis field current, as shown by the graph in Fig. 12. The effect is attributed to cross-saturation. The wider applications of this are important, namely that it is unwise to assume (as is frequently done in synchronous machine theory) that direct-axis parameters are unaffected by quadrature-axis saturation and vice versa. It is not suggested, however, that these results are in any way typical of a normal salient-pole synchronous machine.

The remaining quantity in the armature equation is the rotational inductance with the short-circuited turns. Measurements of this inductance gave a value close to that obtained

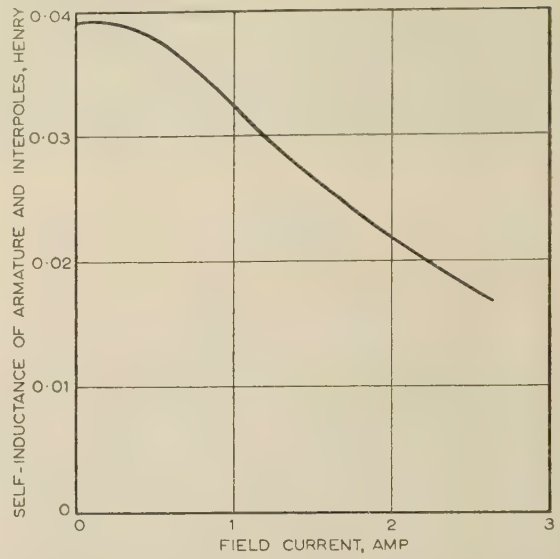

Fig. 12.—Variation of self-inductance of the armature-with-interpoles with field current, showing dependence of a quadrature-axis parameter upon a direct-axis quantity.

in Section 7.3.1 for the reciprocal quantity. The term $\omega(M'_{24} - M'_{34})I_4$ has the value $0{\cdot}333I_4$ and represents the amount by which the generated voltage of the machine is modified by the presence of underwound or overwound interpoles. Fig. 10 shows that in the actual machine the departure from linear commutation is so small that the effect of the term is negligible—0·6 volt on full load.

Experience has shown, however, that for low-voltage, heavy-current machines with few interpole turns the term may be of appreciable significance.

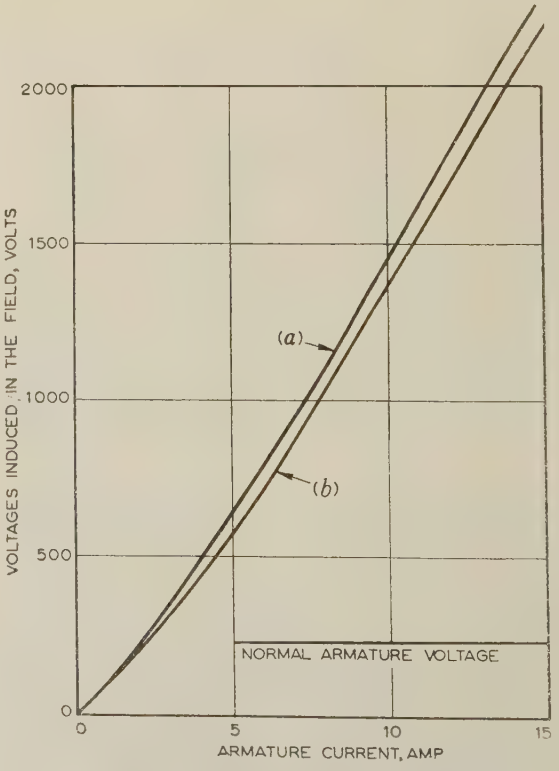

Fig. 13.—Voltages induced in field by armature, due to (*a*) generator and (*b*) transformer action.

(7.3.3) **The Field Inductances.**

The mutual inductance between the short-circuited turns and the field was next measured, and from the results the voltage induced in the field by the continued reversal of current in the short-circuited turns position was calculated. The results are shown graphically in Fig. 13. It will be seen that this voltage reaches a magnitude of 1 880 volts at full load.

Measurements of the rotational inductance between the armature and field similarly enabled the voltage generated in the field by the rotation of the current-carrying armature to be calculated. These results are also plotted in Fig. 13. Here again, for normal armature current, the generated voltage is very high—2 000 volts.

Since the argument of the equivalence of the transformer and generator voltages induced in the field winding is one of the keystones of the theoretical analysis given earlier, it would have been gratifying if the two voltages plotted in Fig. 13 had been identical. They do, in fact, show a mean deviation of about 5%. This difference is, however, definitely attributable to saturation differences and to experimental error, and not to any fault in the theory. On the contrary, the close agreement of the curves is considered adequate proof of the arguments in Section 5.3. The main armature consists of two sets of 34 coils as against the two sets of two in the short-circuited turns. For similar currents, therefore, the ampere-turns, and hence the saturation, will be different.

(8) CONCLUSION

The author believes that the merits of the unified-machine theory are such that it will eventually replace the classical theory altogether. It cannot do this, however, until it is quite comprehensive; at present it ignores completely the process of commutation. It is hoped that this gap will be filled by the theory of commutation given in the paper, which may also, perhaps, shed new light on the mechanism of commutation. It certainly shows a physical relation between the slip-ring and commutator machines which is of intrinsic interest and which may be compared with the purely mathematical analogy between the two classes of machine developed by Park and stressed by Kron. The conclusion to be drawn is that the performance of any electrical machine may be developed from the simple case of two coils with relative angular movement.

(9) ACKNOWLEDGMENT

The author is indebted to Professor J. M. Meek for his encouragement and help.

(10) REFERENCES

(1) PARK, J. H.: 'Two-Reaction Theory of Synchronous Machines', *Transactions of the American I.E.E.*, (i) 1929, **48**, p. 716, and (ii) 1933, **52**, p. 352.

(2) BLONDEL, A.: 'The Methods of Calculation of the Armature Reactions (Direct and Transverse) of Alternators', Transactions of the International Electrical Congress, St. Louis, 1904, **1**, p. 635.

(3) LIWSCHITZ-GARIK, M., and WHIPPLE, C. C.: 'Electrical Machinery', Vol. II (Van Nostrand, New York, 1946).

(4) DOHERTY, R. E., and NICKLE, C. A.: 'Synchronous Machines—III', *Transactions of the American I.E.E.*, 1927, **46**, p. 1.

(5) FORTESCUE, C. L.: 'Method of Symmetrical Co-ordinates applied to the Solution of Polyphase Networks', *ibid.*, 1918, **37**, p. 1027.

(6) KRON, G.: 'Non-Riemannian Dynamics of Rotating Electrical Machinery', *Journal of Mathematics and Physics*, 1934, **13**, p. 103.

(7) KRON, G.: 'The Application of Tensors to the Analysis of Rotating Electrical Machinery', *General Electric Review*, 1935 to 1938. Published in book form 1938 and 1942.

(8) KRON, G.: 'Short Course in Tensor Analysis' (John Wiley, 1942).

(9) GIBBS, W. J.: 'Tensors in Electrical Machine Theory' (Chapman and Hall, 1952).

(10) LYNN, J. W.: 'The Tensor Equations of Electrical Machines', *Proceedings I.E.E.*, Monograph No. 117 S, January, 1955 (**102** C, p. 149).

(11) APPENDIX

If the relation between the actual and transformed currents is given by the matrix equation

$$I = CI'$$

it can easily be shown[8, 9] that, for invariant power, the relation between the voltages is given by

$$V' = C_t V$$

and that between the impedances by

$$Z' = C_t Z C$$

The appropriate form of C has been given in eqn. (7).

The new currents are found from the inverse relation

$$I' = C^{-1} I$$

which gives

$$\begin{bmatrix} I_1 \\ I_2 \\ I_q \\ I_d \end{bmatrix} = \begin{bmatrix} 1 & & & \\ & 1 & & \\ & & \cos\theta & \sin\theta \\ & & -\sin\theta & \cos\theta \end{bmatrix} \times \begin{bmatrix} I_1 \\ I_2 \\ I_3 \\ I_4 \end{bmatrix} = \begin{bmatrix} I_1 \\ I_2 \\ I_3\cos\theta + I_4\sin\theta \\ -I_3\sin\theta + I_4\cos\theta \end{bmatrix}$$

Since the inverse of C is equal to its transpose, a similar relation holds between the original and transformed voltages.

At this point it is interesting to note that, if the rotor carries balanced sinusoidal currents and runs at synchronous speed,

$$I_3 = \sqrt{2}[I\cos(\omega t - \phi)] \quad \text{and} \quad I_4 = \sqrt{2}[I\sin(\omega t - \phi)]$$

where I is the r.m.s. value of the rotor currents and ϕ their phase displacement with respect to the rotor voltages. Since $\theta = \omega t + \delta$, where δ is the load angle, it follows that the transformed rotor currents are direct currents:

$$I_q = \sqrt{2}[I\cos(\delta + \phi)] \quad \text{and} \quad I_d = -\sqrt{2}[I\sin(\delta + \phi)]$$

Similarly the transformed voltages are direct voltages:

$$V_q = \sqrt{2}(V\cos\delta) \quad \text{and} \quad V_d = -\sqrt{2}(V\sin\delta)$$

The two equations also show the physical significance of the rotor-current transformations. The rotor m.m.f.'s are resolved into their components along the direct and quadrature axes of the stator. Historically, this physical resolution of m.m.f.'s was developed first, and the mathematical transformation deduced from it.

The transformed impedance matrix is easily found, if it is remembered that the operator p acts upon the product of all the terms to its right.

Matrix multiplication is not commutative, and the preservation of the correct order of the terms is essential. In the expression C_tZC, the p in Z does not act upon the θ terms in C_t since C_t comes before Z. It does, however, act upon the product of the θ terms in Z, the θ terms in C and the current terms. These latter terms must be understood, since whilst the expression pI has significance the term p alone, which would otherwise occur, is meaningless. With this in mind the analysis is simple.

First,

$$ZC = \begin{array}{|c|c|c|c|} \hline R_1 + L_1p & & & M_1p \\ \hline & R_2 + L_2p & M_2p & \\ \hline -M_1p\sin\theta & M_2p\cos\theta & R_3\cos\theta + (L_a - L_b)p\cos\theta & -R_3\sin\theta - (L_a + L_b)p\sin\theta \\ \hline M_1p\cos\theta & M_2p\sin\theta & R_3\sin\theta + (L_a - L_b)p\sin\theta & R_3\cos\theta + (L_a + L_b)p\cos\theta \\ \hline \end{array}$$

For the second stage, the following simple identities involving the differential of a product are required:

$$(\cos\theta\, p\cos\theta + \sin\theta\, p\sin\theta)I = (p)I$$
$$(\cos\theta\, p\sin\theta - \sin\theta\, p\cos\theta)I = (d\theta/dt)I = (\omega)I$$

Whilst the current does not appear in the impedance matrix its presence must always be understood.

Secondly, then

$$Z' = C_tZC = \begin{array}{|c|c|c|c|} \hline R_1 + L_1p & & & M_1p \\ \hline & R_2 + L_2p & M_2p & \\ \hline -\omega M_1 & M_2p & R_3 + L_qp & -\omega L_d \\ \hline M_1p & \omega M_2 & \omega L_q & R_3 + L_dp \\ \hline \end{array}$$

where $L_d = L_a + L_b$ and $L_q = L_a - L_b$, as in eqn. (9).

It is of interest at this point to apply the transformed equations to the case of a simple salient-pole machine without damper windings. The second row and column disappear, and since for balanced operation it has been seen that the transformed currents and voltages are direct, it follows that the p terms also vanish. Under these conditions the matrix voltage equation may be expanded to read

$$V_1 = R_1I_1$$

$$V\sin\delta = -\omega L_qI\cos(\delta + \phi) + R_3I\sin(\delta + \phi)$$

$$V\cos\delta = -(1/\sqrt{2})\omega M_1I_1 + R_3I\cos(\delta + \phi) + \omega L_dI\sin(\delta + \phi)$$

The first equation is trivial. The second and third apply to motor operation. If the signs of I and, for convenience, of I_1 are reversed to apply to generator operation, it is easily seen that the equations are satisfied by the normal voltage (rotating vector) diagram of the salient-pole alternator drawn in terms of its synchronous reactances.[3, 4] This is yet a further instance of the close interrelation between commutator and slip-ring machines.

It remains to justify the expression for the torque given in eqn. (10), which was of a different form from that of the slip-ring primitive.

It can be shown that $\partial L/\partial\theta$ transforms according to the law

$$(\partial L/\partial\theta)' = C_t(\partial L/\partial\theta)C$$

and that by direct evaluation (p is absent)

$$(\partial L/\partial\theta)' = \begin{array}{|c|c|c|c|} \hline & & -M_1 & \\ \hline & & & M_2 \\ \hline -M_1 & & & L_q - L_d \\ \hline & M_2 & L_q - L_d & \\ \hline \end{array}$$

It will be noted that, since p is absent from the expressions, this torque matrix is still symmetric. It also contains non-zero terms in the stator rows.

The alternative expression is derived as follows. The coefficient of ω in the transformed impedance matrix is

$$G = \begin{array}{|c|c|c|c|} \hline & & & \\ \hline & & & \\ \hline -M_1 & & & -L_d \\ \hline & M_2 & L_q & \\ \hline \end{array}$$

Now, $$I_t'GI' = \tfrac{1}{2}I_t'(G + G_t)I' + \tfrac{1}{2}I_t'(G - G_t)I'$$

But $(G - G_t)$ is a skew-symmetric matrix, and therefore its quadratic form with I' is identically zero, as may easily be proved by direct multiplication. Furthermore, since

$$(G + G_t) = (\partial L/\partial\theta)'$$

it follows that $$T = I_t'GI'$$

gives the torque. This result could equally well be achieved by consideration of the power balance of the transformed equations. The G form of the torque has the advantage that it may be written directly from the transformed equations, without the necessity of a separate transformation for $\partial L/\partial\theta$. It has the disadvantage that it does not appear symmetric and therefore is not convincing without the above justification.

621.526 : 621.372.63

The Institution of Electrical Engineers
Monograph No. 303 M
Apr. 1958
©

DESIGN OF SAMPLING SERVO SYSTEMS IN THE *z*-PLANE

By T. M. H. REENSKAUG, Graduate, and J. H. WESTCOTT, Ph.D., Associate Member.

(*The paper was first received 27th June, 1957, and in revised form 12th February, 1958. It was published as an* INSTITUTION MONOGRAPH *in April, 1958.*)

SUMMARY

The paper summarizes the basic concepts of the sequence-transform theory, particularly emphasizing the non-physical form of samples assumed for mathematical convenience. In dealing with inverse transforms, it introduces some typical transient modes due to poles of the transform function $Y(z)$.

It is shown that the root-locus method is well suited to the design of sampling control systems; also that the passage of time can be described by a system of moving zeros in the complex z-plane. This provides a complete picture of the response of a system to a given input, both at the sampling instants and between them.

Barker has suggested a particular form of stabilizing network which has the advantage of introducing a modifying function $U(z)$ which is independent of the rest of the system. This work has been extended by showing the limitations of the method and by giving a table of the networks required to realize some functions $U(z)$.

Finally, two examples are worked out in some detail to illustrate the theory, and a brief description of an experimental unit is included for completeness.

LIST OF SYMBOLS

In general, capital letters are used for sequence-transform expressions, and lower-case letters for the corresponding time functions and their Laplace transforms.

$A(m)$ = Coefficient of partial fraction term of $G(z, m)$.
α, β = Reciprocals of time-constants.
a, b = Positive constants, zeros of $U(z)$. $a = \varepsilon^{-\alpha\tau}$, $b = \varepsilon^{-\beta\tau}$.
c, d = Poles of $U(z)$.
δ = A delay measured as a fraction of a sampling interval. $0 \leqslant \delta \leqslant 1$.
$\delta(t - n\tau)$ = A Dirac impulse of infinite height and unit area at $t = n\tau$.
ε = Base of natural logarithms.
F, f = Driving function (forcing function).
$f^*(t) = f(t)$ sampled.
G, g = Output function.
H, h = Subsidiary feedback transfer function.
K = Frequency-independent open-loop gain.
m = Inter-sample time parameter measured as a fraction of the sampling interval. $0 \leqslant m \leqslant 1$, $m = 1 - \delta$.
n = Sample number, the sampling instants being $0, \tau, 2\tau, \ldots, n\tau, \ldots$
$0[Y(z)]$ = Order of $Y(z)$, i.e. difference between the degrees of numerator and denominator of $Y(z)$.
p = Laplace transformer operator. The Laplace transform is defined by $f(p) = \int_0^\infty f(t)\varepsilon^{-pt}dt$.
q = A positive integer.
$R(z, m)$ = Ratio of modified to ordinary pulse transfer functions, $= Y(z, m)/Y(z)$ or $W(z, m)/W(z)$.
S = A sampling device producing Dirac impulses of area proportional to the instantaneous value of the input signal.
t = Time.
τ = Sampling interval. Used as unit of time in most of the paper.
V, v; U, u = Two cascaded filters.
$U(z)$ = Effect of subsidiary feedback on open-loop transfer function.
$v(p) = h(p)/p$.
W, w = Open-loop transfer function, the corresponding impulse response.
Y, y = Overall transfer function, the corresponding impulse response.
z = The sequence-transform operator. ($z = \varepsilon^{p\tau}$ and is therefore an advance operator.)
θ, ϕ = Two cascaded filters separated by a sampler.
λ = An integer measuring a delay in terms of sampling intervals.

(1) INTRODUCTION

There has recently been considerable interest in sampling servo systems.[2, 3, 4] The reason is that in many practical cases the information used for feedback is only available at discrete instants. This could be inherent in the system, as in a chemical plant containing an automatic analyser operating on a batch basis. Sometimes it is introduced intentionally, usually in order to facilitate time-sharing of equipment. This is particularly the case if costly equipment such as computers is involved, but other factors, such as weight, may be the determinants.

An excellent survey of the many methods available for treating sampling systems is given in Reference 1. The present paper is only concerned with the sequence-transform method, and in particular with working in the complex z-plane. The basic theory used in the paper is described by Barker,[5] but a short summary is included here for completeness. Also included in the first Section are diagrams and a discussion of the responses due to different types of poles of the transfer function $G(z, m)$.

The application of the root-locus method to sampling-control systems is discussed in Section 2. Also shown is a method of picturing a complete response, both at the sampling instants and between them, in the complex z-plane by a system of poles and moving zeros. The method of stabilization by employing local feedback across the clamp suggested by Barker is discussed further, and the limitations of the method are given.

(1.1) Sampling Systems

A sampling system may be defined as a system whose input is applied at discrete instants and may be represented basically by the block diagram in Fig. 1. The input signal $f(p)$ is first sampled by means of a device S, and the resulting sampled signal $f^*(p)$ is

Correspondence on Monographs is invited for consideration with a view to publication.
Mr. Reenskaug is at the Imperial College of Science and Technology, University of London.
Dr. Westcott is Reader in Electrical Engineering at the Imperial College of Science and Technology, University of London.

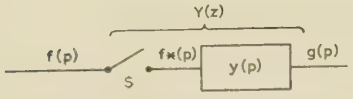

Fig. 1.—Basic sampled system.

applied to the filter proper $y(p)$. In the sequence-transform theory the following assumptions are made:

(*a*) The sampling is performed at regular intervals, τ, in time.

(*b*) The sampling device S is such that its output is in the form of Dirac impulses of infinite height and of area equal to the instantaneous value of the input signal at the sampling instants. The sampling action may be represented by the equation

$$f^*(t) = \sum_{n=0}^{\infty} f(t)\delta(t - n\tau) \quad . \quad . \quad . \quad . \quad (1)$$

where $\delta(t)$ is a Dirac impulse. The corresponding Laplace transform is

$$f^*(p) = \sum_{n=0}^{\infty} f(n\tau)\varepsilon^{-pn\tau} \quad . \quad . \quad . \quad . \quad (2)$$

(*c*) The output of the system is considered at the sampling instants only by imagining there is a sampler in series with it. As will be shown later, no information need be lost owing to this limitation.

(*d*) The system is assumed linear. In this context, linearity is defined by the superposition property, and the sampler therefore falls within the definition.

(1.2) The Sequence Transform

Sampling a function $f(t)$ according to the definition in Section 1.1, the sampler output is given by eqn. (2). Making the substitution

$$z = \varepsilon^{p\tau} \quad . \quad . \quad . \quad . \quad . \quad . \quad . \quad . \quad (3)$$

the equation becomes

$$F(z) = \sum_{n=0}^{\infty} f(n\tau)z^{-n} \quad . \quad . \quad . \quad . \quad . \quad (4)$$

which is defined as the sequence transform of $f(t)$. The summation can usually be performed, giving the sequence transform in closed form. From the defining equation (3) it can be seen that z is the opposite of a delay, or an advance operator.

The inversion integral corresponding to eqn. (4) can, by a transformation from the p-domain, be shown to be

$$f(n\tau) = \frac{1}{2\pi j}\oint F(z)z^{n-1}dz \quad . \quad . \quad . \quad . \quad (5)$$

the integration being performed round a large circle with centre at the origin of the z-plane.

The sequence transform can be obtained by following the steps indicated above, or by using tables (see Section 8.1 or Reference 5).

(1.3) The Pulse Transfer Function

Just as the impulse response of a continuous filter is of great utility, so the response of a sampling system to a unit input will be found useful. A unit input is defined as a signal of arbitrary form, of unit amplitude at zero time and zero at all other sampling instants; thus

$$f(n\tau) = 1; \ (n = 0)$$
$$= 0; \ (n \neq 0)$$

or

$$F(z) = 1$$

If the signal going into the sampler S (Fig. 1) is such a unit input, its output, and therefore the input to the filter proper, will be a single Dirac impulse at zero time. The filter output will be its indicial response $y(t)$. The sequence transform of this response is the pulse transfer function (p.t.f.) of the filter:

$$Y(z) = \sum_{n=0}^{\infty} y(n\tau)z^{-n} \quad . \quad . \quad . \quad . \quad . \quad (6)$$

As an illustration of a pulse transfer function, the simplest possible case of a sampler working alone will be considered. This corresponds to Fig. 1 with $y(p) = 1$. The response of such a system to a unit input is simply $\delta(t)$, giving an output sequence $\delta(t)$, 0, 0, 0, . . . The p.t.f. is therefore $Y(z) = \delta(t)$. It is kept in this form since the amplitude of a Dirac impulse at zero time is open to argument.

It can be shown[5] that the response of a system with p.t.f. $Y(z)$ to a signal whose sequence transform is $F(z)$ is

$$G(z) = F(z)Y(z) \quad . \quad . \quad . \quad . \quad . \quad (7)$$

(1.4) Effect of a Pure Time Delay

If the filter contains a pure time delay $\lambda\tau$ which is an exact multiple of the sampling interval, the effect of this delay is easily shown to be a multiplication of the p.t.f. by a factor $z^{-\lambda}$:

$$Y_1(z) = \sum_{n=0}^{\infty} y(n\tau - \lambda\tau)z^{-n} = z^{-\lambda}\sum_{n=0}^{\infty} y(n\tau)z^{-n} = z^{-\lambda}Y(z) \quad (8)$$

If the delay is a fraction of the sampling interval, $\delta\tau$ say, the new pulse transfer function may be written

$$Y(z, \delta) = \sum_{n=0}^{\infty} y(n\tau - \delta\tau)z^{-n} \quad . \quad . \quad . \quad (9)$$

or, if $m = 1 - \delta$,

$$Y(z, m) = z^{-1}\sum_{n=0}^{\infty} y(n\tau + m\tau)z^{-n} \quad . \quad . \quad . \quad (10)$$

where m is an inter-sample time parameter starting at zero at a sampling instant and increasing with time to 1 at the next sampling instant. The modified p.t.f. $Y(z, m)$ will be found very useful for determining the inter-sample response of sampling systems. Tables of the modified transforms may be found in Section 8.1 or in Reference 5.

(1.5) Cascaded Networks

As pointed out by Barker,[5] the p.t.f. of two filters $U(z)$ and $V(z)$ in cascade, formally written $[VU](z)$, is only equal to the product $V(z)U(z)$ if the two filters are separated by a sampler. The reason for this is that $V(z)$ is the p.t.f. corresponding to $v(p)$ preceded by a sampler (see Fig. 1).

Sometimes the network $v(p)$ may be split into two parts separated by a sampler. Denoting these two parts by $\theta(p)$ and $\phi(p)$, the p.t.f. $[VU](z)$ is equal to $\Theta(z)[\Phi U](z)$. The operation of lumping the part $\phi(p)$ with the following filter and then finding the p.t.f. of the combination may be written as an operational instruction thus: $\Theta(z)*\phi(p)$, leaving the second filter unspecified.

(1.5.1) The Clamp.

The impulsive output of the sampler assumed in the theory must in some way be smoothed to be practically realizable. Commonly used for this purpose is the clamp, which is a device that has a constant output throughout a sampling interval and adjusts this output to be equal to the instantaneous value of the input signal at every sampling instant. Such a clamping action is illustrated in Fig. 2. The clamp may be looked upon as

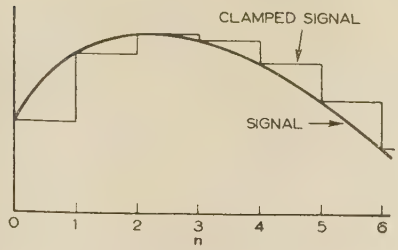

Fig. 2.—Clamping action.

forming a step function at a sampling instant and another of equal magnitude but opposite sign one sampling interval later. The formation of the step function at a sampling instant can be represented by a sampler, forming a Dirac impulse, followed by a pure integrator forming the step. The negative delayed step may be obtained by delaying the input to the sampler by τ and inverting it. This can be done by a unit having the p.t.f. $-1/z$, since $1/z$ is a delay operator. The complete clamp is therefore represented by a unit $(1 - z^{-1})$ followed by a sampler and a pure integrator as shown in Fig. 3. This Figure also

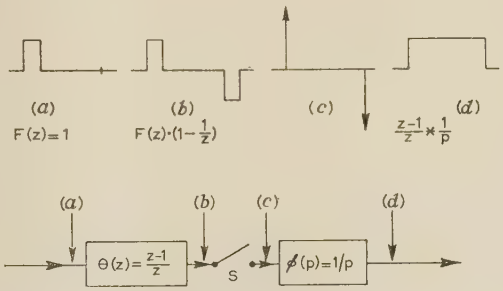

Fig. 3.—Partitioning of clamp transfer function.
Waveform (*a*) represents unit input.
Waveform (*d*) represents clamp output.

shows the waveforms at different points in the clamp due to a unit input. The clamp may now be described by the operational instruction $(1 - z^{-1})*p^{-1}$. It is shown in Section 2.3 that the factor $(1 - z^{-1})$ may be modified without altering its multiplicative property.

(1.6) The Inverse Transform

A given sequence-transform expression $G(z)$ may be inverted by the inversion integral, eqn. (5), or by using Tables of transform (see Section 8.1 or Reference 5). Partial fraction expansion is used where necessary. $G(z)$ may also be expanded in a series of z^{-1}; the coefficients of this series is equal to the output sequence. The coefficient of z^0 is the value of the response at $n = 0$, while that of z^1 is the value at $n = -1$ or $t = -\tau$. Since a physical system can have no response before the input is applied, it follows that the order of the p.t.f. must be zero or less.

(1.6.1) Response Due to Poles of $G(z, m)$.

The root-locus method of design is discussed in Section 2.1. The usefulness of this approach depends to a large extent on a knowledge of the transient modes due to individual poles in the z-plane. Since they are different from the modes of continuous systems, they are discussed here in some detail. The pulse transfer function $Y(z, m)$ is assumed expanded into partial fractions. The denominators will not be functions of the inter-sample time parameter m, since the modes of the system are time-independent; but the coefficients will be, and they determine the inter-sample response of the system.

(a) Simple Real Positive Pole.

The unit input response due to a pole of the form $A(m)z/(z - a)$ for $a \geqslant 0$ is very similar to the response due to a negative real pole of the Laplace transform. The response is $A(m)a^n$, i.e. an exponentially varying sequence as shown in Fig. 4(*a*). Since

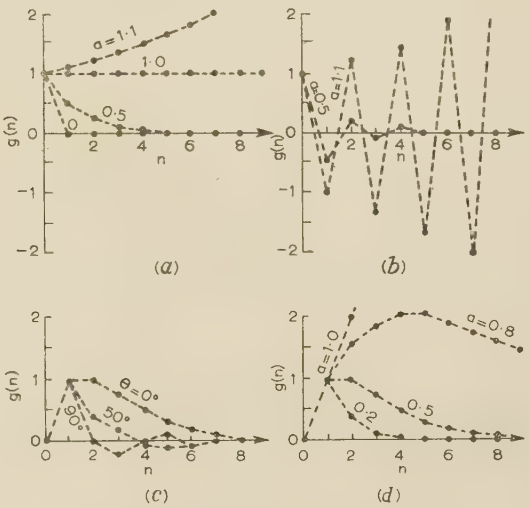

Fig. 4.—Response due to poles of $G(z)$.

(*a*) $G(z) = \dfrac{z}{z - a}$; $g(n) = a^n$; $a \geqslant 0$

(*b*) $G(z) = \dfrac{z}{z + a}$; $g(n) = (-1)^n a^n$; $a > 0$

(*c*) $G(z) = \dfrac{z}{z^2 - 2az\cos\theta + a^2}$; $g(n) = a^{n-1}\dfrac{\sin n\theta}{\sin\theta}$; $a = \frac{1}{2}$

(*d*) $G(z) = \dfrac{z}{(z - a)^2}$; $g(n) = na^{n-1}$

a is positive, the sequence will increase monotonically for $a > 1$ and decrease monotonically for $a < 1$. If $a = 0$, the response will become zero within one sampling interval. The form of the response between the sampling instants is completely determined by $A(m)$, its amplitude being weighted by the exponential term a^n. The dotted lines joining function values at the sampling instants in Fig. 4 have therefore no physical significance.

If the partial fraction expansion term is divided by z, i.e. if the term becomes $A(m)/(z - a)$, the effect is to delay the response by one sampling interval (see Section 1.4).

(b) Simple Real Negative Pole.

The response in this case, shown in Fig. 4(*b*), is identical to that for a positive real pole but for the factor $(-1)^n$, which makes the sequence oscillate between positive and negative values. The appropriate sequence-transform expression is $A(m)z/(z + a)$ for $a > 0$, and the response is $A(m)(-a)^n$.

(c) A Pair of Complex Simple Poles.

A typical term of the partial fraction expansion is here $A(m)z/(z^2 - 2az\cos\theta + a^2)$, the poles being at $z = ae^{\pm j\theta}$. The response is $g(n, m) = A(m)a^{n-1}(\sin n\theta)/(\sin\theta)$. The sequence $g(n)$ has been plotted in Fig. 4(*b*) for different values of θ at $a = 1/2$. Here again the inter-sample response is determined by $A(m)$, and altering the power of z in the numerator will shift the response to the right or left.

(d) Double Real Pole.

The term in the partial-fraction expansion could be $A(m)z/(z - a)^2$, the corresponding response being $g(n, m) = A(m)na^{n-1}$. The sequence $g(n)$ has been plotted for different values of a in Fig. 4(*d*). A different power of z in the

numerator of the partial-fraction term results in a shift of the complete response.

(1.7) Stability

As has been brought out qualitatively by the above inverse transforms, the stability criterion in the z-plane is that no poles of the pulse transfer function $Y(z, m)$ can lie outside the unit circle with centre at the origin. By the defining equation $z = \varepsilon^{p\tau}$, this unit circle is the conformal representation of the imaginary axis in the p-plane. The stability criterion is therefore strictly analogous to the criterion in the p-plane that no poles of the transfer function may lie in the right-half plane.

Note that the stability criterion must be applied to the complete transfer function $Y(z, m)$ and not to the transfer function describing the system at the sampling instants only, $Y(z)$. If the latter criterion only is satisfied, there may be oscillations in the steady state which have nodes at the sampling instants. An example of this is given in Reference 6.

(2) CLOSED-LOOP SYSTEMS

A single-loop sampled servo system is shown in Fig. 5. Its transfer function is similar to the one for continuous systems, namely

$$Y(z) = \frac{KW_1(z)}{1 + K[W_1W_2](z)} \quad . \quad . \quad . \quad (11)$$

This transfer function represents the system at the sampling instants only. In order to obtain an expression which describes

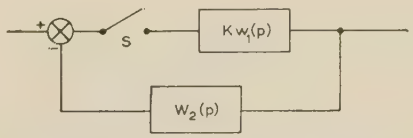

Fig. 5.—Closed-loop system.

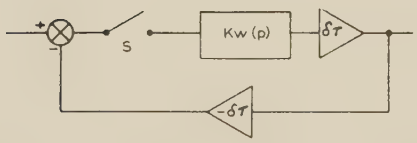

Fig. 6.—System with hypothetical delays for determination of the inter-sample response.

the system at all times, a delay may be cascaded with $Y(z)$ as described in Section 1.6. A better method is due to Barker,[5] and is shown diagrammatically in Fig. 6. A fictitious delay $\delta\tau$ is inserted in the forward path and an equal and opposite delay in the feedback path. The loop then remains unchanged, but the sequence as evaluated at the output terminals may be made to represent any point between the sampling instants by varying $\delta = 1 - m$. The pulse transfer function of such a system is, from eqn. (11),

$$Y(z, m) = \frac{KW(z, m)}{1 + KW(z)} \quad . \quad . \quad . \quad . \quad (12)$$

the loop being closed with unity feedback for simplicity.

If the filter $w(p)$ can be regarded as being partitioned by a sampler, e.g. as the clamp in Fig. 3, the delay $\delta\tau$ modifies the last part, $[\Phi U](z)$, of the p.t.f. only. This is evident, since the delay is introduced at the end of $w(p)$ and therefore does not affect the signals passing through the sampler.

(2.1) The Root-Locus Method

The root-locus method, well known from the design of continuous servo systems by Laplace transforms, is admirably suited to the synthesis of sampled-data systems in the z-plane. The method of constructing the loci is identical in both cases, but the conclusions that can be drawn from them are unfortunately different.

The closed-loop transfer function of a sampling servo system is given by eqn. (11). Assuming unity feedback, it becomes

$$Y(z) = \frac{KW(z)}{1 + KW(z)} \quad . \quad . \quad . \quad . \quad (13)$$

Its characteristic equation may be written $1 + KW(z) = 0$, or in vector form $KW(z) = 1 \angle \pm(2q+1)\pi$, where $q = 0, 1, 2, 3, \ldots$ The root-locus method then consists in plotting the loci satisfying the phase part of this equation, and marking along them the values of K which make the modulus unity.

A thorough discussion of the root-locus method as applied to Laplace transform expressions has been given by Evans.[7] For completeness, a few rules for the construction of the loci are given here.

(*a*) A complete root-locus always joins a pole to a zero; the roots are at the pole positions for $k = 0$ and traverse the loci travelling towards the zero positions as k increases to infinity.

(*b*) The number of separate loci equals the number of poles of $W(z)$.

(*c*) If the order of $W(z)$ is $-r$, i.e. if there is an rth-order zero at infinity, there are r asymptotes at angles $\pm 180°/r$, $\pm 540°/r$, $\pm 900°/r$, etc.

(*d*) The asymptotes intersect at a point on the real axis, not necessarily the origin.

(*e*) The loci include those sections of the real axis which are to the left of an odd number of poles and zeros of $W(z)$.

(*f*) The point of departure from the real axis can be found by considering a point slightly displaced from it. The net change in phase angle must be zero at the point of departure.

(*g*) The loci will always be symmetrical about the real axis since complex poles can occur only in conjugate pairs.

If one is studying the effect on the root-locus of altering the pole-zero pattern, it is often convenient to bear in mind the analogy between a two-dimensional flow field and the root-locus. A description of this analogy is given in Reference 8, but for a qualitative idea it is sufficient to consider the poles as sources and the zeros as sinks. The constant-angle loci, of which the 180° locus is a special case, are then represented by the flow lines.

(2.2) Determination of Pole-Zero Pattern for Modified P.T.F.

There has been a tendency in the past to analyse sampling systems in two separate stages, first considering the response at the sampling instants and then the inter-sample response. This is a reasonable procedure when dealing with servo systems, since the loop is closed at the sampling instants only. It would be illuminating, however, if it were possible to treat the system as a whole, finding some way of describing it at all times by a continuous process. This can in fact be done by using the $Y(z, m)$ notation and describing the response by a system of poles and moving zeros in the z-plane.

The equation in z and m describing the system in Fig. 6 is eqn. (12), which may be written in the form

$$Y(z, m) = R(z, m)\frac{KW(z)}{1 + KW(z)} \quad . \quad . \quad . \quad (14)$$

where $R(z, m) = W(z, m)/W(z)$. The poles and zeros of the latter part of eqn. (14) are found by the normal root-locus method as outlined in Section 2.1. In addition, there are the poles of $R(z, m)$, which are independent of K and also m since the modes of the system are time-independent. Finally, there

are the zeros of $R(z, m)$ whose movement will determine the inter-sample response.

If, as is common in practical systems, the response is continuous, it will be found that as $m \to 1$, a zero of $R(z, m)$ tends to the origin, and as $m \to 0$, a zero tends to infinity. The inversion integral is eqn. (5): $g(n) = (1/2\pi j) \oint G(z) z^{n-1} dz$. Owing to the factor z^{n-1}, a zero is added at the origin at every sampling instant. This may be identified as the zero of $R(z, m)$ moving to the origin as $m \to 1$. In other words, passage of time may be represented by a system of moving zeros in the z-plane, one arriving at the origin and becoming stationary at every sampling instant, and another coming into the finite plane from infinity so that the number of moving zeros is always the same. Since only one zero arrives at the origin at each sampling instant and complex zeros can only occur in conjugate complex pairs, one would expect the zeros to move along the real axis.

If there are discontinuities in the response at the sampling instants, a zero will arrive from infinity into the finite plane at each such instant, and a zero will jump from some point to the origin. This jump is to be expected, since a discontinuity in the response can only be achieved by a discontinuous movement of at least one zero.

(2.3) Stabilization

The simplest way to stabilize a system in terms of the root-locus is to add poles and zeros to the complex z-plane in order to shape the locus into a desired form. Additional poles and zeros are unfortunately difficult to obtain because the p.t.f. of two cascaded networks is not, in general, equal to the product of the individual p.t.f.'s (see Section 1.5).

If a clamp is used, however, there is a particular type of stabilizer due to Barker[5] which overcomes this difficulty. It consists of a subsidiary feedback across the clamp, as shown in Fig. 7(*b*). The clamp is here shown in the partitioned form

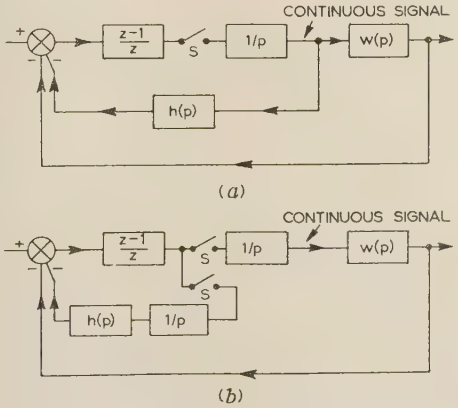

Fig. 7.—Two equivalent block diagrams of stabilized system.

described in Section 1.5.1, and is equivalent to Fig. 7(*b*) with the integrator $1/p$ inserted in the feedback and forward paths separately. Because of the feedback, the operational instruction of the clamp can be modified to

$$\frac{z-1}{z} U(z) * \frac{1}{p} \quad . \quad . \quad . \quad . \quad . \quad (15)$$

where $U(p)$ represents a modifying factor due to $h(p)$ which can be inserted without affecting the pulse transfer function of the rest of the system.

Considering the subsidiary feedback loop, the modifying function $U(z)$ is given by eqn. (11), where $W_1(z) = \dfrac{z-1}{z}$ and $[W_1 W_2](z) = \dfrac{z-1}{z} \cdot V(z)$, since the two networks are separated by a sampler.

$$\frac{z-1}{z} U(z) = \frac{\dfrac{z-1}{z}}{1 + \dfrac{z-1}{z} V(z)}; \quad \text{where } v(p) = \frac{h(p)}{p}$$

$$U(z) = \frac{z}{z + (z-1)V(z)} \quad . \quad . \quad . \quad . \quad . \quad (16)$$

and

$$V(z) = \frac{z}{z-1} \frac{1 - U(z)}{U(z)} \quad . \quad . \quad . \quad . \quad . \quad (17)$$

The feedback across the clamp does not alter the multiplicative property of its pulse transfer function, since the unit $(z-1)U(z)/z$ is still separated from the rest of the filter by a sampler. The pulse transfer function of the modified clamp in operational instruction form is therefore eqn. (15).

In Section 1.3.1 it was shown that the order of the pulse transfer function must be zero or less. Since both $U(z)$ and $V(z)$ must obey this rule, it follows from eqn. (17) that $U(z)$ is restricted to be of zero order. Poles and zeros may therefore be added to the root-locus at will in equal numbers. In addition there is, of course, the normal condition that complex poles or zeros must appear in conjugate pairs. The expressions for $h(p)$ tend to become rather complicated, and for this reason a short table of $U(z)$, $h(p)$ and networks realizing $h(p)$ has been compiled and is given in Section 8.2.

As an example of a modifying function, consider $U(z) = (z-a)/(z-d)$, where $a > 0$. By eqn. (17),

$$V(z) = \frac{z}{z-1} \frac{1 - \dfrac{z-a}{z-d}}{\dfrac{z-a}{z-d}} = \frac{a-d}{1-a} \frac{(1-a)z}{(z-1)(z-a)}$$

From Section 8.1, the corresponding expression for $v(p)$ is

$$v(p) = \frac{a-d}{1-a} \frac{\alpha}{p(p+\alpha)}, \text{ where } \alpha = \log_e (1/a)$$

or

$$h(p) = pv(p) = \frac{a-d}{1-a} \frac{\alpha}{p+\alpha}$$

which can immediately be realized by network (*a*) in Fig. 17 if the gain $K = (a-d)/(1-a)$ and $\alpha = \log_e (1/a) = 1/RC$.

(3) EXAMPLES

In this Section two examples of sampling servo systems are worked out in detail. The first example, a clamped single-lag system, is very simple and could easily be done by purely analytical means. It has been done by a combination of graphical and analytical methods here, however, in order to illustrate the complementary nature of the two methods. The second example is a pure double-integrator system which is used to illustrate the method of stabilization described in Section 2.3 and a graphical procedure for determining the response of the system.

(3.1) Single-Lag System

The system block diagram is shown in Fig. 8. The operational instruction for the clamp is given in Section 1.5.1 as $(z-1)/z * 1/p$. The factor $1/p$ lumped with the lag term $K\alpha/(p+\alpha)$ is

$$\phi(p)\, u(p) = \frac{K\alpha}{p(p+\alpha)}$$

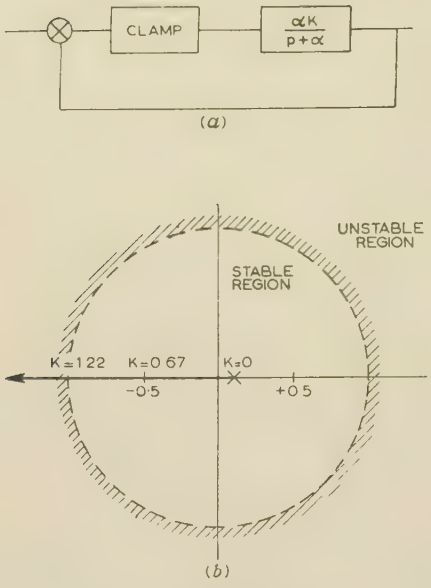

Fig. 8.—Single-lag system.
(*a*) Block diagram.
(*b*) Root-locus diagram.

From Section 8.1, the corresponding p.t.f. is

$$[\Phi U](z) = (1-a)K\frac{z}{(z-1)(z-a)}, \quad \text{where } \begin{matrix} a = \varepsilon^{-\alpha\tau} \\ \tau = 1 \end{matrix}$$

and

$$R(z, m) = \frac{z(1-a^m) - (a-a^m)}{(1-a)z}$$

The open-loop transfer function is therefore

$$W(z, m) = R(z, m)(1-a)K\frac{z-1}{z}\frac{z}{(z-1)(z-a)}$$

$$= R(z, m)\frac{(1-a)K}{z-a}$$

The root-locus diagram corresponding to $W(z)$ is easily plotted by the rules given in Section 2.1, namely

(*a*) The locus starts at the pole of $W(z)$ at $z = a$ and terminates at the zero at infinity.
(*b*) There is only one locus, since there is only pole of $W(z)$.
(*c*) There is one asymptote at 180°.
(*d*) Irrelevant.
(*e*) The locus includes the part of the real axis to the left of $z = a$.
(*f*) There is no point of departure from the real axis.

This is sufficient information to plot the locus [see Fig. 8(*b*)]. The value of gain is given by the modulus condition $|(1-a)KW(z)| = 1$ or $K = |(z-a)/(1-a)|$ when z is on the locus. The system is on the verge of instability when $z = -1$ or $K = (1+a)/(1-a)$. In this example, α is taken as 2·3 or $a = \varepsilon^{-2\cdot3} = 0\cdot1$, giving a maximum gain of 1·22.

From the root-locus diagram, a closed-loop pole is chosen which is expected to give the desired response, and the corresponding value of gain is evaluated. Let the pole be at $z = z_1$ and the gain be $K = K_1$. The step response of the system is given by eqn. (7): $G(z, m) = F(z)\,Y(z, m)$, where $F(z) = z/(z-1)$.

$$G(z, m) = \frac{z}{z-1}R(z, m)\frac{(1-a)K_1}{z-z_1}$$

$$= \frac{z}{z-1}\frac{(1-a^m)z - (a-a^m)}{(1-a)z}\frac{(1-a)K_1}{z-z_1}$$

$$= K_1\frac{(1-a^m)z - (a-a^m)}{(z-1)(z-z_1)}$$

This expression does not appear in Section 8.1 as it stands, but by splitting it into a sum the individual parts may be found; thus

$$G(z, m) = \frac{K_1}{1-z_1}\left[(1-a^m)\frac{(1-z_1)z}{(z-1)(z-z_1)} - (a-a^m)\frac{1-z_1}{(z-1)(z-z_1)}\right]$$

The first term appears directly; the second is of the same form, but delayed one sampling interval in time; thus

$$g(n, m) = \frac{K_1}{1-z_1}[(1-a^m)(1-z^n) - (a-a^m)(1-z^{n-1})]$$

$$= \frac{K_1}{1-z_1}\{(1-a) - [a^m(1-z_1) - (a-z_1)]z_1^{n-1}\}$$

Alternatively, $G(z, m)$ may be expanded into partial fractions and the inverse transforms found for the individual fractions which will yield the same result.

The response can be seen to depend on two time-constants; the open-loop time-constant $1/\alpha$ determines the inter-sample response, and the closed-loop time-constant $1/(\log z_1)$ determines the response at the sampling instants. This is fully to be expected, since the loop is effectively closed at the sampling instants only. The response for $K_1 = 0\cdot67$, $z_1 = -0\cdot5$, has been plotted in Fig. 9 ($a = 0\cdot1$).

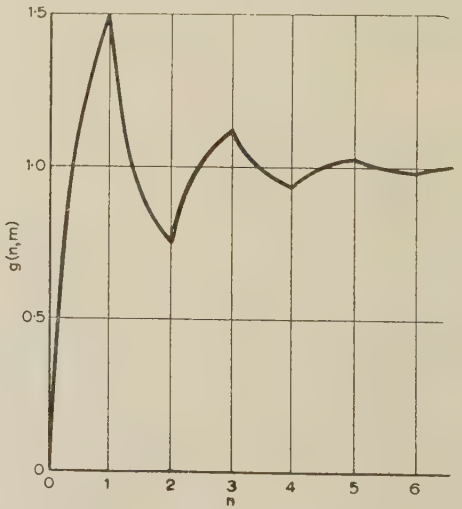

Fig. 9.—Step-function response of single-lag system. $K = 0\cdot67$.

(3.2) Double-Integrator System

The block diagram for a pure double-integrator system with clamp is shown in Fig. 10(*a*). Its open-loop transfer function is found in the same way as before, and is

$$W(z) = \frac{K}{2}\frac{z+1}{(z-1)^2}$$

$$R(z, m) = \frac{m^2z^2 + (1+2m-2m^2)z + (1-m)^2}{z(z+1)}$$

The numerator of $R(z, m)$ is in the form of a parabola in m, indicating that this is the form of the inter-sample response.

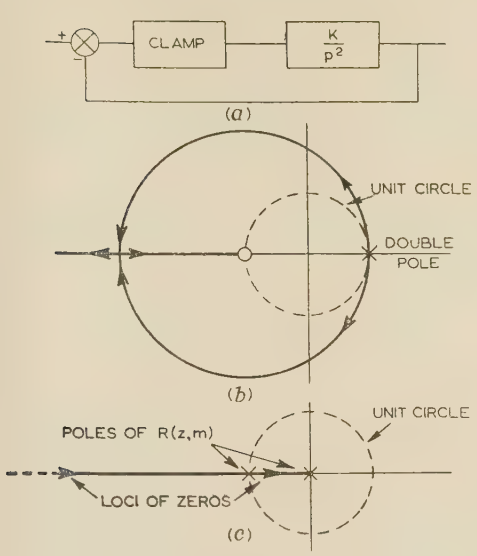

Fig. 10.—Double-integrator system.

(*a*) Block diagram.
(*b*) Root-locus diagram.
(*c*) $R(z, m)$ diagram.

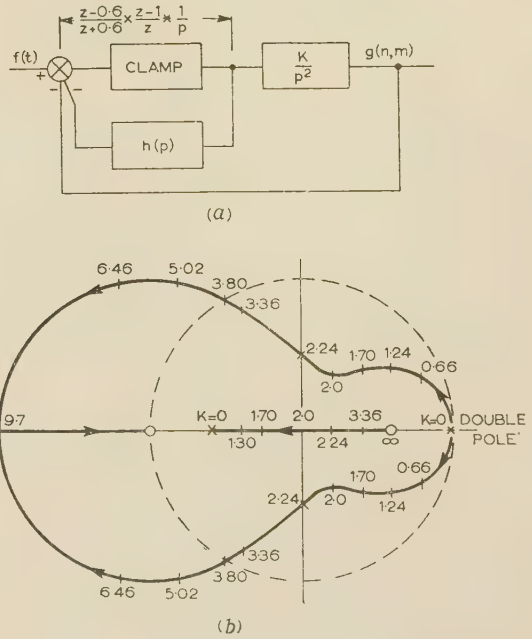

Fig. 11.—Stabilized double-integrator system.

(*a*) Block diagram.
(*b*) Root-locus diagram.

This could of course be predicted from physical considerations of the system. $R(z, m)$ has two zeros moving along the negative real axis, one from infinity to (-1) and the other from (-1) to the origin in each sampling interval. A diagram showing the poles of $R(z, m)$ and also the locus of its zeros is given in Fig. 10(*c*). In the z-domain, passage of time is represented by this movement of zeros coming from infinity and accumulating at the origin. For a complete representation of $R(z, m)$, the coefficient of z^2 in the numerator must be taken into account thus: $R(z, m) = m^2(z - z_1)(z - z_2)/z(z + 1)$.

The root-locus diagram corresponding to $W(z)$ is given in Fig. 10(*b*). It consists of a circle of radius 2 and with centre at $(-1 + j0)$ and the negative real axis $z \leqslant -1$. The circular locus is never inside the stability circle and neither is the locus on the real axis. The system is therefore unstable for all values of gain.

In order to stabilize the system the locus has to be distorted so that it is in the stable region for at least some values of gain. This can be done by adding a zero inside the locus on the positive real axis, its effect being to pull the locus towards it. The pole which has to be added, together with the zero, can be placed somewhere on the negative real axis in the stable region, resulting in a modifying function of the form $U(z) = (z - a)/(z - d)$. The new system is shown in Fig. 11(*a*) and the resulting root-locus in Fig. 11(*b*) for $a = +0{\cdot}6$ and $d = -0{\cdot}6$. The necessary filter $h(p)$ is given in Section 8.2.

The open-loop transfer function now becomes

$$W(z) = \frac{K}{2}\,\frac{(z-a)(z+1)}{(z-d)(z-1)^2}$$

$R(z, m)$ remains unchanged.

A graphical method will be used here to determine the system response to a step-function input. One of the advantages of this method, is that, once the response for one set of parameters has been calculated, the necessary parameter changes to obtain the required response can be estimated. This is because the relative importance of the different terms of the inversion is clear throughout the analysis.

The closed-loop transfer function of the system considered in this example will be of the form

$$Y(z,m) = \left[m^2\frac{(z-z_1)(z-z_2)}{z(z+1)}\right]\left[\frac{K}{2}\,\frac{(z-a)(z+1)}{(z-z_3)(z^2-2rz\cos\theta+r^2)}\right] \quad . \quad . \quad . \quad . \quad (18)$$

where the first term is $R(z, m)$ and the second corresponds to the root-locus.

The residue at a pole $z = z_0$ is obtained by measuring the magnitude and phase angle of the vector joining the point z_0 to each of the other poles and zeros in turn, and then substituting the values of these vectors in eqn. (18).

The complete pole-zero pattern required to find the response to a given forcing function is found by the superposition of three pole-zero patterns: (i) of $R(z, m)$; (ii) from the root-locus plot and (iii) of the forcing function. Such a pattern is given in Fig. 12; it represents the system for $K = 1{\cdot}7$ ($r = 0{\cdot}59$ and

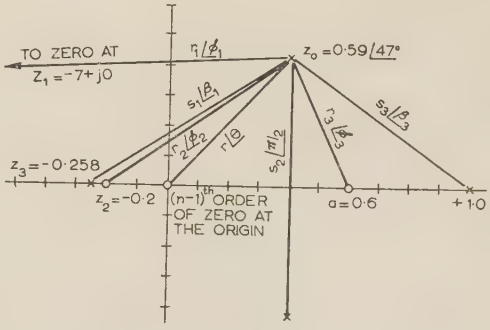

Fig. 12.—Pole-zero pattern for calculation of step-response.

$\theta = 47°$), $m = 0{\cdot}46$, and the input is a step-function, $F(z) = z/(z - 1)$. The order of the zero at the origin is $(n - 1)$, the third sampling interval has been chosen here for illustration The residue at the pole $z = z_0$ is

$$\frac{r_1 r_2 r_3 r^2}{s_1 s_2 s_3} \angle \phi_1 + \phi_2 + \phi_3 + 2\theta - \beta_1 - \pi/2 - \beta_3$$
$$= 1{\cdot}81 \angle -21^\circ$$

The residue at the other complex pole is, by symmetry, $1{\cdot}81 \angle +21^\circ$, and the effect of the conjugate pair of poles is therefore $1{\cdot}81 \times 2\cos 21^\circ = 3{\cdot}39$. The residues at the other poles are similarly found, and the value of the response at this point in time is the sum of the residues multiplied by the factor $Km^2/2$. The value is 1·60. The response for the same value of m in other sampling intervals may be found by altering the order of the zero at the origin, and for other values of m by calculating the new position of the zeros of $R(z, m)$. The complete response has been plotted in Fig. 13.

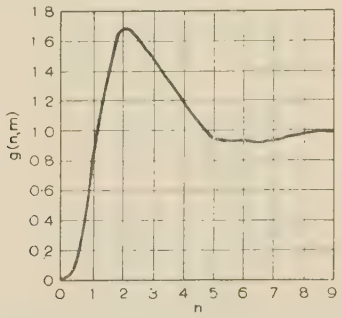

Fig. 13.—Step-response of stabilized double-integrator system.

(4) EXPERIMENT

A short description of an experiment verifying the results of Section 3.1, concerned with a single-lag system, is included here as an indication of a simple experimental technique for handling sampling systems.

The system was represented on a small electronic analogue computer, all elements being orthodox with the exception of the clamping device. This is in fact a time demodulator used for some radar work.[10] The circuit diagram of the clamp is given in Fig. 14; its operation is as follows. On the arrival of a

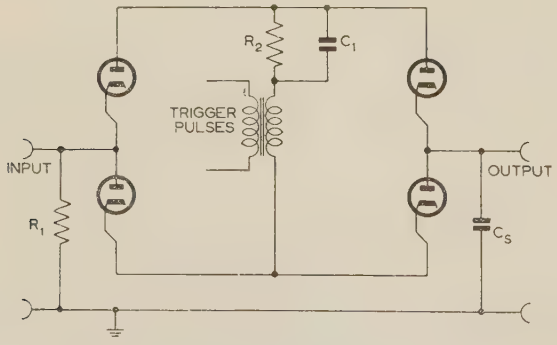

Fig. 14.—A simple clamp.
$R^1 = 470\,\Omega$
$R^2 = 470\,\Omega$
$C_1 = 0{\cdot}01\,\mu F$
$C_s = 0{\cdot}04\,\mu F$
Diodes = 6H6

trigger pulse, the four diodes are biased into the conducting region, connecting the storage capacitor C_s to the input and also charging the capacitor C_1. When the trigger pulse is removed, the charge on C_1 will bias the diodes beyond cut-off, thus isolating the storage capacitor. The clamp has to work into a very high resistance in order to avoid droop of the clamped voltage; in this case it was working into an open grid. With a 1 : 1 isolating transformer, and with no special precautions as to balancing of the circuit, the residuals of the trigger pulse appearing at the output terminals were of the order of 0·5 volt, while the signals were kept of the order of 35 volts. The trigger pulses were obtained from a monostable multivibrator via a cathode-follower stage, their amplitude being approximately 100 volts.

The system was connected as shown diagrammatically in Fig. 15. The gain was set by measuring the loop gain with the

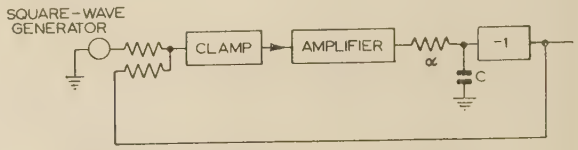

Fig. 15.—Analogue of a single-lag system.

capacitor C open-circuited, and the time-constant $1/\alpha$ by measuring the gain reduction when the capacitor C was inserted, all measurements being done at sampling frequency.

The measured reponse was in complete agreement with the response calculated in Section 3.1 and plotted in Fig. 9.

(5) CONCLUSION

The sequence-transform method applied to sampling systems is the logical analogy of the Laplace transform method used for continuous systems. It is therefore not surprising to find that the development of the two methods follows very similar lines. Since, however, a sampling system has two distinct modes of behaviour—one at the sampling instants and one between them—two variables are necessary to describe it completely. This increases somewhat the complexity of the algebra involved, but does not make the fundamental conception any more difficult. The variables chosen in the modified sequence-transform theory, z and m, are mutually independent and no substantial simplification can be expected by using any other pair of variables.

There seems to be no reason why further development should not lead to a sequence-transform theory just as useful and comprehensive as the Laplace transform theory. This involves finding suitable design criteria in the complex z-plane. One such criterion which has been suggested is the conformal representation in the z-plane of the line of constant damping coefficient in the p-plane. This transformation results in part of a logarithmic spiral, and, owing to the branch point at $p = 0$, a region of the z-plane corresponds to a multiple of regions in the p-plane, with the resulting ambiguity of interpretation. The criterion must therefore include some information as to system bandwidth to have any meaning, and since this is not always convenient a better criterion should be sought. One possibility would be a statistical design procedure. For continuous systems, this involves correlation functions. Since these are derived by time-shift considerations, and the operator z represents a time shift, the resulting sequence-transform expressions might be simpler than the corresponding Laplace transform expressions. This should be a rewarding field for further study.

(6) ACKNOWLEDGMENTS

The work described in the paper was carried out in the Electrical Engineering Department of the Imperial College of Science and Technology, and the authors wish to thank Professor A. Tustin for his encouragement and interest in the work. They are also indebted to Dr. P. F. Blackman for the loan of his complex-plane computer and much valuable advice. A grant

Table 1

TRANSFORM PAIRS

$y(p)$	$y(n)$	$Y(z)$	$R(z, m)$
1	$\delta(t)$	$\delta(t)$	$0;\ (m \neq 0)$
$\frac{1}{p}$	1	$\frac{z}{z-1}$	$\frac{1}{z}$
$\frac{1}{p^2}$	n	$\frac{z}{(z-1)^2}$	$\frac{1+(z-1)m}{z} = m\frac{z+(1-m)/m}{z}$
$\frac{1}{p^3}$	$\frac{n^2}{2}$	$\frac{z(z+1)}{2(z-1)^3}$	$\frac{m^2z^2+(1+2m-2m^2)z+(1-m)^2}{z(z+1)}$
$\frac{1}{p+\alpha}$	$a^n;\ a = \varepsilon^{-\alpha\tau}$	$\frac{z}{z-a}$	$\frac{a^m}{z}$
$\frac{\alpha}{p(p+\alpha)}$	$1-a^n$	$\frac{(1-a)z}{(z-1)(z-a)}$	$\frac{z(1 \quad a^m) \cdot (a-a^m)}{(1-a)z}$
$\frac{\beta}{(p+\alpha)^2+\beta^2}$	$a^n \sin(n\beta)$	$\frac{az\sin\beta}{z^2-2az\cos\beta+a^2}$	$a^m\frac{z\sin(m\beta)+a\sin(1-m)\beta}{az\sin\beta}$

Table 2

REALIZATION OF STABILIZING FUNCTION

$U(z)$	$h(p)$	
	$h_1(p)$	$h_2(p)$
$\frac{z-a}{z-d}$	$\frac{a-d}{1-a}\frac{\alpha}{p+\alpha}$	
$\frac{z+a}{z-d}$	$\frac{-(a+d)}{1+a}\frac{\alpha^2+\pi^2}{(p+\alpha)^2+\pi^2}$	
$\frac{(z-a)(z-b)}{(z-c)(z-d)}$	$\frac{(a-c)(a-d)}{(a-b)(1-a)}\frac{\alpha}{p+\alpha}$	$\frac{(c-b)(b-d)}{(a-b)(1-b)}\frac{\beta}{p+\beta}$
$\frac{(z-a)(z+b)}{(z-c)(z-d)}$	$\frac{(a-c)(a-d)}{(a+b)(1-a)}\frac{\alpha}{p+\alpha}$	$\frac{-(b+c)(b+d)}{(a+b)(1+b)}\frac{\beta^2+\pi^2}{(p+\beta)^2+\pi^2}$
$\frac{(z+a)(z+b)}{(z-c)(z-d)}$	$\frac{(a+c)(a+d)}{(b-a)(1+a)}\frac{\alpha^2+\pi^2}{(p+\alpha)^2+\pi^2}$	$\frac{(b+c)(b+d)}{(a-b)(1+b)}\frac{\beta^2+\pi^2}{(p+\beta)^2+\pi^2}$
$\frac{(z-a)(z-b)}{z^2-2dz\cos\phi+d^2}$	$\frac{a^2-2ad\cos\phi+d^2}{(a-b)(1-a)}\frac{\alpha}{p+\alpha}$	$\frac{b^2-2bd\cos\phi+d^2}{(b-a)(1-b)}\frac{\beta}{p+\beta}$
$\frac{(z-a)(z+b)}{z^2-2dz\cos\phi+d^2}$	$\frac{a^2-2ad\cos\phi+d^2}{(a+b)(1-a)}\frac{\alpha}{p+\alpha}$	$\frac{b^2+2bd\cos\phi+d^2}{-(a+b)(1+b)}\frac{\beta^2+\pi^2}{(p+\beta)^2+\pi^2}$
$\frac{(z+a)(z+b)}{z^2-2dz\cos\phi+d^2}$	$\frac{a^2+2ad\cos\phi+d^2}{(b-a)(1+a)}\frac{\alpha^2+\pi^2}{(p+\alpha)^2+\pi^2}$	$\frac{b^2+2bd\cos\phi+d^2}{(a-b)(1+b)}\frac{\beta^2+\pi^2}{(p+\beta)^2+\pi^2}$

from the Royal Norwegian Council for Industrial and Scientific Research to one of the authors (T. M. H. R.) is also gratefully acknowledged.

(7) REFERENCES

(1) MURPHY, G. J., and ORMSBY, R. D.: 'A Survey of Techniques for the Analysis of Sampled-Data Control Systems', *Transactions of the Institute of Radio Engineers*, PGAC—2, February, 1957.

(2) MACCOLL, L. A.: 'Fundamental Theory of Servomechanisms' (Van Nostrand, 1945), Chapter 10.

(3) HUREWICZ, W.: 'Filters and Servo Systems with Pulsed Data', Chapter 5 of M.I.T. Radiation Laboratory Series, **25** (McGraw-Hill, 1947).

(4) LAWDEN, D. F.: 'A General Theory of Sampling Servo Systems', *Proceedings I.E.E.*, Monograph No. 4, July, 1951 (**98**, Part IV, p. 31).

(5) BARKER, R. H.: 'The Pulse Transfer Function and its Application to Sampling Servo Systems', *ibid.*, Monograph No. 43, July, 1952 (**99**, Part IV, p. 302), and 'Addendum', *ibid.* (**102** C, p. 291).

(6) BOOTHROYD, A. R., and WESTCOTT, J. H.: 'Application of the Sequence Transform Analysis to the Design of Sampling Control Systems', Royal Aircraft Establishment Technical Note No. GW 405, 1956.

(7) EVANS, W. R.: 'Control-System Dynamics' (McGraw-Hill, 1954), Chapter 7.

(8) BOOTHROYD, A. R., CHERRY, E. C., and MAKAR, R.: 'An Electrolytic Tank for the Measurement of Steady-State Response, Transient Response and Allied Properties of Networks', *Proceedings I.E.E.*, Paper No. 835, May, 1949 (**96**, Part I, p. 163).

(9) JURY, E. I.: 'Correlation between Root-Locus and Transient Response of Sampled-Data Control Systems', *Transactions of the American I.E.E.*, 1956, **74**, Part II, p. 427.

(10) CHANCE, B.: 'Amplitude and Time Demodulation', Chapter 14 of M.I.T. Radiation Laboratory Series, **19** (McGraw-Hill, 1949), p. 519.

(8) APPENDICES

(8.1) Pulse Transform Pairs

A short list of Laplace transfer functions $y(p)$ of the system in Fig. 1, together with the corresponding pulse transfer functions $Y(z)$, is given in Table 1. The modified transfer functions $Y(z, m)$ are given in the form $R(z, m) = Y(z, m)/Y(z)$. The Table has been derived from the more complete list of transforms given by Barker.[5] The unit of time is taken as the sampling interval, $\tau = 1$.

(8.2) Realization of Stabilizer

By eqn. (17) and the Table of inverse transforms in Section 8.1, the (Laplace) transfer function of the filter $h(p)$ may be found for different functions $U(z)$. This has been done for some first- and second-order forms of $U(z)$ in Table 2. In this work, both $U(z)$ and $V(z)$ have been assumed stable, so that the poles and zeros of $U(z)$ must lie within the unit circle in the z-plane. Further, since $a = \varepsilon^{-\alpha\tau}$ and $b = \varepsilon^{-\beta\tau}$, both a and b must be positive. The restrictions on the constants are therefore

$$0 < a < 1;\ 0 < b < 1;\ -1 < c < +1;\ -1 < d < +1$$

The functions $h(p)$ of Table 2 may be realized by paralleling networks as shown in Fig. 16; the only two types of network

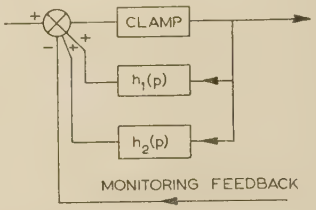

Fig. 16.—Realization of stabilizer.

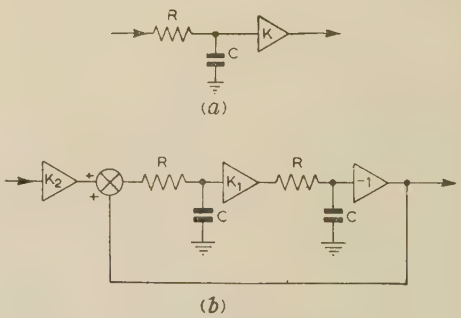

Fig. 17.—Circuits realizing $h(p)$.
$RC = 1/\alpha$; $K_1 = (\pi/\alpha)^2$; $K_2 = (1 + 1/K_1)K$.

needed to realize the functions are shown in Fig. 17. The (Laplace) transfer function of the network of Fig. 17(*a*) is

$$K\frac{\alpha}{p + \alpha} \quad . \quad . \quad . \quad . \quad . \quad . \quad (19)$$

and the transfer function of the network in Fig. 17(*b*) is

$$K\frac{\alpha^2 + \pi^2}{(p + \alpha)^2 + \pi^2} \quad . \quad . \quad . \quad . \quad . \quad (20)$$

if $K_1 = (\pi/\alpha)^2$ and $K_2 = \left(1 + \frac{1}{K_1}\right)K$.

The terms of $h(p)$ in Table 2 may readily be associated with the terms of eqns. (19) and (20), thus realizing the networks.

521.313.33

The Institution of Electrical Engineers
Monograph No. 304 U
May 1958
©

THE CIRCUIT THEORY AND CALCULATIONS OF POLYPHASE INDUCTION MACHINES

By N. KESAVAMURTHY, M.A., M.Sc.(Tech.), Graduate, and R. E. BEDFORD, B.Sc., Ph.D.

(*The paper was first received* 14*th May*, 1957, *and in revised form* 22*nd January*, 1958. *It was published as an* INSTITUTION MONOGRAPH *in May*, 1958.)

SUMMARY

The paper examines in a systematic manner the nature of the various circuits and circuit parameters of both wound-rotor and squirrel-cage induction machines. From these the basic voltage and torque equations are deduced. Substitute variables are then introduced to enable the equations to be made to depend on the speed rather than the position of the rotor, thus making the differential equations linear with constant coefficients for the important case of constant angular velocity of the rotor.

In order that the theory formulated may be of value in practice, methods of evaluation of the various circuit parameters from the physical dimensions of the machine are developed. For these the existing methods available for conventional design constants have had to be considerably modified. The circuit parameters are computed for an actual machine and compared against test results.

LIST OF PRINCIPAL SYMBOLS

The M.K.S. system of units is used. The values shown in square brackets in this and succeeding Sections refer to the experimental machine discussed in Section 11.

a, b, c = Subscripts representing phase windings, or circuits, of the stator.

$r1, r2 \ldots rS$ = Subscripts representing any of the S circuits, or phases, of the rotor.

re = Subscript representing the end-ring circuit of a squirrel-cage rotor.

$v_a, v_b, v_c, v_{r1} \ldots v_{rS}, v_{re}$ = Voltages applied to the circuits denoted by $a, b, c, r1 \ldots re$.

$v_{s\alpha}, v_{s\beta}, v_{so}$ = Substitute variables for stator voltages.

$v_{r\alpha}, v_{r\beta}, v_{ro}$ = Substitute variables for rotor voltages.

$i_a, i_b, i_c, i_{r1} \ldots i_{rS}, i_{re}$ = Currents in circuits denoted by $a, b, c, r1 \ldots rS, re$.

$i_{s\alpha}, i_{s\beta}, i_{so}$ = Substitute variables for stator currents.

$i_{r\alpha}, i_{r\beta}, i_{ro}$ = Substitute variables for rotor currents.

$\Phi_a, \Phi_b, \Phi_c, \Phi_{r1} \ldots \Phi_{rS}$ = Fluxes linking circuits denoted by $a, b, c, r1 \ldots rS$.

$\Phi_{r\alpha}, \Phi_{r\beta}, \Phi_{ro}$ = Substitute variables for rotor fluxes.

R_a, R_b, R_c = Resistances of stator windings.

$R_{r1r1} \ldots R_{rSrS}, R_{rere}$ = Resistances of rotor circuits denoted by $r1, r2 \ldots rS, re$.

R_{mn} = Resistance mutual to circuits m and n, where m and n range over all circuits $r1, r2 \ldots rS, re$.

R_{rre} = Mutual resistance between the end-ring circuit and any one of the S circuits $r1, r2 \ldots rS, re$.

$R_{r\alpha}, R_{r\beta}, R_{ro}$ = Substitute variables for rotor resistances.

L_{mn} = Mutual inductance between circuits m and n, where m and n range over all circuits $a, b, c, r1, r2, \ldots rS, re$.

L_{mm} = Self-inductance of circuit m.

L_{rs} = Component of mutual inductance between any one of the stator and any one of the rotor circuits.

L_{rre} = Mutual inductance between any one of the rotor circuits and the end-ring (re) circuit.

L_{sre} = Mutual inductance between any one of the stator circuits and the end-ring (re) circuit.

$L_{r\alpha}, L_{r\beta}, L_{ro}$ = Substitute variables for rotor inductances.

h_1 = Radius of rotor surface [0·081 75 m].

h_2 = Inner radius of stator surface [0·082 5 m].

S = Number of slots on the rotor [44].

T = Torque.

g = Gap length [0·75 mm].

l_e = Effective length of the stator or rotor, i.e. gross length corrected for ventilating ducts and end fringing [0·118 5 m].

p = Number of poles [4].

q_s = Number of slots per pole per phase on stator [3].

s = Fractional slip.

K_μ = Permeability factor.

k_{bns} = Breadth factor of the stator for the nth harmonic [$\sin 30n/3 \sin 10n$].

k_{pns} = Pitch factor of the stator for the nth harmonic [$\cos 20n$].

k_g = Carter's gap-extension coefficient [1·2].

τ = Pole pitch as measured on the stator surface.

θ = Angular displacement, in electrical degrees, from the a phase axis of the rotor circuit, $r1$.

ψ = Angle, in electrical degrees, between the axes of two adjacent rotor circuits.

ω = Angular frequency of the supply voltage to the stator.

μ_0 = Permeability of free space [$4\pi \times 10^{-7}$ H/m].

ϕ = Angle between the axes of the actuating phase and a coil.

(1) INTRODUCTION

Ever since its invention, the polyphase induction motor has been the subject of many investigations, notably with the aid of the revolving field concept and circle diagrams and equivalent circuits based on this concept. Treatment on these lines has proved extremely useful in visualizing and analysing steady-state performance of the machine. However, for the study of transient phenomena and other special problems this concept is inadequate. With a view to removing this inadequacy there has been a growing tendency to analyse the machine from the point of view of the theory of coupled circuits. The works of Kron,[1] Koenig[2] and Lyon[3] are concerned to a large extent with the development of such a circuit theory for various classes of machines. However, a detailed circuit theory of induction machines, particularly those with squirrel-cage rotors, does not appear to exist in the literature.

The paper examines in a systematic manner the nature of the various circuits and circuit parameters of both wound-rotor and

Correspondence on Monographs is invited for consideration with a view to publication.

Mr. Kesavamurthy and Dr. Bedford are in the Electrical Engineering Department, Indian Institute of Technology, Kharagpur.
Dr. Bedford is temporarily in the Electrical Engineering Department, University of Illinois, U.S.A., as Visiting Assistant Professor.

squirrel-cage induction machines, and obtains the basic voltage and torque equations for these types of machines. Substitute variables are introduced so that these equations can be made to depend on the speed rather than the position of the rotor, thereby enabling the differential equations to be linear with constant coefficients for the important case of constant angular velocity of the rotor. In order that the theory enunciated may be of value in practice, methods of evaluating the various circuit parameters from the physical dimensions of the machine are developed, taking into account the presence of slots, ducts, overhang and saturation. For these the existing methods have had to be considerably modified. The circuit parameters are computed for an actual machine from its dimensions and compared against test results.

(2) ELECTRICAL CIRCUITS OF THE MACHINE

The paper is confined to an induction machine having three phases on the stator. In the case of the wound rotor, the rotor is assumed to have S symmetrical phases wound for the same number of poles as the stator, whilst, for the squirrel cage, it is assumed that there are S equally spaced bars on the rotor.

The three phases a, b and c may be regarded as constituting the three stator circuits, and the currents in these are designated i_a, i_b, i_c respectively.

For a slip-ring induction motor the S phases $r1$, $r2$ . . . rS, constitute the S rotor circuits. The various rotor currents are designated i_{r1}, i_{r2} . . . i_{rS}.

For a squirrel-cage winding consisting of a single cage with S bars, the number of circuits necessary can be formulated from the following considerations. The number of branches in this winding is $3S$, whilst the number of independent nodes is $(2S - 1)$. Consequently, the number of independent loops is $(S + 1)$. For the purpose of formulating a circuit theory, therefore, a squirrel cage must be split up into $(S + 1)$ circuits. It is convenient to make these circuits as nearly similar to one another as possible because this will lead to symmetrical relationships for the inductance and resistance parameters. One suitable choice of rotor circuit is shown in Fig. 1, where the squirrel cage

Fig. 1.—Circuits of a squirrel-cage rotor.

is represented as a pancake arrangement. In this Figure the first rotor circuit consists of the cage bars 1 and $(k + 1)$, where k is any arbitrarily chosen integer, and the portions of the end-rings between these bars. In what follows, this rotor circuit is referred to as the $r1$ rotor circuit. In a similar manner the nth rotor circuit consists of the nth and the $(n + k)$th bars and the portion of the end-rings between them. Proceeding thus we obtain the S rotor circuits, $r1$, $r2$ . . . rS. The $(S + 1)$th rotor circuit may conveniently be chosen round any one of the two end-rings. This last circuit is referred to as the re circuit. The various rotor currents are correspondingly designated i_{r1}, i_{r2} . . . i_{rS} and i_{re}.

(3) FLUX LINKAGES WITH CIRCUITS

The net flux linking any circuit m may be written

$$\Phi_m = \sum_n L_{mn} i_n \qquad . . . . . \quad (1)$$

where n ranges over all the stator and rotor circuits, and L_{mn} is the mutual inductance between circuits m and n.

For a squirrel-cage machine the various flux-linkage relations are

For the stator

$$\left.\begin{aligned}
\Phi_a &= L_{aa}i_a + L_{ab}i_b + L_{ac}i_c + \sum_{n=1}^{S} L_{arn}i_{rn} + L_{are}i_{re} \\
\Phi_b &= L_{ba}i_a + L_{bb}i_b + L_{bc}i_c + \sum_{n=1}^{S} L_{brn}i_{rn} + L_{bre}i_{re} \\
\Phi_c &= L_{ca}i_a + L_{cb}i_b + L_{cc}i_c + \sum_{n=1}^{S} L_{crn}i_{rn} + L_{cre}i_{re}
\end{aligned}\right\}$$

For the rotor

$$\left.\begin{aligned}
\Phi_{r1} &= L_{r1a}i_a + L_{r1b}i_b + L_{r1c}i_c + \sum_{n=1}^{S} L_{r1rn}i_{rn} + L_{r1re}i_{re} \\
\Phi_{r2} &= L_{r2a}i_a + L_{r2b}i_b + L_{r2c}i_c + \sum_{n=1}^{S} L_{r2rn}i_{rn} + L_{r2re}i_{re} \\
&\quad . \qquad . \qquad . \qquad . \qquad . \\
\Phi_{rS} &= L_{rSa}i_a + L_{rSb}i_b + L_{rSc}i_c + \sum_{n=1}^{S} L_{rSrn}i_{rn} + L_{rSre}i_{re}
\end{aligned}\right\} \quad (2)$$

and

$$\left.\begin{aligned}
\Phi_{re} &= L_{rea}i_a + L_{reb}i_b + L_{rec}i_c + \sum_{n=1}^{S} L_{rern}i_{rn} + L_{rere}i_{re}
\end{aligned}\right\}$$

The flux-linkage relationships for a machine with a phase-wound rotor are identical with those given above, except for the fact that Φ_{re}, i_{re} and the inductance term associated with the re circuit do not exist.

(4) BASIC VOLTAGE EQUATIONS

In normal operation the voltages applied to the rotor circuits are zero both for the phase-wound and the squirrel-cage machines. For impressed voltages v_a, v_b and v_c on the stator phases of a three-phase machine the equations of voltages are

$$\left.\begin{aligned}
v_a &= \frac{d}{dt}\Phi_a + i_a R_a \\
v_b &= \frac{d}{dt}\Phi_b + i_b R_b \\
v_c &= \frac{d}{dt}\Phi_c + i_c R_c
\end{aligned}\right\} \qquad . . . . . \quad (3a)$$

where $R_a = R_b = R_c$ = the resistance of a stator phase.

The voltage equations for the rotor circuits are

$$\left.\begin{aligned}
v_{r1} &= \frac{d}{dt}\Phi_{r1} + i_{re}R_{r1re} + \sum_{n=1}^{S} R_{r1rn}i_{rn} \\
v_{r2} &= \frac{d}{dt}\Phi_{r2} + i_{re}R_{r2re} + \sum_{n=1}^{S} R_{r2rn}i_{rn} \\
&\quad . \qquad . \qquad . \qquad . \qquad . \\
v_{rS} &= \frac{d}{dt}\Phi_{rS} + i_{re}R_{rSre} + \sum_{n=1}^{S} R_{rSrn}i_{rn}
\end{aligned}\right\} \qquad . . \quad (3b)$$

and

$$\left.\begin{aligned}
v_{re} &= \frac{d}{dt}\Phi_{re} + i_{e}R_{re} + \sum_{n=1}^{S} R_{rnre}i_{re}
\end{aligned}\right\}$$

where R_{mn} is the resistance mutual to the circuits m and n. Of course, for the phase-wound rotor the last equation does not hold. Further, there is no mutual resistance between any two rotor circuits, and hence only the R_{mn} terms will figure in the above equations.

(5) BASIC TORQUE EQUATION

The net torque developed by the machine can be readily obtained from considerations of energy. In a motor, for example, the equation for torque becomes

$$T = \tfrac{1}{4} p \sum i_m \frac{\partial \Phi_m}{\partial \theta} \quad . \quad . \quad . \quad . \quad . \quad (4)$$

(6) NATURE OF CIRCUIT RESISTANCES AND INDUCTANCES

In a squirrel-cage rotor, as regards the stator there are only self-resistances, whilst as regards the rotor both self- and mutual-resistances exist. Because of the symmetry of the rotor circuits chosen, for the circuits $r1$, $r2$ . . . rS the following relationships are satisfied by the mutual-resistance terms

$$R_{rmrn} = R_{r(m+q)r(n+q)} \text{ and } R_{r1rq} = R_{r1r(S+2-q)} \quad . \quad (5)$$

where q is any integer. Also, the mutual resistance between the re circuit and any one of the S circuits $r1$, $r2$ . . . rS is the same for all circuits and is henceforth designated R_{rre}.

As regards inductances, it is apparent that if the angle between the axes of two adjacent rotor circuits is ψ electrical degrees, the mutual inductances between phase a on the stator and the various rotor circuits may be written

$$\left.\begin{aligned} L_{r1a} &= L_{rs}\cos\theta + \sum_{k=3,5,} L_{rks}\cos k\theta \\ L_{r2a} &= L_{rs}\cos(\theta+\psi) + \sum_{k=3,5,} L_{rks}\cos k(\theta+\psi) \\ L_{rSa} &= L_{rs}\cos[\theta+(S-1)\psi] + \sum_{k=3,5,} L_{rks}\cos k(\theta+(S-1)\psi) \end{aligned}\right\} \quad (6)$$

The mutual inductance between phases b and c and these rotor circuits is obtained by substituting $(\theta - 120°)$ and $(\theta + 120°)$ respectively for θ in the above equations. For the simplifying assumption of sinusoidally distributed phase windings $L_{rks} = 0$, $(k \neq 1)$. Clearly, also, the mutual inductance between the rotor circuit re and any one of the stator circuits is the same for all stator circuits, and hence

$$L_{are} = L_{bre} = L_{cre} = L_{sre} \text{ (say)} \quad . \quad . \quad . \quad (7)$$

Also, neglecting the influence of slots,

$$L_{aa} = L_{bb} = L_{cc} \quad . \quad . \quad . \quad . \quad . \quad (8)$$

whilst $$L_{ab} = L_{bc} = L_{ca} = L_{abo} = L_{sm}\cos(2\pi/3) \quad . \quad . \quad (9)$$

where $L_{ms}\cos(2\pi/3)$ is the component of mutual inductance due to the fundamental air-gap flux produced by a steady unit current through the actuating phase.

Similarly, for the rotor,

$$L_{r1r1} = L_{r2r2} = \ldots = L_{rSrS} \quad . \quad . \quad . \quad (10)$$

and, because of the symmetry of the circuits chosen,

$$L_{rmrn} = L_{r(m+q)(n+q)} \text{ and } L_{r1r(S+2)-q} = L_{r1rq} \quad . \quad (11)$$

where q is any integer. Also, the mutual inductance between any one of the $r1$, $r2$ . . . rS circuits and the re circuits is the same for all these circuits and may be taken as L_{rre}.

(7) TRANSFORMATION OF EQUATIONS TO A REFERENCE FRAME FIXED TO THE STATOR

In what follows we shall concern ourselves with the circuit theory of a squirrel-cage induction machine since this is more complex than for the wound-rotor type. The equations for a wound-rotor machine can always be obtained by neglecting the mutual-resistance terms and the quantities associated with the end-ring circuit.

(7.1) Flux-Linkage Relationships

Substituting the values of inductances as defined in Section 6 in eqns. (2) we have the flux-linkage relationships as functions of θ. Considerable simplification can be effected in the form of these equations by means of a transformation which eliminates θ.

Such a transformation consists in defining new fluxes $\Phi_{r\alpha}$, $\Phi_{r\beta}$ and Φ_{ro} as

$$\left.\begin{aligned} \Phi_{r\alpha} &= \Phi_{r1}\cos\theta + \Phi_{r2}\cos(\theta+\psi) + \Phi_{r3}\cos(\theta+2\psi) + \ldots \\ &\qquad + \Phi_{rS}\cos[\theta+(S-1)\psi] \\ \Phi_{r\beta} &= \Phi_{r1}\sin\theta + \Phi_{r2}\sin(\theta+\psi) + \Phi_{r3}\sin(\theta+2\psi) + \ldots \\ &\qquad + \Phi_{rS}\sin(\theta+(S-1)\psi] \\ \Phi_{ro} &= \Phi_{r1} + \Phi_{r2} + \Phi_{r3} + \ldots + \Phi_{rS} \end{aligned}\right\} \quad (12)$$

On carrying through this transformation and bearing in mind that $S\psi = 2p\pi$, it will be found that

$$\left.\begin{aligned} \Phi_{r\alpha} &= \tfrac{1}{2}Si_aL_{rs} + \tfrac{1}{2}Si_bL_{rs}\cos 120° \\ &\qquad + \tfrac{1}{2}Si_cL_{rs}\cos 240° + i_{r\alpha}L_{r\alpha} + i_{r\beta}L_{r\beta} \\ \Phi_{r\beta} &= \tfrac{1}{2}Si_bL_{rs}\sin 120° + \tfrac{1}{2}Si_cL_{rs}\sin 240° \\ &\qquad - i_{r\alpha}L_{r\beta} + i_{r\beta}L_{r\alpha} \\ \Phi_{ro} &= i_{ro}L_{ro} + Si_{re}L_{rre} \end{aligned}\right\} \quad (13)$$

where

$$\left.\begin{aligned} L_{r\alpha} &= L_{r1r1} + L_{r1r2}\cos\psi + \ldots + L_{r1rS}\cos(S-1)\psi \\ L_{r\beta} &= L_{r1r2}\sin\psi + L_{r1r3}\sin 2\psi + \ldots \\ &\qquad + L_{r1rS}\sin(S-1)\psi \\ L_{ro} &= L_{r1r1} + L_{r1r2} + L_{r1r3} + \ldots + L_{r1rS} \end{aligned}\right\} \quad (14)$$

and

$$\left.\begin{aligned} i_{r\alpha} &= i_{r1}\cos\theta + i_{r2}\cos(\theta+\psi) + \ldots \\ &\qquad + i_{rS}\cos[\theta+(S-1)\psi] \\ i_{r\beta} &= i_{r1}\sin\theta + i_{r2}\sin(\theta+\psi) + \ldots \\ &\qquad + i_{rS}\sin[\theta+(S-1)\psi] \\ i_{ro} &= i_{r1} + i_{r2} + i_{r3} + \ldots + i_{rS} \end{aligned}\right\} \quad (15)$$

Clearly $L_{r\beta} = 0$, since $L_{r1rq} = L_{r1r(S-q+2)}$ [see eqn. (11)] and $\sin q\psi = -\sin(S-q)\psi$.

(7.2) Voltage Equations

The rotor voltages can similarly be transformed by means of the substitute voltages $v_{r\alpha}$, $v_{r\beta}$, v_{ro} defined by

$$\left.\begin{aligned} v_{r\alpha} &= v_{r1}\cos\theta + v_{r2}\cos(\theta+\psi) + \ldots \\ &\qquad + v_{rS}\cos[\theta+(S-1)\psi] \\ v_{r\beta} &= v_{r1}\sin\theta + v_{r2}\sin(\theta+\psi) + \ldots \\ &\qquad + v_{rS}\sin[\theta+(S-1)\psi] \\ v_{ro} &= v_{r1} + v_{r2} + \ldots + v_{rS} \end{aligned}\right\} \quad (16)$$

On carrying out the necessary simplifications using eqn. (3) and bearing in mind the relationships between the various mutual resistances given in Section 6, it will be found that

$$\left.\begin{aligned} 0 = v_{r\alpha} &= \tfrac{1}{2}SL_{rs}\left[\frac{di_a}{dt} + \frac{di_b}{dt}\cos(2\pi/3) + \frac{di_c}{dt}\cos(4\pi/3)\right] \\ &\quad + L_{r\alpha}\frac{di_{r\alpha}}{dt} + L_{r\beta}\frac{di_{r\beta}}{dt} + R_{r\alpha}i_{r\alpha} + R_{r\beta}i_{r\beta} \\ &\quad + \left\{\tfrac{1}{2}SL_{rs}[i_b\sin(2\pi/3) + i_c\sin(4\pi/3)] \right. \\ &\qquad \left. + L_{r\alpha}i_{r\beta} - L_{r\beta}i_{r\alpha}\right\}\frac{d\theta}{dt} \\ 0 = v_{r\beta} &= \tfrac{1}{2}SL_{rs}\left[\frac{di_b}{dt}\sin(2\pi/3) + \frac{di_c}{dt}\sin(4\pi/3)\right] \\ &\quad + L_{r\alpha}\frac{di_{r\beta}}{dt} - L_{r\beta}\frac{di_{r\alpha}}{dt} + R_{r\alpha}i_{r\beta} + R_{r\beta}i_{r\alpha} \\ &\quad - \left\{\tfrac{1}{2}SL_{rs}[i_a + i_b\cos(2\pi/3) + i_c\cos(4\pi/3)] \right. \\ &\qquad \left. + L_{r\alpha}i_{r\alpha} + L_{r\beta}i_{r\beta}\right\}\frac{d\theta}{dt} \\ 0 = v_{ro} &= L_{ro}\frac{di_{ro}}{dt} + SL_{rre}\frac{di_{re}}{dt} + R_{ro}i_{ro} \end{aligned}\right\} \quad (17)$$

and

$$\left.\begin{aligned} 0 = v_{re} &= L_{sre}\frac{d}{dt}(i_a + i_b + i_c) \\ &\qquad + L_{rre}\frac{di_{ro}}{dt} + L_{rere}\frac{di_{re}}{dt} + R_{re}i_{re} \end{aligned}\right\}$$

where

$$\left.\begin{aligned} R_{r\alpha} &= R_{r1r1} + R_{r1r2}\cos\psi + \ldots + R_{r1rS}\cos(S-1)\psi \\ R_{r\beta} &= R_{r1r2}\sin\psi + R_{r1r3}\sin 2\psi + \ldots \\ &\qquad + R_{r1rS}\sin(S-1)\psi \\ R_{ro} &= R_{r1r1} + R_{r1r2} + \ldots + R_{r1rS} \end{aligned}\right\} \quad (18)$$

Clearly

$$R_{r\beta} = 0, \text{ since } R_{r1rq} = R_{r1r(S+2-q)} \text{ and } \sin q\psi = -\sin(S-q)\psi$$

By the use of substitute rotor currents $i_{r\alpha}$, $i_{r\beta}$, i_{ro} defined by eqn. (15) it will be found that the stator voltage equations also become functions of $d\theta/dt$ instead of θ. Their form, however, can be made still more elegant by defining new stator voltages $v_{s\alpha}$, $v_{s\beta}$, and v_{so} and new stator currents $i_{s\alpha}$, $i_{s\beta}$, i_{so} by means of the equations

$$\left.\begin{aligned} v_{s\alpha} &= v_a + v_b\cos(2\pi/3) + v_c\cos(4\pi/3) \\ v_{s\beta} &= v_b\sin(2\pi/3) + v_c\sin(4\pi/3) \\ v_{so} &= v_a + v_b + v_c \end{aligned}\right\} \quad . \quad . \quad (19)$$

and

$$\left.\begin{aligned} i_{s\alpha} &= i_a + i_b\cos(2\pi/3) + i_c\cos(4\pi/3) \\ i_{s\beta} &= i_b\sin(2\pi/3) + i_c\sin(4\pi/3) \\ i_{so} &= i_a + i_b + i_c \end{aligned}\right\} \quad . \quad . \quad (20)$$

On carrying through these substitutions in the equations for stator and rotor voltages and simplifying, the following equations are obtained:

$$\left.\begin{aligned} v_{s\alpha} &= R_a i_{s\alpha} + (L_{aa} - L_{ab})\frac{di_{s\alpha}}{dt} + \frac{3}{2}L_{rs}\frac{di_{r\alpha}}{dt} \\ v_{s\beta} &= R_a i_{s\beta} + (L_{aa} - L_{ab})\frac{di_{s\beta}}{dt} + \frac{3}{2}L_{rs}\frac{di_{r\beta}}{dt} \\ v_{so} &= R_a i_{so} + (L_{aa} + 2L_{ab})\frac{di_{so}}{dt} + \frac{3}{2}L_{sre}\frac{di_{re}}{dt} \\ v_{r\alpha} &= \frac{1}{2}SL_{rs}\frac{di_{s\alpha}}{dt} + \frac{1}{2}SL_{rs}i_{s\beta}\frac{d\theta}{dt} \\ &\qquad + R_{r\alpha}i_{r\alpha} + L_{r\alpha}\frac{di_{r\alpha}}{dt} + L_{r\alpha}i_{r\beta}\frac{d\theta}{dt} \\ v_{r\beta} &= -\tfrac{1}{2}SL_{rs}i_{s\alpha}\frac{d\theta}{dt} + \frac{1}{2}SL_{rs}\frac{di_{s\beta}}{dt} \\ &\qquad - L_{r\alpha}i_{r\alpha}\frac{d\theta}{dt} + R_{r\alpha}i_{r\beta} + L_{r\alpha}\frac{di_{r\beta}}{dt} \\ v_{ro} &= R_{ro}i_{ro} + L_{ro}\frac{di_{ro}}{dt} + SL_{rre}\frac{di_{re}}{dt} \\ v_{re} &= L_{sre}\frac{di_{so}}{dt} + L_{rre}\frac{di_{ro}}{dt} + R_{rere}i_{re} + L_{rere}\frac{di_{re}}{dt} \end{aligned}\right\} \quad (21)$$

since, for a symmetrical machine, $L_{r\beta} = 0$. These equations constitute the basic voltage equations of the induction machine with squirrel-cage rotor.

(7.3) Physical Interpretation of the Voltage Equations for a Symmetrical Machine

From eqns. (13), (19), (20) and (21), when simplified and reduced, it is seen that for a symmetrical machine

$$\left.\begin{aligned} v_{s\alpha} &= R_a i_{s\alpha} + \left(L_{aa} - L_{ab} - \frac{3SL_{rs}^2}{4L_{r\alpha}}\right)\frac{di_{s\alpha}}{dt} + \left(\frac{3L_{rs}}{2L_{r\alpha}}\right)\frac{d\Phi_{r\alpha}}{dt} \\ v_{s\beta} &= R_a i_{s\beta} + \left(L_{aa} - L_{ab} - \frac{3SL_{rs}^2}{4L_{r\alpha}}\right)\frac{di_{s\beta}}{dt} + \left(\frac{3L_{rs}}{2L_{r\alpha}}\right)\frac{d\Phi_{r\beta}}{dt} \\ v_{r\alpha} &= \frac{d\Phi_{r\alpha}}{dt} + \Phi_{r\beta}\frac{d\theta}{dt} + R_{r\alpha}I_{r\alpha}; \\ v_{r\beta} &= \frac{d\Phi_{r\beta}}{dt} - \Phi_{r\alpha}\frac{d\theta}{dt} + R_{r\beta}i_{r\beta} \end{aligned}\right\} \quad (22)$$

From these equations it may be concluded that the machine may be replaced by a pair of coils along each of the α- and β-axes (which are in quadrature) and acted upon by the direct- and quadrature-axis fluxes $\Phi_{r\alpha}$, $\Phi_{r\beta}$ respectively.

(7.4) Torque Equations

From eqn. (4) the torque equation in terms of these substitute variables can be readily obtained. With the necessary simplification the expression for torque reduces to

$$T = \tfrac{1}{4}pL_{rs}(i_{s\beta}i_{r\alpha} - i_{s\alpha}i_{r\beta}) \quad . \quad . \quad . \quad . \quad . \quad (23)$$

In order that this circuit theory may be of practical use it is essential that methods should be available for computing from the dimensions of the machine the various circuit parameters that occur in these equations. Whilst there is a considerable amount of literature dealing with the evaluation of conventional design constants from machine dimensions, none exists wherein

methods of evaluating circuit parameters of the type discussed are presented. However, in what follows, many methods used for evaluating conventional design constants are here adopted for determining the circuit constants.

(8) EVALUATION OF SELF- AND MUTUAL INDUCTANCES OF STATOR PHASES

Both kinds of inductance associated with the stator phases may be regarded as due to air-gap fluxes, slot fluxes and overhang fluxes.

(8.1) Component of Inductance due to Air-Gap Fluxes

To compute this component it is necessary to determine the field distribution produced in the air-gap when a unit current is sent through any one stator phase. Obviously, this field distribution will be profoundly influenced by the presence of slots and ducts and also by saturation in the iron. In order to simplify the problem we shall initially ignore the presence of slots and also the ampere-turns expended on the iron paths. On this basis it is now possible to associate a scalar magneto-static potential (s.m.p.) with the stator and rotor surfaces as discussed in Section 14.1. This results in a radial flux density at the stator surface given by B_{h2} [eqns. (39) and (40)]. When the actuating winding carries unit current, the flux linking N turns, having k_{bns} and k_{pns} as the winding factors for the nth harmonic, is given by

$$\frac{\mu_0 2 l_e N^2}{\pi p}\int_{\lambda-\frac{1}{2}\pi}^{\lambda+\frac{1}{2}\pi} h_2 B_{h2} d\theta = \frac{\mu_0^2 N^2 l_e}{\pi}\sum_{n=1,3}^{\infty}\frac{k_{bns}^2 k_{pns}^2}{n}\left(\frac{h_2^{np}+h_1^{np}}{h_2^{np}-h_1^{np}}\right)\cos n\lambda$$

where λ is the angle between the axes of the actuating phase and the coil in question. Hence, the self-inductance due to air-gap fluxes ($\lambda = 0$) is

$$L_{aa(\text{air-gap})} = \frac{\mu_0 4 N^2 l_e h_2}{\pi g p}\sum_{n=1,3}^{\infty}\left(\frac{k_{bns}^2 k_{pns}^2}{n^2}\right)[=0{\cdot}2239\,\text{H}] \quad (24)$$

since, in practice, the air-gap length $g \ll h_1$. In a similar manner the mutual inductance between phases a and b in a machine is given by

$$L_{ab(\text{air-gap})} = \frac{\mu_0 4 N^2 l_e h_2}{\pi p g}\sum_{n=1,3}^{\infty}\frac{k_{bns}^2 k_{pns}^2}{n^2}\cos n\lambda \quad . \quad (25)$$

$$[= -0{\cdot}1069H \text{ for } \lambda = 2\pi/3]$$

(8.1.1) Correction for Slots and Finite Permeability.

In order to allow for the presence of slots the gap length may be regarded as being $k_g g$. Despite this correction the inductance values are bound to be too high because of the assumption that the iron is of infinite permeability. The s.m.p. difference actually operating across the air-gap at any point on the stator surface is only a part of that calculated on the basis of infinite permeability. It is clear that this ratio will vary from point to point along the surface because of the variation in flux densities. A strict allowance for this effect is therefore out of the question, and recourse must be had to approximate methods. In what follows a 'permeability factor' K_μ defined by the expression $K_\mu \times$ (inductance computed on basis of infinite permeability) = (actual inductance), is used. This factor may therefore be regarded as averaging out the effects of saturation. In the case of balanced 3-phase supplies, to compute for K_μ determine (*a*) the flux per pole, (*b*) the areas and lengths of the magnetic circuit, taking the length of path in the core as 2/3 of the pole pitch, (*c*) the flux density in each path at 60 electrical degrees from zero point, and (*d*) the ampere-turns for each path at 60°. The ratio of gap ampere-turns to the total ampere-turns is then reckoned as the saturation factor.

(8.2) Component of Inductance due to Slot Fluxes

Assuming that the flux passes straight across the slot, the self-inductance per slot for a slot shown in Fig. 2 and carrying current in the same direction in both layers[4] is

$$L'_{aa(\text{slot flux})} = \frac{\mu_0 n_s^2 l_e}{4}\left[\frac{4d_5}{w_1}+\frac{8d_4}{(w_1+w_2)}+\frac{4d_3+d_2}{w_2}+\frac{4(d_1-d_2)}{3w_2}\right]$$
$$[=294{\cdot}5\times10^{-7}\,\text{H}]$$

where n_s = Number of conductors per slot [38].

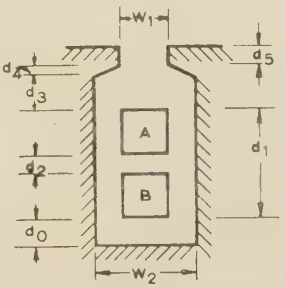

Fig. 2.—Stator slot dimensions.
$w_1 = 0{\cdot}3175$ cm. $d_2 = 0{\cdot}0508$ cm.
$w_2 = 1{\cdot}113$ cm. $d_3 = 0{\cdot}381$ cm.
$d_0 = 0{\cdot}0508$ cm. $d_4 = 0{\cdot}3175$ cm.
$d_1 = 1{\cdot}956$ cm. $d_5 = 0$.

Similarly, the self-inductance per slot for the bottom layer alone carrying current is

$$L''_{aa(\text{slot flux})} = \frac{\mu_0 n_s^2 l_e}{4}\left[\frac{d_5}{w_1}+\frac{2d_4}{(w_1+w_2)}+\frac{2(d_1-d_2)+3d_3}{3w_2}\right]$$
$$[=1037\times10^{-7}\,\text{H}]$$

Also the self-inductance per slot for the top layer alone carrying current is

$$L'''_{aa(\text{slot flux})} = \frac{\mu_0 n_s^2 l_e}{4}\left[\frac{d_5}{w_1}+\frac{2d_4}{(w_1+w_2)}+\frac{d_3}{w_2}+\frac{(d_1-d_2)}{6w_2}\right]$$
$$[=576{\cdot}5\times10^{-7}\,\text{H}]$$

Thus,

$$L_{aa(\text{slot flux})} = L'_{aa}\delta_1 + L''_{aa}\delta_2 + L'''_{aa}\delta_3\ [=0{\cdot}00247\,\text{H}]$$

where δ_1, δ_2, and δ_3, denote the number of slots pertaining to the respective cases.

Proceeding in a similar manner, the mutual inductance per slot in top and bottom layers is

$$L'_{aa(\text{slot flux})} = -\frac{\mu_0 n_s l_e}{4}\left[\frac{(d_1-d_2)}{4w_2}+\frac{d_3}{w_2}+\frac{2d_4}{(w_1+w_2)}+\frac{d_5}{w_1}\right]$$
$$[=6{\cdot}53\times10^{-5}\,\text{H}]$$

Hence

$$L_{ab(\text{slot flux})} = \delta_4 L'_{ab(\text{slot flux})}[=-5{\cdot}23\times10^{-4}\,\text{H}] \quad (26)$$

where δ_4 denotes the number of slots to be considered [8].

(8.3) Component of Inductance due to Overhang Fluxes

A rigorous analytical computation for various types of end-winding configurations is practically impossible. In what follows we shall attempt to deduce expressions for the self- and mutual inductances due to overhang fluxes for machines with diamond windings using the formula deduced by Alger.[4]

Alger's analysis is for balanced 3-phase operation and is based on a resolution of the overhang currents into an axial system and a peripheral system of currents. The expression given for the end-leakage reactance due to axial currents is

$$X_{ea} = \frac{789 \times 10^{-8} m f D_1 N^2 k_{b1s}^2 \tan\alpha}{p^2}\left(\frac{\nu\pi - \sin\nu\pi}{\pi}\right) \quad [=0{\cdot}5489 \text{ ohm}] \quad (27)$$

where m = Number of stator phases [3].
ν = Ratio of coil span to pole pitch [7/9].
D_1 = Mean diameter of the overhang [0·222 m].
f = Supply frequency [50 c/s].

$$\sin\alpha = \frac{w + c}{w + t}[=17/22].$$

where w = Slot width [0·011 1 m].
t = Tooth width [0·006 4 m].
c = Coil end clearance [0·002 4 m].

The end-leakage reactance due to peripheral currents is similarly given thus

$$X_{pe} = \frac{319{\cdot}7 \times 10^{-8} m f N^2 k_{p1s}^2 k_{b1s}^2}{p^2}[D_1 \log(4D_1/r_1) - 1{\cdot}75D_1] \quad [=0{\cdot}7017 \text{ ohm}] \quad (28)$$

where r = Half depth of stator slot, [0·012 7 m].

The net reactance in a 3-phase machine is the sum of X_{ea} and X_{pe}, and the effective inductance per phase is obtained by dividing this reactance by $2\pi f$. For computing the self-inductance due to overhang fluxes we multiply the effective inductance by 2/3, whilst the mutual inductance is taken as $-1/3$ of the effective inductance. This type of division is adopted because it is the ratio in which the inductances due to the fundamental component of air-gap fluxes divide themselves. Thus,

$$L_{aa\,(\text{overhang})} = \frac{1}{2\pi f}\frac{2}{3}(X_{ea} + X_{pe}), \quad [=2{\cdot}66 \times 10^{-3} \text{ H}]$$

and

$$L_{ab\,(\text{overhang})} = -(1/6\pi f)(X_{ea} + X_{pe}), \quad [=-1{\cdot}34 \times 10^{-3} \text{ H}]$$

Summarizing, the total self- and mutual inductances of the stator phase are respectively given by

$$L_{aa} = \frac{K_\mu}{k_g}L_{aa\,(\text{air-gap})} + L_{aa\,(\text{slot flux})} + L_{aa\,(\text{overhang})} \quad (29)$$

$$[=0{\cdot}1788 \text{ H for } K_\mu = 0{\cdot}93,\ k_g = 1{\cdot}2]$$

and

$$L_{ab} = \frac{K_\mu}{k_g}L_{ab\,(\text{air-gap})} + L_{ab\,(\text{slot flux})} + L_{ab\,(\text{overhang})} \quad (30)$$

$$[=0{\cdot}0847 \text{ for } K_\mu = 0{\cdot}93,\ k_g = 1{\cdot}2]$$

(9) EVALUATION OF SELF- AND MUTUAL INDUCTANCES OF ROTOR CIRCUITS

Here also the computation of the inductances depends on air-gap fluxes, slot fluxes and overhang fluxes.

(9.1) Component of Inductance due to Air-Gap Fluxes

In the case of squirrel-cage rotors, to compute the inductances between the $r1$ and any other circuit, say the rn, we proceed as before by initially neglecting this influence of slots and saturation, and defining a s.m.p. along the stator and rotor surfaces as shown in Section 14.2. The flux linkage per ampere with the rn circuit (comprised of cage bars n and $n + k$ and the portion of the end-rings) is then, from eqn. (40),

$$\frac{\mu_0 k l_e}{S}\int_{[2(n-1)/S]-(k/S)}^{[2(n-1)/S]+(k/S)} B_{h1}h_1 d\theta = \sum_{m=1,2,3} L'_{mr}\cos(n-1)\frac{2m\pi}{S}$$

where

$$L'_{mr} = \mu_0 l_e \frac{h_2^{2m} + h_1^{2m}}{(h_2^{2m} - h_1^{2m})}\left(\frac{4}{m\pi}\right)\sin^2\frac{mk\pi}{S} = \frac{\mu_0 4 h_1 l_e}{m^2 g\pi}\sin^2\left(\frac{mk\pi}{S}\right) \quad . \quad . \quad . \quad . \quad (31)$$

Thus the component of inductance due to air-gap fluxes between the $r1$ and rn circuits is $L'_{mr}\cos[(n-1)2m\pi/S]$. These values have to be corrected using the factors K_μ and k_g, as in the other cases. Furthermore, the effects of skew have to be taken into account. It is shown in Section 14.3 that each harmonic component of any inductance between $r1$, $r2$ . . . rn circuits is multiplied by the square of the skew factor k_{rsm}^2 for that harmonic, whilst any inductance between the stator circuit and one of $r1$, $r2$ . . . rn circuits is multiplied by k_{rsm}, where $k_{rsm} = \sin(mx/p)/(x/p)$ and x/p = angle of skew [10° or 0·174 5 rad]. Thus the component of inductance due to air-gap fluxes between the $r1$ and rn circuits is

$$L_{r1rn\,(\text{air-gap})} = \frac{K_\mu}{k_g}\sum_{m=1,2,3} L_{mr}\cos\frac{\pi(n-1)2m}{S}$$

where $L_{mr} = L'_{mr}k_{rsm}^2$ (32)

$$[L_{1r} = 7{\cdot}2 \text{ H}; L_{2r} = 3{\cdot}5 \text{ H}; L_{3r} = 0{\cdot}74 \text{ H}; L_{4r} = 0; L_{5r} = 0{\cdot}224 \text{ H}; L_{6r} = 0{\cdot}28 \text{ H}]$$

(9.2) Component of Inductance due to Slot Fluxes

In the case of bars of circular section, assuming the flux to pass straight across the slot, the inductance is known to be

$$L_{bs} = 0{\cdot}623\mu_0 l_e \ [=1 \times 10^{-7}\text{H}]$$

As regards mutual inductance, clearly all circuits, other than $r(k+1)$ and $r(S+1-k)$ circuits, have no mutual inductances due to slot fluxes, whilst these circuits have a mutual inductance with the $r1$ circuit equal to the inductance of one slot.

(9.3) Component of Inductance due to End-Ring of a Squirrel-Cage Rotor

Note that the rotor end may be taken to be a flux line. On this basis, using the method of magnetic images applicable to iron of infinite permeability, the field linkages when a unit current is sent through the end-rings are equal to those produced with one ring. When two equal coaxial rings are spaced apart by a distance equal to twice that by which an end-ring overhangs the rotor, both rings carry equal currents in opposite directions. The inductance of one end-ring is then clearly the self-inductance of one such ring minus the mutual inductance between the two rings. The Rayleigh–Niven formula for the self-inductance of a single-turn coil of circular cross-section of diameter D [$= 15{\cdot}1 \times 10^{-2}$m] and radius of cross-section r [$= 0{\cdot}8 \times 10^{-2}$m] is

$$L = 2\pi D\left[\left(1 + \frac{r^2}{2D^2}\right)\log\frac{4D}{r} + \frac{r^2}{6D^2} - 1{\cdot}75\right] \times 10^{-7}, \quad [=2{\cdot}43 \times 10^{-7}\text{H}]$$

whilst the Maxwell formula for the mutual inductance between two similar coaxial coils is

$$M = 2\pi D\left[\left(1 + \frac{3d^2}{4D^2}\right)\log\frac{2D}{d} - \left(2 + \frac{d^2}{D^2}\right)\right] \times 10^{-7}, \quad [=1{\cdot}573 \times 10^{-7}\text{H}]$$

where d is the projection of the end-ring over the iron $[0{\cdot}813 \times 10^{-2}\text{m}]$. The self-inductance of the end-ring is therefore $L - M$. It must be noted that r is the effective radius of the section of the end-ring and may be taken as $\sqrt{(a/\pi)}$, where a is the area of section. The quantity L_{eo} appearing in the computation is taken as the inductance associated with a portion of the end-ring between two adjacent bars. Taking both rings into account, the approximate equation is

$$L_{eo} = 2(L - M)/S, \quad [= 3{\cdot}884 \times 10^{-9}\text{H}] \quad . \quad . \quad (33)$$

Summarizing,

$$\left.\begin{aligned}
L_{r1r1} &= 2L_{bs} + kL_{eo} + \frac{K_\mu}{k_g}\sum_{m=1,2}^{\infty} L_{mr}, \qquad [= (K_\mu 101{\cdot}2 + 2{\cdot}42) \times 10^{-7}] \\
L_{r1r2} &= 0 + (k-1)L_{eo} + \frac{K_\mu}{k_g}\sum_{m=1,2}^{\infty} L_{mr}\cos\frac{2m\psi}{p} \\
L_{r1r3} &= 0 + (k-2)L_{eo} + \frac{K_\mu}{k_g}\sum_{m=1,2}^{\infty} L_{mr}\cos\frac{2\cdot 2m\psi}{p} \\
&\ldots\ldots\ldots\ldots \\
L_{r1rk} &= 0 + L_{eo} + \frac{K_\mu}{k_g}\sum_{m=1,2}^{\infty} L_{mr}\cos\frac{(k-1)2m\psi}{p} \\
&\ldots\ldots\ldots\ldots \\
L_{r1r(k+1)} &= -L_{bs} + 0 + \frac{K_\mu}{k_g}\sum_{m=1,2}^{\infty} L_{mr}\cos\frac{k2m\psi}{p} \\
L_{r1r(k+2)} &= 0 + 0 + \frac{K_\mu}{k_g}\sum_{m=1,2}^{\infty} L_{mr}\cos(k-1)\frac{2m\psi}{p} \\
&\ldots\ldots\ldots\ldots \\
L_{r1r(S-k+1)} &= -L_{bs} + 0 + \frac{K_\mu}{k_g}\sum_{m=1,2}^{\infty} L_{mr}\cos\frac{(S-k)2m\psi}{p} \\
L_{r1r(S-k+2)} &= 0 + L_{eo} + \frac{K_\mu}{k_g}\sum_{m=1,2}^{\infty} L_{mr}\cos\frac{(S-k+1)2m\psi}{p} \\
L_{r1r(S-1)} &= 0 + (k-2)L_{eo} + \frac{K_\mu}{k_g}\sum_{m=1,2}^{\infty} L_{mr}\cos\frac{(S-S+2)2m\psi}{p} \\
L_{r1rS} &= 0 + (k-1)L_{eo} + \frac{K_\mu}{k_g}\sum_{m=1,2}^{\infty} L_{mr}\cos\frac{(S-S+1)2m\psi}{p}
\end{aligned}\right\} \quad (34)$$

(9.4) The Inductance, $L_{r\alpha}$

In actual computation, the value that sufficiently represents the rotor inductances in a symmetrical machine is the quantity $L_{r\alpha}$, given by

$$L_{r\alpha} = L_{r1r1} + L_{r1r2}\cos\psi + \ldots + L_{r1rS}\cos(S-1)\psi$$

From eqn. (34) it is clear that the part of $L_{r\alpha}$ due to slot fluxes alone is

$$L_{r\alpha\,(\text{slot fluxes})} = 2L_{bs}(1 - \cos k\psi)$$

since $S\psi = p\pi$, p being an even number.

Also, the part of $L_{r\alpha}$ due to overhang fluxes is

$$\begin{aligned}
L_{r\alpha\,(\text{overhang})} &= kL_{eo} + 2L_{eo}[(k-1)\cos\psi + (k-2)\cos 2\psi + \ldots \\
&\qquad + (k-k+1)\cos\psi] \\
&= \frac{(1-\cos k\psi)}{(1-\cos\psi)}L_{eo}
\end{aligned}$$

Next, to compute the part of $L_{r\alpha}$ due to air-gap fluxes alone, we consider separately the cases when S is odd and even.

(*a*) *For S odd.*—Here the part of $L_{r\alpha}$ due to air-gap fluxes is

$$\frac{K_\mu}{k_g}\left[\sum_{m=1,2}^{\infty} L_{mr} + 2\sum_{n=1,2}^{\frac{1}{2}(S-1)}\left(\sum_{m=1,2}^{\infty} L_{mr}\cos\frac{2mn\psi}{p}\cos n\psi\right)\right] = \frac{K_\mu}{k_g}\left[\sum_{\substack{m=(qS-\frac{1}{2}p)\\ q=1,2}} \tfrac{1}{2}SL_{mr} + \sum_{\substack{m=qS+\frac{1}{2}p\\ q=0,1,2}} \tfrac{1}{2}SL_{mr}\right]$$

Substituting for L_{mr} we find that the above expression simplifies to

$$L_{r\alpha\,(\text{air-gap})} = \frac{K_\mu}{k_g}(1 - \cos k\psi)SL_{rro}$$

where $L_{rro} = \dfrac{1}{\pi}(l_e h_1/g)\left[\dfrac{k^2_{rs(S-\frac{1}{2}p)}}{(S-\frac{1}{2}p)^2} + \dfrac{k^2_{rs(2S-\frac{1}{2}p)}}{(2S-\frac{1}{2}p)^2} + \dfrac{k^2_{rs(\frac{1}{2}p)}}{(\frac{1}{2}p)^2} + \ldots + \dfrac{k^2_{rs(S-\frac{1}{2}p)}}{(S+\frac{1}{2}p)^2} + \dfrac{k^2_{rs(2S+\frac{1}{2}p)}}{(2S+\frac{1}{2}p)^2}\right]$

$[= 0{\cdot}1039 \times 10^{-5}\text{H}]$

(*b*) *For S even.*

It can be shown that for this case

$$L_{r\alpha\,(\text{air-gap})} = \frac{K_\mu}{k_g}(1 - \cos k\psi)(S+2)L_{rro}$$

Thus

$$\begin{aligned}
L_{r\alpha} &= L_{r\alpha\,(\text{air-gap})} + L_{r\alpha\,(\text{slot flux})} + L_{r\alpha\,(\text{overhang})} \\
&= (1 - \cos k\psi)\left[\frac{K_\mu}{k_g}(S+2)L_{rro} + 2L_{bs} + \frac{L_{eo}}{1-\cos\psi}\right], \ S \text{ even} \quad . \quad . \quad . \quad . \quad (35) \\
&= (1 - \cos k\psi)\left[\frac{K_\mu}{k_g}SL_{rro} + 2L_{bs} + \frac{L_{eo}}{1-\cos\psi}\right], \ S \text{ odd} \quad (36)
\end{aligned}$$

$[= (K_\mu 953{\cdot}1 + 2{\cdot}95) \times 10^{-7}\text{H}]$

(9.5) The Inductance $L_{r\beta}$

As shown in Section 7.1 for a symmetrical machine, $L_{r\beta} = 0$.

(10) MUTUAL INDUCTANCE BETWEEN CIRCUITS ON THE STATOR AND CIRCUITS ON THE ROTOR

(10.1) Inductance due to Air-Gap Fluxes

To compute the mutual inductance between a stator phase and any one of the rotor circuits $r1$, $r2 \ldots rS$, we note that a current through phase a results in a scalar potential distribution throughout the air-gap, and the radial flux density, B'_{h1}, at the rotor surface ($r = h_1$) is given in Section 14.1. A full-pitched coil on the rotor with its axis making an angle α electrical degrees has flux linkages given by

$$\frac{\mu_0 h_1 l_e}{p}\int_{(-\pi+2\alpha)/p}^{(\pi+2\alpha)/p} B'_{h1}\,d\theta = \frac{2\mu_0 h_1 l_e}{p}\sum_{n=1,3}^{\infty}(-1)^{1/2(n-1)}4a_{ns}\frac{h_1^{1/2np}h^{1/2np}}{h_2^{np} - h_1^{np}}\cos n\alpha$$

Hence, for a distributed winding having N_r turns per phase on the rotor, with pitch and distribution factor for the nth harmonic given by $k_{bnr}k_{pnr}$, the mutual flux linkages are

$$\mu_0 N_r k_{bnr}k_{pnr}\left(\frac{2h_1 l_e}{p}\right)\sum_{n=1,3}^{\infty}(-1)^{1/2(n-1)}\frac{4a_{ns}(h_1h_2)^{1/2np}}{h_2^{np} - h_1^{np}}\cos n\alpha$$

where a_{ns} is computed for a current of 1 amp through the stator phase.

For the case of squirrel-cage rotors, the flux linkage per unit current with a circuit α electrical degrees away from the rotor is

$$L_{ar1} = \frac{2h_1 l_e}{p} \int_{(-k\psi+2\alpha)/p}^{(k\psi+2\alpha)/p} B'_{h1} h_1 d\theta$$

$$= K_\mu l_e \frac{\mu_0 8N}{k_g g p^2} \sum_{q=1,3}^{\infty} \left[\left(\frac{2h_1 + pg}{q^2} \right) k_{bqs} k_{pqs} k'_{rsq} \sin \tfrac{1}{2} qk \right] \cos q\theta$$

$$= \sum_{q=1,3}^{\infty} \frac{K_\mu}{k_g} L_{mq} \cos q\theta, \text{ say.}$$

$$[= K_\mu (0{\cdot}8968 \times 10^{-3} \cos\theta - 0{\cdot}03215 \times 10^{-4} \cos 3\theta)\,\text{H}] \quad . \quad . \quad . \quad . \quad (37)$$

where $k'_{rsq} = k_{rsm}$ for $m = \frac{1}{2}qp$ and is the skew factor for the rotor bar (see Section 14.3). The above expression is corrected for permeability and air-gap extension.

(10.2) Component of Inductance due to Overhung Fluxes

Following Alger, the mutual reactance due to axial currents may be taken, for the case of balanced polyphase supplies, as $-\left(\frac{0{\cdot}8D_2}{D_1}\right)^{1/2p} \times$ (Self-reactance due to axial current in the stator), whilst the mutual reactance due to peripheral currents is

$$\frac{D \log_\varepsilon \frac{4D}{R} - 2D}{D_1 \log_\varepsilon \frac{4D_1}{r_1} - 1{\cdot}75D_1} \times \begin{pmatrix} \text{Self-reactance per phase} \\ \text{due to axial currents} \end{pmatrix} \quad (38)$$

The mutual inductance between stator and rotor during balanced operation due to axial and peripheral currents may be obtained from the above expression on dividing by $2\pi f$. It is suggested that these inductances multiplied by $(2/3)(2/S)$ may be regarded as the maximum value of the mutual inductance between the stator and rotor circuits, the inductance being assumed to vary as a sinusoidal function of the rotor position.

In the above expressions

$$D = (D_1 D_2)^{1/2}$$

where D_1 is the mean diameter of the stator overhang, and D_2 that of the rotor overhang.

$$R = [\tfrac{1}{4}(D_1 - D_2)^2 + (Y_1 - Y_2)^2]^{1/2}$$

where $Y_1 = \frac{\nu\pi D_1}{4p}\left(1 + \frac{\nu^2}{5}\right) \tan\alpha$

and $Y_2 = \frac{\nu_r \pi D_2}{4p}\left(1 + \frac{\nu_r^2}{5}\right) \tan\alpha_r$

ν, ν_r, α, α_r, being as defined in Section 8.3.

In the case of a squirrel-cage rotor it is also necessary to compute the mutual inductance between the stator overhang and the rotor end-ring. As shown by Alger, this may be taken as two-thirds of the mutual inductance between stator and rotor circuits due to peripheral and axial currents.

(11) APPLICATION OF THE THEORY AND ITS EXPERIMENTAL VERIFICATION

The circuit constants mentioned above were estimated for an experimental squirrel-cage induction motor having the following specification:

440 volts, 14 h.p., 4 pole, 3-phase, 50 c/s delta connected, 3 slots/pole/phase, double-layer winding with 38 conductors per slot and chorded by 2 slots. The dimensions of parts of the machine and the computed values have been given in brackets in the preceding Sections (see List of Principal Symbols).

The permeability factor, K_μ, was estimated for various voltages as outlined in Section 8.1.1; the values are

Voltage	50–250 V	320 V	440 V
K_μ	0·93	0·83	0·67

Several of the estimated inductances were compared with values obtained experimentally. At first the cage was removed and replaced by a few circuits wound on the rotor. The stator self- and mutual inductances were obtained in the usual manner. The mutual inductance between a stator phase and a rotor circuit was computed for various positions of the rotor and a curve of inductance as a function of position was plotted. The fundamental component of the curve is taken to represent $L_{ar1} \cos\theta$. Next, to determine the inductance between rotor circuits, a known current was passed through the $r1$ circuit and the voltages induced in others were measured. This voltage divided by the product of the number of turns in each of the circuits in question gives the reactance operation for a single turn in each. To measure the self-inductance of a rotor circuit it was found advisable to wind an additional coil following the actuating coil.

Table 1 shows a comparison between the experimental and computed values. The computation of the short-circuit and no-load currents is based on eqn. (21). It is claimed that the agreement is within about 4%.

Table 1

COMPARISON OF CALCULATED AND EXPERIMENTAL VALUES FOR THE CIRCUIT PARAMETERS

	Calculated	Experimental
L_{aa}, henry	0·1788 ($K_\mu = 0{\cdot}93$)	0·184
L_{ab}, henry	0·0847 ($K_\mu = 0{\cdot}93$)	0·0875
L_{ar1}, henry	$0{\cdot}834 \times 10^{-3}$ ($K_\mu = 0{\cdot}93$)	$0{\cdot}853 \times 10^{-3}$
L_{r1r1}, henry	$1{\cdot}456 \times 10^{-5}$	$1{\cdot}57 \times 10^{-5}$
X_m, ohms	83·93 ($K_\mu = 0{\cdot}93$)	86
I_{sc}, amperes	67 ($K_\mu = 0{\cdot}67$)	71
I_0, amperes	7·0 ($K_\mu = 0{\cdot}93$)	7·3
Z_{sc}, ohms	$2{\cdot}95 + j7{\cdot}26$ ($K_\mu = 0{\cdot}67$)	

(12) ACKNOWLEDGMENTS

The authors are grateful to the Director of the Indian Institute of Technology, Kharagpur (India), for granting facilities for the work described in the paper.

(13) REFERENCES

(1) KRON, G.: 'Equivalent Circuit of Electrical Machines' (John Wiley and Sons, Inc., 1951).

(2) KOENIG, H. E.: 'Application of Network Theory to the Analysis of Rotating Machinery—Part I', *Transactions of the American I.E.E.*, 1954, **73**, Part I, p. 162.

(3) LYON, W. V.: 'Transient Analysis of Alternating Current Machinery' (John Wiley and Sons, Inc., 1954).
(4) ALGER, P. L.: 'The Nature of Polyphase Induction Motors' (John Wiley and Sons, Inc., 1951).

(14) APPENDICES

(14.1) Field Distribution in the Air-Gap due to a Current through a Distributed Winding on either the Stator or the Rotor

For a pole pitch τ, the s.m.p. distribution due to a single full-pitched coil can be expressed in the Fourier form as

$$G_x = \sum_{n=1,3} (-1)^{1/2(n-1)} \frac{2i}{n\pi} \cos\left(\frac{\pi n x}{\tau}\right)$$

For a double-layer winding, in general, by superposition

$$G_x = \sum_{n=1,3} (-1)^{1/2(n-1)} \frac{4i}{n} k_{bn} k_{pn} \cos(\pi n x/2\tau)$$

Thus the s.m.p. on the stator surface ($r = h_2$) is of the form

$$G_{h2} = \sum_{n=1,3} a_{ns} \cos(np\theta/2)$$

whilst, by symmetry, the potential of the rotor surface may be treated as zero. The scalar potential at any point (r, θ) in the air-gap must satisfy the Laplace equation in the polar form. The solution for this field is found to be

$$G_{r,\theta} = \sum \frac{h_2^{1/2np} a_{ns}}{h_2^{np} - h_1^{np}} (r^{1/2np} - h_1^{np} r^{-1/2np}) \cos \tfrac{1}{2} np\theta \quad \ldots \quad (39)$$

The radial flux density at any point (r, θ) is given by

$$B_r = -\mu_0 \frac{\partial G_{r,\theta}}{\partial r} \quad \ldots \quad (40)$$

whence $B_{h2} = (B_r)_{r=h_2}$ and $B_{h1} = (B_r)_{r=h_1}$

In the case of a current through a distributed winding on the rotor, the s.m.p. can be defined for the rotor surface in a similar manner and the flux density can be computed. On this basis the flux densities at the rotor and stator surfaces are given by

$$\left.\begin{aligned} B'_{h1} &= \mu_0 \sum \tfrac{1}{2} np \frac{a_{nr}}{h_2^{np} - h_1^{np}} (h_2^{np} h_1^{-1} + h_1^{np-1}) \cos \frac{np\theta}{2} \\ \text{and} \quad B'_{h2} &= \mu_0 \sum \frac{npa_{nr}}{h_2^{np} - h_1^{np}} [h_1^{1/2np} h_2^{1/2(np-1)}] \cos \frac{np\theta}{2} \end{aligned}\right\} \quad (41)$$

(14.2) Field Distribution in the Air-Gap of a Cylindrical-Rotor Machine due to a Single-Turn Winding on the Rotor

For computing self- and mutual inductances between rotor circuits and between rotor and stator circuits it becomes necessary to find the field distribution when a current is sent through a circuit such as the $r1$. By arguments similar to that used earlier, a zero s.m.p. being assigned to the stator surface, the rotor surface can be regarded as having a potential distribution similar to that shown in Fig. 3, where θ' is measured in mechanical degrees and the coil sides are at PP', the origin being taken at the centre of the coil. The coil spans an angle equal to k rotor-slot pitches, namely $2k\pi/S$.

This potential distribution, in the Fourier form, becomes

$$= \sum_{n=1,2,3} a_{mr} \cos m\theta'$$

where $a_{mr} = (2i_{r1}/\pi m) \sin(mk\pi/S)$, since $S\psi = p\pi$

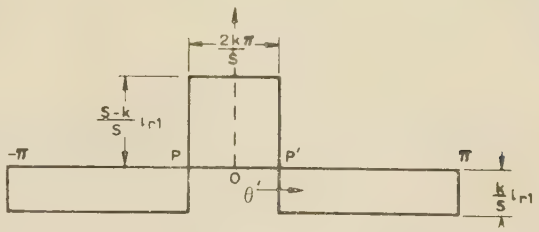

Fig. 3.—Scalar-magnetostatic-potential distribution due to a current in the $r1$ circuit of the rotor.

Solving the Laplace equation for the air-gap,

$$G_{r,\theta} = \sum_{m=1,2} \frac{h_1^m a_{mr}}{(h_2^{2m} - h_1^{2m})} (h_2^{2m} r^{-m} - r^m) \cos m\theta'$$

At the rotor surface the flux density is given by

$$B_{h1} = \sum_{m=1} \frac{ma_{mr}\mu_0}{(h_2^{2m} - h_1^{2m})} [(h_2^{2m} h_1^{-1} + h_1^{(2m-1)}] \cos m\theta' \quad (42)$$

(14.3) Influence of Skew on the Inductances

Consider a squirrel-cage rotor with bars skewed through an angle of x electrical degrees. The average flux density along a line parallel to the axis on the rotor surface may then be deduced from the following considerations. Let this line make an angle θ' with the axis of the $r1$ circuit, the term 'axis' meaning a straight line on the rotor surface parallel to the axis of the shaft and passing through the mid-point of the circuit. Then the flux density along this line due to a circuit with unskewed bars having its axis at an angle θ mechanical degrees away is

$$B_{h1} = \mu_0 \sum_{m=1,2}^{\infty} \frac{ma_{mr}}{(h_2^{2m} - h_1^{2m})} [h_2^{2m} h_1^{-1} + h_1^{(2m-1)}] \cos m(\theta' - \theta)$$

The average flux density along this line due to the skewed coil may be regarded as the average flux density due to a uniformly distributed winding each side of which extends over x electrical degrees. This average flux density at θ' is

$$\frac{p\mu_0}{2} \int_{-x/p}^{x/p} B_{h1} d\theta = \sum_{m=1,2}^{\infty} \frac{ma_{mr}\mu_0}{(h_2^{2m} - h_1^{2m})} [h_2^{2m} h_1^{-1} + h_1^{(2m-1)}] k_{rsm} \cos m\theta'$$

where $k_{rsm} = \sin(mx/p)/(mx/p)$, the skew factor for the mth harmonic.

The flux linkage with the rn circuit, assuming it to consist of parallel sides, is the integral of the above over the range $\frac{2(n-1)\pi + k\pi}{S}$ and $\frac{2(n-1)\pi - k\pi}{S}$. This yields

$$\mu_0 \sum_{m=1,2} \frac{4(h_2^{2m} + h_1^{2m}) k_{rsm}}{(h_2^{2m} - h_1^{2m}) m\pi} \cos \frac{2m(n-1)\pi}{S} \sin^2\left(\frac{mk\pi}{S}\right)$$
$$= \sum A_{mr} \cos \frac{\pi 2m(n-1)}{S}, \text{ (say)}$$

The flux linkage with a circuit, per metre length of rotor, with conductors parallel to the rotor axis, and at an angle θ away from the above is

$$\sum_{m=1,2}^{\infty} A_{mr} \cos m\left[\frac{2(n-1)\pi}{S} + \theta\right]$$

Thus the flux linkage with the skewed circuit, which may be

regarded as equivalent to a single turn with each side distributed over a geometrical angle of $(2x/p)$ is

$$\frac{p}{2x}\int_{-x/p}^{x/p}\sum_{m=1,2}^{\infty} A_{mr}\cos m\left[\frac{2(n-1)\pi}{S}+\theta\right]d\theta = \sum_{m=1,2}^{\infty} L_{mr}\cos\frac{2m(n-1)\pi}{S} \quad (43)$$

where $L_{mr} = \frac{2k_{rsm}^2 h_1}{m^2\pi g}\left(1 - \cos\frac{2mk\psi}{p}\right)$, on simplification.

By arguments similar to the above it is clear that the average gap flux-density distribution of the qth harmonic linking with a stator phase is now merely multiplied by the skew factor for the qth harmonic, yielding eqn. (37) for the inductance between stator and rotor circuits.

621.376.3:621.372

The Institution of Electrical Engineers
Monograph No. 305 R
May 1958
©

THE RESPONSE OF A NETWORK TO A FREQUENCY-MODULATED INPUT VOLTAGE

By J. W. HEAD, M.A., and C. G. MAYO, M.A., B.Sc., Member.

(*The paper was first received 5th November*, 1957, *and in revised form 5th January*, 1958. *It was published as an* INSTITUTION MONOGRAPH *in May*, 1958.)

SUMMARY

If a voltage $v(t)$ is applied to a network of admittance* Y, the resultant current $I(t)$ can be obtained by three different methods:

(*a*) By symbolic calculus, in which an image or transform V of $v(t)$ is found and $I(t)$ is determined by applying the inverse transform to the product VY: this leads to difficulties in the f.m. case because V cannot be conveniently formulated.

(*b*) By the convolution integral derived from $v(t)$ and the response $y(t)$ of the admittance Y to unit impulse. Well-known formulae are here derived by this method, together with an additional formula applicable to a typical amplifier-discriminator system in which the distortion imposed by the admittance is separated from mere delay.

(*c*) By operational calculus, in which the admittance Y is regarded as an operator, a function of d/dt, and the input voltage $v(t)$ is the operand. The same formulae are here derived more simply by operational calculus.

(1) INTRODUCTION

If a voltage $v(t)$ is applied to an admittance Y, the formal solution in terms of symbolic calculus (or the Fourier integral) amounts in essence to finding first the image (or the spectrum) of $v(t)$. For a f.m. signal, however, this image (or spectrum) consists of a very complicated series of sidebands involving Bessel-function coefficients. The analysis does not yield a simple approximation like the 'quasistationary' solution derived by van der Pol,[1] and will not be discussed further.

An alternative approach, discussed in Section 2, is to determine the response $y(t)$ of the admittance Y to unit-impulse input. The resulting current $I(t)$ is then the convolution integral of $v(t)$ and $y(t)$. This approach leads easily to the quasistationary solution already mentioned. The weakness of this solution is that it does not in itself distinguish distortion from mere delay; a way of allowing for the delay content of the admittance Y is proposed in Section 3, and applied to a typical amplifier and discriminator.

A third possible method of attack is to regard Y as an operator, a function of d/dt, and $v(t)$ as the operand. Operational calculus, as opposed to symbolic calculus, is somewhat out of fashion at present, and the writers believe that this eclipse is not justified.[2] It is used here, in Section 4, to derive all the results obtained in Sections 2 and 3 more simply. Questions of convergence are best considered in terms of operational calculus, and are briefly discussed.

(2) FORMULATING THE PROBLEM: EVALUATING THE RESPONSE IN TERMS OF THAT OF THE NETWORK TO UNIT STEP

We shall take the input signal to be

$$v_1(t) = \varepsilon^{j\omega_0 t}F(t) = \varepsilon^{j\omega_0 t + j\mu\int g(\tau)d\tau} = \varepsilon^{j\omega_0 t + js(t)} \quad . \quad (1)$$

where the carrier frequency $\omega_0/2\pi$ will be taken as 10·7 Mc/s in numerical calculations while the maximum frequency deviation $\mu/2\pi$ will be taken as 75 kc/s, so that $\sigma\,(=\mu/\omega_0)$ is a small quantity of order 0·007. In eqn. (1) $|g(t)| \leqslant 1$; $g(t)$ depends upon the programme being transmitted, and we may therefore have available only statistical data. We do know, however, that the programme is unlikely to contain any appreciable components at frequencies higher than 10 kc/s. This means that the maximum numerical value of $g'(t)$ is small compared to μ; the maximum numerical value of $g''(t)$ is small compared to μ^2, and so on.

Now suppose that the response of the network of admittance Y to unit-impulse input is $y(t)$; we shall consider later the form of Y likely to occur in practice. The current $I(t)$ in the network when any signal $v(t)$ is applied is given by

$$I(t) = \int_0^t v(t-\lambda)y(\lambda)d\lambda \quad . \quad . \quad . \quad . \quad . \quad (2)$$

The convolution integral, eqn. (2), can be derived from elementary considerations in the time world alone which do not require the use of symbolic or operational calculus. We are not interested in the transients caused by starting the signal $v(t)$ at zero time; we prefer to consider $v(t)$ as a stationary time series. As the impedance Y necessarily has a dissipative character, any transients due to switching on the signal will have disappeared if t is regarded as sufficiently large. The simplest way to allow for this is to replace the upper limit of integration in eqn. (2) by ∞, and to ignore any finite change in the lower limit. Thus the modified version of eqn. (2), to allow for the fact that we consider $v(t)$ as a stationary time series and are not interested in transients associated with a particular time of switching-on, is

$$I(t) = \int_0^\infty v(t-\lambda)y(\lambda)d\lambda \quad . \quad . \quad . \quad . \quad (3)$$

We regard eqn. (3) as our basic starting-point, from which all the results we require will be derived.

A general formula can be obtained by expanding $v(t-\lambda)$ as a Taylor series in powers of λ. We shall assume that the series is convergent. Conditions of convergence are clearer in the operational form of solution discussed later. Substitution of the Taylor series in eqn. (3) gives

$$I(t) = \int_0^\infty \sum_{r=0}^{\infty} \frac{1}{r!}y(\lambda)(-\lambda)^r\frac{d^r v(t)}{dt^r}d\lambda \quad . \quad . \quad . \quad (4)$$

We also assume that we can reverse the order of the limiting processes in eqn. (4), and that we can integrate term by term, so that

$$I(t) = \sum_{r=0}^{\infty} \frac{1}{r!}\frac{d^r v(t)}{dt^r}\int_0^\infty y(\lambda)(-\lambda)^r d\lambda \quad . \quad . \quad . \quad (5)$$

Now consider the integral

$$Y_r(p) = \int_0^\infty \varepsilon^{-p\lambda}y(\lambda)(-\lambda)^r d\lambda \quad . \quad . \quad . \quad . \quad (6)$$

* Admittance may be generalized to transfer function.

Correspondence on Monographs is invited for consideration with a view to publication.
Mr. Head and Mr. Mayo are with the British Broadcasting Corporation.

which is somewhat more general than that associated with a typical term of the summation eqn. (5), but reduces to the integral involved in eqn. (5) if p is zero; in eqn. (6) p is any number independent of λ. We already know that Y can if we wish be expressed as a function of p in the form

$$Y = \int_0^\infty y(\lambda)\varepsilon^{-p\lambda}d\lambda \quad . \quad . \quad . \quad . \quad . \quad (7)$$

since $y(t)$ is the response of the admittance Y to unit impulse. If we now differentiate eqn. (7) with respect to p, the only term involving p on the right-hand side of eqn. (7) is $\varepsilon^{-p\lambda}$, so that the differentiation under the integral sign merely introduces an extra factor $(-\lambda)$; the limits are independent of p. Thus

$$\frac{dY}{dp} = \int_0^\infty y(\lambda)(-\lambda)\varepsilon^{-p\lambda}d\lambda \quad . \quad . \quad . \quad . \quad (8)$$

and repeating this process gives

$$\frac{d^rY}{dp^r} = \int_0^\infty y(\lambda)(-\lambda)^r\varepsilon^{-p\lambda}d\lambda \quad . \quad . \quad . \quad . \quad (9)$$

so that, substituting back in eqn. (5) and letting p tend to zero, we have

$$I(t) = \sum_{r=0}^{\infty} \frac{1}{r!}\left[\frac{d^rY}{dp^r}\right]_{p=0} \frac{d^rv(t)}{dt^r} \quad . \quad . \quad . \quad (10)$$

Eqn. (10) is a perfectly general result, whatever the nature of the input voltage $v(t)$ and the network admittance Y. We have in effect only assumed that we knew the formula giving the impedance of a network in terms of its response to unit impulse and vice versa. This does not require us to speculate on the precise meaning and significance of p, except in so far as questions of convergence are concerned. It is, however, easier to postpone consideration of convergence until we consider the operational method of attack in Section 3.

If we suppose that

$$v(t) = \varepsilon^{jkt}w(t) \quad . \quad . \quad . \quad . \quad . \quad . \quad (11)$$

$I(t)$ in eqn. (3) becomes

$$I(t) = \varepsilon^{jkt}\int_0^\infty \varepsilon^{-jk\lambda}w(t-\lambda)y(\lambda)d\lambda \quad . \quad . \quad . \quad (12)$$

If $w(t)$ is now expanded in a Taylor series instead of $v(t)$, we can reduce eqn. (12) with the aid of eqn. (9) to

$$I(t) = \varepsilon^{jkt}\sum_{r=0}^{\infty}\frac{1}{r!}\left[\frac{d^rY(p)}{dp^r}\right]_{p=jk}\frac{d^rw(t)}{dt^r} \quad . \quad . \quad (13)$$

Eqn. (13) is a well-known result, given, for example, by van der Pol[1] [his eqn. (34)]. It is applicable to all types of modulation.

For the particular case of frequency modulation, where $v(t)$ is $v_1(t)$ given by eqn. (1), it is convenient in eqn. (12) to take

$$k = \omega_0 \quad w(t) = \varepsilon^{js(t)} \quad . \quad . \quad . \quad . \quad (14)$$

Alternatively, we can in this case expand $s(t-\lambda)$ by Taylor's theorem instead of $w(t-\lambda)$. This gives

$$I(t) = \varepsilon^{j\omega t}\int_0^\infty \varepsilon^{-j\omega_0\lambda}y(\lambda)d\lambda\varepsilon^{js(t)-j\lambda s'(t)+\frac{1}{2}j\lambda^2s''(t)-\ldots}$$

$$= \varepsilon^{j\omega_0t+js(t)}\int_0^\infty \varepsilon^{-j\lambda[\omega_0+s'(t)]}y(\lambda)d\lambda\varepsilon^{\frac{1}{2}j\lambda^2s''(t)+\cdots} \quad . \quad (15)$$

If in eqn. (15) we replace the last exponential by unity, we obtain the quasistationary approximation

$$I(t) = Y(p)\varepsilon^{j\omega_0t+js(t)} \quad . \quad . \quad . \quad . \quad . \quad (16)$$

where p is replaced by $j[\omega_0 + s'(t)]$, that is, $p/2\pi j$ is the 'instantaneous frequency'. This result was also obtained by van der Pol. The first terms neglected by the quasistationary approximation are those in which the last exponential factor of eqn. (15) is replaced by

$$\tfrac{1}{2}j\lambda^2s''(t) + \tfrac{1}{6}j\lambda^3s'''(t) \quad . \quad . \quad . \quad . \quad . \quad (17)$$

and, when the terms in eqn. (17) are allowed for in eqn. (15), eqn. (16) becomes

$$I(t) = [Y(p) + \tfrac{1}{2}jY''(p)s''(t) + \tfrac{1}{6}jY'''(p)s'''(t) + \ldots]\varepsilon^{j\omega_0t+js(t)} \quad (18)$$

where p is replaced by $j[\omega_0 + s'(t)]$ after differentiation. Now $I(t)$ in eqn. (18) differs from a constant multiple of $v_1(t)$ but the difference is not necessarily all distortion. If, for example, $I(t)$ was a constant multiple of $v(t-\tau)$, where τ was constant, the response $I(t)$ would be merely delayed by a time τ. This is not distortion. Further examination of eqn. (18) is necessary to separate the distortion from the delay, and this involves analysis of $Y(p)$. For the type of admittance likely to occur in practice, however, it appears to be advantageous to replace the quasistationary solution by a different type of solution in which a suitable delay factor is separated out from $Y(p)$ at an earlier stage.

It will be helpful, however, first to consider the question of frequency changing. We have seen that if the signal represented by eqn. (11) is applied to the network of admittance Y, the response $I(t)$ is given by eqn. (12). Now the envelope $I_0(t)$ of the response is $I(t)\varepsilon^{-jkt}$, so that

$$I_0(t) = \int_0^\infty \varepsilon^{-jk\lambda}w(t-\lambda)y(\lambda)d\lambda \quad . \quad . \quad . \quad (19)$$

Now suppose the frequency is changed by $K/2\pi$ cycles per second, so that the applied voltage, instead of eqn. (11), is

$$\bar{v}(t) = \varepsilon^{j(k+K)t}w(t) \quad . \quad . \quad . \quad . \quad . \quad (20)$$

and that the impedance Y is replaced by Y_1 in such a way that the envelope is unaltered. The resulting current is

$$\bar{I}(t) = \varepsilon^{j(k+K)t}\int_0^\infty \varepsilon^{-j(k+K)\lambda}w(t-\lambda)y_1(\lambda)d\lambda \quad . \quad . \quad (21)$$

where $y_1(t)$ is the response of the impedance Y_1 to unit impulse. The envelope $\bar{I}_0(t)$ is obtained by omitting the factor $\varepsilon^{j(k+K)t}$ from eqn. (21). If $\bar{I}_0(t) = I_0(t)$, we must have

$$\varepsilon^{-jK\lambda}y_1(\lambda) = y(\lambda) \quad . \quad . \quad . \quad . \quad . \quad (22)$$

Combining eqns. (7) and (22), we deduce

$$Y_1(p) = Y(p + jK) \quad . \quad . \quad . \quad . \quad . \quad (23)$$

Now the response of a band-pass filter is generally expressed, at least approximately, in terms of the deviation of the frequency from the mid-band frequency, and eqn. (23) simply means that the effect of frequency changing is to replace one band-pass filter by another of equal bandwidth etc., only the mid-band frequency being altered. This changed mid-band frequency can be reduced to zero; the band-pass structure then becomes the equivalent low-pass structure. This happens if the admittance Y is a band-pass filter having mid-band frequency $\omega_0/2\pi$ and K is taken as ω_0. We then know that Y can be expressed as a function of $(p - j\omega_0)$, say

$$Y = Y_2(p - j\omega_0) \quad . \quad . \quad . \quad . \quad . \quad (24)$$

so that after frequency-changing which reduces the mid-band frequency to zero, the effective impedance becomes $Y_2(p)$.

In practice Y is not strictly a function of $(p - j\omega_0)$ but rather of $\frac{1}{2}(p/\omega_0 + \omega_0/p)$.* If we consider a f.m. signal of the form of eqn. (1), however, and write

$$p = j\omega_0(1 + x) \quad . \quad . \quad . \quad . \quad . \quad . \quad (25)$$

then x cannot numerically exceed the small quantity $\mu/\omega_0 = \sigma$, which is of order 0·007 if the maximum frequency deviation $\mu/2\pi$ is 75 kc/s and $\omega_0/2\pi$ is 10·7 Mc/s. Substituting from eqn. (25) and expanding in powers of x, we have

$$\frac{p}{\omega_0} + \frac{\omega_0}{p} = 2jx[1 - \tfrac{1}{2}x + \tfrac{1}{2}x^2 - \ldots] \quad . \quad . \quad (26)$$

so the error in neglecting all but the first term of eqn. (26) is of the order of $\frac{1}{2}\sigma$ or 0·35%. If this error is neglected, eqn. (26) means that Y can be regarded as a function of jx or $(p - j\omega_0)/\omega_0$, in such a way that the original band-pass admittance is replaced by the equivalent low-pass admittance for the signal $\exp[js(t)]$. Thus what we really require to calculate is

$$I(t) = \int_0^\infty \varepsilon^{js(t-\lambda)} f(\lambda) d\lambda \quad . \quad . \quad . \quad . \quad (27)$$

where $f(t)$ is the response to unit impulse, not of the original band-pass structure, but of its low-pass equivalent. This low-pass equivalent is obtained by expressing the band-pass admittance as a function of deviation x from the mid-band frequency, and then replacing x by $p/j\omega_0$, and the error committed is of order 0·35%.

(3) EXTRACTION OF A SUITABLE DELAY FACTOR FROM THE EQUIVALENT LOW-PASS ADMITTANCE

We have seen that in order to calculate the effect of the input f.m. signal [eqn. (1)] on the network whose admittance is Y, we can use eqn. (27), i.e. we regard Y as a band-pass admittance and replace it by the equivalent low-pass structure whose admittance we shall call $\eta(p)$. The input signal, eqn. (1), is correspondingly replaced by $\exp[js(t)]$. The error involved in this simplification is of order 0·35% at most.

In practice, the form of this low-pass admittance equivalent to the given band-pass admittance is not in essence different from

$$\eta(p) = 1/2\alpha^2\left(1 + \frac{p}{\alpha\omega_0} + \frac{p^2}{2\alpha^2\omega_0^2}\right) \quad . \quad . \quad . \quad (28)$$

Since $$\varepsilon^{p/\alpha\omega_0} = 1 + p/\alpha\omega_0 + p^2/2\alpha^2\omega_0^2 + \ldots \quad . \quad . \quad (29)$$

we shall write $\eta(p)$ in eqn. (28) in the form

$$\eta(p) = \varepsilon^{-p/\alpha\omega_0}[1 + \phi(p)]/2\alpha^2 \quad . \quad . \quad . \quad (30)$$

where $$\phi(p) = \left(\frac{p^3}{6\alpha^3\omega_0^3} + \frac{p^4}{24\alpha^4\omega_0^4} + \ldots\right)\varepsilon^{-p/\alpha\omega_0} \quad . \quad . \quad (31)$$

so that if $|p|$ is small compared with $\alpha\omega_0$, $|\phi(p)|$ is small compared with unity, $|\phi'(p)|$ is small compared with $1/\alpha\omega_0$ and $|\phi''(p)|$ is small compared with $1/\alpha^2\omega_0^2$, but $|\phi'''(p)|$ is of order $1/\alpha^3\omega_0^3$.

If $\eta(p)$ were not given strictly by eqn. (28), eqn. (31) could contain an additional small term in p^2, and eqn. (33) would then contain a corresponding additional term in d^2w/dt^2.

Now, corresponding to the first term $(1/2\alpha^2)\exp(-p/\alpha\omega_0)$ in eqn. (30), $f(\lambda)$ in eqn. (27) will have a term $(1/2\alpha^2)U(t - 1/\alpha\omega_0)$, where $U(x)$ is the unit step-function, zero for $x < 0$, $\frac{1}{2}$ for $x = 0$ and 1 for $x > 0$. It is equally well known that if the response of an admittance $\phi(p)$ to unit-impulse excitation is $\psi(t)$, the response of the admittance $\varepsilon^{-\gamma p}\phi(p)$ is $\psi(t - \gamma)$. In order, therefore, to evaluate eqn. (27) when $f(t)$ is the response of the admittance (30) to unit-impulse excitation, we have only to consider the response of the terms

$$p^3/6\alpha^3\omega_0^3, \quad p^4/24\alpha^4\omega_0^4 \ldots \quad . \quad . \quad . \quad . \quad . \quad (32)$$

to unit-impulse excitation. But the response of an admittance p^r to such excitation is $d^rU(t)/dt^r$, and therefore substitution in eqn. (27) and repeated integration by parts finally gives

$$I(t) = \frac{1}{2\alpha^2}\left[w(t - 1/\alpha\omega_0) + \frac{1}{6\alpha^3\omega_0^3}\frac{d^3}{dt^3}w(t - 1/\alpha\omega_0) + \frac{1}{24\alpha^4\omega_0^4}\frac{d^4}{dt^4}w(t - 1/\alpha\omega_0) + \ldots\right] \quad . \quad (33)$$

Eqn. (33) and other formulae for output current like eqns. (10) and (18) have been derived by assuming only that if we know the admittance of a network we know the response of that network to unit-impulse excitation; otherwise all mathematical manipulations have taken place entirely within the time world. At present, symbolic calculus is commonly used to determine theoretically the response of a network to unit-impulse or any other excitation, and we have therefore by implication used it here, but the meaning and significance of the results is not associated with or dependent upon symbolic calculus. Indeed, it has become clear to anyone versed in operational calculus (in which p stands for d/dt) that all the results obtained above could have been more quickly and simply derived operationally. Such derivation is therefore carried out in Section 4.

(4) OPERATIONAL DERIVATION OF RESULTS ALREADY OBTAINED

For operational calculus, we assume that p is equivalent to d/dt and p^r to d^r/dt^r. Eqn. (2) is then replaced by

$$I(t) = Y(p)v(t) \quad . \quad . \quad . \quad . \quad . \quad . \quad . \quad (34)$$

so that p's and t's both appear on the right-hand side. Some doubt has recently been cast on the validity of operational calculus; the authors believe that such doubt is not justified, provided that sufficient care is taken concerning the limits of the integration corresponding to the operator p^{-1}. This matter is discussed more fully in Reference 2, in which the use of operational methods has also been validated in problems of the present kind in which stochastic processes are involved. Here we shall merely assume that any algebraic manipulation of $Y(p)$ and of $v(t)$ is permissible, provided only that there is no alteration of the order of terms as between p-terms and t-terms. Thus, starting from eqn. (34), when $v(t)$ is given by eqn. (11) we use the fact that by Leibnitz's theorem

$$p^r[\varepsilon^{jkt}w(t)] = \varepsilon^{jkt}(p + jk)^r w(t) \quad . \quad . \quad . \quad (35)$$

to obtain $$I(t) = \varepsilon^{jkt}Y(p + jk)w(t) \quad . \quad . \quad . \quad . \quad (36)$$

which is equivalent to eqn. (23). If we expand $Y(p)$ in a Maclaurin series (whose convergence is discussed later) and operate with the successive terms on $v(t)$, we obtain eqn. (10) immediately, and if we expand $Y(p + jk)$ in eqn. (36) in a Taylor series we likewise obtain eqn. (13) immediately. Applying eqn. (13) to the f.m. case where $k = \omega_0 + s'(t)$* and $w(t)$ is $\exp j[s(t) - ts'(t)]$, we obtain the quasistationary approxi-

* In the case (usual in broadcast receiver design) of so-called transformer coupling, the circuit is not confluent, that is p/ω_0 may occur without a corresponding term in ω_0/p. In such non-confluent terms, p/ω_0 can be replaced by j and ω_0/p by $-j$ with an error of, at most, μ/ω_0 or 0·7% for the f.m. conditions here considered.

* The fact that k depends on t does not debar it from being regarded as constant, since it is independent of p.

mation [eqn. (16)] immediately. Again, eqn. (27), with due regard to eqn. (28), becomes

$$I(t) = \frac{1}{2\alpha^2}\varepsilon^{-p/\alpha\omega_0}[1 + \phi(p)]w(t) \quad . \quad . \quad . \quad (37)$$

from which eqn. (33) is immediately deducible.

(5) EFFECT OF THE DISCRIMINATOR

Eqn. (33) appears to be the most useful form for $I(t)$ in the f.m. case, when the signal is applied to one stage of the i.f. coupling circuits, and the effect of a number of such stages is to introduce additional delay and to modify the coefficients of the differentiated terms in eqn. (33) without greatly affecting their relative unimportance. Now the discriminator can be regarded as presenting an admittance

$$Y_3(p) = \left(\frac{p}{\omega_0} + \frac{\omega_0}{p}\right)\Big/ D(p) \quad . \quad . \quad . \quad . \quad (38)$$

where $D(p)$ can be treated as if it were part of the amplifier, and therefore omitted from our present discussion. The behaviour of one particular type of discriminator is discussed fully elsewhere.[3] The low-pass equivalent of the effective part of eqn. (38) is then

$$\eta_3(p) = 2p/\omega_0 \quad . \quad . \quad . \quad . \quad . \quad . \quad (39)$$

so that the current, $I_3(t)$, allowing for the discriminator is

$$I_3(t) = \frac{2}{\omega_0}\frac{d}{dt}\left\{\varepsilon^{js(t-\beta)}[1 + \Delta(t)]\right\} \quad . \quad . \quad . \quad (40)$$

where β is the total delay introduced by the i.f. stages and the denominator $D(p)$ of eqn. (38), and $\Delta(t)$ represents the additional terms introduced by applying eqn. (33) to these i.f. stages in succession.

(6) CONVERGENCE

Since the applied voltage is regarded as a stationary time series, we are not interested in transients associated with the fact that the applied voltage $v(t)$ is really switched on at zero time and therefore preferably written $v(t)U(t)$, where $U(t)$ is the unit step-function. We should therefore regard p^rK as zero if r is positive and K is a constant. The nature of the expression $p^rv(t)$, and therefore the convergence of a series in which $p^rv(t)$ is a typical term, depends upon the nature of $v(t)$, which determines the effect of p, or d/dt, on it. The convergence or otherwise of the series is usually obvious once $p^rv(t)$ has been formulated as a time function. In symbolic calculus the criteria of convergence are less obvious. If we require the time function $z(t)$ corresponding to a given p-expression $\zeta(p)$, which can be expressed as a series of negative powers of p having a_s/p^s as a typical term, it has been suggested that the series $\Sigma a_s t^s/s!$ is convergent for all values of t with sum to infinity $z(t)$, provided that there is any range of positive real values of p for which the p-series $\Sigma a_s/p^s$ converges with sum to infinity $\zeta(p)$.

In the case of frequency modulation, we are concerned with the convergence of eqn. (33), which was derived from the expansion of

$$\phi(p) = \frac{\varepsilon^{p/\alpha\omega}}{1 + (p/\alpha\omega_0) + (p^2/2\alpha^2\omega_0^2)} - 1 \quad . \quad . \quad (41)$$

in eqn. (31) as a series in powers of $p/\alpha\omega_0$, which we shall now call ξ for brevity. Now one way of obtaining this series expansion is to write

$$\psi(\xi) = \frac{1}{1 + \xi + \frac{1}{2}\xi^2} = \frac{1}{\left(1 + \frac{1}{\sqrt{2}}\xi\varepsilon^{j\pi/4}\right)\left(1 + \frac{1}{\sqrt{2}}\xi\varepsilon^{-j\pi/4}\right)}$$

$$= \frac{1}{i\sqrt{2}}\left(\frac{\varepsilon^{j\pi/4}}{1 + \frac{1}{\sqrt{2}}\xi\varepsilon^{j\pi/4}} - \frac{\varepsilon^{-j\pi/4}}{1 + \frac{1}{\sqrt{2}}\xi\varepsilon^{-j\pi/4}}\right) \quad . \quad (42)$$

and expand the last member of eqn. (42) in ascending powers of ξ. The expansion is convergent for $|\xi| < \sqrt{2}$ if ξ is an ordinary number; since the exponential series for $\exp \xi$ is convergent for all ξ, the series for $\phi(p)$ obtained from the product $\psi(\xi)\exp\xi$ is convergent also for $|\xi| < \sqrt{2}$. But ξ is not an ordinary number; ξ^r is proportional to d^r/dt^r in eqn. (33), so we have to consider next

$$d^r[\varepsilon^{js(t)}]/dt^r \quad . \quad . \quad . \quad . \quad . \quad . \quad . \quad (43)$$

which can be obtained explicitly. If $y = \exp z$, where z is a function of t, and $z_1, z_2 \ldots z_r$ are the first r derivatives of z with respect to t,

$$y_r = \frac{d^r y}{dt^r} = \varepsilon^z[z_1^r + \binom{r}{2}z_1^{r-2}z_2 + \binom{r}{3}z_1^{r-3}z_3 + \ldots + z_r + 3\binom{r}{4}z_1^{r-4}z_2^2 + 10\binom{r}{5}z_1^{r-5}z_2z_3 + \ldots] \quad . \quad (44)$$

where $\binom{r}{s}$ denotes the binomial coefficient $\dfrac{r!}{s!(r-s)!}$

Terms involving squares and products of derivatives of z above the first only arise for $r \geqslant 4$. This series is finite: all combinations of $z_1^p z_2^q z_3^k \ldots$ appear such that $p + 2q + 3k \ldots = r$.

Now $s(t)$ contains frequencies up to 10 kc/s but mainly in the region 100 c/s–2 kc/s, whereas the maximum frequency deviation, $\mu/2\pi$, is 75 kc/s. We can therefore reasonably take the maximum numerical value of z_r to be $(0{\cdot}05)^{r-1}\mu^r$. If all the z_r terms had their maximum numerical values simultaneously and in phase, the first row of terms in eqn. (44) would make a total contribution to $|y_r|$ of

$$C_r = \mu^r[20 \times 1{\cdot}05^r - 19 - r] \quad . \quad . \quad . \quad (45)$$

There is a very large number of the remaining terms of eqn. (44) for large values of r, but they involve at worst powers of 0·05 at least as high as the second, and this would appear to prevent the total contribution of such terms from being comparable with C_r in eqn. (45). For purposes of convergence, only the term $20(1{\cdot}05\mu)^r$ in eqn. (45) matters. It means that the general term of the series [eqn. (33)] is numerically less than 20 times the general term of the series S obtained by substituting $1{\cdot}05\mu$ for p in eqn. (41). The corresponding value of ξ is about 0·35 if α is of order $3\sigma = 3\mu/\omega_0$, and 0·35 is much less than $\sqrt{2}$. Hence the series S, and therefore the series in eqn. (33), is rapidly convergent.

(7) ACKNOWLEDGMENT

The authors wish to thank the Chief Engineer of The British Broadcasting Corporation for permission to publish the paper.

(8) REFERENCES

(1) VAN DER POL, B.: 'The Fundamental Principles of Frequency Modulation', *Journal I.E.E.*, 1946, **93**, Part III, p. 153.

(2) PROCTOR WILSON, W., MAYO, C. G., and HEAD, J. W.: 'Notes on Operational Calculus'. (Not yet published.)

(3) MAYO, C. G., and HEAD, J. W.: 'The Foster–Seeley Discriminator', *Electronic and Radio Engineer*, 1958, **35**, No. 2, p. 44.

621.372.6.01

The Institution of Electrical Engineers
Monograph No. 306 M
June 1958
©

AN EXACT THEORY OF *N*-COMPONENT STEADY-STATE OPERATORS FOR LINEAR CIRCUITS

By A. J. O. CRUICKSHANK, B.Sc., Ph.D., Associate Member.

(*The paper was first received 7th January, and in revised form 21st March*, 1958. *It was published as an* INSTITUTION MONOGRAPH *in June*, 1958.)

SUMMARY

A theory of *N*-component operators is given for steady-state calculations in linear circuits with inputs of periodic, but non-sinusoidal, form. If the input waveforms have a finite number, *M*, of harmonic components, *N* may be chosen such that an exact theory results. The theory supplements an approximate one of the same nature recently published.[4] The central feature of the method is the decomposition of any periodic function with *M* harmonic components into a number of samples of the same form, but of magnitudes equal to the ordinates of the function at equal intervals τ throughout the period, and displaced in the time-axis by successive intervals τ. By appropriate choice of the sampling function, an exact representation may be obtained.

A shift operator u is now introduced which translates any periodic function one interval τ to the right. By this means it is possible to express a periodic function with *M* harmonics as a product of a polynomial in u and the basic sampling function. This polynomial in u, of order $N - 1$, gives an *N*-component operator representing the waveform. The representation is, in a sense, analogous to that used in vector algebra, where an arbitrary sinusoidal wave may be written as the product of a polynomial in j, such as $a + jb$, with a basic sinusoidal reference wave. The theory gives rise to the fundamental results $u^N = 1$ and $u^N = -1$ for general, and odd harmonic only, waveforms respectively, and using these a standard form for an *N*-component operator may be obtained.

Differential and integral operators are developed and rules are given for obtaining the *N*-component operator corresponding to an impedance, admittance or transfer function. The algebra of *N*-component operators is summarized and the solution of a simple circuit examined by way of illustration. The process of inverting an operator requires the solution of *N* simultaneous equations, and an alternative method of procedure is considered. Simple expressions result for power and r.m.s. values.

The application to linear circuits is advantageous in the case when the input is known graphically or numerically and a similar description of the output is desired. It is therefore an alternative method of procedure to Fourier analysis, calculation of the responses to the harmonic components, and subsequent point-by-point plotting of the output. The theory may also be applied to the solution of non-linear circuits by continued approximation, but, as this technique is the same as for the approximate operators already dealt with, it is not considered in the paper.

(1) INTRODUCTION

Of recent years there has been much interest in the calculation of network and system responses by methods based on the expression of time functions by a series of numbers representing the values of the function at a number of equally spaced points. The procedures, which are known generally as 'time-series' methods and which are now well established, have been developed in a number of different forms, each suited to the particular problem under investigation. The essence of all the methods, however, is the use of an interpolating or sampling function which is taken in varying amounts at equally spaced instants, and the time function is built up by summing these varying amounts.

There are two main features which result, depending on the shape of the sampling function or unit chosen, and on the manner in which the time origin is introduced. These are the accuracy of representation and the emergence of 'single-sided' or 'double-sided' series. By a single-sided series is meant one having a definite starting point, usually the time origin, and developing to the right as time increases. A double-sided series, on the other hand, has a central ordinate, again usually at $t = 0$, and develops in both directions. Both types contain an infinite number of terms, which, for stable responses, will become smaller and smaller. The distinction between single- and double-sided series appears most prominently in the rule for the division of two series. In the former, polynomial division is valid, but in the latter it is invalid, at least in its normal form. In consequence, in the second case, an inversion process takes its place, and this is in general a more complicated process to carry out.

The original work of Tustin[1] on time-series introduced as sampling function the 'delta' unit, i.e. an isosceles triangle of unit height and base twice the interval between pulses, and other pulse shapes were also given. The theory, which was concerned with functions and responses zero for negative time, gave rise to single-sided series and was approximate in principle. In another field of study, Shannon[2] showed that any band-limited time function could be exactly represented by its values at sampling points equally spaced τ sec apart, where 2τ is the period of the highest frequency component present in the time function, provided that the sampling function chosen was the pulse of shape $\sin(\pi t/\tau)/(\pi t/\tau)$. Thomson[3] chose this shape of pulse for his theory of time series, which is therefore in principle an exact theory. Further, the particular problem of waveform transmission with which Thomson was concerned led to his adoption of double-sided series, and the resulting algebra differs from that of other methods in substituting inversion for division. All the methods of time series, however, have been devoted to problems of transient response, for both linear and non-linear systems. A periodic analogue of the technique was introduced recently by the author,[4] but the general forms and rules which were found to apply indicate that a more correct description of this development would be an *N*-component algebra of generalized steady-state operators. In Reference 4, an essentially geometric approach was employed, and the interpolating function, instead of being a non-periodic delta unit, was a periodic delta-unit waveform. The theory was in consequence approximate, and, further, division of operators was accomplished by inversion of the divisor. The extension that is presented in this paper is that the theory is now made exact. This is brought about by the use of the periodic sampling function $\sin(\pi t/\tau)/\sin(\pi t/N\tau)$, where $N\tau$ is equal to the half-period or complete period, depending on whether the periodic function being represented has odd only, or odd and even harmonics in the waveform. In each case N is the number of ordinates at intervals τ throughout the half

Correspondence on Monographs is invited for consideration with a view to publication.
Dr. Cruickshank is in the Electrical Engineering Department, University of St. Andrews, Queen's College, Dundee.

or complete period respectively, and $2N\tau/(N-1)$ is the period of the highest frequency component.

Apart from different rules for forming the differential and integral N-component operators, the algebra is the same as for the approximate theory. Use is made of a shift operator u which translates the waveform one interval τ to the right, and impedance, admittance and transfer-function operators are obtained in the general form $A = \sum_{k=0}^{N-1} A_k u^k$ as before. The fundamental relations $u^N = -1$, and $u^N = 1$ are obtained. As the application of the exact theory differs only slightly from the application of the approximate theory, only a few remarks concerning this are included, and further information may be obtained from Reference 4.

(2) N-COMPONENT OPERATORS

The theory about to be presented is concerned with periodic functions having a finite number of harmonics. If this number of harmonics, including the fundamental, is M, it will be shown that it is possible to express the wave exactly by $2M$ independent numbers in conjunction with an appropriate sampling function; further, that these $2M$ independent numbers are the ordinates of the wave at equal intervals τ throughout the period, or, in the case of waves having only odd harmonics, throughout the half-period. It is reasonable to expect this result as, from the viewpoint of the harmonics, $2M$ independent numbers are required to state their amplitudes and phases.

(2.1) Basis

The sampling functions chosen are $S(t) = \sin N\omega t/(N \sin \omega t)$, where N is even for those waveforms having only odd harmonics, and $R(t) = \sin \frac{1}{2}N\omega t/(N \sin \frac{1}{2}\omega t)$, where N is odd, for periodic functions in general. The trigonometrical expansions of these are

$$S(t) = \frac{2}{N}[\cos \omega t + \cos 3\omega t + \ldots + \cos (N-1)\omega t] \quad . \quad (1)$$

and

$$R(t) = \frac{1}{N} + \frac{2}{N}[\cos \omega t + \cos 2\omega t + \ldots + \cos \tfrac{1}{2}(N-1)\omega t] \quad . \quad (2)$$

There are $M = \frac{1}{2}N$ components in the first of these expressions and $M = \frac{1}{2}(N-1)$ in the second. The functions are shown in Figs. 1(*a*) and 1(*b*), in which, for comparison, are given also the periodic delta unit waveforms corresponding to them. The zeros of $S(t)$ occur at $t = k\pi/(N\omega)$, $k = 1, 2, \ldots, 2N-1$, with the exception of $k = N$, when $S(t) = -1$. The zeros of $R(t)$ occur at $t = k2\pi/(N\omega)$, $k = 1, 2, \ldots, N-1$. At $t = 0$, $S(t)$ and $R(t)$ both equal unity. It follows therefore, that if we are proposing to sample any waveform $f(t)$, having only M harmonics including the fundamental, using the function $R(t)$, a choice of the sampling instants equal to $t = k\tau = k2\pi/(N\omega)$ will result in a contribution from only one sample at any particular sampling instant, since at that instant zeros of all the other samples occur. Analytically this may be shown as follows.

Let $f(t)$ be written as the sum of a number of samples, using $R(t)$ delayed by successive amounts τ. We have then $f(t) = \sum_{k=0}^{N-1} a_k R(t - k\tau)$. By setting $t = k\tau, k = 0, 1, \ldots, N-1$, in turn we have $a_k = f(k\tau)$. Writing the ordinate values $f(k\tau) = f_k$, we have therefore

$$f(t) = \sum_{k=0}^{N-1} f_k R(t - k\tau) \quad . \quad . \quad . \quad . \quad . \quad (3)$$

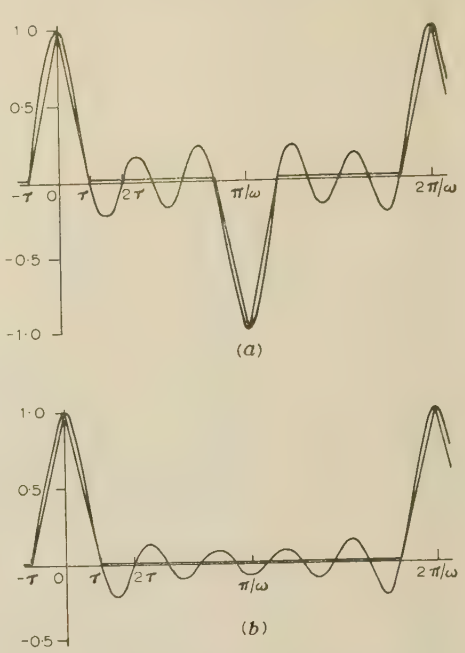

Fig. 1.—The sampling functions $S(t)$ and $R(t)$.
(*a*) $S(t) = (\sin N\omega t)/(N \sin \omega t)$, for $N = 6$.
(*b*) $R(t) = (\sin \frac{1}{2}N\omega t)/(N \sin \frac{1}{2}\omega t)$, for $N = 11$.

The wave is represented exactly by its ordinates at the N instants $t = 0, \tau, 2\tau, \ldots, (N-1)\tau$. If $f(t)$ has no d.c. component, however, these N numbers are not independent. Remembering that $R(t)$ has average value $1/N$, the additional relation obtained from eqn. (3) is

$$\sum_{k=0}^{N-1} f_k/N = 0 \quad . \quad . \quad . \quad . \quad . \quad . \quad (4)$$

so that in all there are $N-1$ independent numbers representing the wave. This is the same as $2M$, i.e. twice the number of components present. The case of only odd harmonics is similar. We have

$$f(t) = \sum_{k=0}^{N-1} f_k S(t - k\tau) \quad . \quad . \quad . \quad . \quad . \quad (5)$$

where $\tau = \pi/(N\omega)$. There are $N = 2M$ independent numbers in this case.

The above results are equivalent to the statement that a wave containing harmonics up to the mth requires, for its exact description, $N = 2m + 1$ equally spaced ordinates throughout the period. If there is no d.c. component, $2m$ of these numbers are independent; if there is a d.c. component the $2m + 1$ numbers are all independent. Further, if only odd harmonics up to the mth are present, the number of equally spaced ordinates throughout the half-cycle required for the exact description of the wave is $N = m + 1$.

For example, the wave $v(t) = \cos \omega t + 0{\cdot}5 \cos 3\omega t + 0{\cdot}5 \cos 5\omega t$ has three odd harmonic components, the highest of order 5. It can therefore be represented exactly by eqn. (5) with $N = 6$. We have $\tau = \pi/(6\omega)$ and $V_k = v(k\tau)$, $k = 0, 1, 2, \ldots, 5$, i.e. V_k is the set of six numbers 2·000, 0·433, 0·250, 0, −0·250, −0·433. The following Section shows how this set of N numbers can be formed into an algebraic N-component operator.

(2.2) N-Component or U-Operators

A theory of N-component operators may be developed on the above basis by introducing a fundamental operator u, whose

effect is to translate any time function to the right by one interval τ, that is, $uf(t) = f(t - \tau)$. In general the relation is $u^k f(t) = f(t - k\tau)$, where k is any integer, positive, negative or zero. It follows therefore that $u^{-k}u^k f(t) = f(t)$, i.e. u^{-k} is the inverse of u^k. For periodic waves in general, with the complete cycle divided into N parts, we have

$$u^N = 1 \quad . \quad . \quad . \quad . \quad . \quad . \quad . \quad (6a)$$

For odd harmonics only, $N\tau = \pi/\omega$, and

$$u^N = -1 \quad . \quad . \quad . \quad . \quad . \quad . \quad . \quad (6b)$$

Using this operator eqns. (3) and (5) become

$$f(t) = \sum_{k=0}^{N-1} f_k u^k R(t) \quad . \quad . \quad . \quad . \quad . \quad (7)$$

$$f(t) = \sum_{k=0}^{N-1} f_k u^k S(t) \quad . \quad . \quad . \quad . \quad . \quad (8)$$

These may be written in the simple form

$$f = \sum_k f_k u^k \quad . \quad . \quad . \quad . \quad . \quad . \quad (9)$$

where k is summed* over the integral values from zero to $N - 1$. Eqn. (9) may be termed the operator form of the waveform $f(t)$, in the same way that

$$V = V_0 j^0 + V_1 j^1 = V_0 + jV_1$$

is the operator form of the sinusoidal wave corresponding to V.

Further, any expression such as $a + bu^\alpha + cu^\beta + \ldots$, containing a finite number of terms, may be reduced to the form $\sum_k A_k u^k$, where some of the A_k may be zero, by the substitution $u^N = 1$ or $u^N = -1$ as the case may be. This is analogous to reducing $a + jb + j^2c + j^3d$, for example, to $(a - c) + j(b - d)$, by substituting $j^2 = -1$. The forms $\sum_k A_k u^k$, $\sum_l f_l u^l$ will be termed N-component operators, or u-operators for short, and denoted simply by A, f respectively.

(2.2.1) Differential and Integral Operators.

In this Section an operator p is developed such that p operating on a waveform $f(t)$, written pf, results in an operator representing the waveform $f'(t)$, where $f'(t)$ is the derivative with respect to time of $f(t)$. This may be found as follows. We have

$$f(t) = \sum_k f_k R(t - k\tau) = \sum_k f_k u^k R(t)$$

and

$$f'(t) = \sum_k f_k R'(t - k\tau) = \sum_k f_k u^k R'(t)$$

Since $R'(t)$, the derivative of $R(t)$, contains the same number of harmonics as $R(t)$, it may be written according to eqn. (7)

$$R'(t) = \sum_k R'_k u^k R(t) \quad . \quad . \quad . \quad . \quad . \quad (10)$$

where R'_k is the ordinate of $R'(t)$ at $t = k\tau$.

By substitution in the expression for $f'(t)$, therefore,

$$f'(t) = \sum_k f'_k u^k R(t) = (\sum_j f_j u^j)(\sum_l R'_l u^l) R(t) \quad . \quad . \quad (11)$$

or, in operator form $f' = fp$. The differential operator is therefore

$$p = \sum_l R'_l u^l = \sum_k R'_k u^k \quad . \quad . \quad . \quad . \quad (12)$$

* Unless stated otherwise $\sum_k$ will in future denote summation with respect to k over the N values from zero to $N - 1$. Similarly for any other index letter written in this fashion.

Similarly for waves having only odd harmonics, the differential operator is $\sum_k S'_k u^k$, where S'_k is the ordinate of $S'(t)$ at $t = k\tau$.

By applying these results, the following operators are obtained:

General waveforms

$$p = \tfrac{1}{2}\omega \sum_{k=1}^{N-1} [(-1)^k \operatorname{cosec}(k\pi/N)] u^k \quad (N \text{ odd}) \quad . \quad (13)$$

Odd harmonics only

$$p = \omega \sum_{k=1}^{N-1} [(-1)^k \operatorname{cosec}(k\pi/N)] u^k \quad (N \text{ even}) \quad . \quad (14)$$

An alternative series form for each of the coefficients R'_k and S'_k may be written, namely

$$R'_k = -\frac{2\omega}{N} \sum_{m=1}^{(N-1)/2} m \sin(2mk\pi/N) \quad . \quad . \quad . \quad (15)$$

$$S'_k = -\frac{2\omega}{N} \sum_{m=1,3\ldots}^{N-1} m \sin(mk\pi/N) \quad . \quad . \quad . \quad (16)$$

The summation in this last result takes place over only odd values of m. Note that there is no coefficient of u^0 in the operators, eqns. (13) and (14). The differential and integral operators for several values of N are given in Section 6.

The integral operators are calculated in an analogous fashion. Integrating

$$R(t) = \frac{1}{N} + \frac{2}{N}[\cos\omega t + \cos 2\omega t + \cos 3\omega t + \quad + \cos \tfrac{1}{2}(N-1)\omega t]$$

gives

$$\int R(t) = \frac{t}{N} + \frac{2}{N\omega} \sum_{m=1}^{(N-1)/2} \frac{\sin m\omega t}{m}$$

Let us write the periodic part of this as $W(t)$. Then we have

$$f(t) = \sum_k f_k R(t - k\tau) = \sum_k f_k u^k R(t)$$

and

$$\int f(t) = \sum_k f_k \int R(t - k\tau)dt = \sum_k f_k W(t - k\tau)$$

since $\sum_k f_k t/N$ is zero for waveforms with zero average value.

Hence

$$\int f(t)dt = \sum_k f_k u^k W(t) = (\sum_k f_k u^k)(\sum_l W_l u^l) R(t)$$

The integral operator is therefore $p^{-1} = \sum_{k=1}^{N-1} W_k u^k$, where

$$W_k = \frac{2}{N\omega} \sum_{k=1}^{(N-1)/2} \frac{\sin 2mk\pi/N}{m} \quad (N \text{ odd}) \quad . \quad . \quad (17)$$

For waveforms with odd harmonics only, writing $\int S(t)dt = V(t)$, where $V(t) = (2/N\omega) \sum_{m=1,3\ldots}^{N-1} (\sin m\omega t)/m$, the operator is

$$p^{-1} = \sum_{k=1}^{N-1} V_k u^k,$$

where

$$V_k = \frac{2}{N\omega} \sum_{m=1,3\ldots}^{N-1} \frac{\sin mk\pi/N}{m} \quad (N \text{ even}) \quad . \quad . \quad (18)$$

The summation in the above expression takes place over odd values of m only.

(2.3) Operation on a Waveform

From the manner in which the differential and integral operators have been developed, it will be seen that an operator

$\boldsymbol{A}$ operates on a waveform f according to the simple rule of polynomial multiplication. If $g(t)$ is the waveform resulting from the operation of $\boldsymbol{A}$ on $f(t)$, we have

$$f(t) = \sum_k f_k u^k R(t)$$

$$g(t) = \sum_k g_k u^k R(t)$$

where $\sum_k g_k u^k = (\sum_j f_j u^j)(\sum_l A_l u^l)$, the product on the right-hand side being subsequently reduced by the substitution $u^N = 1$. We have

$$\boldsymbol{Af} = \boldsymbol{fA}$$

$$(\sum_j f_j u^j)(\sum_l A_l u^l)$$

$$= \sum_{j,l} f_j A_l u^{j+l}$$

$$= \sum_{k,j} f_j A_{k-j} u^k$$

That is, the kth component of $\boldsymbol{g}$ is $g_k = \sum_j f_j A_{k-j} = \sum_j f_j A_{N+k-j}$. For example, $g_0 = f_0 A_0 + f_1 A_{N-1} + f_2 A_{N-2} + \ldots + f_{N-1} A_1$. The substitution $A_{k-j} = A_{N+k-j}$ is made for all $k - j < 0$. For the case of waveforms having only odd harmonics $A_{k-j} = -A_{N+k-j}$, since $u^N = -1$.

For example, the current waveform $i(t) = \sin \omega t + 0{\cdot}5 \sin 2\omega t + 0{\cdot}5 \cos 3\omega t$ has both even and odd harmonics and therefore requires a choice of N odd and equal to 7. In operator form the current is

$$\boldsymbol{I} = \sum_j I_j u^j = 0{\cdot}5000 + 0{\cdot}8144u + 1{\cdot}0697u^2 - 0{\cdot}0683u^3 - 0{\cdot}1541u^4 - 0{\cdot}4463u^5 - 1{\cdot}7244u^6$$

Let this current be passed through an impedance given by

$$\boldsymbol{Z} = \sum_l Z_l u^l = 2{\cdot}0000 - 1{\cdot}1523u + 0{\cdot}6395u^2 - 0{\cdot}5129u^3 + 0{\cdot}5129u^4 - 0{\cdot}6395u^5 + 1{\cdot}1523u^6$$

This operator in fact corresponds to the impedance $2 + j1$ ohms, and has been obtained in the manner indicated in the immediately following Section.

The current $\boldsymbol{I}$ operating on $\boldsymbol{Z}$ gives the voltage drop:

$$\boldsymbol{IZ} = \boldsymbol{V} = \sum_k V_k u^k$$

where the components of $\boldsymbol{V}$ are given by

$$V_k = \sum_j I_j Z_{k-j} \quad \text{for} \quad k = 0, 1, 2, \ldots 6$$

Further, since $u^7 = 1$ in this case, we set $Z_{k-j} = Z_{7+k-j}$ for all $k - j < 0$. That is,

$$V_0 = I_0 Z_0 + I_1 Z_6 + I_2 Z_5 + I_3 Z_4 + I_4 Z_3 + I_5 Z_2 + I_6 Z_1$$
$$V_1 = I_0 Z_1 + I_1 Z_0 + I_2 Z_6 + I_3 Z_5 + I_4 Z_4 + I_5 Z_3 + I_6 Z_2$$

and so on. Numerical evaluation of the above components is most easily carried out using a desk calculating machine and the 'movable strip' technique. The resultant or product operator is

$$\boldsymbol{V} = 3{\cdot}000 + 1{\cdot}376u + 2{\cdot}196u^2 - 1{\cdot}881u^3 + 0{\cdot}882u^4 - 3{\cdot}196u^5 - 2{\cdot}394u^6$$

(3) APPLICATION

(3.1) Impedance, Admittance and Transfer-Function Operators

The differential and integral operators of the preceding Section are used to form N-component operators corresponding to any impedance, admittance or transfer function. If we have an impedance $Z(p)$, then the N-component operator corresponding to this is formed by replacing p by the expression given for $\boldsymbol{p}$. Similarly with admittances and transfer functions. For example, the series circuit having impedance $R + pL$ yields the operator

$$\boldsymbol{Z} = R + \boldsymbol{p}L = \sum_k Z_k u^k$$

and so on. For $N = 6$, say (odd harmonics only), the steady-state impedance $R + j\omega L$ will give

$$R + \omega(-2{\cdot}000u + 1{\cdot}155u^2 - 1{\cdot}000u^3 + 1{\cdot}155u^4 - 2{\cdot}000u^5)L$$

i.e. an expression of the form $\sum_k Z_k u^k$.

(3.2) Algebra of N-Component Operators

The algebra of N-component operators has already been given in Reference 4. It will suffice therefore to summarize the results.

(3.2.1) Unit Operator: Addition and Subtraction: Multiplication.

The unit operator is one in which the coefficients of all powers of u vanish with the exception of the coefficient of u^0, which is unity.

The sum or difference of two operators is formed by taking the sum or difference of corresponding components, i.e.

$$\sum_k A_k u^k \pm \sum_k B_k u^k = \sum_k (A_k \pm B_k) u^k$$

The product of two operators is formed according to the rule previously given for the operation by an operator on a waveform, i.e. $\boldsymbol{AB} = \boldsymbol{C}$, where $C_k = \sum_j A_j B_{k-j}$. Multiplication of N-component operators is commutative, i.e. $\boldsymbol{AB} = \boldsymbol{BA}$.

(3.2.2) Inversion: Division.

Division of operators is accomplished by a process of inversion. Suppose $\boldsymbol{A}$ is the operator to be inverted and that its inverse is $\boldsymbol{A}^{-1} = \boldsymbol{B}$. Then $\boldsymbol{AB} = \boldsymbol{1}$, the unit operator. This gives the set of equations $\sum_j A_j B_{k-j} = C_k$, $k = 0, 1, 2 \ldots (N-1)$, where $C_0 = 1$, and $C_k = 0$ for $k \neq 0$. By solving this set of equations the required coefficients of $\boldsymbol{B}$ may be found. A formal statement for the inverse has been given,[4] but in practice it is better to solve the equations by a short method, such as that due to Crout.[5] None the less there is considerable labour attached to inverting.

An alternative concept of the inverse of an operator for any circuit is that it is simply the response of that circuit to a unit waveform input, that is, the response to $R(t)$ or $S(t)$, and this may be calculated from the known harmonic components of these functions. Viewed in this fashion, the response of a circuit to any input is therefore a selection of unit waveform responses, taken in proportion to the input ordinates at N points, and given the correct delays $k\tau$, $k = 0, 1, 2, \ldots, (N-1)$. The calculation of the inverse in this fashion requires less labour for simple circuits, but for more complex circuits it would be more lengthy than the method of solving the equations.

(3.3) Power and R.M.S. Values

It is shown below that the power represented by two waves $\boldsymbol{V}$ and $\boldsymbol{I}$ is simply $(\boldsymbol{V} \cdot \boldsymbol{I})/N = (\sum_k V_k I_k)/N$, being the scalar product of the two N-component operators. Likewise the mean square value of a voltage $\boldsymbol{V}$ is $\sum_k V_k^2/N$, and the r.m.s. value the square root of this. These are analogous results to those giving the power in two complex waves of voltage and current in terms of

the harmonic powers, and the mean square value in terms of the harmonic mean square values.

If we have $V(t) = \sum_k V_k R(t - k\tau)$ and $I(t) = \sum_k I_k R(t - k\tau)$, the average power is

$$(\omega/2\pi)\int_0^{2\pi/\omega} V(t)I(t)dt$$

$$= (\omega/2\pi)\int_0^{2\pi/\omega} \sum_{j,k} V_j I_k R(t - j\tau)R(t - k\tau)dt$$

$$= (\omega/2\pi)\int_0^{2\pi/\omega} \sum_k V_k I_k R^2(t - k\tau)dt$$

$$+ (\omega/2\pi)\int_0^{2\pi/\omega} \sum_{j,k} V_j I_k R(t - j\tau)R(t - k\tau)dt \quad (j \neq k)$$

For the function $R(t) = 1/N + (2/N)\sum_{m=1}^{(N-1)/2} \cos m\omega t$, the second of these integrals is zero, and the first integral gives $\sum_k V_k I_k/N$. A similar result holds for waves having only odd harmonics. By putting $I(t) = V(t)$, the mean square value of a waveform V is $\sum_k V_k^2/N$.

(3.4) Circuit Example

Consider the circuit shown in Fig. 2, having the fundamental branch impedance $Z_1 = 1 + j1$, $Z_2 = 1 - j2$, and $Z_3 = 1 + j3$.

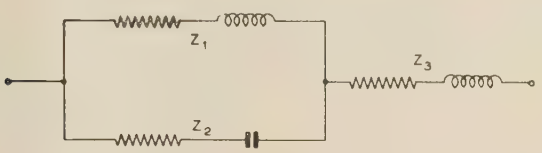

Fig. 2.—Illustrative series-parallel circuit.

Suppose the voltage applied to this circuit is $v(t) = \cos \omega t + 0{\cdot}5 \cos 3\omega t + 0{\cdot}5 \cos 5\omega t$. This is simply an arbitrarily selected complex wave having three odd-harmonic components. In operator form it is

$$V = 2{\cdot}000 + 0{\cdot}433u + 0{\cdot}250u^2 + 0{\cdot}000u^3 - 0{\cdot}250u^4 - 0{\cdot}433u^5$$

where N has been taken equal to 6 in order to give an exact representation, and V_k is equal to $v(k\tau)$.

The operator forms for the impedances are obtained by replacing $j\omega$ and $-j/\omega$ by the differential and integral operators of Section 6, taken for N equal to 6. Thus, using three decimal places only,

$$Z_1 = 1 + 1(-2{\cdot}000u + 1{\cdot}155u^2 - 1{\cdot}000u^3 + 1{\cdot}155u^4 - 2{\cdot}000u^5)$$

$$Z_2 = 1 + 2(0{\cdot}311u + 0{\cdot}231u^2 + 0{\cdot}289u^3 + 0{\cdot}231u^4 + 0{\cdot}311u^5)$$

$$Z_3 = 1 + 3(-2{\cdot}000u + 1{\cdot}155u^2 - 1{\cdot}000u^3 + 1{\cdot}155u^4 - 2{\cdot}000u^5)$$

The admittance is $(Z_1 + Z_2)/(Z_1Z_2 + Z_2Z_3 + Z_3Z_1)$. We have $Z_1Z_2 = 2{\cdot}999 - 1{\cdot}378u + 1{\cdot}617u^2 - 0{\cdot}422u^3 + 1{\cdot}617u^4 - 1{\cdot}378u^5$, using the multiplication rule given, and similarly for Z_2Z_3 and Z_3Z_1. The sum $Z_1Z_2 + Z_2Z_3 + Z_3Z_1$ is $-24{\cdot}009 + 6{\cdot}034u + 6{\cdot}163u^2 - 6{\cdot}844u^3 + 14{\cdot}165u^4 - 35{\cdot}546u^5$. Let this be denoted by $\boldsymbol{A} = \sum_k A_k u^k$, say, and its inverse by $\boldsymbol{B} = \sum_j B_j u^j$. Then from the relation $\boldsymbol{AB} = \mathbf{1}$, we have the equations $\sum_j A_{k-} B_j = C_k$, where $C_k = 1$ for $k = 0$, and $C_k = 0$ for $k = 1, 2, \ldots, (N - 1)$. From these equations the coefficients B_k may be found. In fact the equations are

$$-24{\cdot}009B_0 + 35{\cdot}546B_1 - 14{\cdot}165B_2 + 6{\cdot}844B_3 - 6{\cdot}163B_4 - 6{\cdot}034B_5 = 1{\cdot}000 \quad (k = 0)$$

$$6{\cdot}034B_0 - 24{\cdot}009B_1 + 35{\cdot}546B_2 - 14{\cdot}165B_3 + 6{\cdot}844B_4 - 6{\cdot}163B_5 = 0 \quad (k = 1)$$

and so on. The result is

$$\boldsymbol{A}^{-1} = \boldsymbol{B} = 10^{-1}(0{\cdot}2264 + 0{\cdot}5146u + 0{\cdot}3413u^2 + 0{\cdot}0916u^3 - 0{\cdot}0929u^4 - 0{\cdot}1286u^5)$$

The admittance is

$$\boldsymbol{Y} = 0{\cdot}0622 + 0{\cdot}1208u + 0{\cdot}0562u^2 + 0{\cdot}529u^3 + 0{\cdot}0212u^4 + 0{\cdot}0395u^5$$

and the current is

$$\boldsymbol{I} = \boldsymbol{VY} = 0{\cdot}168 + 0{\cdot}296u + 0{\cdot}208u^2 + 0{\cdot}179u^3 + 0{\cdot}081u^4 + 0{\cdot}044u^5$$

The above ordinates give the required waveform and the r.m.s. value is $[\sum_k I_k^2/N]^{1/2} = 0{\cdot}182$.

From this simple example it will be seen that practically all the labour of calculation lies in obtaining the admittance, for which it is necessary to invert an N-component operator. In view of the nature of the equations giving the unknown components of the inverse operator, i.e. the cyclic type of coefficient array obtained, it is possible that a simpler method of inverting can be found, and if so, this would be highly advantageous.

The alternative method of calculating the admittance, i.e. by calculating the unit waveform response, has some merit in this simple case. The unit waveform is, for $N = 6$, $S(t) = \frac{1}{3}(\cos \omega t + \cos 3\omega t + \cos 5\omega t)$. The response to this, evaluated at points $t = k\tau$, $k = 0, 1, 2, \ldots, (N - 1)$, is $0{\cdot}068 + 0{\cdot}119u + 0{\cdot}050u^2 + 0{\cdot}055u^3 + 0{\cdot}027u^4 + 0{\cdot}037u^5$, which is the admittance $\boldsymbol{Y}$. The discrepancy in the figures is due entirely to taking only three decimal places for the operators $\boldsymbol{p}$ and $\boldsymbol{p}^{-1}$ in the first calculation, and is not due to any error in principle.

(3.5) Conditions of Application

Application of the foregoing theory to linear circuit work would be advantageous in the circumstance of the input being known numerically or graphically, and a similar description of the response being desired. In this case there is no need for Fourier analysis of the input, or summation and point-by-point plotting of the output. If the Fourier components of the input were known and an output waveform was required, there would be little to choose between proceeding by the above method and by the usual method of calculating the harmonic components. The calculation of inverses requires the solution of N simultaneous equations, and it would therefore be fair to say that this amount of labour should be compared with the amount necessary in a Fourier analysis. There would seem to be the probability, however, when large numbers of calculations require the use of computers, that the method suggested might be more suited than the harmonic components method.

Although having a limited application in linear circuits, its application to non-linear circuits by a method of continued approximation seems most advantageous. There are other methods, of course, available in this case using successive corrections to Fourier components, but, generally speaking, these only hold for sinusoidal applied forces. This application has already been dealt with in Reference 4.

(4) CONCLUSION

An exact theory of N-component operators for linear circuits has been given, and its conditions of application discussed. The

theory is intended to supplement an approximate one of the same nature. The relationship of the theory to time-series methods has been pointed out. As a practical method of calculation the theory has a limited application in linear circuits, and a more advantageous one in the approximate solution of non-linear circuits. As a theoretical development it provides an alternative decomposition of periodic functions to Fourier series, and, while this aspect has not yet been properly examined, it is suggested that the theory may be of assistance in investigating the stability of non-linear circuits. It is a further interesting point to note that, for $N = 2$, the sampling function $S(t)$ reduces to $\cos \omega t$, the shift operator u becomes j^{-1} and normal vector algebra results. That is to say, vector algebra, suitable for waves having only a fundamental component, is a particular case of the foregoing theory.

(5) REFERENCES

(1) TUSTIN, A.: 'A Method of Analysing the Behaviour of Linear Systems in Terms of Time Series', *Journal I.E.E.*, 1947, **94**, Part IIA, p. 130.

(2) OLIVER, M., PIERCE, J. R., and SHANNON, C. E.: 'The Philosophy of Pulse-Code-Modulation', *Proceedings of the Institute of Radio Engineers*, 1948, **36**, p. 1324.

(3) THOMSON, W. E.: 'A Theory of Time Series for Waveform Transmission Systems', *Proceedings I.E.E.*, Monograph No. 53 R, October, 1952 (**99**, Part IV, p. 397).

(4) CRUICKSHANK, A. J. O.: 'Generalized Operators for the Approximate Steady-State Analysis of Linear and Non-Linear Circuits', *ibid.*, Monograph No. 256 M, October, 1957 (**105** C, p. 76).

(5) CROUT, P. D.: 'A Short Method for Evaluating Determinants and Solving Systems of Linear Equations with Real or Complex Coefficients', *Transactions of the American I.E.E.*, 1941, **60**, p. 1235.

(6) APPENDICES

(6.1) Differential Operators

The following columns give differential operators for values of N from 4 to 9. The operators for which N is even apply to waveforms having only odd harmonics and are calculated from eqn. (14), omitting the factor ω. Those operators for which N is odd apply in general and are calculated from eqn. (13), omitting the factor $\omega/2$. The factors ω and $\omega/2$ are to be subsequently inserted depending on the input fundamental frequency.

k	$N=4$	$N=5$	$N=6$	$N=7$	$N=8$	$N=9$
1	−1·414 21	−1·701 30	−2·000 00	−2·304 57	−2·613 13	−2·923 80
2	1·000 00	1·051 46	1·154 70	1·278 96	1·414 21	1·555 72
3	−1·414 21	−1·051 46	−1·000 00	−1·025 69	−1·082 39	−1·154 70
4		1·701 30	1·154 70	1·025 69	1·000 00	1·015 43
5			−2·000 00	−1·278 96	−1·082 39	−1·015 43
6				2·304 57	1·414 21	1·154 70
7					−2·613 13	−1·555 72
8						2·923 80

(6.2) Integral Operators

The following columns give integral operators for values of N from 4 to 9. The operators for N even and N odd are restricted as in the previous Section. For N even they are calculated from eqn. (18), omitting the factor $1/\omega$; for N odd, from eqn. (17), omitting the factor $2/\omega$.

	$N=4$	$N=5$	$N=6$	$N=7$	$N=8$	$N=9$
1	0·471 405	0·248 990	0·311 111	0·201 996	0·232 522	0·167 708
2	0·333 333	0·022 451	0·230 940	0·071 043	0·175 093	0·078 494
3	0·471 405	−0·022 451	0·288 889	0·052 563	0·212 941	0·072 169
4		−0·248 990	0·230 940	−0·052 563	0·180 953	0·007 011
5			0·311 111	−0·071 043	0·212 941	−0·007 011
6				−0·201 996	0·175 093	−0·072 169
7					0·232 522	−0·078 494
8						−0·167 708

621.373.4.072.9

The Institution of Electrical Engineers
Monograph No. 307 R
June 1958
©

ON THE DISCRIMINATION OF A SYNCHRONIZED OSCILLATOR AGAINST INTERFERENCE ACCOMPANYING THE SYNCHRONIZING SIGNAL

By R. SPENCE, B.Sc.(Eng.), and A. R. BOOTHROYD, Ph.D., Graduates.

(*The paper was first received 4th December, 1957, and in revised form 22nd March, 1958. It was published as an* INSTITUTION MONOGRAPH *in June, 1958.*)

SUMMARY

An oscillator may be synchronized by an injected signal if the frequency of the signal is close enough to the natural frequency of the oscillator, and if its amplitude is sufficiently large. The output of the oscillator then contains only the frequency of the injected synchronizing signal. In practice an interfering signal is usually present in the input to the oscillator together with the synchronizing signal, and an important property of the synchronized oscillator is its discrimination against the interfering signal even when the difference between the interfering and synchronizing frequencies is infinitesimal. The response of the oscillator to the interfering signal is investigated under conditions where the interference component of the oscillator output is small; the response is found to be linear, and the discrimination is expressed analytically. Good agreement between theory and experiment is obtained.

LIST OF SYMBOLS

v = Oscillator tuned-circuit voltage.
α, γ = Constants of the differential equation of the oscillator.
$H(t)$ = Forcing function of the oscillator.
a_0 = Amplitude of free oscillation.
ω_0 = Natural (angular) frequency of the oscillator.
ω_1 = Synchronizing frequency.
ω_2 = Interfering frequency.
$\sigma_1 = \frac{\Delta_1}{\alpha} = \frac{2(\omega_0 - \omega_1)}{\alpha}$
$\sigma_2 = \frac{\Delta_2}{\alpha} = \frac{2(\omega_0 - \omega_2)}{\alpha} = e$
$\sigma_{12} = \frac{\Delta_{12}}{\alpha} = \frac{2[\omega_0 - (2\omega_1 - \omega_2)]}{\alpha} = f$
$\sigma_{1\,crit}$ = Value of σ_1 at which synchronization ceases.
A = Amplitude of the synchronizing sinusoidal forcing function.
B = Amplitude of the interfering sinusoidal forcing function.
$F_1 = -A\omega_0/a_0\alpha$
$F_2 = -B\omega_0/a_0\alpha$
b_1, b_2 = Sine and cosine components of the output of ω_1.
b_3, b_4 = Sine and cosine components of the output of ω_2.
b_5, b_6 = Sine and cosine components of the output of $2\omega_1 - \omega_2$.
$\rho_1 = (b_1^2 + b_2^2)/a_0^2$
$\rho_2 = (b_3^2 + b_4^2)/a_0^2$
$\rho_3 = (b_5^2 + b_6^2)/a_0^2$
$\rho_s = c = (b_1^2 - b_2^2)/a_0^2$
$\rho_m = d = 2b_1b_2/a_0^2$
D = Discrimination of the oscillator against the interference of frequency ω_2.
V = Diode forward voltage.
I = Diode forward current.
a, I_s = Diode constants.
$g = 1 - 2\rho_1$

Correspondence on Monographs is invited for consideration with a view to publication.
The authors are in the Department of Electrical Engineering, Imperial College of Science and Technology, University of London.

(1) INTRODUCTION

A synchronized oscillator—that is, an oscillator whose frequency is identical with that of an injected synchronizing sinusoid—has a number of practical applications.[1, 2, 3, 4] Among these are carrier generation in communication systems, the reduction of the depth of modulation of an a.m. signal, and the improvement of the signal/noise ratio of a noisy signal.

The synchronized oscillator is especially suited to these applications because it has the property of discriminating against a small-amplitude interfering signal* which may accompany the synchronizing signal. Some discrimination may result from the selectivity of the oscillator's tuned circuit, but this cannot explain the fact that there may be discrimination against the smaller-amplitude interfering signal even when its frequency is infinitesimally different from that of the synchronizing signal. In this latter case, the discrimination is due solely to the non-linearity of the oscillator. This effect cannot, therefore, be explained by a linear analysis of the circuit, and non-linear circuit analysis must be used.

This problem has been studied extensively by Tucker,[1, 2, 3] and by Tucker and Jamieson,[4] and many interesting results have been obtained. Expressions for the response to the interfering signal in a synchronized oscillator were obtained for the cases where the interference frequency is (*a*) far removed from the oscillator frequency, and (*b*) near, but not in, the synchronizing range of the oscillator. Tucker[3] suggests that a general solution of the case where the frequency of the interfering signal lies in the synchronizing range may not be practicable, and he obtains a restricted solution based on the assumption that the selectivity of the oscillator may be neglected. This assumption implies, in effect, that the synchronizing and natural oscillation frequencies differ negligibly, or that the oscillator has no frequency-determining network.

In the present paper no such limitations are assumed, and the solutions obtained are quite general. The solutions of the non-linear differential equation of the oscillator are obtained by the method of van der Pol.[5] The 'phase-plane' approach of Andronov and Witt[6] is introduced, leading to the same solutions, and their method of analysis is used to verify the 'mathematical stability'† of these solutions.

In Section 2 the oscillator under consideration is introduced, and its non-linear differential equation discussed; this equation is solved for the case of a single injected synchronizing signal. A full treatment of the methods of analysis used is given by Stoker.[7]

Section 3 discusses the behaviour of the oscillator when the injected forcing function consists of a synchronizing sinusoid and an interfering sinusoid of a similar order of frequency. The response of the oscillator is derived for the condition where the interference component of the oscillator output is small; this leads to a completely general expression for the discrimination against the interfering signal.

* In describing the interfering signal as small, reference is being made to conditions at the output of the oscillator. The reason for this unusual definition will be apparent in Section 3.

† For an explanation of this expression see Section 2.2.

It should be mentioned that, although the injected interfering signal suffers discrimination, the oscillator itself introduces interference in the form of an intermodulation signal, by reason of its non-linear action. The level of this latter interference in the output of the oscillator is expressed analytically: it is generally lower than that of the interfering signal.

A transistor oscillator was used in the verification of the theory, and excellent agreement was obtained.

(2) TUNED OSCILLATOR WITH ONE INJECTED SINUSOID

(2.1) The Oscillator

The oscillator considered is a tuned oscillator whose forced behaviour is described by the non-linear differential equation

$$\frac{d^2v}{dt^2} + \frac{d}{dt}(-\alpha v + \gamma v^3) + \omega_0^2 v = H(t) \quad . \quad . \quad (1)$$

where v is the oscillator tuned-circuit voltage, ω_0 is the natural frequency of the oscillator, and $H(t)$ is the forcing function.

A physical representation of this equation is shown in Fig. 1(*a*). The parallel tuned circuit is made regenerative by the negative

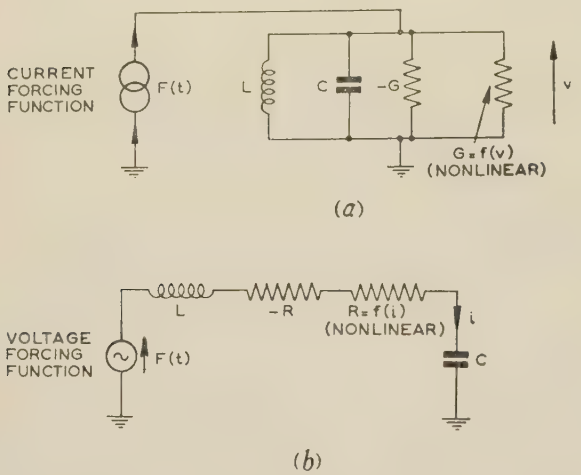

Fig. 1.—Simple equivalent forms of the oscillators considered.

(*a*) $H(t) = \frac{dF}{dt} = C\frac{d^2v}{dt^2} - G\frac{dv}{dt} + \frac{d}{dt}[f(v)v] + \frac{v}{L}$

where $f(v)v \propto v^3$ in the case considered.

(*b*) $H(t) = \frac{dF}{dt} = L\frac{d^2i}{dt^2} - R\frac{di}{dt} + \frac{d}{dt}[f(i)i] + \frac{i}{C}$

where $f(i)i \propto i^3$ in the case considered.

conductance, with limiting effected by the non-linear positive conductance. Fig. 1(*b*) shows a dual circuit representation described by the same form of equation but with current as the independent variable. This paper is concerned with the analysis of oscillatory systems of the general type defined in Fig. 1, the voltage differential equation (1) being considered specifically. The tuned-grid oscillator is an example of a circuit described by this equation (see Reference 7, p. 148).

It may be argued that the ideal non-linearity considered is not realized in practice. It is, however, usual in the analysis of such systems to represent the non-linearity by a power series, and to truncate it at the cubic, so that the first time derivative of only v, v^2 and v^3 remains in the differential equation. If such a simplification is not made, the solution of the oscillator becomes an extremely difficult task. It is considered that such a simplification is a reasonable compromise between utility and complexity. It has also been assumed that the non-linearity is skew-symmetrical about the quiescent operating point, and hence the non-linear quadratic term $d(v^2)/dt$ has been omitted, leaving $d(\gamma v^3)/dt$ as the only non-linear term.

(2.2) The Method of van der Pol for Analysis of the Oscillator with One Injected Sinusoid

If the free behaviour of the oscillator is described by the non-linear differential equation

$$\frac{d^2v}{dt^2} + \frac{d}{dt}(-\alpha v + \gamma v^3) + \omega_0^2 v = 0 \quad . \quad . \quad . \quad (2)$$

where α/ω_0 is small, it may be referred to as a nearly sinusoidal oscillator, and the harmonic content of its output is small: many tuned oscillators can be so described.

Suppose a sinusoid of frequency ω_1 to be injected, such that the forced behaviour of the oscillator is described by the equation

$$\frac{d^2v}{dt^2} + \frac{d}{dt}(-\alpha v + \gamma v^3) + \omega_0^2 v = A\omega_0^2 \sin \omega_1 t \, . \quad . \quad (3)$$

then, if the amplitude A is sufficiently large, and ω_1 is sufficiently close to ω_0, the output will be a single frequency ω_1, again with little harmonic content. Consequently, it might appear reasonable to attempt to solve eqn. (3) by substituting a solution

$$v(t) = b_1 \sin \omega_1 t + b_2 \cos \omega_1 t \quad . \quad . \quad . \quad . \quad (4)$$

This would lead to solutions for b_1 and b_2 in terms of the variables A, ω_1 and the oscillator constants. It may be, however, that such a solution is unstable in the sense that, if the oscillation is made to deviate slightly from this solution, for example owing to noise or changing oscillator parameters, it never returns, but tends to another, stable, state of oscillation.*

In order to be able to establish the stability of the solutions, van der Pol assumed that b_1 and b_2 in eqn. (4) were not constant, but slowly varying functions of time, i.e.

$$v(t) = b_1(t) \sin \omega_1 t + b_2(t) \cos \omega_1 t \quad . \quad . \quad . \quad (5)$$

$b_1(t)$ and $b_2(t)$ can represent the process of divergence from or convergence to the solution given by the constants in eqn. (4). Because $b_1(t)$ and $b_2(t)$ are slowly varying functions of time the following inequalities exist:

$$\frac{\dot{b}_1}{\omega_0} \ll b_1, \quad \frac{\dot{b}_2}{\omega_0} \ll b_2, \quad \frac{\ddot{b}_1}{\omega_0^2} \ll \frac{\dot{b}_1}{\omega_0}, \quad \frac{\ddot{b}_2}{\omega_0^2} \ll \frac{\dot{b}_2}{\omega_0} \quad . \quad . \quad (6)$$

where the dot notation is used to represent differentiation with respect to time.

The method of solution is first to assume that α/ω_0 and $(\omega_0 - \omega_1)/\omega_0$ are small, and to specify that the maximum values of b_1 and b_2 are of the same order as a_0, the free oscillation amplitude, so that it follows from eqn. (6) that $\dot{b}_1/a_0\omega_0$ and $\dot{b}_2/a_0\omega_0$ are small and that $\ddot{b}_1/a_0\omega_0^2$ and $\ddot{b}_2/a_0\omega_0^2$ are very small. Then the solution (5) is substituted in eqn. (3). All terms in which the coefficient is very small, or the product of two small terms, are neglected, as also are terms of frequency $3\omega_1$. All the remaining terms contain $\sin \omega_1 t$ or $\cos \omega_1 t$, and the next step in the analysis is to equate the coefficients of $\sin \omega_1 t$ and $\cos \omega_1 t$ on each side of the equality sign. This results in the following first-order linear differential equations:

$$2\dot{b}_1 + b_2\Delta_1 - \alpha b_1\left(1 - \frac{b_1^2 + b_2^2}{a_0^2}\right) = 0 \quad . \quad . \quad (7)$$

* A useful analogy is a solid pendulum placed with its centre of gravity directly above its axis of rotation; its state is unstable since any slight disturbance displaces it, causing it to seek a position of stable equilibrium, with its centre of gravity directly below the axis of rotation.

$$2\dot{b}_2 - b_1\Delta_1 - \alpha b_2\left(1 - \frac{b_1^2 + b_2^2}{a_0^2}\right) = -A\frac{\omega_0^2}{\omega_1} \simeq -A\omega_0 \quad (8)$$

with $$\Delta_1 = 2(\omega_0 - \omega_1), \quad a_0^2 = 4\alpha/3\gamma \quad . \quad . \quad . \quad (9)$$

where a_0 is the amplitude of free (unforced) oscillation, and where use has been made of the approximation

$$\Delta_1 \simeq (\omega_0^2 - \omega_1^2)/\omega_1$$

By assuming that b_1 and b_2 are constant (i.e. that the output contains only one frequency, ω_1, and hence that the oscillator is synchronized) $\dot{b}_1$ and $\dot{b}_2$ may be put equal to zero. Eqns. (7) and (8) are thereby reduced to simple algebraic form and may be solved to give b_1 and b_2 and hence the output amplitude* of frequency ω_1.

The stability of the solutions is determined by replacing b_1 and b_2 in eqns. (7) and (8) by $b_1 + \delta b_1$ and $b_2 + \delta b_2$, and obtaining linear differential equations for δb_1 and δb_2. The form of the roots of these equations indicates the stability, i.e. whether, in effect, a small disturbance δb_1 of b_1 (say) tends to increase with time (instability) or tends to zero (stability).

The results obtained by van der Pol's method may conveniently be illustrated in a response diagram, as shown in Fig. 2.

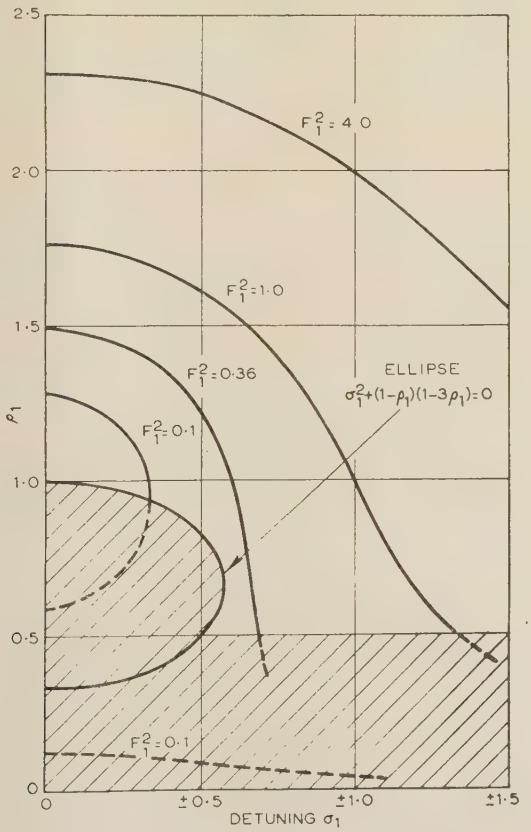

Fig. 2.—Response curves of the forced oscillator described by eqn. (3).
—— Stable solution.
---- Unstable solution.
The region of instability is cross-hatched.

The co-ordinates and the running parameter have been normalized for convenience, according to the following relations:

$$\sigma_1 = \frac{\Delta_1}{\alpha}, \quad \rho_1 = \frac{b_1^2 + b_2^2}{a_0^2}, \quad F_1 = -\frac{A\omega_0}{a_0\alpha} \quad . \quad (10)$$

* The restriction that the maximum values of b_1 and b_2 be of the same order as a_0 is removed if only the steady-state solution for the output amplitude is considered.

The abscissa is a measure of the detuning of ω_1 from ω_0, and the ordinate is proportional to the square of the normalized output amplitude. Sample response curves for various values of the injection amplitude A, and hence of F_1, have been plotted, and the region of instability is indicated by cross-hatching.

The results are described mathematically as follows. The (implicit) expression for the response curves is

$$\rho_1\sigma_1^2 + \rho_1(1 - \rho_1)^2 = F_1^2 \quad . \quad . \quad . \quad . \quad (11)$$

and the region of instability includes the area $\rho_1 < 0\cdot5$ and the area within the ellipse

$$\sigma_1^2 + (1 - \rho_1)(1 - 3\rho_1) = 0 \quad . \quad . \quad . \quad (12)$$

A useful, and explicit, condition for synchronization is found from the stability criteria and eqn. (11) to be

$$2F_1^2 > \sigma_1^2 + 0\cdot25$$
$$\text{or} \quad > 2\sigma_1^2, \text{ whichever is the smaller} \quad . \quad . \quad . \quad (13)$$

The condition $2F_1^2 > 2\sigma_1^2$ (which is approximate) holds for small values of F_1, and the condition $2F_1^2 > \sigma_1^2 + 0\cdot25$ (which is accurate) for large values of F_1.

(2.3) The Method of Andronov and Witt

Assuming the oscillator to be synchronized, the solution can be represented by eqn. (5), with b_1 and b_2 constant. Hence the behaviour of a synchronized oscillator can be represented by one point in a plane with axes b_1 and b_2. From eqns. (7) and (8) it is possible to obtain an expression for db_2/db_1 which defines the direction of motion of the representative point of the oscillator for any values of b_1 and b_2. (The representative point, describing the state of the synchronized oscillator, may move, for example, when the injection amplitude is increased.) In general

$$\frac{db_2}{db_1} = \frac{P(b_1, b_2)}{Q(b_1, b_2)} \quad . \quad . \quad . \quad . \quad . \quad . \quad (14)$$

and if the values of db_2/db_1 at points in the b_1b_2-plane are indicated by 'flow lines', a representation similar to that of Fig. 3 may be obtained. The point representing the state of

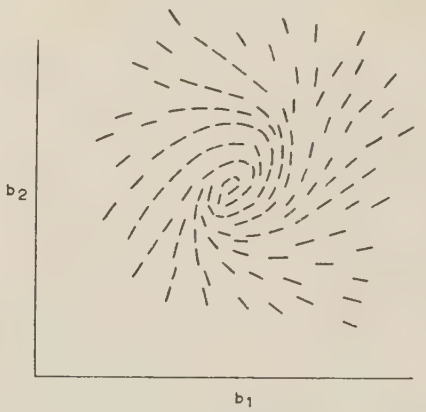

Fig. 3.—Plot of the flow-lines of slope db_2/db_1 in the b_1b_2-plane of the oscillator.

the oscillator will move along the flow lines in its vicinity, and it is possible to place arrows on these flow lines which indicate the direction of movement of the point with the passage of time. It will normally be found that the representative point tends, with time, to a particular point in the b_1b_2-plane. At such a point it is found that the values of P and Q in eqn. (14) are

simultaneously zero, and the point is called a singular point of the first-order differential equation (14). Such a designation also applies, and the condition $P = Q = 0$ holds, at a similar point for which the arrows on the flow lines are reversed, leading away from the point; such a singular point represents an unstable condition.

Andronov and Witt,[6] in the first part of their paper, used the fact that a solution of frequency ω_1 corresponds to a singular point of eqn. (14) to obtain the solutions (the locations of the singular points) and to investigate their stability.

To determine the location of the singular points (for there are usually more than one for a given value of ω_1 and A) P and Q of eqn. (14) are made zero. In the case under consideration it follows from eqns. (7) and (8) that

$$\frac{db_2}{db_1} = \frac{P(b_1, b_2)}{Q(b_1, b_2)} = \frac{-A\omega_0 + \alpha b_2(1-\rho_1) + b_1\Delta_1}{\alpha b_1(1-\rho_1) - b_2\Delta_1} \quad . \quad (15)$$

By equating P and Q to zero the same expressions as were obtained previously by van der Pol's method result for the location of the singular points and also for the output amplitude.

The determination of the stability of the singular points, and hence also of the solutions, of eqn. (15) follows according to the criteria of Poincaré[8] for the stability of singular points of first-order differential equations. Although the conclusions are the same as those arrived at by the method of van der Pol, the approach of Andronov and Witt to the study of the stability of solutions gives a deeper insight into the behaviour of the oscillator.

(3) OSCILLATOR WITH TWO INJECTED SINUSOIDS

The problem under consideration is the behaviour of a synchronized oscillator when the synchronizing signal is accompanied by an interfering signal. Both signals are considered to be sinusoidal. The behaviour of the system is described mathematically by the non-linear differential equation

$$\frac{d^2v}{dt^2} + \frac{d}{dt}(-\alpha v + \gamma v^3) + \omega_0^2 v = A\omega_0^2 \sin\omega_1 t + B\omega_0^2 \sin\omega_2 t \quad . \quad . \quad . \quad . \quad (16)$$

Experiments with an oscillator described approximately by eqn. (16) indicated that the only frequencies of any importance in the output of the oscillator, as judged by their component amplitudes, are ω_1, ω_2 and the intermodulation product $2\omega_1 - \omega_2$. Consequently, following the approach of van der Pol, a solution

$$\left.\begin{aligned} v(t) = {} & b_1(t)\sin\omega_1 t + b_2(t)\cos\omega_1 t \\ & + b_3(t)\sin\omega_2 t + b_4(t)\cos\omega_2 t \\ & + b_5(t)\sin(2\omega_1 - \omega_2)t + b_6(t)\cos(2\omega_1 - \omega_2)t \end{aligned}\right\} \quad . \quad (17)$$

is assumed, the quantities b_1, b_2, b_3, b_4, b_5 and b_6 being slowly varying functions of time.

In order to obtain a simple solution to the problem it is most important to specify the relative magnitudes of the various quantities which appear when the solution (17) is substituted in the non-linear differential equation (16). This was done for the case of one injected signal (Section 2.2) by grouping the quantities under the headings of 'small' and 'very small'. Because of the very large number of quantities under consideration in the present case, it is convenient to separate them into groups which are defined as being small of first, second or third order. Those which are small of first order are of the same order of magnitude as those classed as 'small' in Section 2.2. Those which are small of second order would come under the 'very small' classification of Section 2.2. There is also a group of quantities which are much smaller than those in the 'very small' group; these quantities are said to be small of third order.

So that the order of smallness of the various quantities involved can be specified, the following four assumptions are made:

(*a*) The oscillator is nearly sinusoidal in operation.

(*b*) ω_1 and ω_2 are not far removed from ω_0 (<20% deviation, for example).

(*c*) b_3, b_4, b_5 and b_6 are of an order smaller than b_1 and b_2, i.e. the interference and intermodulation components of the oscillator output are small.

(*d*) The maximum values of b_1 and b_2 are of the same order as a_0.

From these four assumptions it is possible to compile a table (Table 1) showing the order of smallness of the quantities involved in the solution of eqn. (16).

Table 1

DEFINITION OF THE ORDER OF SMALLNESS OF SIGNIFICANT QUANTITIES IN THE ANALYSIS

Small of first order	Small of second order	Small of third order
α/ω_0	$\frac{\dot{b}_3}{a_0\omega_0}$, $\frac{\dot{b}_4}{a_0\omega_0}$	$\frac{\ddot{b}_3}{a_0\omega_0^2}$, $\frac{\ddot{b}_4}{a_0\omega_0^2}$
$\frac{(\omega_0-\omega_1)}{\omega_0}$, $\frac{(\omega_0-\omega_2)}{\omega_0}$		
$\frac{\omega_0-(2\omega_1-\omega_2)}{\omega_0}$	$\frac{\dot{b}_5}{a_0\omega_0}$, $\frac{\dot{b}_6}{a_0\omega_0}$	$\frac{\ddot{b}_5}{a_0\omega_0^2}$, $\frac{\ddot{b}_6}{a_0\omega_0^2}$
$\frac{b_3}{a_0}$, $\frac{b_4}{a_0}$, $\frac{b_5}{a_0}$, $\frac{b_6}{a_0}$	$\frac{\ddot{b}_1}{a_0\omega_0^2}$, $\frac{\ddot{b}_2}{a_0\omega_0^2}$	
$\frac{\dot{b}_1}{a_0\omega_0}$, $\frac{\dot{b}_2}{a_0\omega_0}$		

The assumed solution (17) is substituted in the non-linear differential equation (16). Any terms containing components of frequencies other than ω_1, ω_2 or $2\omega_1 - \omega_2$ are neglected. By equating coefficients of the sine and cosine of $\omega_1 t$, $\omega_2 t$ and $(2\omega_1 - \omega_2)t$ on each side of the equality sign six equations are obtained. In these equations the terms are all of a specified degree of smallness, and in each equation only those terms which are small of the two least orders are retained, i.e. if terms with orders of smallness n, $n+1$, $n+2$ . . . are present, orders n and $n+1$ only are retained. The following equations then result.*

$$2\dot{b}_1 + b_2\Delta_1 - \alpha b_1(1-\rho_1) = 0 \quad . \quad . \quad . \quad (18)$$

$$2\dot{b}_2 - b_1\Delta_1 - \alpha b_2(1-\rho_1) = \frac{-A\omega_0^2}{\omega_1} \simeq -A\omega_0 \quad . \quad . \quad . \quad . \quad (19)$$

$$2\dot{b}_3 + b_4\Delta_2 - \alpha b_3(1-2\rho_1) + \alpha b_5\rho_s + \alpha b_6\rho_m = 0 \quad . \quad . \quad . \quad (20)$$

$$2\dot{b}_4 - b_3\Delta_2 - \alpha b_4(1-2\rho_1) - \alpha b_6\rho_s + \alpha b_5\rho_m = \frac{-B\omega_0^2}{\omega_2} \simeq -B\omega_0 \quad . \quad . \quad . \quad . \quad (21)$$

$$2\dot{b}_5 + b_6\Delta_{12} - \alpha b_5(1-2\rho_1) + \alpha b_3\rho_s + \alpha b_4\rho_m = 0 \quad . \quad . \quad . \quad (22)$$

$$2\dot{b}_6 - b_5\Delta_{12} - \alpha b_6(1-2\rho_1) - \alpha b_4\rho_s + \alpha b_3\rho_m = 0 \quad . \quad . \quad . \quad (23)$$

* An idea of the necessity of specifying the order of smallness of the various quantities involved in the analysis may be gained from the fact that, after substituting eqn. (17) in eqn. (16) and neglecting all the trigonometric functions indicated, there are about 200 terms, including first- and second-order derivatives, whereas, if the smaller terms are neglected as mentioned above, the number of terms is reduced to 50 (before collection and simplification), and there are only first-order derivatives present, as eqns. (18)–(23) show.

where $\Delta_2 = 2(\omega_0 - \omega_2)$, $\Delta_{12} = 2[\omega_0 - (2\omega_1 - \omega_2)]$. (24)

$$\rho_s = \frac{b_1^2 - b_2^2}{a_0^2}, \quad \rho_m = \frac{2b_1 b_2}{a_0^2} \quad . \quad . \quad . \quad . \quad (25)$$

Comparison of eqns. (18) and (19) with eqns. (7) and (8) respectively shows that they are identical, and indicates that, within the accuracy of the assumptions made, the presence of a small-amplitude interfering signal has no effect on the response of the oscillator to the synchronizing signal of frequency ω_1.

Following van der Pol, a steady state is assumed, so that b_1, b_2, b_3, b_4, b_5 and b_6 become constants, and

$$\dot{b}_1 = \dot{b}_2 = \dot{b}_3 = \dot{b}_4 = \dot{b}_5 = \dot{b}_6 = 0 \quad . \quad . \quad . \quad (26)$$

Substituting eqn. (26) in eqns. (18) and (19) the response of frequency ω_1 is obtained, and is identical with that obtained when no interfering signal is present, as seen above. Substitution of eqn. (26) in eqns. (20), (21), (22) and (23) leads to four algebraic equations. These may be solved to obtain expressions for b_3, b_4, b_5 and b_6. As these expressions are rather complicated they are given in the Appendix. Here, as with the case of one injected sinusoid, the condition (*d*) of Section 3, that the maximum values of b_1 and b_2 are of the same order as a_0, is removed for the steady-state solutions. The interest, however, is in the amplitudes of the output components. The amplitude of the component at the synchronizing frequency ω_1 is given by eqn. (11). The output amplitudes at frequencies ω_2 and $2\omega_1 - \omega_2$ have been normalized in the conventional manner with respect to a_0:

$$\rho_2 = \frac{b_3^2 + b_4^2}{a_0^2}, \quad \rho_3 = \frac{b_5^2 + b_6^2}{a_0^2} \quad . \quad . \quad . \quad (27)$$

such that ρ_2 is a measure of the square of the output amplitude of frequency ω_2, and ρ_3 is similarly related to the output of frequency $2\omega_1 - \omega_2$. Using this notation, the expressions for ρ_2 and ρ_3 are found to be

$$\rho_2 = F_2^2 \left\{ \frac{\sigma_{12}^2 + (1 - 2\rho_1)^2}{[\sigma_2^2 + (1 - 2\rho_1)^2][\sigma_{12}^2 + (1 - 2\rho_1)^2] + \rho_1^4 - 2\rho_1^2[\sigma_{12}\sigma_2 + (1 - 2\rho_1)^2]} \right\} \quad . \quad . \quad . \quad . \quad . \quad . \quad (28)$$

$$\rho_3 = F_2^2 \left\{ \frac{\rho_1^2}{[\sigma_2^2 + (1 - 2\rho_1)^2][\sigma_{12}^2 + (1 - 2\rho_1)^2] + \rho_1^4 - 2\rho_1^2[\sigma_{12}\sigma_2 + (1 - 2\rho_1)^2]} \right\} \quad . \quad . \quad . \quad . \quad . \quad . \quad (29)$$

where

$$F_2 = -B\omega_0/a_0\alpha \quad . \quad . \quad . \quad . \quad . \quad (30)$$

$$\sigma_2 = \Delta_2/\alpha, \quad \sigma_{12} = \Delta_{12}/\alpha \quad . \quad . \quad . \quad . \quad (31)$$

Examination of eqn. (28) reveals the most important result that the response to the interfering signal is linear, no matter what the interfering or synchronizing frequency. This fact makes calculation of the response very much easier than if the response had been non-linear.

The equations for ρ_2 and ρ_3 are complicated. This is only to be expected, however, for quite an accurate solution of a non-linear differential equation such as eqn. (16). A useful simplification occurs if $\omega_1 = \omega_0$, i.e. if the synchronizing frequency is the same as the natural frequency of the oscillator. In such a case the simplifying relations $\sigma_1 = 0$ and $\sigma_{12} = -\sigma_2$ may be used. It may then be shown that, as the interference detuning σ_2 is increased, i.e. ω_2 moved away from ω_0, the value of ρ_2 is asymptotic to the simple curve

$$\rho_2 = \frac{F_2^2}{\sigma_2^2 + (1 - 2\rho_1)^2} \quad . \quad . \quad . \quad . \quad (32)$$

The same expressions for b_3, b_4, b_5 and b_6 and hence for ρ_2 and ρ_3 are obtained by the method of Andronov and Witt. The algebraic manipulations involved in arriving at the result are exactly the same; only the theoretical basis of the initial steps differs. Thus in van der Pol's method, putting $\dot{b}_1 = \dot{b}_2 = 0$ because of the assumed steady-state solution, and in the method of Andronov and Witt, putting $P = Q = 0$ because a solution corresponds to a singular point of the differential equation (15).

The above solutions for b_3, b_4, b_5 and b_6 may be shown to be stable both by the method used by van der Pol and by the criteria of Poincaré used by Andronov and Witt.

(3.1) The Discrimination against the Interfering Signal

It is not immediately obvious from eqns. (28) and (11) that the interfering signal can suffer discrimination, but this may be verified by sample calculations and observed experimentally. The discrimination D will be defined by the equation

$$D = \frac{\text{Voltage gain to the synchronizing signal of frequency } \omega_1}{\text{Voltage gain to the interfering signal of frequency } \omega_2} \quad . \quad . \quad . \quad (33)$$

such that, for discrimination to occur, D must be greater than unity. It follows that

$$D = \frac{F_2}{F_1}\sqrt{\frac{\rho_1}{\rho_2}} \quad . \quad . \quad . \quad . \quad . \quad . \quad . \quad (34)$$

and the substitution of eqns. (11) and (28) in eqn. (34) gives the following general expression for the discrimination:

$$D^2 = \frac{[\sigma_2^2 + (1 - 2\rho_1)^2][\sigma_{12}^2 + (1 - 2\rho_1)^2] + \rho_1^4 - 2\rho_1^2[\sigma_{12}\sigma_2 + (1 - 2\rho_1)^2]}{[\sigma_1^2 + (1 - \rho_1)^2][\sigma_{12}^2 + (1 - 2\rho_1)^2]} \quad . \quad . \quad . \quad . \quad (35)$$

Owing to the complexity of this expression, its significance is not immediately apparent. The variation of D with the interference detuning σ_2 is shown graphically in Fig. 4 for various values of σ_1 and ρ_1. With $\omega_1 = \omega_0$, and with infinitesimal difference between the interfering and synchronizing frequencies, such that $\sigma_2 = 0$, the discrimination decreases as ρ_1 (and hence the amplitude of the injected synchronizing signal) is increased; for example, if $\rho_1 = 1{\cdot}5$ [Fig. 4(*a*)], the discrimination is $4{\cdot}8$ dB, rising to $11{\cdot}2$ dB at $\sigma_2 = \pm 1$, whereas, with a larger amplitude of injected synchronizing signal, such that $\rho_1 = 3{\cdot}0$ [Fig. 4(*b*)], the discrimination is $4{\cdot}1$ dB, rising to only $5{\cdot}3$ dB at $\sigma_2 = \pm 1$.

It should be noted that D is a measure of the discrimination against the signal of frequency ω_2, and is not really a measure of the discrimination against interference, since the presence of the intermodulation frequency $2\omega_1 - \omega_2$ in the output may also be said to constitute interference.

At no stage in the solution of the problem has it been assumed that the amplitude of the injected interfering signal is smaller than that of the injected synchronizing signal, i.e. that $B < A$, although in practice this is very often the case. The only assumption made regarding the relative amplitudes of interfering and synchronizing signals refers to conditions at the output of the oscillator. This fact is most important. It would appear, therefore, that if condition (*c*) of Section 3 is satisfied, i.e. if b_3, b_4, b_5 and b_6 are of an order smaller than b_1 and b_2, then it is possible for the injected interfering signal to be of larger

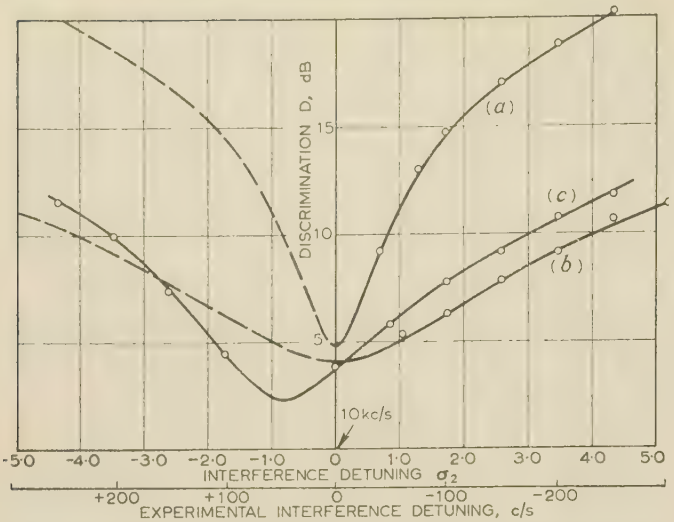

Fig. 4.—Variation of discrimination D with σ_2 for a number of values of σ_1 and ρ_1.

(*a*) $\sigma_1 = 0$, $\rho_1 = 1{\cdot}5$ (symmetrical about $\sigma_2 = 0$)
(*b*) $\sigma_1 = 0$, $\rho_1 = 3{\cdot}0$ (symmetrical about $\sigma_2 = 0$)
(*c*) $\sigma_1 = -1$, $\rho_1 = 2{\cdot}0$

—— Theoretical curve.
Points marked are experimental.

amplitude than the injected synchronizing signal, even though it is of smaller amplitude in the output, the discrimination being due to the selectivity of the tuned circuit together with the non-linearity. For the role of the synchronizing signal to be preserved in such a case, the frequency of the interfering signal would, of course, have to be sufficiently far removed from ω_1, since the discrimination is a minimum when σ_1 and σ_2 are approximately equal, as Fig. 4(*c*) shows. If the frequency of this larger-amplitude 'interfering' signal were made very nearly equal to the 'synchronizing' signal in frequency, the designations 'interfering' and 'synchronizing' would then need to be interchanged.

(4) EXPERIMENTAL VERIFICATION

(4.1) The Circuit

The non-linear differential equation (1) was found to be synthesized quite accurately by the tuned-collector transistor oscillator circuit of Fig. 5. In this circuit, limiting is defined by the non-linear law of two point-contact diodes connected back-to-back.

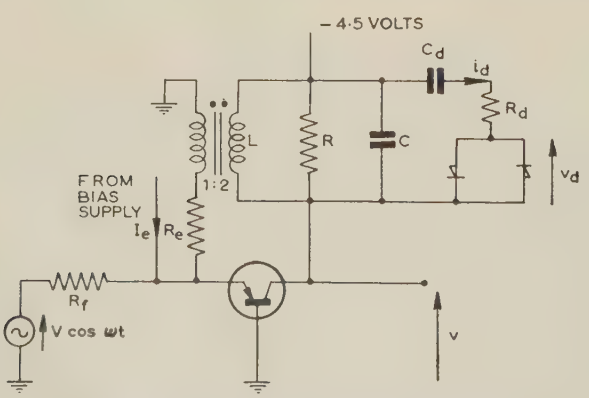

Fig. 5.—The tuned-collector transistor oscillator operating at 10 kc/s.

$R_e = 600\,\Omega$, $R = 4\,\text{k}\Omega$, $R_f = 100\,\text{k}\Omega$,
$L = 6{\cdot}4\,\text{mH}$, $C = 0{\cdot}044\,\mu\text{F}$, $C_d = 2\,\mu\text{F}$.
Transistor type OC71, crystal diodes type CG6E.

It may be shown that maximum regeneration results for a turns ratio of very nearly 2 : α_N, where α_N is the current amplification factor of the transistor; a ratio of 2 : 1 is used in the experimental circuit. The emitter is heavily biased ($I_e \simeq 5\,\text{mA}$) and the amplitude of oscillation of v is kept low (<300 mV peak-to-peak) for two reasons: first to ensure that the non-linearity of the emitter can be neglected, and second so that the non-linear characteristic of the diode limiting circuit may contain no power of v higher than the third.

Assuming that over the region of interest the conduction characteristic of each diode follows the ideal-diode law

$$I = I_s(\varepsilon^{aV} - 1) \quad . \quad . \quad . \quad . \quad . \quad (36)$$

where I and V are the diode forward current and voltage respectively, and I_s and a are constants, then, if V is sufficiently small, eqn. (36) can be approximated by

$$I = I_s\left(aV + \frac{a^2}{2!}V^2 + \frac{a^3}{3!}V^3 + \frac{a^4}{4!}V^4 + \frac{a^5}{5!}V^5\right) \quad . \quad (37)$$

If the two diodes are identical, the conduction characteristic $i_d = f_1(v_d)$ of the two diodes connected back-to-back, as in Fig. 5, can easily be obtained from eqn. (37).* It will contain only the first, third and fifth powers of v_d. To determine the conduction characteristic $i_d = f(v)$ of the back-to-back diodes in series with R_d, the relation $i_d = f_1(v_d)$ must first be inverted to the form $v_d = f_2(i_d)$. From this expression one can proceed to the characteristic $v = f_3(i_d)$ by including the resistance R_d. A final inversion of $v = f_3(i_d)$ to $i_d = f(v)$ gives the required conduction characteristic. It contains only the first, third and fifth powers of v, and an examination of the quintic coefficient shows that the latter can be made zero by setting

$$R_d = 1/18aI_s \quad . \quad . \quad . \quad . \quad . \quad . \quad (38)$$

The conduction characteristic of the limiting circuit then contains only linear and cubic terms, and the behaviour of the experimental oscillator circuit is described quite accurately by eqn. (1). Under these conditions, the values of F and σ are found to be given by†

$$F = \frac{\alpha_N R R_0}{R_f(R - R_0)a_0}V \quad . \quad . \quad . \quad . \quad . \quad (39)$$

$$\sigma = \frac{2CRR_0}{(R - R_0)}(\omega_0 - \omega) \quad . \quad . \quad . \quad . \quad (40)$$

where the subscript 1 or 2 is appended to F, σ, and ω according to whether $V = A$ or B respectively.

The subscript 12 is appended to σ when $\omega = 2\omega_1 - \omega_2$; a_0 is the amplitude of free oscillation; and R_0 is the value of R required just to extinguish oscillations.

(4.2) Measurements

Two point-contact crystal diodes with almost identical characteristics were selected and the required value of R_d to give only a cubic non-linearity was calculated from eqn. (38) to be 1130 ohms. Experiments were carried out with the oscillator of Fig. 5, with a natural frequency of about 10 kc/s and with one injected frequency to ascertain whether this value of R_d resulted in the behaviour described by eqn. (3). The method used was to approximate a theoretical response curve (ρ_1 versus σ_1) experimentally, and compare theoretical and experimental values of F_1 and $\sigma_{1\,crit}$, where $\sigma_{1\,crit}$ is the critical value of σ_1 at which synchronization ceases. The theoretical and experimental curves

* Small symbols are used in the remainder of the discussion, representing time-varying quantities.

† The circuit of Fig. 7 is such that, when F is given by eqn. (39), the approximations indicated in eqns. (8), (19) and (21) do not need to be made.

were adjusted so that they coincided at $\sigma_1 = 0$, and values of F_1 and $\sigma_{1\,crit}$ were obtained for a number of values of R_d. It was found that the best fit between theoretical and experimental values of F_1 and $\sigma_{1\,crit}$ occurred for $R_d = 900$ ohms. For this value of R_d the calculated F_1 was about 2% too low and the calculated $\sigma_{1\,crit}$ about 2% too high. An experimental response curve, with $R_d = 900$ ohms, is shown in Fig. 6, and is seen to agree with theory quite closely; it was therefore decided to use

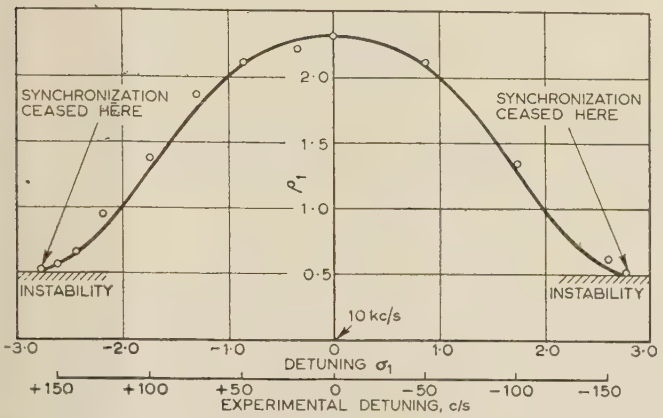

Fig. 6.—Experimental response curve for the oscillator of Fig. 5 with $R_d = 900$ ohms with one injected signal.

Theoretical value of $|F_1| = 2{\cdot}00$.
Experimental value of $|F_1| = 1{\cdot}99$.
—— Theoretical curve.
Points marked are experimental.

the circuit of Fig. 5, with $R_d = 900$ ohms, for the verification of any theory pertaining to a system described by eqn. (1). The condition for synchronization was investigated experimentally and showed reasonable agreement with eqn. (13), as is seen from Fig. 7.

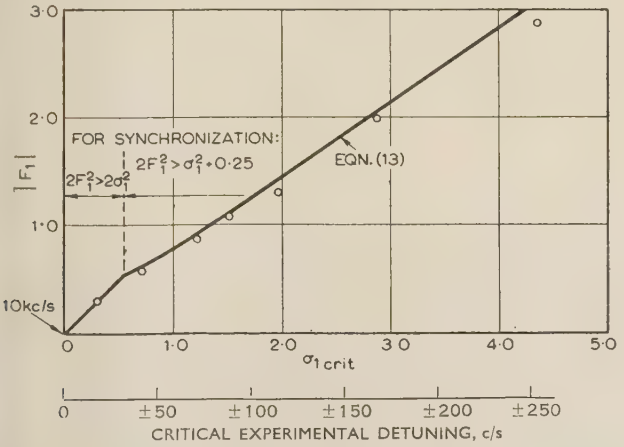

Fig. 7.—Verification of the condition for synchronization of the circuit of Fig. 5 with $R_d = 900$ ohms, showing maximum detuning $\sigma_{1\,crit}$ for synchronization as a function of $|F_1|$.

—— Theoretical curve.
Points marked are experimental.

Experimental results obtained with both a synchronizing and an interfering signal are presented in Figs. 4 and 8, showing excellent agreement with theory. The three graphs of Fig. 4 are of the discrimination D plotted against the interference detuning σ_2 for a number of values of ρ_1 and σ_1. Fig. 8 is a plot of the output level of the intermodulation frequency, relative to the output of the synchronizing signal, to a base of interference detuning σ_2, the output level of the interfering signal being shown

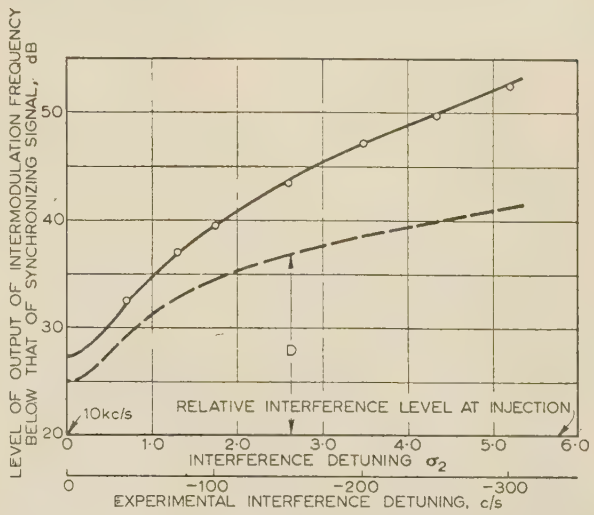

Fig. 8.—Variation of the output of the intermodulation frequency $2\omega_1 - \omega_2$ with σ_2 for the case $\sigma_1 = 0$, $\rho_1 = 1{\cdot}5$.

—— Theoretical curve (symmetrical about $\sigma_2 = 0$).
Points marked are experimental.
---- Theoretical curve of the relative output level of the interfering signal.

for reference. The injected amplitude of the interfering signal was one-tenth of that of the synchronizing signal in the cases considered. The linearity of the response to the interfering signal was, in fact, verified experimentally. In this verification it was found that the linearity ceased to hold when the output amplitude of the interfering signal was greater than 0·4 of the output amplitude of the synchronizing signal. At such an amplitude of the interfering signal condition (*c*) of Section 3 is violated to quite a large degree.

It was verified that, if the interference detuning σ_2 is sufficiently large, the amplitude of the injected interfering signal can exceed that of the synchronizing signal while still allowing discrimination to occur. In the experiment ρ_1 was set at 1·5, and with $\omega_1 = \omega_0$ and the interference detuning σ_2 set nearly equal to 4·0, the discrimination remained sensibly constant as the level of the injected interfering signal was raised from 20 dB below to 10 dB above that of the synchronizing signal.

(5) CONCLUSIONS

A solution has been obtained for the non-linear differential equation (16), representing the synchronization of an oscillator in the presence of interference, and an expression for the discrimination against the interfering signal has been derived. The discrimination is expressed as a continuous function for frequency separations ranging from zero (i.e. infinitesimal) to some 20% of the natural oscillation frequency. Under the assumptions made, the response to the interfering signal is shown to be linear. The validity of the method of solution and its accuracy have been verified experimentally, very close agreement between measured and theoretical results having been obtained. Moreover, the assumptions made are considered to be realistic in practice.

Experimental results also appear to indicate that the simple circuit of Fig. 5 is a suitable electrical analogue of the non-linear differential equation (1) and may therefore be useful in any experimental investigations of systems described by eqn. (1), electrical or otherwise.

(6) ACKNOWLEDGMENTS

The authors wish to express their gratitude to Mr. C. M. Phillips of the Signals Research and Development Establishment, Ministry of Supply, for his continued encouragement of

the research reported herein. Robert Spence is gratefully indebted to The Institution of Electrical Engineers for the award of the Swan Memorial Scholarship.

(7) REFERENCES

(1) TUCKER, D. G.: 'The Synchronization of Oscillators', *Electronic Engineering*, 1943, **15**, pp. 412 and 457; 1943, **16**, pp. 26 and 114.
(2) TUCKER, D. G.: 'Forced Oscillations in Oscillator Circuits and the Synchronization of Oscillators', *Journal I.E.E.*, 1945, **92**, Part III, p. 226.
(3) TUCKER, D. G.: 'Non-linear Regenerative Circuits', *Wireless Engineer*, 1947, **24**, p. 178.
(4) TUCKER, D. G., and JAMIESON, G. G.: 'Discrimination of a Synchronized Oscillator against Interfering Tones and Noise', *Proceedings I.E.E.*, Monograph No. 146 R, March, 1956 (**103** C, p. 129).
(5) VAN DER POL, B.: 'Forced Oscillations in a Circuit with Non-linear Resistance', *Philosophical Magazine*, 1927, **3**, p. 65.
(6) ANDRONOV, A., and WITT, A.: 'Zur Theorie des Mitnehmens von van der Pol', *Archiv für Elektrotechnik*, 1930, **24**, p. 99.
(7) STOKER, J. J.: 'Nonlinear Vibrations' (Interscience Publishers, New York, 1950).
(8) STOKER, J. J.: *Ibid.*, p. 152 and pp. 26–45.

(8) APPENDIX

The expressions for b_3, b_4, b_5 and b_6 are found to be:

$$\frac{b_3}{a_0} = F_2\left[\frac{f\rho_1^2 - e(f^2+g^2)}{(e^2+g^2)(f^2+g^2) + \rho_1^4 - 2\rho_1^2(fe+g^2)}\right] \quad (41)$$

$$\frac{b_4}{a_0} = F_2\left[\frac{g\rho_1^2 - g(f^2+g^2)}{(e^2+g^2)(f^2+g^2) + \rho_1^4 - 2\rho_1^2(fe+g^2)}\right] \quad (42)$$

$$\frac{b_5}{a_0} = F_2\left[\frac{d\rho_1^2 - g(gd+ce) - f(-gc+ed)}{(e^2+g^2)(f^2+g^2) + \rho_1^4 - 2\rho_1^2(fe+g^2)}\right] \quad (43)$$

$$\frac{b_6}{a_0} = F_2\left[\frac{-c\rho_1^2 + f(gd+ce) - g(-gc+ed)}{(e^2+g^2)(f^2+g^2) + \rho_1^4 - 2\rho_1^2(fe+g^2)}\right] \quad (44)$$

where

$$\left.\begin{aligned} c &= \rho_s \\ d &= \rho_m \\ e &= \sigma_2 \\ f &= \sigma_{12} \\ g &= 1 - 2\rho_1 \end{aligned}\right\} \quad (45)$$

Note that

$$\rho_s^2 + \rho_m^2 = \rho_1^2 \quad (46)$$

and also that the denominators of eqns. (41), (42), (43) and (44) are identical.

621.311.1.016.35: 621.372.5

The Institution of Electrical Engineers
Monograph No. 308 S
July 1958
©

THE ENERGY-INTEGRAL CRITERION OF TRANSIENT STABILITY LIMITS OF POWER SYSTEMS

By P. D. AYLETT, Ph.D., M.Sc.(Eng.), Wh.Sc., Associate Member.

(*The paper was first received 27th February, and in revised form 8th May*, 1958. *It was published as an* INSTITUTION MONOGRAPH *in July*, 1958.)

SUMMARY

Methods have been devised, in the study of second-order non-linear differential equations, for identifying the nature of the phase-plane trajectories, without having to find the solutions to the equations. These methods are applied to determine the transient stability limits for a power system with two machines and are shown to be equivalent to establishing the energy integrals of the system. Formulae are derived for the critical switching time taking resistance into account. The methods are then generalized for multi-machine systems both with and without an infinite busbar, and the energy integrals are given. The application of these integrals, in conjunction with step-by-step integration, to find the critical switching time for a fault is described. An example of a three-machine system solved by the conventional and by the new methods is given.

LIST OF SYMBOLS

θ = Rotor angle, rad.
$\dot{\theta} = v$, velocity of slip with respect to synchronous speed, rad/s or rad/(generalized time unit).
t = Time, sec.
τ = Generalized time.
B = Generalized mechanical torque.
T_{mr} = Mechanical torque per unit of the rth machine.
T_{mr} = Electrical torque per unit of the rth machine.
M_r = Inertia constant, kW-sec^2/kVA radians of the rth machine.
V_r = Voltage per unit behind transient reactance of the rth machine.
Z_{rr} = Driving-point impedance.
Z_{pr} = Transfer impedance.
ϕ_{pr} = Complement of impedance angle.

(1) INTRODUCTION

When a power system is being designed it is usual to attempt to establish by means of analytical procedures that the system has adequate transient stability margins. The method of doing this, which has been well described in the literature,[1] amounts to the solution of the simplified electro-dynamical differential equations of the system by means of numerical step-by-step integration. The solutions obtained are in terms of the machine rotor angles as functions of time. When the relative rotor angles appear to be increasing indefinitely, the system is said to be unstable, and when they appear to be going towards zero the system is said to be stable. When there are more than two machines there is, at present, no definite criterion for stability. In this paper, a new approach has been made to the subject, based upon the methods used in the study of non-linear mechanics. The electro-dynamical equations of a power system are non-linear, but by finding the singular points of the differential equations, and obtaining an energy integral, a definite criterion for stability may be obtained. This appears as a generalization of the well-known equal-angle criterion for two machines, but in order to obtain solutions in systems with many machines certain approximations are necessary.

The use of the energy-integral method has several advantages. First, a definite value is obtained for the time in which a fault must be cleared by carrying out only one forward integration. Secondly, the stability or otherwise of the system can be determined mathematically, instead of attempting to assess the general nature of the solution from the slope of the rotor-angle/time curves. Perhaps the most important fact is that the new approach provides a basis for future theoretical work in a field where empirical methods have hitherto been the rule. The application of these methods to a two-machine case is first developed, in order to provide a simple basis for extension of the ideas to systems with many machines.

(2) TRANSIENT STABILITY, TWO-MACHINE CASE

(2.1) Nature of Problem

Transient stability problems involve consideration not of the solutions of the differential equations for a system, but of the general nature of these solutions. The problem is thus particularly suitable for investigation by topological methods developed in the field of non-linear mechanics.[2,3] Results for second-order non-linear differential equations are well established, and the two-machine system, subject to the usual assumption of constant flux leakages in the machines, is characterized by equations of this type.

The differential equations for any system with no more than two synchronous machines can be reduced to the form

$$\ddot{\theta} = B - \sin\theta \quad . \quad . \quad . \quad . \quad . \quad . \quad (1)$$

(see Appendix 7.1)

where differentiation is carried out with respect to a generalized time variable.

Introducing the slip velocity v, this may be written

$$v\frac{dv}{d\theta} = B - \sin\theta \quad . \quad . \quad . \quad . \quad . \quad (2)$$

and integrating,

$$\frac{v^2}{2} = B\theta + \cos\theta - B\theta_0 - \cos\theta_0 \quad . \quad . \quad . \quad (3)$$

when the initial conditions are

$$v = 0, \theta = \theta_0$$

(2.2) Phase-Plane Trajectories

Eqn. (3) expresses the law of conservation of energy for the system, that kinetic energy, $v^2/2$, and potential energy $(-B\theta - \cos\theta)$ are together equal to a constant $(-B\theta_0 - \cos\theta_0)$.

In the nomenclature adopted by writers in the field of non-

Correspondence on Monographs is invited for consideration with a view to publication.

Dr. Aylett was formerly with the Central Electricity Generating Board, and is now Head of the Department of Electrical Engineering, Brunel College of Technology.

linear mechanics, the plane of the variables v, θ, is the phase plane, and a curve corresponding to eqn. (3) is a phase-plane trajectory.

It will be noticed that the phase-plane trajectories, as the name implies, are not solutions to the differential equation (1), since time does not appear as a variable. A trajectory is the path of a representative point. There is an infinity of solutions corresponding to different time origins for a given trajectory. The motion of a representative point along a trajectory corresponds to one of the solutions.

Two types of trajectories can be obtained, normal trajectories and degenerate trajectories, or singular points. For all normal trajectories $dv/d\theta$ is determinate, but for a singular point $dv/d\theta$ is indeterminate. Thus the singular points for eqn. (2) occur at

$$v = 0, B - \sin\theta = 0 \quad . \quad . \quad . \quad . \quad . \quad (4)$$

as can be seen from eqn. (2).

The singular points correspond to points of stable and unstable equilibrium. If,

$B > 1$, there are no singular points.
$B = 1$, there is one singular point at $\theta = \pi/2$.
$B < 1$, there are two singular points, P_1 and P_2 given by $\theta_1 = \arcsin B$ and $\theta_2 = \pi - \arcsin B$.

Poincaré[4] has shown how to classify the singular points of both conservative and dissipative systems of the second order. In this case θ_1 is a point of stable equilibrium, a vortex point, and θ_2 is a point of unstable equilibrium, a saddle point.

The nature of the phase-place trajectories for $B < 1$ is shown in Fig. 1. These trajectories are obtained from eqn. (3), each

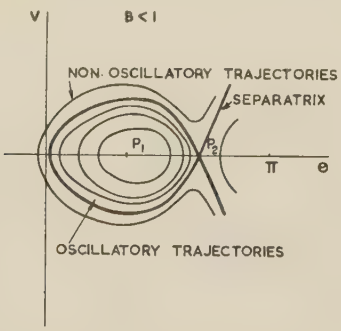

Fig. 1.—Phase-plane trajectories for two-machine case.

trajectory corresponding to different values of θ_0. Three kinds of trajectory can be distinguished; those around the point of stable equilibrium, P_1, which are oscillatory; those approaching the point of unstable equilibrium, P_2, which are non-oscillatory; and a single trajectory which enters P_2. This last trajectory divides the region of oscillatory trajectories from the region of non-oscillatory trajectories, and is called the separatrix.

(2.3) The Critical Switching-Time Problem

(2.3.1) The Critical Switching-Angle.

The critical switching-angle problem is the one which occurs most frequently. It arises as follows:

'A power system is in a condition of stable equilibrium and the accelerations are zero. A fault occurs on the electrical system changing the parameters of the differential equation. In practical cases the electrical power output is reduced, and with the mechanical power input remaining the same, the machines will accelerate. After a certain interval of time, the fault is cleared from the system and the differential equation has a third set of parameters.'

This is the system whose stability must be investigated. The effect of the fault is to give the machine a certain velocity and angle when projected into the final unfaulted condition.

The problem is illustrated in Fig. 2. Initially the velocity is

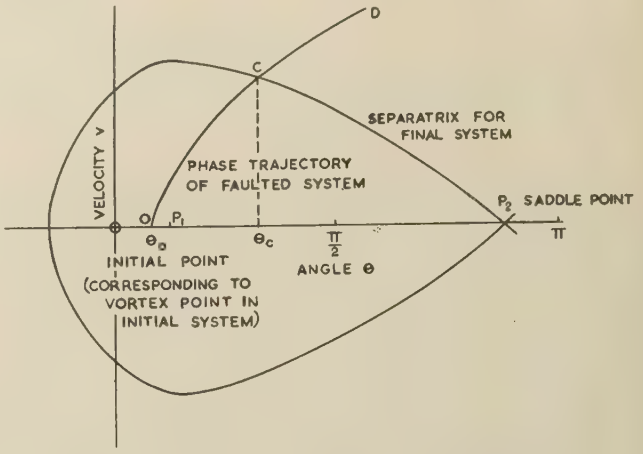

Fig. 2.—Critical switching angle.

zero, and the system parameters are such that $B = B_0$. The initial angle is therefore

$$\theta_0 = \arcsin B_0 \quad . \quad . \quad . \quad . \quad . \quad . \quad (5)$$

There is then a fault and B becomes larger, changing from B_0 to B_f, where B_f is usually greater than unity. The representative point follows the phase trajectory for the faulted system OCD. The fault is now cleared and B becomes B_c less than unity. If the representative point is on the portion of the trajectory OC at this time, it will follow an oscillatory trajectory, but if it is on the portion CD, a non-oscillatory trajectory. If it is at C at the clearing time, it will follow the separatrix to the saddle point P_2, which, however, it will not reach in a finite time. The angle θ_c corresponding to a point C is the critical switching angle. An expression for this angle, derived in Appendix 7.1, is

$$(B_f - CB_c)\theta_c + \cos\theta_c - C\cos(\theta_c - \phi_c)$$
$$= B_f\theta_0 - CB_c(\pi - \theta_{1c} + \phi_c) + \cos\theta_0 + C\cos\theta_{1c} \quad . \quad (6)$$

This equation cannot be directly solved in the general case, but often the quantities $(B_f - CB_c)$ and ϕ_c will be small, and an iterative method may be used to find a good approximate solution quickly. It is shown in Appendix 7.1 that, for certain cases, eqn. (6) reduces to the expression

$$(1 - C)\cos\theta_c = \cos\theta_0 + C\cos\theta_{1c} - B_f[\pi - (\theta_0 + \theta_{1c})] \quad . \quad (7)$$

which corresponds to that given in Reference 1 for the case where there is no resistance.

The critical switching angle has been found, but it is the critical switching time which is required. This is the time required for the representative point to traverse the trajectory OCD in Fig. 2 from O to C.

(2.3.2) Approximate Formulae for the Critical Switching Time

The differential equation of the system under fault conditions is given by

$$\frac{d_2\theta}{d\tau^2} = B_f - \sin\theta \quad . \quad . \quad . \quad . \quad . \quad (8)$$

It is required to find the solution of $\tau = F(\theta)$ and to find the value τ_c corresponding to

$$\tau_c = F(\theta_0) - F(\theta_c) \quad . \quad . \quad . \quad . \quad . \quad (9)$$

where θ_c is determined by eqn. (6).

Also
$$\tau_c = \int_{\theta_0}^{\theta_c} \frac{d\theta}{v} \quad . \quad . \quad . \quad . \quad . \quad . \quad (10)$$

Integrating eqn. (8) once and substituting in eqn. (10)

$$\tau_c = \frac{1}{\sqrt{2}} \int_{\theta_c}^{\theta_0} \frac{d\theta}{\sqrt{(B_f\theta + \cos\theta - B_f\theta_0 - \cos\theta_0)}} \quad . \quad (11)$$

The expression cannot be integrated, except for the case where $B_f = 0$, when an expression in terms of elliptic integrals is obtained. In general, either an approximate, numerical or mechanical method of integration must be used. Numerical step-by-step integration is well known, and the method that will be presented here consists in replacing the expression under the root sign in eqn. (11) by another expression which can be integrated.

In practical problems, the range of integration θ_0 to θ_c is less than π, and over this range the cos θ term may be expanded as a power series in θ.

In addition, in almost all generator problems $0 > \theta_0 > \frac{\pi}{2}$, and if τ_c is not to be infinite, $B_f\theta_c$ must be greater than 0·725.

This means that the cos θ term may be replaced by the series terminated at θ^2, and this will give a sufficiently accurate solution in practical cases. If a higher degree of accuracy is required the series may be carried to the terms of the third and fourth power, when solutions in terms of elliptic integrals will be obtained.

The details of the quadratic approximation are given in Appendix 7.1, and the formula for the switching time is found to be

$$\tau_c = \sqrt{\frac{2}{a}}[\arccos\sqrt{R}/(R + \theta_m)] \quad . \quad . \quad . \quad (12)$$

where
$$\theta_m = (\theta_c - \theta_0)/2$$

$$a = \frac{\sin(\theta_m + \theta_0)\sin\theta_m - 2\sin(\theta_m/2 + \theta_0)\sin\theta_m/2}{\theta_m^2} \quad . \quad (13)$$

and
$$R = \frac{B_f\theta_m - \sin(\theta_m + \theta_0)\sin\theta_m}{2a\theta_m}$$

Eqns. (6), (12) and (13) enable the critical switching time to be calculated for any two-machine system where there is only one change of system connections following the fault.

(2.3.3) Use of Step-by-Step Integration in Conjunction with the Energy Integral.

The method described above of finding τ_c is not easily applied when there are two or more system changes subsequent to fault. In system studies, these conditions arise when there is sequential clearance of circuit-breakers, or reclosure following fault clearance. In order that these problems may be investigated easily, a new method of deciding the stability status of a trajectory is introduced here, and it will later be generalized for systems containing more than two machines. It has been shown in Section 2.2 that, if the representative point is within the area bounded by the separatrix at the instant of switching, it will follow a stable trajectory, and if outside, an unstable trajectory. If the representative point is on the boundary at the time of switching, this is the critical switching time.

The separatrix represents a particular solution of the differential equation in the phase-plane, and this solution can be expressed as an energy relationship. The differential equation for the unfaulted system can be written

$$M\ddot{\theta} = T_{mc} - T_{ec}\sin(\theta + \phi_c) \quad . \quad . \quad . \quad . \quad (14)$$

The reduction of the general two-machine system to this form is shown in Appendix 7.1.

The saddle point is at

$$\theta'_{1c} = \pi - \arcsin(T_{ec}/T_{mc}) - \phi_c = \pi - \theta_{1c} - \phi_c$$

Multiply eqn. (14) by $\dot{\theta}$, and integrating with θ and θ_{1c} as limits,

$$Mv^2/2 = T_{mc}\theta + T_{ec}\cos(\theta + \phi_c) - T_{mc}(\pi - \theta_{1c} - \phi_c) + T_{ec}\cos\theta_{1c} \quad . \quad (15)$$

where
$$\theta'_{1c} = \arcsin(T_{ec}/T_{mc})$$

The energy equation (15) is satisfied on the separatrix, and the corresponding energy curve is given in Fig. 3.

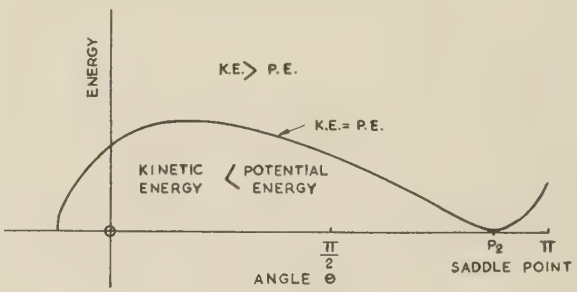

Fig. 3.—Energy curve.

Writing eqn. (15) in a new form with an arbitrary constant A

$$\frac{Mv^2}{2} - [T_{mc}\theta + T_{ec}\cos(\theta + \phi_c) - T_{mc}(\pi - \theta_{1c} - \phi_c) + T_{ec}\cos\theta_{1c}] = A \quad . \quad (16)$$

The instant of changing to the unfaulted system will be characterized by certain definite value of v and θ, and if these are substituted in eqn. (16) a value for A will be obtained.

If A is zero, eqn. (15) is satisfied, and this must be the critical switching time. Since the kinetic energy term is always positive it is clear that A must take negative to positive values when passing from the stable to the unstable region. The criterion of stability is thus given by

$A < 0$—stable
$A = 0$—critical
$A > 0$—unstable

The general method of solving a two-machine transient stability problem is, for the final unfaulted system, as follows:

(*a*) Find the saddle point.

(*b*) Establish the energy equation, giving a zero of energy (a minimum) at the saddle point.

(*c*) Substitute appropriate values of v and θ from the faulted system and test for stability by eqn. (16).

The use of the energy integral in this way can greatly reduce the amount of step-by-step integration necessary, since a solution need be carried on only until the instant corresponding to the critical switching time. In addition, a definite criterion for stability is available, and this means that only one forward integration need be carried out to obtain a result which is definite.

Most transient stability problems involve more than two

machines. In the next Section, therefore, this method will be generalized for multi-machine systems.

(3) TRANSIENT-STABILITY MULTI-MACHINE SYSTEMS

(3.1) General

In testing a power system for transient stability, either by using a network analyser or by calculation, a fault is assumed of a certain duration, and the motion of the machine is calculated by step-by-step integration forward in time. In general, the mechanical powers are fixed prior to the fault and cannot satisfy the condition that the accelerations become zero. Thus the system is said to be stable if the relative accelerations appear to be tending to zero. There has been no precise criterion available such as was obtained for the two-machine problem, and conclusions concerning stability have been obtained by judgment and experience. Certainly if two step-by-step integrations are carried out for different fault durations, two fault times can be found, such that the relative machine angles, during the first 360° in one case, appear to go on to small values, and in the other, to go to continuously increasing values. In the two-machine problem it has been shown that the phase-plane is divided into a zone of stable and unstable trajectories for certain values of a parameter B. The terms 'stable' and 'unstable' refer to the type of trajectory from the point of view of the synchronous operation of the power system—both trajectories are stable in the mathematical sense. It appears likely that some similar division exists for the $2(n-1)$ dimensional phase space of an n-machine system. Indeed, the fact that the transient-stability problem is posed at all presupposes such a division of the phase space into stable and unstable zones. It would be expected that the surface of division, the separatrix, in the phase space passes through the saddle point or rather a point analogous to the saddle point of the two-machine system. If the integral can be found to give the equation of the separatrix, this can be used to test for stability by the method given in Section 2.3.3.

The extension of these concepts to multi-machine systems is beset by many difficulties. There exists no general mathematical background such as has been provided by Poincaré and other workers for two-variable systems. The simple ideas cannot merely be used without development since multi-machine systems produce new phenomena not existing in two-machine system. Three difficulties arise: first, it is difficult to find the singular points; secondly, many singular points exist, and a special one of these must be identified; thirdly, it is only possible to carry out an exact integration where there is no resistance in the system. The difficulties can be met in various ways, and it will be shown that practical use can be made of these new energy methods.

(3.2) The Energy Integral

(3.2.1) Systems with Finite Inertia.

The differential equations for an n-machine system may be written in the form

$$M_r\ddot{\theta}_r = T_{mr} - T_{er} \quad . \quad . \quad . \quad . \quad . \quad (17)$$

where there are n equations, with values of r from 1 to n.

Now
$$T_{er} = \sum_{p=1}^{p=r-1} S_{rp} - S_{rr} + \sum_{p=r+1}^{p=n} S_{rp} \quad . \quad . \quad . \quad (18)$$

where
$$S_{rp} = \frac{V_r V_p}{Z_{rp}} \sin(\theta_r - \theta_p - \phi_{rp}) \quad . \quad . \quad . \quad (19)$$

where p takes values from 1 to n.

A set of $n(n-1)/2$ relative acceleration equations can be established from the set of n eqns. (17) by combining every possible pair of equations.

Consider for example the rth and pth equations of the n set. Multiply the rth equation by M_p and the pth equation by M_r and subtract,

$$M_pM_r(\ddot{\theta}_r - \ddot{\theta}_p) = M_pT_{mr} - M_rT_{mp} - M_pT_{er} + M_rT_{ep} \quad . \quad (20)$$

Now $n(n-1)/2$ equations of this type can be established. If each equation is multiplied by the integration factor for the left-hand side $\dot{\theta}_{rp}$, and the whole set is added together, an integrated expression can be found of the form,

$$\sum_{r=1}^{r=n-1}\sum_{p=r+1}^{p=n} \frac{M_pM_r}{2\sum_{r=n}^{r=n} M_r}\dot{\theta}_{rp}^2 = \sum_{r=1}^{r=n-1}\sum_{p=r+1}^{p=n} \frac{(M_pT_{mr} - M_rT_{pm})}{\sum_{r=1}^{r=n} M_r}\theta_{rp}$$

$$+\int_{\theta_0}^{\theta}\sum_{r=1}^{r=n-1}\sum_{p=r+1}^{p=n}\left[M_p\sum_{p=1}^{p=n}\frac{E_rE_p}{Z_{rp}}\sin(\theta_r - \theta_p - \phi_{rp}) - M_r\sum_{r=1}^{r=n}\frac{E_rE_p}{Z_{rp}}\sin(\theta_p - \theta_r - \phi_{rp})\right]\dot{\theta}_{rp}d\tau \quad . \quad (21)$$

It should be noted that the terms $p = r$ in the integral produce constant terms. These should be written with a minus sign. It will be found in practice that part of this integral can be found directly, i.e. where the p's and r's in one sine term equal the r's and p's in the other.

There are $n(n-1)^2$ terms under the integral sign of the right-hand side of the equation, and of these, $n(n-1)$ terms can be exactly integrated, i.e. $1/(n-1)$ of the whole number of terms. Thus for two machines all the terms may be integrated, for three, one half of the terms, for four, one third of the terms, and so on. In fact, the situation is rather more favourable than this, because of the terms that cannot be integrated exactly, each pair of θ_{pr} and θ_{rp} form the equivalent to a single term of the kind that can be integrated. Thus, for three machines, there are 12 terms, of which six can be exactly integrated and the remaining six terms become three terms if certain of the ϕ_{pr} terms are neglected; thus the two-thirds of the final terms can be directly integrated without approximation. In general $2/n$ of the terms of the final expression can be integrated exactly, and the remainder approximately.

The integral can be found directly, and eqn. (21) can be much simplified if all the small angles ϕ_{pr} are neglected. If at the same time the values of the mechanical power T_{mr} are changed so that eqn. (20) is satisfied at the critical point, the integral will be correct at this point. It is not thought that this assumption will produce large errors in the integral since each of the angles ϕ_{pr} appears also as $\phi_{rp}(= -\phi_{pr})$.

As an example, the integral for a three-machine system is given in Appendix 7.2.

For all $\phi_{pr} = 0$ the corresponding general expression is

$$\sum_{r=1}^{r=n-1}\sum_{p=r+1}^{p=n}\frac{M_pM_r}{2\sum_{r=n}^{r=n} M_r}\dot{\theta}_{rp}^2 = \sum_{r=1}^{r=n-1}\sum_{p=r+1}^{p=n}\frac{V_rV_p}{Z_{rp}}[\sin\theta_{rpc}(\theta_{rp} - \theta_{rpc}) + \cos\theta_{rp} - \cos\theta_{rpc}] \quad . \quad . \quad . \quad . \quad (22)$$

(3.2.2) System with an Infinite Inertia.

If the velocity of one of the machines in the system is fixed, absolute, rather than relative accelerations determine the stability criteria. In practice, this arises when a small power system is connected to a large power system. The machines in the large system can be assumed to have infinite inertia, or at certain points there is assumed to be an infinite busbar. Under this

circumstance the general expression (22), derived when all the ϕ_{pr} were assumed to be zero and the mechanical powers are changed to satisfy eqn. (17), reduces to

$$\sum_{r=1}^{r=n} \frac{M_r\theta_r^2}{2} = \sum_{r=1}^{r=n-1}\sum_{p=r+1}^{p=n} \frac{V_rV_p}{Z_{rp}}[\sin\theta_{rpc}(\theta_{rp}-\theta_{rpc})+\cos\theta_{rp}-\cos\theta_{rpc}] \quad . \quad . \quad . \quad . \quad (23)$$

(3.3) Singular Points of the Differential Equations for Multi-Machine Systems

The singular points are obtained by equating eqn. (20) to zero, and then solving the equations for the $(n-1)$ independent θ variables.

In order to employ the energy integrals usefully it is necessary to find, and generally classify, the singular points. This has been done for the equivalent of a two-machine system but higher-order systems have been little explored. In these systems a large number of singular points may be found. A three-machine system with no resistance, for example, has been found to have as many as six singular points for certain values of the parameters.

Only the singular point which displays stable vortex properties for all variables will give a point of stable equilibrium for the power system. The other singular points will display saddle-type or unstable vortex-type properties. It is a particular saddle-type point which is required in order to find the constant for the energy integral.

(3.3.1) Finding the Singular Points.

The singular points can be found by graphical methods for a three-machine system or by using a network analyser for all systems.

The problem is to solve the simultaneous eqns. (20) when the left-hand sides are zero. The network analyser is simple to use where the absolute accelerations are to be zero because then $T_{er} = T_{mr}$. However, where the relative accelerations are required to be zero, the network analyser must be balanced for some absolute acceleration a, which is constant for all machines but different for each singular point, so that for the rth machine,

$$\frac{T_{mr}-T_{er}}{M_r} = a$$

An example given later shows that this can be done with reasonable accuracy on a network analyser for a three-machine system. For systems with more machines, some modification could be made to the analyser to facilitate the work. Where there is an infinite busbar in the system, eqn. (17) applies, $a = 0$, and balancing becomes a simple matter.

(3.3.2) Identification of Singular Points.

There exists a large literature on the classification of singular points in the sense that this reduces to the problem of finding the extrema of the potential-energy expression and distinguishing the various types of extrema (maximum, minimum and saddle-type). In practice, it is required not so much to distinguish between maximum, minimum and saddle points, but to decide which of a number of saddle points should be used to define the constant of integration of the energy integral. This can only be settled by considering the topology of the phase-plane trajectories in a particular case. To explore the whole phase-plane (or space) is a large undertaking, and it is suggested that the following practical rules will enable the correct saddle point to be found.

(*a*) Set the equations, and select the variables so that the T_{mr}'s are, as far as possible, positive. In a given case some of the T_{mr}'s may be negative, but the sense of the variables should be selected so that the equations reduce predominantly to the form in which T_{mr} is positive and T_e is negative. It is clearly necessary for stability to be possible, for the mechanical torques to be a driving force, and the electrical torques to be a resisting force.

(*b*) The saddle point to be selected is that which gives a maximum angle in the positive direction of the variables.

It is appreciated that the selection of the correct saddle point may be difficult in some cases. It is considered that some more definite criterion can be developed if further work is undertaken.

(3.4) Energy Integral in Transient Stability Studies

The method is a generalization of that already presented for two machines in Section 2.3.3. The energy integral for the n-machine case as developed in Section 3.2 specifies a $2(n-1)$-degree surface. If this surface passes through a saddle point it will, under certain conditions, separate the regions of stable and unstable trajectories in the phase space, i.e. it will be the separatrix.

The transient-stability problem consists in determining the position of the representative point of the system with respect to the separatrix. It is required to find whether the representative point is in the region of stable or unstable trajectories, i.e. whether it is inside or outside the separatrix. This is not difficult to determine since the kinetic-energy term of the energy integral is always positive.

The separatrix is given by eqn. (22), where θ_{rpc} then represents the co-ordinates of the saddle point.

Consider a system subject to a disturbance. At some time t, the system velocities and angles are given by $\dot{\theta}_{rpo}$, θ_{rpo}, and the system has been changed to the configuration used to determine eqn. (22) above.

Substituting the velocity and angle in eqn. (22) and rewriting the equation in a new form with a constant A on the right-hand side,

$$\sum_{r=1}^{r=n-1}\sum_{p=r+1}^{p=n} \frac{M_pM_r}{2\sum_{r=1}^{r=n} M_r}\dot{\theta}_{rpo}^2 - \sum_{r=1}^{r=n-1}\sum_{p=r+1}^{p=n} \frac{V_rV_p}{Z_{rp}}[\sin\theta_{rpc}(\theta_{rpo}-\theta_{rpc})+\cos\theta_{rpo}-\cos\theta_{rpc}] = A \quad . \quad (24)$$

If $A < 0$ the system will be stable,
$A = 0$ the system will be critical,
$A > 0$ the system will be unstable.

The particular form of the integral used is immaterial. The form based upon absolute accelerations could equally well have been used if the system had an infinite busbar, and a rather simpler expression would have been obtained.

(3.5) Example of the Use of the Energy Integral

The example is of a three-machine transient-stability study, and the system to be studied with its initial conditions, as set up on a network analyser, is shown in Fig. 4(*a*). In order to check the method, the problem was first solved by step-by-step integration in the conventional fashion. The swing curve for a fault clearance time of 0·15 sec and reclosure of the line at 0·325 sec is given in Fig. 4(*b*). This appears to be just unstable. The results of a swing calculation for a fault clearing time of 0·15 sec and reclosure in 0·30 sec appeared to give a stable condition.

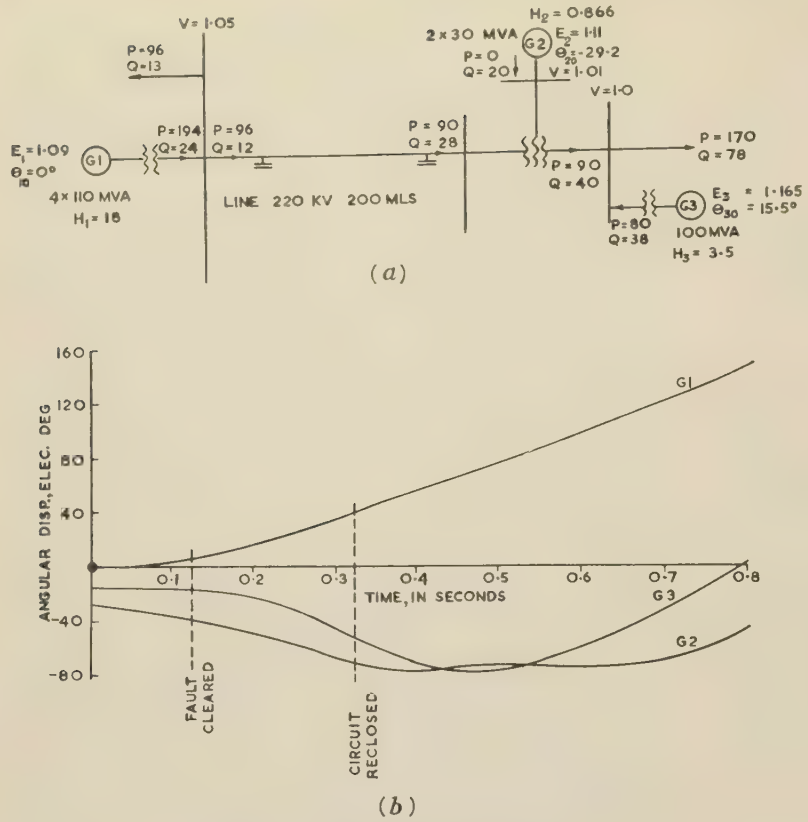

Fig. 4.—Three-machine problem.
(*a*) Initial conditions.
(*b*) Swing curves.

The following procedure must be adopted in order to use the energy-integral method of solving the critical switching-time problem.

(*a*) Set up the post-fault system. In this case, it happens to be the same as the pre-fault system, since the faulted line is first switched out, and then reconnected after an interval of time.
(*b*) Find the transfer and driving-point impedances, and the generator voltages 'behind transient reactance'.
(*c*) Set up the integral, using the expression based upon relative accelerations.
(*d*) Find the singular points, in this case using the criterion of zero *relative* accelerations.
(*e*) Select the saddle-type point, which gives large angles (around π) for those variables, which have positive resultant mechanical powers, or the least negative mechanical powers.

The generator equations for this system, obtained as above, are, on a 100 MVA base,

$$\left.\begin{aligned}\frac{18}{\pi 50}\ddot{\theta}_1 &= 0{\cdot}72 - 0{\cdot}577\sin(\theta_{12}+8°) - 1{\cdot}032\sin(\theta_{13}-8)\\ \frac{0{\cdot}866}{\pi 50}\ddot{\theta}_2 &= 0{\cdot}26 + 0{\cdot}577\sin(\theta_{12}-8) - 0{\cdot}90\sin(\theta_{23}+10)\\ \frac{3{\cdot}5}{\pi 50}\ddot{\theta}_3 &= 0{\cdot}17 + 1{\cdot}032\sin(\theta_{13}+8) + 0{\cdot}90\sin(\theta_{23}-10)\end{aligned}\right\} \quad (25)$$

The equivalent mechanical powers for the relative acceleration equations will be

$$\begin{aligned}T_{m12} &= 0{\cdot}866 \times 0{\cdot}72 - 18 \times (-0{\cdot}26) = 5{\cdot}305\\ T_{m13} &= 3{\cdot}5 \times 0{\cdot}72 - 18 \times 0{\cdot}17 = -0{\cdot}54\\ T_{23} &= 3{\cdot}5(-0{\cdot}26) - 0{\cdot}866 \times 0{\cdot}27 = -1{\cdot}06\end{aligned}$$

Thus the singular point which must be found is in the region where $(\theta_{12}, \theta_{13}, \theta_{23})$ is $(\pi, \pi, 0)$.

For the zero relative-acceleration criterion, it is necessary to balance the network analyser so that $\ddot{\theta}_1 = \ddot{\theta}_2 = \ddot{\theta}_3 = a$, some unknown constant, which will be positive.

In the study of the network analyser the quantities measured on the analyser are the angles and electrical powers for each machine. The mechanical powers are known; balance is secured when the quantities

$$\frac{T_{m1} - T_{e1}}{H_1}, \quad \frac{T_{m2} - T_{e2}}{H_2}, \quad \frac{T_{m3} - T_{e3}}{H_3} \text{ are equal.}$$

In this study, which was first carried out by this method, this was found to be difficult. However, the provision of a special wattmeter which would enable the values $(T_{m1} - T_{e1})/H_1$, etc., to be read off directly would greatly assist in obtaining balance.

The solution found in the neighbourhood of $\theta_{12} = \pi$, $\theta_{13} = \pi$ was $\theta_{12c} = 193°$, $\theta_{13c} = 167°$, and hence $\theta_{23c} = -26°$.

If the small angles due to the resistive part of the transfer impedances are assumed to be zero, and the mechanical powers are modified so that the integral remains zero at the saddle point, the expression to be used is that given in eqn. (23).

Substituting the values, we have

$$\frac{1}{2\pi 50}(0{\cdot}697\dot{\theta}_{12}^2 + 2{\cdot}82\dot{\theta}_{13}^2 + 0{\cdot}136\dot{\theta}_{23}^2)$$

$$-(0{\cdot}361\theta_{12} - 0{\cdot}051\theta_{13} + 0{\cdot}557\cos\theta_{12} + 1{\cdot}032\cos\theta_{13}\, 0{\cdot}90\cos\theta_{23} + -0{\cdot}329) = A$$

From the step-by-step integration of the system under fault conditions, the velocities and angles are found to be

Time	θ_{12}	$\dot{\theta}_{12}$	θ_{13}	$\dot{\theta}_{13}$	θ_{23}	$\dot{\theta}_{23}$
sec	deg	rad/s	deg	rad/s	deg	rad/s
0·30	101	5·79	80·6	7·71	−20·4	1·92
0·35	122·6	7·54	107·7	9·46	−14·9	1·92
0·40	150·6	9·77	138·9	10·89	−11·7	1·02
0·45	186·8	12·64	173·9	12·22	−12·9	−0·42

Substituting the angles and velocities given above we have

Time	A	
sec		
0·30	−0·55	Stable
0·35	0·30	Unstable

By linear interpolation, the critical switching time is

$$0{\cdot}30 + \frac{0{\cdot}55}{0{\cdot}85} \times 0{\cdot}05 = 0{\cdot}33\,\text{sec}$$

In the actual study undertaken by conventional methods it was concluded that 0·325 sec was the critical switching time. There is thus no appreciable difference in the time found by each method.

The positions of the singular points were also found by plotting the two independent relative acceleration equations obtained from eqn. (25). These are shown in Fig. 5.

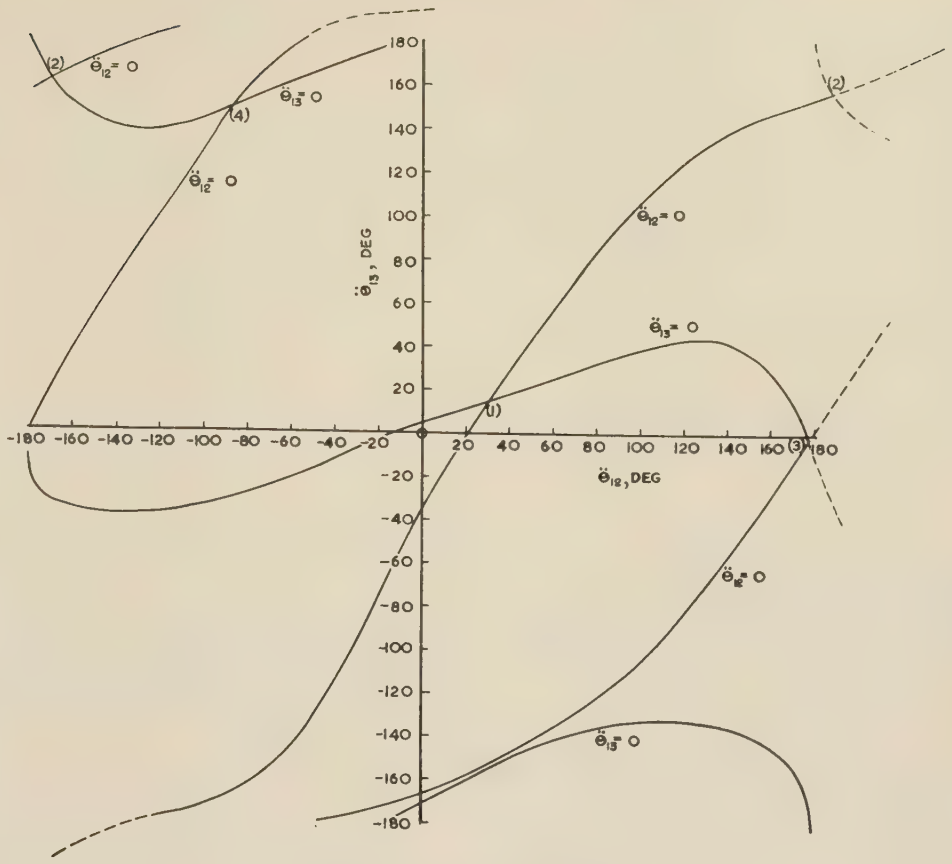

Fig. 5.—Three-machine problem.
Relative acceleration equations.

The four roots are

	θ_{12}	θ_{13}	θ_{23}
(i)	29	15	−14
(ii)	187	158·5	−28·5
(iii)	177	−15	168
(iv)	−82·5	154	−123·5

The last three roots give unstable trajectories and the singular point of interest is (ii). It will be noted that the values are 3–5% different from those obtained by using the network analyser.

Again, substituting the angles and velocities from above, we have

Time	A	
sec		
0·30	−0·54	Stable
0·35	0·31	Unstable

By linear interpolation, the critical switching time is found to be $0{\cdot}30 + \frac{0{\cdot}54}{0{\cdot}85} \times 0{\cdot}05 = 0{\cdot}33$ sec.

Thus the inaccuracy in the determination of the angles on the network analyser did not affect the results.

(4) CONCLUSIONS

In the paper, the author has attempted to give a new orientation to the study of power-system transient stability limits by introducing the concept of energy integrals and singular points used in the general study of non-linear differential equations. In Section 2.3 these methods are applied to the two-machine stability problem, and an equation is given for the critical switching angle, which, for the first time, includes the effect of resistance. An approximate, but sufficiently accurate, expression for the critical time is also derived, and the two equations taken together constitute a complete solution for the two-machine case.

The carrying out of a transient-stability study by the established methods[6] where there are more than two machines requires a large expenditure of effort. The actual process of forward integration, using the electrical powers obtained from a network analyser, is lengthy. In addition, a number of forward integrations with different clearing times—two is the minimum—must be carried out in order to establish the critical time. The establishment of the energy integral may require some effort, but a definite value for critical switching time is obtained with only one short forward integration. If there are many types and situations of fault to be studied which result in a common unfaulted system, as would be the case in a study of auto-reclosing, the same integral may be used in each case.

It is true that some approximations are necessary in order to establish the integral, but the nature of these is such that they will partly cancel out in the integral, and have little effect on the final result.

So far only three-machine problems have been studied in detail, but a surprisingly large range of problems can be reduced to this without a great loss in accuracy. The method is, however, capable of development and this work is now being undertaken for systems with a larger number of machines. It is thought that the energy-integral method can be applied easily when a digital computer is used for transient stability studies. Once the correct value of the constant for the energy integral is established by finding the co-ordinates of the important saddle point, the value of the integral can be found at each step by appropriate operations on the instantaneous velocities and angles which are naturally available during the process of forward integration. When the value of the integral is zero, the critical time can be printed out by the computer, since this is the only information actually required.

The development of methods for investigating non-linear systems with many variables is important in many fields of engineering, and it is hoped that the paper will make some contribution to this subject.

(5) ACKNOWLEDGMENTS

The author is grateful for the assistance afforded by Dr. J. R. Mortlock and Mr. M. Whitelegg in carrying out the network-analyser study. Valuable advice and assistance was given at every stage by Prof. M. W. Humphrey Davies, and this is much appreciated.

(6) REFERENCES

(1) CRARY, S. B.: 'Power System Stability', Vol. II (Chapman and Hall Ltd., London, 1947).

(2) KRYLOFF, H. M., and BOGOLIUBOFF, N.: 'Introduction to Non-Linear Mechanics' (free translation by S. Lefschetz, Princetown University Press, 1943).

(3) MINORSKY, N., and EDWARDS, J. W.: 'Introduction to Non-Linear Mechanics' (Ann Arbor, Michigan, 1947).

(4) POINCARÉ, H.: 'Sur les courbes difinies par une equation differentielle', Ouevres Vol. 1 (Gauthier-Villars, Paris, 1892).

(5) SUMMERS, I. H., and MCCLURE, J. B.: 'Progress in the Study of System Stability', *Transactions of the American I.E.E.*, 1930, **49**, pp. 132–158.

(6) LYON, G.: 'Some Experience with a British A.C. Network, Analyser', *Proceedings I.E.E.*, Paper No. 959 S, March, 1950 (**97**, Part II, p. 697).

(7) APPENDICES

(7.1) Derivation of Critical Clearing-Time Formulae for the Two-Machine Case

(7.1.1) Critical Clearing Angle.

The general expression for a two-machine system may be written

$$\left.\begin{aligned} M_1\ddot{\theta}_1 &= T_{m1} - \frac{V_1^2}{Z_{11}}\sin\phi_{11} - \frac{V_1V_2}{Z_{12}}\sin(\theta_{12}-\phi_{12}) \\ M_2\ddot{\theta}_2 &= T_{m2} - \frac{V_2^2}{Z_{22}}\sin\phi_{22} + \frac{V_1V_2}{Z_{12}}\sin(\theta_{12}+\phi_{12}) \end{aligned}\right\} \quad (26)$$

This may be reduced to a relative acceleration equation

$$M_{12}\ddot{\theta}_{12} = T_{m12} - T_{e12}\sin\theta'_{12} \quad . \quad . \quad . \quad . \quad (27)$$

where

$$M_{12} = \frac{M_1M_2}{M_1+M_2}$$

$$\left.\begin{aligned} T_{m12} &= \frac{\left(T_{m1} - \frac{V_1^2}{Z_{11}}\sin\phi_{11}\right)M_2 - \left(T_{m2} - \frac{V_2^2}{Z_{22}}\sin\phi_{22}\right)M_1}{M_1+M_2} \\ \theta_{12} &= \theta_{12} + \phi'_{12};\ \phi'_{12} = \arctan\left(\frac{M_1-M_2}{M_1+M_2}\tan\phi_{12}\right) \\ T_{e12} &= \frac{V_1V_2}{Z_{12}}\sqrt{\left[1 - \frac{4M_1M_2\sin^2\phi_{12}}{(M_1+M_2)^2}\right]} \end{aligned}\right\} \quad (28)$$

Eqn. (27) may be easily reduced to

$$\frac{d^2\theta}{d\tau^2} = B - \sin\theta \quad . \quad . \quad . \quad . \quad . \quad (29)$$

where

$$\left.\begin{aligned} B &= \frac{T_{m12}}{T_{e12}},\ \theta = \theta'_{12} \\ \tau &= \sqrt{\frac{T_{e12}}{M_{12}}}t \end{aligned}\right\} \quad . \quad . \quad . \quad . \quad (30)$$

From eqn. (29) it is shown in Section 2.2. that

$$\frac{v^2}{2} = B\theta + \cos\theta - B\theta_0 - \cos\theta_0 \quad . \quad . \quad . \quad (31)$$

for the condition $v = 0$ at $\theta = \theta_0$.

The expression for the critical switching angle θ_c can now be derived.

For the faulted system,

$$\frac{v^2}{2} = B_f\theta + \cos\theta - B_f\theta_0 - \cos\theta_0 \quad . \quad . \quad (32)$$

For the final system, the electrical parameters are changed, and

$$M_{12}\theta_{12} = T_{m12c} - T_{e12c}\sin\theta'_{12c} \quad . \quad . \quad . \quad (33)$$

which can be reduced to

$$\frac{d^2\theta}{d\tau^2} = C[B_c - \sin(\theta - \phi_c)] \quad . \quad . \quad . \quad . \quad (34)$$

where

$$\tau = \sqrt{\frac{T_{e12f}}{M_{12}}}t;\ \theta = \theta_{12} + \phi'_{12f};\ \phi'_{12f} = \arctan\left(\frac{M_1-M_2}{M_1+M_2}\tan\phi_{12f}\right) \quad . \quad . \quad . \quad . \quad (35)$$

$$B_c = \frac{T_{m12c}}{T_{e12c}}$$

$$T_{e12c} = \frac{V_1V_2}{Z_{12c}}\sqrt{\left[1 - \frac{4M_1M_2}{(M_1+M_2)^2}\sin^2\phi_{12c}\right]}$$

$$\phi_c = (\phi_{12f} - \phi_{12c}) \qquad C = \frac{T_{e12c}}{T_{e12f}}$$

Where the suffix f is added, the parameters refer to the faulted system.

Now eqn. (34) may be integrated as before, giving

$$\frac{v^2}{2} = C[B_c\theta + \cos(\theta - \phi_c) - B_c\theta_0 - \cos(\theta_0 - \phi_c)] \quad . \quad (36)$$

It is required to find the point C given in Fig. 2, the intersection of the faulted system trajectory with the separatrix in the final system.

Eqn. (36) will give the separatrix if

$$\theta_0 = \pi - \arcsin B_c + \phi_c \quad . \quad . \quad . \quad . \quad . \quad (37)$$

i.e. $\theta_0 = \pi - \theta_{1c} + \phi_c$, where θ_{1c} is the angle of the vortex point. Substituting for θ_0 in eqn. (36) gives

$$\frac{v^2}{2} = C[B_c\theta + \cos(\theta - \phi_c) - B_c(\pi - \theta_{1c} + \phi_c) + \cos\theta_{1c}] \quad . \quad (38)$$

The critical switching angle θ_c will correspond to the intersection of the trajectories given by eqns. (32) and (38).

Substituting θ_c for θ in each, and equating and rearranging gives

$$(B_f - CB_c)\theta_c + \cos\theta_c - C\cos(\theta_c - \phi_c)$$
$$= B_f\theta_0 - CB_c(\pi - \theta_{1c} + \phi_c) + \cos\theta_0 + C\cos\theta_{1c} \quad . \quad (39)$$

Now if $\phi_{12c} = \phi_{12f}$ then $\phi_c = 0$

and $T_{m12c} = T_{m12f}$

whence $B_c = \dfrac{T_{m12c}}{T_{e12c}} = \dfrac{T_{e12f}}{T_{e12c}} \times \dfrac{T_{m12c}}{T_{e12f}} = \dfrac{B_f}{C}$

Under these conditions eqn. (39) reduces to

$$(1 - C)\cos\theta_c = \cos\theta_0 + C\cos\theta_{1c} - B_f[\pi - (\theta_0 + \theta_{1c})] \quad (40)$$

(7.1.2) Derivation of Approximate Formula for Critical Clearing Time. It is proposed to replace the expression under the root sign in eqn. (11) by a quadratic in θ. The expression can then be integrated in terms of inverse trigonometrical functions.

It is useful to change the variable so that the limits of integration are $\pm\theta_m$, where

$$\theta_m = \frac{\theta_c - \theta_0}{2}$$

The expression under the root sign in eqn. (11) becomes

$$F_1(\theta) = B_f\theta + \cos(\theta_m + \theta_0)\cos\theta - \sin(\theta_m + \theta_0)\sin\theta + B_f\theta_m - \cos\theta_0 \quad . \quad (41)$$

If a quadratic function $F_2(\theta)$ is used to replace $F_1(\theta)$ in the equation in such a way that the functions have equal value at $-\theta_m$, 0 and θ_m and if

$$F_2(\theta) = [(\theta_m + R)^2 - (\theta_m - R)^2]a \quad . \quad . \quad . \quad (42)$$

then a and R will have the values given in eqn. (13). The critical clearing time may be found by replacing $F_1(\theta)$ by $F_2(\theta)$ in eqn. (11) and then integrating, giving eqn. (12).

(7.2) The Energy Integral for the Three-Machine Case

The differential equations are

$$\left.\begin{aligned}
M_1\ddot{\theta}_1 &= T_{m1} - \frac{V_1^2}{Z_{11}}\sin\phi_{11} - \frac{V_1V_2}{Z_{12}}\sin(\theta_{12} - \phi_{12}) - \frac{V_1V_3}{Z_{13}}\sin(\theta_{13} - \phi_{13})\\
M_2\ddot{\theta}_2 &= T_{m2} - \frac{V_2^2}{Z_{22}}\sin\phi_{22} + \frac{V_2V_1}{Z_{12}}\sin(\theta_{12} + \phi_{12}) - \frac{V_2V_3}{Z_{13}}\sin(\theta_{23} - \phi_{23})\\
M_3\ddot{\theta}_3 &= T_{m3} - \frac{V_3^2}{Z_{33}}\sin\phi_{33} + \frac{V_3V_1}{Z_{13}}\sin(\theta_{13} + \phi_{13}) - \frac{V_3V_2}{Z_{23}}\sin(\theta_{23} + \phi_{23})
\end{aligned}\right\} \quad . \quad (43)$$

These equations arise from the general expression when

$$\theta_1 - \theta_2 = \theta_{12} = -\theta_{21}, \text{ etc.}$$

The relative acceleration equations for every possible combination of the machines [i.e. $n(n-1)/2$ equations] must be established. Each equation must then be multiplied by the appropriate relative velocity, and the resulting equations added together. For three machines, this gives

$$M_1M_2\ddot{\theta}_{12}\dot{\theta}_{12} + M_2M_3\ddot{\theta}_{23}\dot{\theta}_{23} + M_1M_3\ddot{\theta}_{13}\dot{\theta}_{13}$$
$$= T_{m12}\dot{\theta}_{12} + T_{m23}\dot{\theta}_{23} + T_{m31}\dot{\theta}_{31}$$
$$- \frac{V_1V_2}{Z_{12}}[M_2\sin(\theta_{12} - \phi_{12}) + M_1\sin(\theta_{12} + \phi_{12})]\dot{\theta}_{12}$$
$$- \frac{V_2V_3}{Z_{13}}[M_3\sin(\theta_{23} - \phi_{23}) + M_2\sin(\theta_{23} + \phi_{23})]\dot{\theta}_{23}$$
$$- \frac{V_1V_3}{Z_{13}}[M_3\sin(\theta_{13} - \phi_{13}) + M_1\sin(\theta_{13} + \phi_{13})]\dot{\theta}_{13}$$
$$- \frac{V_1V_2}{Z_{12}}M_3[\sin(\theta_{12} - \phi_{12})\dot{\theta}_{13} - \sin(\theta_{12} + \phi_{12})\dot{\theta}_{23}]$$
$$- \frac{V_2V_3}{Z_{23}}M_1[\sin(\theta_{23} + \phi_{23})\dot{\theta}_{13} - \sin(\theta_{23} - \phi_{23})\dot{\theta}_{12}]$$
$$- \frac{V_1V_3}{Z_{13}}M_2[\sin(\theta_{13} - \phi_{13})\dot{\theta}_{12} - \sin(\theta_{13} + \phi_{13})\dot{\theta}_{23}] \quad (44)$$

where

$$\left.\begin{aligned}
T_{m12} &= M_2\left(T_{m1} - \frac{V_1^2}{Z_{11}}\sin\phi_{11}\right) - M_1\left(T_{m2} - \frac{V_2^2}{Z_{22}}\sin\phi_{22}\right)\\
T_{m13} &= M_3\left(T_{m1} - \frac{V_1^2}{Z_{11}}\sin\phi_{11}\right) - M_1\left(T_{m3} - \frac{V_3^2}{Z_{33}}\sin\phi_{33}\right)\\
T_{m23} &= M_3\left(T_{m2} - \frac{V_2^2}{Z_{22}}\sin\phi_{22}\right) - M_2\left(T_{m3} - \frac{V_3^2}{Z_{33}}\sin\phi_{33}\right)
\end{aligned}\right\} \quad . \quad (45)$$

The first three terms containing sines on the right-hand side of eqn. (44) can be directly integrated, but not the last three terms.

One method of approximation is to assume that ϕ_{12}, ϕ_{13} and ϕ_{23} are zero in the last three terms only. The first of this group of terms then becomes

$$\frac{V_1V_2}{Z_{12}}M_3[\sin\theta_{12}(\dot{\theta}_{13} - \dot{\theta}_{23})] = M_3\frac{V_1V_2}{Z_{12}}\sin\theta_{12}\dot{\theta}_{12} \quad . \quad (46)$$

and similarly for the other two terms, and all can then be integrated.

Greater simplicity will be obtained at some sacrifice in accuracy if the small angles ϕ_{12}, ϕ_{13}, etc., are assumed to be zero in all terms of eqn. (44). If at the same time the values of T_{m12}, T_{m13} and T_{m23} are modified so that eqn. (20) is satisfied, the integral

will then have the correct value in the region of greatest interest, close to the singular (saddle) point.

Then

$$\left.\begin{aligned} T_{m12} &= \frac{V_1V_2}{Z_{12}}\sin\theta_{12c} + \frac{V_1V_3}{Z_{13}}\sin\theta_{13c} \\ T_{m13} &= \frac{V_1V_2}{Z_{12}}\sin\theta_{12c} + \frac{V_2V_3}{Z_{23}}\sin\theta_{23c} \\ T_{m23} &= \frac{V_1V_3}{Z_{13}}\sin\theta_{13c} + \frac{V_2V_3}{Z_{23}}\sin\theta_{23c} \end{aligned}\right\} \quad \ldots \quad (47)$$

and eqn. (25) reduces to

$$\left.\begin{aligned} &\frac{1}{2(M_1+M_2+M_3)}(M_1M_2\dot{\theta}_{12}^2 + M_2M_3\dot{\theta}_{23}^2 + M_1M_3\dot{\theta}_{13}^2) \\ &\quad = \frac{V_1V_2}{Z_{12}}[\sin\theta_{12c}(\theta_{12}-\theta_{12c}) + \cos\theta_{12} - \cos\theta_{12c}] \\ &\quad + \frac{V_2V_3}{Z_{23}}[\sin\theta_{23c}(\theta_{23}-\theta_{23c}) + \cos\theta_{23} - \cos\theta_{23c}] \\ &\quad + \frac{V_1V_3}{Z_{13}}[\sin\theta_{13c}(\theta_{13}-\theta_{13c}) + \cos\theta_{13} - \cos\theta_{13c}] \end{aligned}\right\} \quad (48)$$

This gives a simple equation to use in practical problems such as the example given in Section 3.5.

621.372.45: 621—52

The Institution of Electrical Engineers
Monograph No. 309 M
July 1958
©

MULTI-GAIN REPRESENTATION FOR A SINGLE-VALUED NON-LINEARITY WITH SEVERAL INPUTS, AND THE EVALUATION OF THEIR EQUIVALENT GAINS BY A CURSOR METHOD

By M. J. SOMERVILLE, B.Sc., Graduate, and D. P. ATHERTON, B.Eng., Student.

(*The paper was first received 26th February, and in revised form 15th May*, 1958. *It was published as an* INSTITUTION MONOGRAPH *in July*, 1958.)

SUMMARY

A general method is described for calculating the equivalent gain through a non-linear element for a signal of known amplitude probability distribution, in the presence of other, uncorrelated, signals or disturbances, also of known amplitude-probability distributions. A cursor method for calculating the equivalent gains is developed, and cursor results are verified by theoretical and experimental points, for the equivalent gains of Gaussian and sinusoidal signals applied together to certain non-linearities. An example is given, showing how the behaviour of a non-linear feedback system may be analysed when two signals of different amplitude probabilities are applied to it.

It is shown also that the equivalent gain to a Gaussian noise signal in the presence of other signals applied to a single-valued non-linearity has the same value as the incremental d.c. gain through the non-linearity (with the input signals present). Experimental results are given using this as a method of obtaining the value of equivalent gain.

(1) INTRODUCTION

When several inputs are applied together to a non-linear element, the output consists of components due to each separate input, plus harmonics and cross-modulation products of the inputs. It is desirable to replace such a non-linearity by an equivalent linear gain (defined as being that which minimizes mean-square error[1]), since calculations on its effect in a feedback system are thereby facilitated. If these inputs to the non-linear element are of different amplitude probabilities or different magnitudes of similar waveforms, the equivalent linear gains (of all the signals) do not have the same values, and each separate gain is a function, not only of the magnitude of the particular input, but also of the magnitudes of each other input. An approximate method[2] which has been used to simplify calculation of the equivalent gain of a non-linear element with two input signals A and B assumes that the gain for each signal has the same value k_{AB} (Fig. 1); the equivalent gain is then effectively

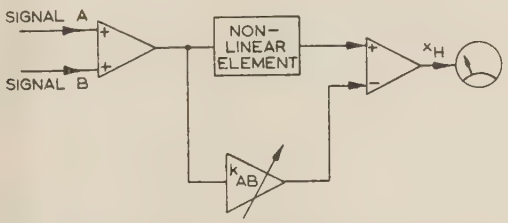

Fig. 1.—Simplified single equivalent gain for two signals to a non-linear element.

that which gives minimum mean-square error between the output of the non-linearity and that of the equivalent linear gain. This method is found to give reasonable accuracy for a combination of a sine wave with Gaussian noise applied to a saturation non-linearity, but large discrepancies can result if this simplifying approximation is made for certain other non-linear elements. In the precise method of calculation the equivalent gain for each input signal is effectively that which gives minimum mean-square error as the equivalent gain for that particular signal is varied (Fig. 2). Separate minimizations of error are carried out to

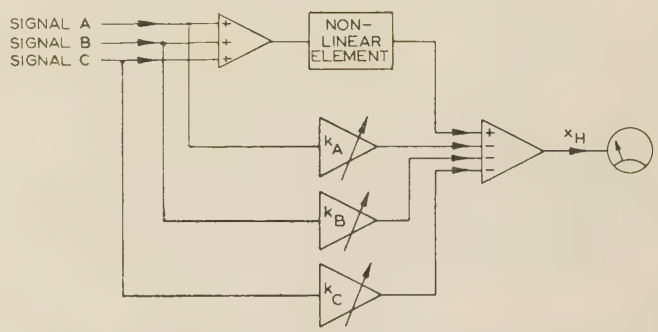

Fig. 2.—Multi-gain representation of a non-linear element.
k_A, k_B and k_C are adjusted separately to give a minimum mean-square value for x_H.

find the equivalent gains for each of the other signals. The representation of a non-linearity by a particular equivalent gain for each of the input signals will thus result in a smaller mean-square error than if the simplifying approximation, that all equivalent gains have the same value, is taken.

The equivalent gain for a very small sinusoidal signal applied with other input signals to a single-valued non-linearity will have the same value as the incremental d.c. gain (in the presence of the same input signals) through the non-linearity. If one of the input signals is a Gaussian noise signal x_i, for which $p(x_i) = [1/\sqrt{(2\pi)}\sigma]\varepsilon^{-x_i^2/2\sigma^2}$, it may be considered as being composed of a large number of small sinusoidal signals $c_n \cos(\omega_n t + \phi_n)$ (see Reference 3), where ϕ_n is randomly distributed, with a uniform probability distribution from 0 to 2π, and c_n are constants describing the frequency spectrum of the noise signal. Thus the gain for each of the small sinusoidal components of the noise will equal the incremental d.c. gain which occurs when all the input signals (including the Gaussian signal itself) are present. The equivalent gain for the whole Gaussian signal will thus have the same value as that of each of its components, and the gain for any Gaussian input signal in the presence of other signals applied to a non-linearity, has therefore the same value as the incremental d.c. gain with all these inputs present. A proof of this property is given in Section 4.

(2) THEORETICAL ANALYSIS OF EQUIVALENT GAINS

A single-valued non-linearity is assumed to have the characteristic $v_0 = f(v_i)$, v_0 and v_i being the output and input signals respectively. An input $v_i = (\beta + x + y)$ is applied to the non-linearity (Fig. 3). β is the d.c. level of the input;

Correspondence on Monographs is invited for consideration with a view to publication.
The authors are in the Electrical Engineering Laboratories, University of Manchester.

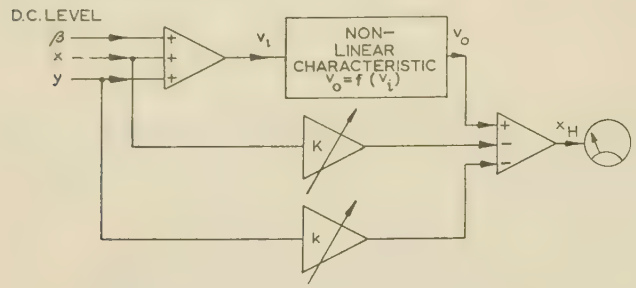

Fig. 3.—Equivalent gains for signals x and y.

a.c. inputs x and y are taken to have zero average value and are assumed to be uncorrelated. In the general case, x is the signal for which the equivalent linear gain is to be determined, and y is the sum of all other signals $y_1 \ldots y_n$. The amplitude probability distributions of x and y are respectively written $q(x)$ and $p(y)$. For simplicity, y will first be assumed to represent only one signal. The general case where $y = y_1 + \ldots y_n$ is treated in Section 10.1.

For the input $(\beta + x + y)$ to the non-linearity, the output is $v_0 = f(\beta + x + y)$, while that from the equivalent linear gains has the value $(Kx + ky)$. The difference x_H between the outputs from the non-linearity and equivalent linear gains represents cross-modulation products and harmonics of the input signals, and also includes the d.c. level λ at the output from the non-linearity.

The instantaneous value of this difference or error is

$$x_H = f(\beta + x + y) - (Kx + ky) \quad . \quad . \quad . \quad (1)$$

and its mean-square value is

$$M = \lim_{T \to \infty} \frac{1}{T} \int_0^T x_H^2 dt \quad . \quad . \quad . \quad . \quad . \quad . \quad . \quad (2)$$

x_H is a function of x and y, both of which are functions of time and are partly defined by their amplitude probability distributions $q(x)$ and $p(y)$. The probability that x lies between x and $(x + dx)$ while y also lies between y and $(y + dy)$ is $q(x)dx \,.\, p(y)dy$, provided that x and y are uncorrelated. This joint probability is in fact the proportion of time spent in this condition, and the corresponding contribution to the integral of eqn. (2) is therefore $x_H^2 q(x)dx \,.\, p(y)dy$. For all values of y, with x between x and $(x + dx)$, the total of such contributions is

$$\int_{y=-\infty}^{y=+\infty} x_H^2 q(x)p(y)dxdy$$

The total contribution from the sum of these components for all values of x is thus the mean-square error M, and has the value

$$M = \int_{x=-\infty}^{x=+\infty} \int_{y=-\infty}^{y=+\infty} x_H^2 q(x)p(y)dxdy \quad . \quad . \quad . \quad (3)$$

Putting the value of x_H from eqn. (1) into eqn. (3) gives

$$M = \int_{x=-\infty}^{x=+\infty} \int_{y=-\infty}^{y=+\infty} [f^2(\beta + x + y) - 2f(\beta + x + y)(Kx + ky) + (Kx + ky)^2]q(x)p(y)dxdy \quad (4)$$

As the value of K is adjusted, a minimum mean-square error is obtained when $\partial M/\partial K = 0$;

$$\text{i.e. } \frac{\partial M}{\partial K} = \int_{x=-\infty}^{x=+\infty} \int_{y=-\infty}^{y=+\infty} [-2f(\beta + x + y)x + 2Kx^2 + 2kxy]q(x)p(y)dxdy = 0$$

Now

$$\int_{x=-\infty}^{x=+\infty} \int_{y=-\infty}^{y=+\infty} 2kxyq(x)p(y)dxdy = 2k \int_{x=-\infty}^{x=+\infty} xq(x)dx \int_{y=-\infty}^{y=+\infty} yp(y)dy$$

$$= 0 \text{ if } \int_{-\infty}^{+\infty} xq(x)dx = 0$$

$$\text{or if } \int_{-\infty}^{+\infty} yp(y)dy = 0$$

Thus the above part of the expression for $\partial M/\partial K$ is zero if the average value of x or of y is zero. This assumption was in fact made at the outset to make this term zero. The condition that the input signals x and y have zero average level does not restrict the analysis, as may at first appear to be the case, but means simply that the gain to a signal which is made up of a d.c. component plus an a.c. component (of zero average level) must be represented by two different gains, one for the d.c. and the other for the a.c. component. The latter is the equivalent gain K (or k) and the former is represented by the incremental gain for d.c., and has the same value for all d.c. components, which are lumped together for convenience to give the d.c. level β at the input.

Thus,

$$\frac{\partial M}{\partial K} = 0 \text{ when } \int_{x=-\infty}^{x=+\infty} \int_{y=-\infty}^{y=+\infty} [-2f(\beta + x + y)x + 2Kx^2]q(x)p(y)dxdy = 0$$

Whence

$$K = \frac{\int_{x=-\infty}^{x=+\infty} \int_{y=-\infty}^{y=+\infty} xf(\beta + x + y)q(x)p(y)dxdy}{\int_{x=-\infty}^{x=+\infty} \int_{y=-\infty}^{y=+\infty} x^2 q(x)p(y)dxdy}$$

But $\int_{y=-\infty}^{y=+\infty} p(y)dy = 1$, therefore

$$K = \frac{1}{\bar{x}^2} \int_{x=-\infty}^{x=+\infty} \int_{y=-\infty}^{y=+\infty} xf(\beta + x + y)q(x)p(y)dxdy \quad . \quad (5)$$

where $\bar{x}^2$ is the mean-square value of the input x. Similarly, differentiating M [eqn. (4)] with respect to k, and putting $\partial M/\partial k = 0$ gives

$$k = \frac{1}{\bar{y}^2} \int_{y=-\infty}^{y=+\infty} \int_{x=-\infty}^{x=+\infty} yf(\beta + x + y)p(y)q(x)dydx \quad . \quad (6)$$

where $\bar{y}^2$ is the mean-square value of the input y.

As y tends to zero and $\int_{-\infty}^{+\infty} p(y)dy = 1$, eqn. (5) gives the usual expression for the equivalent gain K of a signal x in the presence of a d.c. input β,

$$K = \frac{1}{\bar{x}^2} \int_{x=-\infty}^{x=+\infty} xf(\beta + x)q(x)dx \quad . \quad . \quad . \quad . \quad (7)$$

(3) TWO-STAGE EVALUATION OF K

For a d.c. input γ applied to the non-linearity together with the inputs $(\beta + y)$, the d.c. output from the non-linearity has a value

$$g(\gamma) = \int_{y=-\infty}^{y=+\infty} f(\gamma + \beta + y)p(y)dy \quad . \quad . \quad . \quad (8)$$

Suppose now that the function $g(\gamma)$ given by eqn. (8) is the characteristic of a single-valued non-linearity, and that the

nput x is applied to it. The equivalent gain K_x of the signal x through this non-linearity with characteristic $g(\gamma)$ has then the value [cf. eqn. (7)]

$$K_x = \frac{1}{\bar{x}^2}\int_{x=-\infty}^{x=+\infty} xg(x)q(x)dx \quad . \quad . \quad . \quad . \quad (9)$$

Putting in the value of $g(x)$ obtained from eqn. (8) gives

$$K_x = \frac{1}{\bar{x}^2}\int_{x=-\infty}^{x=+\infty} x \int_{y=-\infty}^{y=+\infty} f(x+\beta+y)p(y)dyq(x)dx$$

$$= \frac{1}{\bar{x}^2}\int_{x=-\infty}^{x=+\infty}\int_{y=-\infty}^{y=+\infty} xf(\beta+x+y)q(x)p(y)dxdy$$

Comparison with eqn. (5) shows that $K_x = K$, i.e. the equivalent gain through the non-linearity for a signal x in the presence of signals $(\beta + y)$ is equal to the gain of x applied alone to the 'effective non-linearity' with the d.c. input/output characteristic $g(\gamma)$ of eqn. (8).

This result, proved above for y a single signal, is shown in Section 10.2 to be true also for the general case when $y = y_1 + \ldots y_n$.

The process of evaluating the equivalent gain K may now be done by a relatively simple two-stage method, in which the characteristic $g(\gamma)$ is first calculated, and the gain of the signal x through this effective non-linearity is then obtained. This method proves particularly amenable to the use of cursors[4] (Section 5), one to obtain the characteristic $g(\gamma)$ and another to evaluate the equivalent gain of x through the non-linear characteristic $g(\gamma)$. In the general case (Section 10.3) n d.c. cursors are used to construct the characteristic $g(\gamma)$, one cursor being required for each of the inputs $y_1 \ldots y_r \ldots y_n$.

The equivalent gain k_r for the signal y_r may be evaluated in the same way as that described above, and is the gain of the signal y_r through the 'effective non-linearity' represented by the d.c. input/output curve when inputs $(\beta + x + y - y_r)$ are applied to the non-linear element.

(4) INCREMENTAL D.C. GAIN

It follows from Section 3 that the gain for a very small sinusoidal signal will have the same value as the slope at the origin of the d.c. input/output curve for the non-linear element with all the inputs applied. This slope is the incremental d.c. gain through the non-linearity, and its value is of some importance, since incremental (Nyquist) stability of a feedback loop containing the non-linear element will be determined by the magnitude and sign of the gain to small sinusoidal signals.

For an input $(\beta + x + y)$ to the non-linearity, the d.c. output λ has the value [cf. derivation of eqn. (3)]

$$\lambda = \int_{x=-\infty}^{x=+\infty}\int_{y=-\infty}^{y=+\infty} f(\beta+x+y)q(x)p(y)dxdy$$

$\frac{d\lambda}{d\beta}$ = incremental d.c. gain

$$= \int_{x=-\infty}^{x=+\infty}\int_{y=-\infty}^{y=+\infty} \frac{d}{d\beta}f(\beta+x+y)q(x)p(y)dxdy$$

Now,

$$\frac{d}{d\beta}f(\beta+x+y) = \frac{d}{dx}f(\beta+x+y) = \frac{d}{dy}f(\beta+x+y)$$

Thus

$$\frac{d\lambda}{d\beta} = \int_{y=-\infty}^{y=+\infty} p(y)\left\{\int_{x=-\infty}^{x=+\infty} q(x)d[f(\beta+x+y)]\right\}dy$$

$$= \int_{y=-\infty}^{y=+\infty} p(y)\left\{\Big[f(\beta+x+y)q(x)\Big]_{-\infty}^{+\infty} - \int_{x=-\infty}^{x=+\infty} f(\beta+x+y)d[q(x)]\right\}dy$$

Assuming $q(x) = 0$ at $x = \pm\infty$

$$\frac{d\lambda}{d\beta} = -\int_{y=-\infty}^{y=+\infty} p(y)\left\{\int_{x=-\infty}^{x=+\infty} f(\beta+x+y)d[q(x)]\right\}dy \quad . \quad (10)$$

When the signal x has a Gaussian amplitude probability distribution, $q(x) = \frac{1}{\sqrt{(2\pi)\sigma}}\varepsilon^{-x^2/2\sigma^2}$, where σ is the r.m.s. value $\bar{x}$ of the signal x,

$$d[q(x)] = \frac{1}{\sqrt{(2\pi)\sigma}}\left(\frac{-2x}{2\sigma^2}\right)\varepsilon^{-x^2/2\sigma^2}dx = -\frac{x}{\bar{x}^2}q(x)dx$$

Putting this value for $d[q(x)]$ into eqn. (10) gives

$$\frac{d\lambda}{d\beta} = \frac{1}{\bar{x}^2}\int_{x=-\infty}^{x=+\infty}\int_{y=-\infty}^{y=+\infty} xf(\beta+x+y)q(x)p(y)dxdy \quad (11)$$

Comparison of eqn. (11) with eqn. (5) shows that, for a Gaussian signal x, its equivalent gain in the presence of signals $(\beta + y)$ is equal to the incremental d.c. gain through the non-linearity in the presence of the inputs $(\beta + x + y)$, i.e.

$$K = d\lambda/d\beta \quad . \quad . \quad . \quad . \quad . \quad . \quad (12)$$

Section 10.4 gives a proof of eqn. (12) for the general case when $y = y_1 + \ldots y_n$. Thus, if several Gaussian signals are included among the inputs $x, y_1, \ldots y_n$, then each of the Gaussian signals has the same value of equivalent gain, equal to the incremental d.c. gain. This fact enables all Gaussian signals at the input to a non-linear element to be conveniently lumped together as a single Gaussian signal of mean-square value equal to the sum of the mean-square values of each component. This technique is used in the example given in Section 7.

Eqn. (12) provides a useful practical method for measuring the equivalent gain for a Gaussian signal. Direct measurement is obtained, for example, by adjusting the gain k_A (input A in Fig. 2 being the Gaussian signal) to give a minimum mean-square error. The accuracy obtained by this method is usually low (about $\pm 20\%$) since the null of the mean-square error can be obscured by the presence of cross-modulation products and harmonics. Also, since the mean-square null instrument must have a long time-constant to smooth out random low-frequency fluctuations,[5] it can take a considerable time to obtain the null balance. Measurement of incremental d.c. gain, on the other hand, does not involve a null adjustment, and can give good accuracy. To obtain an accurate measurement of incremental d.c. gain by this method, only a small d.c. increment should be applied to the non-linearity, the corresponding d.c. increment at the output should be measured on an instrument with a long time-constant to smooth out random low-frequency fluctuations, and several points for positive and negative increments should be taken to allow, by interpolation, for curvature of the d.c. input/output characteristic.

(5) CURSORS FOR CALCULATING EQUIVALENT GAINS

Two cursors are required to evaluate equivalent gains by the method outlined in Section 3; a 'd.c. cursor' to give the effective

non-linear characteristic $g(\gamma)$ in the presence of signals $(\beta + y)$, and an 'a.c. cursor'[4] to give the equivalent gain of the signal x through the effective non-linear characteristic $g(\gamma)$.

In the general case, $y = y_1 + \ldots y_r + \ldots y_n$ (Section 10.3), the d.c. cursor for y_r is applied to the equivalent non-linear characteristic $g_{r-1}(\gamma_{r-1})$ to obtain the equivalent non-linear characteristic $g_r(\gamma_r)$. This procedure is repeated n times for $r = 1$ to $r = n$, starting with $g_0(\gamma_0) = f(\beta + \gamma_0)$, the actual non-linearity, until $g(\gamma) = g_n(\gamma_n)$ is obtained.

The a.c. cursor for x is applied to the effective non-linear characteristic $g(\gamma)$ to give the equivalent gain K to the signal x. When the equivalent gains $k_1 \ldots k_n$ for all the signals $y_1 \ldots y_n$ are required as well as that for x, the procedure will be similar to that described above for x, and in this case both a d.c. and an a.c. cursor will be required for each of the signals applied to the non-linearity.

(5.1) The D.C. Cursor

In the general case (Section 10.3),

$$g_r(\gamma_r) = \int_{y_r=-\infty}^{y_r=+\infty} g_{(r-1)}(\gamma_r + y_r)p_r(y_r)dy_r \quad . \quad . \quad (13)$$

If y is a single signal, eqn. (13) reduces to

$$g(\gamma) = \int_{y=-\infty}^{y=+\infty} f(\gamma + \beta + y)p(y)dy$$

The general eqn. (13) may be rewritten

$$g_r(\gamma_r) = \int_0^1 g_{(r-1)}(\gamma_r + y_r)d\left[\int p_r(y_r)dy_r\right] \quad . \quad (14)$$

The value of $\int_{-\infty}^{Y} p_r(y_r)dy_r$ increases continuously from zero with $Y = -\infty$, to $+1$ with $y = +\infty$. If N values of Y ($Y_1 \ldots Y_R \ldots Y_N$) are obtained, such that

$$\int_{-\infty}^{Y_1} p_r(y_r)dy_r = \frac{1}{2N} \ldots \int_{Y_R}^{Y_{(R+1)}} p_r(y_r)dy_r = \frac{1}{N} \ldots \int_{Y_N}^{+\infty} p_r(y_r)dy_r = \frac{1}{2N}$$

the values Y_R then represent the most probable values (i.e. mean position) of y_r over the range

$$\frac{1}{N}(R-1) \leqslant \int_{-\infty}^{y_r} p_r(y_r)dy_r \leqslant \frac{R}{N}$$

Thus the integral of eqn. (14) may now be evaluated approximately by the summation

$$g_r(\gamma_r) = \frac{1}{N}\sum_{R=1}^{R=N} g_{(r-1)}(\gamma_r + Y_R) \quad . \quad . \quad . \quad (15)$$

Taking $N = 20$ usually gives a reasonably accurate result. The values of Y_R for sinusoidal and Gaussian signals are calculated in Section 10.5 and tabulated in Table 1 for the case when $N = 20$.

Fig. 4 gives a diagrammatic representation of the values of Y_R, for the cases when $\hat{E} = 1{\cdot}0h$ and $2^{1/2}\sigma = 1{\cdot}0h$ (i.e. equal powers of sinusoidal and noise signals, normalized relative to $\hat{E} = h$). If Fig. 4(*a*) or (*b*) is drawn on tracing paper, it can be used as a d.c. cursor by placing it over a graph of the non-linear characteristic (or effective non-linear characteristic), when the intersections of the vertical lines $y_r = Y_1 \ldots Y_R \ldots Y_N$ with the non-linear characteristic $g_{(r-1)}(\gamma_{r-1})$ give the values $g_{r-1}(\gamma_r + Y_R)$. Thus, to obtain the d.c. output $g_r(\gamma_r)$ for an input γ_r, the d.c. cursor for y_r is placed over the characteristic $g_{r-1}(\gamma_{r-1})$, with its origin at the point $\gamma_{r-1} = \gamma_r$, and the values

Table 1

VALUES OF Y_R ON D.C. CURSOR FOR (*a*) SINUSOIDAL AND (*b*) GAUSSIAN SIGNALS

R	1	2	3	4	5	6	7	8	9	10	11 ... 20
$\int_{-\infty}^{Y_R} p(y)dy$	0·025	0·075	0·125	0·175	0·225	0·275	0·325	0·375	0·425	0·475	0·525 ... 0·975
(*a*) Sine: $Y_R/\hat{E}$	−0·997	−0·972	−0·924	−0·853	−0·760	−0·649	−0·523	−0·383	−0·233	−0·079	+0·079 ... +0·997
(*b*) Gaussian: $Y_R/2^{1/2}\sigma$ ..	−1·386	−1·018	−0·813	−0·661	−0·534	−0·423	−0·321	−0·225	−0·134	−0·044	+0·044 ... +1·386

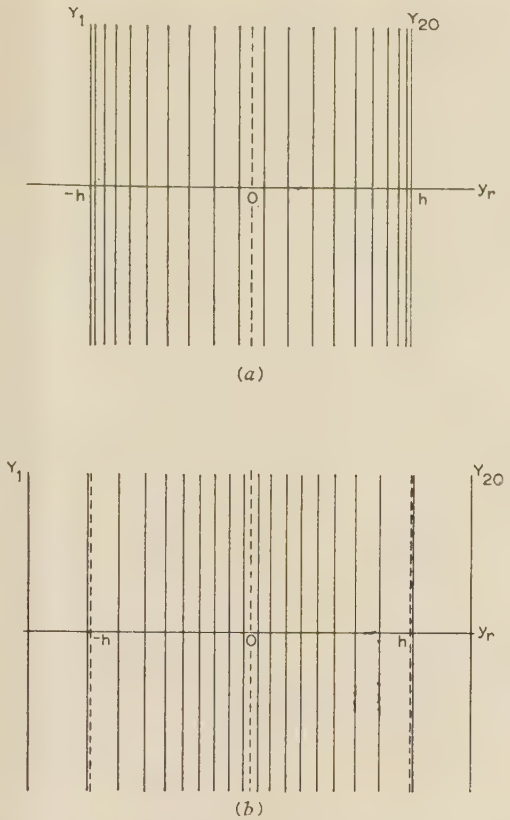

Fig. 4.—D.C. cursors.
(*a*) For sinusoidal signal.
(*b*) For Gaussian noise signal [$\hat{E} = \sqrt{(2)}\sigma = 1{\cdot}0h$].

$g_{r-1}(\gamma_r + Y_R)$ are summated [eqn. (15)]. This process is repeated for a range of values of γ_r to obtain points for the curve $g_r(\gamma_r)$.

The d.c. cursors of Fig. 4 are of use only for the one signal magnitude and must be redrawn for each required value. Fig. 5 shows the d.c. cursor for a sinusoidal signal drawn (cf. Reference 4) in such a way as to enable it to be used over a range of normalized values of $\hat{E}$ between 0 and $2h$. In using this cursor,

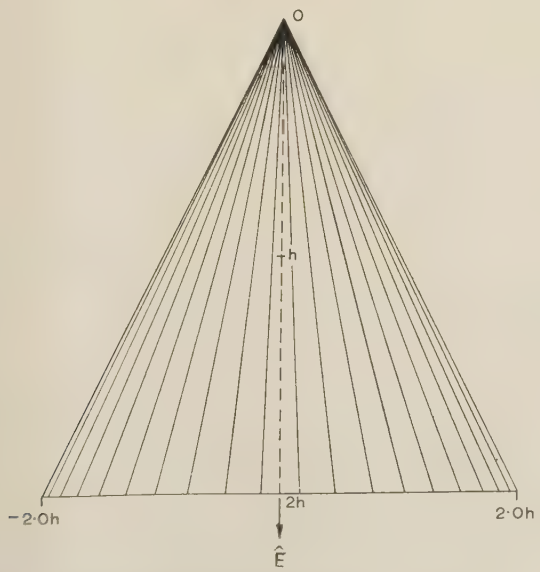

Fig. 5.—D.C. cursor for sinusoidal signals of magnitudes 0 to $2{\cdot}0h$.

the point Y_R on the particular horizontal line corresponding to the required value of $\hat{E}$ is made to coincide with the curve $g_{(r-1)}[\gamma_{(r-1)}]$ by moving the cursor vertically. The ordinate of this point of coincidence gives only one of the N values $g_{(r-1)}(\gamma_r + Y_R)$, and the cursor has to be manipulated in the above manner for each of the N values to be taken. Since the cursors of Fig. 4 prove somewhat easier and quicker in use than that of Fig. 5, the former would be used in preference to the latter, as is convenient, for example, when only the gain for the signal x is required, in the presence of constant amounts of signals $y = y_1 + \ldots y_n$.

(5.2) The A.C. Cursor

From eqn. (9) (and Section 10.2) the equivalent gain for a signal x is

$$K = \frac{1}{\bar{x}^2}\int_{-\infty}^{+\infty} g(x)xq(x)dx$$

Since $\bar{x}$ is the r.m.s. value of the input signal, the r.m.s. output $\phi(x)$ from the equivalent gain has the value

$$\phi(x) = K\bar{x} = \int_{-\infty}^{+\infty} g(x)\frac{x}{\bar{x}}q(x)dx$$

which may be written

$$\phi(x) = \int_{x=-\infty}^{x=+\infty} g(x)d\left[\int \frac{x}{\bar{x}}q(x)dx\right] \quad . \quad . \quad . \quad (16)$$

The value of $\int_{-\infty}^{X} \frac{x}{\bar{x}}q(x)dx$ increases in value as X moves from $-\infty$ to zero, but starts to decrease for positive X, and becomes zero for $X = +\infty$, since x has been taken to have zero d.c. component.

Thus $$-\int_{-\infty}^{0} \frac{x}{\bar{x}}q(x)dx = \int_{0}^{\infty} \frac{x}{\bar{x}}q(x)dx = \frac{x_{av}}{2\bar{x}} = \frac{1}{2F}$$

where x_{av} is the average value of the signal x, and F is its form factor, r.m.s./average.

An approximate evaluation of the above integral may now be obtained, as follows, in the same way as was used for derivation of eqn. (15) for the d.c. cursor. N values of X ($X_1 \ldots X_R \ldots X_N$) are thus calculated, such that, for negative X,

$$\int_{-\infty}^{X_1} \frac{x}{\bar{x}}q(x) = \frac{-1}{2F}\frac{1}{2N}\cdots\int_{X_R}^{X_{(R+1)}} \frac{x}{\bar{x}}q(x)dx$$
$$= \frac{-1}{2F}\frac{1}{N}\cdots\int_{X_{(N/2)}}^{0} \frac{x}{\bar{x}}q(x)dx = \frac{-1}{2F}\frac{1}{2N}$$

and for positive X,

$$\int_{0}^{X_{(N/2+1)}} \frac{x}{\bar{x}}q(x)dx = \frac{1}{2F}\frac{1}{2N}\cdots\int_{X_R}^{X_{(R+1)}} \frac{x}{\bar{x}}q(x)dx$$
$$= \frac{1}{2F}\frac{1}{N}\cdots\int_{X_N}^{\infty} \frac{x}{\bar{x}}q(x)dx = \frac{1}{2F}\frac{1}{2N}$$

Then the integral of eqn. (16) may be evaluated approximately by the summation

$$\phi(x) = \frac{1}{2F}\left[-\sum_{R=1}^{R=N/2} g(X_R) + \sum_{R=N/2+1}^{R=N} g(X_R)\right] \quad . \quad (17)$$

Table 2

VALUES OF X_R FOR (*a*) SINUSOIDAL AND (*b*) GAUSSIAN SIGNALS

R	1	2	3	4	5	6	7	8	9	10	11 ... 20
$F\int_{-\infty}^{X_R}\frac{x}{\bar{x}}q(x)dx$	0·025	0·075	0·125	0·175	0·225	0·275	0·325	0·375	0·425	0·475	0·525 ... 0·975
(*a*) Sine: $X_R/\bar{E}$ .. .. ($F = 1{\cdot}111$)	−0·999	−0·989	−0·968	−0·937	−0·893	−0·835	−0·740	−0·662	−0·529	−0·312	+0·312 ... +0·999
(*b*) Gaussian: $X_R/2^{1/2}\sigma$ ($F = 1{\cdot}253$)	−1·733	−1·379	−1·177	−1·025	−0·893	−0·773	−0·658	−0·536	−0·403	−0·231	+0·231 ... +1·733

(N is an even number.) The values X_R for a sinusoidal and for a Gaussian signal are calculated in Reference 4 for the case when $N = 20$, and are reproduced in Table 2.

The values of X_R shown in Table 2 are now used to construct an a.c. cursor[4] which is similar to the d.c. cursors (Figs. 4 and 5). The a.c. cursor is used in much the same way as was the d.c. cursor, to obtain the ordinates $g(X_R)$ which are summated and divided by $2F$ to give the value of $\phi(x)$ for the particular input-signal magnitude, x.

When an input signal contains d.c. as well as a.c., it is split into the separate components x_0 (d.c. level) and x (a.c. with zero d.c. level), since the d.c. gain is specified by the incremental d.c. gain, and the gain for x is its equivalent gain K. (It is necessary to split up the signal in this way, since the gain K and the incremental d.c. gain $d\lambda/d\beta$ do not in general have the same value.) The equivalent non-linear characteristic $g(\gamma)$ for the signals y together with all d.c. components other than x_0 is then constructed so that, in determining the equivalent gain K for various magnitudes of the a.c. component x, the cursor must each time be used on the modified characteristic $g(\gamma + x_0)$.

(5.3) Evaluation of the Joint Probability $p(y)$ for Signals $y_1 + \ldots y_n$

The equivalent non-linear characteristic $g(\gamma)$ may be obtained by a method alternative to that described in Section 5.1, by determining the overall amplitude probability distribution $p(y)$ ($y = y_1 + \ldots y_n$), when, from eqn. (8),

$$g(\gamma) = \int_{-\infty}^{+\infty} f(\gamma + \beta + y)p(y)dy \quad . \quad . \quad . \quad (18)$$

In certain cases, this method can prove simpler and quicker than that of Section 5.1. For example, if the gain for the signal x is required for a range of values of y (the relative values of $y_1 \ldots y_n$ remaining constant), then determination of the characteristic $g(\gamma)$ for each new value of y involves only a single-stage cursor operation to evaluate eqn. (18), whereas use of the method of Section 5.1 would require n stages of cursor operation.

The total amplitude probability distribution $t_2(z_2)$ for a signal $z_2 = y_1 + y_2$ is obtained from the convolution integral

$$t_2(z_2) = \int_{y_2=-\infty}^{y_2=+\infty} p_1(z_2 - y_2)p_2(y_2)dy_2 \quad . \quad . \quad . \quad (19)$$

For a signal $z_3 = y_1 + y_2 + y_3 = z_2 + y_3$,

$$t_3(z_3) = \int_{y_3=-\infty}^{y_3=+\infty} t_2(z_3 - y_3)p_3(y_3)dy_3$$

Putting in the value of $t_2(z_3 - y_3)$ from eqn. (19),

$$t_3(z_3) = \int_{y_3=-\infty}^{y_3=+\infty}\int_{y_2=-\infty}^{y_2=+\infty} p_3(y_3)p_2(y_2)p_1[z_3-(y_2+y_3)]dy_3dy_2$$

To obtain the probability distribution $p(y)$ when $y = y_1 + \ldots y_n$, convolution integrals

$$t_r(z_r) = \int_{y_r=-\infty}^{y_r=+\infty} t_{(r-1)}(z_r - y_r)p_r(y_r)dy_r \quad . \quad . \quad . \quad (20)$$

are carried out, from $r = 2$ to $r = n$, to give

$$t_n(z_n) = p(y) = \int_{y_n=-\infty}^{y_n=+\infty}\ldots\int_{y_2=-\infty}^{y_2=+\infty} p_n(y_n)\ldots p_2(y_2)$$
$$p_1[y - (y_2 + \ldots y_n)]dy_n \ldots dy_2 \quad (21)$$

Eqn. (20) can be written

$$t_r(z_r) = \int_0^1 t_{(r-1)}(z_r - y_r)d\left[\int p_r(y_r)dy_r\right] \quad . \quad (22)$$

Comparing eqn. (22) with eqn. (14), it is seen that an approximate evaluation for $t_r(-z_r)$ may be obtained by using the d.c. cursor for the signal y_r on the characteristic $t_{r-1}(-z_{r-1})$, in just the same manner as was described in Section 5.1, where the characteristic $g_r(\gamma_r)$ was constructed from $g_{r-1}(\gamma_{r-1})$. Thus the total amplitude probability distribution $p(y)$ is obtained by applying the d.c. cursor in a total of $(n-1)$ stages.

Now, rewriting eqn. (18) in the form

$$g(\gamma) = \int_0^1 f(\gamma + \beta + y)d\left[\int p(y)dy\right]$$

the effective characteristic $g(\gamma)$ may be constructed from the actual non-linear characteristic using the d.c. cursor for the signal y. The values Y_R for this cursor may be obtained from graphical integration of the curve $p(y)$.

(6) THEORETICAL AND EXPERIMENTAL EQUIVALENT GAINS

Theoretical results for the 'dead-space' non-linear characteristic (Fig. 6) have been constructed by the cursor method,

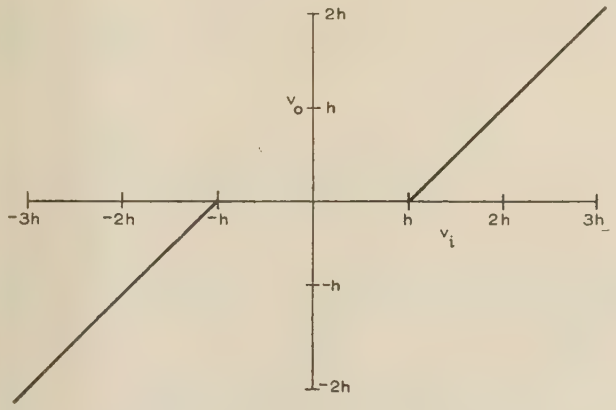

Fig. 6.—'Dead-space' non-linear characteristic.

and with check points obtained, when possible, by calculation. (Even for only two inputs to the non-linearity, the purely theoretical evaluation of their equivalent gains can be extremely complex, and the integrations would often have to be evaluated by numerical methods.) For convenience, the signals x and y are written in normalized form, relative to the fixed reference level h. A signal of r.m.s. value $\bar{x}$ is taken to have a normalized value $2^{1/2}\bar{x}/h$: in this way a sinusoidal signal of peak value h has a normalized value of unity.

The curves of Fig. 7 are for an input to the dead-space non-linear characteristic consisting of a sinusoidal signal plus Gaussian noise, of normalized values P_n and σ_n respectively. For $P_n \simeq 1{\cdot}0$ and low values of σ_n (e.g. $P_n = 1{\cdot}0$, $\sigma_n = 0{\cdot}5$), the difference in equivalent gain K to signal P_n and the equivalent gain k to noise σ_n is appreciable. These results for the dead-space characteristic may be used to construct curves for the same inputs to other non-linear characteristics. A 'limit' non-linear characteristic represented by Fig. 8 may be written $[1 - D.S.(h)]$, where $D.S.(\theta)$ denotes a dead-space characteristic with 'break' points at $\pm\theta$, and with unity slope for inputs of magnitude greater than θ. The 'limited field of view'* (l.f.v.) non-linear

* An example of this type of non-linear characteristic is that of certain radar direction-sensing aerials, where the error signal from the aerial becomes zero for large positive or negative angular displacements.

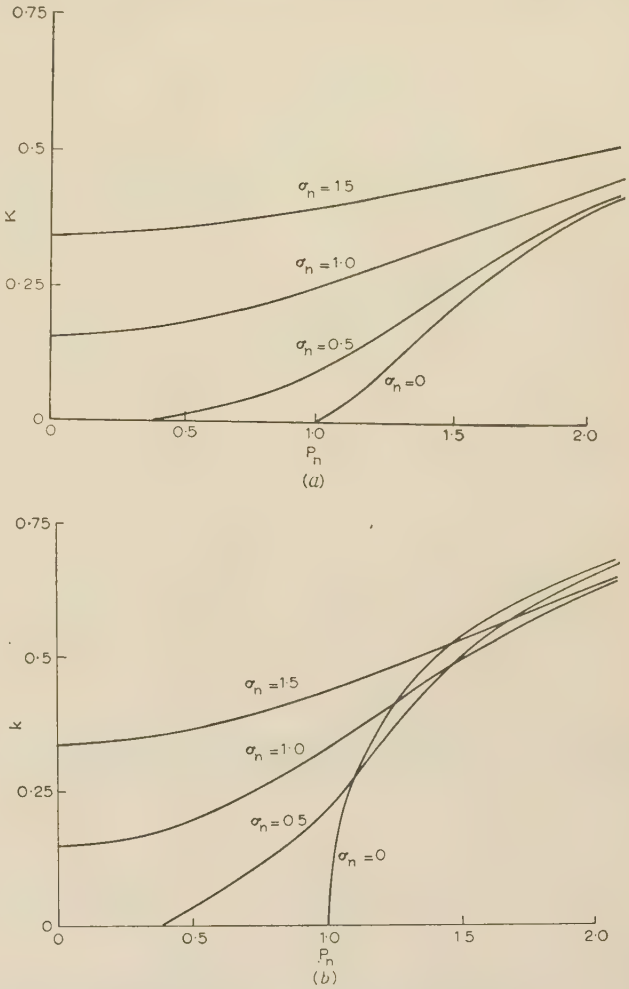

Fig. 7.—Equivalent gains for a sinusoidal signal plus Gaussian noise applied to a 'dead-space' non-linearity.
(*a*) Gain K for a sinusoidal signal P_n.
(*b*) Gain k for Gaussian noise σ_n.

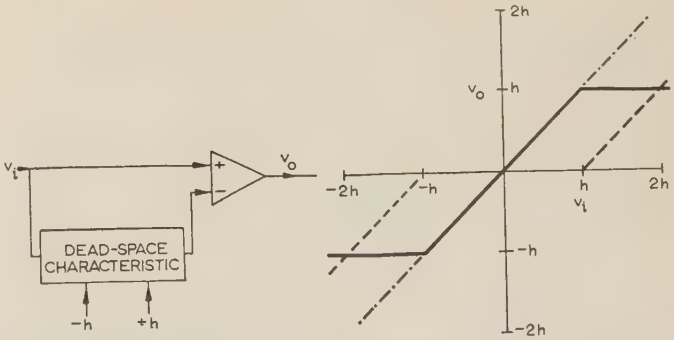

Fig. 8.—Construction of a limit characteristic from a 'dead-space' characteristic.

characteristic shown in Fig. 9 may be written $[1 - 2D.S.(h) + D.S.(2h)]$. Equivalent gains for sine wave plus noise signal to these non-linearities are shown in Figs. 10 and 11, together with experimental points.

Theoretical results for three signals applied to the dead-space non-linearity of Fig. 6 are shown in Fig. 12. The three signals taken are two sine waves (P_n and S_n) of unrelated frequencies, and Gaussian noise (σ_n). Equivalent gains for these

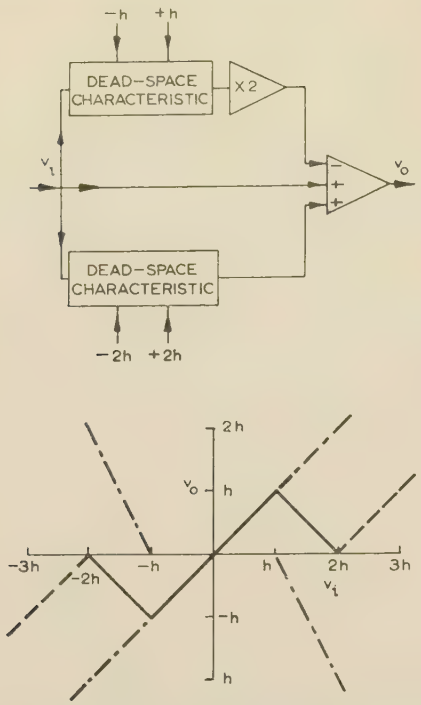

Fig. 9.—Construction of a 'limited-field-of-view' (l.f.v.) characteristic from 'dead-space' characteristics.

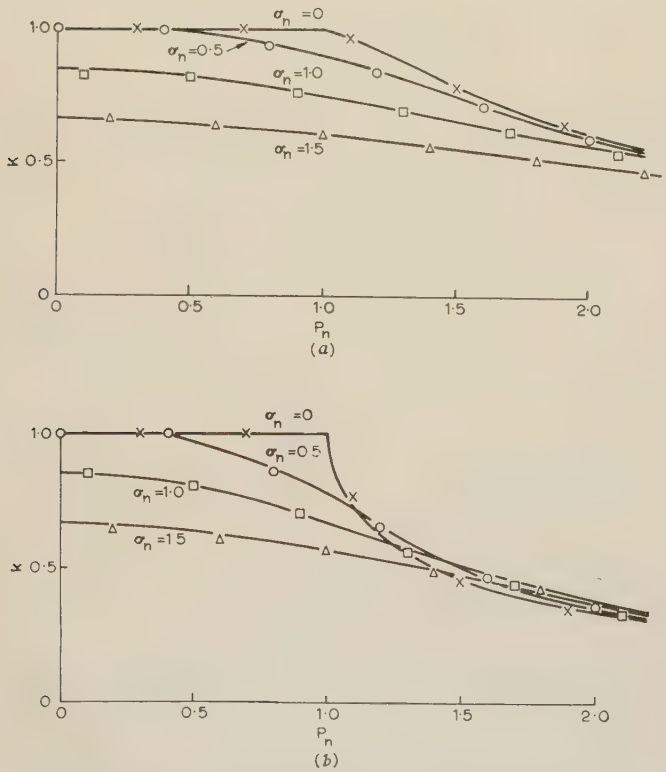

Fig. 10.—Equivalent gains through the limit non-linearity for a sinusoidal signal plus Gaussian noise.
(*a*) Gain K for a sinusoidal signal P_n.
(*b*) Gain k for Gaussian noise σ_n.

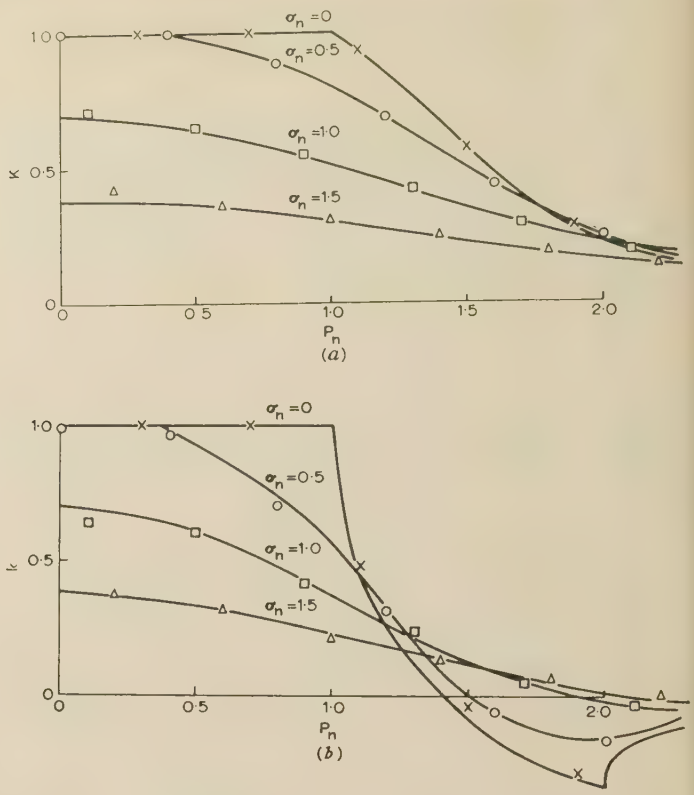

Fig. 11.—Equivalent gains through an l.f.v. non-linearity for a sinusoidal signal plus Gaussian noise.
(*a*) Gain K for a sinusoidal signal P_n.
(*b*) Gain k for Gaussian noise σ_n.

three signals through an l.f.v. non-linearity have been obtained from those for dead-space (Fig. 12), and are shown in Fig. 13 together with experimental points.

(7) DETERMINATION OF OPERATING POINTS ON THE NON-LINEAR CHARACTERISTIC

When the non-linear element is included in a feedback loop, the operating point for each signal is a function of all the other signals present at the input to the non-linearity. Thus, if the non-linearity is represented by N different equivalent gains, the operating point is obtained, in effect, by the solution of N simultaneous equations. If a mathematical solution is to be attempted, it is first necessary to represent the gains K and $k_1 \ldots k_n$ by equations involving the magnitudes of all the signals $x, y_1 \ldots y_n$. For example, with sine waves and Gaussian signals applied to the non-linear characteristic of Fig. 14B, an approximate expression which holds over a limited range of values for P_n and σ_n can be obtained from the curves of Fig. 16: for small deviations of P_n and σ_n about a normalized value 1·0, $K \simeq 3{\cdot}2 + 1{\cdot}5(P_n - 1{\cdot}0) + 2{\cdot}8(\sigma_n - 1{\cdot}0)$ and $k \simeq 3{\cdot}96 + 1{\cdot}96(\sigma_n - 1{\cdot}0) + 2{\cdot}8(P_n - 1{\cdot}0)$. When only two different equivalent gains are needed to specify the non-linear element, a relatively simple graphical construction can be used to find the operating points. To illustrate this construction, the second-order feedback system of Fig. 14A containing a hard-spring non-linear characteristic (Fig. 14B) will be analysed. The three inputs to the system are a sine wave of frequency $1{\cdot}5\omega_0$ and two Gaussian noise signals ν_{n1} and ν_{n2}, the frequency spectrum of ν_{n1} having 6 dB per octave low-frequency attenuation from $\omega_0/8$ and 6 dB per octave high-frequency attenuation from $\omega_0/4$, and ν_{n2} having a similar spectrum with low-frequency attenuation

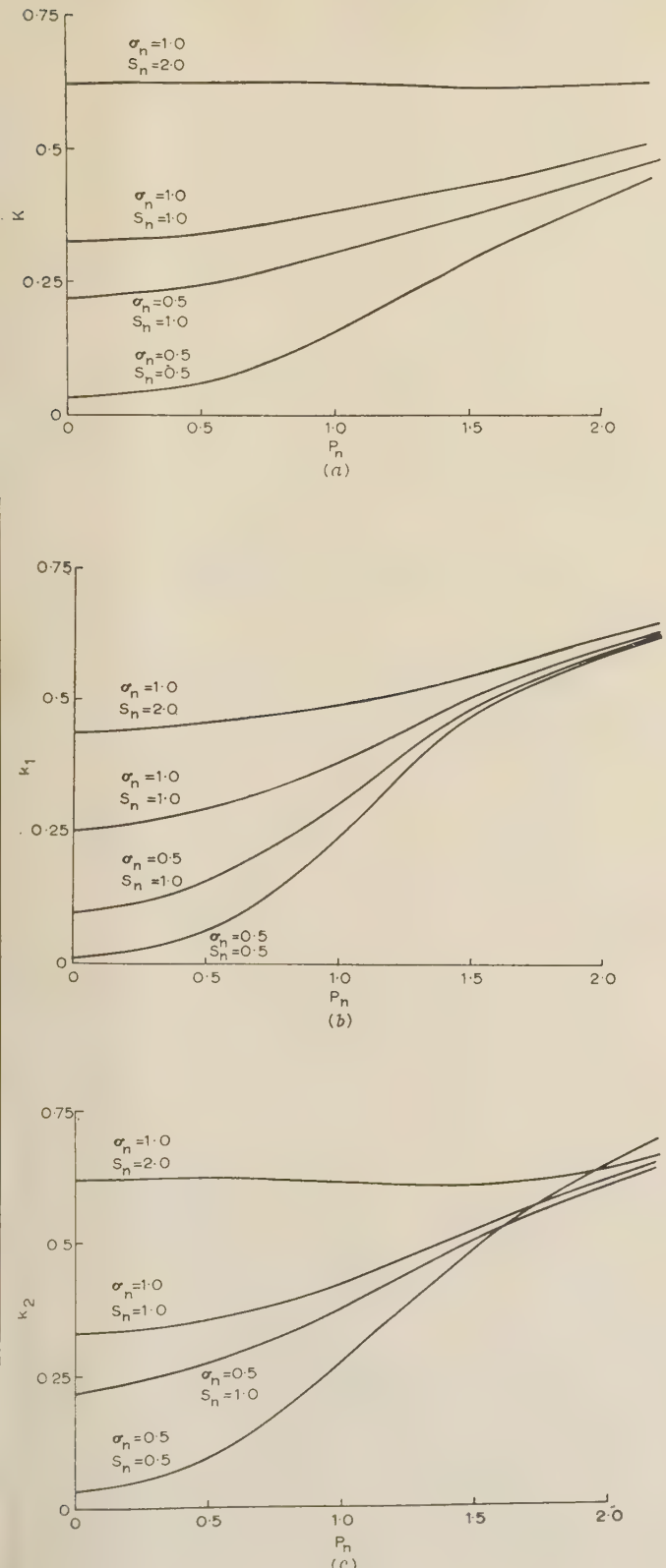

Fig. 12.—Equivalent gains through a 'dead-space' non-linearity for two sinusoidal signals plus Gaussian noise.

(*a*) Gain K for a sinusoidal signal P_n.
(*b*) Gain k_1 for a sinusoidal signal S_n.
(*c*) Gain k_2 for Gaussian noise σ_n.

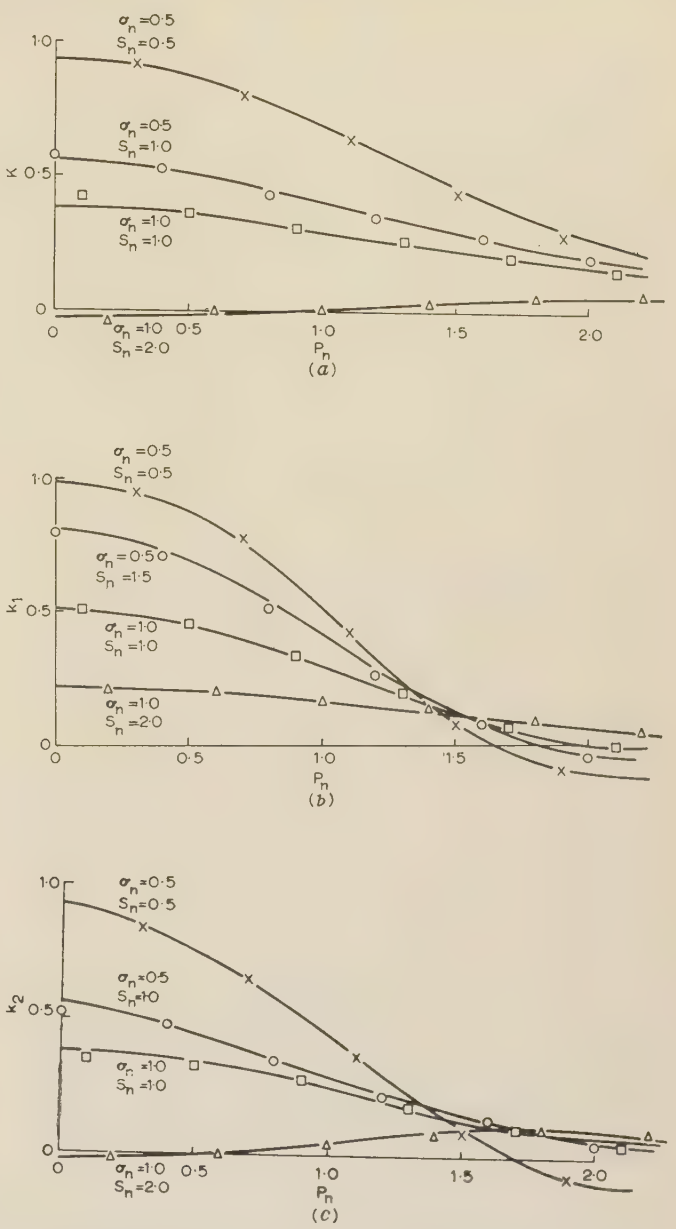

Fig. 13.—Equivalent gains through an l.f.v. non-linearity for two sinusoidal signals plus Gaussian noise.

(*a*) Gain K for a sinusoidal signal P_n.
(*b*) Gain k_1 for a sinusoidal signal S_n.
(*c*) Gain k_2 for Gaussian noise σ_n.

beginning at ω_0 and high-frequency attenuation beginning at $2\omega_0$. These noise signals are present in the ratio $\nu_{n1}^2 : \nu_{n2}^2 = 4 : 1$, and, having the same value of equivalent gain, can be considered as a composite noise signal of total noise power $\nu_n^2 = \nu_{n1}^2 + \nu_{n2}^2$.

For a signal v_i applied to the system, the signal v_0 at the input to the non-linear element has the value

$$v_0 = v_i \frac{(p/\omega_0)^2}{[(p/\omega_0)^2 + K_{eq}] + K_{eq}\alpha(p/\omega_0)} \quad . \quad . \quad (23)$$

where K_{eq} is the value of equivalent gain through the non-linear element, and α is the damping factor $T\omega_0$, which is taken to have a value 0·2.

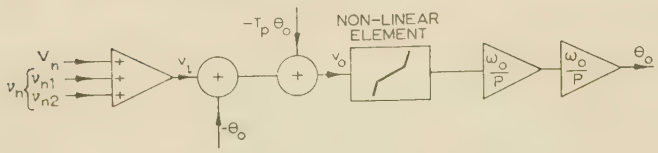

Fig. 14A.—Non-linear feedback system.

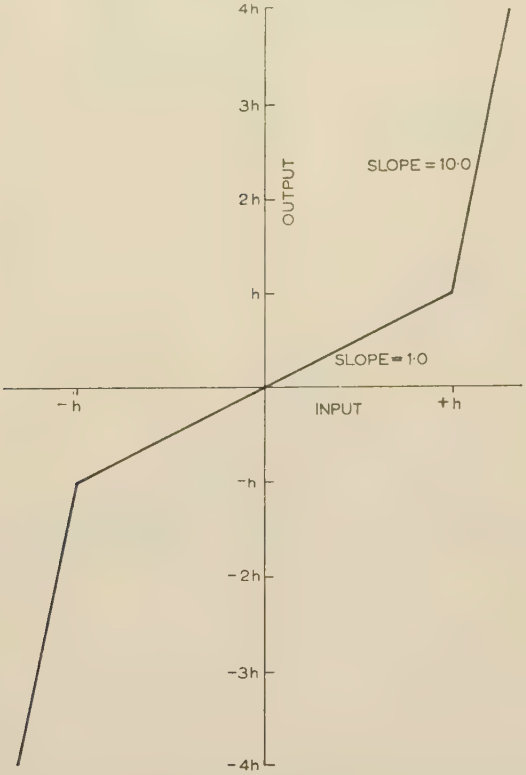

Fig. 14B.—'Hard-spring' characteristic.

For a sinusoidal input signal V_n of frequency $1{\cdot}5\omega_0$ the signal P_n at the input to the non-linear element has a magnitude

$$P_n = V_n \frac{2{\cdot}25}{(1{\cdot}09K^2 - 4{\cdot}5K + 5{\cdot}06)^{1/2}} \quad . \quad . \quad (24)$$

where K is the equivalent gain to a sine wave.

The ratio P_n/V_n is plotted in Fig. 15 [curve (*a*)] for a range of values of K from 1 to 5.

An expression similar to that of eqn. (24) can be obtained for each of the noise signals by integration over the power spectrum of the noise signal. The power spectrum $\Phi(\omega)$ of the input noise signals is given by

$$\Phi(\omega) = \frac{2(\omega_1 + \omega_2)}{\pi} \left| \frac{p}{(p + \omega_1)(p + \omega_2)} \right|^2 \nu^2$$

where ω_1 and ω_2 are respectively the frequencies at which low- and high-frequency attenuations of 6dB per octave begin, and ν^2 is the total power of the input noise signal.

From eqn. (23), the power gain $G(\omega)$ from the noise input to the input of the non-linear element is, for $\alpha = 0{\cdot}2$,

$$G(\omega) = \left| \frac{p^2}{p^2 + 0{\cdot}2k\omega_0 p + k\omega_0^2} \right|^2$$

in which $p = j\omega$ and k is the equivalent gain for a noise signal.

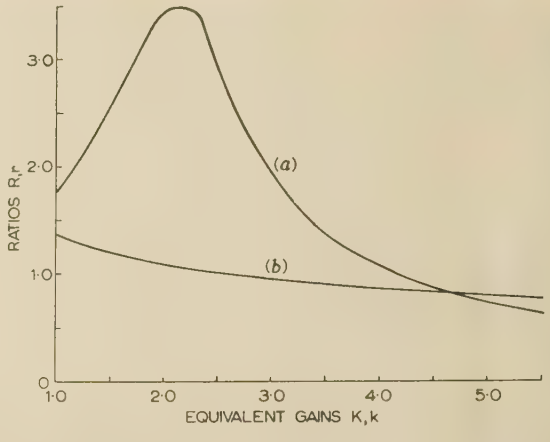

Fig. 15.—Magnitudes of signal and noise to the non-linear element.

(*a*) Variation of the sinusoidal signal applied to the non-linear element, with the equivalent gain K.
(*b*) Variation of the noise signal applied to the non-linear element, with the equivalent gain k.

$$R = \frac{\text{Signal amplitude to non-linear element}}{\text{Input signal amplitude}}$$

$$r = \frac{\text{R.M.S. noise to non-linear element}}{\text{R.M.S. noise input}}$$

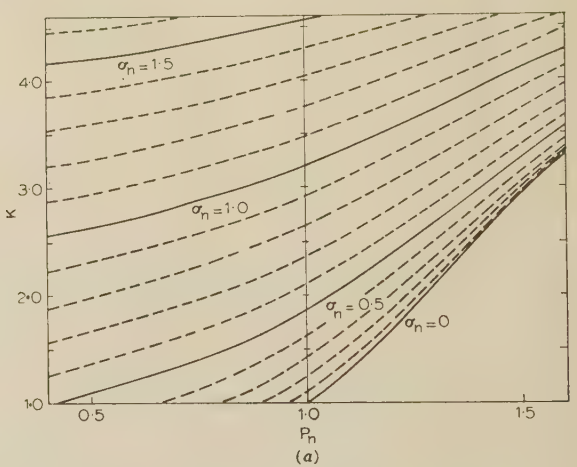

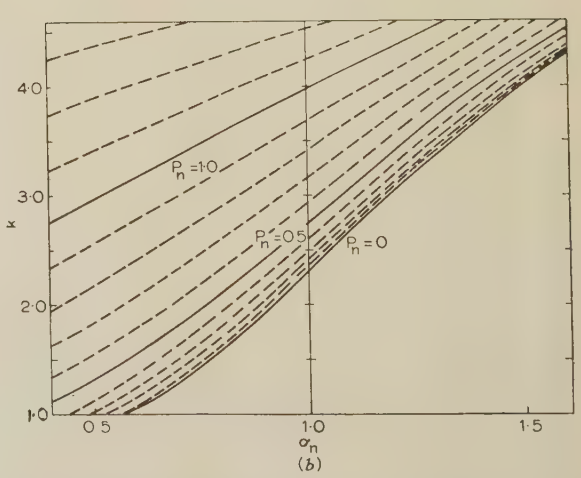

Fig. 16.—Detailed equivalent-gain curves through the 'hard-spring' characteristic of Fig. 15 for a sinusoidal signal plus Gaussian noise.

(*a*) Gain K for a sinusoidal signal P_n.
(*b*) Gain k for a Gaussian noise σ_n.

The power spectrum at the input to the non-linear element is now $\Phi(\omega)G(\omega)$, and its total noise power σ^2 has the value

$$\sigma^2 = \int_0^\infty \Phi(\omega)G(\omega)d\omega \quad . \quad . \quad . \quad . \quad (25)$$

This integral is evaluated in Section 10.6 to give the results

$$\sigma_{n1}^2 = \nu_{n1}^2 \frac{(0{\cdot}2 + 413{\cdot}3k)}{(0{\cdot}2 + 16{\cdot}48k + 220{\cdot}4k^2)}$$

$$\sigma_{n2}^2 = \nu_{n2}^2 \frac{(1 + 6{\cdot}30k)}{(1 + 1{\cdot}55k + 0{\cdot}42k^2)}$$

The total input noise power ν_n^2 is made up from ν_{n1}^2 and ν_{n2}^2 in the ratio 4 : 1, so that $\nu_{n1}^2 = \frac{4}{5}\nu_n^2$ and $\nu_{n2}^2 = \frac{1}{5}\nu_n^2$. Thus

$$\sigma_n^2 = \sigma_{n1}^2 + \sigma_{n2}^2 = \nu_n^2 \left[\frac{4}{5}\frac{(0{\cdot}2 + 413{\cdot}3k)}{(0{\cdot}2 + 16{\cdot}48k + 220{\cdot}4k^2)} + \frac{1}{5}\frac{(1 + 6{\cdot}30k)}{(1 + 1{\cdot}55k + 0{\cdot}42k^2)}\right]$$

The ratio σ_n/ν_n obtained from the above expression is plotted in Fig. 15 [curve (*b*)] for values of k from 1 to 5.

Using the equivalent gain curves of Fig. 16(*a*), the curve (*a*) of Fig. 15 showing variation of P_n with K can be converted to a curve of P_n against σ_n', the noise required at the input to the non-linear element, together with P_n, to give the gain K to P_n. Similarly the equivalent gain curves of Fig. 16(*b*) can be used to convert curve (*b*) of Fig. 15 to a curve of σ_n against P_n'. The curves P_n, σ_n' and σ_n, P_n' are plotted together in Fig. 17 for

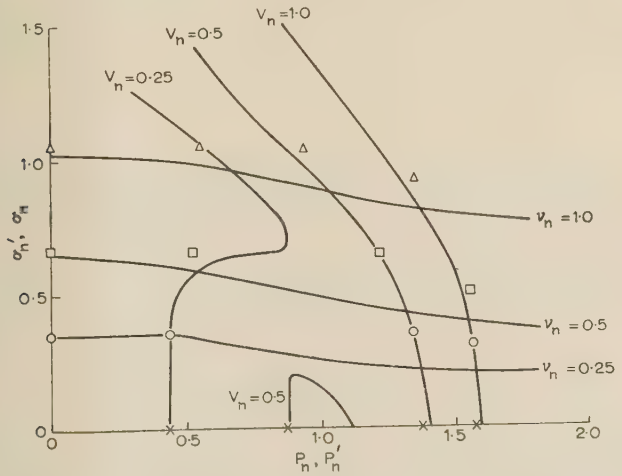

Fig. 17.—Determination of operating points on the non-linear characteristic.

several values of P_n and σ_n. Intersections of these curves now give the operating points for the particular values of V_n and ν_n. Experimentally determined operating points are also shown in Fig. 17. For $V_n = 0{\cdot}5$ and ν_n somewhat less than 0·25, it will be seen from Fig. 17 that three intersections can occur: this indicates the existence of a jump in operating conditions.[6]

For large numbers of inputs to a system such as that considered above, the problem is best simplified, if possible, so that only two different equivalent gains need be considered, when the analysis can be effected as shown in the example. To help achieve this simplification, all Gaussian signals may be considered together, very low-frequency inputs may sometimes be ignored if the signal they produce at the input to the non-linear element is small, and high-frequency inputs may be assumed to feed direct to the non-linear element, since the signal fed back at high frequencies is small.

(8) CONCLUSIONS

The multi-gain analysis of single-valued non-linearities is simplified by the introduction of the 'effective non-linear characteristic' which can be calculated for each signal. Further simplification can be obtained in that the equivalent gain curves for, say, a 'dead-space' characteristic can be used to obtain the curves for other more complex segmented characteristics. Also, the fact that the gain for all Gaussian signals in the input is the same enables these signals to be lumped together, as in the example dealt with in Section 7. Equality of gain for Gaussian signal with incremental d.c. gain is of use in experimental determination of the equivalent gain for noise, but it is also of significance, for example, when there is a reversal in sign of the equivalent gain for noise, as with the l.f.v. non-linear characteristic [Figs. 11(*b*) and 13(*b*)], under which conditions d.c. instability of a feedback loop containing the non-linear element would take place.

If each of a large number of inputs to a non-linearity is small compared with the total input signal, the absence of any one will not much influence the total probability distribution of the rest. The effective non-linear characteristic for each of the signals is therefore about the same and may be assumed nearly linear over a small central portion, so that the gains for each of these signals may be expected to be the same. Under these conditions it may sometimes be justifiable to consider a single equivalent gain for all the signals, its value being equal to the incremental d.c. gain through the non-linear element, in the presence of all the inputs.

The spectrum of the distortion products x_H which occurs with a noise signal plus several other inputs to a non-linearity is of some interest, the low-frequency spectrum[5] in x_H usually being of particular importance since this appears as a permanent error signal, whereas the high-frequency part of x_H may be sufficiently attenuated by the filtering action of the servo loop to be ignored. In the example dealt with in Section 7, it will be seen that, at the actual operating point, the noise signal is considerably greater than that predicted. This increase is found to be caused by cross-modulation products of the noise and sine wave, which in this example can have a considerable magnitude at the effective natural frequency of the feedback loop.

(9) REFERENCES

(1) Booton, R. C.: 'Non-linear Control Systems with Statistical Inputs', Report No. 61, Dynamic Analysis and Control Laboratory, M.I.T.

(2) Nikiforuk, P. N., and West, J. C.: 'The Describing-Function Analysis of a Non-linear Servomechanism Subjected to Stochastic Signals and Noise', *Proceedings I.E.E.*, Monograph No. 207 M, November, 1956 (**104** C, p. 193).

(3) Rice, S. O.: 'Mathematical Analysis of Random Noise', *Bell System Technical Journal*, 1944, **23**, p. 282.

(4) Douce, J. L.: 'A Note on the Evaluation of the Response of a Non-linear Element to Sinusoidal and Random Signals', *Proceedings I.E.E.*, Monograph No. 257 M, October, 1957 (**105** C, p. 88).

(5) West, J. C., and Douce, J. L.: 'Frequency Spectrum Distortion of Random Signals in Non-linear Feedback Systems'. To be published.

(6) West, J. C., and Nikiforuk, P. N.: 'The Behaviour of a Remote-Position-Control Servo Mechanism with Hard Spring Characteristics', *Proceedings I.E.E.*, Paper No. 1621 M, February, 1954 (**101**, Part II, p. 481).

(10) APPENDICES

(10.1) Equivalent Gain for a Signal x in the Presence of n Other Signals

An input $(\beta + x + y)$ is applied to the non-linear element, where β is the total d.c. level at the input, x is a single a.c. signal, and y is the sum of all other signals $y_1 \ldots y_n$. All input signals are assumed to be uncorrelated with one another.

The output from the non-linear system is $v_0 = f(\beta + x + y)$, and that from the equivalent gains has the value $Kx + (k_1y_1 + \ldots k_ny_n)$. The difference $x_H = \{f(\beta + x + y) - [Kx + (k_1y_1 + \ldots k_ny_n)]\}$, which has a mean-square value $M = \lim_{T\to\infty} \frac{1}{T}\int_0^T x_H^2 dt$.

Extending the argument used to obtain eqn. (3) gives for the general case

$$M = \int_{x=-\infty}^{x=+\infty} \int_{y_1=-\infty}^{y_1=+\infty} \ldots \int_{y_n=-\infty}^{y_n=+\infty} x_H^2 q(x)p_1(y_1) \ldots p_n(y_n)dxdy_1 \ldots dy_n$$

Now

$$x_H^2 = \{[f(\beta+x+y)]^2 - 2f(\beta+x+y)[Kx+(k_1y_1+\ldots k_ny_n)] + [Kx + (k_1y_1 + \ldots k_ny_n)]^2\}$$

and

$$\frac{\partial}{\partial K}(x_H^2) = \{0 - 2xf(\beta + x + y) + 2x[Kx + (k_1y_1 + \ldots k_ny_n)]\}$$

Thus

$$\frac{\partial M}{\partial K} = \int_{x=-\infty}^{x=+\infty} \int_{y_1=-\infty}^{y_1=+\infty} \ldots \int_{y_n=-\infty}^{y_n=+\infty} [-2xf(\beta+x+y) + 2Kx^2 + 2x(k_1y_1+\ldots k_ny_n)] q(x)p_1(y_1)\ldots p_n(y_n)dxdy_1\ldots dy_n$$

Now

$$\int_{x=-\infty}^{x=+\infty} \int_{y_1=-\infty}^{y_1=+\infty} \ldots \int_{y_n=-\infty}^{y_n=+\infty} 2x(k_1y_1 + \ldots k_ny_n)q(x)p_1(y_1)\ldots \ldots p_n(y_n)dxdy_1 \ldots dy_n = 0$$

since $\int_{-\infty}^{+\infty} xq(x)dx = 0$ (i.e. x has zero d.c. level)

so that $\frac{\partial M}{\partial K} = 0$ when

$$\int_{x=-\infty}^{x=+\infty} \int_{y_1=-\infty}^{y_1=+\infty} \ldots \int_{y_n=-\infty}^{y_n=+\infty} Kx^2q(x)p_1(y_1)\ldots p_n(y_n)dxdy_1\ldots dy_n = \int_{x=-\infty}^{x=+\infty} \int_{y_1=-\infty}^{y_1=+\infty} \ldots \int_{y_n=-\infty}^{y_n=+\infty} xf(\beta+x+y)q(x)p_1(y_1)\ldots \ldots p_n(y_n)dxdy_1\ldots dy_n$$

The left-hand side of this equation has the value $K\int_{-\infty}^{+\infty} x^2q(x)dx$, since $\int_{-\infty}^{+\infty} p_r(y_r)dy_r = 1$

Hence

$$K = \frac{1}{\bar{x}^2}\int_{x=-\infty}^{x=+\infty} \int_{y_1=-\infty}^{y_1=+\infty} \ldots \int_{y_n=-\infty}^{y_n=+\infty} xf(\beta + x + y)q(x)p_1(y_1)\ldots \ldots p_n(y_n)dxdy_1\ldots dy_n$$

(10.2) Proof that the Gain K for the Signal x Equals the Gain of x through the Effective Non-linear Characteristic $g(\gamma)$

The d.c. value $g(\gamma)$ of the output from the non-linear element, when a d.c. input γ is applied together with inputs $\beta + y_1 + \ldots y_n$, has the value

$$g(\gamma) = \lim_{T\to\infty} \frac{1}{T}\int_0^T f(\gamma + \beta + y)dt$$

An expression may be obtained for $g(\gamma)$ in terms of the amplitude probability distributions of the signals $y_1 \ldots y_n$, by using the same argument as that by which eqn. (3) was derived. Whence

$$g(\gamma) = \int_{y_1=-\infty}^{y_1=+\infty} \ldots \int_{y_n=-\infty}^{y_n=+\infty} f(\gamma + \beta + y)p_1(y_1)\ldots p_n(y_n)dy_1\ldots dy_n$$

If the signal x were now applied alone to the equivalent non-linear characteristic $g(\gamma)$ its gain would have the value [eqn. (9)]

$$K_x = \frac{1}{\bar{x}^2}\int_{x=-\infty}^{x=+\infty} xg(x)q(x)dx$$

Putting in the above value of $g(\gamma)$,

$$K_x = \frac{1}{\bar{x}^2}\int_{x=-\infty}^{x=+\infty} \int_{y_1=-\infty}^{y_1=+\infty} \ldots \int_{y_n=-\infty}^{y_n=+\infty} xf(\beta + x + y)q(x)p_1(y_1)\ldots \ldots p_n(y_n)dxdy_1\ldots dy_n$$

Comparison of this expression with that for the equivalent gain K, derived in Section 10.1, shows that $K_x = K$.

(10.3) Derivation of the Characteristic $g(\gamma)$

When a d.c. signal γ_1 is applied to the non-linear element together with the input $(\beta + y_1)$, the d.c. output $g_1(\gamma_1)$ has the value

$$g_1(\gamma_1) = \int_{y_1=-\infty}^{y_1=+\infty} f(\gamma_1 + \beta + y_1)p_1(y_1)dy_1$$

If a d.c. signal γ_2 is now applied together with the signal y_2 to a non-linearity having a characteristic the same as the effective characteristic $g_1(\gamma_1)$ above, the d.c. output has the value

$$g_2(\gamma_2) = \int_{y_2=-\infty}^{y_2=+\infty} g_1(\gamma_2 + y_2)p_2(y_2)dy_2 = \int_{y_2=-\infty}^{y_2=+\infty} \int_{y_1=-\infty}^{y_1=+\infty} f(\gamma_2+\beta+y_1+y_2)p_1(y_1)p_2(y_2)dy_1dy_2$$

Repeating the above process, $g_r(\gamma_r) = \int_{y_r=-\infty}^{y_r=+\infty} g_{r-1}(\gamma_r + y_r)p_r(y_r)dy_r$,

and if r has values 1 to n (corresponding to signals $y_1 \ldots y_n$) then

$$g_n(\gamma_n) = \int_{y_n=-\infty}^{y_n=+\infty} \ldots \int_{y_1=-\infty}^{y_1=+\infty} f(\gamma_n + \beta + y_1 + \ldots y_n)p_1(y_1)\ldots \ldots p_n(y_n)dy_1\ldots dy_n$$

This expression for $g_n(\gamma_n)$ is the same as that obtained in Section 10.2 [i.e. $g_n(\gamma_n) = g(\gamma)$] and $g(\gamma)$ can therefore be obtained by the above process of n integrations, using the d.c. cursors described in Section 5.1.

(10.4) Proof that, for a Gaussian Signal, $K = \frac{d\lambda}{d\beta}$ (General Case)

An input $(\beta + x + y)$ is applied to the non-linear element, where β is the total d.c. level, x is a single a.c. signal, and y is

all other a.c. signals $y_1 \ldots y_n$. The d.c. output from the non-linearity has the value

$$\lambda = \lim_{T\to\infty} \frac{1}{T}\int_0^T f(\beta + x + y)dt$$

which, from Section 10.2, may be expressed

$$\lambda = \int_{x=-\infty}^{x=+\infty}\int_{y_1=-\infty}^{y_1=+\infty}\cdots\int_{y_n=-\infty}^{y_n=+\infty} f(\beta + x + y)q(x)p_1(y_1)\ldots p_n(y_n)dxdy_1\ldots dy_n$$

Now, $$\frac{d}{d\beta}f(\beta + x + y) = \frac{d}{dx}f(\beta + x + y)$$

Therefore

$$\frac{d\lambda}{d\beta} = \int_{y_1=-\infty}^{y_1=+\infty}\cdots\int_{y_n=-\infty}^{y_n=+\infty}\left\{\int_{x=-\infty}^{x=+\infty} q(x)d[f(\beta + x + y)]\right\} p_1(y_1)\ldots p_n(y_n)dy_1\ldots dy_n$$

Integrating by parts,

$$\int_{x=-\infty}^{x=+\infty} q(x)d\Big[f(\beta + x + y)\Big] = \Big[q(x)f(\beta + x + y)\Big]_{-\infty}^{+\infty} - \int_{x=-\infty}^{x=+\infty} f(\beta + x + y)d[q(x)]$$

For x a Gaussian signal,

$$q(x) = \frac{1}{\sqrt{(2\pi)}\sigma}\varepsilon^{-x^2/2\sigma^2}$$

and $d[q(x)] = \dfrac{-x}{\bar{x}^2}q(x)dx$, where $\bar{x}^2 = \sigma^2$.

Also, $\Big[q(x)f(\beta + x + y)\Big]_{-\infty}^{+\infty} = 0$ since $q(x) = 0$ and $f(\beta + x + y)$ is finite, at $x = \pm\infty$.

Thus,

$$\frac{d\lambda}{d\beta} = \frac{1}{\bar{x}^2}\int_{x=-\infty}^{x=+\infty}\int_{y_1=-\infty}^{y_1=+\infty}\cdots\int_{y_n=-\infty}^{y_n=+\infty} xf(\beta + x + y)q(x)p_1(y_1)\ldots p_n(y_n)dxdy_1\ldots dy_n$$

This expression for $d\lambda/d\beta$ corresponds exactly with that for the equivalent gain, derived in Section 10.1, i.e. for a Gaussian signal in the presence of other signals with which it is uncorrelated, $K = d\lambda/d\beta$.

(10.5) Calculation of the Ordinate Y_R for D.C. Cursors

(a) Sine Signal $y = \hat{E}\sin\omega t$

$$p(y) = \frac{1}{\pi\hat{E}\sqrt{[1-(y/\hat{E})]}} \text{ for } |y/\hat{E}| \leqslant 1, \text{ and } p(y) = 0 \text{ for } |y/\hat{E}| > 1$$

Within the limits

$$|y/\hat{E}| \leqslant 1, \int p(y)dy = \left[\frac{1}{\pi}\sin^{-1}(y/\hat{E})\right]$$

From Section 5.1,

$$\int_{-\hat{E}}^{Y_R} p(y)dy = \frac{1}{2N}(2R-1) \text{ where } R = 1 \text{ to } N \text{ and } \left|\frac{Y_R}{\hat{E}}\right| \leqslant 1.$$

Thus

$$\frac{1}{\pi}\left[\sin^{-1}\left(\frac{Y_R}{\hat{E}}\right) - \sin^{-1}(-1\cdot 0)\right] = \frac{(2R-1)}{2N}$$

whence $$\frac{Y_R}{\hat{E}} = \sin\left[\frac{\pi}{2}\frac{(2R-N-1)}{N}\right]$$

(b) Gaussian Signal

$$p(y) = \frac{1}{\sqrt{(2\pi)}\sigma}\varepsilon^{-y^2/2\sigma^2}$$

From Section 5.1,

$$\int_{-\infty}^{Y_R}\frac{1}{\sqrt{(2\pi)}\sigma}\varepsilon^{-y^2/2\sigma^2}dy = \frac{(2R-1)}{2N}$$

whence

$$\frac{(2R-1)}{2N} = 0\cdot 5\left[1 + \text{erf}\left(\frac{Y_R}{2^{1/2}\sigma}\right)\right], \text{ where erf } z = \frac{2}{\sqrt{\pi}}\int_0^z \varepsilon^{-x^2}dx$$

and erf $(-z) = -$ erf z.

Thus $$\text{erf}\left(\frac{Y_R}{2^{1/2}\sigma}\right) = \frac{(2R-N-1)}{N}$$

(10.6) Solution of Equation (25)

From eqn. (25),

$$\sigma^2 = \nu^2\frac{2(\omega_1+\omega_2)}{\pi}\int_0^\infty\left|\frac{p^3}{(p+\omega_1)(p+\omega_2)(p^2+0\cdot 2k\omega_0 p + k\omega_0^2)}\right|^2 d\omega$$

where $p = j\omega$.

This can be written in the form

$$\sigma^2 = \nu^2\frac{2(\omega_1+\omega_2)}{\pi}\int_0^\infty\left|\frac{p^3}{d_4p^4 + d_3p^3 + d_2p^2 + d_1p + d_0}\right|^2 d\omega$$

in which $d_0 = k\omega_0^2\omega_1\omega_2$ $\quad d_1 = k\omega_0^2(\omega_1+\omega_2) + 0\cdot 2k\omega_0\omega_1\omega_2$, $d_2 = k\omega_0^2 + 0\cdot 2k\omega_0(\omega_1+\omega_2) + \omega_1\omega_2$, $\quad d_3 = 0\cdot 2k\omega_0 + (\omega_1+\omega_2)$, $\quad d_4 = 1$.

From Reference 2, the solution of this integral is

$$\sigma^2 = \nu^2(\omega_1+\omega_2)\frac{(-d_0d_3 + d_1d_2)}{d_4(-d_0d_3^2 - d_1^2d_4 + d_1d_2d_3)}$$

For $\nu = \nu_{n1}$, $\omega_1 = \omega_0/8$ and $\omega_2 = \omega_0/4$, and evaluation of the above expression gives

$$\sigma_{n1}^2 = \nu_{n1}^2\frac{(0\cdot 2 + 413\cdot 3k)}{(0\cdot 2 + 16\cdot 48k + 220\cdot 4k^2)}$$

Similarly, for $\nu = \nu_{n2}$, $\omega_1 = \omega_0$ and $\omega_2 = 2\omega_0$,

$$\sigma_{n2}^2 = \nu_{n2}^2\frac{(1 + 6\cdot 30k)}{(1 + 1\cdot 55k + 0\cdot 42k^2)}$$

DISCUSSION ON

'NON-LINEAR DISTORTION IN TRANSISTOR AMPLIFIERS AT LOW SIGNAL LEVELS AND LOW FREQUENCIES'*

Miss L. Luz (*communicated*): Previous work done by the writer and by Dr. Meyer can be extended to medium frequencies. In the monograph the assumption is made that all elements of the transistor are frequency-independent real quantities. It does not seem necessary to make this assumption; the same expressions in fact can be used to calculate the 2nd harmonic distortion factor at any frequency if the complex parameters of the transistor are known at this given frequency.

2nd Harmonic Distortion at 100 *kc/s.*—The expressions obtained for the common-base configuration are

$$K_d^b = \left|\frac{i_{c2}^b}{i_{c1}^b}\right| = \left|\frac{h_{21}^b K_A - (R_g + h_{11}^b)K_B}{D_1^b}\right| i_{c1}^b \quad . \quad (A)$$

where

$$K_A = \frac{1}{4}\frac{\partial h_{11}^b}{\partial I_e^b}\frac{(1 + h_{22}^b R_L)^2}{(h_{21}^b)^2} - \frac{1}{2}\frac{\partial h_{11}^b}{\partial V_c^b}\frac{1 + h_{22}^b R_L}{h_{21}^b}R_L + \frac{1}{4}\frac{\partial h_{12}^b}{\partial V_c^b}R_L^2$$

$$K_B = \frac{1}{4}\frac{\partial h_{21}}{\partial I_e^b}\left(\frac{1 + h_{22}^b R_L}{h_{21}^b}\right)^2 - \frac{1}{2}\frac{\partial h_{21}^b}{\partial V_c^b}\frac{1 + h_{22}^b R_L}{h_{21}^b}R_L + \frac{1}{4}\frac{\partial h_{22}}{\partial V_c^b}R_L^2$$

$$D_1^b = -\left[R_L(h_{11}^b h_{22}^b - h_{12}^b h_{21}^b) + R_g(1 + h_{22}^b R_L) + h_{11}^b\right]$$

The expressions obtained for the common-emitter configuration are

$$K_d^e = \left|\frac{i_{c2}^e}{i_{c1}^e}\right| = \left|\frac{h_{21}^e K_c - (R_g + h_{11}^e)K_D}{D_1^e}\right| i_{c1}^e \quad . \quad . \quad (B)$$

where

$$K_c = \frac{1}{4}\frac{\partial h_{11}^e}{\partial I_b^e}\left(\frac{1 + h_{22}^e R_L}{h_{21}^e}\right)^2 - \frac{1}{2}\frac{\partial h_{11}^e}{\partial V_c^e}\frac{1 + h_{22}^e R_L}{h_{21}^e}R_L + \frac{1}{4}\frac{\partial h_{12}^e}{\partial V_c^e}R_L^2$$

$$K_D = \frac{1}{4}\frac{\partial h_{21}^e}{\partial I_b^e}\left(\frac{1 + h_{22} R_L}{h_{21}^e}\right)^2 - \frac{1}{2}\frac{\partial h_{21}^e}{\partial V_c^e}\frac{1 + h_{22}^e R_L}{h_{21}^e}R_L + \frac{1}{4}\frac{\partial h_{22}^e}{\partial V_c^e}R_L^2$$

$$D_1^e = -\left[R_L(h_{11}^e h_{22}^e - h_{12}^e h_{21}^e) + R_g(1 + h_{22}^e R_L) + h_{11}^e\right]$$

Both expressions were checked experimentally using a junction transistor type 3X/302 having a common-emitter cut-off frequency of approximately 10 kc/s. The calculations and measurements were made at 100 kc/s, the parameters being directly measured at this frequency.

The results are shown in Fig. A. Quite good agreement between calculated and measured 2nd harmonic distortion factors can be seen. Different values of R_g (internal impedance of signal generator) were considered.

Calculation from an Equivalent Circuit.—If the parameters of an equivalent circuit are known then the *h*-parameters of a transistor can be calculated at any given frequency. From these the 2nd harmonic distortion can be calculated for a particular value of R_g. The natural equivalent circuit shown in Fig. B could be used for this purpose.[A] It is claimed that in a medium

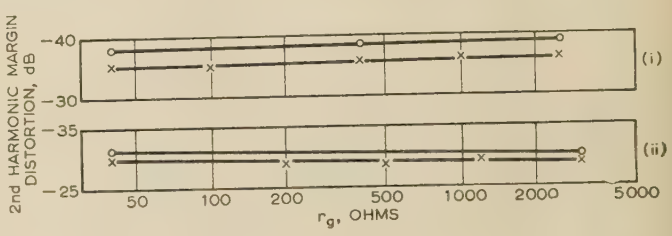

Fig. A

(i) Output distortion factor of common-base configuration as a function of internal resistance of signal generator.
(ii) Output distortion factor of common-emitter configuration as a function of internal resistance of signal generator.

$R_L = 4{\cdot}7$ kilohms; $V_e = 6$ volts; $I_e = 3$ mA; $V_{out} = 4{\cdot}7$ volts (d.a.p.); $f = 100$ kc/s
○ Calculated. × Measured.

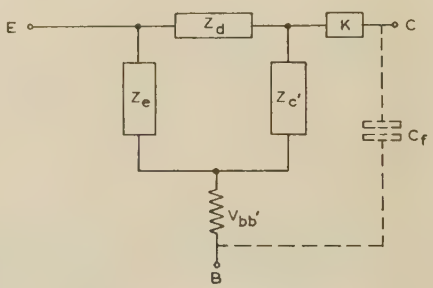

Fig. B.—Natural equivalent circuit.

$$Z_e = \frac{1}{g_e + j\omega C_e}$$
$$Z_{c'} = \frac{1}{g_{c'} + j\omega C_{c'}}$$
$$Z_d = r_d + j\omega L_d$$

frequency range L_d and C_f can be neglected[B] and the circuit then contains seven parameters, which must be measured in order to calculate the *h*-parameters.

For the common-emitter configuration, the *h*-parameters deduced from the natural equivalent circuit will be

$$h_{11}^e = r_{bb'} + \frac{1}{g_e + j\omega C_e} \quad . \quad . \quad . \quad . \quad . \quad . \quad . \quad . \quad (C)$$

$$h_{21}^e = \frac{1}{(g_e + j\omega C_e)r_d} \quad . \quad . \quad . \quad . \quad . \quad . \quad . \quad . \quad (D)$$

$$h_{12}^e = \frac{g_{c'} + j\omega C_{c'}}{K(g_e + j\omega C_e)} \quad . \quad . \quad . \quad . \quad . \quad . \quad . \quad . \quad (E)$$

$$h_{22}^e = \frac{1}{K}\left[(g_{c'} + j\omega C_{c'}) + \frac{1}{r_d} + \frac{g_{c'} + j\omega C_{c'}}{(g_e + j\omega C_e)r_d}\right] \quad . \quad (F)$$

* MEYER, N. I.: Monograph No. 209 R, November 1956 (see 104 C, p. 208).

For the common-base configuration they will be

$$h^b_{11} = \frac{r_d\{(g_e + j\omega C_e)[K(g_{c'} + j\omega C_{c'}) + r_{bb'}] + K(g_{c'} + j\omega C_{c'})r_{bb'}\}}{K(g_{c'} + j\omega C_{c'})[r_d + (g_e + j\omega C_e)] + r_{bb'}(r_d + g_e + j\omega C_e + g_{c'} + j\omega C_{c'})} \quad \text{(G)}$$

$$h^b_{21} = \frac{[r_d + (g_{c'} + j\omega C_{c'})]r_{bb'} + (g_e + j\omega C_e)[K(g_{c'} + j\omega C_{c'}) + r_{bb'}]}{[r_d + (g_{c'} + j\omega C_{c'})]r_{bb'} + (g_e + j\omega C_e)[K(g_{c'} + j\omega C_{c'}) + r_{bb'}] + Kr_d(g_{c'} + j\omega C_{c'})} \quad \text{(H)}$$

$$h^b_{12} = \frac{r_{bb'}[(g_e + j\omega C_e) + (g_{c'} + jwC_{c'}) + r_d] + (g_{c'} + j\omega C_{c'})(g_e + j\omega C_e)}{r_{bb'}[(g_{c'} + j\omega C_{c'}) + (g_e + j\omega C_e) + r_d] + K(g_{c'} + j\omega C_{c'})(g_e + j\omega C_e + r_d)} \quad \text{(J)}$$

$$h_{22} = \frac{r_d + (g_e + j\omega C_e) + (g_{c'} + j\omega C_{c'})}{K(g_{c'} + j\omega C_{c'})(r_d + g_e + j\omega C_e) + r_{bb'}(g_{c'} + j\omega C_{c'})} \quad \text{(K)}$$

The seven necessary measurements are $r_{bb'}$, g_e, C_e, h^e_{120} (l.f. value of h^e_{12}), h^e_{220} (l.f. value of h^e_{22}), h^e_{210} (l.f. value of h^e_{21}) and ω_c (angular frequency at which $|h^e_{12}|$ is 3 dB higher than h^e_{12}).

From these measurements all the remaining four factors that appear in expressions (C)–(K) can be calculated as follows:

$$r_d = \frac{1}{g_e h^e_{210}}$$

$$K = \frac{1}{h^e_{120}\left(\frac{r_d h^e_{220}}{h^e_{120}} - 1\right)}$$

$$g_{c'} = Kh^e_{120}g_e$$

$$C_{c'} = \frac{g_{c'}}{\omega_c}$$

Experimental verification for the common-emitter configurations was made using the same junction transistor, type 3X/302, as above.

The results of measurements and calculations are shown in Fig. C. The agreement obtained between measured and calculated values falls off above 10 kc/s; this is thought to be due to neglecting L_d and C_f in the equivalent circuit used to calculate the h-parameters.

References

(A) Lo, A. W., *et al.*: 'Transistor Electronics' (Prentice-Hall, 1955), p. 240 *et seq.*

(B) *Ibid.*, p. 244.

Dr. N. I. Meyer (*in reply*): I would like to present a short résumé of our latest results in this field.

In September, 1957, an extensive theoretical and experimental investigation was started in our laboratory with the purpose of finding values for the 2nd and 3rd harmonic distortions in junction transistors as a function of d.c. conditions, frequency, load impedance, Z_1, and the internal impedance, Z_g, of the signal generator. The experimental investigation included both low- and high-frequency transistor types in the frequency range from 1 kc/s to 100 kc/s. The ranges of emitter current and collector voltage were 1 to 15 mA and −1 to −15 volts, while Z_g and Z_1 were varied from 10 ohms to 10 kilohms and from 50 ohms to 25 kilohms. These values refer to the common-base configuration.

The results of the investigation are currently being published in a series of laboratory progress reports (in Danish). The first part, which includes a theoretical treatment of almost-linear, complex 2-poles and 4-poles, and extends the work described in the monograph to medium frequencies, is already in print.

The theoretical and experimental results obtained show that the expressions found for low-frequency distortion can be applied in the same form at higher frequencies, provided that the complex parameters, corresponding to the proper frequencies, are inserted. These results apparently agree with the experimental conclusions reached by Miss Luz.

The same progress report cites a few of the experimental results on 2nd and 3rd harmonic distortion in a low-frequency transistor of type OC76. The measured values agree well with theoretical results calculated from h-parameters that have been derived, as functions of d.c. conditions and frequency, directly from the physical design parameters of the transistor.

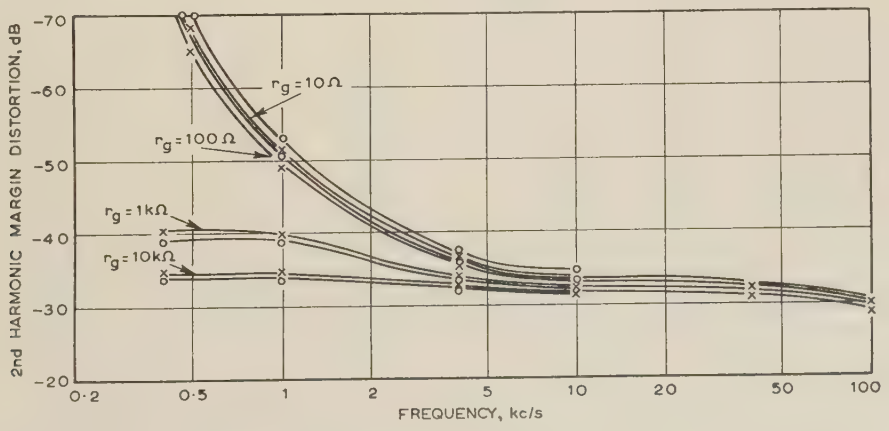

Fig. C.—Output distortion factor of common-emitter configuration as a function of frequency for different internal resistances of signal generator.

R_L = 4·7 kilohms; V_o = 6 volts; I_o = 3 mA; V_{out} = 4·7 volts (d.a.p.).

○ Calculated. × Measured.

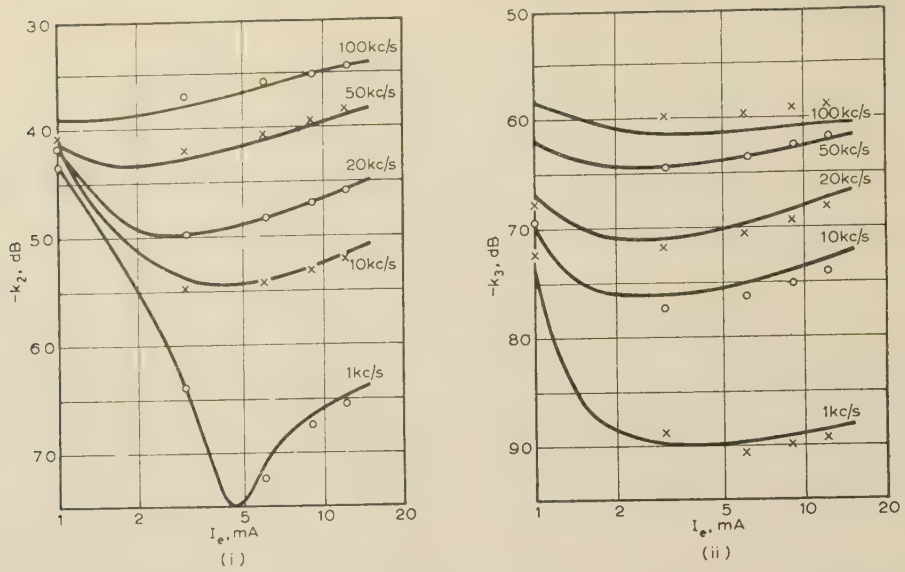

Fig. D

(i) Second-harmonic distortion factor, and
(ii) Third-harmonic distortion factor as a function of emitter direct current for common-base configuration.

Load resistance, $R_1 = 5$ kilohms.
Source resistance, $R_g = 100$ ohms.
Base-collector bias, $V_c = -3$ volts.
Collector alternating current, $i_c = 0{\cdot}1$ mA (r.m.s.).

○ × Calculated.
—— Measured.

It is planned to publish an English translation of the report. Fig. D provides an example of the preliminary results. The 2nd harmonic distortion factor, k_2, is defined as the ratio of amplitudes of the 2nd harmonic and the fundamental component of the collector alternating current. An analogous definition is used for the 3rd harmonic distortion factor, k_3.

DISCUSSION ON
'THE SLIDING CONTACT OF GRAPHITE AND COPPER'*

Dr. D. A. Bell (*communicated*): I should like the author's views on the suggestion of Shobert† that the voltage drop between brush and copper in steady running conditions is largely associated with the work function of an insulating film of liquid or gas which the current traverses by quantum-mechanical tunnel effect. The author states that coherer bridges are formed under the negative brush at a temperature approximating to the melting point of the metal, but Holm‡ states that melting of copper does not occur because the greater part of the voltage drop across the junction occurs in the carbon. Is there any way of observing directly the temperature of the contact areas on the copper?

Dr. W. Davies (*in reply*): In reply to Dr. Bell, I must point out that the contact resistance does not seem to be noticeably affected by the 'tunnel' resistance of adsorbed films of liquid or gas—see, for example, my Fig. 14, where the 'tunnel' resistance of an adsorbed film of water alone is seen to be quite negligible. It is worth noting also that, in an experiment with dry nitrogen, an increase in the pressure of this gas from 0·1 to 760 mm Hg resulted in a decrease of about 20% in the kinetic friction, but produced no really measurable change in the contact resistance. The conclusion here is that a film of the gas was formed aerodynamically under the brush and extended even into the actual contact areas; however, it must have been extremely thin in these latter regions, and conduction through it was almost certainly by way of the tunnel effect.

In actual fact the influence of adsorbed water on the contact resistance seems to be markedly dependent upon the partial pressure of ambient oxygen. It appears then that this water, which may be chemisorbed at the oxide surface, does not simply form a superficial discrete film through which the current might be expected to pass by virtue of the tunnel effect.

With regard to Dr. Bell's second point, reference to my Fig. 4 shows that for a current of 20 amp in a negative brush the voltage drop in the contact is 0·15 volt in vacuum, and about 0·45 volt in dry oxygen at a pressure of 50 mm Hg. The oxide (the reoxidized coherer bridges) under these latter conditions accounts for a voltage drop of 0·3 volt. This value is of course somewhat less than that needed for the maintenance of molten bridges, but since it was measured by an ordinary voltmeter it seems to be distinctly possible that rather higher transient voltages of short duration were developed across the oxide film. In such circumstances the bridges when first formed would be in a molten state.

The main point, however, is that these bridges are in an activated condition when reoxidation occurs.

The difficulty of direct measurement of the temperature at the contact areas of a current-carrying sliding pair is clearly very great, and I am not aware of any really satisfactory method for making such measurements.

* Davies, W.: Monograph No. 271 U, December, 1957 (see 105 C, p. 203).
† Shobert, E. I.: 'Electrical Resistance of Carbon Brushes on Copper Rings', *Transactions of the American I.E.E.*, 1954, 73, Part IIIA, p. 788.
‡ Holm, E.: 'Contribution to the Theory of the Contact between a Carbon Brush and a Copper Collector Ring', *Journal of Applied Physics*, 1957, 28, p. 1171.

DISCUSSION ON

'THE STATISTICAL BASIS OF IMPULSE TESTING'*

Dr. R. Hancox (*communicated*): In Section 8 Dr. Lewis has discussed the accuracy to be expected in a limited series of impulse tests which take the form of Bernoulli trials. The statistical variation of the number of breakdowns S_N obtained in a series of N trials at a fixed voltage is shown to follow a binomial distribution, having a maximum standard deviation when the probability of breakdown p is equal to $0{\cdot}5$. From this it is concluded that the 50% breakdown criterion often specified in impulse tests is not necessarily the best which could be adopted, since the estimate of the probability of breakdown S_N/N is least accurate at the 50% breakdown point. It is often of greater interest, however, to consider the accuracy with which the voltage, as opposed to the probability of breakdown, is determined in such tests. This may be calculated if the distribution of the probability of breakdown p with voltage v is known, and the values of p and v are found for which it is a maximum.

Taking an approximate form for the distribution of S_N [eqn. (9)], it can be shown that the values of p which may result in a given value of $S_N/N = P$ being obtained in an experiment cover the range

$$\Delta p \simeq \frac{2f\sqrt{[NP(1-P)]}}{N+f^2} \quad . \quad . \quad . \quad . \quad \text{(A)}$$

where f is a factor determined by the confidence limits required. For any given distribution of the probability of breakdown this may be rewritten as the range of voltages Δv which could give a particular experimental result. If Δv has a minimum value when $p = 0{\cdot}5$, the 50% breakdown criterion can be obtained more accurately than any other from a statistical point of view. Alternatively, if Δv is not a minimum when $p = 0{\cdot}5$, it may be advantageous to choose a different criterion. The distribution of p which gives the boundary condition, Δv independent of voltage, may be found, and if Δp is small it is given by

$$p = \tfrac{1}{2}\left(1 + \sin \pi/2 \frac{v - V_0}{V_s}\right) \quad . \quad . \quad . \quad . \quad \text{(B)}$$

when $-V_s \leqslant v - V_0 \leqslant V_s$.

The variation of p with voltage which is most often used to represent the results of impulse breakdown tests is the normal or Gaussian distribution, and this can be shown to give a minimum value for Δv when $p = 0{\cdot}5$. Therefore, the 50% breakdown criterion can be assumed to give the greatest statistical accuracy unless it is known that the variation of the probability of breakdown with voltage differs appreciably from the normal distribution.

Dr. T. J. Lewis (*in reply*): Dr. Hancox has made an important contribution concerning the accuracy of measurement of impulse tests. As stated in Section 8 of the paper, for any given value of p there is a dispersion in the value of S_N which has a maximum when $p = 0{\cdot}5$. Eqn. (A) is a statement of what might be called the converse effect; namely, if a given value of S_N ($=NP$, say) is found in a test, there is a range Δp which could give this. Δp also involves a constant f which is related in a complicated way with a required minimum probability of obtaining S_N. In fact Δp lies symmetrically about the point

$$p = \frac{2P + \dfrac{f^2}{N}}{2\left(1 + \dfrac{f^2}{N}\right)}$$

If the minimum probability is high, f is small and

$$p \simeq P \text{ and } \Delta p \simeq 2f[P(1-P)/N]^{1/2}$$

As might be expected Δp has a maximum f/N when $p = P = 0{\cdot}5$. Eqn. (A) may be illustrated by reference to Fig. 6 of the paper, in which, as an artificial example, if $N = 10$ and a minimum probability of about 1% is required for $S_N/N = 0{\cdot}27$, then p might range between about $0{\cdot}1$ and $0{\cdot}5$.

Dr. Hancox has rightly stressed that in practice it will be the range of voltage Δv rather than the range of probability Δp that will be more important. If Δp is small, i.e. f small, then

$$\Delta v \simeq \left(\frac{dv}{dp}\right)_{p=P} \Delta p$$

Eqn. (B) gives the required form of p such that dv/dp changes to keep Δv constant over the whole range of p. The more important problem, however, is given a particular form of p as a function of v, to determine the value of p for which Δv is a minimum. It is clear from the behaviour of Δp that, if dp/dv should change little over a range about $p = 0{\cdot}5$, then Δv will not be a minimum at that point. This has been stated less precisely in Section 8 of the paper.

It is true that if p is represented as a function of v by a normal distribution then Δv is a minimum at $p = 0{\cdot}5$, but it is also true that quite a small change in slope dp/dv could alter this fact. For example, if the slope of the $p - v$ curve at $p = 0{\cdot}8$ were increased by 20% above that for a normal distribution function, then a minimum of Δv would occur at $p = 0{\cdot}8$ and not at $p = 0{\cdot}5$.

Since there is no *a priori* reason why a normal distribution function should be assumed for p, it is not necessarily correct to infer that the 50% breakdown criterion is the best. Some knowledge of the characteristic is required in any specific case before the minimum point can be found. Unfortunately, the determination of this very characteristic involves the same procedures and accuracies that are under discussion.

* Lewis, T. J.: Monograph No. 249 M, July, 1957 (see 105 C, p. 27).

INDEX TO VOLUME 105, PART C

1958

ABBREVIATIONS
(P)—Paper. (D)—Discussion.

Printed in Great Britain by
UNWIN BROTHERS LIMITED, WOKING AND LONDON

PROCEEDINGS OF THE INSTITUTION OF ELECTRICAL ENGINEERS

PART C—MONOGRAPHS, SEPTEMBER 1958

CONTENTS

Declaration on Fair Copying.—Within the terms of the Royal Society's Declaration on Fair Copying, to which The Institution subscribes, material may be copied from issues of the *Proceedings* (prior to 1949, the *Journal*) *which are out of print and from which reprints are not available.* The terms of the Declaration and particulars of a Photoprint Service afforded by the Science Museum Library, London, are published in the *Journal* from time to time.

Bibliographical References.—It is requested that bibliographical reference to an Institution paper should always include the serial number of the paper and the month and year of publication, which will be found at the top right-hand corner of the first page of the paper. This information should precede the reference to the Volume and Part.
Example.—SMITH, J.: 'Reflections from the Ionosphere', *Proceedings I.E.E.*, Paper No. 3001 R, December, 1954 (102 B, p. 1234)

Published by The Institution, Savoy Place, London, W.C.2. *Telephone:* Temple Bar 7676. *Telegrams:* 'Voltampere, Phone, London.'
Printed by Unwin Brothers Limited, Woking and London.